Publication Date (Web): November 22, 2013 | doi: 10.1021/bk-2013-1144.fw001

Green Polymer Chemistry: Biocatalysis and Materials II

In Green Polymer Chemistry: Biocatalysis and Materials II; Cheng, H., et al.;
ACS Symposium Series; American Chemical Society: Washington, DC, 2013.

Publication Date (Web): November 22, 2013 | doi: 10.1021/bk-2013-1144.fw001

In Green Polymer Chemistry: Biocatalysis and Materials II; Cheng, H., et al.;
ACS Symposium Series; American Chemical Society: Washington, DC, 2013.

ACS SYMPOSIUM SERIES **1144**

Green Polymer Chemistry: Biocatalysis and Materials II

H. N. Cheng, Editor
Southern Regional Research Center
Agricultural Research Service
U.S. Department of Agriculture
New Orleans, Louisiana

Richard A. Gross, Editor
Rensselaer Polytechnic Institute
Troy, New York

Patrick B. Smith, Editor
Michigan Molecular Institute
Midland, Michigan

Sponsored by the
ACS Division of Polymer Chemistry, Inc.

American Chemical Society, Washington, DC

Distributed in print by Oxford University Press

Publication Date (Web): November 22, 2013 | doi: 10.1021/bk-2013-1144.fw001

Library of Congress Cataloging-in-Publication Data

Green polymer chemistry : biocatalysis and biomaterials II / H. N. Cheng, Richard A. Gross, Patrick B. Smith, editors.
p. cm. -- (ACS symposium series ; 1144)
Includes bibliographical references and index.
ISBN 978-0-8412-2895-5 (alk. paper)
1. Biodegradable plastics--Congresses. 2. Environmental chemistry--Industrial applications--Congresses. 3. Biopolymers--Congresses. I. Cheng, H. N. II. Gross, Richard A., 1957-. III. Smith, Patrick B.
TP1180.B55G74 2010
547′.7--dc22

2010023453

The paper used in this publication meets the minimum requirements of American National Standard for Information Sciences—Permanence of Paper for Printed Library Materials, ANSI Z39.48n1984.

PRINTED IN THE UNITED STATES OF AMERICA

Publication Date (Web): November 22, 2013 | doi: 10.1021/bk-2013-1144.fw001

Foreword

The ACS Symposium Series was first published in 1974 to provide a mechanism for publishing symposia quickly in book form. The purpose of the series is to publish timely, comprehensive books developed from the ACS sponsored symposia based on current scientific research. Occasionally, books are developed from symposia sponsored by other organizations when the topic is of keen interest to the chemistry audience.

Before agreeing to publish a book, the proposed table of contents is reviewed for appropriate and comprehensive coverage and for interest to the audience. Some papers may be excluded to better focus the book; others may be added to provide comprehensiveness. When appropriate, overview or introductory chapters are added. Drafts of chapters are peer-reviewed prior to final acceptance or rejection, and manuscripts are prepared in camera-ready format.

As a rule, only original research papers and original review papers are included in the volumes. Verbatim reproductions of previous published papers are not accepted.

ACS Books Department

Publication Date (Web): November 22, 2013 | doi: 10.1021/bk-2013-1144.fw001

In Green Polymer Chemistry: Biocatalysis and Materials II; Cheng, H., et al.;
ACS Symposium Series; American Chemical Society: Washington, DC, 2013.

Publication Date (Web): November 22, 2013 | doi: 10.1021/bk-2013-1144.ot001

Editors' Biographies

H. N. Cheng

H. N. Cheng (Ph.D., University of Illinois) is currently a research chemist at Southern Regional Research Center of the U.S. Department of Agriculture in New Orleans, where he works on projects involving improved utilization of commodity agricultural materials, green chemistry, and polymer reactions. Prior to 2009 he was with Hercules Incorporated where he was involved (at various times) with new product development, team and project leadership, new business evaluation, pioneering research, and supervision of analytical research. Over the years, his research interests have included NMR spectroscopy, polymer characterization, biocatalysis and enzymatic reactions, functional foods, and pulp and paper technology. He is an ACS and a POLY Fellow and has authored or co-authored 174 papers, 24 patent publications, co-edited 8 books, and organized or co-organized 22 symposia at national meetings since 2003.

Richard A. Gross

Professor Richard A. Gross (Ph.D., Polytechnic University) was on the faculty of University of Massachusetts (Lowell) from 1988−1998. From 1998 to June 2013 he occupied the Herman F. Mark Chair Professorship at Polytechnic University (New York). Since July 1, 2013 Gross assumed a Constellation Chaired Professorship at Rensselaer Polytechnic Institute (RPI) and is also a member of RPI's Departments of Chemistry and Biology as well as Biomedical Engineering. His research is focused on developing biocatalytic routes to biobased materials including monomers, macromers, prepolymers, polymers, surfactants, and other biochemicals. He combines chemical methods with cell-free and whole-cell biocatalytic systems to investigate biotransformations, such as whole-cell routes to biosurfactants, ω-hydroxylation of fatty acids, protease-catalyzed transformations to polypeptides, and lipase-catalyzed routes to biomaterials. He has over 400 publications in peer-reviewed journals, has been cited approximately 7000 times, has edited 6 books, and has granted and filed a total of 26 patents. Gross has founded and directed several major research centers and assumed a large number of editorial assignments. He is also the recipient of numerous awards, including the 2003 Presidential Green Chemistry Award in the academic category. In 2007, he was inducted into the American Institute for Medical and Biological Engineering. In 2010, he was selected as the Turner Alfrey Visiting Professor. He founded SyntheZyme, LLC in 2009 and serves as its Chief Technology officer. SyntheZyme was established to commercialize technologies developed in Gross's laboratory.

In Green Polymer Chemistry: Biocatalysis and Materials II; Cheng, H., et al.;
ACS Symposium Series; American Chemical Society: Washington, DC, 2013.

Patrick B. Smith

Patrick B. Smith currently serves as a Research Scientist at Michigan Molecular Institute. He received a Ph.D. in Physical Chemistry from Michigan State University and joined The Dow Chemical Company, rising to the rank of Fellow prior to his retirement in 2007. During his time at Dow, he served with Cargill Dow Polymers which launched the Ingeo™ line of poly(lactic acid) products. He consulted for Archer Daniels Midland (ADM) between 2007and 2010, as their R&D leader for the Telles joint venture that commercialized poly(hydroxyalkanoates) and on ADM's biobased propylene glycol effort. He was elected as ACS Fellow in 2013.

Publication Date (Web): November 22, 2013 | doi: 10.1021/bk-2013-1144.ot001

Epilogue

Thus far, with a tired but eager pen,
The editors have pursued their story,
Where *enzymes* are showcased time and again
In examples that boast of their glory.
Like magic potions that were once believed,
They have charmed both research and industry;
Through them improved reactions are achieved
With less waste and more skillful chemistry.
Likewise, *biobased know-how* is the best thing
In material science right now that we need.
Its vogue is due to prudent managing
That permits many projects to proceed.
We celebrate both fields in this book
And hope that you agree with our outlook.

H. N. Cheng
June 2013
(A parody on William Shakespeare's *Henry V*, Epilogue)

Publication Date (Web): November 22, 2013 | doi: 10.1021/bk-2013-1144.ot002

In Green Polymer Chemistry: Biocatalysis and Materials II; Cheng, H., et al.;
ACS Symposium Series; American Chemical Society: Washington, DC, 2013.

Publication Date (Web): November 22, 2013 | doi: 10.1021/bk-2013-1144.pr001

Preface

Green polymer chemistry is a very active area of research that has attracted the attention of the scientific community and the public at large. Developments in this area are stimulated by health and environmental concerns, interest in sustainability, desire to decrease the dependence on petroleum, and opportunity to design and produce "green" products and processes. A large number of publications have appeared, and many new methodologies have been reported.

In consideration of the rapid advances in this area, we organized an international symposium on "Green Polymer Chemistry: Biocatalysis and Biobased Materials" at the American Chemical Society (ACS) national meeting in Philadelphia, PA in August 2012. The symposium was very successful, with a total of 63 papers and active participation and discussions among the leading researchers. Whereas all aspects of Green Polymer Chemistry were covered, a particular emphasis was placed on *biocatalysis* and *biobased materials.* Biocatalysis involves the use of enzymes, microbes, and higher organisms to carry out chemical reactions. It provides exciting opportunities to manipulate polymer structures, to discover new reaction pathways, and to devise environmentally friendly processes. It also benefits from innovations in biotechnology which enables cheaper and improved enzymes to be made and customized polymeric materials to be produced *in vivo* using metabolic engineering. Biobased materials also represent an equally exciting opportunity that has found many industrial and medical applications. There is commonality with biocatalysis because many biobased products are biodegradable, where enzymes and/or microbes are involved.

In view of the success of the Philadelphia symposium, and the fact that this field is multidisciplinary where publications tend to be spread out over journals in different disciplines, we decided to edit this book in order to gather the information on the latest developments in one place. We have asked many of the symposium presenters to contribute chapters to this book, where they report either original results or write special reviews of their ongoing work. We hope this book provides a good representation of what is happening in the forefront of research in green polymer chemistry.

Among the 28 chapters, the following topics are covered that interweave concepts of polymers, materials, biocatalysis, and biotechnology:

1. New biobased materials
   - Renewable raw materials (e.g., polysaccharides, proteins, triglycerides, lignin)
   - Novel bioprocesses and biobased products

In Green Polymer Chemistry: Biocatalysis and Materials II; Cheng, H., et al.;
ACS Symposium Series; American Chemical Society: Washington, DC, 2013.

- Biocatalyzed synthetic and natural polymers
- Silicone bioscience and biomaterials

2. New or improved biocatalysts (e.g., enzymes, whole-cells, and cell extracts)
   - Improved biocatalysts (enzyme engineering, metabolic pathway engineering)
   - Enzyme immobilization and assembly
   - Enzyme-polymer bioconjugates

3. Biotransformations with enzymes, whole cells, and cell-extracts
   - Polymer synthesis through biocatalysis
   - Grafting and functionalization reactions
   - Hydrolysis, degradation, and remediation

4. Other innovative techniques
   - Chemo-enzymatic approaches
   - Genetic PEGylation
   - Microwave-assisted reactions

It may be noted that among the 96 authors who contribute to this book, 70 work in academia, 2 in industry, and 24 in government labs. They are international in scope, with 56 from the United States, 2 from Latin America, 5 from Europe, and 33 from Asia.

This book is targeted for scientists and engineers in multiple disciplines (chemists, biochemists, chemical engineers, agronomists, biochemical engineers, material scientists, microbiologists, molecular biologists, and enzymologists) as well as graduate students who are engaged in research and applications of polymer biocatalysis and biobased materials. It can also be a useful reference book for people who are interested in these topics.

We appreciate the efforts of the authors to submit their manuscripts and their cooperation during the peer review process. We are also grateful to our many anonymous reviewers for their hard work. Thanks are also due to the ACS Division of Polymer Chemistry, Inc. for sponsoring the 2012 symposium.

H. N. Cheng
Southern Regional Research Center
Agricultural Research Service
U.S. Department of Agriculture
1100 Robert E. Lee Blvd.
New Orleans, Louisiana 70124

Richard A. Gross
Department of Chemistry and Chemical Biology
Rensselaer Polytechnic Institute
Cogswell Laboratories
110 8th Street
Troy, New York 12180-3590

Patrick B. Smith
Michigan Molecular Institute
1910 West St. Andrews Road
Midland, Michigan 48640

Publication Date (Web): November 22, 2013 | doi: 10.1021/bk-2013-1144.pr001

Publication Date (Web): November 22, 2013 | doi: 10.1021/bk-2013-1144.ch001

Chapter 1

Green Polymer Chemistry: A Brief Review

H. N. Cheng,*,[1] Patrick B. Smith,[2] and Richard A. Gross[3]

[1]Southern Regional Research Center, Agriculture Research Service, U.S. Department of Agriculture, 1100 Robert E. Lee Blvd., New Orleans, Louisiana 70124
[2]Michigan Molecular Institute, Midland, Michigan 48640
[3]Department of Chemistry and Chemical Biology, Rensselaer Polytechnic Institute, 110 8th Street, Troy, New York 12180-3590
***E-mail: hn.cheng@ars.usda.gov**

This review briefly surveys the research done on green polymer chemistry in the past few years. For convenience, these research activities can be grouped into 8 themes: 1) greener catalysis, 2) diverse feedstock base, 3) degradable polymers and waste minimization, 4) recycling of polymer products and catalysts, 5) energy generation or minimization during use, 6) optimal molecular design and activity, 7) benign solvents, and 8) improved syntheses or processes in order to achieve atom economy, reaction efficiency, and reduced toxicity. All these areas have attracted worldwide attention, with contributions variously from academic, industrial, and government laboratories. Many new promising technologies are being developed. Whereas most aspects of green polymer chemistry are covered in this review, special attention has been paid to biocatalysis and biobased materials due to the specific research interests of the authors. Appropriate examples are provided, taken particularly from the articles included in this symposium volume.

In Green Polymer Chemistry: Biocatalysis and Materials II; Cheng, H., et al.;
ACS Symposium Series; American Chemical Society: Washington, DC, 2013.

Publication Date (Web): November 22, 2013 | doi: 10.1021/bk-2013-1144.ch001

Introduction

Green chemistry is the design of chemical products and processes that reduce or eliminate the use or generation of hazardous substances (*1*, *2*). Because of environmental concerns, energy demands, global warming, and interest in sustainability, this concept has become very popular. Several books and review articles have appeared in the past few years on this topic (*1–6*).

There is also increasing interest in green polymer chemistry. This can be seen in the number of books (*7–9*) and reviews (*10*, *11*) on this topic. We have previously (*12*) categorized the developments in green polymer chemistry into eight pathways (Table 1). These pathways also appear to be consistent with most of themes discussed in recent articles and books on green chemistry (*1–6*).

Table 1. Major pathways for green polymer chemistry

Major Pathways	*Examples*
Greener catalysts	Biocatalysts, such as enzymes and whole cells
Diverse feedstock base	Biobased building blocks and agricultural feedstock (sugars, peptides, triglycerides, lignin). Natural fillers in composites. CO_2 as monomer.
Degradable polymers and waste minimization	Natural renewable materials. Some polyesters and amides.
Recycling of polymer products and catalysts	Many degradable polymers can potentially be recycled. Immobilized enzymes can be reused.
Energy generation or minimization of use	Biofuels. Reactive extrusion method. Microwave-assisted synthesis.
Optimal molecular design and activity	Improved enzymes. Metabolic engineering. Protein synthesis.
Benign solvents	Water, ionic liquids, or reactions without solvents
Improved syntheses and processes	atom economy, reaction efficiency, toxicity reduction.

The aim of this article is not to provide a comprehensive review of green polymer chemistry but to highlight major developments in this area, using selective literature and emphasizing research reported in this symposium volume (*13–39*). A particular emphasis is placed on biocatalysis (e.g., (*40–47*)) and biobased materials (e.g., (*48–55*)). Biocatalysis involves the use of enzymes, microbes, and higher organisms to facilitate chemical reactions. Because the reaction conditions are often mild, water-compatible, and environmentally friendly, they are good examples of green polymer chemistry. Likewise, many biobased materials are biodegradable and recyclable, and their use represents an exemplar of green polymer chemistry.

In Green Polymer Chemistry: Biocatalysis and Materials II; Cheng, H., et al.;
ACS Symposium Series; American Chemical Society: Washington, DC, 2013.

Publication Date (Web): November 22, 2013 | doi: 10.1021/bk-2013-1144.ch001

Biocatalysts

As noted earlier, biocatalysis is an accepted method for green polymer chemistry. Several reviews (*40–43*) and books (*44–47*) are available. There are also ample examples of biocatalysis in this book. A total of 15 articles deal with biocatalysis and biotransformations. Among them, 11 articles deal with enzymes (*13–23*) and 4 deal with whole cells and their biotransformations (*24–27*).

Campbell et al (*13*) provided a good overview of the perspectives and opportunities offered by enzyme-based technologies. As expected, lipases are the most often used enzymes for synthesis. For example, Jiang (*14*) reviewed the synthesis of high purity amino-bearing copolyesters via lipase catalysis. Hunley et al (*15*) described their comprehensive metrology approach to identify key parameters to control enzymatic ring-opening polymerization of lactones. Barrera-Rivera and Martinez-Richa (*16*) used *Yarrowia lipolytica* lipase to synthesize biodegradable polyesters via ring-opening polymerization of cyclic esters, including oligomeric diols, which could be subsequently converted to biodegradable linear polyester urethanes. Mahapatro and Negron (*17*) reviewed the microwave-assisted polymerizations, particularly lipase-catalyzed polymerization of caprolactone. Puskas et al (*18*) utilized lipase-catalyzed transesterification to functionalize poly(ethylene glycol) (PEG). Poojari and Clarson (*19*) reviewed a wide range of lipase-catalyzed reactions involving poly(dimethylsiloxane).

Kawai et al (*20*) constructed mutant cutinases using random and site-directed mutagenesis to improve activity and thermal stability and studied their hydrolytic mechanisms on polyesters. Gitsov and Simonyan (*21*) made polymer-modified laccase complexes and produced copolymers of bisphenol A and diethyl stilbestrol with them. Kadokawa (*22*) used phosphorylase-catalyzed α-glycosylation to make new polysaccharides, such as branched anionic polysaccharides and amylose-grafted heteropolysaccharides. Renggli et al (*23*) reviewed the technique of biocatalytic atom transfer radical polymerization (ATRP), where metalloproteins (e.g., horseradish peroxidase and hemoglobin) were employed to polymerize vinyl monomers under ATRP conditions.

As for whole-cell approaches, Nduko at al (*24*) reviewed the microbial production of lactate-based polyesters, including the optimization of culture conditions, metabolic engineering of bacteria, directed evolution of lactate-polymerizing enzyme, and copolymerization with lactate. Abdala et al (*25*) reported on the microbial synthesis of poly(R-3-hydroyoctanoate), its characterization, and its nanocomposite with thermally reduced graphene. Tomizawa et al (*26*) provided a mini-review of their work on poly(hydroxyalkanoate) production by marine bacteria, using sugars, plant oils, and three unsaturated fatty acids as sole carbon sources. Tada et al (*27*) coupled PEG to antibodies and oligonucleotides (through chemical means) to solubilized them in organic media. In addition, a genetic-encoding approach was devised for the site-specific incorporation of PEG into t-RNA. The techniques of PEGylated biopolymers and the methodology for gene PEGylation seem to be promising new tools for the synthesis of designed (bio-)macromolecular structures

In Green Polymer Chemistry: Biocatalysis and Materials II; Cheng, H., et al.;
ACS Symposium Series; American Chemical Society: Washington, DC, 2013.

Publication Date (Web): November 22, 2013 | doi: 10.1021/bk-2013-1144.ch001

Diverse Feedstock Base

There is growing interest in biobased materials, partly due to the uncertainly with petroleum-based raw materials and partly due to the increasing appreciation of the limited resources of the world and the need for sustainability. Several reviews (*48–51*) and books (*52–55*) are available on the use of natural renewable materials as raw materials for synthesis and polymerization or as ingredients for commercial products. In this book, 12 articles (*28–39*) are primarily involved with biobased raw materials or products.

Several of these articles deal with polyesters. Thus, Ishii et al (*28*) carried out polycondensation reaction on caffeic acid (a precursor in the biosynthesis of lignin) and measured the thermal properties. Tsui et al (*29*) made films and foams of poly(3-hydroxybutyrate-co-3-hydroxyvalerate) blended with silk fibroin and studied their properties. Zhang et al (*30*) monitored the polycondensation reaction of adipic acid and trimethylolpropane using ^{1}H and ^{13}C NMR as a function of time. Mahmood et al (*31*) carried out direct fluorination of polyhydroxyalkanoates at elevated pressure with elemental F_2/N_2 gas mixture and characterized the product.

Hablot et al (*32*) reviewed their work using all parts of soybean as raw materials for conversion to value-added products, including ozonation of oil triglycerides to produce polyols, reactions of proteins to polyurethanes, dimer acids to polyurethanes, and silylation of triglycerides. Biswas et al (*33*) summarized their work involving common beans, particularly the extrusion cooking of whole beans as food, use of bean as fillers in polymeric composites, extraction of triglyceride oils and phenolic phytochemicals from beans, and conversion of bean starch to ethanol. Dowd and Hojilla-Evangelista (*34*) prepared protein isolates from cottonseed meals and characterized the solubility and the functional properties of the protein isolates. Cheng et al (*35*) hydrogenated triglycerides using Ni, Pt and Pd catalysts and obtained oils with distinct amounts of mono- and di-enes, which could be derivatized to produce specific biobased products.

Chung et al (*36*) developed new lignin-based graft copolymers via ATRP and click chemistry; these hybrid materials had a lignin center and poly(n-butyl acrylate) or polystyrene grafts. Fundador et al (*37*) prepared xylan esters with different alkyl chain lengths (C2-C12) and measured the mechanical and crystallization properties of these esters. Wang and Shi (*38*) converted modified starches into thermoplastic materials; new high-value products were then made from these materials using plasticizers or appropriate blends. Cheng et al (*39*) added cotton gin trash as filler in low-density polyethylene; the resulting composites are likely to be useful in applications where reduced cost is desirable and reductions in mechanical properties are acceptable.

Degradable Polymers and Waste Minimization

Because of ongoing interest in degradability, many degradable polymers have been reported. These can be categorized (*56*, *57*) into three groups: a) synthetic polymers, such as condensation polymers, water-soluble polymers, and addition polymers with pro-oxidants or photosensitizers; b) biobased polymers, such as

In Green Polymer Chemistry: Biocatalysis and Materials II; Cheng, H., et al.;
ACS Symposium Series; American Chemical Society: Washington, DC, 2013.

polysaccharides, proteins, lipids, and semi-natural polymers, c) polyblends, e.g., blends of synthetic and biobased polymers, and biopolymer blends. Biobased polymers are beneficial in that many of them are biodegradable, often minimize waste, and mitigate disposal problems. Biocatalysis is also helpful because the ensuing products are potentially biodegradable, and the biocatalysts themselves are usually biodegradable.

It may be noted that almost all the polymers described in this book (polyesters, polyamides, polypeptides, polysaccharides, proteins, triglycerides, lignin, PEG) are biodegradable or potentially biodegradable. Most of the enzymes used are hydrolases (e.g., lipases, cutinase) (*13–19*), and these can be employed for synthesis or for polymer degradation and hydrolysis. Whereas polyethylene itself is not degradable, the incorporation of a agri-based filler (*33*, *39*) is a known tactic to improve the degradability of polyethylene.

Publication Date (Web): November 22, 2013 | doi: 10.1021/bk-2013-1144.ch001

Recycling of Polymer Products and Catalysts

Many of the degradable polymers can be potentially recycled. Certainly agricultural raw materials and bio-based building blocks are amenable to enzymatic or microbial breakdown and (if economically justifiable) can be candidates for recycling. Currently even many plastics (e.g., polyesters, polyolefins, poly(vinyl chloride), polystyrene) are being recycled (*58*, *59*).

Recycling is also important for biocatalysts in order to decrease process cost; this is one of the reasons for the use of immobilized enzymes. Several examples of immobilized enzymes appear in this book (*14*, *15*, *17–19*), particularly Novozym® 435 lipase from Novozymes A/S, which is an immobilized lipase from *Candida antarctica*.

Energy Generation and Minimization of Use

As global demand for energy continues to rise, it is desirable to decrease energy use in industrial processes. Biocatalysis is potentially beneficial in this regard because their use often involves lower reaction temperatures and mild reaction conditions (*13–27*). Other examples of energy savings in this book are microwave-assisted reactions (*17*), reactive extrusion technique (*38*) and extrusion cooking (*33*). An active area of current research is biofuels, and many review articles are available (*60–63*). An example of this technology in this book is shown for the conversion of bean starch to ethanol (*33*).

Molecular Design and Activity

In biochemistry, a good example of molecular design is genetic engineering, which permits modification of protein structure in order to optimize a particular activity. For example, Kawai et al (*20*) used random and site-specific mutagenesis to improve activity and thermostability of cutinase. In designing new lactate polymers, Nduko et al (*24*) modified the bacteria via metabolic engineering. Tada, et al (*27*) utilized a genetic method to incorporate PEG into a peptide.

In Green Polymer Chemistry: Biocatalysis and Materials II; Cheng, H., et al.;
ACS Symposium Series; American Chemical Society: Washington, DC, 2013.

In a different enzyme design, Gitsov and Simonyan (*21*) made supramolecular complexes of laccase, which facilitated one-pot copolymerization reactions.

In product development, structure-property and structure-activity correlations are often employed as part of synthetic design, and several articles on syntheses in this book implicitly incorporated this tactic (e.g., (*25*, *27*, *29*, *35*, *37*, *38*)).

Benign Solvents

A highly desirable goal of green chemistry is to replace organic solvents in chemical reactions with water. Biocatalytic reactions are highly suited for this. In fact, several enzymatic reactions and whole-cell biotransformations in this book were done in water (e.g., (*22*, *25*, *26*, *38*)). An alternative is to carry out the reaction without any solvents, as exemplified by several articles in this book (*17–19*, *28*, *31*, *35*).

Improved Syntheses and Processes

Optimization of experimental parameters in synthesis and process improvement during scale-up and commercialization are part of the work that synthetic scientists and polymer engineers do. The use of biocatalysis can potentially improve processes because enzymatic reactions often involve fewer by-products and less (or no) toxic chemical reagents. An example is the use of biocatalysts instead of copper in ATRP (*23*). Hablot et al (*32*) illustrated an example of process improvement in their effort to ozonize soybean oil to generate polyols. Hunley et al (*15*) identified the key parameters to control enzymatic ring-opening polymerization of lactone, which aided the design of better reaction conditions and next generation catalysts.

Polymer blends and composites are often produced as part of the strategy towards improved products and processes. In this book, examples of polyblends include poly(hydroalkanoate)/silk fibroin (*29*), poly(vinyl alcohol)/bean (*33*), modified starch/polyester and modified starch/polyester/poly(vinyl alcohol) (*38*). Examples of polymeric composites include poly(hydroxyalkanoate)/graphene (*25*), polylactate/bean and polyethylene/bean (*33*), and polyethylene/cotton gin trash (*39*).

Conclusion

From the foregoing discussion, it is clear that green polymer chemistry is very much an active area of research and development. Both *biocatalysis* and *biobased materials* hold much promise as platforms for innovative research and product developments (*64–66*). These areas have attracted the attention of many R&D personnel from academic, industrial, and government laboratories. An impressive array of new structures and new methodologies have been developed. The key to commercial viability is the cost versus benefit of the polymers in use relative to alternatives. For commodity applications like coatings, adhesives, packaging, and construction, cost is a major constraint, but for biomaterials, pharmaceuticals, and

In Green Polymer Chemistry: Biocatalysis and Materials II; Cheng, H., et al.;
ACS Symposium Series; American Chemical Society: Washington, DC, 2013.

Publication Date (Web): November 22, 2013 | doi: 10.1021/bk-2013-1144.ch001

personal care there is more latitude. In view of the wide range of applications, as exemplified by the articles given in this symposium volume, we expect to see continued vigor and vitality in these fields in the future.

Acknowledgments

Thanks are due to the authors of various chapters of this symposium volume for their contributions and for their cooperation during the peer review process. Mention of trade names or commercial products in this publication is solely for the purpose of providing specific information and does not imply recommendation or endorsement by the U.S. Department of Agriculture. USDA is an equal opportunity provider and employer.

References

1. Horvath, I. T.; Anastas, P. T. *Chem. Rev.* **2007**, *107*, 2169–2173.
2. *Green Chemistry: Challenging Perspectives*; Tundo, P., Anastas, P. T., Eds.; Oxford University Press: Oxford, U.K., 2000.
3. *Introduction to Green Chemistry*; Matlack, A. S., Ed.; Marcel Dekker: New York, 2001.
4. *Green Chemistry: An Introductory Text*; Lancaster, M., Ed.; Royal Society of Chemistry: Cambridge, U.K., 2002.
5. *Green Chemistry and Catalysis*; Sheldon, R. A., Arends, I., Hanefeld, U., Eds.; Wiley-VCH: Weinheim, Germany, 2007.
6. *Green Chemistry and Engineering*; Doble, M., Kumar, A., Eds.; Academic Press: Burlington, MA, 2007.
7. *Green Plastics: An Introduction to the New Science of Biodegradable Plastics*; Stevens, F. S., Ed.; Princeton University Press: Princeton, NJ, 2002.
8. *Green Polymer Chemistry: Biocatalysis and Biomaterials*; Cheng, H. N., Gross, R. A., Eds.; ACS Symposium Series 1043; American Chemical Society: Washington, DC, 2010.
9. *Green Polymerization Methods: Renewable Starting Materials, Catalysis and Waste Reduction*; Mathers, R. T.; Meier, M. A. R., Eds.; Wiley-VCH: Weinheim, Germany, 2011.
10. Mulhaupt, R. *Macromol. Chem. Phys.* **2013**, *214*, 159–174.
11. Williams, C. K.; Hillmyer, M. A. *Polym. Rev.* **2008**, *48*, 1–10.
12. *Green Polymer Chemistry: Biocatalysis and Biomaterials*; Cheng, H. N., Gross, R. A., Eds.; ACS Symposium Series 1043; American Chemical Society: Washington, DC, 2010; pp 1−14.
13. Campbell, A. S.; Dong, C.; Wu, N.; Dordick, J. S.; Dinu, C. Z. Enzyme-Based Technologies: Perspectives and Opportunities. In *Green Polymer Chemistry: Biocatalysis and Materials II*; Cheng, H. N., Gross, R. A., Smith, P. B., Eds.; ACS Symposium Series 1144; American Chemical Society: Washington, DC, 2013; Chapter 2.

14. Jiang, Z. Lipase-Catalyzed Synthesis of Poly(amine-co-esters) and Poly(lactone-co-β-aminoesters). In *Green Polymer Chemistry: Biocatalysis and Materials II*; Cheng, H. N., Gross, R. A., Smith, P. B., Eds.; ACS Symposium Series 1144; American Chemical Society: Washington, DC, 2013; Chapter 3.
15. Hunley, M. T.; Orski, S. V.; Beers, K. L. Metrology as a Tool to Understand Immobilized Enzyme Catalyzed Ring-Opening Polymerization. In *Green Polymer Chemistry: Biocatalysis and Materials II*; Cheng, H. N., Gross, R. A., Smith, P. B., Eds.; ACS Symposium Series 1144; American Chemical Society: Washington, DC, 2013; Chapter 4.
16. Barrera-Rivera, K. A.; Martínez-Richa, A. Syntheses and Characterization of Aliphatic Polyesters via *Yarrowia lipolytica* Lipase Biocatalysis. In *Green Polymer Chemistry: Biocatalysis and Materials II*; Cheng, H. N., Gross, R. A., Smith, P. B., Eds.; ACS Symposium Series 1144; American Chemical Society: Washington, DC, 2013; Chapter 5.
17. Mahapatro, A.; Negrón,T. D. M. Microwave Assisted Biocatalytic Polymerizations. In *Green Polymer Chemistry: Biocatalysis and Materials II*; Cheng, H. N., Gross, R. A., Smith, P. B., Eds.; ACS Symposium Series 1144; American Chemical Society: Washington, DC, 2013; Chapter 6.
18. Puskas, J. E.; Seo, K. S.; Castaño, M.; Casiano, M.; Wesdemiotis, C. Green Polymer Chemistry: Enzymatic Functionalization of Poly(ethylene glycol)s Under Solventless Conditions. In *Green Polymer Chemistry: Biocatalysis and Materials II*; Cheng, H. N., Gross, R. A., Smith, P. B., Eds.; ACS Symposium Series1144; American Chemical Society: Washington, DC, 2013; Chapter 7.
19. Poojari, Y.; Clarson, S. J. Biocatalysis for the Preparation of Silicone Containing Copolymers. In *Green Polymer Chemistry: Biocatalysis and Materials II*; Cheng, H. N., Gross, R. A., Smith, P. B., Eds.; ACS Symposium Series 1144; American Chemical Society: Washington, DC, 2013; Chapter 8.
20. Kawai, F.; Thumarat, U.; Kitadokoro, K.; Waku, T.; Tada, T.; Tanaka, N.; Kawabata, T. Comparison of Polyester-Degrading Cutinases from Genus Thermobifida. In *Green Polymer Chemistry: Biocatalysis and Materials II*; Cheng, H. N., Gross, R. A., Smith, P. B., Eds.; ACS Symposium Series 1144; American Chemical Society: Washington, DC, 2013; Chapter 9.
21. Gitsov, I.; Simonyan, A. "Green" Synthesis of Bisphenol Polymers and Copolymers, Mediated by Supramolecular Complexes of Laccase and Linear-Dendritic Block Copolymers. In *Green Polymer Chemistry: Biocatalysis and Materials II*; Cheng, H. N., Gross, R. A., Smith, P. B., Eds.; ACS Symposium Series 1144; American Chemical Society: Washington, DC, 2013; Chapter 10
22. Kadokawa, J. Synthesis of New Polysaccharide Materials by Phosphorylase-catalyzed Enzymatic alpha-Glycosylations Using Polymeric Glycosyl Acceptors. In *Green Polymer Chemistry: Biocatalysis and Materials II*; Cheng, H. N., Gross, R. A., Smith, P. B., Eds.; ACS Symposium Series 1144; American Chemical Society: Washington, DC, 2013; Chapter 11.

23. Renggli, K.; Spulber, M.; Pollard, J.; Rother, M.; Bruns, N. Biocatalytic ATRP: Controlled Radical Polymerizations Mediated by Enzymes. In *Green Polymer Chemistry: Biocatalysis and Materials II*; Cheng, H. N., Gross, R. A., Smith, P. B., Eds.; ACS Symposium Series 1144; American Chemical Society: Washington, DC, 2013; Chapter 12.
24. Nduko, J. M.; Matsumoto, K.; Taguchi, S. Microbial Plastic Factory: Synthesis and Properties of the New Lactate-Based Biopolymers. In *Green Polymer Chemistry 2: Biocatalysis and Biobased Materials*; Cheng, H. N., Gross, R. A., Smith, P. B., Eds.; ACS Symposium Series 1144; American Chemical Society: Washington, DC, 2013; Chapter 13.
25. Abdala, A.; Barrett, J.; Srienc, F. Synthesis of Poly-(R)-3 Hydroxyoctanoate (PHO) and Its Graphene Nanocomposites. In *Green Polymer Chemistry: Biocatalysis and Materials II*; Cheng, H. N., Gross, R. A., Smith, P. B., Eds.; ACS Symposium Series 1144; American Chemical Society: Washington, DC, 2013; Chapter 14.
26. Tomizawa, S.; Chuah, J.; Ohtani, M.; Demura, T.; Numata, K. Biosynthesis of Polyhydroxyalkanoate by a Marine Bacterium Vibrio sp. Strain Using Sugars, Plant Oil and Unsaturated Fatty Acids As Sole Carbon sources. In *Green Polymer Chemistry: Biocatalysis and Materials II*; Cheng, H. N., Gross, R. A., Smith, P. B., Eds.; ACS Symposium Series 1144; American Chemical Society: Washington, DC, 2013; Chapter 15.
27. Tada, S.; Abe, H.; Ito, Y. PEGylated Antibodies and DNA in Organic Media and Genetic PEGylation. In *Green Polymer Chemistry: Biocatalysis and Materials II*; Cheng, H. N., Gross, R. A., Smith, P. B., Eds.; ACS Symposium Series 1144; American Chemical Society: Washington, DC, 2013; Chapter 16.
28. Ishii, D.; Maeda, H.; Hayashi, H.; Mitani, T.; Shinohara, M.; Yoshioka, K.; Watanabe, T. Effect of Polycondensation Conditions on Structure and Thermal Properties of Poly(caffeic acid). In *Green Polymer Chemistry: Biocatalysis and Materials II*; Cheng, H. N., Gross, R. A., Smith, P. B., Eds.; ACS Symposium Series 1144; American Chemical Society: Washington, DC, 2013; Chapter 17.
29. Tsui, A.; Hu, X.; Kaplan, D. L.; Frank, C. W. Biodegradable Films and Foam of Poly(3-Hydroxybutyrate-co-3-hydroxyvalerate) Blended with Silk Fibroin. In *Green Polymer Chemistry: Biocatalysis and Materials II*; Cheng, H. N., Gross, R. A., Smith, P. B., Eds.; ACS Symposium Series 1144; American Chemical Society: Washington, DC, 2013; Chapter 18.
30. Zhang, T.; Howell, B. A.; Martin, P. K.; Martin, S. J.; Smith, P. B. The Synthesis and NMR Characterization of Hyperbranched Polyesters from Trimethylolpropane and Adipic Acid. In *Green Polymer Chemistry: Biocatalysis and Materials II*; Cheng, H. N., Gross, R. A., Smith, P. B., Eds.; ACS Symposium Series 1144; American Chemical Society: Washington, DC, 2013; Chapter 19.
31. Mahmood, S. F.; Lund, B. R.; Yagneswaran, S.; Aghyarian, S.; Smith, Jr., D. W. Direct Fluorination of Poly(3-hydroxybutyrate-co)-hydroxyhexanoate. In *Green Polymer Chemistry: Biocatalysis and Materials II*; Cheng, H. N.,

Publication Date (Web): November 22, 2013 | doi: 10.1021/bk-2013-1144.ch001

Gross, R. A., Smith, P. B., Eds.; ACS Symposium Series 1144; American Chemical Society: Washington, DC, 2013; Chapter 20.
32. Hablot, E.; Graiver, D.; Narayan, R. Biobased industrial products from soybean biorefinery. In *Green Polymer Chemistry: Biocatalysis and Materials II*; Cheng, H. N., Gross, R. A., Smith, P. B., Eds.; ACS Symposium Series 1144; American Chemical Society: Washington, DC, 2013; Chapter 21.
33. Biswas, A.; Lesch, W. C.; Cheng, H. N. Applications of Common Beans in Food and Biobased Materials. In *Green Polymer Chemistry: Biocatalysis and Materials II*; Cheng, H. N., Gross, R. A., Smith, P. B., Eds.; ACS Symposium Series 1144; American Chemical Society: Washington, DC, 2013; Chapter 22.
34. Dowd, M. K.; Hojilla-Evangelista, M. Preparation and Characterization of Protein Isolate from Glandless and Glanded Cottonseed. In *Green Polymer Chemistry: Biocatalysis and Materials II*; Cheng, H. N., Gross, R. A., Smith, P. B., Eds.; ACS Symposium Series 1144; American Chemical Society: Washington, DC, 2013; Chapter 23.
35. Cheng, H. N.; Rau, M.; Dowd, M. K.; Easson, M. W.; Condon, B. D. Hydrogenated Cottonseed Oil as Raw Material for Biobased Materials. In *Green Polymer Chemistry: Biocatalysis and Materials II*; Cheng, H. N., Gross, R. A., Smith, P. B., Eds.; ACS Symposium Series 1144; American Chemical Society: Washington, DC, 2013; Chapter 24.
36. Chung, H.; Al-Khouja, A.; Washburn, N. R. Lignin-Based Graft Copolymers via ATRP and Click Chemistry. In *Green Polymer Chemistry: Biocatalysis and Materials II*; Cheng, H. N., Gross, R. A., Smith, P. B., Eds.; ACS Symposium Series 1144; American Chemical Society: Washington, DC, 2013; Chapter 25.
37. Fundador, N. G. V.; Enomoto-Rogers, Y.; Iwata, T. Esterification of Xylan and Its Applicaion. In *Green Polymer Chemistry: Biocatalysis and Materials II*; Cheng, H. N., Gross, R. A., Smith, P. B., Eds.; ACS Symposium Series 1144; American Chemical Society: Washington, DC, 2013; Chapter 26.
38. Wang, J. H.; Shi, B. Converting Polysaccharides into High Value Water Dispersible Thermoplastic Materials. In *Green Polymer Chemistry: Biocatalysis and Materials II*; Cheng, H. N., Gross, R. A., Smith, P. B., Eds.; ACS Symposium Series 1144; American Chemical Society: Washington, DC, 2013; Chapter 27.
39. Cheng, H. N.; Dowd, M. K.; Finkenstadt, V. L.; Selling, G. W.; Evangelista, R. L.; Biswas, A. Use of Cotton Gin Trash and Compatibilizers in Polyethylene Composites. In *Green Polymer Chemistry: Biocatalysis and Materials II*; Cheng, H. N., Gross, R. A., Smith, P. B., Eds.; ACS Symposium Series 1144; American Chemical Society: Washington, DC, 2013; Chapter 28.
40. Gross, R. A.; Kumar, A.; Kalra, B. *Chem. Rev.* **2001**, *101*, 2097–2124.
41. Kobayashi, S.; Uyama, H.; Kimura, S. *Chem. Rev.* **2001**, *101*, 3793–3818.
42. Kobayashi, S.; Makino, A. *Chem. Rev.* **2009**, *109*, 5288–5353.
43. Cheng, H. N.; Gu, Q.-M. *Polymers* **2012**, *4*, 1311–1330 (Special Issue on Enzymes in Monomer and Polymer Synthesis).

44. *Biocatalysis in Polymer Chemistry*; Loos, K., Ed.; Wiley-VCH: Weinheim, Germany, 2011.
45. *Polymer Biocatalysis and Biomaterials II*; Cheng, H. N., Gross, R. A., Eds.; ACS Symposium Series 999; American Chemical Society: Washington, DC, 2008.
46. *Polymer Biocatalysis and Biomaterials*; Cheng, H. N., Gross, R. A., Eds.; ACS Symposium Series 900; American Chemical Society: Washington, DC, 2005.
47. *Biocatalysis in Polymer Science*; Gross, R. A., Cheng, H. N., Eds.; ACS Symposium Series 840; American Chemical Society: Washington, DC, 2002.
48. Roach, P.; Eglin, D.; Rohde, K.; Perry, C. C. *J. Mater. Sci.: Mater. Med.* **2007**, *18*, 1263.
49. Meier, M. A. R.; Metzgerb, J. O.; Schubert, U. S. *Chem. Soc. Rev.* **2007**, *36*, 1788–1802.
50. Bhardwaj, R.; Mohanty, A. K. *J. Biobased Mater. Bioenergy* **2007**, *1* (2), 191–209.
51. Raquez, J.-M.; Deléglise, M.; Lacrampe, M.-F.; Krawczak, P. *Prog. Polym. Sci.* **2010**, *35*, 487–509.
52. *Biobased Monomers, Polymers, and Materials*; Smith, P. B., Gross, R. A., Eds.; ACS Symposium Series 1105; American Chemical Society: Washington, DC, 2012.
53. *Degradable Polymers and Materials: Principles and Practice*, 2nd ed.; Khemani, K., Scholz, C., Eds.; ACS Symposium Series 1114; American Chemical Society: Washington, DC, 2012.
54. *Natural Fibers, Biopolymers, and Biocomposites*; Mohanty, A. K., Misra, M., Drzal, L. T., Eds.; CRC Press: Boca Raton, FL, 2005.
55. *Bio-Based Polymers and Composites*; Wool, R., Sun, X. S., Eds.; Elsevier: Burlington, MA, 2005.
56. Cheng, H. N. An Overview of Degradable Polymers. In *Degradable Polymers and Materials: Principles and Practice*, 2nd ed.; Khemani, K., Scholz, C., Eds.; ACS Symposium Series 1114; American Chemical Society: Washington, DC, 2012; pp xiii−xiv.
57. Khemani, K.; Scholz, C. Introduction and Overview of Degradable and Renewable Polymers and Materials. In *Degradable Polymers and Materials: Principles and Practice*, 2nd ed.; Khemani, K., Scholz, C., Eds.; ACS Symposium Series 1114; American Chemical Society: Washington, DC, 2012; pp 3−10
58. *Polymer Recycling: Science, Technology, and Applications*; Scheirs, J., Ed.; Wiley: New York, 1998.
59. Bayer, F. L *Food Addit. Contam.* **1997**, *14*, 661–670.
60. Naik, S. N.; Goud, V. V.; Rout, P. K.; Dalai, A. K. *Renewable Sustainable Energy Rev.* **2010**, *14*, 578–597.
61. Damartzis, T.; Zabaniotou, A. *Renewable Sustainable Energy Rev.* **2011**, *15*, 366–378.
62. Carroll, A.; Somerville, C. *Annu. Rev. Plant Biol.* **2009**, *60*, 165–182.

Publication Date (Web): November 22, 2013 | doi: 10.1021/bk-2013-1144.ch001

63. Ragauskas, A. J.; Williams, C. K.; Davison, B. H.; Britovsek, G.; Cairney, J.; Eckert, C. A.; Frederick, W. J., Jr.; Hallett, J. P; Leak, D. J.; Liotta, C. L.; Mielenz, J. R.; Murphy, R.; Templer, R.; Tschaplinski, T. *Science* **2006**, *311*, 484–489.
64. Dale, B. E. *J. Chem. Technol. Biotechnol.* **2003**, *78*, 1093–1103.
65. Babu, R. P.; O'Connor, K.; Seeram, R. *Prog. Biomater.* **2013**, *2*, 8, DOI:10.1186/2194-0517-2-8.
66. Bomgardner, M. *Chem. Eng. News* **2013**, *91* (26), 14 (July 1, 2013).

Publication Date (Web): November 22, 2013 | doi: 10.1021/bk-2013-1144.ch001

Publication Date (Web): November 22, 2013 | doi: 10.1021/bk-2013-1144.ch002

Chapter 2

Enzyme-Based Technologies: Perspectives and Opportunities

Alan S. Campbell,[1] Chenbo Dong,[1] Nianqiang Wu,[2] Jonathan S. Dordick,[*,3] and Cerasela Zoica Dinu[*,1]

[1]Department of Chemical Engineering, West Virginia University, Morgantown, West Virginia 26506
[2]Department of Mechanical and Aerospace Engineering, West Virginia University, Morgantown, West Virginia 26506
[3]Department of Chemical and Biological Engineering, Rensselaer Polytechnic Institute, Troy, New York 12180
[*]E-mail: dordick@rpi.edu (J.S.D.); cerasela-zoica.dinu@mail.wvu.edu (C.Z.)

Enzymes are biological catalysts that are currently used for biocatalysis, biofuel synthesis and biological fuel cell production, for biosensors, as well as as active constituents of surfaces with antifouling and decontamination properties. This review is focused on recent literature covering enzyme-based technologies with emphasis on enzymes as preferred catalysts that provide environmentally friendly, inexpensive and easy to use alternatives to existing decontamination technologies against a wide variety of pathogens, from bacteria to spores.

In Green Polymer Chemistry: Biocatalysis and Materials II; Cheng, H., et al.; ACS Symposium Series; American Chemical Society: Washington, DC, 2013.

Publication Date (Web): November 22, 2013 | doi: 10.1021/bk-2013-1144.ch002

Introduction

Enzymes are biological catalysts with high selectivity and specificity (*1*, *2*) that are employed in a wide range of applications from industrial catalysis (*3–6*), to biofuel (*7–10*) and biofuel cell production (*11–13*), from biosensing (*14–16*), to pharmaceutical and agrochemical synthesis (*17–19*), and in surface active materials with antifouling (*20–22*) or decontamination (*23*, *24*) capabilities. Their high specificity and selectivity have enabled enzyme-based industrial processes with high yields and fewer harmful byproducts than those resulting from traditional chemical processes (*3*, *4*, *8*). Furthermore, enzymes operate at much milder conditions of temperature, pressure and pH than conventional catalysts (*1*, *2*), thereby providing substantial energy and manufacturing costs savings (*3*, *25*). However, there are a number of practical problems associated with the development of enzyme-based technologies *in vitro*. For instance, enzyme isolation and purification is laborious and costly (*18*) and most of the isolated enzymes have optimum activity in water-based environments. Further, in such applications (*26*) their increased specificity and selectivity could lead to narrow-ranged and focused catalysis, thus enzyme-based systems with short operational lifetimes (*1*, *2*).

Enzyme immobilization is used as a viable alternative to overcome the limitations of enzyme-based applications *in vitro* and to ensure high enzyme activity retention and high operational stability (*2*, *27*). The choice of immobilization technique is determined by considering both chemical and physical properties of the enzymes and of the support surfaces. As such, immobilization has been achieved by entrapping enzymes into polymer matrices (*28*, *29*), Langmuir-Blodgett films (*30*, *31*), solid- (*32*) or liquid- (*33*) based membranes, or simply by attachment of enzymes onto solid supports (either by covalent or physical immobilization) (*16*, *34*, *35*). This review is focused on the current trends in enzyme-based technologies and our own research aimed at developing decontamination platforms based on enzymes and capable of neutralizing bacteria, viruses and spores (*23*, *24*, *36*). Various enzyme immobilization strategies are discussed and further insights into the next generation of surface decontamination technologies are provided, outlining the studies that are underway to enable these technologies to be self-sustainable (i.e. operate under ambient conditions without external addition of the enzyme substrate).

Industrial Catalysis

Biocatalysis (*25*) has gained widespread use across several industries including food processing, specialty and commodity chemicals, and in pharmaceuticals production (*5*, *17*, *18*). For example, in pharmaceutical and chemical industries, enzymes are used to circumvent the often complicated steps required by chemical synthesis and separation in order to generate compounds of high purity, typically chiral, while having a much lower environmental impact (*3*, *17*, *18*). A hypothetical process is shown in Figure 1a; the image shows a nanoparticle-enzyme-based packing technology developed for large-scale industrial reacting.

In Green Polymer Chemistry: Biocatalysis and Materials II; Cheng, H., et al.;
ACS Symposium Series; American Chemical Society: Washington, DC, 2013.

Publication Date (Web): November 22, 2013 | doi: 10.1021/bk-2013-1144.ch002

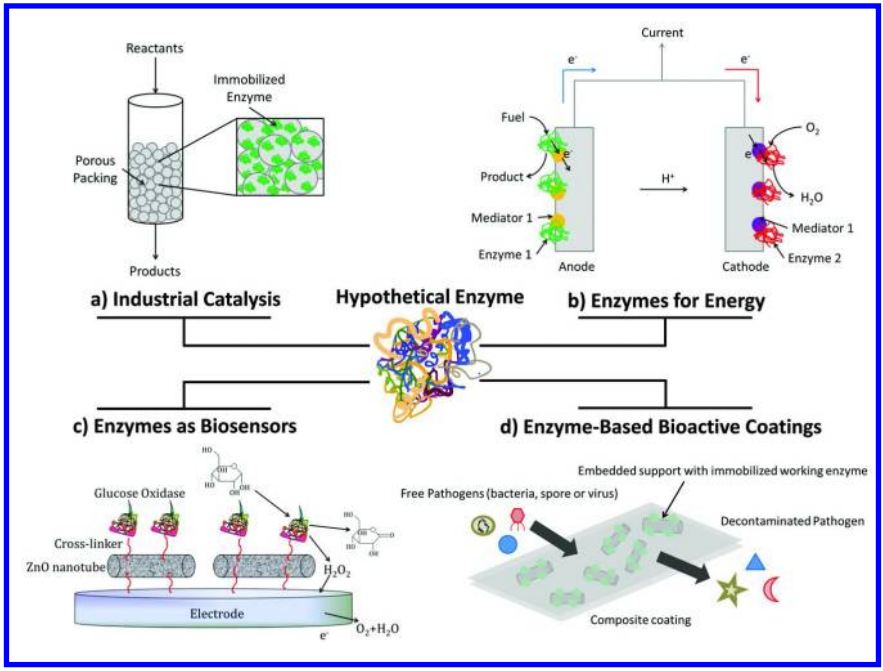

Figure 1. Schematic diagrams for the applications of enzymes as biological catalysts currently used for industrial-based membrane separation (a), biological fuel cell (b), as core components in biosensors (c), and as active constituents of surfaces with antifouling and decontamination properties (d). (see color insert)

The industrial use of enzymes has been influenced by the emerging technologies that allowed recombinant technology or genetic engineering (*3*, *17*, *18*) to be implemented for the generation of enzymes with improved catalytic properties and selectivity (*25*, *37*), as well as by the development of immobilization and polymer-based crosslinking techniques that allow enhanced enzyme stability (*1*, *2*, *23*). Specifically, when an enzyme is immobilized onto the surface of a chosen support it can become partially denatured, i.e., the secondary and tertiary structural features of the enzyme can be altered, thus reducing its activity (*38*). Furthermore, enzyme-enzyme aggregation can occur at high surface loadings, which can further reduce enzyme activity (*39*). Immobilization and crosslinking of enzymes onto nanoscale supports, such as carbon nanotubes, are not only capable of increasing enzyme activity and stability in extreme conditions (*1*, *23*), but could also allow for enzyme retention and thus reusability in several reaction processes. Activies of the enzymes immobilized at the nanoscale support have been found to be influenced by the properties of the support (i.e., surface curvature, surface chemistry, etc.) as well as by the immobilization method being

In Green Polymer Chemistry: Biocatalysis and Materials II; Cheng, H., et al.;
ACS Symposium Series; American Chemical Society: Washington, DC, 2013.

used (covalent versus physical) (*39*). For example, when Dinu et al. immobilized perhydrolase S54V (AcT) onto single-walled carbon nanotubes (SWNTs), the immobilization process yielded ~20% of the specific activity compared to the activity of free enzyme in solution. However, when the enzyme was crosslinked using aldehyde dextran prior to immobilization onto the SWNTs, ~40% specific activity was retained (*23*). These advantages of using enzyme immobilization or enzyme crosslinking might reduce the high cost associated with enzyme production and use (*18*, *27*).

Enzymes for Energy: Biofuel Synthesis and Biological Fuel Cells

Publication Date (Web): November 22, 2013 | doi: 10.1021/bk-2013-1144.ch002

Enzymes are at the forefront of several emerging energy technologies that will help to revolutionize energy production on both the macro- and micro-scales. Energy-based applications of enzymes include: biofuel synthesis, and enzyme biofuel cell production.

With the costs of fossil fuels on the rise and a greater push for more environmentally friendly energy sources, biofuels represent a valuable alternative energy source, with enzymatic processing being a critical component of the process (*8*, *40*). Generally, biofuels are produced via the biochemical conversion (e.g., hydrolysis, esterification or transesterification) of renewable biomass, either chemically or enzymatically (*7*, *10*). Biofuels such as bioethanol and biodiesel are a classification of fuels derived from biomass conversion. In the United States, bioethanol manufactured from cornstarch was widely used in recent years (*41*). Biodiesel is produced from a variety of sources through the transesterification of alkyl esters from feedstock and not only is more environmentally-friendly but also can be used with a higher efficiency than traditional gasoline (*41*). The selectivity and biocompatibility of enzymes lead to a more efficient process with fewer unwanted byproducts than traditional chemical processing (*8*). The large loading requirements and inherent cost of enzymes have reduced the enthusiasm for industrial scale use of enzymes for biofuel production (*8*). However, the economic viability of enzymatic processes can be improved through enzyme immobilization onto solid supports to allow for large-scale production (*27*) and reusability (*42*).

Biological fuel cells transform the chemical energy of organic compounds, such as glucose or ethanol, into electricity by using enzymes as the catalyst (*11*, *12*, *43*). Figure 1b shows a schematic diagram of an enzyme-based fuel cell. The biofuel reaction is catalyzed by two different enzymes; the oxidation of the enzyme at the anode interface transfers the electrons to the cathode and onto a second enzyme to lead to electric current production. Enzyme functionality and specificity allow the construction of the fuel cells without a membrane separating the anode and cathode (*12*, *43*). Due to this feature, enzyme-based fuel cells can be easily miniaturized to allow incorporation into implantable biomedical devices such as artificial organs, micro-pumps, micro-valves, pacemakers and sensors (*13*, *43*) further decreasing the risk of cytotoxicity associated with the implants (*13*).

Publication Date (Web): November 22, 2013 | doi: 10.1021/bk-2013-1144.ch002

Enzymes as Biosensors

Enzyme-based biosensors can be used for recognition and quantification of various analytes from sugar (*44–46*) to hydrogen peroxide (*47*), and from superoxide anions (*48*), to proteins (*49*). Enzyme-based biosensors are formed by immobilizing enzymes onto a wide range of transducers, including electrodes (*50*); the immobilized enzymes create an "open-gate-based electron communication window" with the electrode surface (*51*, *52*). The general physical and chemical properties of the materials used in the construction of biosensors, as well as the working conditions being employed, play a significant role in the performance and the detection capability of the biosensor (*53*). For developing the next generation of viable biosensors with increased flexibility, accuracy, specificity and optimal performance, the proper support materials and enzyme immobilization conditions need to be carefully considered. The examples included below provide a comprehensive guide into current enzyme-based biosensors used in several laboratory and industrial settings.

Glucose detection is of great importance in various fields such as the food industry, quality monitoring processes, and in clinical settings for diabetes diagnosis and therapeutic maintenance (*54*). Due to their high surface area-volume ratio, as well as their low toxicity and ease of fabrication, metal oxide-based and carbon-based nanomaterials are considered excellent candidates for immobilization of glucose oxidase to lead to the next generation of glucose-based biosensors (Figure 1c) (*55*). Zinc oxide nanotubes were recently used in biosensor fabrication that allowed linear detection of glucose in only 3 s, with a limit of detection between 50 μM to 12 mM (*56*); in this example the reaction is catalyzed by the glucose oxidase enzyme which transfers electrons to the support conductive material. Similarly, glucose oxidase-tetragonal pyramid-shaped zinc oxide nanostructure biosensors allowed detection in a range of 50 μM to 8.2 mM (*57*). In other settings, glucose oxidase was immobilized onto platinum multi-walled carbon nanotube-alumina-coated silica nanocomposites to form biosensors that displayed wide linear detection up to 10.5 mM and response time of less than 5 s (*58*). Lastly, bionanocomposites comprising glucose oxidase-platinum-functional graphene-chitosan complexes were used to achieve a detection limit of 0.6 μM (*59*). For clinical application, a multi-layer cadmium telluride quantum dot-glucose oxidase conjugate biosensor was developed to detect glucose concentrations in serum; such a biosensor allowed glucose detection with minimal pretreatment of the sample and with increased accuracy (*60*).

Lactose is a metabolic byproduct regulated by the food industry (*61*, *62*). Novel, rapid, simple and inexpensive biosensors that allow precise detection of lactose were constructed by integrating 3-mercapto propionic acid functionalized gold electrodes and beta-galactosidase-glucose oxidase-peroxidase-mediator tetrathiafulvalene combined membranes (*63*). Such biosensors exhibited a linear detection range of 1.5 μM to 120 μM, with a detection limit of 0.46 μM. Furthermore, such biosensors had a working lifetime of nearly 1 month.

Hydrogen peroxide is the byproduct of several biochemical oxidation processes, as well as an essential mediator in clinical, pharmaceutical, food

In Green Polymer Chemistry: Biocatalysis and Materials II; Cheng, H., et al.;
ACS Symposium Series; American Chemical Society: Washington, DC, 2013.

industry and environment (*64*). Fast, accurate and reliable detection of hydrogen peroxide was achieved using horseradish or soybean peroxidase enzyme-based systems. For instance, horseradish peroxidase was immobilized onto gold functionalized titanium dioxide nanotubes (*65*) or onto chitosan-based nanocomposites (*66*) to allow the construction of biosensors with a detection range from 5 μM to 400 μM (measurement limit of 2 μM) and hydrogen peroxide detection ranging from 0.6 μM and 160 μM (detection limit of 0.15 μM) respectively. Similarly, soybean peroxidase-based biosensors were formed by immobilization of the enzyme onto single-walled carbon nanohorns and showed linear detection ranging from 20 μM to 1.2 mM (detection limit of 0.5 μM) (*67*).

Biological analytes ranging from superoxide anions to proteins have been detected using enzyme-based biosensors. The superoxide anion is mostly regarded as toxic leading to cellular death and mutagenesis (*68*). Recently, a novel disposable superoxide anion biosensor based on the enzyme superoxide dismutase was fabricated (*48*). Such a biosensor was able to detect superoxide anions in a range from 0.08 μM to 0.64 μM; furthermore, this biosensor showed increased sensitivity, accuracy and long term stability. Also, a horseradish peroxidase-gold nanoparticles-carbon nanotube hybrid biosensor proved to have excellent ability to detect human IgG protein for advancing immuno-analysis assays (*69*).

Enzyme amperometric biosensors have also been developed and employed for the detection, monitoring and reporting of biochemical analytes related to a wide range of pathologies ranging from diabetes to trauma-associated hemorrhage (*53*). Implantable enzyme amperometric biosensors must recognize, transmute and generate physicochemical signals that are proportional to the chemical potential (concentration) of the analytes they are intended to be measured. Kotanen et al. have summarized the properties of such biosensors, as well as the conditions required to ensure enzyme biotransducer performance such as the stability, substrate interference, or mediator selection. The failures associated with enzyme-based biosensors are mainly due to the degradation of the immobilized enzyme or its denaturation at the interface by unfolding which could lead to loss of biorecognition and thus loss of signal transduction (*51–53*).

Publication Date (Web): November 22, 2013 | doi: 10.1021/bk-2013-1144.ch002

Enzyme-Based Bioactive Coatings

Enzymes can be used to provide biological function to non-biological materials, thus leading to a "bioactive" material or surface (*70*). In many such applications, enzymes are incorporated into paint or polymer-based coatings and subsequently applied to a desired surface (*22*, *24*, *71*). Two of the main areas in which this type of technology is being employed are in the development of antifouling surfaces (*20*, *21*) and surfaces with active decontamination capabilities (*23*, *36*). Figure 1d illustrates the general principle of enzyme-based coatings; enzymes are immobilized onto nanosupports and upon entrapment in composite-based materials they can generate reactive species to prevent biofilm formation or to allow decontamination.

Publication Date (Web): November 22, 2013 | doi: 10.1021/bk-2013-1144.ch002

Enzyme-Based Antifouling Coatings

The main aim of antifouling coatings is to prevent the attachment and growth of living organisms (referred to as a biofilm) onto a surface (*22*). This functionality is vital in many different applications including biomedical implants (*72*), biosensors (*73*) and several types of equipment used in industrial and marine settings (*74*, *75*). There are two major steps in biofilm formation: the initial adhesion of the fouling species, and the proliferation of that species (*22*). To combat adhesion or reduce adhesion strength (*76*), "non-sticky" coatings have been developed (*77*). To deter proliferation, enzyme-based coatings that generate reactive species to prevent biofilm formation have been developed (*22*). Such technologies offer viable alternatives to traditional antifouling coatings that rely on the use of broadly cytotoxic compounds (*78*, *79*), and further provide safer and more environmentally friendly substitutes.

Enzyme-Based Decontamination Coatings

Enzyme-based decontamination platforms have been proposed as viable alternatives to currently available decontamination methods that use harsh chemicals and pose environmental and logistical burdens (*80–82*). Our groups have pioneered research into enzyme-nanomaterial-based coatings to be used as decontamination platforms that exhibit bactericidal, virucidal and sporicidal activities (*23*, *24*, *36*, *83*). For instance, we have shown that upon enzyme immobilization onto carbon-based nanomaterials, including carbon nanotubes, enzyme S54V perhydrolase (AcT) stability is increased under adverse conditions such as high temperature (up to 75°C) as well as over long periods of time and room temperature storage conditions (*23*, *38*, *84*) (Figure 2a,b,c). Also, the conjugates thus formed can further be incorporated into polymer or paint-based coatings without undesired leaching of the enzyme (*23*, *71*).

The decontamination capabilities of such coatings were tested against various pathogens. Peracetic acid generated by carbon nanotube-immobilized S54V perhydrolase in a latex-based coating was found to be able to decontaminate >99% of 10^6 CFU/mL B. *cereus* spores within 1 h (Figure 2d), $4x10^7$ PFU/mL influenza virus in 15 min, and 10^6 CFU/mL E. *coli* in only 5 min, upon addition of the substrates propylene glycol diacetate and hydrogen peroxide (*23*, *83*). With a sustainable substrate source, such coatings can be used in the future as a passive decontamination measure to combat aerosolized anthrax. Additionally, Pangule et al. showed the antimicrobial capabilities of a lysostaphin-based coating. When such coatings were tested against 10^6 CFU/mL of methicillin-resistant *Staphylococcus aureus* (MRSA), >99% killing capability was achieved in only 2 h (*36*). Borkar et al. tested the bactericidal and sporicidal capabilities of two other enzymes incorporated into paint-based coatings, namely laccase and chloroperoxidase. Hypochlorous acid produced by chloroperoxidase in the presence of hydrogen peroxide and Cl^- ions was found to be capable of killing >99% of 10^6 CFU/mL S. *aureus* and E. *coli* after 30 min. Immobilized laccase also showed bactericidal activity in the presence of several mediators with >99% killing achieved in 30 min for S. *aureus* and in 60 min for E. *coli*. The sporicidal

In Green Polymer Chemistry: Biocatalysis and Materials II; Cheng, H., et al.;
ACS Symposium Series; American Chemical Society: Washington, DC, 2013.

capabilities of laccase were also demonstrated with >99% killing of 10^4 CFU/mL B. *cereus* and B. *anthracis* spores in 2 h (*24*). All of these results show the enormous potential of enzyme-based systems for active surface decontamination in multiple situations including hospital and military scenarios (*23*, *24*, *36*, *83*).

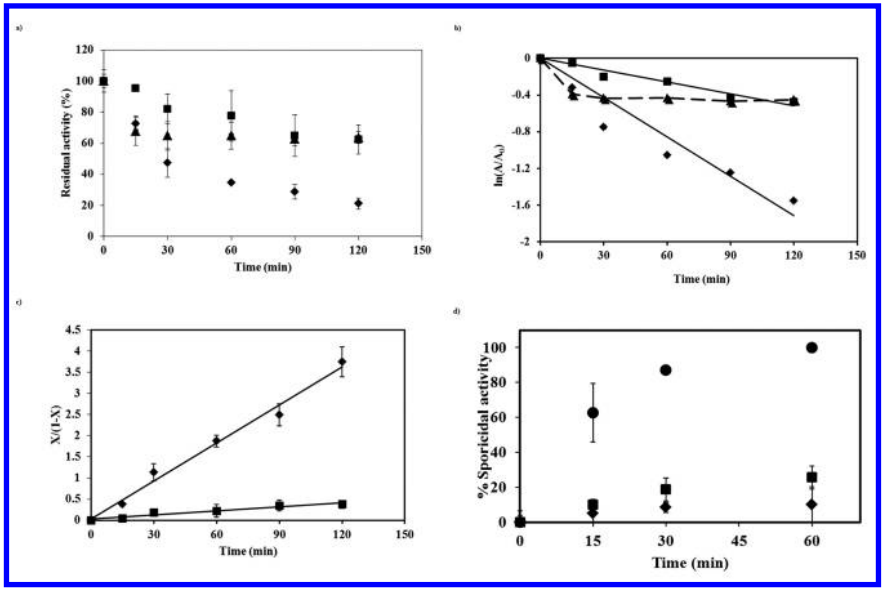

Figure 2. a) Thermal stability of free S54 perhydrolase (AcT; filled diamond), AcT crosslinked with aldehyde dextran (filled squares) and AcT crosslinked with aldehyde dextran and immobilized onto SWNTs (filled triangles) at 75°C. b) and c) Deactivation plots following second order deactivation model. d) Sporicidal activity of cross-linked AcT-nanotube based composites: control films (spores in buffer, filled diamond), films containing cross-linked AcT-nanotube (filled circles) and control spores in PGD and H_2O_2 reaction mixture (filled squares). (Reproduced with permission from reference (23). Copyright 2012 Elsevier).

Conclusions and Future Directions

Recent advances in bioinformatics and molecular biology techniques have allowed production of enzymes with high activity, controlled specificity, and high catalytic power. Simultaneously, recent developments in immobilization of enzymes onto several nanoscale supports that have tailored properties controlled by the user, allowed the development of the next generation of enzyme-based applications as illustrated in this review. Growth in these areas will surely continue. For example, our groups continue to focus on enzyme-based decontamination strategies that will function without addition of external reagents, i.e., either the substrate or the enzyme mediator. Such enzyme-based decontamination strategies aim to be functional by simply relying on ambient conditions and will initiate *in situ* enzymatic generation of decontaminants; such systems are further defined as being self-sustainable. To achieve this goal, we

Publication Date (Web): November 22, 2013 | doi: 10.1021/bk-2013-1144.ch002

are currently investigating a working strategy that allows immobilization of chloroperoxidase enzyme onto titanium dioxide nanosupports. Titanium dioxide is a widely studied photocatalyst that produces hydrogen peroxide from water when excited under UV-light. Hydrogen peroxide generated at the photocatalyst nanointerface could serve as the substrate for enzymatic *in situ* hypochlorous acid generation; hypochlorous acid is a much stronger decontaminant than H_2O_2 (*85*, *86*) and thus has a broader activity range against both bacterial and sporicidal contaminants (*24*). Such strategy may be used in the development of the next generation of self-sustainable decontamination systems upon incorporation into a coating.

A major problem arising from the use of enzymes in a surface coating is enzyme deactivation over time (*25*). We envision the development of layered-based technologies that would allow user-controlled coating performance of such enzyme-based decontamination strategies (Figure 3). Specifically, in a layered system, when the activity of the enzyme on the outer layer of the coating has decreased below an acceptable level, that layer can be peeled away to expose the lower layer, thereby extending the functional lifetime of the coating. Ultimately, the potential for biotechnological application will be whether such systems can be durable and operate over a wide variety of conditions while having increased operational stability, shelf-life and being environmentally and user friendly.

Publication Date (Web): November 22, 2013 | doi: 10.1021/bk-2013-1144.ch002

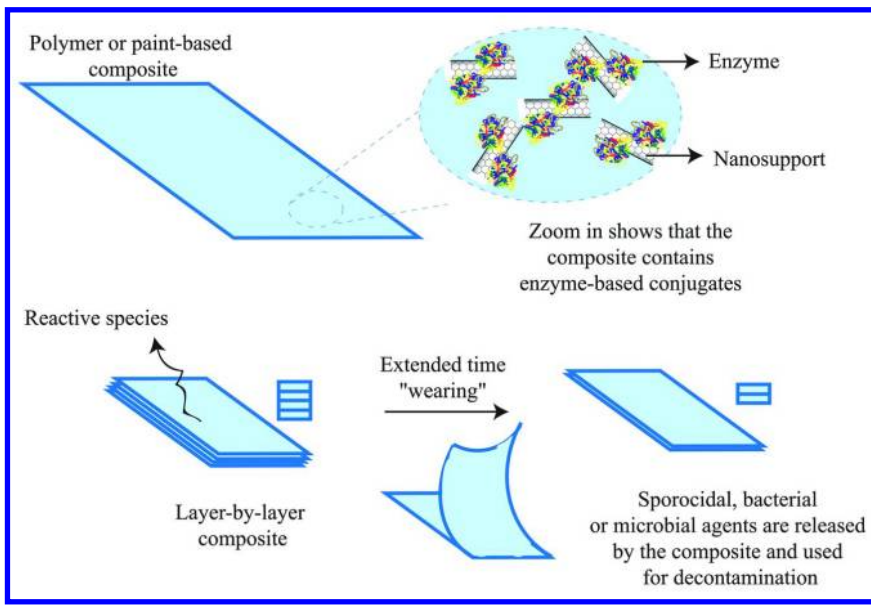

Figure 3. Enzymes are immobilized onto nanosupports and incorporated in composites in a layered technology. When the activity of the enzyme on the outer layer of the coating has decreased below an acceptable level, that layer can be peeled away to expose the lower layer, thereby extending the functional lifetime of the coating. (see color insert)

In Green Polymer Chemistry: Biocatalysis and Materials II; Cheng, H., et al.;
ACS Symposium Series; American Chemical Society: Washington, DC, 2013.

Publication Date (Web): November 22, 2013 | doi: 10.1021/bk-2013-1144.ch002

Acknowledgments

National Science Foundation (CBET-1033266) supported this work.

References

1. Mateo, C.; Palomo, J. M.; Fernandez-Lorente, G.; Guisan, J. M.; Fernandez-Lafuente, R. *Enzyme Microb. Technol.* **2007**, *40* (6), 1451–1463.
2. Garcia-Galan, C.; Berenguer-Murcia, A.; Fernandez-Lafuente, R.; Rodrigues, R. C. *Adv. Syn. Catal.* **2011**, *353* (16), 2885–2904.
3. Schmid, A.; Dordick, J. S.; Hauer, B.; Kiener, A.; Wubbolts, M.; Witholt, B. *Nature* **2001**, *409* (6817), 258–268.
4. Kuddus, M.; Ramteke, P. W. *Crit. Rev. Microbiol.* **2012**, *38* (4), 330–338.
5. Falch, E. A. *Biotechnol. Adv.* **1991**, *9* (4), 643–658.
6. Wong, C. M.; Wong, K. H.; Chen, X. D. *Appl. Microbiol. Biotechnol.* **2008**, *78* (6), 927–938.
7. Mata, T. M.; Sousa, I. R. B. G.; Vieira, S. S.; Caetano, N. S. *Energy Fuels* **2012**, *26* (5), 3034–3041.
8. Zhang, Z. S.; Donaldson, A. A.; Ma, X. X. *Biotechnol. Adv.* **2012**, *30* (4), 913–919.
9. Wang, L.; Templer, R.; Murphy, R. J. *Appl. Energy* **2012**, *99*, 23–31.
10. Menon, V.; Rao, M. *Prog. Energy Combust. Sci.* **2012**, *38* (4), 522–550.
11. Zhang, J. M.; Zhu, Y. H.; Chen, C.; Yang, X. L.; Li, C. Z. *Particuology* **2012**, *10* (4), 450–455.
12. Stolarczyk, K.; Lyp, D.; Zelechowska, K.; Biernat, J. F.; Rogalski, J.; Bilewicz, R. *Electrochim. Acta* **2012**, *79*, 74–81.
13. Ammam, M.; Fransaer, J. *Biosens. Bioelectron.* **2013**, *39* (1), 274–281.
14. Tu, X. M.; Zhao, Y. J.; Luo, S. L.; Luo, X. B.; Feng, L. *Microchim. Acta* **2012**, *177* (1−2), 159–166.
15. Zargoosh, K.; Chaichi, M. J.; Shamsipur, M.; Hossienkhani, S.; Asghari, S.; Qandalee, M. *Talanta* **2012**, *93*, 37–43.
16. Sassolas, A.; Blum, L. J.; Leca-Bouvier, B. D. *Biotechnol. Adv.* **2012**, *30* (3), 489–511.
17. Zaks, A. *Curr. Opin. Chem. Biol.* **2001**, *5* (2), 130–136.
18. Pollard, D. J.; Woodley, J. M. *Trends Biotechnol.* **2007**, *25* (2), 66–73.
19. Adamczak, M.; Krishna, S. H. *Food Technol. Biotechnol.* **2004**, *42* (4), 251–264.
20. Banerjee, I.; Pangule, R. C.; Kane, R. S. *Adv. Mater.* **2011**, *23* (6), 690–718.
21. Magin, C. M.; Cooper, S. P.; Brennan, A. B. *Mater. Today* **2010**, *13* (4), 36–44.
22. Kristensen, J. B.; Meyer, R. L.; Laursen, B. S.; Shipovskov, S.; Besenbacher, F.; Poulsen, C. H. *Biotechnol. Adv.* **2008**, *26* (5), 471–481.
23. Dinu, C. Z.; Borkar, I. V.; Bale, S. S.; Campbell, A. S.; Kane, R. S.; Dordick, J. S. *J. Mol. Catal. B: Enzym.* **2012**, *75*, 20–26.
24. Grover, N.; Borkar, I. V.; Dinu, C. Z.; Kane, R. S.; Dordick, J. S. *Enzyme Microb. Technol.* **2012**, *50* (6−7), 271–279.

25. Bornscheuer, U. T.; Huisman, G. W.; Kazlauskas, R. J.; Lutz, S.; Moore, J. C.; Robins, K. *Nature* **2012**, *485* (7397), 185–194.
26. Karyakin, A. A.; Kotel'nikova, E. A.; Lukachova, L. V.; Karyakina, E. E.; Wang, J. *Anal. Chem.* **2002**, *74* (7), 1597–1603.
27. Sheldon, R. A. *Adv. Syn. Catal.* **2007**, *349* (8−9), 1289–1307.
28. Shi, J.; Claussen, J. C.; McLamore, E. S.; ul Haque, A.; Jaroch, D.; Diggs, A. R.; Calvo-Marzal, P.; Rickus, J. L.; Porterfield, D. M. *Nanotechnology* **2011**, *22* (35).
29. Rubio-Retama, J.; Lopez-Cabarcos, E.; Lopez-Ruiz, B. *Talanta* **2005**, *68* (1), 99–107.
30. Pastorino, L.; Nicolini, C. *Mater. Sci. Eng., C* **2002**, *22* (2), 419–422.
31. Zanon, N. C. M.; Oliveira, O. N.; Caseli, L. *J. Colloid Interface Sci.* **2012**, *373*, 69–74.
32. Pan, C. W.; Chou, J. C.; Sun, T. P.; Hsiung, S. K. *IEEE Sens. J.* **2006**, *6* (2), 269–275.
33. Yabuki, S.; Hirata, Y.; Sato, Y.; Iijima, S. *Anal. Sci.* **2012**, *28* (4), 373–377.
34. Tsai, T. W.; Heckert, G.; Neves, L. F.; Tan, Y. Q.; Kao, D. Y.; Harrison, R. G.; Resasco, D. E.; Schmidtke, D. W. *Anal. Chem.* **2009**, *81* (19), 7917–7925.
35. Hirsh, S. L.; Bilek, M. M. M.; Nosworthy, N. J.; Kondyurin, A.; dos Remedios, C. G.; McKenzie, D. R. *Langmuir* **2010**, *26* (17), 14380–14388.
36. Pangule, R. C.; Brooks, S. J.; Dinu, C. Z.; Bale, S. S.; Salmon, S. L.; Zhu, G. Y.; Metzger, D. W.; Kane, R. S.; Dordick, J. S. *ACS Nano* **2010**, *4* (7), 3993–4000.
37. Jochens, H.; Bornscheuer, U. T. *ChemBioChem* **2010**, *11* (13), 1861–1866.
38. Asuri, P.; Bale, S. S.; Pangule, R. C.; Shah, D. A.; Kane, R. S.; Dordick, J. S. *Langmuir* **2007**, *23* (24), 12318–12321.
39. Asuri, P.; Bale, S. S.; Karajanagi, S. S.; Kane, R. S. *Curr. Opin. Biotechnol.* **2006**, *17* (6), 562–568.
40. Hahn-Hagerdal, B.; Galbe, M.; Gorwa-Grauslund, M. F.; Liden, G.; Zacchi, G. *Trends Biotechnol.* **2006**, *24* (12), 549–556.
41. Solomon, B. D. *Ecol. Econ. Rev.* **2010**, *1185*, 119–134.
42. Xie, T.; Wang, A. M.; Huang, L. F.; Li, H. F.; Chen, Z. M.; Wang, Q. Y.; Yin, X. P. *Afr. J. Biotechnol.* **2009**, *8* (19), 4724–4733.
43. Stolarczyk, K.; Sepelowska, M.; Lyp, D.; Zelechowska, K.; Biernat, J. F.; Rogalski, J.; Farmer, K. D.; Roberts, K. N.; Bilewicz, R. *Bioelectrochemistry* **2012**, *87*, 154–163.
44. Yang, C. Y.; Zhang, Z. J.; Shi, Z. L.; Xue, P.; Chang, P. P.; Yan, R. F. *Talanta* **2010**, *82* (1), 319–324.
45. Manesh, K. M.; Kim, H. T.; Santhosh, P.; Gopalan, A. I.; Lee, K. P. *Biosens. Bioelectron.* **2008**, *23* (6), 771–779.
46. Rakhi, R. B.; Sethupathi, K.; Ramaprabhu, S. *J. Phys. Chem. B* **2009**, *113* (10), 3190–3194.
47. Yin, H. S.; Ai, S. Y.; Shi, W. J.; Zhu, L. S. *Sens. Actuators, B* **2009**, *137* (2), 747–753.
48. Wang, J.; Rennie, K. L.; Gu, W.; Li, H.; Yu, Z.; Lin, X. *Ann. Hum. Biol.* **2009**, *36* (1), 110–21.

Publication Date (Web): November 22, 2013 | doi: 10.1021/bk-2013-1144.ch002

49. Cui, R. J.; Huang, H. P.; Yin, Z. Z.; Gao, D.; Zhu, J. J. *Biosens. Bioelectron.* **2008**, *23* (11), 1666–1673.
50. Cao, Z. J.; Jiang, X. Q.; Xie, Q. J.; Yao, S. Z. *Biosens. Bioelectron.* **2008**, *24* (2), 222–227.
51. Carrara, S.; Ghoreishizadeh, S.; Olivo, J.; Taurino, I.; Baj-Rossi, C.; Cavallini, A.; Op de Beeck, M.; Dehollain, C.; Burleson, W.; Moussy, F. G.; Guiseppi-Elie, A.; De Micheli, G. *Sensors (Basel)* **2012**, *12* (8), 11013–11060.
52. Wang, J. *Electroanalysis* **2005**, *17* (1), 7–14.
53. Kotanen, C. N.; Moussy, F. G.; Carrara, S.; Guiseppi-Elie, A. *Biosens. Bioelectron.* **2012**, *35* (1), 14–26.
54. Rahman, M. M.; Umar, A.; Sawada, K. *Sens. Actuators, B* **2009**, *137* (1), 327–333.
55. Guiseppi-Elie, A.; Lei, C.; Baughman, R. H. *Nanotechnology* **2002**, *13* (5), 559.
56. Kong, T.; Chen, Y.; Ye, Y. P.; Zhang, K.; Wang, Z. X.; Wang, X. P. *Sens. Actuators, B* **2009**, *138* (1), 344–350.
57. Dai, Z. H.; Shao, G. J.; Hong, J. M.; Bao, J. C.; Shen, J. *Biosen. Bioelectron.* **2009**, *24* (5), 1286–1291.
58. Tsai, M. C.; Tsai, Y. C. *Sens. Actuatore, B* **2009**, *141* (2), 592–598.
59. Wu, H.; Wang, J.; Kang, X. H.; Wang, C. M.; Wang, D. H.; Liu, J.; Aksay, I. A.; Lin, Y. H. *Talanta* **2009**, *80* (1), 403–406.
60. Li, X. Y.; Zhou, Y. L.; Zheng, Z. Z.; Yue, X. L.; Dai, Z. F.; Liu, S. Q.; Tang, Z. Y. *Langmuir* **2009**, *25* (11), 6580–6586.
61. Marrakchi, M.; Dzyadevych, S. V.; Lagarde, F.; Martelet, C.; Jaffrezic-Renault, N. *Mater. Sci. Eng., C* **2008**, *28* (5-6), 872–875.
62. Ammam, M.; Fransaer, J. *Sens. Actuators, B* **2010**, *148* (2), 583–589.
63. Conzuelo, F.; Gamella, M.; Campuzano, S.; Ruiz, M. A.; Reviejo, A. J.; Pingarron, J. M. *J. Agric. Food Chem.* **2010**, *58* (12), 7141–7148.
64. Upadhyay, A. K.; Ting, T. W.; Chen, S. M. *Talanta* **2009**, *79* (1), 38–45.
65. Kafi, A. K. M.; Wu, G.; Chen, A. *Biosens. Bioelectron.* **2008**, *24* (4), 566–571.
66. Xi, F. N.; Liu, L. J.; Wu, Q.; Lin, X. F. *Biosens. Bioelectron.* **2008**, *24* (1), 29–34.
67. Shi, L. H.; Liu, X. Q.; Niu, W. X.; Li, H. J.; Han, S.; Chen, J.; Xu, G. B. *Biosens. Bioelectron.* **2009**, *24* (5), 1159–1163.
68. Salimi, A.; Noorbakhsh, A.; Rafiee-Pour, H. A.; Ghourchian, H. *Electroanalysis* **2011**, *23* (3), 683–691.
69. Cui, R. J.; Huang, H. P.; Yin, Z. Z.; Gao, D.; Zhu, J. J. *Biosens. Bioelectron.* **2008**, *23* (11), 1666–1673.
70. de Jonge, L. T.; Leeuwenburgh, S. C. G.; van den Beucken, J. J. J. P.; Wolke, J. G. C.; Jansen, J. A. *Adv. Funct. Mater.* **2009**, *19* (5), 755–762.
71. Dinu, C. Z.; Zhu, G.; Bale, S. S.; Anand, G.; Reeder, P. J.; Sanford, K.; Whited, G.; Kane, R. S.; Dordick, J. S. *Adv. Funct. Mater.* **2010**, *20* (3), 392–398.
72. Pavithra, D.; Doble, M. *Biomed. Mater.* **2008**, *3* (3).

Publication Date (Web): November 22, 2013 | doi: 10.1021/bk-2013-1144.ch002

73. Kuhlmann, J.; Dzugan, L. C.; Heineman, W. R. *Electroanalysis* **2012**, *24* (8), 1732–1738.
74. Asuri, P.; Karajanagi, S. S.; Kane, R. S.; Dordick, J. S. *Small* **2007**, *3* (1), 50–53.
75. Chambers, L. D.; Stokes, K. R.; Walsh, F. C.; Wood, R. J. K. *Surf. Coat. Technol.* **2006**, *201* (6), 3642–3652.
76. Holland, R.; Dugdale, T. M.; Wetherbee, R.; Brennan, A. B.; Finlay, J. A.; Callow, J. A.; Callow, M. E. *Biofouling* **2004**, *20* (6), 323–329.
77. Berglin, M.; Wynne, K. J.; Gatenholm, P. *J. Colloid Interface Sci.* **2003**, *257* (2), 383–391.
78. Volk, R. B. *J. Appl. Phycol.* **2006**, *18* (2), 145–151.
79. Roper, K. E.; Beamish, H.; Garson, M. J.; Skilleter, G. A.; Degnan, B. M. *Mar. Biotechnol.* **2009**, *11* (2), 188–198.
80. Tiller, J. C.; Lee, S. B.; Lewis, K.; Klibanov, A. M. *Biotechnol. Bioeng.* **2002**, *79* (4), 465–471.
81. Cousins, C. M.; Allan, C. D. *J. Appl. Bacteriol.* **1967**, *30* (1), 168–174.
82. *Guidelines for Protecting the Safety and Health of Health Care Workers*; DHHS (NIOSH) Publication Number 88-119; National Institute for Occupational Safety and Health (NIOSH): Washington, DC, 1988; pp 88−119.
83. Grover, N.; Douaisi, M.; Borkar, I.; Lee, L.; Dinu, C.; Kane, R.; Dordick, J. *Appl. Microbiol. Biotechnol.* **2012**, PMID: 23188457.
84. Asuri, P.; Karajanagi, S. S.; Yang, H. C.; Yim, T. J.; Kane, R. S.; Dordick, J. S. *Langmuir* **2006**, *22* (13), 5833–5836.
85. Takahara, Y. K.; Hanada, Y.; Ohno, T.; Ushiroda, S.; Ikeda, S.; Matsumura, M. *J. Appl. Electrochem.* **2005**, *35* (7−8), 793–797.
86. Khodadoust, S.; Sheini, A.; Armand, N. *Spectrochim. Acta, Part A* **2012**, *92*, 91–95.

Publication Date (Web): November 22, 2013 | doi: 10.1021/bk-2013-1144.ch002

Publication Date (Web): November 22, 2013 | doi: 10.1021/bk-2013-1144.ch003

Chapter 3

Lipase-Catalyzed Synthesis of Poly(amine-*co*-esters) and Poly(lactone-*co*-*β*-amino esters)

Zhaozhong Jiang*

Molecular Innovations Center, Yale University,
600 West Campus Drive, West Haven, Connecticut 06516
***E-mail: zhaozhong.jiang@yale.edu**

Candida antarctica lipase B (CALB) was found to be highly tolerant toward tertiary amino functional groups during polyester synthesis. Thus, different types of copolyesters bearing tertiary amino moieties have been successfully prepared in one step without protection and deprotection of the amines using CALB as the transesterification catalyst. Polycondensation between C_4-C_{12} diesters (i.e., from succinate to dodecanedioate) and diethanolamine comonomers with either an alkyl (methyl, ethyl, *n*-butyl, *t*-butyl) or an aryl (phenyl) substituent on the nitrogen led to the formation of various poly(amine-*co*-esters). The hydrophobicity and nitrogen (or charge) density of the poly(amine-*co*-esters), which are crucial for gene delivery applications, can be adjusted by additionally incorporating lactone units into the copolymer chains. For this purpose, lactones with different ring size (C_6-C_{16}), diethyl sebacate (DES), and *N*-methyldiethanolamine (MDEA) were copolymerized to form poly(amine-*co*-ester) terpolymers with a wide range of lactone unit contents (10-80 mol%). A number of these amino-bearing copolyesters

In Green Polymer Chemistry: Biocatalysis and Materials II; Cheng, H., et al.;
ACS Symposium Series; American Chemical Society: Washington, DC, 2013.

exhibited exceedingly high gene transfection efficiency; in particular, ω-pentadecalactone-DES-MDEA terpolymer was remarkably effective in delivering therapeutic genes to inhibit tumor growth in mice *in vivo*. Finally, a new ω-hydroxy *β*-amino ester monomer, [ethyl 3-(4-(hydroxymethyl)piperidin-1-yl)propanoate] was prepared, which underwent either homopolymerization or copolymerization with lactone to form a poly(*β*-amino ester) and poly(lactone-*co*-*β*-amino ester) copolymers. This article provides a brief review on the versatile methods which have been successfully developed for the synthesis of high purity amino-bearing copolyesters via lipase catalysis.

Publication Date (Web): November 22, 2013 | doi: 10.1021/bk-2013-1144.ch003

Introduction

Gene therapy has great potential to treat genetic disorders, including cancers (*1*). Viral vectors, cationic liposomes, cationic polymers are typical carriers that have been developed and evaluated for DNA delivery. Viral vectors are known to possess high gene delivery efficiency, but are limited by their potential in causing adverse immune responses and by their small DNA-loading capabilities (*2*, *3*). Cationic liposomes can be structurally optimized to deliver DNA with high transfection efficiency (*4*, *5*). However, because they are not sufficiently stable under physiological conditions and are highly toxic, such liposomes are often not suitable for *in vivo* gene delivery applications (*6*, *7*). To overcome these problems, various types of polymeric materials containing amine functional groups have been used to serve as non-viral carriers for DNA (or gene) delivery to living cells (*1*). These polymers are capable of condensing plasmid DNA via electrostatic interactions to form nanometer-sized polyelectrolyte complexes (or polyplexes), protecting DNA against extracellular nuclease degradation, and facilitating transportation of DNA into cell compartments through cellular barriers (*8*). Examples of such polymers include poly(dimethylaminoethyl methacrylate), poly(trimethylaminoethyl methacrylate), poly(ethylenimine), poly[α-(4-aminobutyl)-L-glycolic acid] (PAGA), poly(4-hydroxy-L-proline ester) (PHP), poly(L-lysine), poly(*β*-amino esters) (PBAE), and chitosan. Among these polycations, polyesters bearing tertiary amino substituents are particularly promising due to their biodegradability (thus avoiding accumulation of the polymers in the body after repeated administration), low cytotoxicity, and outstanding transfection efficacy (*9*). Nevertheless, few efficient synthetic methods are currently available for preparation of amino-containing polyesters primarily because metal catalysts required for conventional polyester synthesis are often sensitive to and deactivated by amino groups.

In Green Polymer Chemistry: Biocatalysis and Materials II; Cheng, H., et al.;
ACS Symposium Series; American Chemical Society: Washington, DC, 2013.

Publication Date (Web): November 22, 2013 | doi: 10.1021/bk-2013-1144.ch003

In the past two decades, enzymes (e.g., lipases) have been extensively evaluated as environmentally benign, alternative catalysts for polyester preparation (*10–12*). Enzymatic synthesis methods were developed to prepare various types of polyesters via condensation copolymerization of dicarboxylic acids with diols (*13*), transesterification reaction of diesters with diols (*13*, *14*), polymerization of hydroxy acids (*13*), ring-opening polymerization of lactones (*15–17*), and combined ring-opening and condensation copolymerization of lactones with diesters and diols (*18–21*). Lipases are known to be highly tolerant of functional organic moieties (e.g., hydroxyl, vinyl, epoxy) and are ideally suited for synthesis of functional polyesters (*10–12*). Furthermore, enzymatic polymerization catalysis has distinct advantages for producing biomedical polymers due to the high activity and extraordinary selectivity of enzyme catalysts and the high purity of products that are also metal free. This article provides a brief review on several new versatile methods which have been successfully developed in the past a few years for the synthesis of high purity, biodegradable, amino-bearing copolyesters via lipase catalysis.

Poly(amine-*co*-esters) Derived from Diester and Amino Diol Monomers

Synthesis of Poly(amine-*co*-ester) Copolymers via Polycondensation between Diesters and Amino-Substituted Diols

Poly(amine-*co*-esters) bearing tertiary amino groups in the main chain of the polymers were synthesized in one step via copolymerization of diesters with amino-substituted diols using *Candida antarctica* lipase B (CALB) as the catalyst (*22*). Temperature screening experiments showed that the desirable reaction temperature for the copolymerization reactions is in the range between 80 and 90 °C. The synthesis procedures, purification methods, and structural characterization of the copolymers can be found in a previous publication (*22*). The enzymatic reaction appears to be quite general and accommodates a large number of comonomer substrates with various chain length and substituents (Scheme 1). Thus, C_4-C_{12} diesters (i.e., from succinate to dodecanedioate) and diethanolamine comonomers with either an alkyl (methyl, ethyl, *n*-butyl, *t*-butyl) or an aryl (phenyl) substituent on the nitrogen were successfully incorporated into the poly(amine-*co*-ester) chains. The yields and molecular weights of the purified polymers are shown in Table 1 (data taken from reference (*22*)). The observed high tolerance of the lipase toward tertiary amine moieties provides new routes for synthesizing poly(amine-*co*-esters) with diverse chain structures from readily available monomers.

In Green Polymer Chemistry: Biocatalysis and Materials II; Cheng, H., et al.;
ACS Symposium Series; American Chemical Society: Washington, DC, 2013.

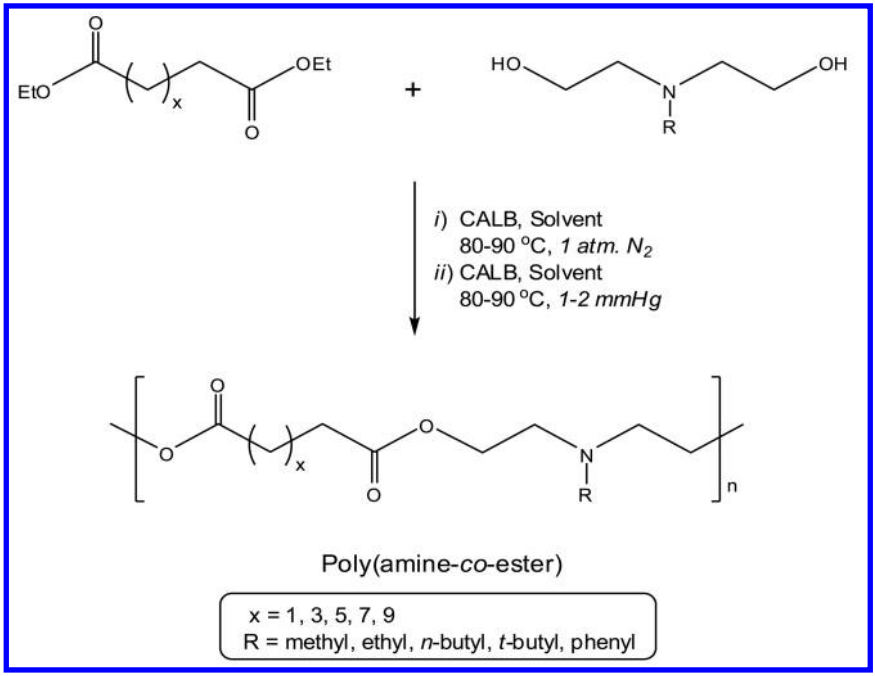

Scheme 1. Two-Stage Process for Copolymerization of Diesters with Amino-substituted Diols

Table 1. Molecular Weight and Isolated Yield of Poly(amine-*co*-esters) Synthesized via Copolymerization between Diesters and Diethanolamine with R-substituent on the Nitrogen[a]

substrates		*isolated polymer*			
diethyl diester	*R in diol*	*name*	*yield (%)*	M_w	M_w/M_n
succinate	methyl	PMSN	82	29500	2.3
adipate	methyl	PMAP	83	29600	2.3
suberate	methyl	PMSR	83	30300	2.4
sebacate	methyl	PMSC	86	31800	2.3
dodecanedioate	methyl	PMDO	87	41200	2.4
sebacate	ethyl	PESC	81	29900	2.3
sebacate	*n*-butyl	PB^{n}SC	80	36000	2.2

Continued on next page.

Table 1. (Continued). Molecular Weight and Isolated Yield of Poly(amine-*co*-esters) Synthesized via Copolymerization between Diesters and Diethanolamine with R-substituent on the Nitrogen[a]

substrates		*isolated polymer*			
diethyl diester	*R in diol*	*name*	*yield (%)*	M_w	M_w/M_n
sebacate	*t*-butyl	PB^{t}SC	80	44500	2.0
sebacate	phenyl	PPSC	88	44200	2.2

[a] Reaction conditions: 1:1 molar ratio of diester to diol; 80 °C, 1 atm nitrogen, 24 h for the first stage oligomerization; 80 °C, 1.6 mmHg vacuum, 72 h for the second stage polymerization.

Publication Date (Web): November 22, 2013 | doi: 10.1021/bk-2013-1144.ch003

Poly(amine-*co*-ester) Properties

The amino-bearing copolyesters readily turned to cationic polyelectrolytes upon protonation at pH of 5-6, which were capable of condensing with polyanionic DNA to form nanometer-sized polyplexes (*23*). In particular, the polyplexes of luciferase DNA (pLucDNA) with poly(*N*-methyldiethyleneamine sebacate) (PMSC) and those of pLucDNA with poly(*N*-ethyldiethyleneamine sebacate) (PESC) possessed desirable particle sizes (40-70 nm) for cellular uptake and were capable of functioning as proton sponges to facilitate endosomal escape after cellular uptake. PMSC and PESC had extremely low cytotoxicity and were highly effective carriers for delivery of genes to various cells (e.g., HEK293, LLC, 9L, V87MG) *in vitro* (*23*). The gene transfection efficiency of PMSC exceeds that of leading commercial products, such as Lipofectamine 2000. Furthermore, the copolymer was substantially more efficient than polyethylenimine (PEI) as gene vector to transfect tumor cells in mice via localized delivery (*23*). Nevertheless, PMSC was ineffective for systemic gene delivery applications due to the low stability of its polyplexes with DNA under physiological conditions (unpublished results).

Poly(amine-*co*-ester) Terpolymers Derived from Lactone, Diester, and Amino Diol Monomers

Synthesis and Structures of Poly(amine-*co*-ester) Terpolymers via Copolymerization of Lactone with Diethyl Sebacate (DES) and *N*-Methyldiethanolamine (MDEA)

The versatility of lipase catalysis has allowed additionally incorporation of lactone units into poly(amine-*co*-ester) chains. Lactone-DES-MDEA terpolymers are of great interest primarily because by incorporating lactone units into PMSC chains, the hydrophobicity and charge density of the resultant lactone-DES-MDEA terpolymers, which are crucial for gene delivery applications, can be effectively controlled by choosing a lactone with a specific

ring size and/or by adjusting lactone unit content in the terpolymers. Thus, various lactones (C_6 to C_{16}) were copolymerized with DES and MDEA to form random poly(amine-*co*-ester) terpolymers with diverse chain structures using a two-stage polymerization process (Scheme 2) (*24*). Such amino-bearing copolyesters would be extremely difficult to synthesize using conventional organometallic catalysts, as metal catalysts are often sensitive to (or deactivated by) organic amines (*25*) and are known to be inefficient for polymerizing large ring lactone monomers (*26*). Because of the high tolerance of the lipase catalyst toward tertiary amines, protection and deprotection of the amino group of MDEA are not necessary during the copolymerization. Additional factors for choosing lactones as comonomers are that they are readily available in various ring sizes and are known to possess low toxicity. For example, polyesters of small lactones, such as poly(ε-caprolactone) and poly(*p*-dioxanone), are commercial biomaterials and have already been used in clinical applications. Large (e.g., C_{16}-C_{24}) lactones and their polyester derivatives are nature products that exist in different bee species (*27–29*). Details regarding the synthesis, purification, and structural characterization of all terpolymers were reported elsewhere (*24*). The compositions, molecular weights and other characterization data of purified 12-dodecanolide-DES-MDEA (DDL-DES-MDEA) terpolymers (II) and 15-pentadecanolide-DES-MDEA (PDL-DES-MDEA) terpolymers (III) are shown in Table 2 (data taken from reference (*24*)). The compositions of the terpolymers were readily controlled by adjusting the corresponding monomer feed ratios (Table 2).

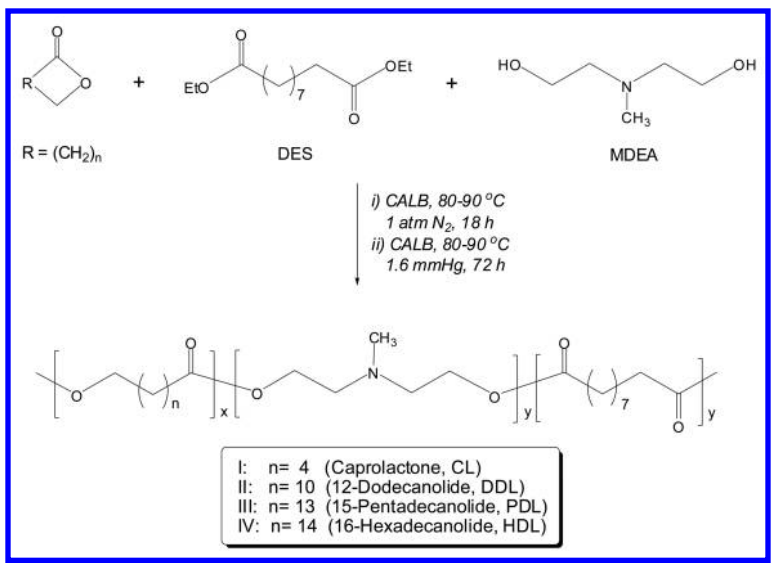

Scheme 2. Synthesis of Lactone-DES-MDEA Terpolymers

Publication Date (Web): November 22, 2013 | doi: 10.1021/bk-2013-1144.ch003

Table 2. Characterization of Selected Lactone-DES-MDEA Terpolymers

Name [a]	*lactone/ DES/MDEA (feed molar ratio)*	*lactone/sebacate/ MDEA (unit molar ratio)* [b]	M_w[c]	M_w-/M_n[c]	*Nitrogen Content (wt%)*
II-10%DDL	10:90:90	10:90:90	24900	1.9	4.6
II-20%DDL	20:80:80	20:80:80	29300	2.0	4.2
II-40%DDL	40:60:60	40:60:60	25800	1.8	3.4
II-60%DDL	60:40:40	60:40:40	47400	2.1	2.4
II-80%DDL	80:20:20	80:20:20	40600	2.1	1.3
III-10%PDL	10:90:90	10:90:90	30700	2.1	4.5
III-20%PDL	20:80:80	20:80:80	38700	2.3	4.1
III-40%PDL	40:60:60	40:60:60	33300	2.1	3.1
III-61%PDL	60:40:40	61:39:39	34500	2.3	2.1
III-82%PDL	80:20:20	82:18:18	41700	2.7	1.0

[a] The polymer names are abbreviated. Polymers II and III represent DDL-DES-MDEA and PDL-DES-MDEA terpolymers, respectively. Each polymer is denoted with x% lactone indicating the lactone unit content [mol% vs. (lactone + sebacate) units] in the polymer. [b] Measured by ^{1}H NMR spectroscopy. [c] Measured by GPC using narrow polydispersity polystyrene standards.

Publication Date (Web): November 22, 2013 | doi: 10.1021/bk-2013-1144.ch003

To elucidate how the polymer chains grow during the copolymerization of lactone with DES and MDEA, PDL-DES-MDEA terpolymerization at different temperatures was studied. Table 3 depicts the changes in polymer molecular weight and polydispersity index as a function of polymerization time for the copolymerization reactions. For all reactions, polymer chains continued to grow during the 72 h polymerization period. The chain growth was faster with increasing reaction temperature from 60 to 90 °C. These results indicate that the molecular weight of the PDL-DES-MDEA terpolymers can be readily controlled by varying the reaction time and/or reaction temperature. The polydispersity of the polymers was higher with increasing polymer molecular weight, but overall the polydispersity values of all products remained relatively low (1.5-1.8).

In Green Polymer Chemistry: Biocatalysis and Materials II; Cheng, H., et al.;
ACS Symposium Series; American Chemical Society: Washington, DC, 2013.

Table 3. Variations of Product Molecular Weight and Polydispersity during the Copolymerization of PDL with DES and MDEA[a]

2nd stage polym. time (h)	*polymer M_w (polydispersity) at reaction temperature*			
	60 °C	*70 °C*	*80 °C*	*90 °C*
4	6800 (1.5)	8100 (1.5)	12100 (1.6)	12700 (1.5)
21	9700 (1.5)	12500 (1.6)	18200 (1.7)	19300 (1.8)
31	10600 (1.6)	13900 (1.6)	20300 (1.8)	21100 (1.8)
47	11500 (1.6)	15500 (1.7)	23800 (1.8)	26100 (1.8)
55	12000 (1.6)	16500 (1.7)	26300 (1.8)	30200 (1.8)
72	13300 (1.6)	19200 (1.7)	32300 (1.8)	39700 (1.8)

[a] Reaction conditions: 2:3:3 (molar ratio) PDL/DES/MDEA, 10 wt% Novozym 435 catalyst (vs. total monomer), 200 wt% diphenyl ether solvent (vs. total monomer); 1 atm nitrogen gas, 19 h for the first stage oligomerization; 1.4 mmHg for the second stage polymerization.

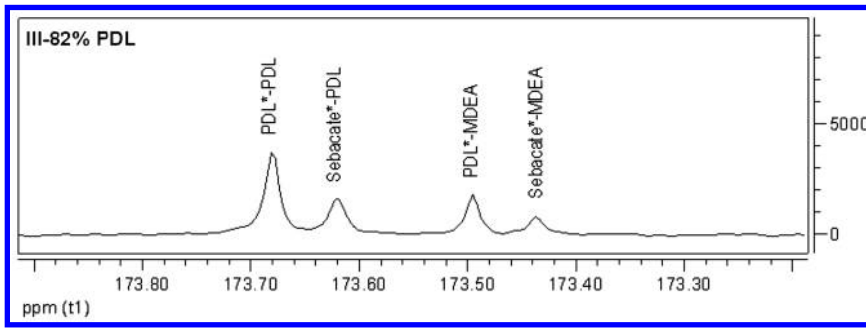

Figure 1. The carbonyl carbon-13 NMR absorptions of PDL-DES-MDEA terpolymer (III).

The molecular structures of the lactone-DES-MDEA terpolymers were fully characterized by both ^{1}H and ^{13}C NMR spectroscopy (*24*). The proton NMR spectra of the lactone-DES-MDEA terpolymers showed that the copolymers contained three different types of repeating units: lactone, *N*-methyldiethyleneamine, and sebacate. Carbon-13 NMR analyses indicate that these repeat units are distributed randomly in the copolymer chains. For example, PDL-DES-MDEA terpolymers exhibited four carbonyl resonance absorptions due to the presence of PDL*-PDL, sebacate*-PDL, PDL*-MDEA, and sebacate*-MDEA diads in the copolymer chains (Figure 1). The abundances of the four diads measured by ^{13}C NMR spectroscopy match remarkably well the theoretical diad distribution values calculated for random copolymers with same compositions (Table 4, data taken from reference (*24*)).

In Green Polymer Chemistry: Biocatalysis and Materials II; Cheng, H., et al.;
ACS Symposium Series; American Chemical Society: Washington, DC, 2013.

Publication Date (Web): November 22, 2013 | doi: 10.1021/bk-2013-1144.ch003

Table 4. Diad Distributions of PDL-DES-MDEA Terpolymers: Experimental Values vs. Theoretical Values Calculated for Random Copolymers

Polymer	*PDL/Seb/ MDEA (unit ratio)*	*PDL*-PDL*		*PDL*-MDEA*		*Seb*-PDL*		*Seb*-MDEA*	
		meas.[a]	*calc.*[b]	*meas.*[a]	*calc.*[b]	*meas.*[a]	*calc.*[b]	*meas.*[a]	*calc.*[b]
III-40%PDL	40:60:60	0.06	0.06	0.18	0.19	0.20	0.19	0.56	0.56
III-82%PDL	82:18:18	0.48	0.48	0.22	0.21	0.20	0.21	0.10	0.09

[a] Measured from ^{13}C NMR spectra. [b] Calculated for a copolymer with statistically random unit distribution in the polymer chains.

Publication Date (Web): November 22, 2013 | doi: 10.1021/bk-2013-1144.ch003

Lactone-DES-MDEA Terpolymer Properties

The physical properties of the poly(amine-*co*-ester) terpolymers vary substantially depending on the ring size of the lactone and its content in the polymers. In general, the terpolymers with a small-ring lactone and a low lactone content are liquids, and those with a large lactone and a high lactone content are waxy or solid materials. Thus, I-(10-80)% CL, II-(10-40)% DDL, III-(10-20)% PDL, and IV-10% HDL were viscous liquids at ambient temperature whereas II-(60-80)% DDL, III-(40-80)% PDL, and IV-(20-80)% HDL were either semi-solid or solid polymers (see the terpolymer structures in Scheme 2).

Among these polymers, all liquid terpolymers were capable of forming polyplexes with DNA in aqueous medium (*24*). Compared to PEI that contains 32.6 wt% nitrogen, the lactone-DES-MDEA terpolymers had a nitrogen content of less than 5 wt%. This low nitrogen content is presumably a major contributor to the minimal cytotoxicity exhibited by these terpolymers. The presence of lactone units in the terpolymer chains can enhance the hydrophobicity of the poly(amine-co-esters). As the result, compared to PMSC/DNA polyplexes, the DNA polyplexes of lactone-DES-MDEA terpolymers could contain more stable hydrophobic domains which non-covalently crosslink the polyplex particles, leading to higher gene delivery efficiency of the terpolymers. Indeed, a number of lactone-DES-MDEA terpolymers, especially those with large lactones and high lactone contents (e.g., II-40%DDL, III-20%PDL), were substantially more effective gene vectors than PMSC, as well as commercial transfection reagents polyethylenimine and Lipofectamine 2000 (*24*). Upon coating with a targeting peptide, III-20%PDL with improved stability was efficient for systemic delivery of therapeutic TRAIL gene to inhibit tumor growth in mice *in vivo* (*24*).

In Green Polymer Chemistry: Biocatalysis and Materials II; Cheng, H., et al.;
ACS Symposium Series; American Chemical Society: Washington, DC, 2013.

Poly(lactone-*co*-*β*-amino esters) Derived from Lactone and ω-Hydroxy *β*-Amino Ester Monomers

Synthesis and Structures of Poly[Ω-pentadecalactone-*co*-3-(4-(methylene)piperidin-1-yl)propanoate] (poly(PDL-*co*-MPP)) via Copolymerization of ω-Pentadecalactone (PDL) with Ethyl 3-(4-(Hydroxymethyl)piperidin-1-yl)propanoate (EHMPP)

Because of the extraordinary tolerance of the lipase catalyst toward tertiary amino functional groups, it is anticipated that ω-hydroxy esters bearing tertiary amino moieties are also suitable monomers for homopolymerization or copolymerization with lactone to form new amino-containing copolyesters. To demonstrate the viability of this synthesis strategy, EHMPP was prepared in quantitative yield under mild conditions via Michael addition reaction of 4-piperidinemethanol with ethyl acrylate (Scheme 3) (*30*). EHMPP underwent condensation polymerization in the presence of CALB catalyst to form poly[3-(4-(methylene)piperidin-1-yl)propanoate] (PMPP) (Scheme 4-A, Table 5) (*30*). Ring-opening and condensation copolymerization of EHMPP with PDL led to the formation of poly(PDL-*co*-MPP) copolymers (Scheme 4-B), whose compositions were readily controlled by varying the monomer feed ratio (Table 5, data taken from reference (*30*)) (*30*). NMR analyses, including statistical analysis on repeating unit sequence distribution, indicate that the poly(PDL-*co*-MPP) copolymers are totally random polymers. The diad distributions of the poly(PDL-*co*-MPP) samples measured by carbon-13 NMR spectroscopy closely match the theoretical values calculated for random copolymers at same compositions (Table 6, data taken from reference (*30*)).

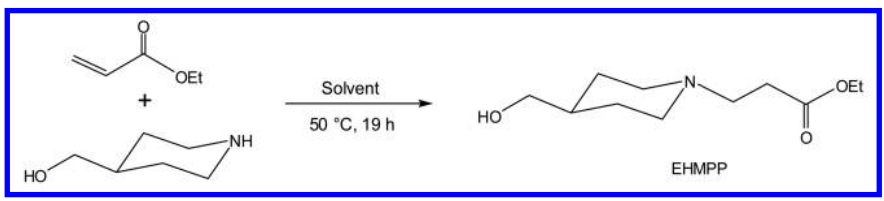

Scheme 3. Synthesis of ω-Hydroxy β-Amino Ester EHMPP

The synthesis methods described in Schemes 3 and 4 can be easily adopted for preparation of analogous ω-hydroxy *β*-amino ester monomers and other poly(lactone-*co*-*β*-amino esters). The current poly(*β*-amino ester), PMPP, differs from the previously reported PBAE (*9*) in that PMPP contains *β-amino monoester repeat units* and the latter polymers contain *β-amino diester units*. In addition, poly(PDL-*co*-MPP) copolymers cannot be synthesized using the conjugate addition method effective for preparation of the previous PBAE copolymers. PMPP and poly(PDL-*co*-MPP) represent a new type of poly(*β*-amino esters), and their capability to serve as non-viral vectors for gene delivery is currently under investigation.

In Green Polymer Chemistry: Biocatalysis and Materials II; Cheng, H., et al.;
ACS Symposium Series; American Chemical Society: Washington, DC, 2013.

Publication Date (Web): November 22, 2013 | doi: 10.1021/bk-2013-1144.ch003

Publication Date (Web): November 22, 2013 | doi: 10.1021/bk-2013-1144.ch003

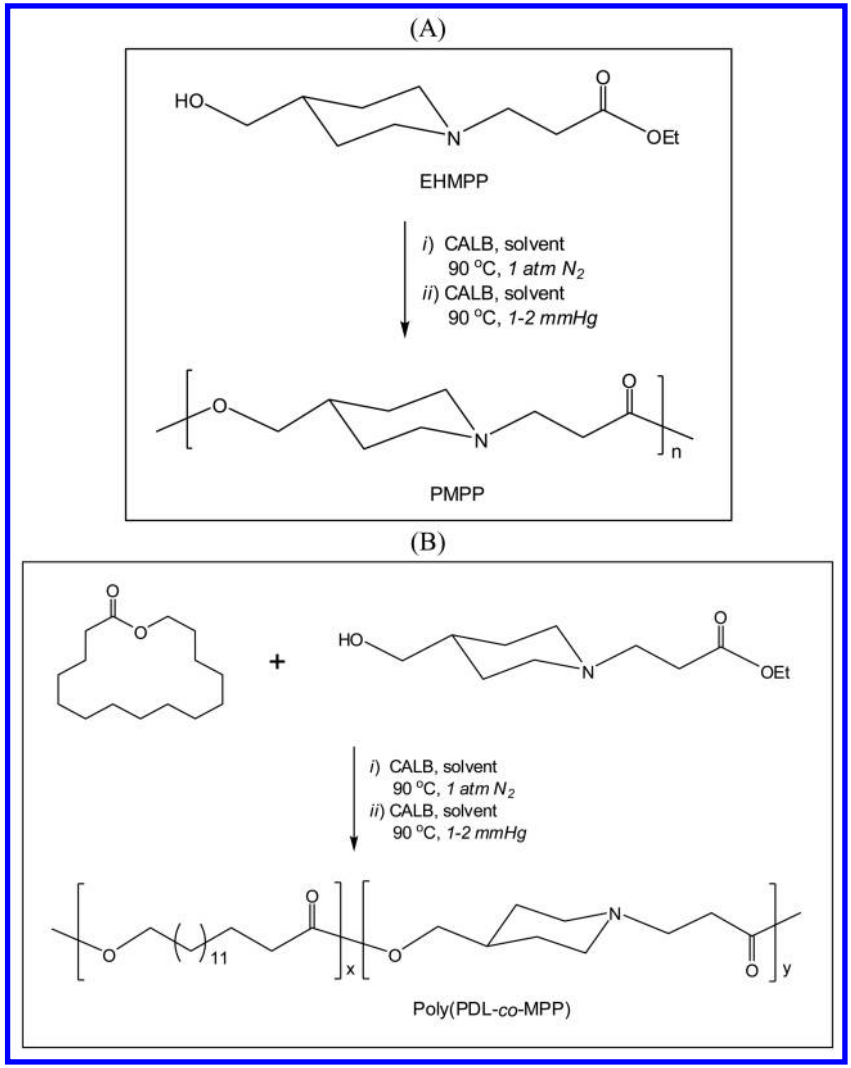

Scheme 4. Enzymatic Synthesis of PMPP and Poly(PDL-co-MPP)

In Green Polymer Chemistry: Biocatalysis and Materials II; Cheng, H., et al.;
ACS Symposium Series; American Chemical Society: Washington, DC, 2013.

Table 5. Characterization of Purified Poly(PDL-*co*-MPP)

PDL/EHMPP (feed molar ratio)	*PDL unit content [a] (mol%)*	*polymer yield (%)*	M_w [b]	M_w/M_n [b]
0:100	0%	82	13200	1.8
20:80	21%	82	15900	1.6
35:65	36%	81	16300	1.6
50:50	51%	84	24800	1.5
65:35	67%	82	24100	1.7
80:20	82%	90	27200	1.6

[a] Calculated from the ^{1}H NMR spectra. [b] Measured by GPC using polystyrene standards.

Table 6. Diad Distributions in Poly(PDL-*co*-MPP) Copolymers

PDL content (mol%)	*PDL*-PDL*		*PDL*-MPP*		*MPP*-PDL*		*MPP*-MPP*	
	Meas.[a]	*Calc.[b]*	*Meas.[a]*	*Calc.[b]*	*Meas.[a]*	*Calc.[b]*	*Meas.[a]*	*Calc.[b]*
36%	0.12	0.13	0.23	0.23	0.23	0.23	0.41	0.41
51%	0.26	0.26	0.25	0.25	0.25	0.25	0.24	0.24
67%	0.45	0.45	0.22	0.22	0.22	0.22	0.11	0.11
82%	0.68	0.67	0.15	0.15	0.15	0.15	0.02	0.03

[a] Measured from ^{13}C NMR spectra. [b] Calculated for a copolymer with statistically random unit distribution in the polymer chains.

Publication Date (Web): November 22, 2013 | doi: 10.1021/bk-2013-1144.ch003

Poly(PDL-*co*-MPP) Properties

Solid state properties of the copolymers were studied and the results are documented in a previous publication (*30*). All synthesized poly(PDL-*co*-MPP) copolymers and PMPP homopolymer are semi-crystalline materials partially due to the rigid piperidine ring structures present in the chains. Wide angle X-ray diffraction measurements showed that the copolymers rich in PDL (≥ 51 mol%) crystallize in poly(PDL) lattice and those with ≤ 21 mol% PDL content develop PMPP-type crystals while in the copolymer with 36 mol% PDL, PMPP-type and poly(PDL)-type crystals co-exist.

In Green Polymer Chemistry: Biocatalysis and Materials II; Cheng, H., et al.;
ACS Symposium Series; American Chemical Society: Washington, DC, 2013.

Conclusions

As discussed in the above sections, enzymatic polymerization methods are promising and highly efficient for synthesis of biodegradable copolyesters containing tertiary amino functional groups, which do not require protection and deprotection of the amines during the polymer synthesis. A variety of monomers, including diesters, amino diols, lactones, and ω-hydroxy amino esters, can serve as suitable substrates for the lipase catalyst to form the copolymer products with diverse chain structures and properties. These newly developed synthesis methods are highly desirable for preparation of efficient, high molecular weight, polycationic gene vectors since their gene delivery capability substantially depends on the repeat unit structures, unit arrangements, and compositions of the polymer chains, which in turn determine the polymer physical properties, such as hydrophobicity, charge density, and solubility. The versatility of enzyme catalysis should allow further incorporation of new unit structures and functionalities into the amino-bearing polyester chains described in this article, which is anticipated to produce next generation of non-viral gene vectors with even higher efficacy.

Publication Date (Web): November 22, 2013 | doi: 10.1021/bk-2013-1144.ch003

Acknowledgments

I wish to thank other team members or collaborators who have contributed greatly to the work described in this article: Dr. Mark Saltzman, Dr. Jiangbing Zhou, Dr. Jie Liu, Christopher J. Cheng, Rachel J. Fields, Elias Quijano, Toral R. Patel, Dr. Joseph M. Piepmeier, Dr. Caroline E. Weller, Dr. Lucrezia Martino, Dr. Mariastella Scandola, and others.

References

1. de Martimprey, H.; Vauthier, C.; Malvy, C.; Couvreur, P. *Eur. J. Pharm. Biopharm.* **2009**, *71*, 490–504.
2. Sheridan, C. *Nat. Biotechnol.* **2011**, *29*, 459.
3. Kay, M. A. *Nat. Rev. Genet.* **2011**, *12*, 316.
4. Felgner, P. L.; et al. *Proc. Natl. Acad. Sci. U.S.A.* **1987**, *84*, 7413–7417.
5. Templeton, N. S.; et al. *Nat. Biotechnol.* **1997**, *15*, 647–652.
6. Al-Dosari, M. S.; Gao, X. *Am. Assoc. Pharm. Sci. J.* **2009**, *11*, 671–681.
7. Tros de Ilarduya, C.; Sun, Y.; Duzgunes, N. *Eur. J. Pharm. Sci.* **2010**, *40*, 159–170.
8. Pack, D. W.; Hoffman, A. S.; Pun, S.; Stayton, P. S. *Nat. Rev. Drug Discovery* **2005**, *4*, 581.
9. Green, J. J.; Langer, R.; Anderson, D. G. *Acc. Chem. Res.* **2008**, *41*, 749.
10. Kobayashi, S.; Makino, A. *Chem. Rev.* **2009**, *109*, 5288–5353.
11. Kobayashi, S. *Macromol. Rapid Commun.* **2009**, *30*, 237–266.
12. Gross, R. A.; Kumar, A.; Kalra, B. *Chem. Rev.* **2001**, *101*, 2097.
13. Uyama, H.; Kobayashi, S. *Adv. Polym. Sci.* **2006**, *194*, 133–158.
14. Azim, H.; Dekhterman, A.; Jiang, Z.; Gross, R. A. *Biomacromolecules* **2006**, *7*, 3093–3097.
15. Matsumura, S. *Adv. Polym. Sci.* **2006**, *194*, 95–132.

16. Jiang, Z.; Azim, H.; Gross, R. A.; Focarete, M. L.; Scandola, M. *Biomacromolecules* **2007**, *8*, 2262–2269.
17. (a) Liu, J.; Jiang, Z.; Zhang, S.; Liu, C.; Gross, R. A.; Kyriakides, T. R.; Saltzman, W. M. *Biomaterials* **2011**, *32*, 6646−6654. (b) Srivastava, R. K.; Albertsson, A. C. *Biomacromolecules* **2006**, *7*, 2531−2538. (c) Srivastava, R. K.; Albertsson, A. C.; *Macromolecules* 2006, *39*, 46-54. (d) Van der Mee, L.; Antens, J.; Van de Kruijs, B.; Palmans, A. R. A.; Meijer, E. W. *J. Polym. Sci., Part A: Polym. Chem.* **2006**, *44* (7), 2166−2176. (e) Magusin, P. C. M. M.; Mezari, B.; Van der Mee, L.; Palmans, A. R. A.; Meijer, E. W. *Macromol. Symp.* **2005**, *230*, 126−132.
18. Namekawa, S.; Uyama, H.; Kobayashi, S. *Biomacromolecules* **2000**, *1*, 335–338.
19. Jiang, Z. *Biomacromolecules* **2008**, *9*, 3246–3251.
20. Mazzocchetti, L.; Scandola, M.; Jiang, Z. *Macromolecules* **2009**, *42*, 7811–7819.
21. Liu, J.; Jiang, Z.; Zhang, S.; Saltzman, W. M. *Biomaterials* **2009**, *30*, 5707–5719.
22. Jiang, Z. *Biomacromolecules* **2010**, *11*, 1089–1093.
23. Liu, J.; Jiang, Z.; Zhou, J.; Zhang, S.; Saltzman, W. M. *J. Biomed. Mater. Res. A* **2011**, *96*, 456–465.
24. Zhou, J.; Liu, J.; Cheng, C. J.; Patel, T. R.; Weller, C. E.; Piepmeier, J. M.; Jiang, Z.; Saltzman, W. M. *Nat. Mater.* **2012**, *11*, 82–90.
25. Stridsberg, K. M.; Ryner, M.; Albertsson, A. C. *Adv. Polym. Sci.* **2002**, *157*, 41–65.
26. Nomura, R.; Ueno, A.; Endo, T. *Macromolecules* **1994**, *27*, 620–621.
27. Hefetz, A.; Fales, H. M.; Batra, S. W. T. *Science* **1979**, *204*, 415–417.
28. Hefetz, A.; Bergstrom, G.; Tengo, J. *J. Chem. Ecol.* **1986**, *12*, 197–208.
29. Duffield, R. M.; Laberge, W. E.; Cane, J. H.; Wheeler, J. W. *J. Chem. Ecol.* **1982**, *8*, 535–543.
30. Martino, L.; Scandola, M.; Jiang, Z. *Polymer* **2012**, *53*, 1839–1848.

Publication Date (Web): November 22, 2013 | doi: 10.1021/bk-2013-1144.ch003

Publication Date (Web): November 22, 2013 | doi: 10.1021/bk-2013-1144.ch004

Chapter 4

Metrology as a Tool To Understand Immobilized Enzyme Catalyzed Ring-Opening Polymerization

Matthew T. Hunley, Sara V. Orski, and Kathryn L. Beers*

Materials Science and Engineering Division, National Institute of Standards and Technology, Gaithersburg, Maryland 20899, United States
***E-mail: beers@nist.gov.**

Enzyme-catalyzed polymerization provides a green alter-native to synthesize biodegradable polyesters over conven-tional heavy metal catalysts. Heterogeneous catalysis, where the enzyme is immobilized onto solid-supports, allows for easy catalyst removal and can increase the commercial feasibility of biocatalysis with a thorough understanding of the reaction kinetics and required process conditons. In this mini-review, we describe our comprehensive metrology approach to fully identify key parameters to control enzymatic ring-opening polymerization (ROP) of lactones: development of predictive models of reaction kinetics, experimental models of the catalyst surface micro-environment, and on-line spectro-scopic analysis of reaction conversion for polyester homo-polymers and copolymers. Quantitative evaluation of enzyme-atic ROP illucidates advantages and limitations of current enzyme-catalyzed polymerizations and aids in the design of better reaction conditions and next generation catalysts.

Introduction

Awareness of sustainability and polymer lifecycle analysis has driven the development of many novel as well as commercial monomers from renewable feedstocks. Many commercially-important bioderivable, degradable polymers, including poly(lactic acid (PLA) and polycaprolactone (PCL), are synthesized

In Green Polymer Chemistry: Biocatalysis and Materials II; Cheng, H., et al.;
ACS Symposium Series; American Chemical Society: Washington, DC, 2013.

via ring-opening polymerization (ROP) using organometallic catalysts. Conventionally, this class of polymers is synthesized in bulk using $Sn(Oct)_2$ as the catalyst for controlled molecular masses and low polydispersities. However, the heavy metal catalyst often remains in the polymer and can pose a risk of toxicity. Recent interest in ROP using enzyme catalysts and organocatalysts (*1*, *2*) suggests that the the same polymers can be controllably synthesized without the presence of toxic metals.

Many different enzymatic catalysts have been identified for the ROP of lactones, cyclic carbonates, and lactides, as well as the polycondensation of carboxylic acids with alcohols (*3–5*). Lipase enzymes traditionally serve as degradation catalysts by cleaving ester linkages into carboxylic acids and alcohols in nature. These same catalysts can be induced to promote polymerization by stressing them in the presence of high concentrations of monomer in organic media. Previous studies have shown that many lipases are highly active under milder conditions than conventional metal catalysts, and the enzyme structure can dictate enhanced selectivity of stereochemistry and polymer structure. Enzymes can also be readily immobilized onto solid supports for heterogeneous catalysts with little loss of activity. One popular commercialized heterogenous enzyme catalyst is *Candida antarctica* Lipase B (CAL B) immobilized on an acrylic resin. Such heterogeneous catalysts can help in achieving proper stoichiometry and allow facile catalyst removal after the reaction. For these reasons, lipase enzymes have received significant interest as "green chemistry" alternatives for heavy metal catalysts.

The commercial adoption of enzymatic catalysts, however, requires a thorough understanding of the kinetic pathways and the catalyst stability. Previous studies have indicated that water content has a tremendous impact on initiation, polymerization kinetics, cyclic formation, polymer molecular mass, and enzyme activity over time. Similarly, copolymerization studies have demonstrated mutual reactivities of a wide range of monomers via the formation of statistical copolymers. These studies have not resulted in a complete framework to fully understand enzyme catalyzed polymerizations. We have approached enzyme catalysis with the objective of enhanced understanding through improved measurement techniques and predictive models. In this mini-review, we focus on the results of our recent work to understand the stability of solid-supported CAL B enzyme, develop a predictive model of polymerization, and improve the metrology through polymerization monitoring and reactor design.

Evaluating Enzyme Catalyst Surface Stability

Heterogeneous catalysts allow for the easy removal and recovery of the catalyst from the reaction mixture for potential reuse in subsequent polymerizations. Catalyst recycling is an important factor in increasing commercial acceptance of CAL B-catalyzed ring-opening polymerizations, as the catalyst must have a high polymer yield to offset the increased production costs associated with enzymes (*6*) over current metallic catalysts.

In Green Polymer Chemistry: Biocatalysis and Materials II; Cheng, H., et al.;
ACS Symposium Series; American Chemical Society: Washington, DC, 2013.

Publication Date (Web): November 22, 2013 | doi: 10.1021/bk-2013-1144.ch004

Publication Date (Web): November 22, 2013 | doi: 10.1021/bk-2013-1144.ch004

CAL B catalyzed ROP of ε-CL yields PCL with high molecular weights, and conversion rates based on choice of reaction solvent, temperature, and trace water content (*7*, *8*). Decreasing reaction rates over multiple cycles, often indicates enzyme desorption, which limits recyclability and contaminates the PCL product (*9*, *10*). This leaching is frequently attributed to the weak hydrophobic interactions of the enzyme physisorbed at the acrylic resin surface. Quantitative measurement of enzyme desorption to confirm that theory is challenging, however, as concentrations of leached enzyme within the polyester are exceedingly low (*9*). Attempts to measure enzyme leaching have been evaluated indirectly through monitoring monomer conversion over several reuse cycles (*9*) or by elemental analysis of the acrylic resin (*10*). Furthermore, isolating potential causes of catalyst leaching is challenging due to the complex structure of the immobilized catalyst on the surface of a crosslinked, porous, polymer bead. A more direct method is needed to understand the physiochemical interaction between the enzyme and the crosslinked poly(methyl methacrylate) (PMMA) surface, so that optimal process conditions can be used to maintain adequate polymerization control and improve catalyst retention for several reuses.

Quartz crystal microbalance with dissipation monitoring (QCM-D) has been used to characterize in situ enzyme and protein adsorption at surfaces (*11–13*), including CAL B adsorption on self-assembled monolayers (*14–16*). Mass adsorbed on a quartz crystal sensor will cause small changes in resonant frequency (*f*) and energy dissipation (D) of the oscillating sensor (*17*). These changes can be used to determine mass and viscoelastic properties of an adsorbed layer through Kelvin-Voigt visoelastic models (*18*).

The microenvironment of the PMMA bead surface was mimicked by fabrication of a homogenous, highly crosslinked PMMA thin film on a QCM-D sensor. The PMMA chains were covalently crosslinked to the quartz sensor using a photoactivated benzophenone moiety within the polymer thin film and as a self-assembled monolayer on the crystal surface, as depicted in Scheme 1. The dual photochemical process permits efficient covalent attachment of commercially available PMMA to the surface and to other neighboring chains. The flat, 2D PMMA layer replates the chemistry and mechanical properties of the bead surface in QCM-D, where enzyme adsorption, desorption, and changes in viscoelastic properties could be measured in situ as experimental conditions were varied. Enzyme stability was evaluated with increasing water content of toluene and polycaprolactone solutions, and with increasing reactor temperature, mimicking reaction environments where enzyme leaching and changing enzymatic activity has been previously demonstrated. The 2D experimental model was used to quantiatively study the enzyme stability at the polymer surface microenvironment, pinpointing the sources of variation in enzyme affinity for the solid support,

Adsorption of CAL B on the PMMA surface occurred rapidly in the QCM-D cell, as 90% of the enzyme adsorption was complete within 300 s of addition to the QCM-D under flow, resulting in a mass surface coverage of 530 ng/cm^2 ± 63 ng/cm^2, determined by the Sauerbrey equation (equation 1) (*19*). All Sauerbrey masses calculated represent one standard deviation among at least three trials. The overtone is denoted by n and C is a constant dependent on crystal properties, which is 17.7 ng cm^{-2}Hz^{-1}.

In Green Polymer Chemistry: Biocatalysis and Materials II; Cheng, H., et al.;
ACS Symposium Series; American Chemical Society: Washington, DC, 2013.

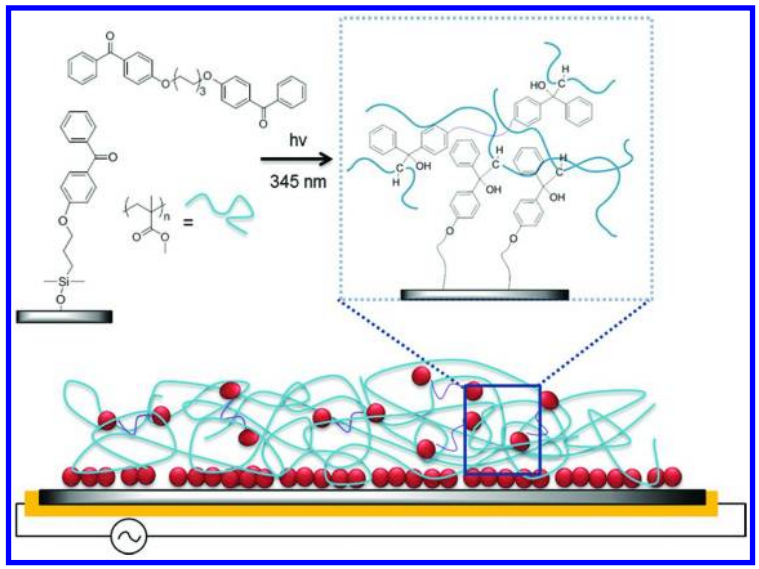

Scheme 1. Depiction of two-dimensional crosslinked PMMA thin film on quartz crystal sensor (side view). Reproduced with permission from reference (19). Copyright 2013 The American Chemical Society.

$$\Delta m = -\frac{C}{n}\Delta f_n \quad (1)$$

Generally, if the ratio of dissipation to frequency, $\Delta D_n/(-\Delta f_n/n)$, is less than 4 x$10^{-7}$ (*20*), the layer on the sensor can be approximated as rigid, which is true for the adsorption of CAL B on crosslinked PMMA.

Enzyme surface stability was first evaluated as a function of increasing the trace water content in reaction solvent (toluene) from 250 ppm to 450 ppm. This range was used to evaluate CAL B at a model surface over a range where the enzyme surface transitions from dehydrated and inactive (≤ 250 ppm) to fully hydrated (≥ 450 ppm) during ε-CL ROP conditions (*9*). Sauerbrey calculations yielded an 8% decrease in mass surface coverage of the enzyme at 350 ppm and a 20.2% decrease at 450 ppm among several trials (*19*). PMMA control samples demonstrated an insignificant mass increase at 450 ppm, due to water adsorption on the PMMA layer. The CAL B desorption from the surface is caused by the disruption of the hydrophobic interaction between the enzyme and the PMMA surface, as the enzyme absorbs water and becomes less rigid.

Formation of the enzyme-activated complex (EAC) was evaluated by measuring adsorption of polycaprolactone (M_n = 10,000 g/mol) to CAL B active sites with increasing water content (250 ppm – 450 ppm). Mass adsorption changes due exclusively to the EAC were evaluated as the difference between enzyme-modified and unmodified PMMA, deconvoluting the mass change of the EAC from non-specific binding of PCL to the surface. The measured increase in mass of the EAC with additional water content was inconsistent with the enzyme loss observed with increasing water concentration in toluene. This difference

In Green Polymer Chemistry: Biocatalysis and Materials II; Cheng, H., et al.;
ACS Symposium Series; American Chemical Society: Washington, DC, 2013.

results from the influence of water on polymerization kinetics (*21*), where the concentration of free polyester chains in solution over those bound to the enzyme increases as trace water content increases. This creates increased diffusion of PCL chains to active enzymes and the water affinity between the enzyme and PCL will retain greater mass at the sensor surface.

The PMMA/CAL B interfacial stability was also evaluated as a function of temperature between 22 °C and 90 °C. Bare crystal and PMMA control samples were measured under identical conditions to determine the response of the CAL B layer corrected for background effects such as temperature dependence on frequency and dissipation of the quartz crystal, as well as the temperature effects on solvent density and viscosity. Mass surface coverage of the CAL B layer decreases with increasing temperature; 90% of the enzyme layer is desorbed at 90 °C (*19*). The frequency and dissipation changes of the CAL B/PMMA and PMMA layers indicate that the enzyme layer becomes more viscoelastic as temperature increases. The ratio of $\Delta D_n/(-\Delta f_n/n)$ for CAL B is right at the approximation threshold, where the film can be approximated as rigid below 50 °C, and viscoelastic above. The CAL B layer therefore remains mostly elastic, with minimal diffusion and relaxation occurring between the surface-bound enzymes. Increasing temperature disrupts the CAL B layer, permitting enzyme diffusion from the PMMA surface, which is reversible upon cooling. Mass loss due to enzyme dehydration will be minimal, however, since only water adsorbed at the enzyme surface can be removed by organic solvents (*22*).

The development of a simplified 2D experimental model of the CAL B/ polymer interface has demonstrated the chemical affinity of CAL B for PMMA on a flat, smooth surface with varying reaction parameters. This model establishes a reproducable in situ model, which may be used to expand enzyme affinity measurements to include more complex interactions induced by a porous particle geometry of the heterogeneous catalyst bead.

Understanding the Kinetic Pathways

Enzyme-catalyzed ring-opening polymerization (ROP) proceeds via several distinct steps which all require the presence of lipase (*8*, *21*). Scheme 2 illustrates the central role of lipase catalyst in the ROP mechanism of ε-caprolactone (ε-CL) (*21*). The active site reacts to open the monomer ring to form the enzyme-activated monomer (EAM) (Step 1 in Scheme 2). The EAM can then react with water to form ring-opened monomer (Step 2), a propagating polymer chain to form polymer (Step 3), or intramolecularly to form cyclics (Step 4). The lipase also reacts with oligomeric and polymeric species to drive these reactions in reverse.

Earlier studies demonstrated the influence of water on initiation and the prevalence of cyclics within the polymer product (*23–25*). However, these early reports had no predictive capabilities. We adopted the generally accepted mechanism (*8*) into a robust kinetic model to track the evolution of all species (including ring-opened monomer, cyclics, and all polymer chains) over the course of polymerization. The results of the kinetic model simulation of ε-CL polymerization using CAL B enzyme are shown in Figure 1. The model monomer

In Green Polymer Chemistry: Biocatalysis and Materials II; Cheng, H., et al.;
ACS Symposium Series; American Chemical Society: Washington, DC, 2013.

Publication Date (Web): November 22, 2013 | doi: 10.1021/bk-2013-1144.ch004

conversion mirrored the experimentally observed monomer conversion to within measurement error, but more impressively the model molar mass distribution showed very similar behavior to the experimental SEC traces. The tailing at high elution times demonstrates the presence of low molar mass cyclic oligomers, even at high monomer conversions. These low molar mass species act as plasticizers with detrimental effects on polymer physical properties.

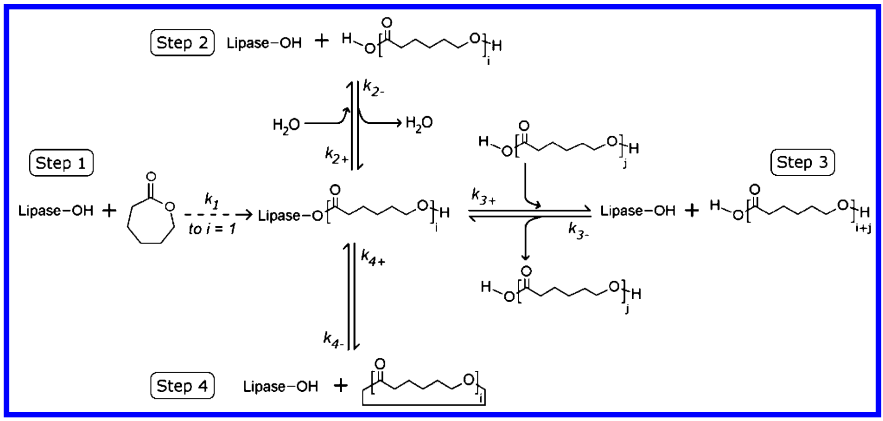

Scheme 2. Kinetic reactions in the enzyme-catalyzed polymerization of ε-caprolactone. Reproduced with permission from reference (21). Copyright 2012 The American Chemical Society.

Another major factor in the enzyme-mediated ROP revealed by the kinetic model is the influence of water, which affects all stages of polymerization from initiation to degradation. The model indicated that the ring-opening reaction proceeded faster with higher water concentrations. Because water affects the release of enzyme-activated monomer (EAM) from the enzyme active sites, lower water concentrations lead to longer residence times of EAM, slowing the overall polymerization rate. Further experiments confirmed the influence of water on M_n. Since each water molecule acts as an initiator, reduction in the water concentration should reduce the number of chains and result in increased M_n at equivalent monomer conversions. Water concentration was controlled rudimentarily through the addition of molecular sieves to the polymerization mixture. The molecular sieves slowly remove water from the reaction mixture, resulting in little change in reaction kinetics during most of the reaction but an increase in M_n at high conversions. Experimental results confirmed the model predictions, demonstrating that the molecular sieves led to a dramatic increase in M_n at high conversion (*26*).

Similarly, the kinetic model provided insight into the enzymatic degradation of polymers. When the starting material is switched from ε-CL to PCL, chain equilibrium reactions dominate (*21*). At long times, the PCL will reach a new equilibrium molecular mass determined by the starting M_n and the amount of additional water present. If the amount of water present is less than the number of polymer chains, then the degradation will first result in a bimodal molecular

In Green Polymer Chemistry: Biocatalysis and Materials II; Cheng, H., et al.;
ACS Symposium Series; American Chemical Society: Washington, DC, 2013.

Publication Date (Web): November 22, 2013 | doi: 10.1021/bk-2013-1144.ch004

mass distribution as a portion of the polymer is degraded to lower molar mass. Afterwards, the enzyme will equilibrate all the chains to a molecular mass consistent for the number of linear chains. This equilibrium molecular mass is slightly higher than the mass of the initially degraded chains. This model behavior was confirmed experimentally.

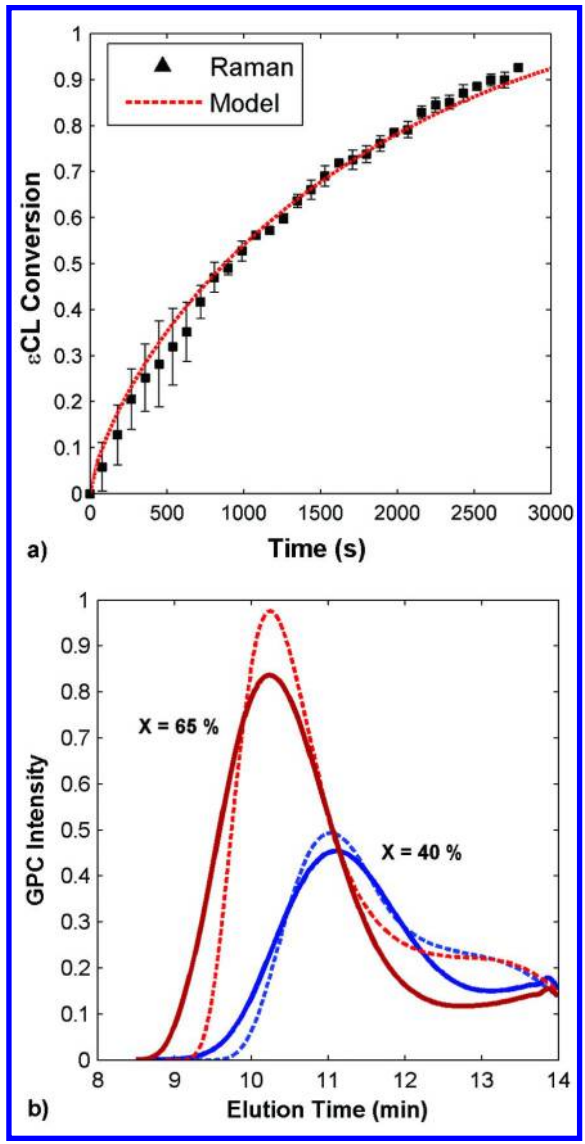

Figure 1. (a) Comparison of experimental (■) and model (---) results for ε-CL ring-opening conversion. (b) Experimental (---) and modeled (–) SEC traces for molecular mass distribution at 40% (blue) and 65% (red) conversion. Reproduced with permission from reference (21). Copyright 2012 The American Chemical Society.

In Green Polymer Chemistry: Biocatalysis and Materials II; Cheng, H., et al.;
ACS Symposium Series; American Chemical Society: Washington, DC, 2013.

Publication Date (Web): November 22, 2013 | doi: 10.1021/bk-2013-1144.ch004

Reaction Monitoring

In addition to the predictive capabilities of the model for enzyme kinetics, on-line reaction monitoring provides a wealth of knowledge about the polymerization. Off-line analytical techniques can be time consuming and labor intensive, and removal and storage of reaction aliquots is difficult for moisture-sensitive reactions such as enzyme-mediated ROP. Enzyme leaching can also contaminate the aliquots and lead to residual polymerization prior to analysis. On-line spectroscopic monitoring via Raman or infrared spectroscopy reduces these concerns and can provide rapid data collection over the entire reaction time.

Raman spectroscopy was used to follow the consumption of ε-CL by monitoring the monomer's anti-symmetric ring stretching absorbance at 696 cm^{-1} (*27*). Figure 2 shows the monomer conversions versus reaction time for the enzyme-catalyzed ROP at different temperatures. The spectroscopic data was confirmed by ^{1}H NMR aliquots taken at specific time intervals, indicating that the consumption of monomer reflected incorporation into the polymer and not just ring-opening. In addition, the spectroscopic method enables a higher data density during the reaction; data collection from reaction aliquots is intrinsically limited to maintain reaction stoichiometry. The conversion data in Figure 2 also indicate that increasing temperature does not have a linear effect on the reaction kinetics. Above 55 °C, increasing the temperature leads to only a minute increase in reaction rate, possibly due to slight denaturation of the enzyme.

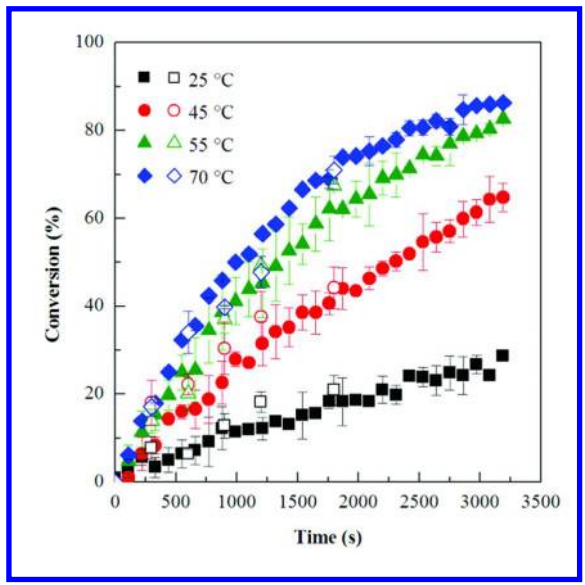

Figure 2. Conversion of ε-CL as a function of reaction times at different temperatures: (black squares) 25 °C, (red circles) 45 °C, (green triangles) 55 °C, (blue diamonds) 70 °C. Open symbols represent NMR data collected off-line, closed symbols represent Raman spectroscopic data. Reproduced with permission from reference (27). Copyright 2012 The Royal Society of Chemistry.

In Green Polymer Chemistry: Biocatalysis and Materials II; Cheng, H., et al.;
ACS Symposium Series; American Chemical Society: Washington, DC, 2013.

Publication Date (Web): November 22, 2013 | doi: 10.1021/bk-2013-1144.ch004

Publication Date (Web): November 22, 2013 | doi: 10.1021/bk-2013-1144.ch004

On-line spectroscopic analysis also enables the simultaneous monitoring of multiple monomers during copolymerizations and provides many more data points in the low conversion regime to decrease measurement uncertainty when calculating reactivity ratios. The properties of copolymers are strongly influenced by the relative reactivities and sequence distributions of different comonomers, but reliable quantification of copolymerization parameters limits the development of structure-property relationships. Conventional linearization techniques to estimate comonomer reactivity ratios depend on measurements of the partial molar conversions of each monomer at low conversions. These values can be accurately measured by NMR or GC, but such offline measurements typically provide one data point per reaction and require extensive experimental work. In situ techniques also allow rapid measurements of multiple reactions at different feed compositions.

We monitored the copolymerization of ε-CL and δ-valerolactone (δ-VL) using in situ Raman spectroscopy. The monomer concentrations profiles are shown in Figure 3. During the first five minutes of copolymerization, the δ-VL concentration remains constant while ε-CL is consumed. Similar induction periods have been observed previously for δ-VL polymerized by enzyme catalysis (*28*). The mechanistic model described earlier allowed us to identify a possible cause of the induction period. At the initial stages of copolymerization, the water present reacts with enzyme-activated monomer to form the ring-opened monomer. Although δ-VL exhibits a faster rate of hydrolysis and rate of propagation (*29*), the ring-opened form (5-hydroxypentanoic acid) undergoes spontaneous cyclization back to the monomer faster than it can be incorporated in the growing oligomers (*30*). The ring-opened form of ε-CL, 6-hydroxyhexanoic acid, undergoes lactonization at a much slower rate. Once the water present in the reaction is incorporated into the growing oligomers, around 5 minutes in this case, the δ-VL is readily incorporated in the polymer.

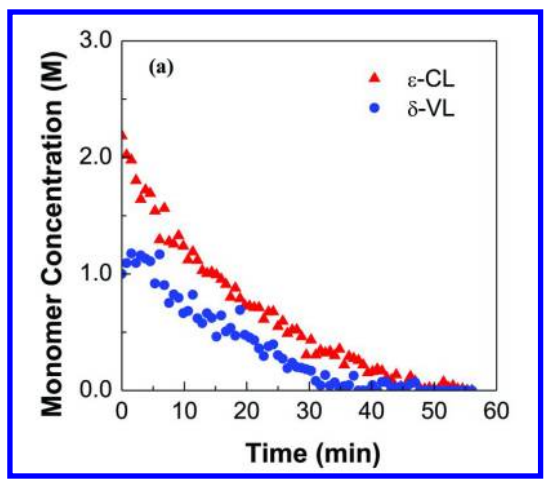

Figure 3. Monomer concentration profiles for enzymatic copolymerization of (red triangles) ε-CL and (blue circles) δ-VL. Reproduced with permission from reference (34). Copyright 2013 The American Chemical Society.

In Green Polymer Chemistry: Biocatalysis and Materials II; Cheng, H., et al.;
ACS Symposium Series; American Chemical Society: Washington, DC, 2013.

Publication Date (Web): November 22, 2013 | doi: 10.1021/bk-2013-1144.ch004

Reactivity ratios are conventionally estimated using linearization techniques such as the Fineman-Ross and Kelen-Tüdös method (K-T method) (*31*, *32*). We were able to use the Raman spectroscopic data to calculate the initial monomer consumption ratio, d[δ-VL]/d[ε-CL], for each starting monomer ratio [δ-VL]/[ε-CL]. Reactivity ratios were then determined using the K-T method as $r_{\varepsilon\text{-}CL} = 0.38 \pm 0.06$ and $r_{\delta\text{-}VL} = 0.29 \pm 0.03$. These reactivity ratios indicate a slightly alternating microstructure, and are similar to ratios reported for the bulk copolymerization catalyzed by $Sn(Oct)_2$ ($r_{\varepsilon\text{-}CL} = 0.25$ and $r_{\delta\text{-}VL} = 0.49$) (*33*).

Conventional reactivity ratio techniques have many problems, however. Due to the low conversion assumption, we only use a small fraction of the collected Raman data. Skeist, along with the work of Meyer and Lowry, developed a model to describe the monomer composition drift during the course of copolymerization. Applying this integrated form of the copolymer composition equation uses the spectroscopic data over the entire course of the copolymerization. Using an error-in-variables-model (EVM) nonlinear regression technique, the data was fit to the model to estimate reactivity ratios (*34*). Figure 4 shows the spectroscopic data with model fits. The model fit the data very well, suggesting that enzyme-catalyed copolymerizations can be effectively described by terminal model kinetics. The results from each reaction were combined to estimate the composite reactivity ratios of $r_{\varepsilon\text{-}CL} = 0.27$ and $r_{\delta\text{-}VL} = 0.39$. Figure 5 shows the reactivity ratios and 95% joint confidence regions (JCRs) from both the K-T method and the EVM method. The EVM method estimates reactivity ratios lower for ε-CL and higher for δ-VL, which is presumably due to the lowered influence of the δ-VL induction period.

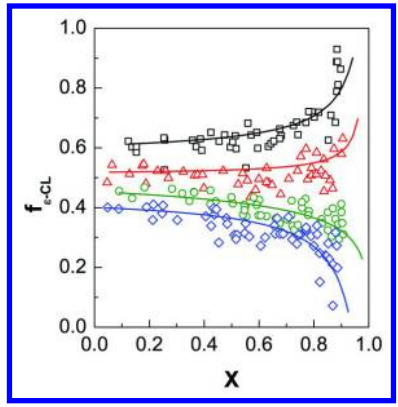

Figure 4. Monomer fraction versus total monomer conversion for enzymatic copolymerizations of ε-CL and δ-VL. The symbols represent experimental data and the solid lines represent the best fit using EVM regression for starting compositions $f_{\varepsilon\text{-}CL,0}$ of (black squares) 0.60, (red triangles) 0.52, (green circles) 0.45, and (blue diamonds) 0.40. Reproduced with permission from reference (34). Copyright 2013 The American Chemical Society.

In Green Polymer Chemistry: Biocatalysis and Materials II; Cheng, H., et al.;
ACS Symposium Series; American Chemical Society: Washington, DC, 2013.

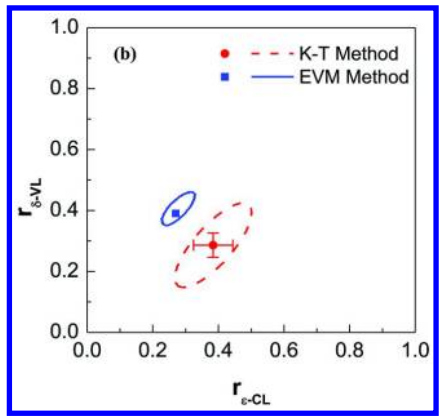

Figure 5. Reactivity ratios and 95% JCRs for the enzymatic copolymerization of ε-CL and δ-VL in toluene. The error bars for the K-T method represent one standard deviation based on linear regression analysis. Reproduced with permission from reference (34). Copyright 2013 The American Chemical Society.

Engineering Control of Ring-Opening Polymerization through Microfluidic Reactor Design

Understanding the mechanism and influence of water, concentration, and temperature in enzyme catalyzed ring-opening polymerization has led to the development of packed bed microfluidic flow reactors to systematically control experimental parameters (*9*, *10*). The development of measurement tools to characterize enzymatic ROP must also coincide with the progress of reactor design to evaluate the advantages afforded to conducting the reaction in a microfluidic system under continuous flow. Accurate determination of process changes involving immobilized enzyme catalyst can compliment advantages of new reactor design and increase the possibilities for scaling up reactors with improved control to commercial reactor sizes.

The packed bed reactor, consisting of a 2 mm x 1 mm x 260 mm (W x D x L) channel cut into a 10 mm thick aluminum block, maintained accurate reaction temperature control to ± 0.5 °C. A depiction of the reactor design is illustrated in Scheme 3.

ROP of ε-CL in the microfluidic reactor was conducted at temperatures between 55 °C – 100 °C and ε-CL conversion was monitored by Raman spectroscopy. The reaction reached final conversion within 240 s for all temperatures studied (Figure 6a). The rate of reaction was calculated for temperatures for the residence time in the columns and calculated from the equation below:

$$-\ln(1-X_t) = k_{app}t$$

where X_t is the monomer conversion for residence time, t, and k_{app} is the apparent rate constant. Residence time in the reactor was controlled by flow rate. Fits of first-order reaction kinetics are shown in Figure 6b, where k_{app} values were

In Green Polymer Chemistry: Biocatalysis and Materials II; Cheng, H., et al.;
ACS Symposium Series; American Chemical Society: Washington, DC, 2013.

between 0.007 s^{-1} to 0.012 s^{-1} for all temperatures studied. This is an order of magnitude increase for batch reactions under the same conditions, (k_{app} values between 0.0004 s^{-1} and 0.0008 s^{-1}). This rate increase is due to the restricted volume in the packed microfluidic chanel, where diffusion length to the enzyme active site is much smaller. In addition, the larger surface area to volume ratio of the microfluidic reactor relative to the batch reactor will result in more availability of enzyme active sites for faster polymerization. Active site availability and short diffusion pathways also can be attributed to the increase in M_n for the microfluidic device over batch reactors.

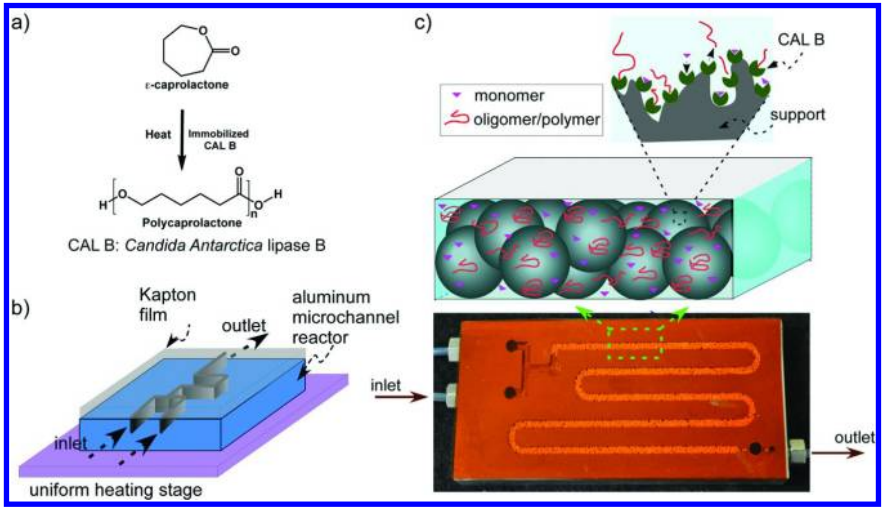

Scheme 3. (a) Ring-opening polymerization of ε-CL catalyzed by CAL B. (b) flow direction in the packed-bed microfluidic device. (c) side view of polymer chains interacting with immobilized CAL B catalyst. (4) picture of N435 packed bed microfluidic device sealed with a Kapton film (orange). Reproduced with permission from reference (9). Copyright 2011 The American Chemical Society.

The microfluidic reactor also allows for control of polymer chain ends not afforded to batch reactors. Water, which plays a critical role in lubrication and activation of the enzymes (*24*), can also act as an initiator, forming more carboxylic acid polymer chain ends. Following on the microreactor development work, investigations into chain end control were compared between batch and microfluidic devices, monitoring reaction conversion by ^{1}H NMR (*10*). Benzyl alcohol initiator was added to batch and microfluidic reactors that were anhydrous (water from solvent and monomer removed) and wet conditions. Initiation of benzyl alcohol was dominant in the microfluidic device, regardless of starting water concentration. The fraction of benzyl chain ends from PCL synthesized in the microfluidic device was greater than 0.98 after 90 s of reaction time. While batch reactors under dry conditions demonstrate fractions of benzyl end groups similar to the microfluidic system , the mass fraction of initiated benzyl alcohol

Publication Date (Web): November 22, 2013 | doi: 10.1021/bk-2013-1144.ch004

in wet conditions leads to greater carboxylic acid chain ends and benzyl alcohol fraction of less than 0.2. Tailored initiators can therefore be introduced into microfluidic reactors under less stringent conditions to incorporate endgroup functionalized polyesters for further postpolymerization reactions.

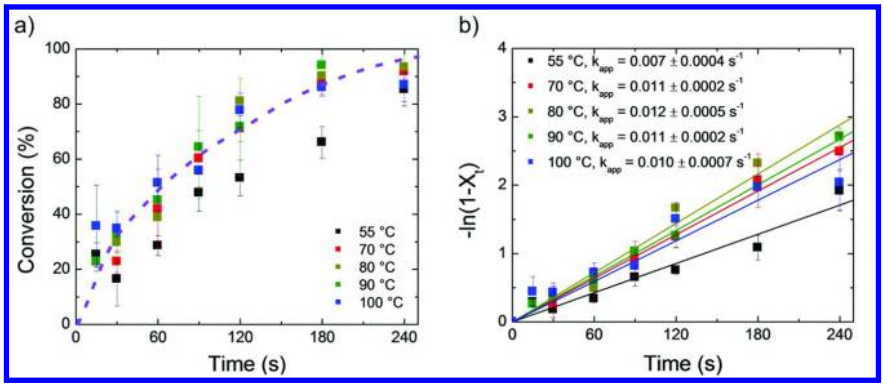

Figure 6. (a) Conversion of ε-CL with residence time for five temperatures. (b) Semilogrithmic conversion data fitted with first order reaction kinetics. Error bars represent one standard uncertainty of the data based on at least three measurements. Reproduced with permission from reference (9). Copyright 2011 The American Chemical Society.

The determination of enzyme activity and stability in microfluidic devices over batch reactions is critical to process development, where improving catalyst reusability can make heterogeneous catalysts more amenable to commercial-scale polymerizations. Previously, enzyme activity over several reuse cycles in the microfluidic device has been controlled by the hydration of the active enzyme site. Rinsing the device with anhydrous toluene caused a dramatic decrease in polymer conversion in subsequent cycles, while a "wet wash" rehydrated the enzymes and kept conversion high at 80%.

Summary and Outlook

A wide-ranging measurement toolbox has been applied to improving understanding of enzyme-catalyzed ring-opening polymerization reactions through measuring the reaction at multiple tiers, from experimentally-validated theoretical reaction models, to on-line reaction monitoring of entire reaction mixtures. Predictive kinetic models detailing the reaction pathways of a propagating chain provide a comprehensive view of the reaction mechanism, which is supported by experimental data. Stability of the enzyme catalyst/solid support interface was measured through 2D experimental models to probe the effects of reaction conditions on catalyst retention. On-line measurement of the bulk ROP reaction mixture using Raman spectroscopy provides kinetic information without disturbing the reaction mixture. Rapid kinetic data collection of ROP is expanded to determine reactivity ratios for lactone copolymerizations

In Green Polymer Chemistry: Biocatalysis and Materials II; Cheng, H., et al.;
ACS Symposium Series; American Chemical Society: Washington, DC, 2013.

Publication Date (Web): November 22, 2013 | doi: 10.1021/bk-2013-1144.ch004

to control material properties. Development of microfluidic reactors imparts rapid polymerization rates with control of polymer endgroups that were quantified in direct comparison with traditional polymerization methods.

These characterization methods can be used to quantify reaction rates and process conditions for current advances in enzyme-catalyzed ROP, including the study of new solid-supported enzymes (*35*), development of novel monomer and co-monomer pairs (*36–38*), and the sythesis of branched polymers (*39*). This comprehensive metrology approach of prediction, simplied surface models, and on-line reaction monitoring can be used to rapidly characterize and optimize novel polymerization systems, including next-generation catalysts, monomers, and reactor systems.

Publication Date (Web): November 22, 2013 | doi: 10.1021/bk-2013-1144.ch004

References

1. Guillaume, S. M.; Carpentier, J.-F. *Catal. Sci. Technol.* **2012**, *2*, 898–906.
2. Kamber, N. E.; Jeong, W.; Waymouth, R. M.; Pratt, R. C.; Lohmeijer, B. G. G.; Hedrick, J. L. *Chem. Rev.* **2007**, *107*, 5813–5840.
3. Kobayashi, S. *Macromol. Rapid Commun.* **2009**, *30*, 237–266.
4. Yang, Y.; Yu, Y.; Zhang, Y.; Liu, C.; Shi, W.; Li, Q. *Process Biochem.* **2011**, *46*, 1900–1908.
5. Yu, Y.; Wu, D.; Liu, C.; Zhao, Z.; Yang, Y.; Li, Q. *Process Biochem.* **2012**, *47*, 1027–1036.
6. Tufvesson, P.; Lima-Ramos, J.; Nordblad, M.; Woodley, J. M. *Org. Process Res. Dev.* **2010**, *15*, 266–274.
7. Kumar, A.; Gross, R. A. *Biomacromolecules* **2000**, *1*, 133–138.
8. Mei, Y.; Kumar, A.; Gross, R. A. *Macromolecules* **2002**, *35*, 5444–5448.
9. Kundu, S.; Bhangale, A. S.; Wallace, W. E.; Flynn, K. M.; Guttman, C. M.; Gross, R. A.; Beers, K. L. *J. Am. Chem. Soc.* **2011**, *133*, 6006–6011.
10. Bhangale, A. S.; Beers, K. L.; Gross, R. A. *Macromolecules* **2012**, *45*, 7000–7008.
11. Kao, P.; Allara, D. L.; Tadigadapa, S. *IEEE Sens. J.* **2011**, *11*, 2723–2731.
12. Liu, S. X.; Kim, J.-T. *J. Lab. Autom.* **2009**, *14*, 213–220.
13. Liu, C.; Meenan, B. J. *J. Bionic Eng.* **2008**, *5*, 204–214.
14. Laszlo, J. A.; Evans, K. O. *J. Mol. Catal. B: Enzym.* **2007**, *48*, 84–89.
15. Laszlo, J. A.; Evans, K. O. *J. Mol. Catal. B: Enzym.* **2009**, *58*, 169–174.
16. Volden, S.; Moen, A. R.; Glomm, W. R.; Anthonsen, T.; Sjöblom, J. *J. Dispersion Sci. Technol.* **2009**, *30*, 865–872.
17. Rodahl, M.; Höök, F.; Fredriksson, C.; Keller, C. A.; Krozer, A.; Brzezinski, P.; Voinova, M.; Kasemo, B. *Faraday Discuss.* **1997**, *107*, 229–246.
18. Voinova, M. V.; Rodahl, M.; Jonson, M.; Kasemo, B. *Phys. Scr.* **1999**, *59*, 391–396.
19. Orski, S. V.; Kundu, S.; Gross, R. A.; Beers, K. L. *Biomacromolecules* **2013**, *14*, 377–386.
20. Reviakine, I.; Johannsmann, D.; Richter, R. P. *Anal. Chem.* **2011**, *83*, 8838–8848.

21. Johnson, P. M.; Kundu, S.; Beers, K. L. *Biomacromolecules* **2011**, *12*, 3337–3343.
22. Idris, A.; Bukhari, A. *Biotechnol. Adv.* **2012**, *30*, 550–563.
23. Varma, I. K.; Albertsson, A.-C.; Rajkhowa, R.; Srivastava, R. K. *Prog. Polym. Sci.* **2005**, *30*, 949–981.
24. Dong, H.; Cao, S.-G.; Li, Z.-Q.; Han, S.-P.; You, D.-L.; Shen, J.-C. *J. Poly. Sci., A: Polym. Chem.* **1999**, *37*, 1265–1275.
25. Bisht, K. S.; Henderson, L. A.; Gross, R. A.; Kaplan, D. L.; Swift, G. *Macromolecules* **1997**, *30*, 2705–2711.
26. Kundu, S.; Johnson, P. M.; Beers, K. L. *ACS Macro Lett.* **2012**, *1*, 347–351.
27. Hunley, M. T.; Bhangale, A. S.; Kundu, S.; Johnson, P. M.; Waters, M. S.; Gross, R. A.; Beers, K. L. *Polym. Chem.* **2012**, *3*, 314–318.
28. López-Luna, A.; Gallegos, J. L.; Gimeno, M.; Vivaldo-Lima, E.; Bárzana, E. *J. Mol. Catal. B: Enzym.* **2010**, *67*, 143–149.
29. Van der Mee, L.; Helmich, F.; De Bruijn, R.; Vekemans, J. A. J. M.; Palmans, A. R. A.; Meijer, E. W. *Macromolecules* **2006**, *39*, 5021–5027.
30. Wiberg, K. B.; Waldron, R. F. *J. Am. Chem. Soc.* **1991**, *113*, 7697–7705.
31. Fineman, M.; Ross, S. D. *J. Polym. Sci.* **1950**, *5*, 259–262.
32. Kelen, T.; Tüdös, F. *J. Macromol. Sci. A* **1975**, *9*, 1–27.
33. Storey, R. F.; Hoffman, D. C. *Makromol. Chem. Macromol. Symp.* **1991**, *42-43*, 185–193.
34. Hunley, M. T.; Beers, K. L. *Macromolecules* **2013**, *46*, 1393–1399.
35. Barrera-Rivera, K. A.; Flores-Carreón, A.; Martínez-Richa, A. Methods in Molecular Biology. In *Lipases and Phospholipases*; Sandoval, G., Ed.; Humana Press: Totowa, NJ, 2012; Vol. 861, pp 485–493.
36. Poulhès, F.; Mouysset, D.; Gil, G.; Bertrand, M. P.; Gastaldi, S. *Polymer* **2012**, *53*, 1172–1179.
37. Frampton, M. B.; Séguin, J. P.; Marquardt, D.; Harroun, T. A.; Zelisko, P. M. *J. Mol. Catal. B: Enzym.* **2013**, *85–86*, 149–155.
38. Ragupathy, L.; Ziener, U.; Dyllick-Brenzinger, R.; Von Vacano, B.; Landfester, K. *J. Mol. Catal B: Enzym.* **2012**, *76*, 94–105.
39. Liu, C.; Jiang, Z.; Decatur, J.; Xie, W.; Gross, R. A. *Macromolecules* **2011**, *44*, 1471–1479.

Publication Date (Web): November 22, 2013 | doi: 10.1021/bk-2013-1144.ch004

Publication Date (Web): November 22, 2013 | doi: 10.1021/bk-2013-1144.ch005

Chapter 5

Syntheses and Characterization of Aliphatic Polyesters via *Yarrowia lipolytica* Lipase Biocatalysis

Karla A. Barrera-Rivera and Antonio Martínez-Richa*

Departamento de Química, División de Ciencias Naturales y Exactas, Universidad de Guanajuato, Noria Alta s/n, Guanajuato, Guanajuato 36050, México
***E-mail: richa@ugto.mx, fionita@ugto.mx**

In 2008, we reported a novel method to isolate lipases from yeasts of *Yarrowia lipolytica*. Isolated lipases were proven to be effective in the ring-opening polymerization of lactones. In the presence of ionic liquids, enzyme increases its activity and yields poly (ε-caprolactone)s (PCLs) with number-average molecular weights (Mn) in the range of 300-9,000 Da. Immobilization of lipases in different matrices was achieved and tested to be effective for the acylation of isosorbide by lactones. A recent application of the obtained immobilized enzymes involves quantitative production of α-ω-telechelic PCL diols (using *Yarrowia lipolytica* lipase immobilized on a macroporous resin Lewatit VP OC 1026), by ring-opening polymerization of CL in presence of diethylene glycol and 1,3-propanediol. Various degradable linear polyester-urethanes have been prepared from synthesized PCL diols and hexamethylenediisocyanate (HDI). Stress-strain tests show the existence of three different regimes during the elongation process, which quotes for the complex morphology present in the obtained polymers.

In Green Polymer Chemistry: Biocatalysis and Materials II; Cheng, H., et al.;
ACS Symposium Series; American Chemical Society: Washington, DC, 2013.

Publication Date (Web): November 22, 2013 | doi: 10.1021/bk-2013-1144.ch005

Introduction

In recent years, environmental concerns have led to a renewed interest in biodegradable polyesters as an alternative to commodity plastics. Since ester linkages are frequently encountered in nature it is reasonable to assume that at least a subset of the polyester family will be environmentally degradable. Random and block copolymers as well as blends have been investigated with regard to controlling the lifetime of biodegradable polymers as well as improving their mechanical properties. Environmental pollution caused by production and disposal of petrochemical - derived plastics have led to pursue strategic alternatives using environmentally benign processes to synthesize plastics that are engineered to degrade - on - demand (*1*).

Enzymatic polymerizations are a powerful and versatile approach which can compete with chemical and physical techniques to produce known materials (such as 'commodity plastics') and also to synthesize novel macromolecules so far not accessible via traditional chemical approaches. Enzymatic polymerizations can prevent waste generation by using efficient catalytic processes with high stereo- and regio–selectivity, prevent or limit the use of hazardous organic reagents by, for instance, using water or ionic liquids as green solvents, design processes with higher energy efficiency and safer chemistry by conducting reactions at low temperatures under ambient atmosphere, and increase atom efficiency by avoiding extensive protection and deprotection steps. Because of these characteristics, enzymatic polymerizations can provide an essential contribution to achieving industrial sustainability in the future (*1*).

Yarrowia lipolytica lipase has demonstrated to be efficient in the synthesis of different biodegradable polyesters, obtained by ring-opening polymerization of cyclic esters. Using biocatalysis with YLL, oligomeric PCL diols can be efficiently produced. These bifunctional monomers can then be used to prepare biodegradable linear polyester urethanes (*2–5*).

Experimental

Materials

ε-CL (Aldrich Chemicals Co.) was dried over calcium hydride and distilled under reduced pressure before use. Chloroform, toluene and methanol were obtained from Karal and used as received. Chloroform-*d* (99.8 %), was obtained from Sigma-Aldrich. Diethylene glycol (DEG), 1,3-propanediol, Lewatit VP OC 1026 and K2629 beads, stannous 2-ethylhexanoate, hexamethylenediisocianate (HDI) and 1,2-dichloroethane anhydrous 99.8 % were purchased from Sigma Aldrich and used as received.

Instrumentation

Solution ^{1}H and ^{13}C-NMR spectra were recorded at room temperature on a Varian Gemini 2000. Chloroform-*d* ($CDCl_3$) was used as solvent. FT-IR spectra were obtained with the ATR technique on films deposited over a diamond crystal

In Green Polymer Chemistry: Biocatalysis and Materials II; Cheng, H., et al.;
ACS Symposium Series; American Chemical Society: Washington, DC, 2013.

on a Perkin-Elmer 100 spectrometer in the 4000-400 cm^{-1} range with an average of 4 scans at 4 cm^{-1} resolution. Gel permeation chromatography multi-angle light scattering (GPC-MALLS) was used to determine molecular weights and molecular weight distributions, M_w/M_n, of macrodiols samples. The chromatographic set-up used consists of an Alliance HPLC Waters 2695 Separation Module having a vacuum degassing facility on online, an auto sampler, a quaternary pump, a columns thermostat, and a Waters 2414 Differential Refractometer for determining the distribution of molecular weight. The temperature of the columns was controlled at 33 °C by the thermostat. MALDI-TOF spectra were recorded in the linear mode in a Voyager DE-PRO time-of-flight mass spectrometer (Applied Biosystems) equipped with a nitrogen laser emitting at λ = 337 nm with a 3 ns pulse width and working in positive-ion mode and delayed extraction. A high acceleration voltage of 20 kV was employed. 2,5-Dihydroxybenzoic acid (DHB) was used as matrix. Samples were dissolved in acetonitrile and mixed with the matrix at a molar ratio of approximately 1:100. Tensile properties were measured in a MTS Synergie 200 testing machine equipped with a 100 N load cell. Type 3 dumbbell test pieces (according to ISO 37) were cut from film. A crosshead speed of 200 mm/min was used. Strain was measured from crosshead separation and referred to 12 mm initial length. Five samples were tested for each polymer composition.

Publication Date (Web): November 22, 2013 | doi: 10.1021/bk-2013-1144.ch005

Synthesis of α-Hydroxyl-ω-(Carboxylic acid) Poly(ε-Caprolactone) with *Yarrowia lipolytica* Lipase

Vials are previously dried and purged with dry nitrogen. In a typical experiment, 1 mL of ionic liquid (1-butylpyridinium tetrafluoroborate [BuPy][BF_4]), 1.0 g of ε-caprolactone (8.76 mmol) and 0.1 g of YLL were placed at 60°C for 24 h, The obtained polymer was purified by five consecutive extractions with 5 mL toluene and the enzyme was filtered off. Toluene was removed by evaporation at reduced pressure. The ionic liquid was recovered and purified by passing them by a column with silica gel and activated charcoal. Polymer was crystallized from cold chloroform/methanol and dried under vacuum. Molecular weights and conversions during reaction were monitored by ^{1}H-NMR.

Synthesis of α,ω-Telechelic Poly(ε-Caprolactone) Diols (HOPCLOH)

PCL diols were prepared using the following molar ratios: DEG1PCL (10 mmol of ε-CL, 1 mmol of DEG), DEG2PCL (10 mmol of ε-CL, 0.5 mmol of DEG), DEG3PCL (10 mmol of ε-CL,0.25 mmol of DEG), PCL-1,3-propanediol (1) (10 mmol ε-CL/0.5 mmol 1,3-prop/12 mg YLL-1026), PCL-1,3-propanediol (2) (10 mmol ε-CL/0.25 mmol 1,3-prop/12 mg YLL-1026), PCL-1,3-propanediol (4) (10 mmol ε-CL/1 mmol 1,3-prop/12 mg YLL-K2629), PCL-1,3-propanediol (5) (10 mmol ε-CL/0.5 mmol 1,3-prop/12 mg YLL-K2629). In all cases 12 mg of immobilized YLL was used. Vials were stoppered with a teflon silicon septum and placed in a thermostated bath at 120 °C for 6 h. No inert atmosphere was used. After the reaction was stopped, the enzyme was filtered off.

In Green Polymer Chemistry: Biocatalysis and Materials II; Cheng, H., et al.;
ACS Symposium Series; American Chemical Society: Washington, DC, 2013.

PCL diols were dried at 70 °C *in vacuo* for 12 h, and stored at ambient temperature in a dessicator at vacuum until used.

Synthesis of PCL Macrodiisocyanate

Dry PCL diol (1.5 g) and HDI in the appropriate amount and 2 mL of 1,2-dichloroethane were charged in a round bottom flask. The catalyst, stannous 2-ethylhexanoate (1% mol by PCL diol moles) was added, and stirred for 4 h at 80 °C. The resulting slurry was poured over teflon petri dishes. The solution was covered by a conical funnel to protect it from dust and to avoid the excessively fast solvent evaporation, and allowed to stand at ambient temperature for 24 h. The film was then released and dried in vacuum. Samples for physical characterization were cut from films, film thickness ranged from 50-80 μm.

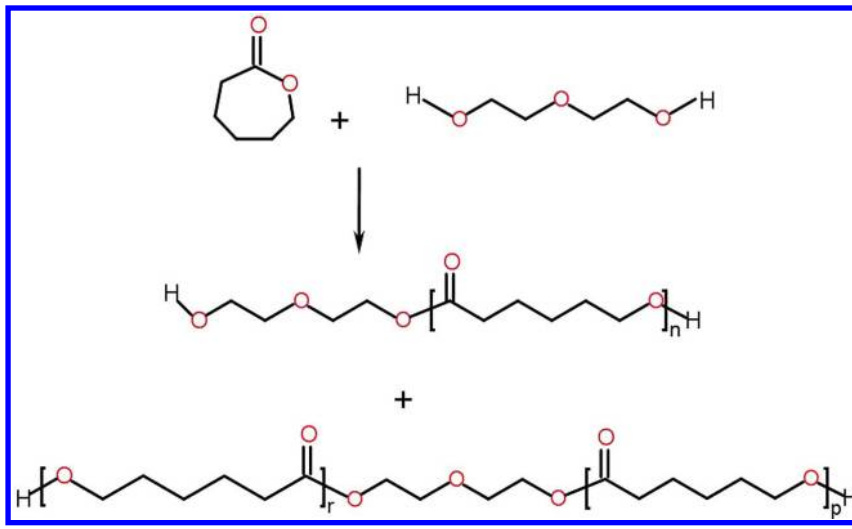

Figure 1. Synthesis of α, ω-telechelic poly(ε-caprolactone) diols (HOPCLOH).

Results and Discussion

α-Hydroxyl-ω-(Carboxylic acid) Poly(ε-Caprolactone)

The synthesis of α-hydroxyl-ω-(carboxylic acid) poly(ε-caprolactone) has a molecular weight of 8000 Da and a polydispersity of 1.6. Monomer conversion was 100%. NMR data for HA-PCL: ^{1}H NMR (200 MHz, $CDCl_3$, ppm) δ 4.031(t, 2H,[CH_2O], 3.613 (t, 2H, [CH_2OH]), 2.363 (t, 2H, [CH_2CO_2H]), 2.28 (t, 2H, [CH_2O_2]), 1.62 (m, 4H, [$(CH_2)_2$]), 1.38 (q, 2H, [CH_2]). ^{13}C NMR (200 MHz, $CDCl_3$, ppm) δ 177.616 (a), 173.944 (j), 173.754 (g), 64.310 (f), 62.679 (q), 34.373 (k), 34.267 (h), 33.812 (b), 32.401 (p), 28.479 (e), 25.664 (d), 25.444 (m), 24.822 (l), 24.716 (i), 24.488 (c). IR (cm^{-1}): 2945(υ_{CH}), 1724 ($\upsilon_{C=O}$), 1166 ($\delta_{O-C=O}$).

In Green Polymer Chemistry: Biocatalysis and Materials II; Cheng, H., et al.;
ACS Symposium Series; American Chemical Society: Washington, DC, 2013.

Publication Date (Web): November 22, 2013 | doi: 10.1021/bk-2013-1144.ch005

In the full MALDI-TOF spectrum given in Figure 2, a series of signals dominate, which can be adscribed to the HA-PCL oligomers doped with Na^+ ions. Small signals due to cyclic species were detected.

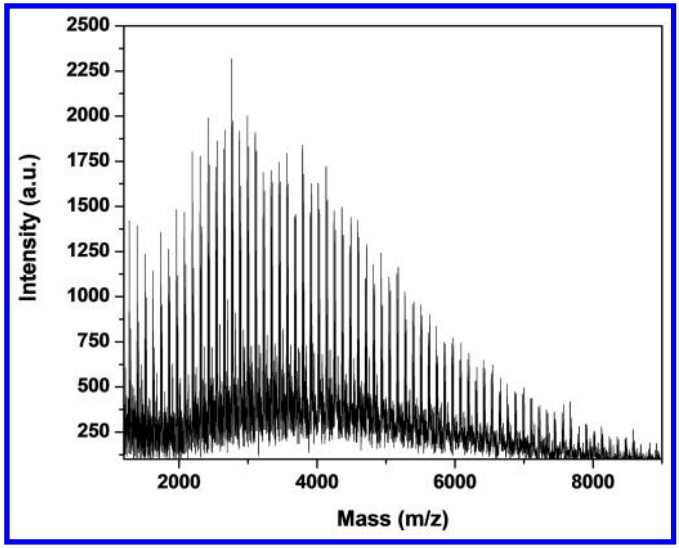

Figure 2. MALDI-TOF spectrum for PCL obtained by enzymatic ROP with 100 mg YLL/ 43.8 mmol ε-CL/100 mg YLL/ 1 mL [BuPy][BF_4] Mn(MALDI)=1754.

Publication Date (Web): November 22, 2013 | doi: 10.1021/bk-2013-1144.ch005

Synthesis of α,ω-Telechelic Poly(ε-Caprolactone) Diols (HOPCLOH)

The synthetic pathway is described in Figure 1. The first step was the formation of the PCL diols by the ring-opening polymerization of ε-CL and using DEG and 1,3-propanediol as initiators in the presence of immbobilized YLL. Under the same conditions, the CL and DEG were allowed to polymerize in the absence of enzyme for control. After precipitation, no corresponding copolymers could be obtained, which indicate that the lipase enzymes actually catalyze the copolymerization of CL and DEG. Results for the synthesized PCL diols are shown in Tables 1 and 2. In Figure 3 the GPC traces of the synthesized PCL-diols are shown.

The stress-strain curves of the different polyester-urethanes are shown in Figures 4 and 5. Characteristic mechanical properties derived from these curves are presented in Tables 3 and 4. Three regimes are visible. First, the behavior at low deformations can be explained as the pure elastic deformation belonging to regular elastomers. Secondly, a zone due to plastic flow is observed. This is much the same for all the polymers studied, indicating a great feasibility for shear induced crystal fragmentation. Thirdly, at strains above 600 % an upswing in

In Green Polymer Chemistry: Biocatalysis and Materials II; Cheng, H., et al.;
ACS Symposium Series; American Chemical Society: Washington, DC, 2013.

some of the curves can be observed, which can be attributed to the strain induced crystallization of soft segment chains.

Observed behavior can be ascribed to the complex morphology that must be present in the obtained polyester-urethanes. Conformational arrangements around torsional angles of the many sequential methylene chains can impose crystallization sites that operate differently during elongation. Also, crystallization is inhibed when flexible DEG chains are inserted in the polyurethane backbone. Various degrees of phase separation and crystallization in the hard segments affect the mechanical properties in a complicated manner (*6*).

Mechanical properties for polyester-urethanes obtained from PCLDEG and HDI strongly depends upon the PCL content in the PCL-diol from which they were derived. Higher number-average molecular weight PCL-diols were obtained when low amounts of DEG were used (see Table 1) this in turn results in a polyster-urethane with a higher PCL content in the repeating unit. It is known that PCL soft segments tend to crystallize, and this fact is reflected in the increase of the observed tensile modulus (*7*). PCLDEG2HDI shows a tensile modulus that is around eleven times higher than PCLDEG1HDI. PCLDEG3HDI has the highest tensile modulus (about twice to that observed for PCLDEG2HDI), but lower stress at break and strain at yield values than the other polymers.

Mechanical properties for samples derived from PCL-1,3 propanodiol (PD) and HDI are shown in Table 3. Obtained polyester-urethanes have similar properties eventhough they were obtained form PCL diols with different molecular weights. This behavior can be adscribed to the fact that only monosubstitution was achieved for all samples (see Table 2).

Publication Date (Web): November 22, 2013 | doi: 10.1021/bk-2013-1144.ch005

Table 1. Molecular weights of the synthesized poly(ε-caprolactone) diols

	***Mn* (GPC)**	***Mw/Mn* (GPC)**
PCLDEG1	4321	1.181
PCLDEG2	5101	1.272
PCLDEG3	7426	1.531
PCL-1,3-propanediol (1)	5475	1.144
PCL-1,3-propanediol (2)	5922	1.136
PCL-1,3-propanediol (4)	3755	1.247
PCL-1,3-propanediol (5)	4099	2.457

In Green Polymer Chemistry: Biocatalysis and Materials II; Cheng, H., et al.;
ACS Symposium Series; American Chemical Society: Washington, DC, 2013.

Table 2. Percent of bisubstitution (% Bi (OH)), monosubstitution (% Mono (OH)) in the synthesized poly(ε-caprolactone) diols

	Mn (Da) ^{1}H-NMR	*% Mono (OH)*	*% Bi (OH)*	*HAPCLOH (%)*
PCLDEG1	836	34	66	8
PCLDEG2	1305	29	71	9
PCLDEG3	1780	23	77	48
PCL-1,3-propanediol (1)	484	94	0	22
PCL-1,3-propanediol (2)	935	94	0	30
PCL-1,3-propanediol (4)	233	95	0	21
PCL-1,3-propanediol (5)	376	81	0	35

Publication Date (Web): November 22, 2013 | doi: 10.1021/bk-2013-1144.ch005

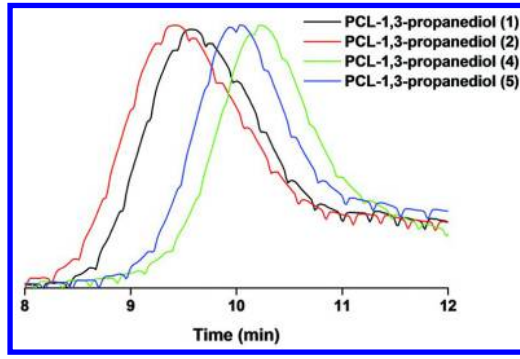

Figure 3. GPC traces showing the incorporation of ε-caprolactone during the synthesis of oligomer.

In Green Polymer Chemistry: Biocatalysis and Materials II; Cheng, H., et al.;
ACS Symposium Series; American Chemical Society: Washington, DC, 2013.

Publication Date (Web): November 22, 2013 | doi: 10.1021/bk-2013-1144.ch005

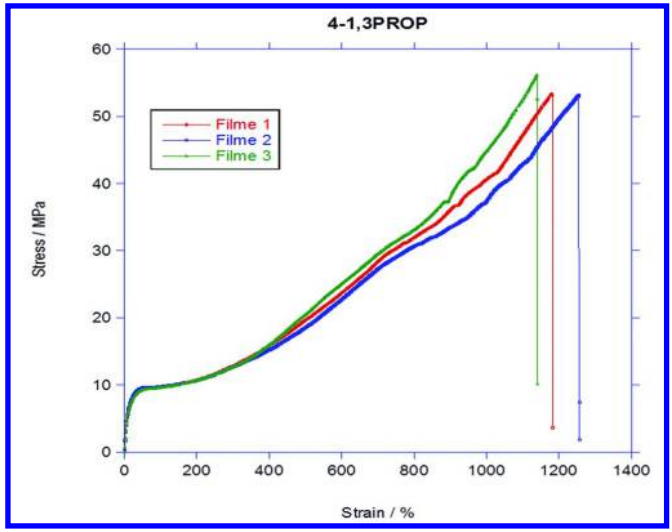

Figure 4. Stress–strain graph for polyester-urethanes obtained from PCL-1,3-propanediol and HDI at room temperature.

Table 3. Mechanical properties of the synthesized polyester-urethanes obtained from PCL-1,3-propanediol and HDI

	Modulus/MPa	*Yield/MPa*	*% at yield*	*Stress at break/ MPa*	*Strain at break/%*
Film 1	100 ± 4	9.6	60	55 ± 3	1180 ± 50
Film 2	105 ± 11	9.7	60	52.7 ± 1.4	1260 ± 20
Film 3	95 ± 4	9.7	63	57 ± 4	1130 ± 40
	100 ± 8	**9.7**	**61**	**54.8 ± 1.7**	**1190 ± 30**

In Green Polymer Chemistry: Biocatalysis and Materials II; Cheng, H., et al.;
ACS Symposium Series; American Chemical Society: Washington, DC, 2013.

Publication Date (Web): November 22, 2013 | doi: 10.1021/bk-2013-1144.ch005

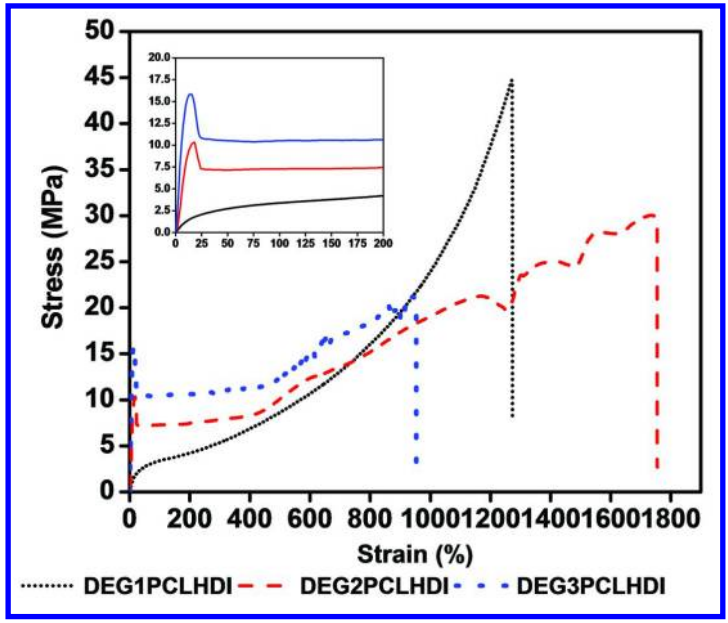

Figure 5. Stress–strain graph for polyester-urethanes obtained from PCLDEG and HDI at room temperature.

Table 4. Mechanical properties of the synthesized polyester-urethanes obtained from PCLDEG and HDI

Polymer	*Modulus (MPa)*	*Strain at yield (%)*	*Stress at break (MPa)*	*Strain at break (%)*
PCLDEG1HDI	11 ± 2.2	67 ± 8	45 ± 6	1434 ± 127
PCLDEG2HDI	122 ± 47	39 ± 2	32 ± 2	1779 ± 137.4
PCLDEG3HDI	228 ± 10	23 ± 3	21 ± 2.2	953 ± 373

Conclusions

High molecular weight aliphatic polyesters were synthesized using a green chemistry route in the presence of ionic liquids. A series of α,ω-telechelic poly (ε-caprolactone) diols were successfully synthesized for the first time, using immobilized lipase from *Yarrowia lipolytica* as catalyst. Results demonstrated that these diols are useful for polyurethane syntheses. All the polyester-urethanes containing 1,3-propanediol have extensive crosslinking and very good mechanical properties (elastomeric properties) with stress at yield over 40 MPa.

In Green Polymer Chemistry: Biocatalysis and Materials II; Cheng, H., et al.;
ACS Symposium Series; American Chemical Society: Washington, DC, 2013.

Publication Date (Web): November 22, 2013 | doi: 10.1021/bk-2013-1144.ch005

Acknowledgments

Financial support by Consejo Nacional de Ciencia y Tecnología (CONACYT), Consejo de Ciencia y Tecnología del Estado de Guanajuato (CONCYTEG) and University of Guanajuato. We are indebted to Ángel Marcos-Fernández and Rosa Lebrón-Aguilar (CSIC, Madrid España) for MALDI-TOF spectra and mechanical properties measurements.

References

1. Loos, K. *Biocatalysis in Polymer Chemistry*; Wiley-VCH Verlag GmbH & Co. KGaA: Weinheim, Germany, 2011.
2. Barrera-Rivera, K. A.; Marcos-Fernández, A.; Martínez-Richa, A. Chemo-Enzymatic Syntheses of Polyester-Urethanes. In *Green Polymer Chemistry: Biocatalysis and Biomaterials*; Cheng, H. N., Gross, R. A., Eds.; ACS Symposium Series 1043; American Chemical Society: Washington, DC, 2010; Chapter 16.
3. Barrera-Rivera, K. A.; Marcos-Fernández, A.; Vera-Graziano, R.; Martínez-Richa, A. Ring-opening polymerization of ε-caprolactone by *Yarrowia lipolytica* lipase in the presence of ionic liquids. *J. Polym. Sci., Part A: Polym. Chem.* **2009**, *47*, 5792–5805.
4. Barrera-Rivera, K. A.; Martínez-Richa, A. One-pot biocatalytic synthesis of sugar based poly (ε-caprolactone). *Macromol. Symp.* **2009**, *283−284*, 144–151.
5. Barrera-Rivera, K. A.; Flores-Carreón, A.; Martínez-Richa, A. Enzymatic ring-opening polymerization of ε-caprolactone by a new lipase from *Yarrowia lipolytica*. *J. Appl. Polym. Sci.* **2008**, *109* (2), 708–719.
6. Prisacariu, C.; Scortanu, E. Morphology of polyurethanes based on the chain extender ethylenglicol and aromatic flexible diisocianates, as revealed by scanning electron microscopy. *Rev. Roum. Chim.* **2008**, *53* (9), 821–825.
7. Kim, B. K.; Lee, S. Y.; Xu, M. Polyurethanes having shape memory effects. *Polymer* **1996**, *37*, 5781–5793.

Publication Date (Web): November 22, 2013 | doi: 10.1021/bk-2013-1144.ch006

Chapter 6

Microwave-Assisted Biocatalytic Polymerizations

Anil Mahapatro*,[1] and Taína D. Matos Negrón[2]

[1]Bioengineering Program & Department of Industrial and Manufacturing Engineering, Wichita State University, Wichita, Kansas 67260, U.S.A.
[2]Center for Materials Research (CMR), Norfolk State University, Norfolk, Virginia 23508, U.S.A.
***E-mail: anil.mahapatro@wichita.edu**

Microwave heating has been gaining interest as an alternative green energy source. Similarly enzymatic assisted polymer chemistry has been gaining interest for its use as a green catalyst. However, microwave (MW) assisted enzymatic polymerizations which combine the benefits of both microwave heating and enzymatic catalysis is an area that is largely unexplored. This chapter focuses on the various microwave assisted organic and polymeric transformations including microwave assisted biocatalytic polymerizations that have been reported in literature in recent years.

Introduction

Microwave heating has been traditionally used as a heating source for food and drinks (*1*). It has however gained attention over the last two decades for its application as a heat source in the chemical industry (*2*, *3*). Microwave (MW) heating has also been gaining increased popularity in green chemistry and technology fields as an alternative heat source (*4*). In recent years microwave synthesizers has become standard equipment in organic and pharmaceutical laboratories (*5*). Figure 1 shows the different microwaves available starting from domestic microwave used for heating food and drinks (Figure 1a) to complex microwave systems that offer several advantages such as precise temperature, pressure control and automated stage (Figure 1b, c and d) (*5*).

In Green Polymer Chemistry: Biocatalysis and Materials II; Cheng, H., et al.;
ACS Symposium Series; American Chemical Society: Washington, DC, 2013.

Figure 1. Selected examples for microwave reactors used for chemical reactions: domestic microwave oven (a), Initiator Eight (Biotage, Sweden) (b), CEM Discover (CEM) (c), and Chemspeed Swave automated microwave synthesizer (Chemspeed, Switzerland) (d). Reproduced with permission from Reference (5) . Copyright 2011 American Chemical Society.

Publication Date (Web): November 22, 2013 | doi: 10.1021/bk-2013-1144.ch006

As seen in Figure 1 microwave technology has come a long way since its original development for heating of food (*5*). Significant improvements in microwave associated technology has resulted in the use of microwave heating in a wide variety of applications such as organic chemistry, polymer chemistry, drug discovery, proteomics and more recently in biotransformations (*2*, *6–9*). Improvements in hardware and software technology of microwave synthesizers allowed for automated reactions using robotic arms (Figure 1b), introduction of flexible platform that could be modified as per individual needs (Figure 1c) such as control of reaction parameters (temperature, pressure), large batch vial with with magnetic stirrer, or a round bottom flask with possibility of refux condenser on the top. Current industrial microwaves (Figure 1d) allows for fully automated systems that not only carry out microwave assisted reaction but can also prepare the vials to be reacted from stock solutions (*5*).

Microwave heating not only provides a safe, clean and convenient way to heat reactions to elevated temperatures, but it also accelerates many syntheses providing selective activation and allows for fast optimization of reactions (*4*, *10*). It also offers benefits to soluble catalysts (including enzymes) over heterogeneous catalysts, in that the use of metals even as catalysts can lead to undesirable arcing when MW is used (*11*, *12*). As the range of techniques for microwave heating has expanded, so have the areas in which it can have a significant effect (*3*). In this mini review we provide an overview of microwave assisted reactions pertaining to organic reactions, polymerizations and microwave assisted biotransformations. Special emphasis is given to microwave assisted biocatalytic lactone polymerizations.

Microwave-Assisted Organic Synthesis

Microwave heating are used to accelerate organic chemical reactions and have become a useful non-conventional energy source for performing organic synthesis (*2*). Initial reports of microwave assisted organic reactions were by Gedye and co-workers (*11*) and Giguere and co-workers (*13*). Since then microwave assisted

In Green Polymer Chemistry: Biocatalysis and Materials II; Cheng, H., et al.;
ACS Symposium Series; American Chemical Society: Washington, DC, 2013.

organic reactions have experienced tremendous growth and has been extensively reviewed (*2*, *12*, *14–18*). This review looks at impact of microwave heating on two traditional organic reactions; Suzuki and Heck Reactions and the Cannizaro reaction.

Suzuki and Heck Reactions (*16*)

The Heck and Suzuki reactions are one of the widely used reactions for the formation of carbon-carbon bonds. These reactions are generally catalyzed by soluble Pd complexes with various ligands (*19*). However, the efficient separation and subsequent recycling of homogeneous transition-metal catalysts remains a scientific challenge (*19*). An example of use for Heck and Suzuki reactions under MW irradiation conditions is schematically represented in Figure 2 (*16*). These C-C coupling reactions proceeded efficiently under the influence of MW, with excellent yield, high turnover number (TON), and high turnover frequency (TOF) (*16*). PEG was found to be an inexpensive and nontoxic reaction medium for the MW-assisted Suzuki cross-coupling of arylboronic acids with aryl halides (*20*). Microwave assisted protocol offers ease of operation and enables recyclability of the catalyst in the case of Suzuki and Heck reactions (*20–22*).

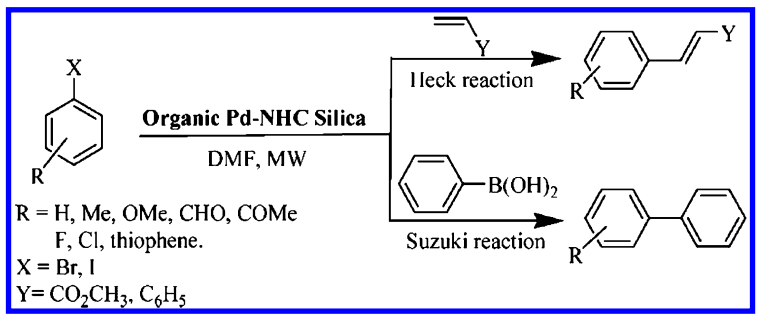

Figure 2. Synthesis of Pd-NHC Organic Silica Catalyst. Reproduced with permission from Reference (16). Copyright 2008 American Chemical Society.

Cannizzaro Reaction (*16*)

The Cannizzaro reaction is the disproportionation of an aldehyde to an equimolar mixture of primary alcohol and carboxylic salt and is restricted to aldehydes that lack α-hydrogens (*16*). Figure 3 depicts a schematic representation of a microwave assisted solvent-free cross-Cannizzaro protocol for the preparation of alcohols from aldehydes using barium hydroxide, Ba(OH)O and paraformaldehyde (*16*, *23*). The operational simplicity, rapid reaction rates, and high yield of pure alcohol make microwave assisted cannizzaro reaction a useful and attractive procedure as compared to traditional heating (*2*, *12*, *23*).

Publication Date (Web): November 22, 2013 | doi: 10.1021/bk-2013-1144.ch006

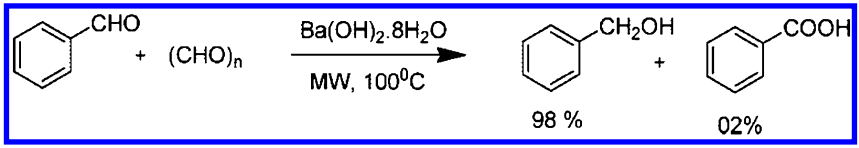

Figure 3. Solvent-Free Cross-Cannizzaro Reaction. Reproduced with permission from Reference (16). Copyright 2008 American Chemical Society.

Microwave-Assisted Polymer Synthesis

Microwave assisted vulcanization of rubber has been reported as early as the 1960's (*24*), however in recent years due to the success of microwave irradiation as a heat source in organic chemistry its use has been explored and reviewed extensively for polymerization reactions (*5*, *25–27*). This mini review focuses on the microwave assisted ring opening polymerizations. Cyclic monomers are able to undergo polymerization by a ring-opening mechanism, which is characterized by an initiation step, the ring-opening of the monomer, and the subsequent chain-growth of the polymer (*26*). Ring-opening polymerization (ROP) technique encompasses a variety of polymer examples some of which include poly(lactic acid) (PLLA), poly(caprolactone) (PCL) and poly-pentadecalactone) (PPDL). The ROP was found to benefit using microwave heating which allowed a control over the polymerizations combined with acceleration of the polymerization rates (*28*). Some examples of the benefit of microwave technology on ring opening polymerizations are illustrated below.

Microwave-Assisted Ring Opening Polymerization (*5*)

In a report by Liu et al. the authors formed copolymers of CL and 2-phenyl-5,5-bis(oxymethyl)trimethylene carbonate (PTC) (*29*). The polymerizations were performed using microwave heating with fixed power mode (50 W) and 180°C in order to study the molar mass dependency on microwave power, reaction time, and temperature. The authors controlled the degree of polymerization (DP) of the PCL chains and the degree of substitution (DS) using microwave power (*29*). They reported that the DP and DS increased proportionally by increasing microwave power, while increase in the irradiation time lead to higher DP and polymer conversions (*5*, *29*). The authors concluded that higher conversion, DP and DS values were obtained with increasing microwave power and were the result of higher localized temperatures that were obtained by the higher microwave power (*5*, *29*). In another report the synthesis of PCL-b-PEGPCL triblock copolymers was reported by Ahmed and co-workers (*30*). They carried out the bulk polymerization at 140°C and formed two different triblock copolymers with varying ratio of PEG/PCL (*30*). Microwave heating exhibited a higher content of triblock structures than observed with traditional heating (*30*).

Publication Date (Web): November 22, 2013 | doi: 10.1021/bk-2013-1144.ch006

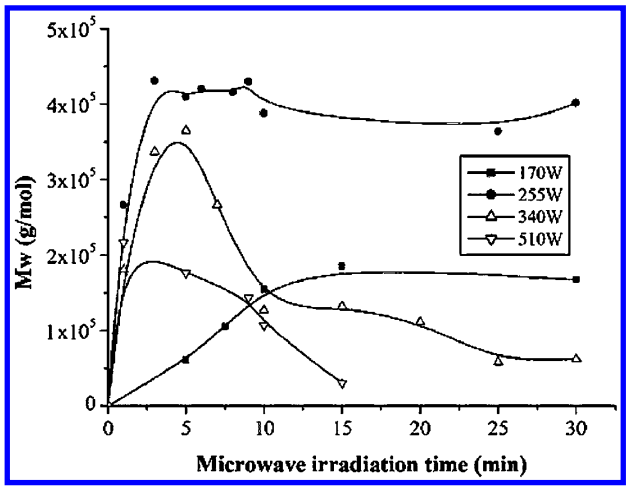

Figure 4. Molecular weight vs irradiation time at different microwave powers for stannous octanoate catalyzed ROP of D,L-lactide. Reproduced with permission from Reference (31). Copyright 2004 John Wiley & Sons.

Shu et al. described the stannous octanoate catalyzed ring opening polymerization of lactide using microwave irradiation (*32*). They reported that efficient heating using microwave resulted in successful polymerization without the need for vacuum or inert atmosphere (*32*). Liu and coworkers investigated the microwave assisted polymerization of lactide emphasizing on the effect of microwave power on polymerization process (*31*). They concluded that, up to 255 W the molecular weight of the polymer increased and reached a maximum when approximately 90% conversion was reached (Figure 4) (*31*). With higher dose of microwave the molecular weight first increased and subsequently decreased due to transesterification reactions (*31*). The synthesis of PLLA-b-PEG diblock copolymers and PLLA-b-PEG-b-PLLA triblock copolymers was reported by Gong and co-workers (*33*, *34*). In both cases the microwave-assisted polymerizations occurred much faster than the ones under conventional heating (*33*, *34*).

The acceleration using microwave-assisted polymerizations allows for the rapid screening and improvement of diverse polymers and copolymers and will therefore be continuously investigated in the future (*5*). Detailed reviews of microwave assisted polymerization have been reported that cover this expanding area extensively (*5*, *25–28*, *31*).

Microwave-Assisted Biocatalytic Polymerizations

Apart from traditional organic chemistry applications, MW has been used in biological sciences for the synthesis of peptides, oligopeptides, carbohydrates and in the field of proteomics (*6*, *7*, *35*, *36*). However only few reports exist on the applications of microwave assisted enzymatic reactions, focusing predominantly

In Green Polymer Chemistry: Biocatalysis and Materials II; Cheng, H., et al.;
ACS Symposium Series; American Chemical Society: Washington, DC, 2013.

on organic small molecule transformations (*7*, *35*, *37–39*). An understanding of this area is poor and often controversial (*40*). Researchers have reported enhancements in the initial rate of reaction (*41*, *42*), product yields (*39*, *43*) and enantioselectivity (*38*) when using microwave heating as compared to conventional heating. Leadbeater and coworkers studied the effect of microwave irradiation on lipase catalyzed transesterification of methyl acetoacetate in toluene (*37*). They found no differences between conventional and microwave heating (*37*). Rejasse et al. investigated the influence of microwave heating on the stability of Candida antarctica Lipase B (CALB) and the kinetics of butyl butyrate synthesis (*44*). They reported an increase in enzymatic stability under microwave field in organic medium suggesting this as a possible explanation for an increase in conversion rates observed for some enzymatic synthesis carried out under microwave heating (*44*).

The field of microwave assisted enzymatic polymerizations has been recently receiving attention for exploiting the synergistic benefits of lipase and microwave heating in the field of polymer chemistry (*9*, *40*, *45*, *46*). Kerep and Ritter investigated the influence of MW irradiation on lipase catalyzed ring opening polymerization of ε-caprolactone (*46*). The polymerization showed a strong dependency on the temperature and polarity of the medium/solvent. While an increase of the polymerization rate was observed for the polymerizations under reflux conditions in diethyl ether, the rates in boiling toluene or benzene decreased (*46*). Moreover, in polar solvents, e.g., THF and dioxane, no polymerization occurred. The differences in case of the nonpolar solvents originate in view of the authors from the milder conditions (lower polymerization temperature) when using diethyl ether, yielding a better spatial fit between the active center of the enzyme and the ester substrate (*46*). The same group reported the polymerization of CL initiated with 2-mercaptoethanol, performed under reflux in diethyl ether for 90 min (*47*). The polymer obtained showed a high chemoselectivity and higher yields under microwave irradiation (*47*). The favoured formation of the thiol end group of the PCL was ascribed to a "microwave effect" caused by the stronger stabilization of a "more ionic" transition state occurring during the microwave-assisted heating as schematically depicted in Figure 5 (*5*).

Recently other researchers in our laboratory investigated the effects of microwave process parameters (power, intensity, MW irradiation time and temperature) on lipase catalyzed polymerization of caprolactone (*40*). A 3-D plot predicting the Mn of the PCL was developed. Figure 6 depicts the 2D screen shot of the developed 3-D plot. Figure 6 shows high Mn along the region where the value for power is low and when time and temperature are high. If one rotates the 3-D view it can be seen that high Mn is around the region obtained using high time and temperature values. Additionally, if we follow the z axis (Power) in the positive direction, we find that the color changes quickly to yellow, green and blue, which correspond with very low Mn. The plot concludes that higher temperatures, longer times, and lower power are required to produce high Mn PCL. The authors conducted the polymerization reaction under the optimal conditions (90°C and 240 min) and obtained PCL with Mn of 20,624.

Publication Date (Web): November 22, 2013 | doi: 10.1021/bk-2013-1144.ch006

Publication Date (Web): November 22, 2013 | doi: 10.1021/bk-2013-1144.ch006

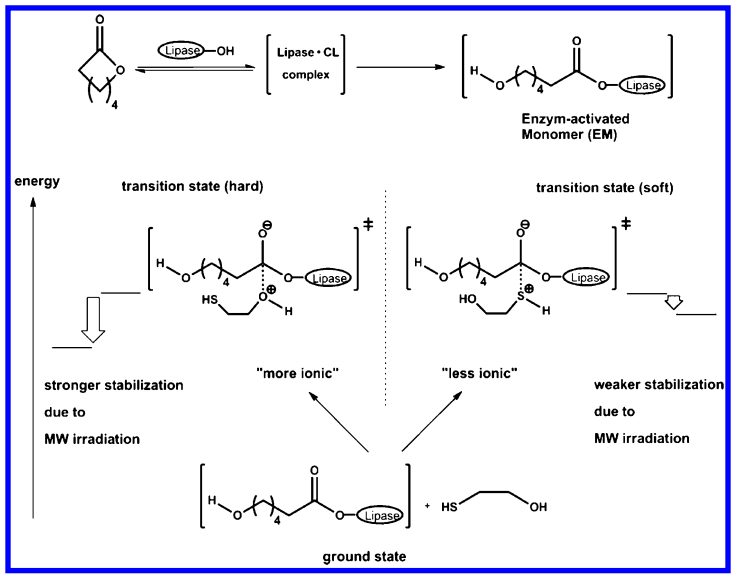

Figure 5. Schematic representation of ROP of caprolactone using 2-mercaptoethanol as initiator in the microwave field. Reproduced with permission from Reference (5). Copyright 2011 American Chemical Society.

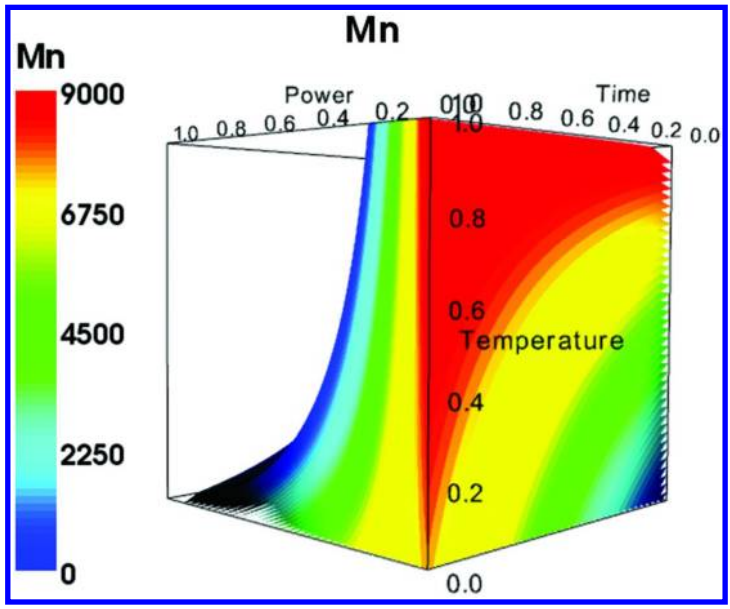

Figure 6. A 2D screen shot of the 3-D model predicting Mn of microwave assisted lipase polymerization of caprolactone . Reproduced with permission from Reference (40). Copyright 2011 Taylor and Francis.

In another report Mahapatro and Matos (*9*), investigated the lipase catalyzed microwave assisted polymerization of pentadecalactone (PDL) schematic represented in Figure 7.

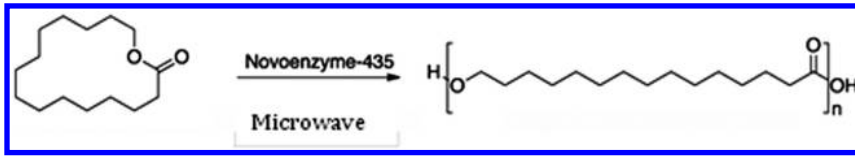

Figure 7. Schematic representation of synergistic microwave and novozyme-435 catalyzed polymerization of ω-pentadecalactone. Reproduced with permission from Reference (9). Copyright 2013 Scientific and Academic Publishing.

Table 1 summarizes the obtained molecular weights, PDI and % yields at different time intervals for microwave assisted lipase catalyzed polymerization of PDL (*9*). Using synergistic lipase and MW irradiation after 240 min (4 hrs) the value of number average molecular weight (Mn) of the polymer obtained was 24,997 g/mol with a polydispersity index (PDI) of 1.93. In contrast the polymer obtained using traditional heating in an oil bath for 240 min gave a Mn of 8,060 g /mol with a PDI of 2.17 (*9*). This confirmed that synergistic effects of MW and lipase catalysis resulted in a significant (three fold) increase in the Mn obtained as compared to traditional oil bath heating within the same time period (*9*). Thermal characterization using thermogravimetric analysis (TGA) of PPDL formed using MW and lipase catalysis showed that microwave heating did not result in a detrimental effect on the thermal properties of the polymer obtained (*9*).

Table 1. Polymerization of ω-Pentadecalactone in Bulk at 70° C Catalyzed by Novozyme-435 under Microwave Conditions (*9*)

Sample	*Mn*	*Mw*	*DPavg*	*PDI*	*% yield*
PPDL- 30 min	13,342	25,953	56	1.94	62
PPDL- 60 min	15,066	32,670	63	2.16	41
PPDL- 120 min	19,406	39,259	81	2.02	61
PPDL- 240 min	24,997	48,459	104	1.93	56
PPDl- 240 min in oil bath*	8,060	17,555	34	2.17	20

* Reaction carried out in using lipase catalysis using conventional heating in oil bath, Mn is number average molecular weight, Mw is weight average molecular weight, DPavg is average degree of polymerization and PDI is polydispersity index.

Publication Date (Web): November 22, 2013 | doi: 10.1021/bk-2013-1144.ch006

Summary

In summary, we reviewed some recent findings in the field of microwave assisted polymerizations with emphasis on microwave assisted biocatalytic polymerizations. Although the area of microwave assisted biocatalytic polymerizations have been relatively less studied, the inherent combined advantages of biocatalytic polymerization and microwave heating offers promise in this growing field.

Acknowledgments

The author, Anil Mahapatro, would like to acknowledge Wichita State University for its financial support.

Publication Date (Web): November 22, 2013 | doi: 10.1021/bk-2013-1144.ch006

References

1. Chandrasekaran, S.; Ramanathan, S.; Basak, T. Microwave food processing—A review. *Food Res. Int.* **2013**, *52*, 243–261.
2. Caddick, S. Microwave assisted organic reactions. *Tetrahedron* **1995**, *51*, 10403–10432.
3. Zovinka, E. P.; Stock, A. E. Microwave Instruments: Green machines for green chemistry? *J. Chem. Educ.* **2010**, *87*, 350–352.
4. Hayes, B. L. *Microwave Synthesis: Chemistry at the Speed of Light*; CEM Publishing: Reading, U.K., 2002; p 292.
5. Kempe, K.; Becer, C. R.; Schubert, U. S. Microwave-assisted polymerizations: Recent status and future perspectives. *Macromolecules* **2011**, *44*, 5825–5842.
6. Leadbeater, N. E. Microwave assisted proteomics. *J. Am. Chem. Soc.* **2009**, *131*, 17523–17523.
7. Karmee, S. K. Application of Microwave Irradiation in Biocatalysis. *Res. J. Biotechnol.* **2006**, *1*, 1.
8. Mavandadi, F.; Pilotti, Å. The impact of microwave-assisted organic synthesis in drug discovery. *Drug Discovery Today* **2006**, *11*, 165–174.
9. Mahapatro, A.; Matos Negrón, T. D. Biodegradable poly-pentadecalactone (PDL) synthesis via synergistic lipase and microwave catalysis. *Am. J. Biomed. Eng.* **2013**, *3*, 9–13.
10. Thostenson, E. T.; Chou, T. W. Microwave processing: Fundamentals and applications. *Composites, Part A* **1999**, *30*, 1055–1071.
11. Gedye, R.; Smith, F.; Westaway, K.; Ali, H.; Baldisera, L.; Laberge, L.; Rousell, J. The use of microwave ovens for rapid organic synthesis. *Tetrahedron Lett.* **1986**, *27*, 279–282.
12. Lidström, P.; Tierney, J.; Wathey, B.; Westman, J. Microwave assisted organic synthesis—A review. *Tetrahedron* **2001**, *57*, 9225–9283.
13. Giguere, R. J.; Bray, T. L.; Duncan, S. M.; Majetich, G. Application of commercial microwave ovens to organic synthesis. *Tetrahedron Lett.* **1986**, *27*, 4945–4948.

14. Wathey, B.; Tierney, J.; Lidström, P.; Westman, J. The impact of microwave-assisted organic chemistry on drug discovery. *Drug Discovery Today* **2002**, *7*, 373–380.
15. Hoz, A. d. l.; Diaz-Ortiz, A.; Moreno, A. Microwaves in organic synthesis. Thermal and non-thermal microwave effects. *Chem. Soc. Rev.* **2005**, *34*, 164–178.
16. Polshettiwar, V.; Varma, R. S. Microwave-assisted organic synthesis and transformations using benign reaction media. *Acc. Chem. Res.* **2008**, *41*, 629–639.
17. Kuhnert, N. Microwave-assisted reactions in organic synthesis—Are there any nonthermal microwave effects? *Angew. Chem., Int. Ed.* **2002**, *41*, 1863–1866.
18. Razzaq, T.; Kappe, C. O. On the energy efficiency of microwave-assisted organic reactions. *ChemSusChem* **2008**, *1*, 123–132.
19. Polshettiwar, V.; Molnár, Á. Silica-supported Pd catalysts for Heck coupling reactions. *Tetrahedron* **2007**, *63*, 6949–6976.
20. Chen, J.; Spear, S. K.; Huddleston, J. G.; Rogers, R. D. Polyethylene glycol and solutions of polyethylene glycol as green reaction media. *Green Chem.* **2005**, *7*, 64–82.
21. Namboodiri, V. V.; Varma, R. S. Microwave-accelerated Suzuki cross-coupling reaction in polyethylene glycol (PEG). *Green Chem.* **2001**, *3*, 146–148.
22. Crozet, M. D.; Castera-Ducros, C.; Vanelle, P. An efficient microwave-assisted Suzuki cross-coupling reaction of imidazo[1,2-a]pyridines in aqueous medium. *Tetrahedron Lett.* **2006**, *47*, 7061–7065.
23. Varma, R. S.; Naicker, K. P.; Liesen, P. J. Microwave-accelerated crossed Cannizzaro reaction using barium hydroxide under solvent-free conditions. *Tetrahedron Lett.* **1998**, *39*, 8437–8440.
24. Linnig, F. J.; Parks, E. J. Natural and synthetic rubbers. *Anal. Chem.* **1963**, *35*, 160–178.
25. Ebner, C.; Bodner, T.; Stelzer, F.; Wiesbrock, F. One Decade of Microwave-Assisted polymerizations: Quo vadis? *Macromol. Rapid Commun.* **2011**, *32*, 254–288.
26. Zhang, C.; Liao, L.; Gong, S. Recent developments in microwave-assisted polymerization with a focus on ring-opening polymerization. *Green Chem.* **2007**, *9*, 303–314.
27. Chauveau, E.; Marestin, C.; Martin, V.; Mercier, R. Microwave-assisted polymerization process: A way to design new, high molecular weight poly(arylimidazole)s. *Polymer* **2008**, *49*, 5209–5214.
28. Hoogenboom, R.; Schubert, U. S. Microwave-assisted polymer synthesis: Recent developments in a rapidly expanding field of research. *Macromol. Rapid Commun.* **2007**, *28*, 368–386.
29. Lu, K.; Yan, G.; Chen, H.; Li, L.; Ai, C.; Yu, X. Microwave-assisted ring-opening copolymerization of epsilon caprolactone and 2-phenyl-5,5-bis(oxymethyl) trimethylene carbonate. *Chin. Sci. Bull.* **2009**, *54*, 3237–3243.

Publication Date (Web): November 22, 2013 | doi: 10.1021/bk-2013-1144.ch006

30. Ahmed, H.; Trathnigg, B.; Kappe, C. O.; Saf, R. Synthesis of poly(ε-caprolactone) diols and EO–CL block copolymers and their characterization by liquid chromatography and MALDI-TOF-MS. *Eur. Polym. J.* **2010**, *46*, 494–505.
31. Zhang, C.; Liao, L.; Liu, L. Rapid ring-opening polymerization of D,L-lactide by microwaves. *Macromol. Rapid Commun.* **2004**, *25*, 1402–1405.
32. Shu, J.; Peng, W.; Tong, Z.; Baoxiu, Z. Microwave-irradiated ring-opening polymerization of D,L-lactide under atmosphere. *J. Appl. Polym. Sci.* **2006**, *100*, 2244–2247.
33. Zhang, C.; Liao, L.; Gong, S. Synthesis of PLLA-MPEG diblock copolymers by microwave-assisted copolymerization of L-lactide and methoxy poly(ethylene glycol). *Macromol. Chem. Phys.* **2007**, *208*, 1122–1128.
34. Zhang, C.; Liao, L.; Gong, S. Microwave-assisted synthesis of PLLA-PEG-PLLA triblock copolymers. *Macromol. Rapid Commun.* **2007**, *28*, 422–427.
35. Maugard, T.; Gaunt, D.; Legoy, M. D.; Besson, T. Microwave-assisted synthesis of galacto-oligosaccharides from lactose with immobilized β-galactosidase from Kluyveromyces lactis. *Biotechnol. Lett.* **2003**, *25*, 623–629.
36. Horchani, H.; Chaâbouni, M.; Gargouri, Y.; Sayari, A. Solvent-free lipase-catalyzed synthesis of long-chain starch esters using microwave heating: Optimization by response surface methodology. *Carbohydr. Polym.* **2010**, *79*, 466–474.
37. Leadbeater, N. E.; Stencel, L. M.; Wood, E. C. Probing the effects of microwave irradiation on enzyme-catalysed organic transformations: the case of lipase-catalyzed transesterifications reactions. *Org. Biomol. Chem.* **2007**, *5*, 1052–1055.
38. Carrillo-Munoz, J.-R.; Bouvet, D.; Guibe-Jampel, E.; Loupy, A.; Petit, A. Microwave-promoted lipase-catalyzed reactions. Resolution of (+-)-1-phenylethanol. *J. Org. Chem.* **1996**, *61*, 7746–7749.
39. Lin, G.; Lin, W.-Y. Microwave-promoted lipase-catalyzed reactions. *Tetrahedron Lett.* **1998**, *39*, 4333–4336.
40. Matos, T. D.; King, N.; Simmons, L.; Walker, C.; McClain, A. R.; Mahapatro, A.; Rispoli, F. J.; McDonnell, K. T.; Shah, V. Microwave assisted lipase catalyzed solvent-free polycaprolactone synthesis. *Green Chem. Lett. Rev.* **2011**, *4*, 73–79.
41. Roy, I.; Gupta, M. N. Applications of microwave in biological sciences. *Curr. Sci.* **2003**, *85*, 1685–1693.
42. Parker, M.-C.; Besson, T.; Lamare, S.; Legoy, M.-D. Microwave radiation can increase the rate of enzyme-catalysed reactions in organic media. *Tetrahedron Lett.* **1996**, *37*, 8383–8386.
43. Yadav, G. D.; Lathi, P. S. Synergism between microwave and enzyme catalysis in intensification of reactions and selectivities: Transesterification of methyl acetoacetate with alcohols. *J. Mol. Catal. A: Chem.* **2004**, *223*, 51–56.

Publication Date (Web): November 22, 2013 | doi: 10.1021/bk-2013-1144.ch006

44. Rejasse, B.; Lamare, S.; Legoy, M. D.; Besson, T. Stability improvement of immobilized *Candida antarctica* lipase B in an organic medium under microwave radiation. *Org. Biomol. Chem.* **2004**, *2*, 1086–1089.
45. Atsushi, Y.; Yoshizawa-Fujita., M.; Yuko, T.; Masahiro, R. In *Microwave-Assisted Enzymatic Polymerization of PLGA Copolymers and Hybridization with Hydroxyapatite*; 238th ACS National Meeting, Washington, DC, 2009.
46. Kerep, P.; Ritter, H. Influence of microwave irradiation on the lipase-catalyzed ring-opening polymerization of ε-caprolactone. *Macromol. Rapid Commun.* **2006**, *27*, 707–710.
47. Kerep, P.; Ritter, H. Chemoenzymatic synthesis of polycaprolactone-block-polystyrene via macromolecular chain transfer reagents. *Macromol. Rapid Commun.* **2007**, *28*, 759–766.

Publication Date (Web): November 22, 2013 | doi: 10.1021/bk-2013-1144.ch006

Publication Date (Web): November 22, 2013 | doi: 10.1021/bk-2013-1144.ch007

Chapter 7

Green Polymer Chemistry: Enzymatic Functionalization of Poly(ethylene glycol)s Under Solventless Conditions

Judit E. Puskas,*[,1,2,3] Kwang Su Seo,[2] Marcela Castaño,[2] Madalis Casiano,[3] and Chrys Wesdemiotis[2,3]

[1]Department of Chemical and Biomolecular Engineering, The University of Akron, Akron, Ohio 44325, U.S.A.
[2]Department of Polymer Science, The University of Akron, Akron, Ohio 44325, U.S.A.
[3]Department of Chemistry, The University of Akron, Akron, Ohio 44325, U.S.A.
***E-mail: jpuskas@uakron.edu**

Enzymes as biocatalysts have been contributing to "Green Polymer Chemistry", providing an alternative to conventional chemical catalysis for polymerization and polymer functionalization. Specifically, enzyme-catalyzed polymer functionalization carried out under solventless conditions is a great advancement in the design of a green process for biomedical applications, where the toxicity of solvents and catalyst residues need to be considered. In this paper, we present quantitative enzyme-catalyzed transesterification of vinyl esters with poly(ethylene glycol)s (PEG)s. Specifically, vinyl methacrylate, vinyl acrylate and vinyl crotonate were transesterified with PEGs in the presence of *Candida antarctica* lipase B (CALB; Novozym® 435) at 50 °C under solventless conditions. ^{1}H and ^{13}C NMR spectroscopy and MALDI-ToF mass spectrometry verified the structure and the purity of the functionalized polymers.

In Green Polymer Chemistry: Biocatalysis and Materials II; Cheng, H., et al.; ACS Symposium Series; American Chemical Society: Washington, DC, 2013.

Publication Date (Web): November 22, 2013 | doi: 10.1021/bk-2013-1144.ch007

Introduction

In tune with the globally increasing interest in "Green or Greener" chemistry, our group has been exploring the power of enzyme catalysis in the functionalization of synthetic polymers. Enzymatic catalysis in organic synthesis has emerged as an attractive "green chemistry" alternative to conventional chemical catalysis. In the past two decades, enzymatic catalysis has been applied to polymer synthesis (*1–5*) and functionalization (*6–11*) with several advantages, including high efficiency, recyclability, the ability to operate under mild conditions, and environmental friendliness (*12*).

All enzymes are classified into six main groups according to the International Union of Biochemistry and Molecular Biology (Figure 1) (*7*, *12*). Today about 3000 enzymes are commercially available and some of them are mutated for industrial applications. Generally, oxidoreductases, hydrolases, and isomerases are relatively stable, and the most widely used catalysts in biotransformations. In contrast, lyases and ligases are present in lesser amounts in living cells and are less stable for isolation or separation from living organisms.

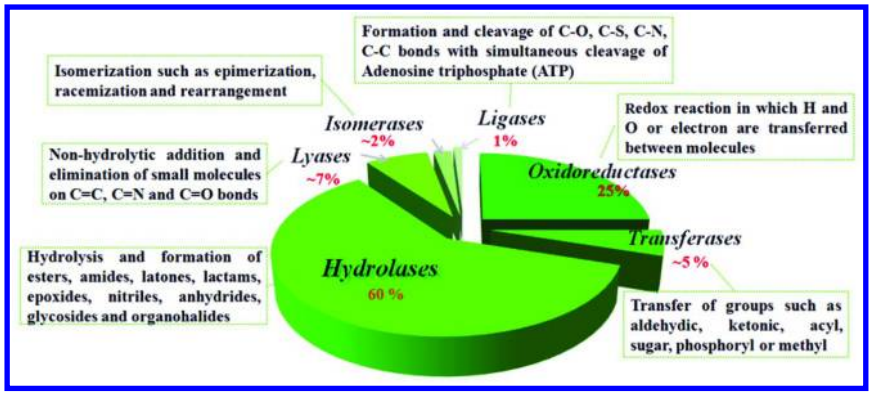

Figure 1. Classification of enzymes. Reproduced with permission from ref. (7). Copyright 2011 Elsevier.

Lipases belong to the group of hydrolyses and are the most popular biocatalysts. They are widely used in esterification, transesterification, aminolysis, and Michael addition reactions in organic solvents (*12*, *13*). The most useful lipases for organic synthesis are: porcine pancreatic lipase (PPL), lipase from *Pseudomoanas cepacia* (Amano lipase PS, PCL), lipase from *Candida rugosa* (CRL), and lipase B from *Candida antarctica* (CALB) (*13*).

CALB is one of the most effective catalysts for transesterification. CALB contains 317 amino acids and the catalytic triad is Ser105- His224-Asp187 (*14*). It has a larger pocket above the Asp-His-Ser triad and a medium-sized pocket below it (Figure 2.) (*9*, *15*, *16*). The top pocket is the "carbonyl" pocket, and the bottom is the "hydroxyl" pocket, represented by different shading in Figure 2.

In Green Polymer Chemistry: Biocatalysis and Materials II; Cheng, H., et al.;
ACS Symposium Series; American Chemical Society: Washington, DC, 2013.

Publication Date (Web): November 22, 2013 | doi: 10.1021/bk-2013-1144.ch007

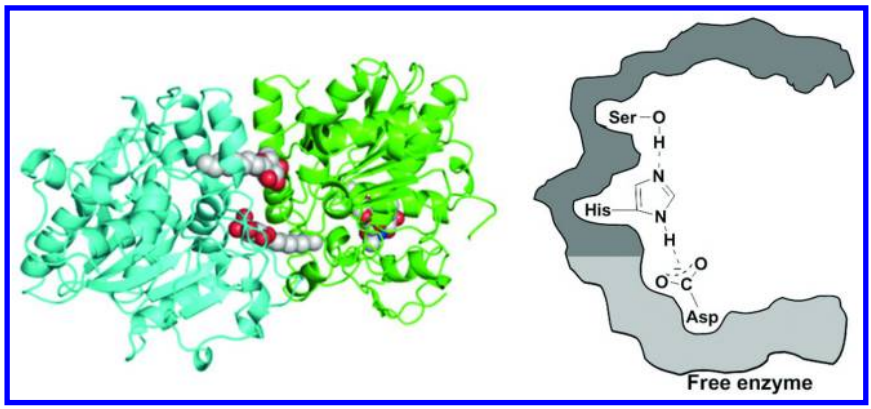

Figure 2. (Left) 3D structure of CALB [Image of PBD ID:1TCB from ref. (15) created with Polyview 3D] and (right) schematic representation of the the catalytic triad of CALB.

Since we will discuss PEG functionalization via transesterification, this reaction will be discussed in more detail.

CALB-Catalyzed Transesterification

Transesterification reactions are generally reversible. In order to shift the equilibrium towards the product, the nucleophilicity of the leaving group of the acyl donor should be reduced by the introduction of electron-withdrawing groups (e.g., trihaloesters, enol esters, oxime esters, anhydrides, etc), described in Scheme 1 (*17*).

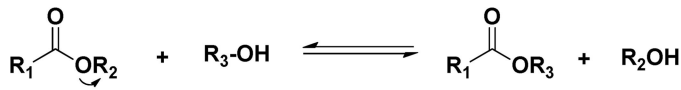

Scheme 1. Transesterification of esters with alcohols.

The use of enol esters (*17*, *18*) such as vinyl or isopropenyl esters appears to be the most useful since it liberates unstable enols as by-products which rapidly tautomerize to give the corresponding aldehydes or ketones. Therefore, the reaction becomes irreversible. Acetaldehyde, which forms during the reactions with vinyl esters, is known to inactivate the lipases from *Candida rugosa* and *Geotrichum candidum* by forming a Schiff's base with the lysine residues of the protein; however most lipases, including CALB, tolerate the liberated acetaldehyde (*18*). Comparison of the catalytic activities of CALB and distannoxane, a conventional tin-based catalyst revealed that the transesterification of vinyl acetate with 2-phenyl-1-propanol catalyzed by CALB was complete in 2 hours, while the traditional tin-based catalyst yielded 95% conversion in 12 hours (Figure 3) (*7*).

In Green Polymer Chemistry: Biocatalysis and Materials II; Cheng, H., et al.;
ACS Symposium Series; American Chemical Society: Washington, DC, 2013.

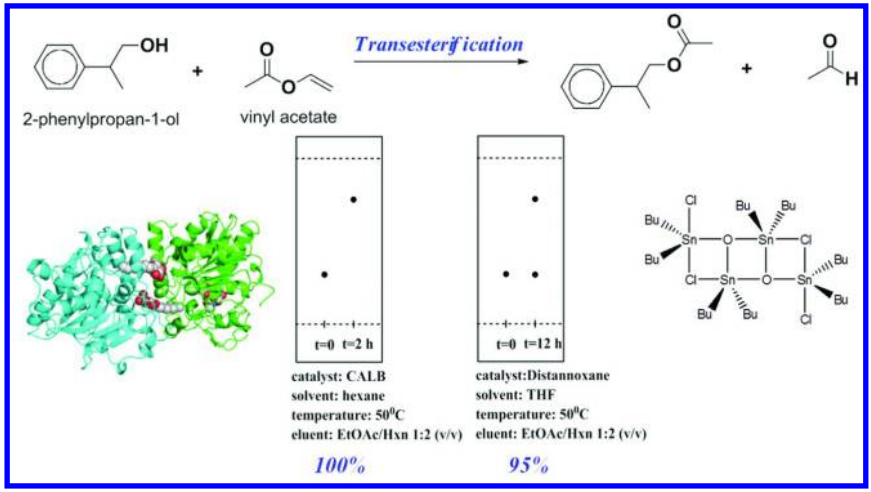

Figure 3. Transesterification of vinyl acetate: comparison of CALB and a tin-based catalyst. Reproduced with permission from ref. (7). Copyright 2011 Elsevier.

The catalytic cycle of the CALB-mediated transesterification shown in Figure 3 can be visualized based on the mechanism described in the literature (*8*, *9*, *13*, *15*). The different shadings in our rendition in Figure 4 represent the carbonyl and hydroxyl pockets of the enzyme. First, the nucleophilic serine (Ser105) residue interacts with the carbonyl group of the vinyl acetate, forming a tetrahedral intermediate which is stabilized by the oxyanion hole of the enzyme via three hydrogen bonds: one from glutamine (Gln106) and two from threonine (Thr40) units. In the second step, the ester bond is cleaved to form the acyl-enzyme complex (AEC) and the first product, vinyl alcohol. Vinyl alcohol will immediately tautomerize to acetaldehyde, rendering the reaction irreversible. In the third step, the alcohol reacts with the acyl-enzyme complex to form a second tetrahedral intermediate which is again stabilized by the oxyanion hole. In the last step, the enzyme is deacylated to form the desired product. The nucleophilic attack by the Ser105 is mediated by the His224-Asp187 pair.

Publication Date (Web): November 22, 2013 | doi: 10.1021/bk-2013-1144.ch007

Publication Date (Web): November 22, 2013 | doi: 10.1021/bk-2013-1144.ch007

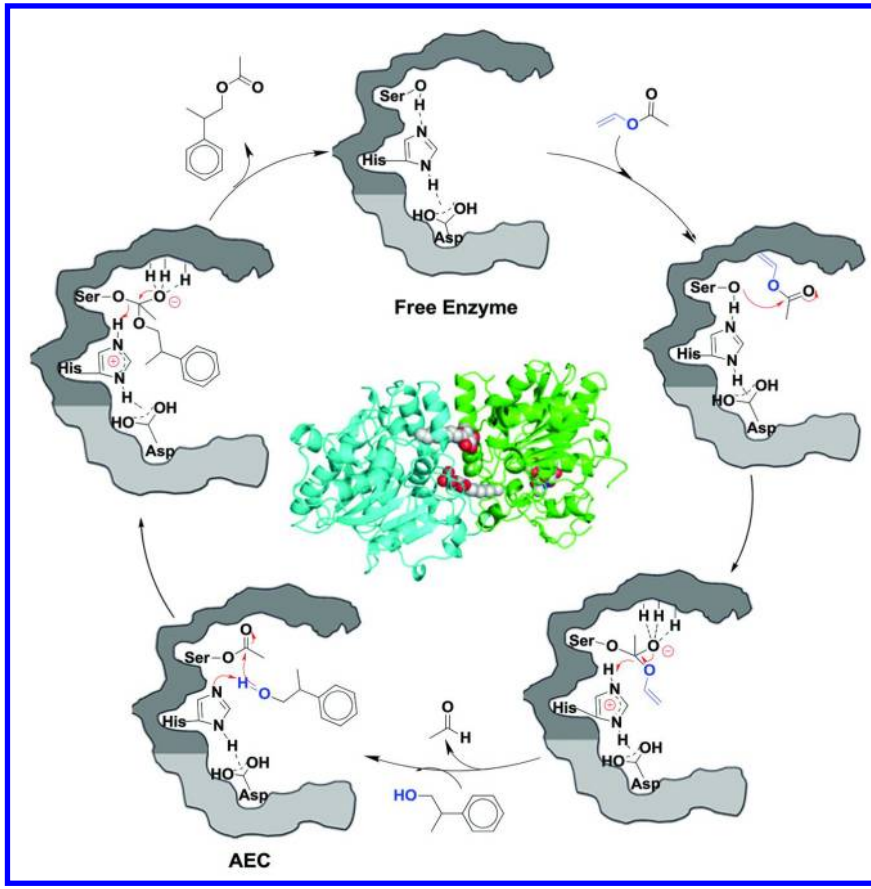

Figure 4. Illustration of the mechanism of CALB-catalyzed transesterification of vinyl acetate with 2-phenylpropane-1-ol. The different shading represents the two enzyme pockets.

Enzymes in the Synthesis of Telechelic Polymers

Before our group had started working on the end-functionalization of preformed synthetic symmetric or asymmetric telechelic polymers, enzymatic catalysis has not been extensively utilized in this area despite the advantages enzymes offer. Telechelic carboxylic acid functionalized PDMSs were reacted with α,β-ethylglucoside at 70 °C under vacuum for 34 hours in the presence of CALB, but the product was a mixture of mono- and difunctional esters (*19*). Recently the synthesis of telechelic methacrylate-functionalized oligoesters by the CALB-catalyzed polycondensation of ethylene glycol, hydroxyethyl methacrylate and divinyl adipate (DVA) was reported (*20*). However, 5-9% of the product was not difunctional methacrylate.

The first examples of quantitative functionalization of telechelic polymers using CALB-catalyzed reactions with and without organic solvents have been reported by our group (*7–11*). The *primary* hydroxyl groups

In Green Polymer Chemistry: Biocatalysis and Materials II; Cheng, H., et al.;
ACS Symposium Series; American Chemical Society: Washington, DC, 2013.

of hydroxyl-functionalized polyisobutylenes (PIBs) were quantitatively methacrylated by transesterification of vinyl methacrylate in the presence of CALB within 24 hours in hexane and 2 hours in bulk, respectively (Scheme 2) (*8*, *9*).

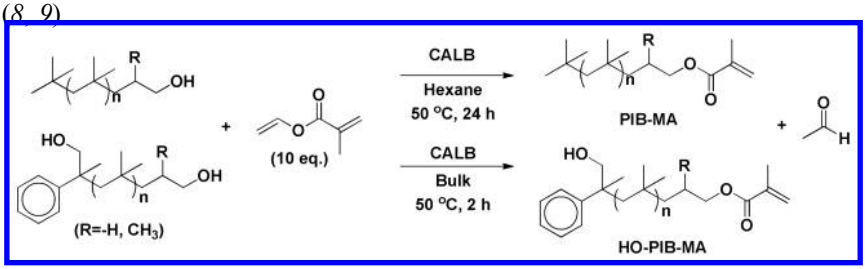

Scheme 2. CALB-catalyzed transesterification of vinyl methacrylate with PIBOHs.

Commercially available polydimethylsiloxanes (PDMS), PDMS-monocarbinol and PDMS-dicarbinols were also methacrylated with vinyl methacrylate under solventless conditions within 2 hours in the presence of CALB (*8*, *9*).

The methacrylation and acrylation of PEGs with various molecular weights and molecular weight distributions in THF were quantitative in 24 hours. Against this background, we investigated the transesterification of vinyl methacrylate, vinyl acrylate and vinyl crotonate with PEGs under solventless conditions

Enzymatic Functionalization of Poly(ethylene glycol)s under Solventless Conditions

Transesterification of Vinyl Acrylate and Vinyl Methacrylate with PEG

Solid low molecular weight PEGs became liquid at 50 °C and were quantitatively functionalized by transesterification. When reacted with vinyl methacrylate (VMA) in the presence of CALB under solventless conditions, the reactions were complete within 4 hours (Scheme 3).

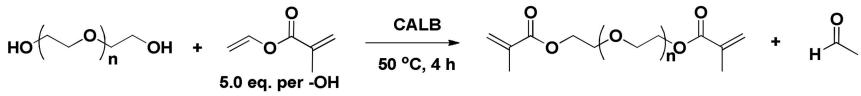

Scheme 3. Enzymatic transesterification of VMA with PEG (M_n = 1000 g/mol; M_w/M_n = 1.08) in the presence of CALB. [VMA] = 8.32 mol/L, [PEG] = 0.83 mol/L; [CALB] = 5.0 × 10^{-4} mol/L.

In the ^{1}H NMR spectrum of Figure 5, the hydroxyl proton signals at δ=4.55 ppm (a, not shown) from the HO-PEG-OH disappeared and the peak corresponding to the methylene protons adjacent to the hydroxyl groups shifted downfield from δ=3.50 to δ=4.22 ppm (b) after the reaction. The new peaks

In Green Polymer Chemistry: Biocatalysis and Materials II; Cheng, H., et al.;
ACS Symposium Series; American Chemical Society: Washington, DC, 2013.

Publication Date (Web): November 22, 2013 | doi: 10.1021/bk-2013-1144.ch007

corresponding to the vinyl [δ=6.07 ppm (e) and δ=5.65 ppm (e′)] and methyl [δ=1.73 ppm (f)] protons of the methacrylate group were observed at the expected positions. The ^{13}C NMR spectrum of the methacrylation product also confirmed the structure of the polymer. The ^{13}C NMR spectrum showed that the carbons connected to the hydroxyl groups at δ=60.13 ppm in the HO-PEG-OH shifted downfield to δ=64.02 ppm (B) and the carbon signals associated with the methacrylate group at δ = 17.95 ppm (G) δ = 136.17 ppm (F), δ = 126.20 ppm (E) and δ = 166.68 ppm (H) appeared after 4 hours reaction.

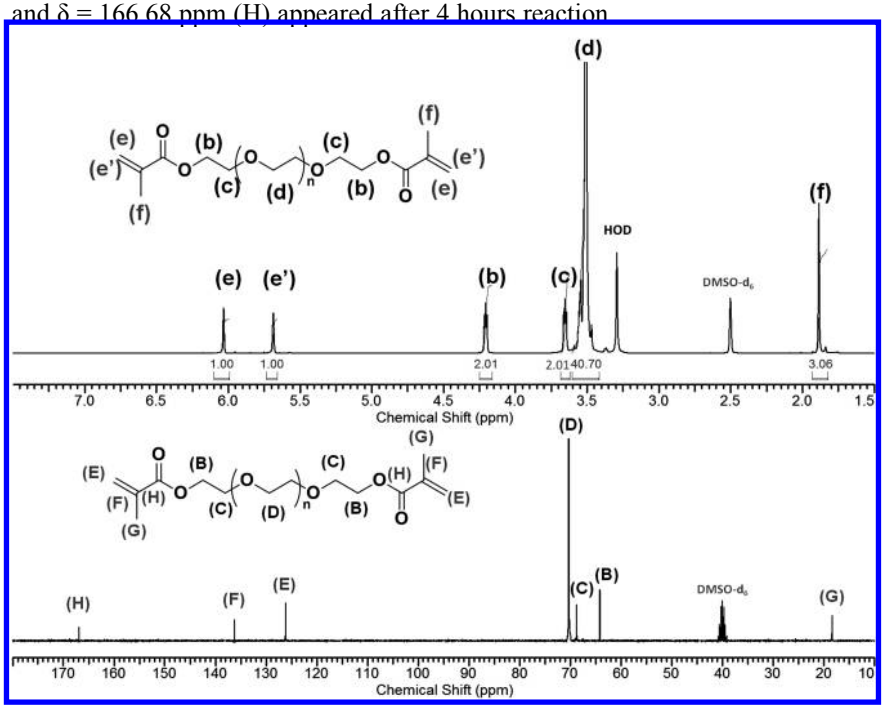

Figure 5. NMR spectra of the methacrylation product of PEG (M_n = 1000 g/mol; M_w/M_n = 1.08): (top) ^1H NMR spectrum and (bottom) ^{13}C NMR spectrum (solvent: DMSO-d_6).

The MALDI-ToF mass spectrum is shown in Figure 6. The peak at *m/z* 1101.61 corresponds to the sodium complex of the 21-mer of PEG dimethacrylate. The calculated monoisotopic mass for this ion is 1101.70 Da [21 × 44.03 (C_2H_4O repeat unit) + 154.08 ($C_8H_{10}O_3$ end groups) + 22.99 (Na^+)]. Within the series, the peaks were separated by 44 Da, corresponding to an ethylene glycol repeating units. The minor distribution of peaks which differ from the main series by 16 *m/z* units (see bottom of Figure 6) was assigned to the K^+ complex of PEG dimethacrylate - it is known that K^+ contamination occurs during sample preparation (*21*). Therefore, MALDI-ToF MS analysis confirmed that the conversion of HO-PEG-OH to PEG dimethacrylate was quantitative within 4 hours of reaction time under solventless conditions.

PEG with 2000 g/mol was also enzymatically methacrylated under the same conditions as above, yielding a very pure product.

In Green Polymer Chemistry: Biocatalysis and Materials II; Cheng, H., et al.;
ACS Symposium Series; American Chemical Society: Washington, DC, 2013.

Publication Date (Web): November 22, 2013 | doi: 10.1021/bk-2013-1144.ch007

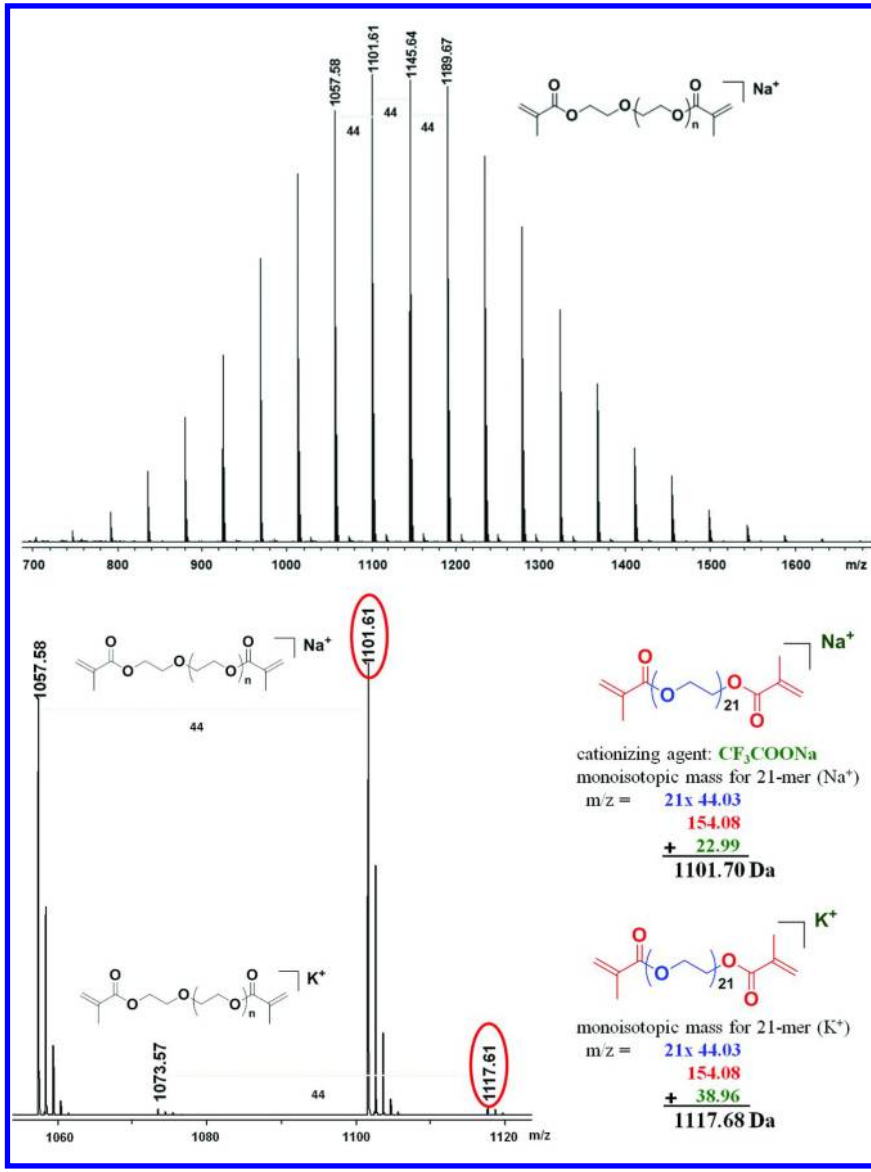

Figure 6. MALDI-ToF mass spectrum of PEG dimethacrylate (M_n=1000 g/mol; M_w/M_n = 1.08).

The same reactions were also carried out with vinyl acrylate, also yielding exceptionally pure products. Figure 7 shows the ^{1}H NMR spectrum of the PEG diacrylate. The peak corresponding to the methylene protons next to hydroxyl group shifted downfield from δ=3.50 to δ=4.42 ppm (b) after 4 hours. New resonances attributed to the vinylidene [δ=6.20 ppm (e)] and vinyl [δ=6.32

ppm (f) and δ=5.97 ppm (e′)] protons appeared with the integration ratios of (b):(e):(f):(e′) as 2:1:1:1. The ^{13}C NMR spectrum of the transesterification product also confirmed the structure of the PEG diacrylate. The carbons connected to the hydroxyl groups in the starting material at δ=60.13 ppm shifted downfield to δ=63.41 ppm (B) and the carbon signals associated with the acrylate group at δ = 166.02 ppm (H), δ = 131.86 ppm (F) and δ = 128.55 ppm (E) appeared after the acrylation.

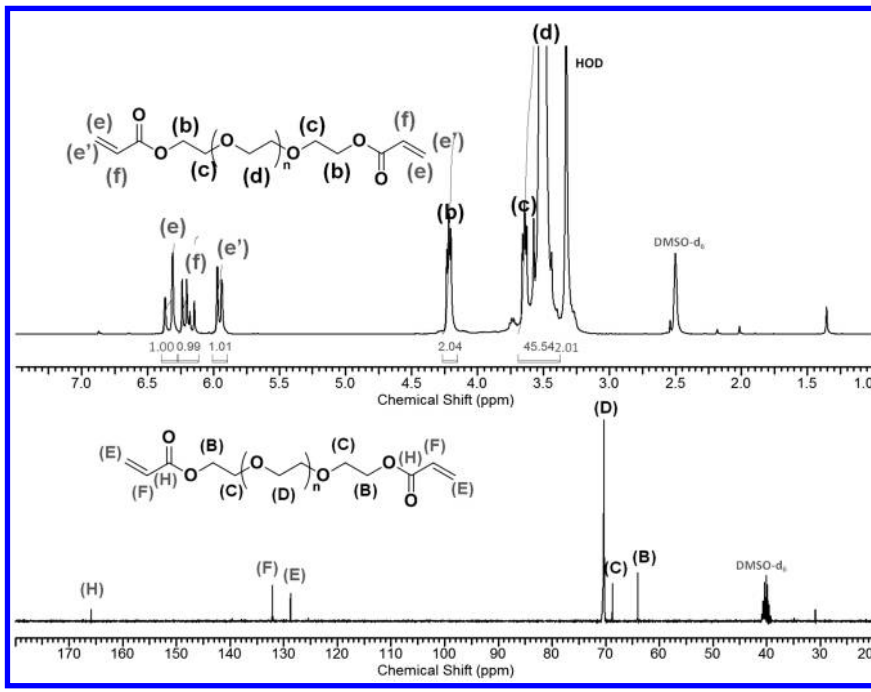

Figure 7. NMR spectra of the acrylation product of PEG (M_n = 1000 g/mol; M_w/M_n = 1.08): (top) ^1H NMR spectrum and (bottom) ^{13}C NMR spectrum (solvent: DMSO-d_6).

Figure 8 shows MALDI-ToF mass spectrum of the transesterification product after 4 hours of reaction. The major distribution corresponds to PEG diacrylate. In the expanded spectrum, the representative peak at *m/z* 1117.65 corresponds to the sodium complex of the 22-mer of PEG diacrylate; its calculated monoisotopic mass is [22 × 44.03 (C_2H_4O repeat unit) + 126.11 ($C_6H_6O_3$ end groups) + 22.99 (Na^+)] 1117.73 Da. The peak at *m/z* 1105.65, which belongs to a minor distribution differing from the main series by 12 *m/z* units, corresponds to α-acetate, ω-acrylate functionalized PEG. The calculated monoisotopic mass for its 22-mer is 1105.75 Da [22 × 44.03 (C_2H_4O repeat unit) + 114.10 ($C_5H_6O_3$ end groups) + 22.99 (Na^+)]. The acetate group most likely came from the vinyl acetate, an impurity found in commercial vinyl acrylate (*22*).

In Green Polymer Chemistry: Biocatalysis and Materials II; Cheng, H., et al.;
ACS Symposium Series; American Chemical Society: Washington, DC, 2013.

Publication Date (Web): November 22, 2013 | doi: 10.1021/bk-2013-1144.ch007

Publication Date (Web): November 22, 2013 | doi: 10.1021/bk-2013-1144.ch007

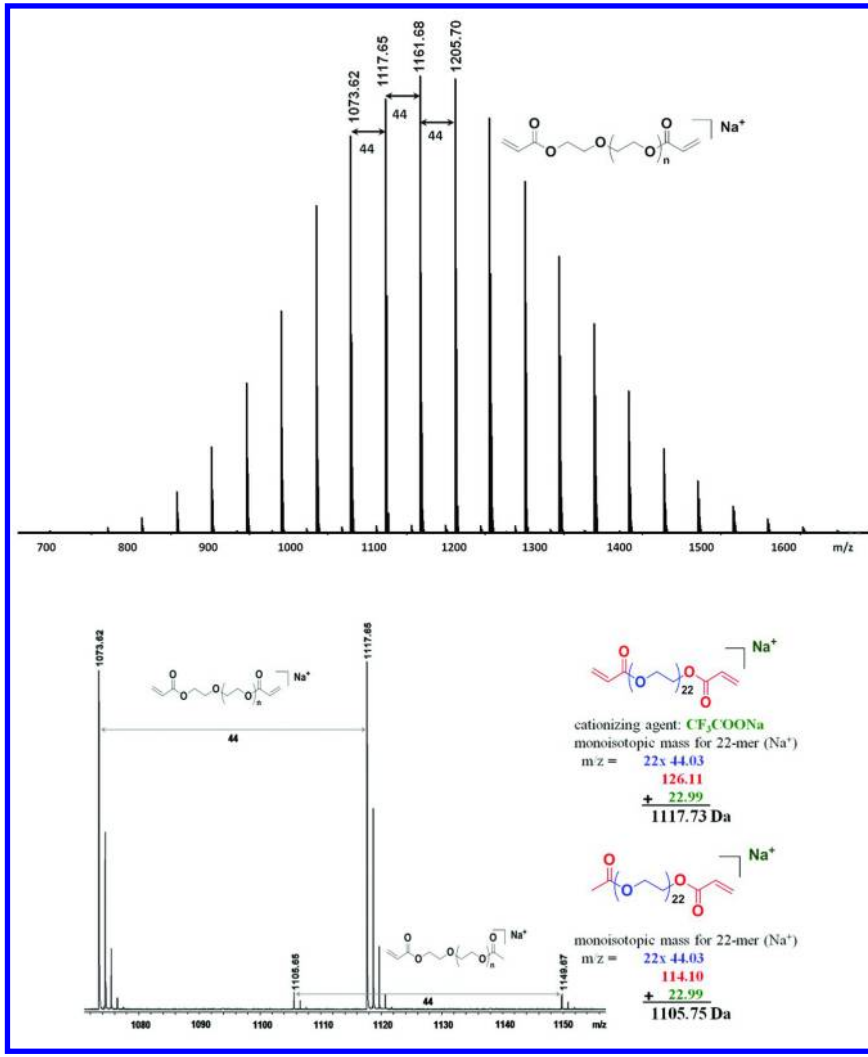

Figure 8. MALDI-ToF mass spectrum of PEG-diacrylate. (M_n = 1000 g/mol; M_w/M_n = 1.08).

Transesterification of Vinyl Crotonate with PEG

Crotonate groups were also successfully introduced at the chain ends of PEG by the transesterification of vinyl crotonate (VC) in the presence of CALB in bulk (Scheme 4).

In Green Polymer Chemistry: Biocatalysis and Materials II; Cheng, H., et al.;
ACS Symposium Series; American Chemical Society: Washington, DC, 2013.

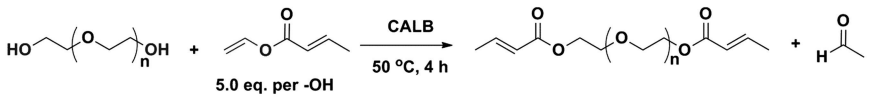

Scheme 4. Transesterification of vinyl crotonate with PEG (M_n = 1000 g/mol; M_w/M_n = 1.08) in the presence of CALB. [VC] = 8.28 mol/L, [PEG] = 0.89 mol/L; [CALB] = 5.5× 10^{-4} mol/L.

NMR spectroscopy and MALDI-ToF mass spectrometry confirmed the single transesterification product without any side products. Figure 9 shows the ^{1}H and ^{13}C NMR spectra of the transesterification product. The triplet peak of the methylene protons adjacent to the hydroxyl groups shifted downfield from δ=3.50 to δ=4.16 ppm (b) after the reaction. New resonances attributed to the methyl [δ=1.85 ppm (g)] and vinyl [δ=6.90 ppm (e) and δ=5.90 ppm (f)] protons of the crotonate group were observed at the expected positions. The ^{13}C NMR spectrum showed that the carbons connected to the hydroxyl groups in the starting material shifted downfield to δ=63.12 ppm (B) and the carbon signals associated with the crotonate group [δ=166.00 ppm (H), δ=145.26 ppm (F), δ=122.10 ppm (E) and δ=17.55 ppm (G)] appeared at the expected positions, confirming the successful functionalization.

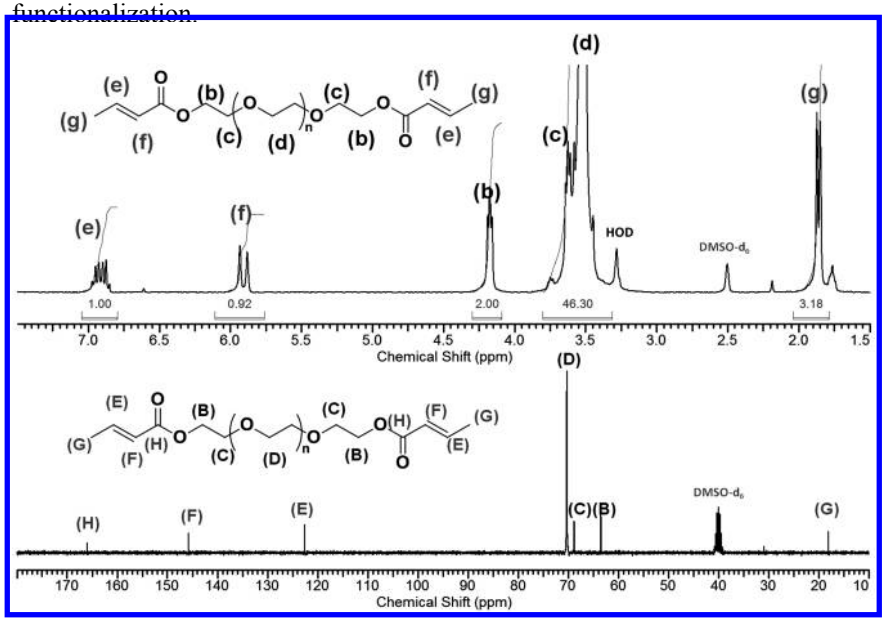

Figure 9. NMR spectra of PEG-dicrotonate (M_n = 1000 g/mol; M_w/M_n = 1.08): (top) ^{1}H NMR spectrum and (bottom) ^{13}C NMR spectrum (solvent: DMSO-d_6).

The MALDI-ToF mass spectrum includes a peak at *m/z* 1101.67 which corresponds to the sodium complex of the 22-mer of PEG dicrotonate (Figure 10). The calculated monoisotopic mass for this ion is 1145.73 Da [22×44.03 (C_2H_4O repeat unit) + 154.08 ($C_8H_{10}O_3$ end groups) + 22.99 (Na^+)]. In the

In Green Polymer Chemistry: Biocatalysis and Materials II; Cheng, H., et al.;
ACS Symposium Series; American Chemical Society: Washington, DC, 2013.

Publication Date (Web): November 22, 2013 | doi: 10.1021/bk-2013-1144.ch007

expanded spectrum, a minor series of peaks were distributed 16 *m/z* units above the main (sodiated) product series; the masses of these products agreed with those of potassiated PEG dicrotonate (1161.68 Da). The calculated monoisotopic mass for the potassiated 44-mer is 1161.70 Da [22x44.03 (C_2H_4O repeat unit) + 154.08 ($C_8H_{10}O_3$ end groups) + 38.96 (K^+)].

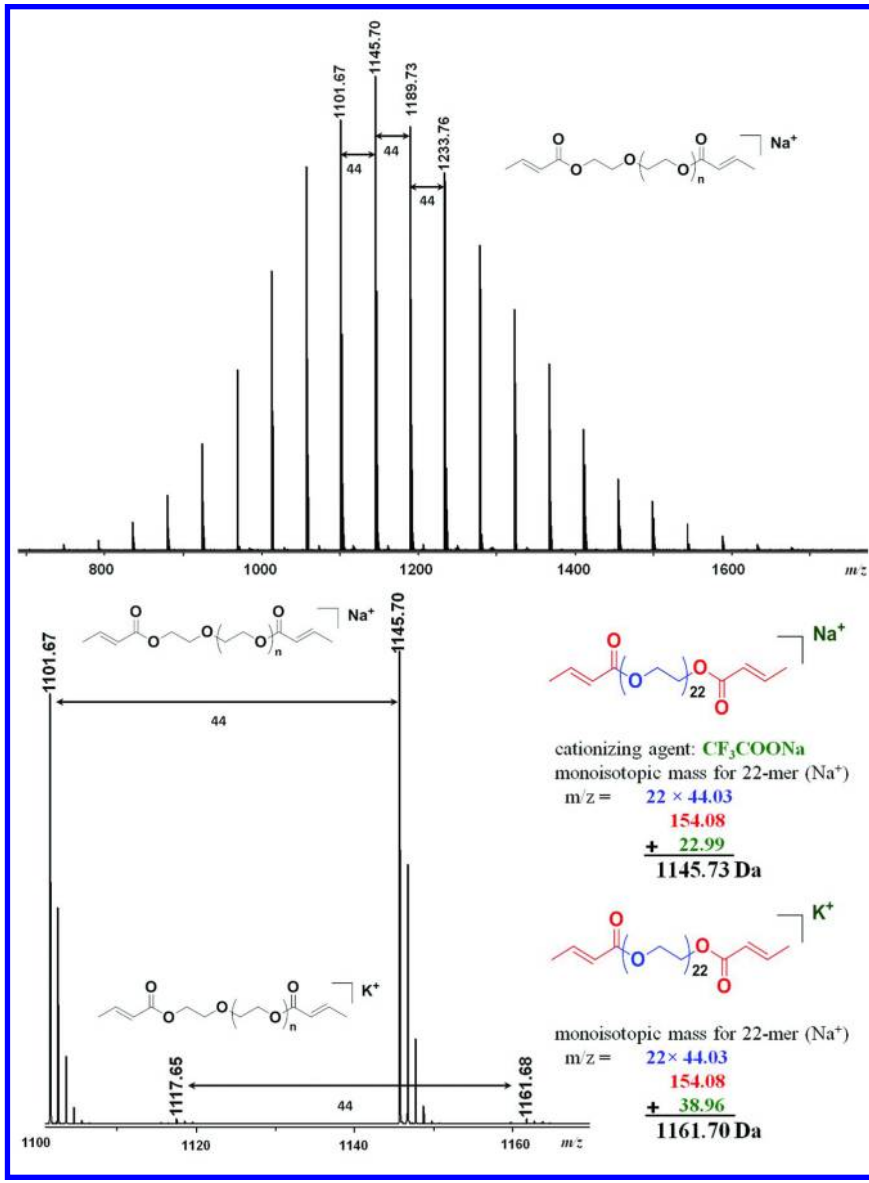

Figure 10. MALDI-ToF mass spectrum of PEG dicrotonate (M_n = 1000 g/mol; M_w/M_n = 1.08).

In Green Polymer Chemistry: Biocatalysis and Materials II; Cheng, H., et al.;
ACS Symposium Series; American Chemical Society: Washington, DC, 2013.

Conclusion

PEGs were successfully functionalized under solventless conditions via CALB-catalyzed transesterification of vinyl esters. ^{1}H and ^{13}C NMR spectroscopy and MALDI-ToF verified the structure and purity of the products. This method provides a convenient and greener process to functionalize PEGs.

Acknowledgments

This work is supported by National Science Foundation NSF under DMR-0804878 and the Ohio Board of Regents. We wish to thank The Ohio Board of Regents and NSF for funds used to purchase the NMR (CHE-0341701 and DMR-0414599) and MS (CHE-1012636 and DMR-0821313) instruments used in this work.

Publication Date (Web): November 22, 2013 | doi: 10.1021/bk-2013-1144.ch007

References

1. Rodney, R. L.; Allinson, B. T.; Beckman, E. J.; Russell, A. J. *Biotechnol. Bioeng.* **1999**, *65*, 485–489.
2. Kobayashi, S.; Makino, A. *Chem. Rev.* **2009**, *109*, 5288–5353.
3. Kadokawa, J.; Kobayashi, S. *Curr. Opin. Biotechnol.* **2010**, *14*, 145–153.
4. Gross, R. A.; Kumar, A.; Kalra, B. *Chem. Rev.* **2001**, *101*, 2097–2124.
5. Sahoo, B.; Bhattacharya, A.; Fu, H.; Gao, W.; Gross, R. A. *Biomacromolecules* **2006**, *7*, 1042–1048.
6. Gubitz, G. M.; Paulo, A. C. *Curr. Opin. Biotechnol.* **2003**, *14*, 577–582.
7. Puskas, J. E.; Seo, K. S.; Sen, M. Y. *Eur. Polym. J.* **2011**, *47*, 524–534.
8. Sen, M. Y. Ph.D. Dissertation, The University of Akron, Akron, OH, 2009.
9. Puskas, J. E.; Sen, M. Y.; Seo, K. S. *J. Polym. Sci. Part A: Polym. Chem.* **2009**, *47*, 2959–2976.
10. Puskas, J. E.; Sen, M. Y.; Kasper, J. R. *J. Polym. Sci. Part A: Polym. Chem.* **2008**, *46*, 3024–3028.
11. Sen, M. Y.; Puskas, J. E.; Ummadisetty, S.; Kennedy, J. P. *Macromol. Rapid Commun.* **2008**, *29*, 1598–1602.
12. Faber, K. *Biotransformations in Organic Chemistry*, 5th ed.; Springer-Verlag: New York, 2004.
13. Bornscheuer, U. T.; Kazlauskas, R. J. *Hydrolases in Organic Synthesis: Regio- and Stereoselective Biotransformations*, 2nd ed.; WileY-VCH Verlag GmbH & Co. KgaA: Weinheim, Germany, 2006.
14. Gotor-Fernández, V.; Busto, E.; Gotor, V. *Adv. Syn. Catal.* **2006**, *348*, 797–812.
15. Uppenberg, J.; Hansen, M. T.; Patkar, S.; Jones, T. A. *Structure* **1994**, *2*, 293–308.
16. Uppenberg, J.; Patkar, S.; Bergfors, T.; Jones, T. A. *J. Mol. Biol.* **1994**, *235*, 790–792.
17. Paravidino, M.; Hanefeld, U. *Green Chem.* **2011**, *13*, 2651–2657.
18. Weber, H. K.; Stecher, H.; Faber, K. *Biotechnol. Lett.* **1995**, *17*, 803–808.

19. Sahoo, B.; Brandstadt, K. F.; Lane, T. H.; Gross, R. a *Org. Lett.* **2005**, *7*, 3857–3860.
20. Eriksson, M.; Hult, K.; Malmström, E.; Johansson, M.; Trey, S. M.; Martinelle, M. *Polym. Chem.* **2011**, *2*, 714–719.
21. Belu, A. M.; DeSimone, J. M.; Linton, R. W.; Lange, G. W.; Friedman, R. M. *J. Am. Soc. Mass Spectrom.* **1996**, *7*, 11–24.
22. Nakagawa, H.; Okimoto, Y.; Sakaguchi, S.; Ishii, Y. *Tetrahedron Lett.* **2003**, *44*, 103–106.

Publication Date (Web): November 22, 2013 | doi: 10.1021/bk-2013-1144.ch007

Publication Date (Web): November 22, 2013 | doi: 10.1021/bk-2013-1144.ch008

Chapter 8

Biocatalysis for Silicone-Based Copolymers

Stephen J. Clarson,* Yadagiri Poojari, and Michael D. Williard

Department of Biomedical, Chemical and Environmental Engineering, and the Polymer Research Centre, University of Cincinnati, Cincinnati, Ohio 45221-0012, U.S.A.
***E-mail: Stephen.Clarson@UC.Edu**

Linear poly(dimethylsiloxane) (PDMS), the most common silicone chain molecule, can form organic-silicone copolymers, which have the unique properties of linear PDMS such as low temperature flexibility, high thermal stability, excellent electrical properties, good gas permeability and excellent biocompatibility, and other system specific properties which depend on the type and nature of the organic segments of the organic-silicone copolymer. However, such organic-silicone copolymers are conventionally synthesized using metal based catalysts under harsh reaction conditions. These harsh conditions can be detrimental to the siloxane bonds in the silicone part of chain backbone. Recently, the novel enzymatic syntheses of organic-silicone copolymers through esterification and transesterification reactions under mild reaction conditions have been reported. The synthesis and properties of some of these organic-silicone copolymers are reviewed and discussed in this chapter.

Introduction

Silicon is the second most abundant element in the Earth's crust after oxygen. It is widely used in the manufacture of siloxane-based materials. Such materials find applications as fluids, gels, rubbers, resins, semiconductors, glasses, ceramics, plastics, mesoporous molecular sieves, optical fibers, coatings, insulators, moisture shields, photoluminescent polymers, and cosmetics (*1*, *2*). The industrial production of silica or siloxane polymers often requires extremes of pH and/or temperature (*3*). In contrast to such industrial methods, many

In Green Polymer Chemistry: Biocatalysis and Materials II; Cheng, H., et al.;
ACS Symposium Series; American Chemical Society: Washington, DC, 2013.

marine and freshwater organisms synthesize large quantities of silica under mild physiological conditions. This process is a known as biosilicification, wherein silica forming proteins biocatalyze the biochemical formation of polysiloxane materials (*4*). The biosilica structures of these organisms provide protection and allows for the survival of a speciesin its natural habitat (or niche) (*4*). Morse and coworkers reported that an enzyme, *silicatein α*, has a serine protease-like active site and it can produce silica or organically modified silica *in vitro* from tetraethoxysilane at neutral pH and at moderate temperatures (*5*, *6*). This discovery has led to increased research interest in the enzymatic synthesis of novel polysiloxane based materials.

Silicones $(RR'SiO)_n$ have been known since the early part of the twentieth century and as commercial materials since the 1940s. Kipping is known for many seminal contributions to mechanistic and preparative organosilicon chemistry (*7*). Silicones, in the absence of acidic or basic catalysts, exhibit exceptional thermal stability. For example, the degradation of dimethylsilicone fluids due to siloxane bond interchanges begins at approximately 350°C (*8*). This thermal stability is being utilized, for instance, in sealing of kitchen appliances, and hair dryers. The relative permittivity of silicone fluids is very low (approximately 2.75). By comparison, the relative permittivity for acetone and water are 20.7 and 78.5, respectively (*9*). These values are not significantly affected by temperature, even at extreme temperatures. The decomposition of silicone in air can lead to the formation of silica, which is an excellent insulator. Thus silicones are useful in wire coating, motor insulators and electrical transformers (*10*).

Dimethylsilicones, also known as linear poly(dimethylsiloxane) (PDMS), are known to possess exceptional hydrophobicity. This property is mainly attributed to the two following characteristics: (i) the methyl groups provide hydrophobic characteristics to the polymer, and (ii) the flexibility of the silicone polymer chain permits the rearrangement of the polymer backbone such that the methyl groups may orient themselves at an interface. The fluid nature of the silicones allows them to wet (spread over) surfaces, presenting a layer of hydrophobic methyl groups at the interface (*11*). The chain flexibility originates from the large bond angle of the Si–O–Si linkages and the low bending force constant for this linkage. The glass transition temperature, T_g of PDMS, which reflects the relative ease of segmental motion in the chain, is typically less than –120°C.

The ability to wet and spread and the intrinsic hydrophobicity of silicones make them among the lowest-surface-energy compounds known (*12*). Hence, silicones are used as release agents to prevent adhesion in many applications. When silicones are chemically combined with hydrophilic species, such as cationic species or poly(ethylene oxide) (PEO), very interesting surfactant properties arise. For example, silicones are used as foam stabilizers for making of polyurethane foams while silicone copolymers are used as defoamers in the pulp & paper and in the food industries (*9*).

Block copolymers are attractive materials because they combine the properties of both of the parent polymers or segments and offer the possibility of tailoring the physico-chemical properties, the thermo-mechanical properties and the processability to obtain new engineered materials. Silicon-containing block copolymers are particularly interesting because of the unique properties

Publication Date (Web): November 22, 2013 | doi: 10.1021/bk-2013-1144.ch008

In Green Polymer Chemistry: Biocatalysis and Materials II; Cheng, H., et al.;
ACS Symposium Series; American Chemical Society: Washington, DC, 2013.

of polysiloxanes. Their exceptional properties such as very low glass transition temperature, low surface energy, high gas permeability, resistance to oxidation and biocompatibility, leads to materials for a wide range of commercially important products and applications (*13*). In the following sections, we will describe some of the applications of enzymes to prepare a variety of silicone containing copolymers.

Results and Discussion

Polysiloxanes

Nishino and coworkers (*14*) have first reported the synthesis of polysiloxanes using lipase D (from *Rhizopus delemar*), which is a stable serine esterase, as a catalyst. The authors used a lipid-coated lipase D in order to catalyze the oligomerization of diethoxydimethylsilane (DEDMS) in isooctane in the presence of 2 wt% water. The lipid-coated lipase system, in which hydrophilic head groups of the lipids interacted with the enzyme surface and the two long lipophilic alkyl chains extend away from its surface, solubilized the enzyme in hydrophobic organic solvents such as isooctane, as shown in Scheme 1. The conversion of the lipids reached over 80% after 20 hours in the presence of an excess amount of the DEDMS monomer. The weight-average molecular weight (M_w) of the product was found to be constant at 1500 g mol^{-1} and the molecular weight distribution (M_w/M_n) was observed to be very narrow at 1.06.

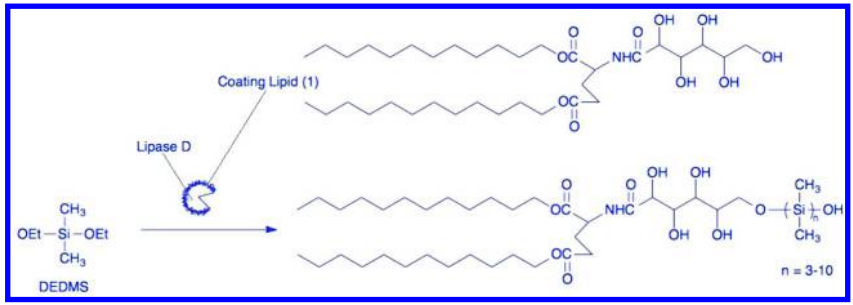

Scheme 1. A lipid (1)-coated lipase catalyzes the oligomerization of diethoxydimethylsilane (DEDMS) in isooctane containing 2 wt% water, where the polymerization occurs at the (–OH) end group of the coated lipid (1) in the enzyme cavity (14).

Followed by these observations, Bassindale and coworkers (*15*, *16*) studied the use of various homologous lipase and protease enzymes to catalyze the formation of molecules with a single siloxane bond during the *in vitro* hydrolysis and condensation of alkoxysilanes under mild reaction conditions. They found that non-specific interactions with trypsin promoted the hydrolysis of alkoxysilanes, while the active site was determined to selectively catalyze the condensation of silanols. One interesting observation was when trypsin from various sources was employed, different extents of conversion were observed. Comparatively, the activity of trypsin obtained from a bovine pancreas was

In Green Polymer Chemistry: Biocatalysis and Materials II; Cheng, H., et al.;
ACS Symposium Series; American Chemical Society: Washington, DC, 2013.

Publication Date (Web): November 22, 2013 | doi: 10.1021/bk-2013-1144.ch008

Publication Date (Web): November 22, 2013 | doi: 10.1021/bk-2013-1144.ch008

greater than the alternate sources of trypsin. Although various sources (e.g. mammalian, fish) of trypsin are similar (e.g. tertiary structure), their selectivity and activity was found to be different due to different optimum pH ranges and/or the levels of calcium (an additive).

Silicone Aliphatic Polyesters

One of the most important features of aliphatic polyesters is their compatibility with the natural environment and their ability to undergo hydrolytic as well as biological degradation. When these linear polymer segments are being incorporated into the silicone backbone chains, a biodegradable silicone fluid or an elastomer can be synthesized for a variety of applications including biomedical implants and personal care products. In fact, for this very same reason, synthesis of linear silicone aliphatic polyesters by the condensation polymerization of 1,3-bis(3-carboxypropyl)tetramethyldisiloxane with alkanediols (1,4-butanediol, 1,6-hexanediol and 1,8-octanediol) using an immobilized lipase B from *Candida antarctica* (Novozym-435®) as a catalyst, as shown in Scheme 2**,** has been reported (*17*). These reactions were performed in the bulk (without the use of any solvent) in the temperature range 50–90°C under reduced pressure (50–300 mmHg, vacuum gauge).

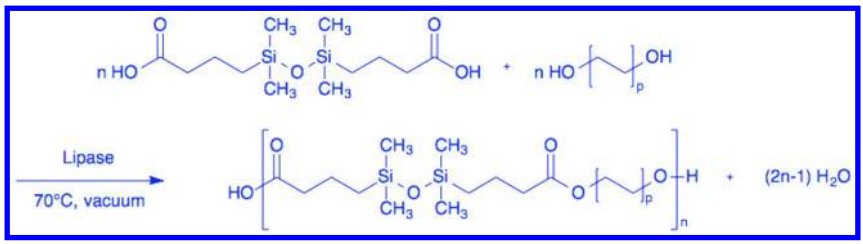

Scheme 2. Lipase (Novozym-435®) catalyzed polyesterification of 1,3-bis(3-carboxypropyl)tetramethyl disiloxane with alkanediol (p = 2, 3 and 4), in the bulk, at 70°C under reduced pressure (17).

The molar mass of the polyesters depended on the reaction temperature, enzyme activity, enzyme concentration, and to a lesser extent on the applied vacuum. For example, when the polyesters were synthesized using 1,4-butanediol, 1,6- hexanediol and 1,8-octanediol in the bulk at 70°C under reduced pressure for 24 hours, the weight average molecular weights obtained were 15,100 g mol^{-1}, 16,000 g mol^{-1}, 16,700 g mol^{-1}, respectively. Thermal analysis of these copolymers revealed no melting phenomenon, which is perhaps due to the presence of the flexible siloxane segments in the backbone of the chains. In addition, the glass transition temperatures of these polyesters were observed around –75°C, which is much higher when compared to that of the PDMS, –125°C. This is presumably a result of the ethylene segments in the system. Also, these enzymatically synthesized low molecular weight silicone polyesters were found to be highly viscous liquids at room temperature, apparently due to the presence of hydrogen bonding between the ester segments.

In Green Polymer Chemistry: Biocatalysis and Materials II; Cheng, H., et al.;
ACS Symposium Series; American Chemical Society: Washington, DC, 2013.

Publication Date (Web): November 22, 2013 | doi: 10.1021/bk-2013-1144.ch008

Silicone Aliphatic Polyesteramides

In another study, lipase catalyzed silicone polyesteramides formed in the bulk at 70°C under reduced pressure (10-20 mmHg) have been reported (*18*). Novozym-435® was used as the enzyme under mild reaction conditions to perform the polycondensation reaction using various feed mole ratios of diethyl adipate (DEA), 1,8-octanediol (OD), and *α,ω*-(diaminopropyl) polydimethylsiloxane (Si-NH_2), as shown in Scheme 3. The authors also synthesized poly(octamethyleneadipate), POA, and poly(*α,ω*-(diaminopropyl)polydimethyl siloxane adipamide), PSiAA, using the same enzyme, and compared their properties with those of the silicone polyesteramides.

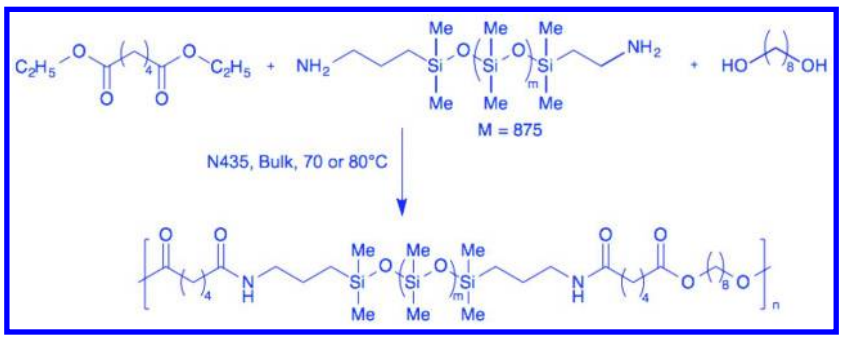

Scheme 3. Lipase (Novozym-435®) catalyzed polymerization of α,ω-(diaminopropyl)poly-dimethyl-siloxanes, diethyl adipate, and 1,8-octanediol at 70°C in the bulk (18).

The relative amounts of amide and ester units in the polymer chain were observed to strongly influence the physical properties of the polyesteramides, for example, the presence of a high content of DEA-OA units resulted in hard solid materials containing a well developed high melting POA-type crystal phase. The observed melting temperature was at around 67°C, which depended on the copolymer composition. However, when the amount of DEA-SiAA segments was increased in the copolymer's composition, the material exhibited a sticky appearance.

Silicone Fluorinated Aliphatic Polyesteramides

The aliphatic fluorocarbon based materials are known for their exceptionally low surface energies, and when combined with the excellent properties of silicones, can produce interesting and useful engineered materials. Efforts were made to synthesize silicone fluorinated aliphatic polyesteramides (SFAPEAs) containing both amide and ester linkages formed by a simultaneous transesterification reaction between *α,ω*-aminopropyl terminated poly(dimethylsiloxane) (APDMS) and diethyl adipate (DEA) with four different fluorinated alkane diol (FAD) monomers, as shown in reaction Scheme 4 (*19*), using Novozym-435® as a catalyst. The DEA was employed to inhibit the phase

In Green Polymer Chemistry: Biocatalysis and Materials II; Cheng, H., et al.;
ACS Symposium Series; American Chemical Society: Washington, DC, 2013.

separation of the FADs and to facilitate the transesterification reactions with the APDMS.

The highest molar masses were obtained when using OFOD, which has an additional methylene (-CH_2-) spacer between the fluorocarbon chain (-CF_2-)$_n$ and the hydroxyl end groups (-OH). The physical state of the fluorosilicones (SFAPEAs) depended upon the relative contents of the fluorinated polyester (FPE) and the silicone polyamide (SPA) in the final product. The FPEs were partially crystalline white solids at room temperature and they became progressively viscous and waxy as the silicone content increased in the fluorosilicones. The thermogravimetric analysis (TGA) revealed a marginal improvement in the degradation characteristics of the fluorosilicones compared to the fluorinated polyesters. It is worth noting that the presence of the fluorinated methylene segments in the polyesters did not improve the thermal degradation behavior. However, the presence of silicone in the fluorosilicones shifted the characteristic polymer degradation to higher temperatures.

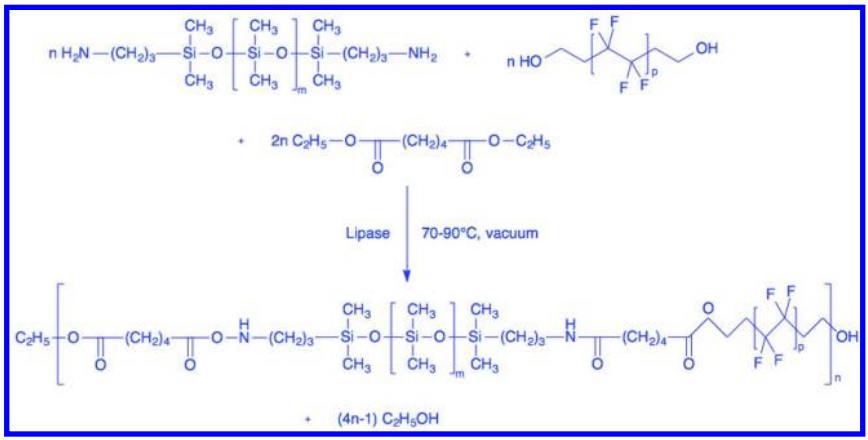

Scheme 4. Lipase (Novozym-435®) catalyzed synthesis of silicone fluorinated aliphatic polyesteramides (SFAPEAs) by the transesterification and amidation of α,ω-aminopropyl terminated poly(dimethylsiloxane) (APDMS) and 3,3,4,4,5,5,6,6-octafluoro 1,8-octanediol (OFOD) with diethyl adipate (DEA), respectively, at temperatures in the range of 70°C to 90°C in the bulk (19).

Silicone Aromatic Polyesters and Silicone Aromatic Polyamides

Linear poly(dimethylsiloxane) (PDMS) and poly(ethylene terephthalate) (PET) are two of the most commercially important polymers. It is well known that PDMS can be prepared either as a fluid, gel, rubber or resin depending on its structure and functionality. On the other hand PET is a thermoplastic with excellent film and fiber forming properties (*20*). Needless to say, PDMS and PET are incompatible with respect to forming binary polymer blends. The coating or grafting of silicones onto PET fibers is another important technology

In Green Polymer Chemistry: Biocatalysis and Materials II; Cheng, H., et al.;
ACS Symposium Series; American Chemical Society: Washington, DC, 2013.

Publication Date (Web): November 22, 2013 | doi: 10.1021/bk-2013-1144.ch008

for improving fiber processing and for surface modification (*21*). However, the conventional copolymerization pathways to PDMS and PET copolymers are paved with difficulties due to both physical incompatibility and chemical convertibility issues regard to the catalysts and temperatures used for esterification and transesterification reactions (*18*). In particular the strong acids typically used in esterification or transesterification reactions can break the siloxane bonds Si–O–Si unless great care is taken. In order to address this problem, a facile enzymatic synthesis of silicone aromatic polyester (SAPE) and silicone aromatic polyamide (SAPA) in toluene under mild reaction conditions was performed as described in the reaction Scheme 5 and Scheme 6 (*22*, *23*).

Publication Date (Web): November 22, 2013 | doi: 10.1021/bk-2013-1144.ch008

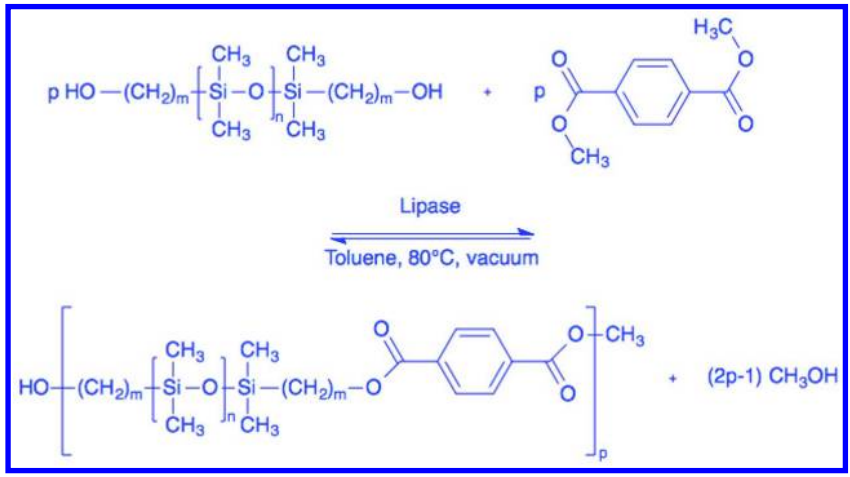

Scheme 5. Lipase (Novozym-435®) catalyzed synthesis of silicone aromatic polyester (SAPE) by the polyesterification of α,ω-(dihydroxy alkyl) terminated poly(dimethylsiloxane) (m ≈ 7, n ≈ 30 and M_n ≈ 2500 g mol^{-1}) with dimethyl terephthalate in toluene at 80°C under reduced pressure (22).

Both the SAPE and SAPA copolymers were found to be amorphous liquids at room temperature, but were also found to contain hard domains resulting from the segregation of the segments of aromatic polyesters and aromatic polyamides, respectively. The SAPAs were highly viscous and sticky glue-like in appearance, probably due to the presence of the hydrogen bonding between the amide linkages when compared to the SAPE polymers. Nevertheless, the thermogravimetric analysis (TGA) of both of these polymer samples displayed minimal residual mass and a very similar solid residue that ranged between 0.25 and 0.5 wt % at 700°C.

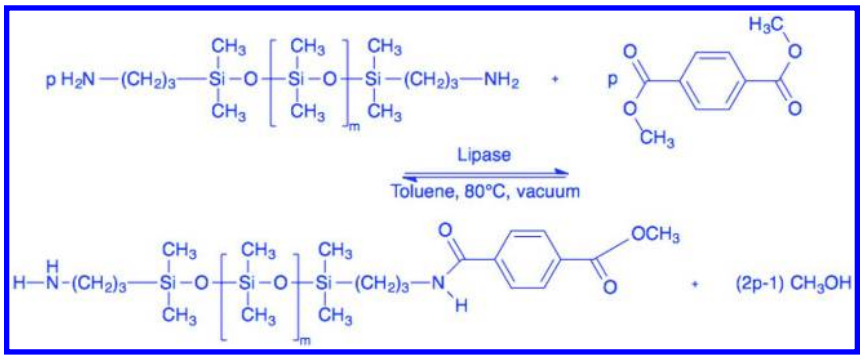

Scheme 6. Lipase (Novozym-435®) catalyzed synthesis of silicone aromatic polyamide (SAPA) by the polyamidation of α,ω-(diaminopropyl) terminated poly(dimethylsiloxane) with dimethyl terephthalate in toluene at 80°C under reduced pressure (23).

Publication Date (Web): November 22, 2013 | doi: 10.1021/bk-2013-1144.ch008

Silicone Polycaprolactones

Biodegradable polymers have generated tremendous research interest in the fields of biomedical, agricultural and industrial applications. One such example is poly(ε-caprolactone) (PCL), which is a semi-crystalline homopolymer having a glass transition temperature of −60°C and melting point in the range 59 to 64°C, depending upon the crystalline nature and thermal history of the PCL. The controlled biodegradation of PCL, depending on chain length and morphology, is ideally suited for both short-term personal care products and long-term drug delivery applications. Copolymers of PCL and silicones, with the excellent properties of both these individual polymers, can be synthesized with tailored properties for interesting products and applications. In one such study, linear poly(ε-caprolactone)–poly(dimethylsiloxane)–poly(ε-caprolactone) triblock copolymers were synthesized using an enzyme under benign reaction conditions (*24*). The copolymerization was performed by the ring-opening polymerization of ε-caprolactone with *α,ω*-(dihydroxyalkyl) terminated PDMS using Novozym-435® as the catalyst in toluene at 70°C, as shown in reaction Scheme 7. The triblock copolymers were found to be semi-crystalline by Differential Scanning Calorimetry (DSC) and X-Ray Diffraction (XRD) analysis. The degree of crystallinity was found to increase with the increased feed ratio of (ε-caprolactone)/(PDMS). The crystal structure of the copolymers was determined by wide-angle X-Ray diffraction (WAXD), and found to be similar to that of the PCL homopolymer. Furthermore, the thermal stability of these copolymers improved over the parent PCL homopolymer with increased mole fraction of the PDMS in the copolymers apparently due to the high thermal stability of PDMS compared to that of the PCL.

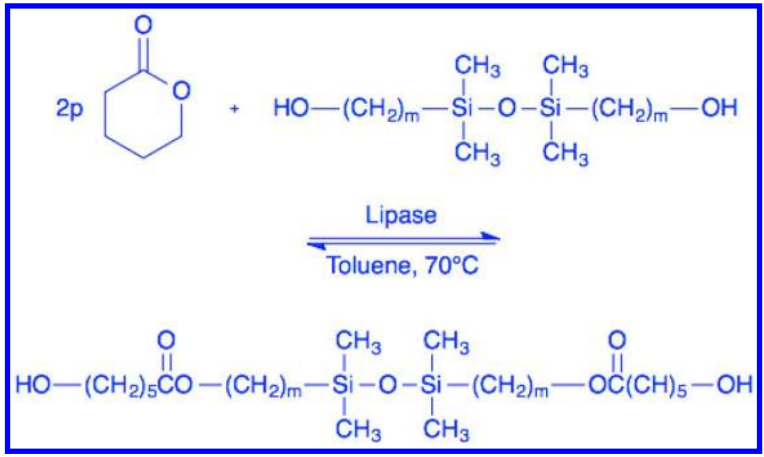

Scheme 7. Lipase (Novozym-435®) catalyzed copolymerization of ε-caprolactone with α,ω-(dihydroxy alkyl) terminated PDMS (m ≈ 7, n ≈ 30 and M_n ≈ 2500 g mol^{-1}) in toluene at 70°C (24).

Silicone Polyethers

Silicone surfactants including silicone-polyethers have been utilized in a variety of products and processes such as polyurethane foam stabilizers and as novel water-in-oil and oil-in-water emulsifiers (*9*). Recently, silicone aliphatic polyethers, in particular poly(dimethylsiloxane)–poly(ethylene glycol) an amphiphilic copolymer, were synthesized in the bulk at 80°C and under reduced pressure (500 mmHg gauge) (*25*). Novozym-435® was utilized for the condensation polymerization of 1,3-*bis*(3-carboxypropyl)tetramethyldisiloxane with poly(ethylene glycol) (PEG) having a number average molar mass, M_n = 400, 1000 and 3400 g mol^{-1}, respectively. This is shown in Scheme 8. The same enzyme was also used to copolymerize *α,ω*-(dihydroxy alkyl) terminated poly(dimethylsiloxane) (HAT-PDMS, M_n = 2500 g mol^{-1}) with *α,ω*-(diacid) terminated poly(ethylene glycol) (PEG, M_n = 600 g mol^{-1}) as shown in Scheme 9. As expected, the thermal stability of these copolymers was found to increase with increased dimethylsiloxane content in the copolymers.

It is worth mentioning here that PEG is a biomedical polymer with excellent biocompatibility. It shows resistance to platelet adsorption and to protein adsorption due to its mobility in aqueous environments (*26*). Indeed, PEG allows biomaterials to retain their excellent water swelling properties, whereas PDMS modifies its surface to inhibit protein adsorption (*13*). Hence, PDMS−PEG copolymers are considered to be ideal candidates as biomaterials for wound dressing applications and also for personal care products.

In Green Polymer Chemistry: Biocatalysis and Materials II; Cheng, H., et al.;
ACS Symposium Series; American Chemical Society: Washington, DC, 2013.

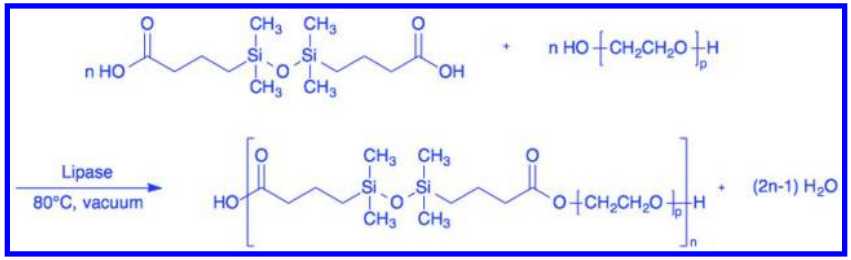

Scheme 8. Lipase (Novozym-435®) catalyzed copolymerization of 1,3-bis(3-carboxypropyl) tetramethyldisiloxane with poly(ethylene glycol) (PEG, M_n = 400, 1000 and 3400 g mol^{-1}, respectively) in the bulk under vacuum at 80°C (25).

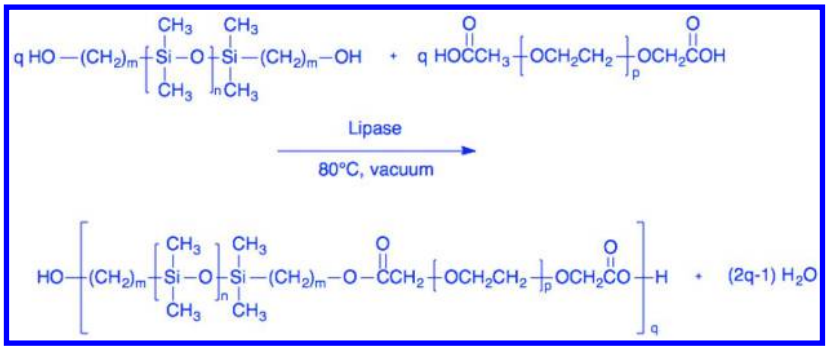

Scheme 9. Lipase (Novozym-435®) catalyzed copolymerization of α,ω-(dihydroxy alkyl) terminated poly(dimethylsiloxane) (HAT-PDMS, m ≈ 7, n ≈ 30 and M_n = 2500 g mol^{-1}) with α,ω-(diacid) terminated poly(ethylene glycol) (PEG, M_n = 600 g mol^{-1}) in the bulk under vacuum at 70°C (25).

Silicone Sugar Conjugates

Braunmühl and coworkers (*27*) have synthesized poly(dimethylsiloxane)s with pendent maltoheptaoside or maltoheptaonamide groups by hydrosilylation and/or amidation reactions. Subsequently, potato phosphorylase was used to catalyze the formation of poly(dimethylsiloxane)-graft-(*α*,1→4)-D-glucopyranose molecules with *α*-D-glucose-1-phosphate in a citrate buffer at 37°C. The amylose side chains were found to have helical structures, but the need for multiple steps and activation chemistry were problematic. A facile enzymatic method was reported by Bishwabhusan and coworkers, who have performed esterification of organo-siloxane carboxylic diacids with the C1-O-alkylated *α,β*- ethyl glucoside by using Novozym-435® as a catalyst (*28*). The pure organo- siloxane-sugar conjugates "Sweet silicones" were prepared in a one-step reaction without protection-deprotection steps and without activation of the acid groups with the integrity of the siloxane bonds, as shown in Scheme 10.

In Green Polymer Chemistry: Biocatalysis and Materials II; Cheng, H., et al.;
ACS Symposium Series; American Chemical Society: Washington, DC, 2013.

Publication Date (Web): November 22, 2013 | doi: 10.1021/bk-2013-1144.ch008

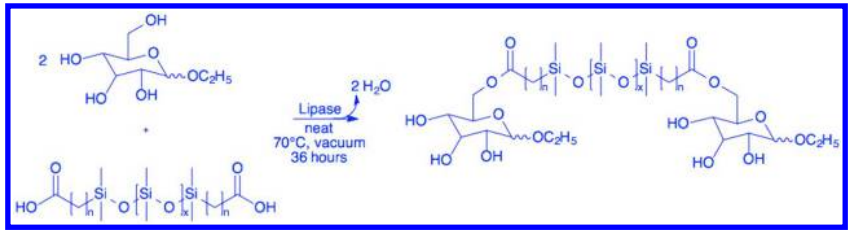

Scheme 10. Lipase (Novozym-435®) catalyzed regioselective formation of ester bonds between organosilicon carboxylic diacids and a C1-O-alkylated sugar under mild reaction conditions (28).

Publication Date (Web): November 22, 2013 | doi: 10.1021/bk-2013-1144.ch008

Stereo-Selective Organosiloxanes

A wide variety of enzymes were utilized for the stereo-selective transformation of organosiloxanes and a couple of examples are discussed here. Kawamoto and coworkers (*29*) have carried out comparative studies of the use of organosilicon compounds ($Me_3Si(CH_2)_nOH$) as acyl acceptor and also the corresponding carbon compounds ($Me_3C(CH_2)_nOH$) in the stereo-selective esterification of 2- (4-chlorophenoxy)propanoic acid by the use of lipase OF 360 of *Candida cylindracea* in water-saturated benzene. The organosilicon compounds were found to be efficient substrates for the esterification of the D-acid enantiomer. For the organosilicon compounds of different chain-length between the silicon atom and the hydroxyl group, trimethylsilylmethanol (n = 1) enabled the esterification reaction to be both fast and highly stereoselective, compared to conventional substrates such as its carbon counterpart. Uejima et al. (*30*) have reported the stereo-selective esterification of three isomers of trimethylsilylpropanol, 1-trimethylsilyl-2-propanol, 1-trimethylsilyl-l-propanol and 2-trimethylsilyl-l-propanol, synthesized with five different types of hydrolases in an organic solvent system and they correlated the findings with the structure of the compounds. The hydrolases were found to be able to esterify these organosilicon compounds, even with β-hydroxyalkylsilanes, which are unstable under the conditions of conventional acid-catalyzed esterification.

Conclusions

The enzymatic synthesis of macromolecules has generated tremendous research interest due to many inherent advantages over conventional synthetic methods. These often utilize inorganic or organic acid catalysts, inorganic or organic base catalysts and / or metal-based catalysts (and often at high temperatures). Given the commercial importance of silicone, it is somewhat surprising that the use of enzymes for synthesis of functional silicones and silicone copolymers has been reported only recently.

With the wide range of applications of silicones and their copolymers we predict that the number of such novel functional silicone based materials and products by enzymatic synthetic routes will increase significantly in the coming years.

On Robert Burns and His Poetry

The "sub-theme" of this ***American Chemical Society*** Symposium Series book is poetry. We shall therefore conclude this chapter with a poem by Robert Burns (1759-1796) of Scotland (*31*):

Epitaph on D— C—

HERE lies in Earth a root of H—l,
Set by the Deil's ain dibble; This
worthless body d—d himself, To
save the L—d the trouble.

[I was born on April 20th, 1959 – two hundred years after the birth of Robert Burns (b. January 25th, 1759). He died on July 21st, 1796 at a tragically young age for such a talented wee laddie. Had the G—d L—d taken me away at age 37 (1996), I would not have had the opportunity to collaborate with Professor Gross. Much much more importantly, I would never have know in *this* world, my beautiful son – Master Samuel S. Clarson (b. July 22, 1999).]

Acknowledgments

We thank the late Professor Robert Burns Woodward (1917-1979) for inspiration (*32*). Professor Clarson never got to meet Professor Woodward … but he did always wonder why the various components of the Waters® chromatography equipment in Tony Semlyen's laboratories at the ***University of York*** were a distinctive "blue" colour.

Professor Clarson would also like to thank Provost Bob Reid of Alcuin College, the ***University of York***, for introducing him to the poetry of Robert Burns. The private "invitation only" Burns Night events in the senior common room were among the many priveledges of being a resident of ***Alcuin College***. The "piping in" of the haggis always brought tears to this proud Scotsman's eyes. The "Tours of Scotland" with Bob Reid (and sometimes with my undergraduate chemistry tutor from ***Alcuin College*** – Dr. John McIntyre) taught me how to enjoy the finest of products from "North of the Border".

We sincerely thank the American public (*33*) for their support of this work through hard–earned money provided to the ***National Science Foundation*** who, in turn, kindly provided some funding to the ***University of Cincinnati*** (Co-PI Clarson) under the ***NSF*** TIE Grant, NSF #0631412. This grant was in collaboration with Professor Richard A. Gross (Co-PI from ***"Brooklyn POLY"***). We thank Professor Gross for helpful discussions throughout our work together. Professor Gross also provided us with some of the materials and with kind help *vis-à-vis* some aspects of the molecular characterization.

We also thank Dr. Michael J. Owen (***Michigan Molecular Institute***) and Mr. Praveen Kumar Balasubramani (the ***University of Cincinnati***) for

In Green Polymer Chemistry: Biocatalysis and Materials II; Cheng, H., et al.;
ACS Symposium Series; American Chemical Society: Washington, DC, 2013.

Publication Date (Web): November 22, 2013 | doi: 10.1021/bk-2013-1144.ch008

carefully reading the manuscript and for making some useful suggestions for its improvement.

Professor Clarson would like to thank Ms. Roxanne L. Hummel and Mr. Jeffrey R. Schaefer for their invaluable professional input and, much more importantly, for their friendship over many many years.

Dr. Poojari is now at the Department of Chemistry, the ***Ohio State University***, Columbus, OH 43210, USA.

References

1. Mark, J. E.; Allcock, H. R.; West, R. *Inorganic Polymers*, 2nd ed.; Oxford University Press: Oxford, U.K., 2005; ISBN 0-19-513119-3.
2. Van Dyke, M. E.; Clarson, S. J.; Arshady, R. In *Introduction to Polymeric Biomaterials*; Arshady R. Ed.; The PBM Series, Vol. 1; Citus Books: London, 2003; pp 109−135; ISBN 1-904536-01-8.
3. Morse, D. E. *Trends Biotechnol.* **1999**, *17*, 230.
4. Shimizu, K.; Cha, J.; Stucky, G. D.; Morse, D. E. *Proc. Natl. Acad. Sci. U.S.A.* **1998**, *95*, 6234.
5. Cha, J. N.; Shimizu, K.; Zhou, Y.; Christiansen, S. C.; Chmelka, B. F.; Stucky, G. D.; Morse, D. E. *Proc. Natl. Acad. Sci. U.S.A.* **1999**, *96*, 361.
6. Zhou, Y.; Shimizu, K.; Cha, J. N.; Stucky, G. D.; Morse, D. E. *Angew. Chem., Int. Ed.* **1999**, *38*, 780.
7. Kipping, F. S. *Proc. Chem. Soc.* **1904**, *20*, 15.
8. Clarson, S. J.; Semlyen, J. A. *Polymer* **1986**, *27*, 91.
9. Brook, M. A. *Silicon in Organic, Organometallic, and Polymer Chemistry*; Wiley: New York, 2000; p 256.
10. Tomanek, A. In *Silicones and Industry*; Hanser (Wacker Chemie): Munich, Germany, 1991.
11. Owen, M. J. In *Silicon-Based Polymer Science: A Comprehensive Resource*; Zeigler, J. M., Fearon, F. W., Eds.; American Chemical Society: ACS Advances in Chemistry Series 224; Washington, DC, 1990; p 705.
12. Owen, M. J. In *Siloxane Polymers*; Clarson, S. J., Semlyen, J. A., Eds.; Prentice Hall: Englewood Cliffs, NJ, 1993; p 309; ISBN 0-13-816315-4.
13. Belorgey, G.; Sauvet, G. In Organosiloxane Block and Graft Copolymers; Jones, R. G., et al., Eds.; *Silicone-Containing Polymers*; Kluwer Academic Publishers: The Netherlands, 2000; p 43.
14. Nishino, H.; Mori, T.; Okahata, Y. *Chem. Commun.* **2002**, 2684.
15. Bassindale, A. R.; Brandstadt, K. F.; Lane, T. H.; Taylor, P. G. *J. Inorg. Biochem.* **2003**, *96*, 401.
16. Bassindale, A. R.; Brandstadt, K. F.; Lane, T. H.; Taylor, P. G. Biocatalysis of Siloxane Bond. In *Polymer Biocatalysis and Biomaterials*; Gross, R. A., Cheng, H. N., Eds.; ACS Symposium Series 900; American Chemical Society: Washington, DC, 2005; p 164.
17. Poojari, Y.; Palsule, A. S.; Cai, M.; Clarson, S. J.; Gross, R. A. *Eur. Poly. J.* **2008**, *44* (12), 4139.

In Green Polymer Chemistry: Biocatalysis and Materials II; Cheng, H., et al.;
ACS Symposium Series; American Chemical Society: Washington, DC, 2013.

18. Sharma, B.; Azim, A.; Azim, H.; Gross, R. A.; Zini, E.; Focarete, M. L.; Scandola, M. *Macromolecules* **2007**, *40*, 7919.
19. Palsule, A. S.; Poojari, Y. *Polymer* **2010**, *51*, 6161.
20. Iroh, J. O. Poly(ethylene terephthalate). In *Polymer Data Handbook*, 2nd ed.; Mark, J. E., Ed.; Oxford University Press: New York, 2009; p 706.
21. Ji, Y. Y.; Chang, H. K.; Hong, Y. C.; Lee, S. H. *Curr. Appl. Phys.* **2009**, *9*, 253.
22. Poojari, Y.; Clarson, S. J. *Chem. Commum.* **2009**, 6834.
23. Poojari, Y.; Clarson, S. J. *Macromolecules* **2010**, *43*, 4616.
24. Poojari, Y.; Clarson, S. J. *Silicon* **2009**, *1*, 165.
25. Poojari, Y.; Clarson, S. J. *J. Inorg. Organomet. Polym.* **2010**, *20*, 46.
26. Park, J. H.; Park, K. D.; Bae, Y. H. *Biomaterials* **1999**, *20*, 943.
27. Braunmühl, V. V.; Jonas, G.; Stadler, R. *Macromolecules* **1995**, *28*, 17.
28. Bishwabhusan, S.; Brandstadt, K. F.; Lane, T. H.; Gross, R. A. *Org. Lett.* **2005**, *18*, 3857.
29. Kawamoto, T.; Sonomoto, K.; Tanaka, A. *J. Biotechnol.* **1991**, *18*, 85.
30. Uejima, A.; Fukui, T.; Fukusaki, E.; Omata, T.; Kawamoto, T.; Sonomoto, K.; Tanaka, A. *Appl. Microbiol. Biotechnol.* **1993**, *38*, 482.
31. Mackay, J. *The Land O'Burns*; HMSO: London, 1996; ISBN 0-11-495766-5.
32. Bowden, M. E.; Benfey, T. *Robert Burns Woodward and the Art of Organic Synthesis*; Publication Number 9; The Beckman Center for the History of Chemistry: Philadelphia, PA, 1992; ISBN 0-941901-08-4.
33. Morgan, E. S. *The Birth of the Republic 1763-89*, 3rd ed.; The University of Chicago Press: Chicago, 1992; ISBN 0-226-53757-9.

Publication Date (Web): November 22, 2013 | doi: 10.1021/bk-2013-1144.ch008

Publication Date (Web): November 22, 2013 | doi: 10.1021/bk-2013-1144.ch009

Chapter 9

Comparison of Polyester-Degrading Cutinases from Genus *Thermobifida*

Fusako Kawai,[*,1] Uschara Thumarat,[2,5] Kengo Kitadokoro,[3] Tomonori Waku,[3] Tomoko Tada,[3] Naoki Tanaka,[3] and Takeshi Kawabata[4]

[1]Center for Nanomaterials and Devices, Kyoto Institute of Technology, Matsugasaki, Sakyo-ku, Kyoto 606-8585, Japan
[2]Division of Applied Biology, Graduate School of Science and Technology, Kyoto Institute of Technology, Matsugasaki, Sakyo-ku, Kyoto 606-8585, Japan
[3]Division of Biomolecular Engineering, Graduate School of Science and Technology, Kyoto Institute of Technology, Matsugasaki, Sakyo-ku, Kyoto 606-8585, Japan
[4]Institute for Protein Research, Osaka University, 3-2 Yamadaoka, Suita, Osaka 565-0871, Japan
[5]Current address: Faculty of Science, King Mongkut's Institute of Technology Ladkrabang, Bangkok 10520, Thailand
[*]E-mail: fkawai@kit.ac.jp

Several specis of genus *Thermobifida* are known to possess two tandem cutinases, which have high identities and similarities with each other. *Thermobifida alba* AHK119 is a moderately thermophilic actinomycete isolated from compost. The strain possesses two tandem cutinase genes (*est1* and *est119*), which were expressed with pQE80L in *E. coli* Rosetta-gami B (DE3) as soluble active proteins with 6xhis at the C-terminal. Recombinant enzymes showed wide substrate specificity toward aliphatic and aliphatic-aromatic polyesters. They share 95% identity and 98% similarity with each other, but differ in activity and thermostability. Divalent cations, especially calcium ion, affected a lot both activity and thermostability of two enzymes. We have constructed mutant enzymes by

In Green Polymer Chemistry: Biocatalysis and Materials II; Cheng, H., et al.; ACS Symposium Series; American Chemical Society: Washington, DC, 2013.

random and site-directed mutagenesis to improve activity and thermostability. The tertiary structure of Est119 was analyzed by X-ray crystallography at 1.68 Å resolution. Based on crystalline structure and 3D modeling, we elucidated the difference of activity and thermostability in two enzymes and suggested amino acids relevant to activity and thermostability. Calcium ion was bound to the surface carboxyl and hydroxyl groups of Est119 on a loop region. Ca^{2+}-bound Est1 displayed higher Tm values than Est1 in the absence of Ca^{2+}, but no different CD spectra were found in Est1 with and without Ca^{2+}. In this report, we will compare two recombinant enzymes and elucidate their reaction mechanisms on polyesters.

Publication Date (Web): November 22, 2013 | doi: 10.1021/bk-2013-1144.ch009

Introduction

Cutinases belong to the lipase family. Not all cutinases can degrade polyester-type plastics, but recent research has shown that some cutinases play major roles in polyester degradation (*1*). Although the potential of cutinases in various applications has been known, detailed molecular characterization of cutinases has not been performed, in contrast with the depth of characterization of true lipases. Most expected application of cutinases is surface hydrophilization/functionalization and recycling of polyesters, especially of poly(ethylene terephthalate) (PET). Cutinases are discriminated from true lipases by their substrate specificity toward *p*-nitrophenyl acyl esters, with a preference for short-chain (C_4-C_6) acyl esters. Additionally, their 3D protein structure lacks a lid covering the active site, a feature that is commonly found and is requisite for interfacial activation in true lipases (*2*). Several cutinases from the genus *Thermobifida* have been cloned as polyester-degrading enzymes and characterized (*3*–*5*). All of these enzymes share a high degree of similarity, but none of them have been crystallized yet.

We have cloned two esterase genes (*est119* and *est1*) from strain AHK119 and expressed in *E. coli* (*6*, *7*). Activity and thermostability of both enzymes were remarkably enhanced by Ca^{2+}. The tertiary structure of the Est119 was analyzed by X-ray crystallography at 1.76 Å resolution. Among homologous cutinases, the lipase from *Streptomyces exfoliates* lipase (1JFR), a microbial homologue of mammalian platelet activating factor acetylhydrolases, has the only known crystal structure, although its function as a polyester-degrading enzyme is unknown (*8*). The crystal structure of Est119 is the first reported structure of a polyester-degrading cutinase among homologous cutinases (*9*).

Materials and Methods

Materials

Poly(caprolactone) (PCL; average mol wt of 40,000) was purchased from Wako Pure Chemical Industries (Japan). Poly(butylene succinate-*co*-adipate) (PBSA; Bionolle® EM-301; weight-average mol wt of 1.0×10^5) and poly(butylene

In Green Polymer Chemistry: Biocatalysis and Materials II; Cheng, H., et al.;
ACS Symposium Series; American Chemical Society: Washington, DC, 2013.

succinate) (PBS; Bionolle® #1020; weight-average mol wt of 1.3×10^5) are products of Showa Denko K. K. (Japan). Ecoflex® and Apexa® 4027 are aliphatic-*co*-aromatic polyesters (*6*). Poly (L-lactic acid) (PLLA; weight-average mol wt of 1.69×10^5) and poly(D-lactic acid) (PDLA; weight-average mol wt of 1.63×10^5) were synthesized, as described previously (*10*). Poly(3-hydroxybutyric acid) was kindly provided by Mitsubishi Gas Chem. Co., Inc. (Japan).

Cloning, Expression, and Purification

Cloning, expression and purification of two cutinases from *T. alba* AHK119 were performed, as described previously (*7*). Each gene (devoid of a sinal peptide) was ligated with pQE80L and transformed into *E. coli* Rosetta-gami B (DE3). Expression of each recombinant enzyme was induced with 0.1 mM isopropyl β-D-1-thiogalactopyranoside (IPTG) as soluble protein in cell-free extract, which was purified by affinity chromatography on a Ni-Sepharose 6 Fast Flow column (GE Healthcare, Sweden).

Assay of Enzymatic Activity

Esterase activity was measured, using *p*-nitrophenyl butyrate (PNPB). Polyesterase activity was confirmed by halo formation of LB agar plates containing 0.1% polyesters or by the decrease of turbidity of 0.05% PBSA suspension in Tris-HCl buffer (pH 7.0).

Measurement of Circular Dichroism (CD) and Differential Scanning Calorimetry (DSC)

CD measurements were carried out with a Jasco spectropolarimeter model J-720 (Tokyo, Japan) at 25 °C, using an optical cell with a path length 0.02 cm. Sample solutions were prepared in 50 mM MES or Tris (pH 7.0). Melting temperature (Tm) was measured with nano-differential scanning calorimeter (Model 6100 NanoII DSC, Calorimetry Sciences Co. Ltd., USA). Samples were deaerated *in vacuo* for 15 min prior to measurements. DSC measurements were carried out under pressure of 3 atm to avoid bubbling of samples and at a heating rate of 1°C/min.

Homology Modeling

A 3D structure of Est119 from *T. alba* AHK119 was modeled with ViewerLite 5.0 software, based on a lipase (1jfr) from *Streptomyces exfoliates* (*8*). A unit structure of PET was placed in the predicted active site as a model substrate. The crystal structure of a true lipase from *Pseudomonas* sp. MIS38 (*11*) was obtained from the NCBI protein database (http://www.ncbi.nlm.nih.gov).

In Green Polymer Chemistry: Biocatalysis and Materials II; Cheng, H., et al.;
ACS Symposium Series; American Chemical Society: Washington, DC, 2013.

Publication Date (Web): November 22, 2013 | doi: 10.1021/bk-2013-1144.ch009

Publication Date (Web): November 22, 2013 | doi: 10.1021/bk-2013-1144.ch009

Results and Discussion

Presence of Tandem Cutinase Genes among Genus *Thermobifida*

Two probable cutinase genes (*est1* and *est119*) were sequenced from *T. alba* AHK119 (*7*). The gene *est1* is located in the upstream of *est119*, which is apart by 506 bp. A homology search and alignment of *Thermobifida* cutinases was performed using the BLAST program (http://blast.genome.jp/) and Clustal W. Phylogenetic ananlysis of Est119 was performed using BLAST tree view based on the neighbor-joining method (*12*). *T. alba, T. cellulosylitica* and *T. fusca* possess two tandem cutinase genes with high sequence identities, which are categorized into cutinase 1 and cutinase 2 groups (Figure 1). Both Est1 and Est119 belonged to cutinase 2 with 95% identity and 98% similarity with each other. The conserved tandem genes enoding cutinases in *Thermobifida* suggest that the ancestor gene was duplicated and distributed among this genus. Chen et al. (*4*) indicated that two enzymes coded by tandem genes exhibit arithmetic effect on hydrolysis of PNPB, but both showed different activity levels, although their difference in amino acid sequences is not much.

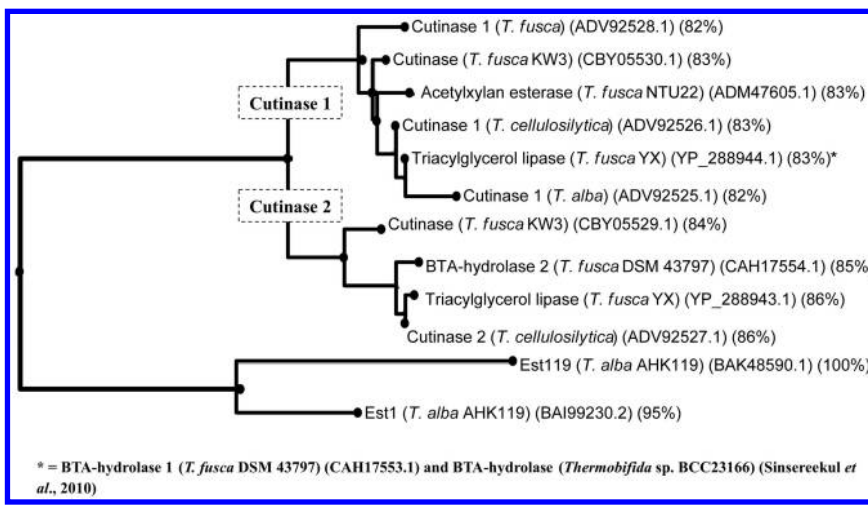

Figure 1. Phylogenic relationship of Est1 and Est119 with cutinase 1 and cutinase 2 from Thermobifida species. Identities were aligned with predicted mature protein sequences and shown in parentheses, employing Est119 as the 100% criterion. (Reproduced with permission from reference (7). Copyright 2011 Springer-Verlag).

In Green Polymer Chemistry: Biocatalysis and Materials II; Cheng, H., et al.;
ACS Symposium Series; American Chemical Society: Washington, DC, 2013.

Both enzymes showed the higher activity on PNPB than PNP-C_2 and PNP-C_8 and displayed approximately the same optimal pH and optimal temperature (around 6.0 and 50 °C). Est 1 had higher activity and thermostability than Est119. Activity and thermostability was enhanced by divalent cations, especially by Ca^{2+}. Presence of Ca^{2+} gave higher melting point (Tm) values (Figure 2) than the absence of Ca^{2+}, but did not change CD spectra (Figure 3), suggesting that Ca^{2+} does not affect the secondary strucure, but tightens the ternary protein structure by bridging surface amino acids with Ca^{2+}.

Publication Date (Web): November 22, 2013 | doi: 10.1021/bk-2013-1144.ch009

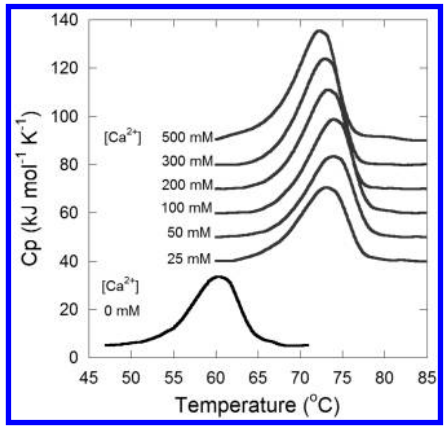

Figure 2. Change of Tm values of Est1 in the presence of Ca^{2+}.

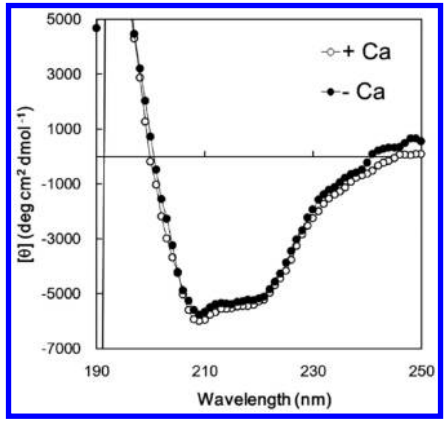

Figure 3. CD spectra of Est 1 in the presence and absence of Ca^{2+}.

In Green Polymer Chemistry: Biocatalysis and Materials II; Cheng, H., et al.;
ACS Symposium Series; American Chemical Society: Washington, DC, 2013.

Random mutagenesis of Est119 was performed by error-prone PCR in the presence of $MnCl_2$ (*13*). Mutants were screened by the size of halos at 37°C on Luria-Bertani agar plates containing 0.5% tributyrin and 0.001% Rhodamin B, 50 μg/ml ampicillin and 1 mM isopropyl β-D-1-thiogalactopyranoside, displaying that replacement of a hydrophilic amino acid to a hydrophobic amino acid in the E1 strand (see Figure 4D) enhances activity probably by hydrophobic interaction with the E2 strand (Especially Ala68Val gave the highest activity) and replacement of Ser219 to proline is requisite for the thermostability. Est 1 already has proline at 219, but not a hydrophobic amino acid at 68. Therefore, Valine was introduced at 68, resulting in that Est 1 (Ala68Val) increased the activity remarkably. Both enzymes made clear zones on polymer-agar plates including Ecoflex®, PCL, PBSA, PBS, PDLA and PLLA, when incubated at 37 °C overnight. Activities were PBSA>PCL, PBS>Ecoflex®>>PDLA. Only a slight halo appeared on PLLA after incubation for a few days. At an elevated temperature around 50°C, degradation rate of PDLA is promoted and considered as practical level. As D-lactica acid is very expensive, use of it is limited to make stereocomplex PLA consisting of PDLA and PLLA. As stereocomplex PLA has a high melting temperature close to that of PET, the future expansion of its application is expected. Recovery and recycling of D-lactic acid from stereocomplex is advantageous, for which the thermostable enzyme is probably useful. Originally strain AHK119 was isolated from compost as a potent degrader for Apexa® (a hydrolysable group is partly introduced in a polyethylene terephthalate (PET)), but Apexa® cannot be emulsified with convensional organic solvents such as methylene chloride or chloroform for use in polymer-agar plates. Apexa® is probably hydrolyzed and depolymerized in compost and depolymerized Apexa® is susceptible to enzymatic hydrolysis. Chen et al. reported that cutinase from *T. fusca* can hydrolyze PET, although they did not show data on the visible surface change of PET by scanning electronscopy. Ronkvist et al. reported hydrolysis of low crystallinity PET (ca. 7% of crystallinity) by a cutinase from *Humicola insolens,* showing the erosion of the PET surface by scanning electronscopy (*14*). Many reports on hydrolysis of PET by cutinases have been reported to show release of terephthalic aicd or weight loss (*15*, *16*). However, practical degradation of commercially available PET has not been accomplished yet. On the other hand, availability of cutinases are obvious for biodegradable polyester films such as Ecoflex®, PBSA, PBS and PLA. Our enzymes can be included as a member of polyesterases that are useful for biological treatment or recycling of biodegradable polyesters. As shown in Figure 1, all the hydrolases from genus *Thermobifida* have high similarities. Differences are mainly found in putative substrate-docking regions posited around the active cavity (Figure 4). Whether a slight difference causes a big difference in the recoginition of substrates or not still remains unsolved.

Publication Date (Web): November 22, 2013 | doi: 10.1021/bk-2013-1144.ch009

Publication Date (Web): November 22, 2013 | doi: 10.1021/bk-2013-1144.ch009

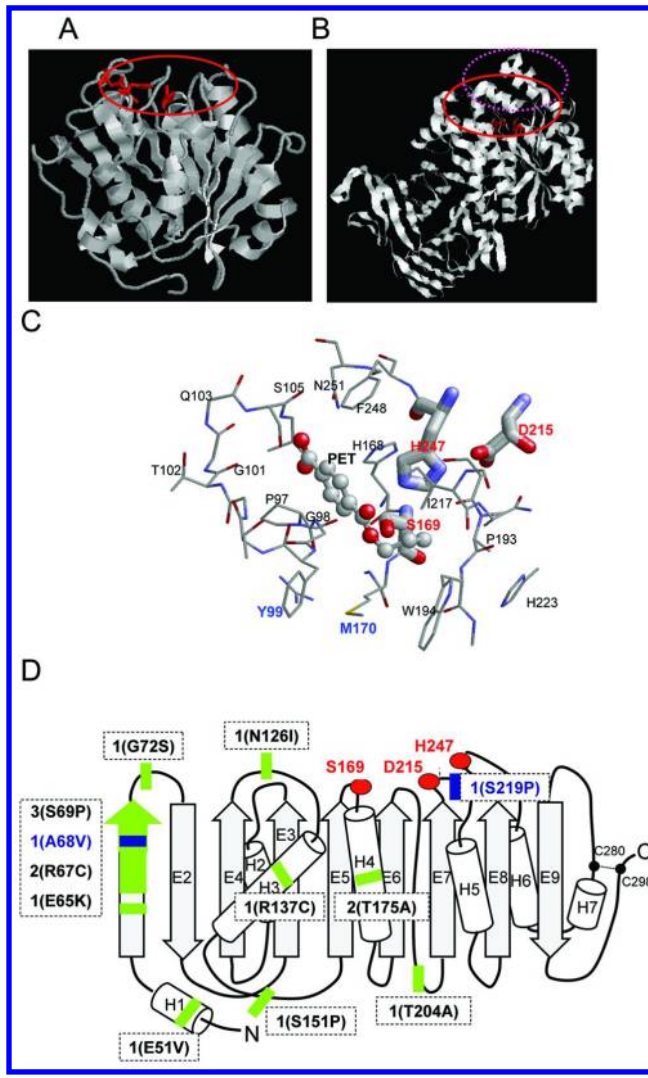

Figure 4. The predicted 3D structure of Est119. A: a ribbon diagram of the predicted 3D structure of Est119. B: The structure of a true lipase from Pseudomonas sp. MIS38. C: The active site residues docked with a monomer unit of PET. D: Topology of the predicted 3D structure of Est119. The amino acid residues in the catalytic triad are shown in red (both A and B). The lid domain of Pseudomonas sp. MIS38 lipase is circled in pink (B). The active site residues are Ser^{169}, His^{247}, and Asp^{215}. The oxyanion hole is formed by the main chin amides of Met^{170} and Tyr^{90} (C). The catalytic triad (S^{169}, D^{215}, and H^{427}) is shown in red. Mutations are shown in green. A68V and S219P are shown in dark blue (D). (Reproduced with permission from reference (7). Copyright 2011 Springer-Verlag). (see color insert)

In Green Polymer Chemistry: Biocatalysis and Materials II; Cheng, H., et al.;
ACS Symposium Series; American Chemical Society: Washington, DC, 2013.

Publication Date (Web): November 22, 2013 | doi: 10.1021/bk-2013-1144.ch009

Crystallography of Est119

As described above, the minor difference might lead to the significant difference in the substrate recoginition. To solve the relationship between the activity and the protein structure, crystallography of this group of enzymes is requisite. We could successfully analyze X-ray diffraction data on Est119 crystals only recently (*9*). This is the first crystallization of a *Thermobifida* polyesterase. The refined model of a crystal at a resolution of 1.76 Å contains two monomers in the asymmetric unit that form a dimmer interface; a single polyethylene glycol (PEG) molecule is bound in an interfacial site formed by both molecules. The crystal structure exhibits an α/β-hydrolase fold consisting of a central twisted nine β-sheet flanked on both sides by nine α-helices (Figure 5). PEG-binding site may suggest a glycol-binding site. The crystal structure of S169A mutant complex with a substrate is currently under investigation to determine the substrate-docking amino acids. When the crysal soaked in $CaCl_2$ solution was analyzed by X-ray crystallography, calcium ion was found to be bound to carbonyl and hydroxyl groups in the loop region, as shown in Figure 6. Taken this result together with CD spectra, it is reasonable to consider that calcium ion bridges surface carbonyl and hydroxyl groups on the enzyme surface and tighten the ternary structure, which might lead to the elevated activity and thermostability.

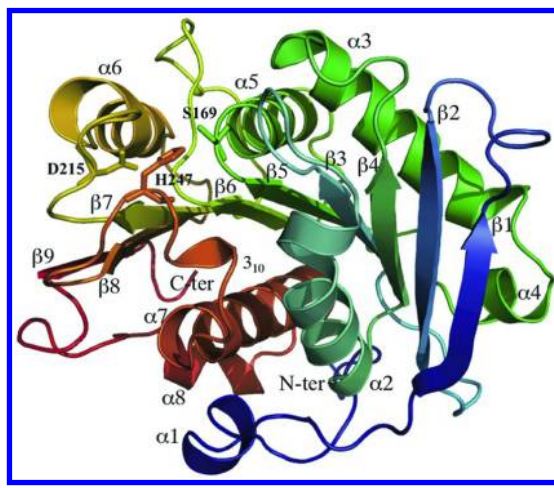

Figure 5. Ribbon diagram of the Est119 monomer; α-helices and β-strands are marked α1-α8 and β1-β9, respectively. The 3_{10} helix is also indicted. The Est119 monomer is shown in a color gradient from blue (N-terminus) to red (C-terminus). The catalytic triad, which is composed of S^{169}, D^{215} and H247, is shown as sticks. (Reproduced with permission from reference (9). Copyright 2012 Elsevier Ltd.). (see color insert)

In Green Polymer Chemistry: Biocatalysis and Materials II; Cheng, H., et al.;
ACS Symposium Series; American Chemical Society: Washington, DC, 2013.

Publication Date (Web): November 22, 2013 | doi: 10.1021/bk-2013-1144.ch009

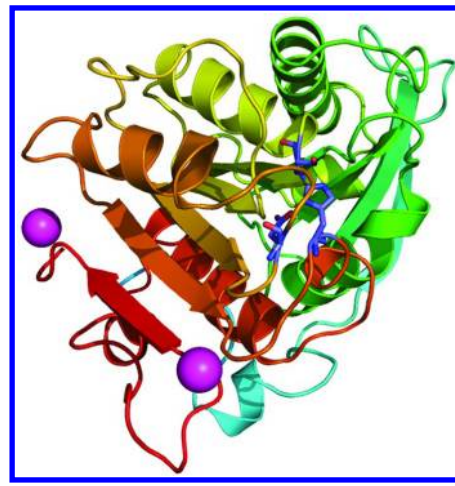

Figure 6. Calcium ions bound to a crystalline Est119. (see color insert)

Conclusion

Genus *Thermobifida* often possesses two tandem genes coding for cutinases. Both cutinases in each strain have high identity and similarity with each other and are categorized into cutinase 1 and cutinase 2 groups. Both cutinases (Est1 and Est119) of *T. alba* strain AHK119 belong to cutinase 2 group with 95% identity and 98% similarity, but they differ in activity and thermostability (Est1 has higher activity and thermostability). Different amino acids are found in loop regions surrounding the active site (probably substrate-docking loops). Divalent cations (especially Ca^{2+}) activated enzyme activity and enhanced thermostability, showing increased Tm values, but did not affect CD spectra. Ala68Val mutation elevated activity. Proline at 219 was requisite for thermostability. The crystalline structure at a resolution of 1.76 Å displayed an α/β-hydrolase fold consisting of a central twisted nine β-sheet flanked on both sides by nine α-helices. Ca^{2+} was found to be bound to the surface carbonyl and hydroxyl groups in the loop region.

Acknowledgments

We would like to thank Institute of Fermentation Osaka for the financial support to F. K. This work was also supported by JSPS Invitation Program fro East Asian Young Researchers.

References

1. Pio, T. F.; Macedo, G. A. *Adv. Appl. Microbiol.* **2009**, *66*, 77–95.
2. Schmid, R. D.; Verger, R. *Angew. Chem., Int. Ed.* **1998**, *57*, 1608–1633.
3. Dresler, K.; Heuvel, J.; Müller, R. J.; Deckwer, W. D. *Bioprocess Biosyst. Eng.* **2006**, *29*, 169–183.

4. Chen, S.; Tong, X.; Woodard, R. W.; Du, G.; Wu, J.; Chen, J. *J. Biol. Chem.* **2008**, *283*, 25854–25862.
5. Acero, E. H.; Ribitsch, D.; Steinkellner, G.; Gruber, K.; Greimel, K.; Eiteljoerg, I.; Trotscha, E.; Wei, R.; Zimmermann, W.; Zinee, M.; Cavco-Paulo, A.; Freddi, G.; Schwab, H.; Guebitz, G. *Macromolecules* **2011**, *44*, 4632–4640.
6. Hu, X.; Thumarat, U.; Zhang, X.; Tang, M.; Kawai, F. *Appl. Microbiol. Biotechnol.* **2010**, *87*, 771–779.
7. Thumarat, U.; Nakamura, R.; Kawabata, T.; Suzuki, H.; Kawai, F. *Appl. Microbiol. Biotechnol.* **2012**, *95*, 419–430.
8. Wei, Y.; Swenson, L.; Castro, C.; Derewenda, U.; Minor, W.; Arai, H.; Aoki, J.; Inoue, K.; Servin-Gonsalez, L.; Derewenda, Z. S. *Structure* **1988**, *6*, 511–519.
9. Kitadokoro, K.; Thumarat, U.; Nakamura, R.; Nishimura, K.; Karatani, H.; Suzuki, H.; Kawai, F. *Polym. Degrad. Stab.* **2012**, *97*, 771–775.
10. Kawai, F.; Nakadai, K.; Nishioka, E.; Nakajima, H.; Ohara, H.; Masaki, K.; Iefuji, H. *Polym. Degrad. Stab.* **2011**, *96*, 1342–1348.
11. Angkawidjaja, C.; You, D. J.; Matsumura, H.; Kuwahara, K.; Koga, Y.; Takano, K.; Kanaya, S. *FEBS Lett.* **2007**, *581*, 5060–5064.
12. Saitou, N.; Nei, M. *Mol. Biol. Evol.* **1987**, *4*, 406–425.
13. Niu, W. N.; Li, Z. P.; Zhang, D. W.; Yu, M. R.; Tan, T. W. *J. Mol. Catal. B: Enzym.* **2006**, *43*, 33–39.
14. Ronkvist, Å. M.; Wenchun, X.; Wenhua, L.; Gross, R. A. *Macromolecules* **2009**, *42*, 5128–5138.
15. Müller, R.-J.; Schrader, H.; Profe, J.; Dresler, K.; Deckwer, W.-D. *Macromol. Rapid Commun.* **2005**, *26*, 1400–1405.
16. Eberl, A.; Heumann, S.; Kotek, R.; Kaufmann, F.; Mitsche, S.; Cavaco-Paulo, A.; Gubitz, G. M. *J. Biotechnol.* **2008**, *135*, 45–51.

Publication Date (Web): November 22, 2013 | doi: 10.1021/bk-2013-1144.ch009

Publication Date (Web): November 22, 2013 | doi: 10.1021/bk-2013-1144.ch010

Chapter 10

"Green" Synthesis of Bisphenol Polymers and Copolymers, Mediated by Supramolecular Complexes of Laccase and Linear-Dendritic Block Copolymers

Ivan Gitsov*,[1,2] and Arsen Simonyan[2]

[1]The Michael M. Szwarc Polymer Research Institute, College of Environmental Sciences and Forestry, State University of New York, Syracuse, New York 13210
[2]Department of Chemistry, College of Environmental Sciences and Forestry, State University of New York, Syracuse, New York 13210
***E-mail: igivanov@syr.edu**

This chapter describes our recent advances on the utilization of polymer-modified laccase complexes for the "green" polymerization of strongly hydrophobic bisphenolic compounds (bisphenol A and stilbestrol) in aqueous systems. Linear-dendritic AB and ABC copolymers, composed of poly(ethylene oxide) and dendritic poly(benzyl ether)s of generations 3 and 2 (G3-PEO13k and G3-PEO13k-G2) easily form stable complex with laccase, isolated from *Trametes versicolor* upon simple mixing and stirring. Compared to the native enzyme these supramolecular systems show improved stability, activity, and overall simplicity in product separation and isolation. The products formed have molecular weights between 500 and 6000 D and are structurally characterized by size-exclusion chromatography in combination with NMR and FT-IR. It is found that the polymers contain predominantly unperturbed phenolic groups suggesting a chain growth mechanism through prevailing C-C coupling. A one-pot copolymerization of bisphenol A and diethylstilbestrol yields copolymers with interesting application potential as macroligands and/or macromonomers.

In Green Polymer Chemistry: Biocatalysis and Materials II; Cheng, H., et al.; ACS Symposium Series; American Chemical Society: Washington, DC, 2013.

Publication Date (Web): November 22, 2013 | doi: 10.1021/bk-2013-1144.ch010

Introduction

Enzymes make a good choice in any chemical transformation due to their inherent chemo-, regio- and stereo selectivity, operation in ambient temperature region, and bio-renewability as well as general lack of undesirable side reactions. However, enzymes, like most proteins, exhibit their (bio)activity almost exclusively in aqueous media. While water is a solvent very often unsuitable for organic chemistry reactions due to poor solubility of the substrates, it is the ultimate "green" solvent and there has been substantial interest recently into modification of existing and developing new organic reactions in this environmentally benign medium (*1*). Laccases (EC 1.10.3.2, p-diphenol:dioxygen oxireductase) are part of a populous family of lignolytic oxidative enzymes. They are copper containing glycoproteins of molecular weights between 50k and 80k Da, depending on the biosource. In the last decade laccase has attracted industrial attention in several areas – dye decolorization (*2*), pulp and paper bleaching (*3*, *4*), food processing (*5*) and bioremediation of polluted waste waters (*6*), as well. Laccase has been employed for the purpose of bisphenol A (BPA) removal by several groups with different success (*7–10*). There are some concerns about the toxicological levels of BPA in the environment. Its annual use has been estimated at 2.8 million tons for 2002 by the Chemical Market Associates, Inc. and has been accompanied by certain unintended amounts released. The pathways of release include but are not limited to a) chemical degradation of the respective polymers (*11*); b) leaching from liquid containers and other plastic products (*12*) and c) direct release from industrial sites. It has been known for a while that BPA is a potent hormone disruptor in mammals due to its estrogenic activity even at fairly low concentrations (*13*, *14*). The known activity of laccase towards a fairly wide range of substrates had already been shown for BPA and extended to oligo- and polymerization reactions of simple phenols (*15*), polyphenols (*16*) and even vinyl derivates (*17*) The first described syntheses that utilized laccase as organic reaction catalyst resorted to the use of biphasic water-organic solvent emulsion (*18*, *19*) or aqueous systems containing significant amounts of organic co-solvents (*20*). These seem to produce the desired materials in low to acceptable yields (typically 40-60%) and in addition to compromised environmental benefits - at the expense of organic-solvent-related rapid decrease in enzyme activity. Immobilization of laccase on solid supports provides some remedy with the possibility of multiple enzyme use sometimes in both aqueous and organic solvents, but it generally hampers seriously the conversion rates due to lack of protein molecule mobility (*21*). This paper reports the use of a supramolecular complex of laccase from *Trametes Versicolor* and linear-dendritic AB and ABC copolymers built of 3-rd (and 2-nd) generation Fréchet-type monodendrons and linear poly(ethylene oxide), PEO, with molecular mass of 13000 Da (*22*), as a green(er) polymerizing agent for two bisphenolic substrates. The polymer-enzyme nanoconstruct can be easily formed by simple addition/stirring of the linear dendritic copolymer to the aqueous enzyme solution (Scheme 1). It has been characterized (*23*), and compared to the native enzyme it has been shown to have superior oxidation activity toward various substrates such as steroids (*24*) and polyaromatic hydrocarbons including fullerene (*25*,

In Green Polymer Chemistry: Biocatalysis and Materials II; Cheng, H., et al.;
ACS Symposium Series; American Chemical Society: Washington, DC, 2013.

26). The proposed system offers a facile route to rigid polymeric constructs rich in functionality and inaccessible by conventional chemistry. Also, a significant operational benefit is presented by the recyclability, enhanced stability, activity, and overall simplicity in product harvesting and isolation. The (co)polymerization process produces predominantly higher molecular mass oligomers (degree of polymerization, DP = 4-12), unlike earlier studies where, at significantly lower substrate loads, dimers and/or unreacted monomers have been the main outcome (*27*, *28*). Diethylstilbestrol (DES), similarly to BPA, is a synthetic, strongly estrogenic but nonsteroidal substance (*29*).

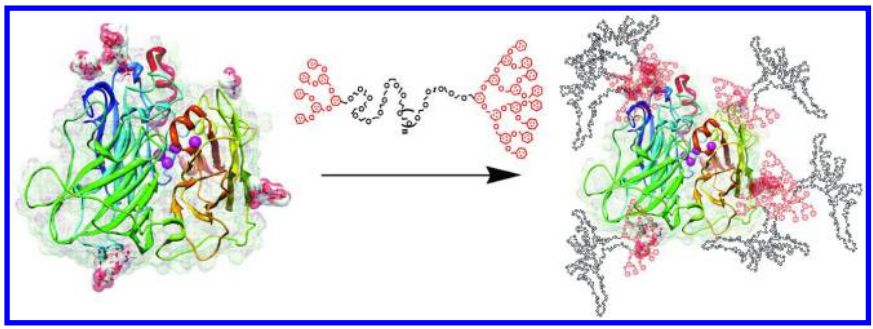

Scheme 1. Formation of a G3-PEO13k-G2/laccase complex.

The structural and chemical peculiarities of the obtained polyphenolic (co)polymeric materials have high potential to render them excellent macroligands and/or macromonomers for further polycondensation.

Experimental

Materials

The linear-dendritic copolymers [G-3]-PEO13k (LD) and [G-3]-PEO13k-[G-2] have a linear poly(oxyethylene) block with molecular weight of 13,000 Da (PEO13k) and were formed via "living" anionic polymerization of ethylene oxide initiated by a third-generation poly(benzyl ether) monodendron, [G-3] and eventual quenching of part of the "living" AB copolymer with a second-generation dendron bromide (*22*). Laccase (TVL) was produced in a three stage procedure using the basidiomycete white rot fungus *Trametes versicolor*. Isolation and purification details are provided elsewhere (*23–26*). Deionized (DI) water, (18.2 MΩ), was produced in a Barnstead Nanopure system. Tetrahydrofuran (THF) was purchased from Aldrich and distilled under nitrogen. Bisphenol A (BPA) and diethylstilbestrol (DES) (>99%) (Figure 1) were purchased from Sigma-Aldrich and used without further purification.

In Green Polymer Chemistry: Biocatalysis and Materials II; Cheng, H., et al.;
ACS Symposium Series; American Chemical Society: Washington, DC, 2013.

Publication Date (Web): November 22, 2013 | doi: 10.1021/bk-2013-1144.ch010

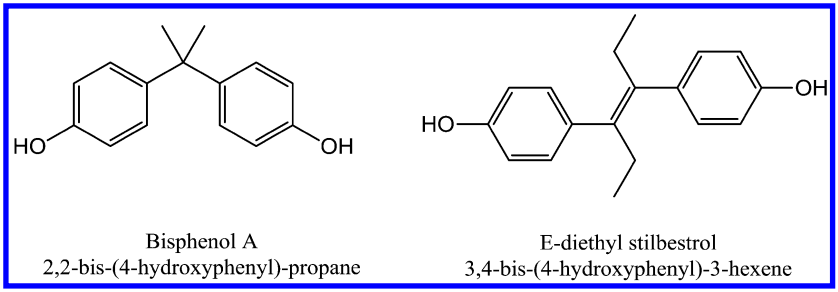

Bisphenol A
2,2-bis-(4-hydroxyphenyl)-propane

E-diethyl stilbestrol
3,4-bis-(4-hydroxyphenyl)-3-hexene

Figure 1. Names and structures of bisphenolic substrates investigated in this study.

Publication Date (Web): November 22, 2013 | doi: 10.1021/bk-2013-1144.ch010

Instrumentation

Size-exclusion chromatography (SEC) in THF was performed on a line consisting of Waters 510 pump, Waters Associates U6K injector, an Applied Biosystems 785A programmable UV-Vis detector and a dual refractive index (dRI) and differential pressure Viscotek Model 250 detector; three 5μm columns PLGel columns (50 Å, 500 Å and a mixed-pore C column) were used for the separations at 40°C and eluent flow at 1 mL/min. Data was acquired and manipulated with OmniSEC 3.1 software package and conventional calibration, based on 27 poly(styrene) standards. ^{1}H NMR spectra were taken on a Bruker Avance instrument (600MHz) in DMSO-d_6 or acetone-d_6. Deuterium exchange with minimal amounts of CH_3OH-d_4 was applied to confirm the phenolic assignments in structural characterizations. UV-Vis spectra were obtained on a Beckman 680B spectrophotometer. Infrared spectra were acquired on a Nicolet Impact 400 FT-IR instrument in solid state (neat sample).

Laccase Modification

All polymer-enzyme complexes (TVL-LD) were prepared by the following protocol: solid 1.4 ± 0.1 mg/mL linear-dendritic diblock copolymer of the type G3-PEO13k (LD) was introduced into a solution of 100× diluted native laccase (TVL) with specific activity of 6.7 μkat/mg. The solution (pH of 6.2-6.7) was stirred at room temperature for 3 hours prior to use. Identical protocol was followed with G3-PEO13k-G2 copolymer.

Polymerization Reactions

The weighed solid substrates (2.5-4 mg/mL) were initially dissolved in a minimal amount of DMSO, typically between 20 and 40 μL, and then their solutions were introduced to the TVL-LD complex while the mixtures were magnetically stirred at room temperature, and in air at atmospheric pressure. When copolymerization was attempted, two substrates were mixed in equimolar

amounts and treated like above. After the end of the reaction, products were separated and purified by the following procedure: initially the aqueous enzyme complex-substrate mixtures were centrifuged at 1000 G-force for 30 min, the clear aqueous solution of polymer-enzyme complex was filtered through 0.45 μm Whatman cellulose filter and kept at 4°C for further reuse. The precipitate (unreacted monomers and polymers formed) was collected, washed twice with DI water and dried at room temperature under vacuum. It was analyzed by SEC in THF. The separation of the oxidation product(s) was achieved by preparative fractionation on the same SEC system - the THF solvent in each fraction was evaporated and the dry contents were analyzed spectroscopically. The solids insoluble in THF were also not noticeably soluble in a number of common solvents probably due to large molecular weight and/or significant branching leading possibly to network formation. All solids were analyzed by photo-acoustic FTIR on a Nicolet Magna-IR 750 instrument where possible. The general sequence of procedures is depicted on the flow chart on Scheme 2.

Publication Date (Web): November 22, 2013 | doi: 10.1021/bk-2013-1144.ch010

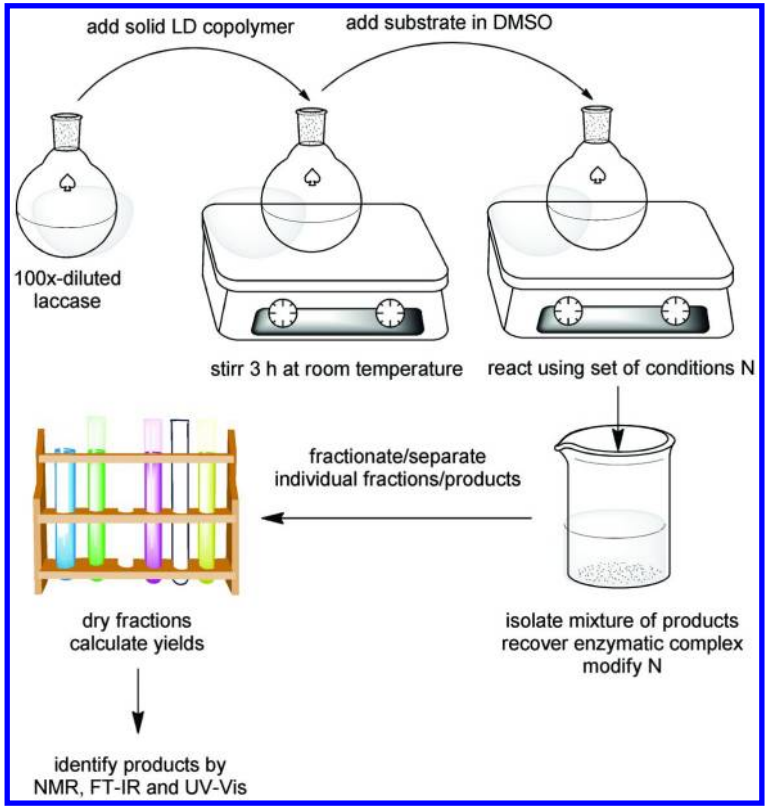

Scheme 2. Flow chart of procedures.

In Green Polymer Chemistry: Biocatalysis and Materials II; Cheng, H., et al.;
ACS Symposium Series; American Chemical Society: Washington, DC, 2013.

Publication Date (Web): November 22, 2013 | doi: 10.1021/bk-2013-1144.ch010

Results and Discussion

The benefit of complexation of laccase with linear-dendritic copolymer stems not only from the increase of substrate uptake, but also from the increase in activity, as found by our previous studies (*23*) The mechanism of complexation involves hydrophobic, π-H and hydrogen bond interactions between the dendritic blocks and the carbohydrate residues of the laccase molecule. The latter seem to be closely positioned to the channels leading to and from the active center of the enzyme, as evidenced by a sharp decrease of the catalytic activity upon their removal (*23*). Optimal concentration of copolymer in the complex was measured to be 1.4 g/L and was found to be independent from the nature of the substrates whose oxidation we have described in previous publications (*22*, *23*). Larger copolymer amounts result in the formation of separate polymeric micelles capable of binding (and thus keeping away from the enzyme active center) significant amounts of the hydrophobic reactants. Lower amounts are not sufficient for the effective substrates solubilization and therefore their oxidation is not quantitative. When no copolymer was used, no significant oxidation was observed due to poor solubilization of the hydrophobic substrates. The mechanism of the polymerization for the substrates in this study is shown on Scheme 3.

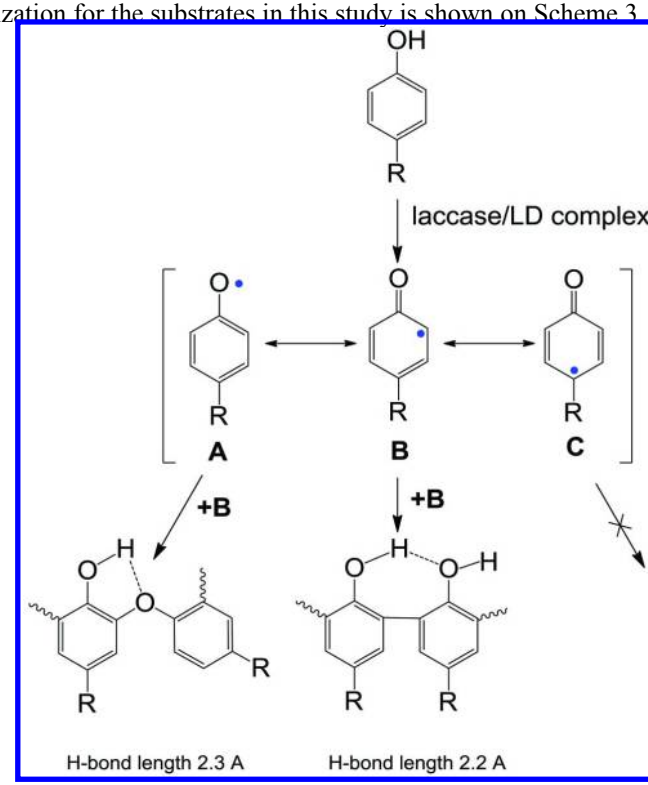

Scheme 3. Intermediate products and tentative reaction paths for bisphenols polymerized with laccase/LD copolymer complex. The hydrogen bond lengths were calculated with HyperChem ver.7.05 by geometrical optimization with the semi-empirical method AM1.

In Green Polymer Chemistry: Biocatalysis and Materials II; Cheng, H., et al.;
ACS Symposium Series; American Chemical Society: Washington, DC, 2013.

Publication Date (Web): November 22, 2013 | doi: 10.1021/bk-2013-1144.ch010

Two types of experiments were done to estimate the polymerization capabilities of our enzyme-linear dendritic copolymer system towards bisphenol A (BPA) and diethylstilbestrol (DES). Firstly the kinetic characteristics were explored and secondly – its recyclability and repeated action toward portions of fresh monomer was also studied.

Bisphenol A

Figure 2 shows an overlay of SEC chromatograms of the solids, collected from a reaction of 2 g/L BPA (44 μmol in 5 mL TvL-LD solution with activity of 12 000 U/mL, determined against syringaldazine) at 0, 2, 12, 18 and 24 h. Similarly to the previous figure, Figure 3 shows an overlay of the eluograms of the products, collected from consecutive polymerizations re-using the same TVL-LD solution, while Figure 4 is a plot of the time evolution of the content of the separated fractions with different molecular weight. In order to explain the cyclic nature of action of the enzyme complex, it is important to note that loading it with quantities of substrate larger than ~ 0.02 M seriously hampers the conversion rate and the overall yield. A similar drop in activity has also been observed in a lesser extent with water-soluble substrates, like syringaldazine, but only when the initial load exceeded 0.04 M (*23*).

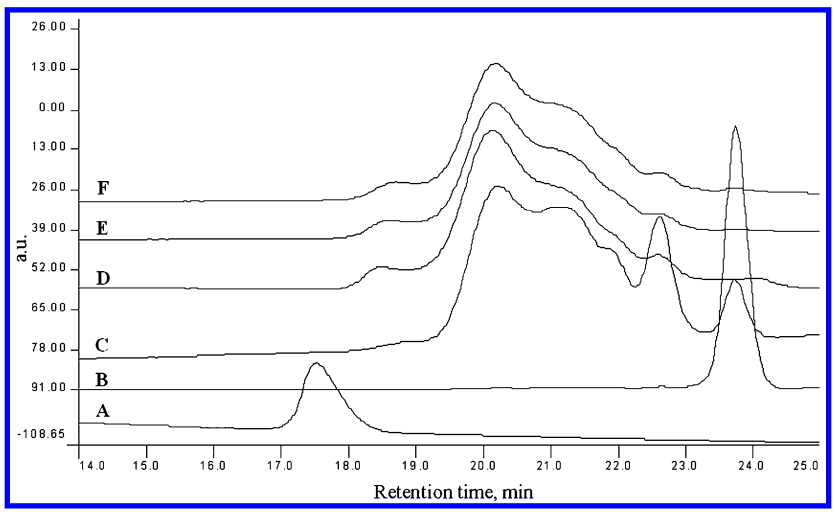

Figure 2. Overlay of SEC chromatograms of: A - G3-PEO13k copolymer and solids collected at: B - 0 h; C - 2 h; D - 12 h; E - 18 h; F - 24 h.

This phenomenon can be explained with the larger mass pressure and hence the driving force at higher concentrations for the hydrophobic substrates to enter the binding sites in the enzyme complex. However, building up high local concentration of substrate contributes to plugging the internal voids and channels of the complex ,where the actual radical recombination takes place, leading to restricted molecular mobility and effective "shut down" of the nanoreactor.

In Green Polymer Chemistry: Biocatalysis and Materials II; Cheng, H., et al.;
ACS Symposium Series; American Chemical Society: Washington, DC, 2013.

Publication Date (Web): November 22, 2013 | doi: 10.1021/bk-2013-1144.ch010

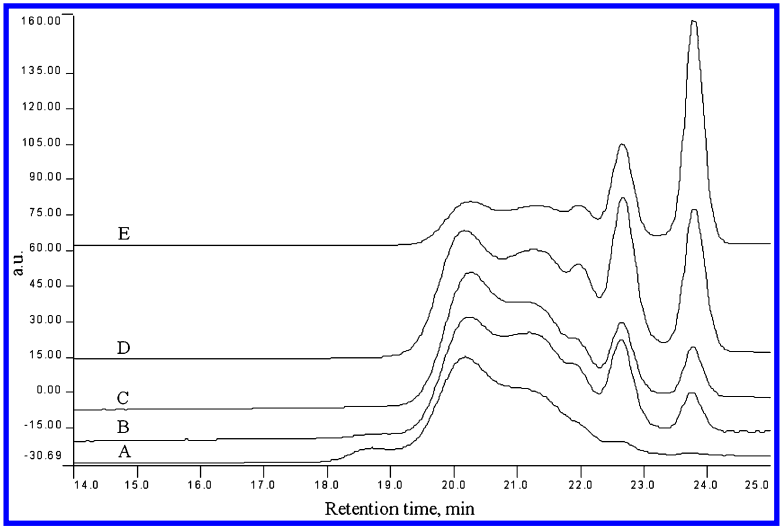

Figure 3. SEC chromatograms of the products, obtained after 24 h with the same recycled solution of the TVL-LD complex: A - cycle 1; B - cycle 2; C - cycle 4; D - cycle 6; E - cycle 8.

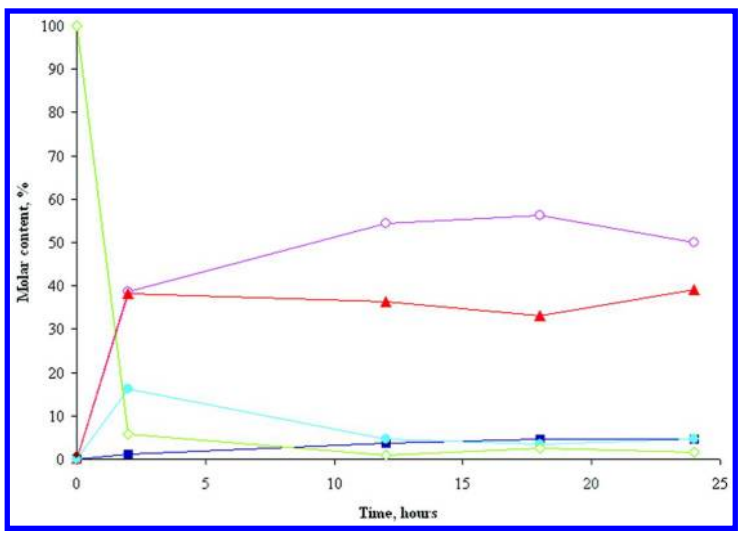

Figure 4. Molar content time evolution of different molecular weight fractions of poly-BPA: (green diamond) BPA monomer; (light blue solid circle) 700 Da [dimer]; (red triangle) 1500 Da; (purple open circle) 3000 Da; (dark blue square) 6000 Da.

It can be seen from the above kinetic data that the major changes in the system occur within the first 12 h of the reaction. Further oxidation for 24 h only slightly increases the fraction of the higher molecular weight material. The amount of free BPA decreases quickly to less than 10% in the first 2 h of the reaction, indicating good substrate-nanoreactor interaction, leading to fast monomer uptake. The molar content of dimeric BPA (~700 Da in THF-SEC) is maximal at 2 h and then slowly decreases, but remains always present in the system at ~5%. Two other fractions are always present at the highest concentrations corresponding to molecular weights 1200-1500 (1.5k) and 2700-3000 Da (3k). Apparently, the formation of these species, which are oligomers with DP ~ 4-6 and DP ~ 8-10, occurs even at the earliest stages and continues throughout the reaction. Interestingly, the trimer peak is just vaguely observable as a shoulder of the tetramer peak at 2 h, but beyond that time it almost disappears. The highest molecular weight fraction of 6000 Da forms slowly and does not exceed 4% molar content (corresponding to ~10% wt), probably due to the larger molecular size (DP ~ 16-20 units of BPA), which hampers both molecular mobility and entrance into the reactive voids of the complex. The above observations can be mechanistically explained by fast initial oxidative polymerization of monomeric BPA that has partitioned into the LD copolymer "supply reservoirs" at the entrance of the enzyme. The obtained pool of primarily dimers and probably some higher oligomers is then re-uptaken and further oxidation into tetramers occurs. The process is repeated further to obtain higher molecular weight polymers. Reactions performed at higher temperature (45°C) lead to an increase in observed molecular weight to 8500 Da and increase in its molar content from 4% to 6% (weight % increases from 10% to ~20%) probably due to both the enhanced mobility of oligomeric and polymeric chains and the expected increase in TvL activity. The observed upper limits in molecular weight may be caused by a decreasing aqueous solubility of the growing polymeric species, which in turn leads to precipitation of the larger chains once they are expelled from the TVL-LD complex. This process further impedes the penetration into the enzymatic nanoreactor and limits the maximum molecular weight at given set of conditions. In that sense, the use of organic co-solvents should increase the yield of higher molecular weight fraction as the solubility and availability of the longer chains would be overall higher. Indeed, a previous report of co-solvents used in quantities up to 1:1, report the highest molecular weight value of 21300 Da in one instance, where *Pycnoporus coccineus* laccase of unknown activity was used in up to 50% 2-propanol (*30*). It is difficult however, to compare results, obtained with enzymes from different biosources as their qualities may vary significantly. Other studies not using organic co-solvents, resorted to increasing the concentration of laccase and reacting for longer time (4 days) to obtain a marginal amount (1.7% yield) of oligomeric material with maximal molecular weight of 1450 Da (*31*). As mentioned earlier, the laccase-copolymer system (TvL-LD) does not cope well when initial substrate loading surpasses 0.02 M. Hence we examined the reusability of the enzymatic solution. The distribution of the products with different molecular weights changed in a quite regular fashion, consistent with enzyme activity decrease. From Figure 3 it can be deduced that lower molecular weight products are favored with each next cycle. The graph

shows that the fractions of unreacted BPA and dimeric BPA increase in direct proportionality with cycle number while the fraction of higher molecular weights (1500 and 3000 Da) decreases. The molar amounts of the latter components each remain around the same levels of ~40% through the 5-th cycle. It is noteworthy that the highest molecular weight fraction of 6000 Da is only formed in fairly small amounts in the second cycle and is not formed during next cycles at all. The reason for this disappearance should be sought in structural changes and reduction of activity of the enzymatic complex in the course of the reaction.

It could be argued that after every next cycle the active centers of the enzyme become increasingly inaccessible due to plugging of the internal voids with higher molecular weight species or irreversible binding of substrates. The possible connectivities between the monomers include Ph-Ph bond at the *ortho-ortho'* positions with preservation of the phenolic –OH groups, and C-O bridge, where one monomer is attached to an *ortho-* position of another by an ether bond (Scheme 3). The second linkage type reduces the overall number of –OH groups. The most abundant 2500-3000 Da (3kDa) fraction of poly(BPA) was isolated by fractional SEC and characterized with respect to the monomer by ^{1}H NMR in acetone-d_6 and by FT-IR spectroscopy of films cast from THF on NaCl plates. The corresponding spectra are presented in Figures 5 and 6. Overall, the NMR signals in the polymer are notably broadened, except for the phenolic protons. They are convenient basis for comparison with the monomeric BPA as their location is either next to new Ph-Ph / Ph-O-Ph bonds, or remains relatively unperturbed if no coupling occurred at the respective phenolic moiety of BPA. Indeed, analysis of the Ph-O**H** region from the polymer shown on Figure 5B reveals three new downfield Ph-O**H** signals at 8.11, 8.36 and 10.82 ppm in addition to a signal very close in value to that of the original phenolic proton at 8.08 ppm (Figure 5A). SEC analyses did not show presence of unreacted bisphenol A, hence the unchanged signal must be from a phenolic moiety, which is close or at the chain end. The first signal downfield at 8.11 ppm belongs probably to phenyl protons next to Ph-Ph bonds, while the second at 8.36 ppm is neighboring a Ph-O-Ph bond and is further downfield due to the higher electron withdrawing capability of a directly connected oxygen atom (see scheme 3). This signal is much smaller compared to the others hinting at the lower abundance of ether linkages as compared to biphenylene ones.

Apart from these, there is a strong signal at the far left, which is probably belonging to phenolic protons participating in multiple intramolecular H-bonding of the type shown on Scheme 3. The bands in the IR spectrum show several notable features. The O-H band is strong like in the starting BPA and probably wider due to extended intra- and intermolecular H-bonding. The Ph-OH stretch from the BPA at 1220 cm^{-1} is preserved as expected, but has developed more complex sub-structure due to the multiple phenolic moieties in different sub-environments. The Ph-O-Ph vibration also contributes to the structure above 1200 cm^{-1} and gives rise to a new typical aryl ether band in the polymeric material at 1010 cm^{-1}. In the fingerprint region it is notable that the band characteristic for 1,4-substituted phenyl rings from the BPA at 825 cm^{-1} is preserved due to the unreacted phenolic moieties, but new poly-substituted benzene ring absorption is also observable at 938 cm^{-1}.

Publication Date (Web): November 22, 2013 | doi: 10.1021/bk-2013-1144.ch010

In Green Polymer Chemistry: Biocatalysis and Materials II; Cheng, H., et al.;
ACS Symposium Series; American Chemical Society: Washington, DC, 2013.

Publication Date (Web): November 22, 2013 | doi: 10.1021/bk-2013-1144.ch010

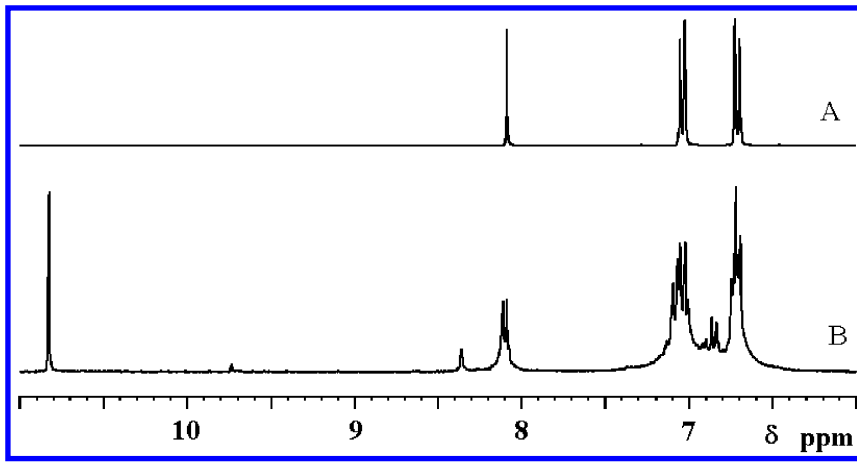

Figure 5. [1]H NMR spectra of A - monomer BPA and B- polymer, poly(BPA).

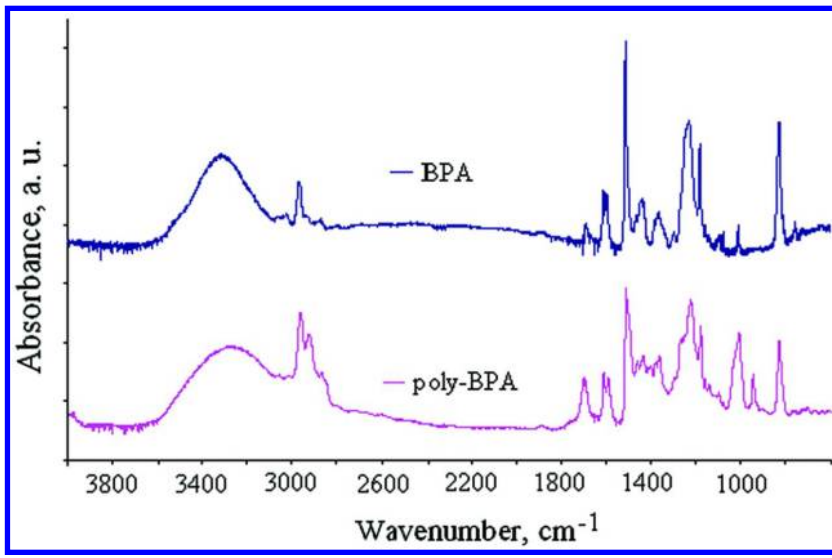

Figure 6. Stack of FT-IR spectra of monomer, BPA and polymer, poly-BPA.

Diethylstilbestrol

Chromatographic data of this substrate is presented in the same order as in previous section: Figure 7 shows an overlay of SEC chromatograms of the solids collected from a reaction of 2.22 g/L DES (33 μmol in 4 mL TvL-LD with activity of 12 000 U/mL, determined against syringaldazine) at 1, 20, 26, 45 and 120 hours; Figure 8 is a plot of the contents of the separate molecular weight fractions in the product mixtures vs. time; Figure 9 shows an overlay of the chromatograms of the poly-DES products collected from consecutive polymerizations (120 h each) re-using the same enzymatic nanoreactor solution.

In Green Polymer Chemistry: Biocatalysis and Materials II; Cheng, H., et al.;
ACS Symposium Series; American Chemical Society: Washington, DC, 2013.

Publication Date (Web): November 22, 2013 | doi: 10.1021/bk-2013-1144.ch010

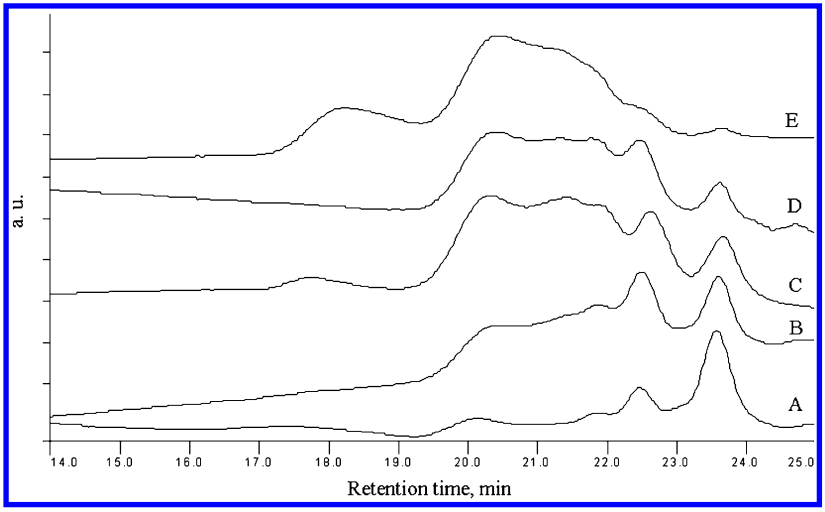

Figure 7. SEC traces of DES polymerization products at A - 1 h; B - 20 h; C - 26 h; D - 45 h; E - 120 h.

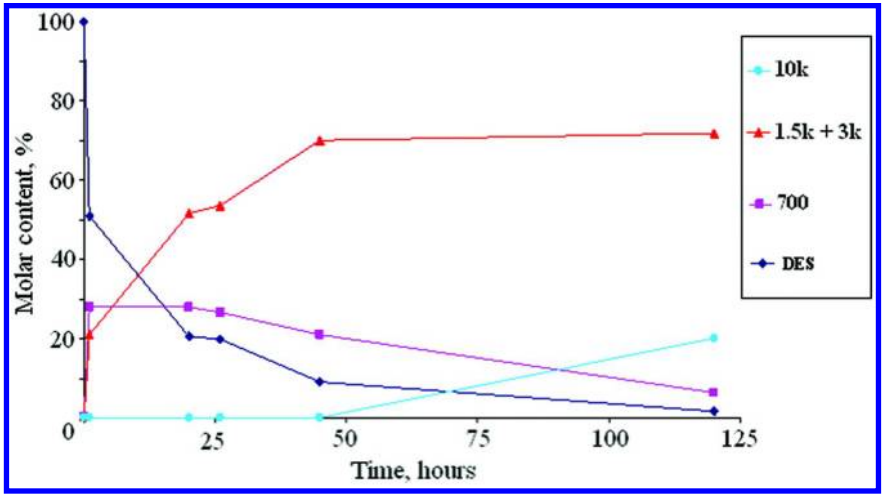

Figure 8. Molar content evolution of different molecular weight fractions of oxidized DES with time; (dark blue diamond) monomer DES; (purple square) dimeric DES; (red triangle) 1500-3000 Da; (light blue circle) 10 000 Da.

It can be noticed that the amount of free DES drops below 10% after 45 hours of the reaction, indicating relatively slow conversion, as compared to BPA. Conversion does not reach 100% even after 5 days (120 h). The molar content of dimeric DES reaches 28% in 1 h and remains at the same level for the next 24 h after which it slowly decreases to levels of about ~10% after 5 days. The two

In Green Polymer Chemistry: Biocatalysis and Materials II; Cheng, H., et al.;
ACS Symposium Series; American Chemical Society: Washington, DC, 2013.

other fractions exhibit very similar molecular weights to the ones from the BPA reactions: 1200-1500 (1.5k) and 2700-3000 (3k), but are more overlapping in this case and hence not calculated jointly. The molar content of those materials increases fairly quickly to ~70% within the first 48 h of the reaction. The above kinetic data shows a much longer time of conversion as compared to BPA. The bulk of the DES monomer takes 48 h to react against 12 h for BPA. It is peculiar that no high molecular weight (above 3000 Da) is present before the 120 h. Also, this fraction possesses relatively higher molecular (~10 000 Da) weight than the corresponding BPA fraction (~6000 Da). The overall slower polymerization of DES is related to the larger size of its molecule, which leads to a smaller diffusion coefficient and slower uptake into the nanoreactor and also contributes to limited mobility inside. Apart from that, although full coplanarity between the middle double bond and the phenyl rings is not possible due to the bulky ethyl residues, poly(DES) has polyconjugated character (seen also in its UV-Vis spectrum, where a batochromic shift occurs from colorless monomer to deep yellow-orange polymer). This stiffens the backbone of the polymer and additionally decreases molecular mobility and diffusion into the nano-sized reactive channels of the complex. In comparison, poly-BPA is more flexible due to the sp^3 carbon atom between the phenolic moieties (additional conjugation occurs only at the newly formed Ph-Ph linkages) and hence benefits from easier transport through the nanoreactor. The differences between BPA and DES polymerization processes can be traced in an enzymatic nanoreactor solution reuse experiment. The relevant chromatograms for DES are presented in Figure 9. The first and most notable difference is that the enzymatic complex could not be reused effectively for more than 4 times as compared to 8 times with BPA. Also, no high molecular weight fraction above 3000 Da was produced beyond the first use, and the 3000 Da fraction quickly decreases to below 10% in the 4-th cycle of use. The conversion decreases linearly with every next use of the complex to drop below 90 % in the second cycle and to ~50% in the last cycle. In comparison, BPA decreases its conversion below 90% after 5 cycles of enzymatic complex reuse. The reuse characteristics of the DES polymerization are in agreement with the kinetic data and point to a stiffer, less mobile polymer chain of poly-DES. This apparently leads to increased plugging of the internal voids of the complex and overall faster decrease in reactivity compared to BPA.

To shed some light on the structure of the obtained poly(DES), the ^{1}H NMR spectrum of an isolated 1,5k-3k fraction was recorded in acetone-d_6 (indicative phenolic –OH region shown on Figure 10, stacked with the respective spectrum of pure DES) Three separate phenolic proton signals can be distinguished. The original spectrum of DES shows two peaks (8.07 and 8.31 ppm) because the compound is a mixture of *cis*- and *trans*- isomers in ratio ~ 1 : 4. In the oligomeric product the peak at 8.31 ppm has shifted slightly upfield and split into two new peaks at 8.26 and 8.23 ppm, respectively. Similarly, the 8.07 ppm Ph-OH signal of the Z-isomer has also shifted upfield by 0.05 ppm. There can be seen a bump of about 10% of the intensity of the main peaks, which is downfield by 0.15 ppm, compared to the original 8.31 ppm Ph-OH peak. These observations are consistent with primarily Ph-Ph coupling and marginally occurring -C-O- type of connectivity between the DES monomers, just as observed with BPA. The

In Green Polymer Chemistry: Biocatalysis and Materials II; Cheng, H., et al.;
ACS Symposium Series; American Chemical Society: Washington, DC, 2013.

Publication Date (Web): November 22, 2013 | doi: 10.1021/bk-2013-1144.ch010

increasing conjugation in the oligomeric molecule causes the slight upfield shifts of the phenolic protons when additional conjugation by Ph-Ph bonding occurs. The main peak at 8.26 ppm is likely belonging to a monomer connected only to one another monomer, while the 8.23 ppm should indicate double linkage. The aromatic proton region is not shown here as it is too crowded due to the presence of both E- and Z- isomers of DES and no structure indicative information is readily useful. Contrary to poly-BPA, no signal above 9 ppm has been observed, indicating different nano-environment and H-bonding patterns in poly-DES.

Publication Date (Web): November 22, 2013 | doi: 10.1021/bk-2013-1144.ch010

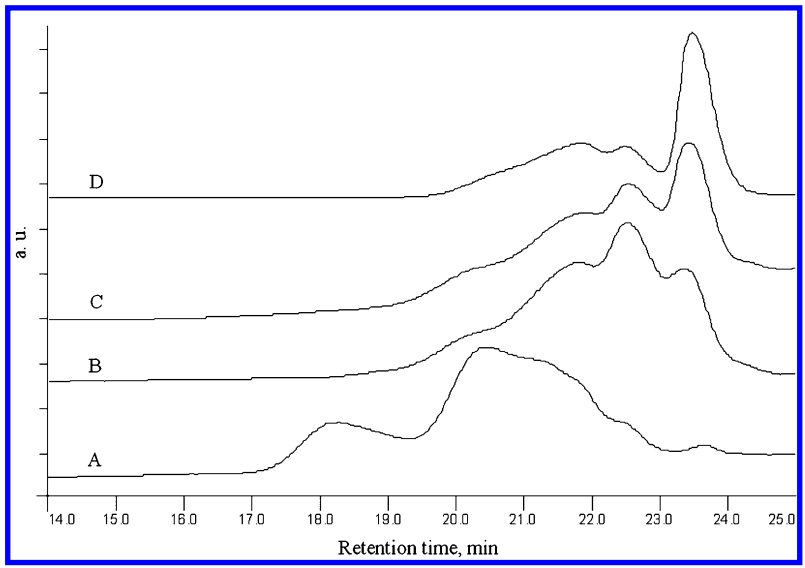

Figure 9. THF SEC chromatograms of the products obtained after 120 h with the same recycled solution of the laccase-LD complex: A - cycle 1; B - cycle 2; C - cycle 3; D - cycle 4.

The FT-IR spectra (Figure 11) are also in good agreement with the previous data and confirm the presence of large number of –OH groups. The ratio between the areas of –OH peaks and C-H for example does not change from DES to poly-DES, prompting preservation of the phenolic moieties. The group of bands between 1258 and 1148 cm^{-1} form a new group of three distinguishable broadened bands – 1233 cm^{-1} (Ph-OH), 1105 cm^{-1} (skeletal vibration of 1,4-substituted Ph-ring) and 1024 cm^{-1} typical for the Ph-O-Ph vibration. Also, a new 950 cm^{-1} band appears, indicating the poly-substitution at phenyl rings.

In Green Polymer Chemistry: Biocatalysis and Materials II; Cheng, H., et al.;
ACS Symposium Series; American Chemical Society: Washington, DC, 2013.

Publication Date (Web): November 22, 2013 | doi: 10.1021/bk-2013-1144.ch010

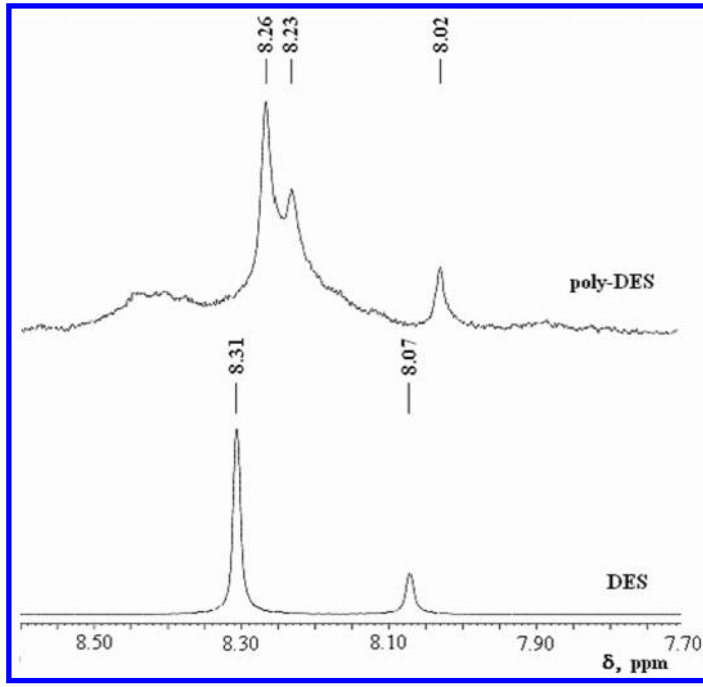

Figure 10. [1]H NMR spectra of monomer, DES and polymer, poly-DES.

Copolymerization of BPA and DES

Based on the reactivity and rate of polymerization from the previous sections, it is envisioned that substrates with similar parameters will be able to copolymerize if introduced together in the nano-reactor. The obtained polymer was characterized by SEC. The resolution of the column set is within 2% for molecular weights below 1000 Da and therefore the method could be used as a reliable analytical source of structural information. Two identical injections were made from the same sample and detected at wavelength corresponding to a UV absorption maximum of BPA and of DES. These wavelengths were determined to be 250 nm for DES and 287 nm for BPA. Then the two chromatograms were overlaid – they are shown on Figure 12. It is easily noticeable that the unreacted monomers elute at different times due to their different molecular weight (and hydrodynamic volume) – 228.3 Da for BPA (Retention time = 23.6 min) and 268.4 Da for DES (Retention time = 23.3 min). However, the peak at 22.6 min corresponding to the dimer is identical at both wavelengths – it has the same elution time and same elution profile. The characteristic peak parameters of the higher DP oligomers and polymers completely coincide, as well, indicating that all products contain both DES and BPA repeating units. To confirm that the dimer is a mixed dimer of both substrates, its elution time was compared to the elution

In Green Polymer Chemistry: Biocatalysis and Materials II; Cheng, H., et al.;
ACS Symposium Series; American Chemical Society: Washington, DC, 2013.

times of dimers from homopolymerization reactions of BPA and of DES. The dimer regions were overlaid and the pattern obtained (Figure 13) indicates that the dimer from the copolymerization reaction is a compound with retention time of 22.6 min in the middle between the respective times of DES_2 (22.4 min) and BPA_2 (22.8 min). The only reasonable explanation of this data is that a mixed dimer and mixed oligomers have been exclusively formed in the copolymerization reaction.

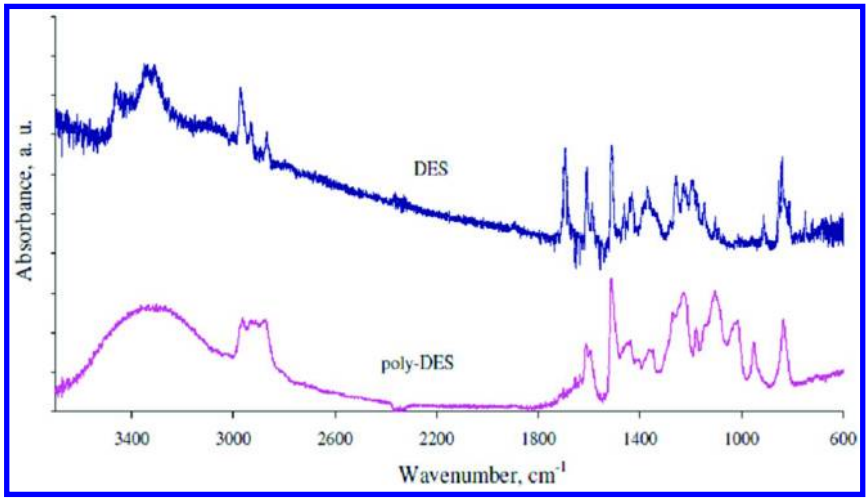

Figure 11. FT-IR spectra of monomer, DES, and polymer, poly-DES.

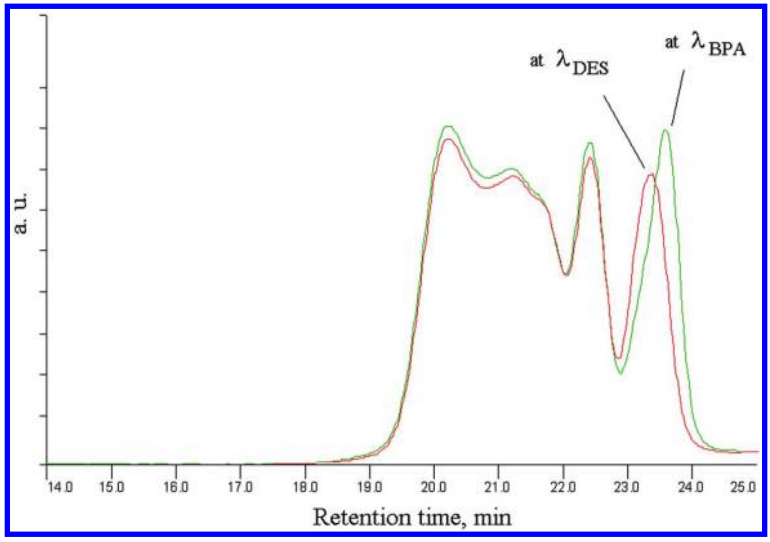

Figure 12. Overlay of SEC-UV traces from two consecutive injections of the same BPA/DES copolymerization mixture, recorded at the specific wavelengths of both comonomers.

In Green Polymer Chemistry: Biocatalysis and Materials II; Cheng, H., et al.;
ACS Symposium Series; American Chemical Society: Washington, DC, 2013.

Publication Date (Web): November 22, 2013 | doi: 10.1021/bk-2013-1144.ch010

Publication Date (Web): November 22, 2013 | doi: 10.1021/bk-2013-1144.ch010

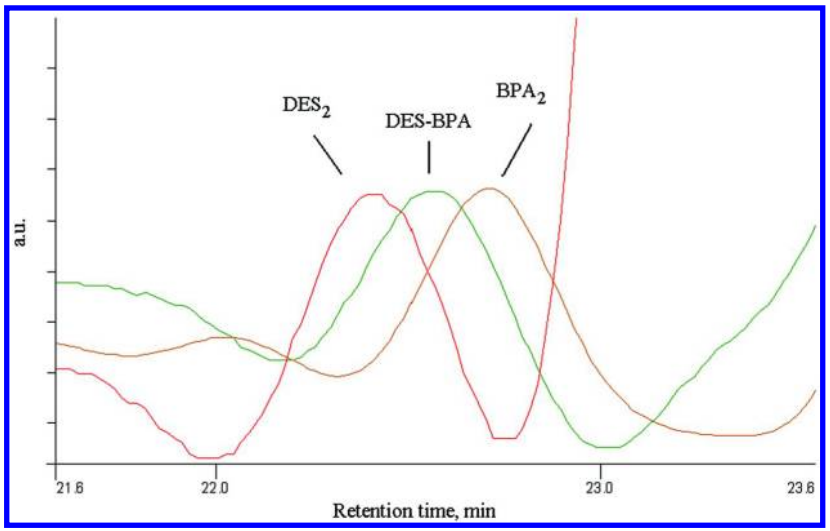

Figure 13. Overlay of SEC-dRI traces showing the dimer regions of BPA-, DES- and BPA/DES polymerization mixtures.

Conclusions

The results of this study indicate that the developed polymer-enzyme nano-reactor offers a convenient and greener approach towards materials that have a strong potential for applications ranging from polyphenolic macromonomers for polyethers and polycarbonates, which are inherently more stable and unable to leach their ingredients (BPA), to macroligands, poly-conjugated materials with specific opto-electronic properties and (co)poly-drugs (DES). The working principle of this particular enzyme system suggests that the polymer-modification concept can also be applied to other (glycoprotein) enzymes possibly dramatically enhancing their substrate range and reactivity (see ref. (*32*) for further developments). A long sought outcome of the development of such reactions would also be the decreased or even eliminated dependence on organic solvents, lower energy consumption and ultimately - a diminished cost of the products. Furthermore, more than one enzyme could be employed and conditions for cascade reactions may be created.

Acknowledgments

This study was made possible through partial funding by the National Science Foundation (CBET 0853454). Gratitude is extended to Dr. Stuart Tanenbaum and Dr. Albert Krastanov for inspirational discussions. Thanks are also due to Mr. Anthony Fuoco who assisted in some of the copolymerizations and in the chromatographic fractionation of the different polymerization mixtures.

References

1. Li, C.; Chen, L. *Chem. Soc. Rev.* **2006**, *35*, 68.
2. Claus, H.; Faber, G.; König, H. *Appl. Microbiol. Biotechnol.* **2002**, *59*, 672.
3. Bajpai, P. *Biotechnol. Prog.* **1999**, *15*, 147.
4. Rochefort, D.; Leech, D.; Bourbonnais, R. *Green Chem.* **2004**, *6*, 14.
5. Minussi, R. C.; Pastore, G. M.; Duran, N. *Trends Food Sci. Technol.* **2002**, *13*, 205and references therein.
6. Torres, E.; Bustos-Jaimes, I.; Borgne, S. *Appl. Catal., B* **2003**, *46*, 1.
7. Diano, N.; Grano, V.; Fraconte, L.; Caputo, P.; Ricupito, A.; Attansio, A.; Bianco, M.; Bencivenga, U.; Rossi, S.; Manco, I.; Mita, L.; Del Pozzo, G.; Mita, D. *Appl. Catal., B* **2007**, *69*, 252.
8. Kim, Y.; Nicell, J. *Bioresource Technol.* **2006**, *97*, 1431.
9. Modaressi, K.; Taylor, K.; Bewtra, J.; Biswas, N. *Water Res.* **2005**, *39*, 4309.
10. Okazaki, S.; Michizoe, J.; Goto, M.; Furusaki, S.; Wariishi, Y.; Tanaka, H. *Enzyme Microb. Technol.* **2002**, *31*, 227.
11. Factor, A. Mechanisms of Thermal and Photodegradations of Bisphenol A Polycarbonate. In *Polymer Durability: Degradation, Stabilization, and Lifetime Prediction*; Clough, R. L., Billingham, N. C., Gillen, K. T., Eds.; Advances in Chemistry Series 249; American Chemical Society: Washington, DC, 1996; pp 59−76.
12. Brede, C.; Fjeldal, P.; Skjevrak, I.; Herikstad, H. *Food Addit. Contam.* **2003**, *20*, 684.
13. Honma, S.; Suzuki, A.; Buchanan, D. L.; Katsu, Y.; Watanabe, H.; Iguchi, T. *Reprod. Toxicol.* **2002**, *16*, 117.
14. Howdeshell, K.; Hotchkiss, A.; Thayer, K.; Vandenbergh, J.; vom Saal, F. *Nature* **1999**, *401*, 763.
15. Ikeda, R.; Sugihara, J.; J. Uyama, H.; Kobayashi, S. *Macromolecules* **1996**, *29*, 8702.
16. Uyama, H.; Kobayashi, S. *Adv. Polym. Sci.* **2006**, *194*, 51.
17. Singh, A.; Kaplan, D. *J. Polym. Environ.* **2002**, *10*, 85.
18. Lugaro, G.; Carrea, G.; Cremonesi, P. *Arch. Biochem. Biophys.* **1973**, *159*, 1.
19. D'Acunzo, F. *J. Mol. Catal. B: Enzym.* **2004**, *31*, 25.
20. Kobayashi, S.; Uyama, H.; Ushiwata, T.; Uchiyama, T.; Sugihara, J.; Kurioka, H. *Macromol. Chem. Phys.* **1998**, *199*, 777.
21. Duran, N.; Rosa, M.; D'Annibale, A.; Gianfreda, L. *Enz. Microb. Technol.* **2002**, *31*, 907.
22. Gitsov, I.; Simonyan, A.; Vladimirov, N. G. *J. Polym. Sci.: Part A: Polym. Chem.* **2007**, *45*, 5136.
23. Gitsov, I.; Hamzik, J.; Ryan, J.; Simonyan, A.; Nakas, J. P.; Krastanov, A.; Omori, Sh.; Cohen, T.; Tanenbaum, S. *Biomacromolecules* **2008**, *9*, 804.
24. Gitsov, I.; Simonyan, A.; Krastanov, A., Tanenbaum, S. Green Oxidation of Steroids in Nanoreactors Assembled from Laccase and Linear-Dendritic Copolymers. In *Polymer Biocatalysis and Biomaterials II*; Gross, R. A.Cheng, H. N., Eds.; ACS Symposium Series 999; American Chemical Society: Washington, DC, 2008; pp 110−128.

25. Gitsov, I.; Lambrych, K.; Lu, P.; Nakas, J.; Ryan, J.; Tanenbaum, S. Nondestructive Regioselective Modification of Laccase by Linear-Dendritic Copolymers: Enhanced Oxidation of Benzo-α-Pyrene in Water. In *Polymer Biocatalysis and Biomaterials*; Gross, R. A.Cheng, H. N., Eds.; ACS Symposium Series 900; American Chemical Society: Washington, DC 2005; pp 80−94.
26. Gitsov, I.; Simonyan, A.; Wang, L.; Krastanov, A.; Tanenbaum, S. W.; Kiemle, D. *J. Polym. Sci., Part A: Polym. Chem.* **2012**, *50*, 119.
27. Uchida, H.; Fukuda, T.; Miyamoto, H.; Kawabata, T.; Suzuki, M.; Uwajima, T. *Biochem. Biophys. Res. Commun.* **2001**, *287*, 355.
28. Fukuda, T.; Uchida, H.; Suzuki, M.; Miyamoto, H.; Morinaga, H.; Nawata, H.; Uwajima, T. *J. Chem. Technol. Biotechnol.* **2004**, *79*, 1212.
29. Toda, K.; Hayashi, Y.; Okada, T.; Morohashi, K.; Saibara, T. *Mol. Cell. Endocrinol.* **2005**, *229*, 119.
30. Mita, N.; Tawaki, S.; Uyama, H.; Kobayashi, S. *Macromol. Biosci.* **2003**, *3*, 253.
31. Uchida, H.; Fukuda, T.; Miyamoto, Y.; Kawabata, T.; Suzuki, M.; Uwajima, T. *Biochem. Biophys. Res. Commun.* **2001**, *287*, 355.
32. Junker, K.; Gitsov, I.; Quade, N.; Walde, P. *Chem. Pap.* **2013**, *67*, in press.

Publication Date (Web): November 22, 2013 | doi: 10.1021/bk-2013-1144.ch010

Publication Date (Web): November 22, 2013 | doi: 10.1021/bk-2013-1144.ch011

Chapter 11

Synthesis of New Polysaccharide Materials by Phosphorylase-Catalyzed Enzymatic α-Glycosylations Using Polymeric Glycosyl Acceptors

Jun-ichi Kadokawa*

Graduate School of Science and Engineering, Kagoshima University, 1-21-40 Korimoto, Kagoshima 890-0065, Japan
***E-mail: kadokawa@eng.kagoshima-u.ac.jp**

This chapter reviews the synthesis of new polysaccharide materials by means of phosphorylase-catalyzed enzymatic α-glycosylations using polymeric glycosyl acceptors (or primers). Glycogen-based polysaccharide materials having the elongated amylose graft-chains were prepared by the phosphorylase-catalyzed successive α-glucosylations (polymerization) using glycogen as a multifunctional polymeric acceptor. Highly branched anionic polysaccharides were also synthesized by the phosphorylase-catalyzed α-glucuronylation of glycogen. The synthesis of amylose-grafted heteropolysaccharides composed of abundant polysaccharide main-chains, such as chitin/chitosan, (carboxymethyl)cellulose, alginate, and xanthan gum, was achieved by the phosphorylase-catalyzed enzymatic polymerization using the corresponding maltooligosaccharide-grafted polysaccharide acceptors.

Introduction

Polysaccharides are naturally occurring carbohydrate polymers, where each monosaccharide residue is linked directly through glycosidic linkage in the main-chain (*1*, *2*). A glycosidic linkage is a type of covalent bond that joins a monosaccharide residue to another group, which is typically another saccharide residue. Natural polysaccharides are found in various sources such as plant,

In Green Polymer Chemistry: Biocatalysis and Materials II; Cheng, H., et al.;
ACS Symposium Series; American Chemical Society: Washington, DC, 2013.

Publication Date (Web): November 22, 2013 | doi: 10.1021/bk-2013-1144.ch011

animal, seaweed, and microbial kingdoms, where they serve as vital materials for important *in vivo* functions, e.g., providing an energy resource, acting as a structural material, and conferring specific biological properties (*1*, *2*). Natural polysaccharides have very complicated structures owing not only to a structural diversity of monosaccharide residues, but also to the differences in stereo- and regio-types of glycosidic linkages. In contrast, the other two major biological polymers, that is, nucleic acids and proteins have relatively simple structures because they are constructed by a type of specific linkage between several kinds of nucleotides and 20 kinds of amino acids, respectively (*3*). The large diversity of polysaccharide structures contributes to serve a whole range of biological functions in the host organism, and a subtle change in the chemical structure has a profound effect on the properties and functions of the polysaccharides (*4–6*). Therefore, the preparation of artificial polysaccharides has attracted increasingly much attention because of their potential applications as materials in the fields related to medicine, pharmaceutics, cosmetics, and food industries.

Figure 1 shows a typical schematic reaction for the formation of a glycosidic linkage, so-called 'glycosylation' for the possible formation of α-(1→4)- and β-(1→4)-linked glucose dimers from two glucose substrates (maltose and cellobiose derivatives, respectively) (*7–9*). For design of the two substrates, that is, glycosyl donor and acceptor, an anomeric carbon (C1) of the glycosyl donor is activated by introducing a leaving group (X), and a hydroxy group in the glycosyl acceptor, which takes part in the reaction, is employed as a free form, whereas the other hydroxy groups in both the donor and acceptor are protected. For stereo- and regioselective construction of the glycosidic linkage, a leaving group, protective groups, a catalyst, and a solvent should appropriately be selected. Although polysaccharide is theoretically produced by the repeated glycosylations, only one kind of linkages among multiple stereo- and regiofashions during the repeated reactions must be constructed to give the products with well-defined structure. As appeared in two representative natural polysaccharides, i.e., cellulose and starch, the importance of the fashions in glycosidic linkages of the polysaccharides is significant for their functions (*10*, *11*). Cellulose and starch are composed of the same structural unit, i.e., an anhydroglucose unit, but are linked through different α-(1→4)- and β-(1→4)-glycosidic linkages, respectively. Owing to the difference in such stereochemistry of glycosidic linkages in cellulose and starch, their roles in nature are completely different; the former is the structural material and the latter acts as the energy resource. From the viewpoint of synthetic chemistry, however, the perfection of the selectivities in glycosidic linkages still remains a difficult barrier in the general chemical glycosylations (*12*).

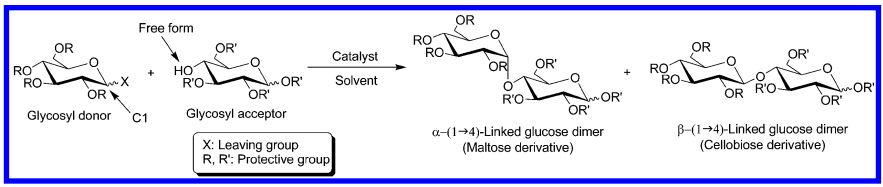

Figure 1. Typical reaction manner of glycosylation between two glucose substrates.

In Green Polymer Chemistry: Biocatalysis and Materials II; Cheng, H., et al.;
ACS Symposium Series; American Chemical Society: Washington, DC, 2013.

Publication Date (Web): November 22, 2013 | doi: 10.1021/bk-2013-1144.ch011

To develop the efficient method for the synthesis of polysaccharides, *in vitro* approach by enzymatic catalysis has been significantly investigated because enzymatic reactions proceed in highly stereo- and regiocontrolled manners. Enzymes are generally categorized into six main classes, which are oxidoreductase (EC1), transferase (EC2), hydrolase (EC3), lyase (EC4), isomerase (EC5), and ligase (EC6) (*13*). In such main classes, transferase and hydrolase have been practically applied as catalysts for the *in vitro* enzymatic synthesis of polysaccharides (*14–19*).

Similar to the general chemical glycosylation as shown in Figure 1, the enzymatic formation of a glycosidic linkage between C1 atom of a monosaccharide and one of hydroxy groups of the other monosaccharide can be realized by the reaction of a activated glycosyl donor at the C1 atom with a glycosyl acceptor (Figure 2), where a glycosyl donor and a glycosyl acceptor can be employed in their unprotected forms beside the anomeric position of the donor (*20*, *21*). In the enzymatic glycosylation, first, the glycosyl donor is recognized by enzyme to form a glycosyl-enzyme intermediate. Then, the intermediate is attacked by the hydroxy group of the glycosyl acceptor in the stereo- and regioselective manners according to specificity of each enzyme under mild conditions, leading to the direct formation of the unprotected glycoside. Thus, repetition of the enzymatic glycosylations, i.e., enzymatic polymerization, forms polysaccharides with well-defined structure. As aforementioned, the enzymes involved in the synthesis of polysaccharides are mainly glycosyl transferases and glycosyl hydrolases. Furthermore, the former is mainly subclassified into synthetic enzymes (Leloir glycosyltransferases) (*22*) and phosphorolytic enzymes (phosphorylases) (*23*, *24*).

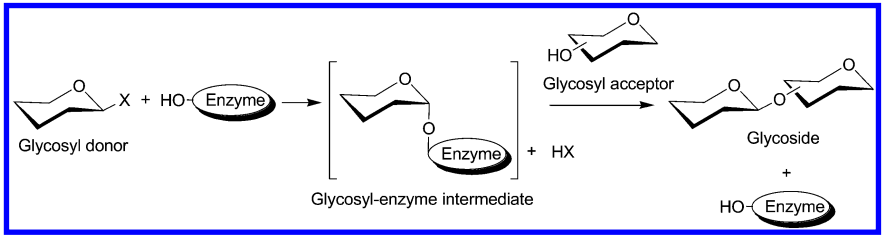

Figure 2. General reaction scheme for enzymatic glycosylation.

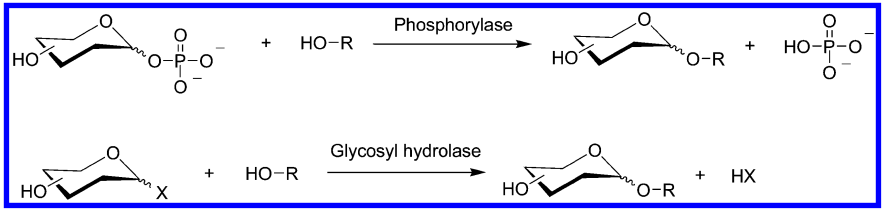

Figure 3. Enzymatic glycosylations catalyzed by phosphorylase and glycosyl hydrolase.

In Green Polymer Chemistry: Biocatalysis and Materials II; Cheng, H., et al.;
ACS Symposium Series; American Chemical Society: Washington, DC, 2013.

Leloir glycosyltransferases are biologically important because they perform the role for synthesizing saccharide chains *in vivo* (*25*). The reactions catalyzed by Leloir glycosyltransferases are irreversible in the synthetic direction due to the requirement for cleavage of the high-energy bond of the glycosyl nucleotide of a substrate in the reaction. However, Leloir glycosyltransferases are generally transmembrane-type proteins, present in less amount in nature, and unstable for isolation and purification. Therefore, *in vitro* enzymatic reaction using Leloir glycosyltransferases is not common for practical synthesis of the polysaccharides.

Phosphorylases are the enzymes that catalyze phosphorolytic cleavage of a glycosidic linkage at a nonreducing end of the saccharide chain in the presence of inorganic phosphate to produce hexose 1-phosphate and the saccharide chain with one smaller degree of polymerization (DP) (*23*, *24*). Because the bond energy of the hexose 1-phosphate product is comparable with that of the glycosidic linkage, the phosphorylase-catalyzed reactions show reversible nature. Therefore, phosphorylases can be employed as a catalyst in the practical synthesis of saccharide chains via glycosylation. In such glycosylation, hexose 1-phosphates are used as a glycosyl donor and a hexose residue is transferred from the donor to a nonreducing end of an appropriate glycosyl acceptor to form a stereo- and regiocontrolled glycosidic linkage accompanied with the production of inorganic phosphate (Figure 3). Of the phophorylases, which have been known so far, α-glucan phosphorylase (glycogen phosphorylase, starch phosphorylase, hereafter, this enzyme is simply called 'phosphorylase' in this chapter) is the most extensively studied (the detailes of the phosphorylase-catalyzed reaction are explained in the next section).

Glycosyl hydrolases have been frequently employed in the hydrolysis of polysaccharides such as starch. The glycosyl hydrolase catalysis using natural polysaccharides readily proceeds in the hydrolysis direction under normal conditions in aqueous media. Because an enzyme-substrate intermediate is formed in the reaction using the activated glycosyl donor, glycosyl hydrolases catalyze a glycosylation *in vitro* to produce a glycoside (Figure 3). This view is based on a hypothesis that the structures of transition states are very similar in both *in vivo* and *in vitro* reactions (*14*, *16*, *17*). For the synthesis of polysaccharides by the glycosyl hydrolase-catalyzed successive enzymatic glycosylations (enzymatic polymerization), therefore, the substrates should be designed as the structure of a transition state analogue. On the basis of this concept, two types of substrates, i.e., glycosyl fluorides and sugar oxazolines, have been designed to be efficiently recognized by glycosyl hydrolases (*15*, *26*). An anomeric carbon of the starting sugars is activated by introducing fluoride or an oxazoline group (1,2-oxazoline derived from 2-acetamido-2-deoxysugar), giving the substrates, which have the structures close to transition states of the suitable enzymatic reactions and efficiently form the enzyme-substrate intermediates. By the enzymatic polymerization of glycosyl fluorides catalyzed by glycosyl hydrolase catalyses, cellulose, amylose, xylan, and related polysaccharides have been synthesized (*14–19*, *27–29*). The glycosyl hydrolase-catalyzed enzymatic polymerization using sugar oxazolines produced chitin, hyaluronan, chondroitin, and related aminopolysaccharides (*16–19*, *30–35*). Cellobiosyl fluoride and *N,N′*-diacetylchitobiose oxazoline are representatively shown in Figure 4, which

In Green Polymer Chemistry: Biocatalysis and Materials II; Cheng, H., et al.;
ACS Symposium Series; American Chemical Society: Washington, DC, 2013.

Publication Date (Web): November 22, 2013 | doi: 10.1021/bk-2013-1144.ch011

are enzymatically polymerized by cellulase and chitinase catalyses, respectively, to give synthetic cellulose and synthetic chitin (*27*, *30*). The manners of both the polymerizations belong to step-growth polymerization; the former proceeds via polycondensation through liberating hydrogen fluoride, whereas the ring-opening polyaddition is the mechanism of the latter case.

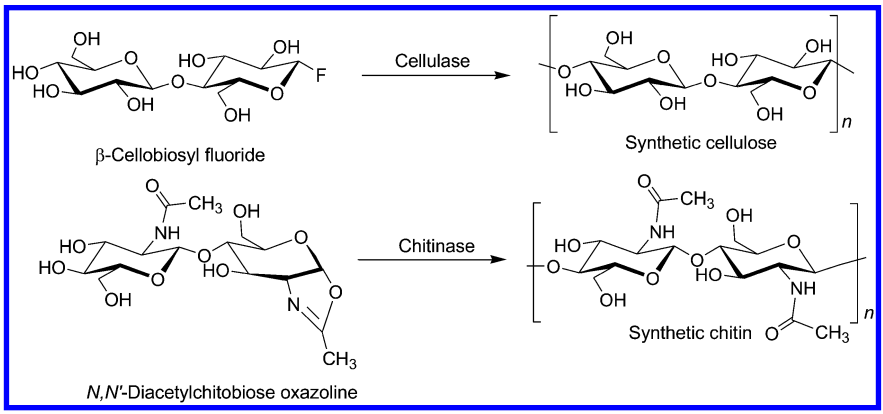

Figure 4. Enzymatic polymerization of cellobiosyl fluoride and N,N'-diacetylchitobiose oxazoline catalyzed by cellulase and chitinase, respectively.

Characteristic Features of Phosphorylase-Catalyzed Enzymatic α-Glycosylations

Phosphorylase catalyzes the reversible phosphorolysis of α-(1→4)-glucans at the nonreducing end, such as glycogen and starch, in the presence of inorganic phosphate, giving rise to α-D-glucose 1-phosphate (Glc-1-P) (*23*, *24*). By means of the reversibility of the reaction, α-(1→4)-glucosidic linkage can be constructed by the phosphorylase-catalyzed α-glucosylation using Glc-1-P as a glycosyl donor (*36–39*). In the α-glucosylation, a glucose residue is transferred from Glc-1-P to a nonreducing end of the acceptor to form α-(1→4)-glucosidic linkage. As the glycosyl acceptor, maltooligosaccharides with DPs higher than the smallest one, which is recognized by phosphorylase, are used. The smallest substrates for the phosphorolysis and glycosylation by potato phosphorylase catalysis are typically maltopentaose (Glc_5) and maltotetraose (Glc_4), respectively. However, it was reported that the smallest substrates accepted by phosphorylase isolated from thermophilic bacterial sources (thermostable phosphorylase) for the former and latter reactions are Glc_4 and maltotriose (Glc_3) (*38*, *40*, *41*). These observations indicate that phosphorylases exhibit different recognition behaviors for the substrates depending on their sources.

Because phosphorylase has shown loose specificity for recognition of the glycosyl donor structure (*42*), the phosphorylase-catalyzed enzymatic α-glycosylations using different hexose 1-phosphates from the native one (Glc-1-P) have been investigated (*43*). Consequently, it has been

In Green Polymer Chemistry: Biocatalysis and Materials II; Cheng, H., et al.;
ACS Symposium Series; American Chemical Society: Washington, DC, 2013.

Publication Date (Web): November 22, 2013 | doi: 10.1021/bk-2013-1144.ch011

found that the following hexose 1-phosphates, that is, α-D-mannose, 2-deoxy-α-D-glucose, α-D-xylose, 2-amino-2-deoxy-α-D-glucose, and 2-formamido-2-deoxy-α-D-glucose 1-phosphates were recognized by phosphorylase as the glycosyl donor, to give the corresponding non-natural oligosaccharides, that is, α-mannosylated, 2-deoxy-α-glucosylated, α-xylosylated, 2-amino-2-deoxy-α-glucosylated, and 2-formamido-2-deoxy-α-glucosylated oligosaccharides, respectively (Figure 5) (*44–49*). Recently, the author also found that thermostable phosphorylase from *Aquifex aeolicus* VF5 (*50*) recognizes α-D-glucuronic acid 1-phsophate (GlcA-1-P) as a new glycosyl donor (*51*). In the thermostable phosphorylase-catalyzed enzymatic α-glucuronylation using Glc_3 as a glycosyl acceptor, a glucuronic acid residue transferred from the donor to a nonreducing end of the acceptor to give α-glucuronylated tetrasaccharide (Figure 6). The reaction is the efficient method to provide anionic oligosaccharides having a glucuronic acid residue at the nonreducing end. Compared with the thermostable phosphorylase, potato phosphorylase did not catalyze the α-glucuronylation using GlcA-1-P.

Publication Date (Web): November 22, 2013 | doi: 10.1021/bk-2013-1144.ch011

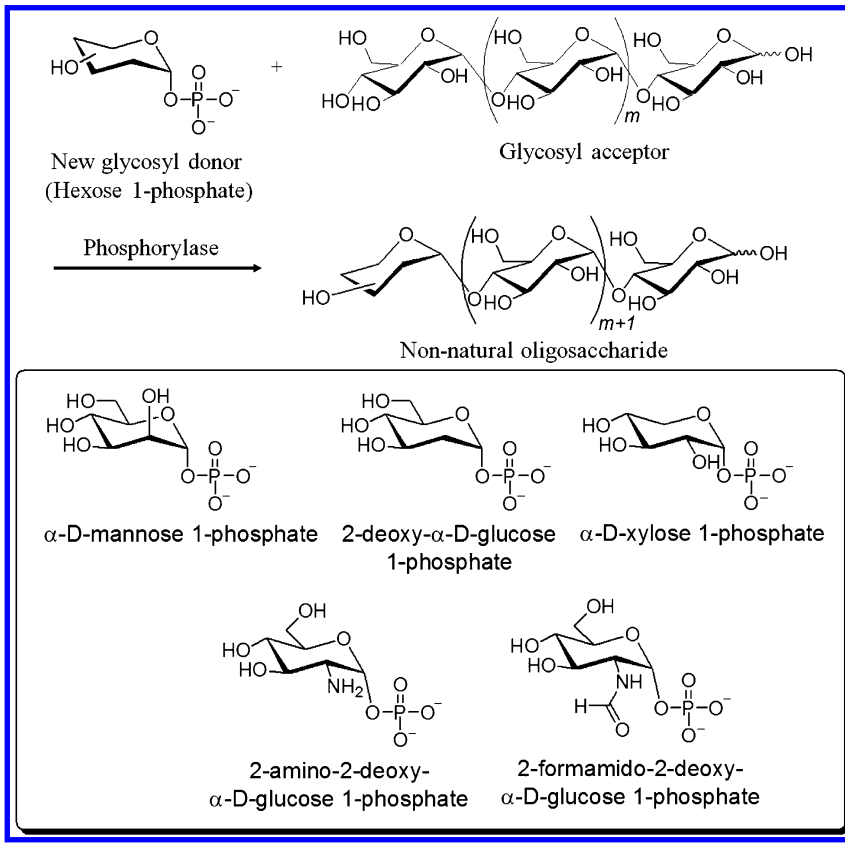

Figure 5. Phosphorylase-catalyzed enzymatic glycosylations using various hexose 1-phosphates as glycosyl donor.

In Green Polymer Chemistry: Biocatalysis and Materials II; Cheng, H., et al.;
ACS Symposium Series; American Chemical Society: Washington, DC, 2013.

Publication Date (Web): November 22, 2013 | doi: 10.1021/bk-2013-1144.ch011

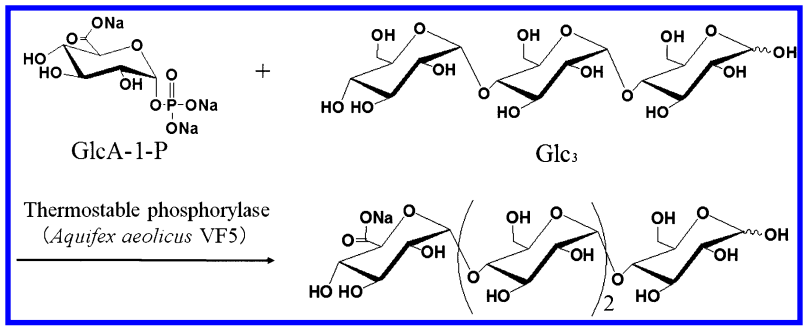

Figure 6. Thermostable phosphorylase-catalyzed enzymatic a-glucuronylation of maltotriose (Glc_3) using GlcA-1-P.

When the excess molar ratio of Glc-1-P to the acceptor is present in the phosphorylase-catalyzed reaction system, the successive α-glucosylations occur as a propagation of polymerization to produce the α-(1→4)-glucan chain, i.e., amylose (Figure 7) (*36–39*). This polymerization manner belongs to chain-growth polymerization and the glycosyl acceptor is often called a 'primer' because the reaction is exactly initiated at a nonreducing end of the acceptor. Therefore, the phosphorylase-catalyzed polymerization proceeds analogously to a living polymerization. Accordingly, the molecular weights of the produced amylose can be controlled by the Glc-1-P/acceptor feed molar ratios and their distribution is a narrow ($M_w/M_n < 1.2$) (*52*).

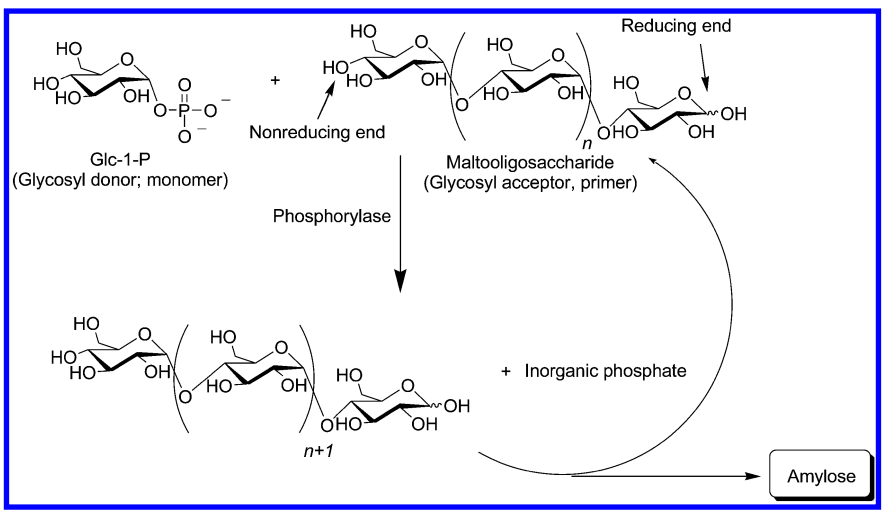

Figure 7. Phosphorylase-catalyzed enzymatic polymerization to produce amylose.

In Green Polymer Chemistry: Biocatalysis and Materials II; Cheng, H., et al.;
ACS Symposium Series; American Chemical Society: Washington, DC, 2013.

Publication Date (Web): November 22, 2013 | doi: 10.1021/bk-2013-1144.ch011

The phosphorylase-catalyzed reactions can take place using the modified maltooligosaccharides as the glycosyl acceptor, whose reducing ends are covalently attached to another material such as a polymeric chain because the reducing end does not participate in the reaction (Figure 8) (*53*). The modified acceptor typically serves multifunctions due to the presence of the plural nonreducing α-(1→4)-linked glucan ends. This is one of the most characteristic and advantageous features of the phosphorylase-catalyzed reactions that are not possible in the glycosyl hydrolase-catalyzed reaction because of the different polymerization manners of the former and latter, i.e., the chain- and step-growth polymerization manners, respectively. This chapter reviews the synthesis of new polysaccharide materials by the phosphorylase-catalyzed enzymatic glycosylations using such multifunctional polymeric glycosyl acceptors, where the reducing ends of plural maltooligosaccharides are covalently attached to the polymeric chain (*54*, *55*).

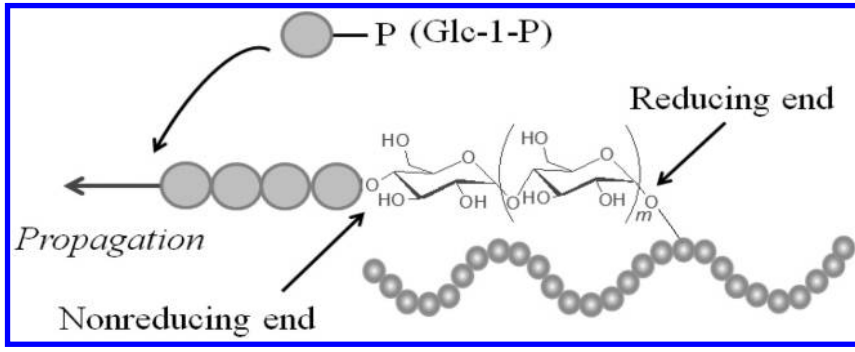

Figure 8. Image for propagation in phosphorylase-catalyzed enzymatic polymerization using modified maltooligosaccharide as glycosyl acceptor, whose reducing end is covalently attached to another polymeric chain.

Preparation of Highly Branched Polysaccharide Materials by Phosphorylase-Catalyzed α-Glycosylations Using Glycogen as Multifunctional Glycosyl Acceptor

Glycogen is known to be a water soluble polysaccharide with high molecular-weight, which is composed of linear chains containing an average of 10 to 14 α-(1→4)-linked glucose residues, interlinked by α-(1→6)-glycosidic linkages to form highly branched structure (*56*, *57*). Besides glycogen being for the *in vivo* phosphorolysis by phosphorylase, it was used as a multifunctional polymeric glycosyl acceptor for the phosphorylase-catalyzed polymerization (Figure 9) because of the presence of a number of the nonreducing α-(1→4)-linked glucan ends (*58*). When the phosphorylase-catalyzed polymerization of Glc-1-P from glycogen was carried out, followed by standing further at room temperature for 24 h, the reaction mixture turned into a hydrogel form. The hydrogelation was caused by the formation of junction zones based on the double helix structure of

In Green Polymer Chemistry: Biocatalysis and Materials II; Cheng, H., et al.;
ACS Symposium Series; American Chemical Society: Washington, DC, 2013.

the elongated amylose chains among glycogen molecules because amylose chains are known to readily form the double helix conformation. The stress-strain curves of the hydrogels obtained by various Glc-1-P/glycogen ratios under compressive mode showed that the properties of the gels were gradually strengthened and then became brittle with increasing amounts of glycogen. Because the number of elongated amylose chains increased with increasing amounts of glycogen, the gel strength increased as more junction zones were formed. However, further increase in the number of junction zones probably induced the brittle nature.

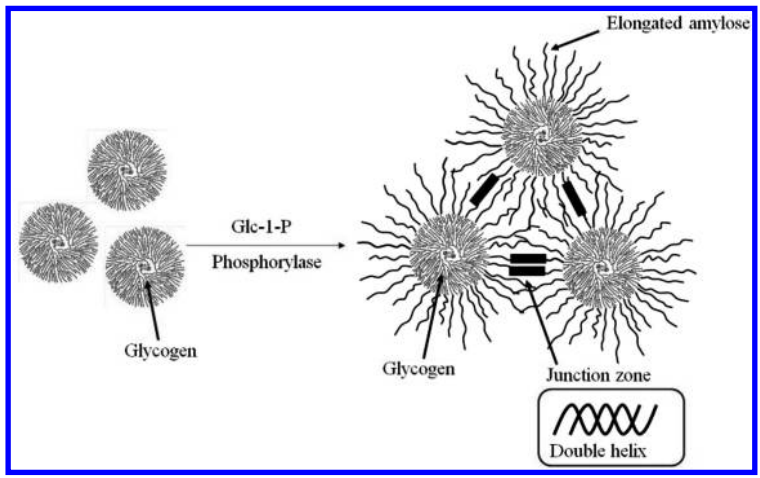

Figure 9. Schematic reaction for phosphorylase-catalyzed polymerization using glycogen to form hydrogel.

The hydrogels were then converted into porous materials by lyophilization of the hydrogels. The stress-strain curves of the porous materials under compressive mode showed that the harder materials were obtained when the amounts of glycogen used for the preparation of the hydrogels increased. This is probably due to the formation of tighter packed networks because the larger number of junction zones were formed from the larger amounts of glycogen. The XRD profile of the porous material showed diffraction peaks due to the crystalline structure of the double helix amylose conformations (*59*). This result indicated that the networks in the porous materials were constructed based on the double helical entanglement of the elongated amylose chains which in turn supported the presence of the junction zones by the double helix formation in the hydrogel.

When an aqueous solution of the porous material was prepared by dissolution in aqueous NaOH solution, followed by neutralization with acetic acid to pH 5.5 – 6.5, it gradually turned into the hydrogel form again (Figure 10(a)-(b)). When the standard iodine-iodide solution was added to the neutralized solution immediately after it was prepared by the same procedure as above, on the other hand, the re-hydrogelation did not take place (Figure 10(c)). In this experiment, iodine was included in the cavity of the elongated amylose helix to form the well-known amylose/iodine inclusion complex, which suppressed the formation of the double helix as the junction zone.

Publication Date (Web): November 22, 2013 | doi: 10.1021/bk-2013-1144.ch011

Publication Date (Web): November 22, 2013 | doi: 10.1021/bk-2013-1144.ch011

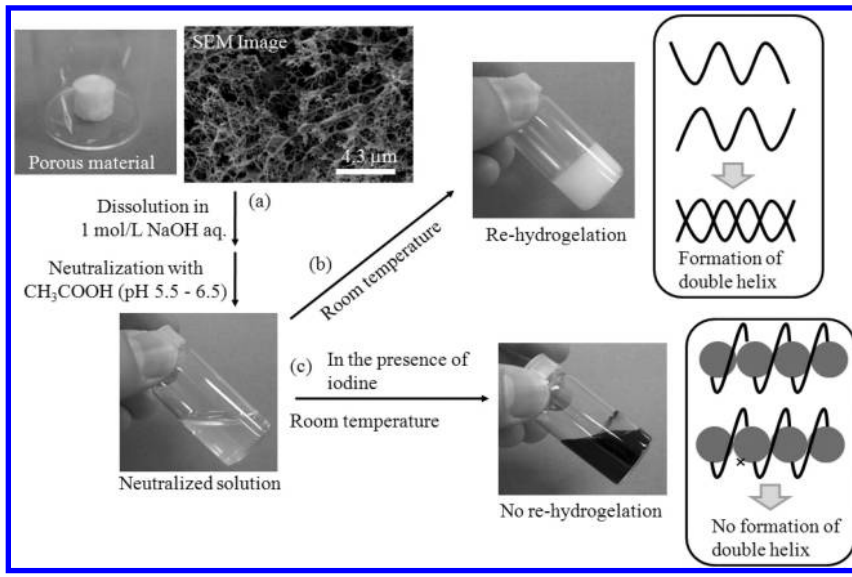

Figure 10. Dissolution of porous material (a), re-hydrogelation (b), and suppression of re-hydrogelation (c).

Anionic polysaccharides in living system are vital materials for important *in vivo* functions as examples of glycosaminoglycans (*60*, *61*). Uronic acids are the representative anionic sugar residues present in such saccharide materials, which have carboxylates as the anionic moiety. Therefore, synthesis of new anionic polysaccharides containing uronic acid residues such as glucuronic acid has been in great demand to exhibit new functions in the research field of glyco-materials. The author reported the synthesis of highly branched anionic glycogens having a number of glucuronic acid residues at nonreducing ends by the aforementioned thermostable phosphorylase-catalyzed α-glucuronylation using glycogen as a multifunctional polymeric glycosyl acceptor and GlcA-1-P as a glycosyl donor (Figure 11). The enzymatic α-glucuronylation of glycogen was carried out using 5 or 30 equiv. of GlcA-1-P for nonreducing ends catalyzed by thermostable phosphorylase from *Aquifex aeolicus* VF5 in 200 mM acetate buffer (pH 6.2) at 50 °C for 48 h. After the reaction, ethanol was added to the reaction mixture to precipitate the product. The precipitate was isolated by filtration and washed with ethanol. The product was dissolved in water and the mixture was subjected to centrifugation to remove the insoluble fraction. The supernatant was dialyzed against water and lyophilized to give the highly branched anionic glycogens.

In Green Polymer Chemistry: Biocatalysis and Materials II; Cheng, H., et al.;
ACS Symposium Series; American Chemical Society: Washington, DC, 2013.

Publication Date (Web): November 22, 2013 | doi: 10.1021/bk-2013-1144.ch011

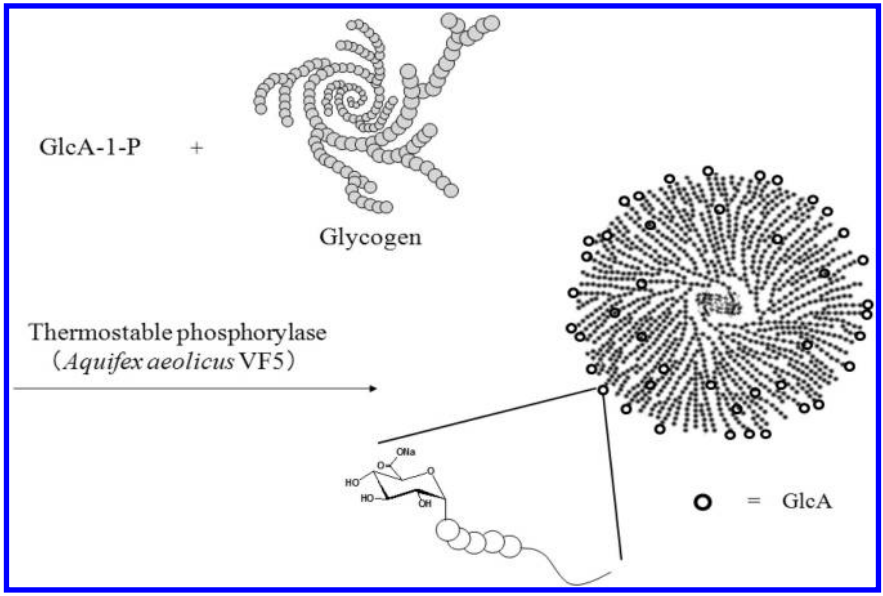

Figure 11. Synthesis of highly branched anionic glycogen by thermostable phosphorylase-catalyzed enzymatic α-glucuronylation of glycogen using GlcA-1-P.

The presence of GlcA residues in the product was confirmed by the IR analysis. First, the product was treated with cation-exchange resin (Amberlite IR-120 plus (H^+ form)) in water for 4 h to convert the sodium carboxylate in GlcA residues to the free carboxylic acid (Figure 12). Then, the IR measurement of the resulting material was conducted. Figure 12 shows the IR spectra of the product before and after the cation-exchange resin treatment. These spectra indicated that the carbonyl absorption due to the carboxylic acid group newly appeared at 1720 cm^{-1} by the treatment, supporting the presence of GlcA residues in the product. The transfer ratio of GlcA residues to the nonreducing ends in glycogen was evaluated by the energy-dispersive x-ray spectroscopic analysis using scanning electron microscope (SEM-EDX analysis). Figure 13 shows the SEM-EDX chart of the product (feed ratio; GlcA-1-P/nonreducing ends = 30). The signal assigned to P element was not detected, indicating that inorganic phosphates released from GlcA-1-P by the phosphorylase catalysis and unreacted GlcA-1-P were removed by the isolation procedure of the product. The transfer ratio of GlcA residues to nonreducing ends by the enzymatic α-glucuronylation was calculated on the basis of the O/Na ratio in the SEM-EDX chart to be 41.2 %. Similarly, the transfer ratio in the product obtained by the reaction in the feed ratio of GlcA-1-P/nonreducing ends = 5 was evaluated as 20.0 %.

In Green Polymer Chemistry: Biocatalysis and Materials II; Cheng, H., et al.;
ACS Symposium Series; American Chemical Society: Washington, DC, 2013.

Publication Date (Web): November 22, 2013 | doi: 10.1021/bk-2013-1144.ch011

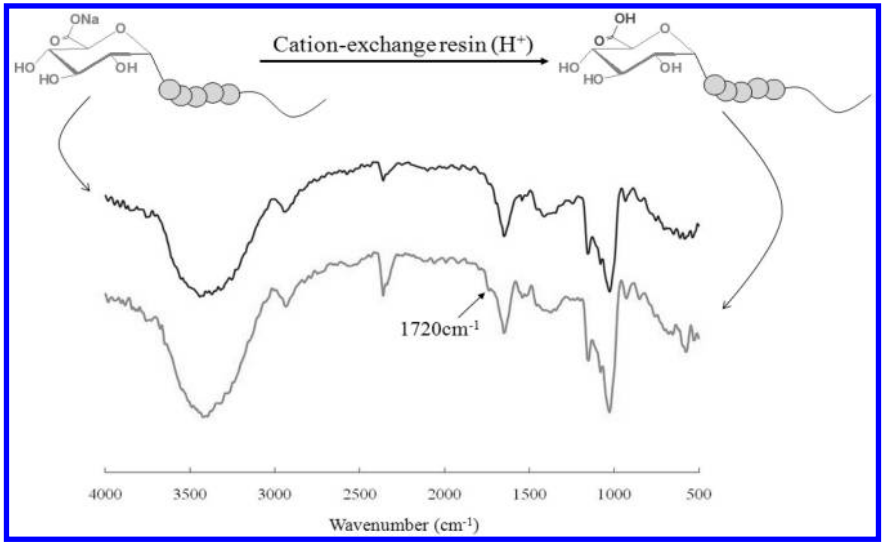

Figure 12. IR spectra of anionic glycogen before and after treatment with cation-exchange resin (H^+).

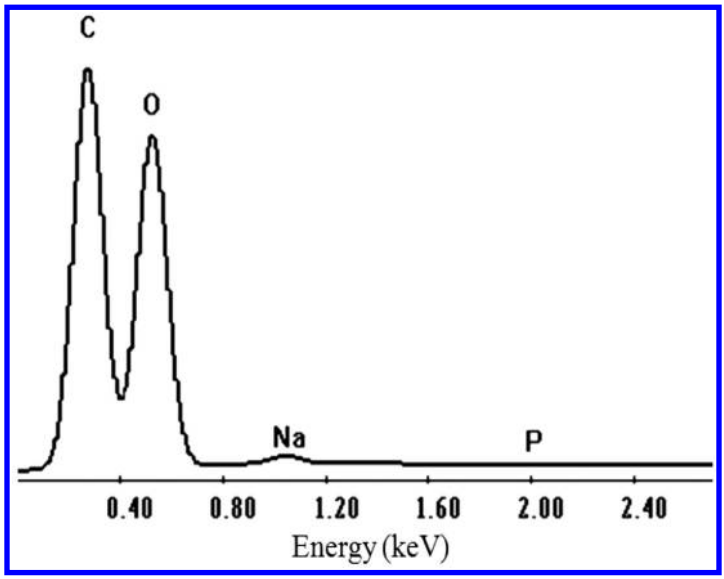

Figure 13. SEM-EDX chart of anionic glycogen.

In Green Polymer Chemistry: Biocatalysis and Materials II; Cheng, H., et al.;
ACS Symposium Series; American Chemical Society: Washington, DC, 2013.

Synthesis of Amylose-Grafted Heteropolysaccharides by Phosphorylase Catalyzed Enzymatic Polymerization Using Maltooligosaccharide-Grafted Polymeric Glycosyl Acceptors

In addition to linear polysaccharides such as cellulose, chitin/chitosan, and amylose, branched structures have often been found in natural polysaccharides, where a polysaccharide of the main-chain accompanies another kinds of branched polysaccharide chains by covalent linkages (*2*). Such chemical structures probably contribute to their promising and high-performance functions in nature. Therefore, the development of efficient methods for the preparation of the branched or grafted artificial polysaccharides using common polysaccharides is a promising topic in carbohydrate and material research fields.

On the basis of the above viewpoint, amylose-grafted heteropolysaccharides have been synthesized by the phosphorylase-catalyzed enzymatic polymerization of Glc-1-P. As aforementioned, maltooligosaccharides as a glycosyl acceptor have to be present to initiate the polymerization. To obtain the amylose-grafted heteropolysaccharides, therefore, the maltooligosaccharides are first introduced onto the polysaccharides of the main-chain by appropriate chemical reactions, and then the phosphorylase-catalyzed polymerization is performed using the products as the multifunctional polymeric glycosyl acceptor (chemoenzymatic method). Two types of chemical reactions have been employed to introduce the maltooligosaccharide chains onto the main-chain polysaccharides; one is reductive amination of maltooligosaccharides with cationic polysaccharides having amino groups using reductants and the other one is condensation of amine-functionalized maltooligosaccharides with anionic polysaccharides having carboxylate groups using condensing agents (Figure 14) (*54*, *55*).

By means of the former approach using chitosan as a cationic polysaccharide, a maltooligosaccharide-grafted chitosan was obtained (*62*, *63*). This material was converted further into a maltooligosaccharide-grafted chitin by *N*-acetylation. Then, the phosphorylase-catalyzed enzymatic polymerization of Glc-1-P from the maltooligosaccharide chains on the chitin and chitosan derivatives was performed to obtain amylose-grafted chitin/chitosan (Figure 15). On the other hand, the latter approach was employed for alginate and xanthan gum as an anionic polysaccharide (*64*, *65*). A maltooligosaccharide having an amino group at a reducing end was first prepared by the reaction of maltooligosaccharide lactone with 2-azidoethylamine, followed by reduction using $NaBH_4$. Then, it was chemically introduced onto alginate or xanthan gum by condensation with carboxylates of the polysaccharides using water-soluble carbodiimide (WSC)/*N*-hydroxysuccinimide (NHS) as the condensing agent to produce maltooligosaccharide-grafted alginate and xanthan gum. Then, the phosphorylase-catalyzed enzymatic polymerization of Glc-1-P from the maltooligosaccharide chains on the products was conducted to produce amylose-grafted alginate and xanthan gum (Figure 15).

The chemoenzymatic approach for amylose-grafted heteropolysaccharides was extended to the synthesis of an amylose-grafted cellulose (Figure 16) (*66*). The two representative natural polysaccharides, cellulose and amylose, are composed of the same structural unit, i.e., an anhydroglucose unit, but linked through the different β-(1→4)- and α-(1→4)-glucosidic linkages, respectively.

In Green Polymer Chemistry: Biocatalysis and Materials II; Cheng, H., et al.;
ACS Symposium Series; American Chemical Society: Washington, DC, 2013.

Publication Date (Web): November 22, 2013 | doi: 10.1021/bk-2013-1144.ch011

Therefore, the amylose-grafted cellulose has a very interesting and unique structure because it is composed of two polysaccharide chains with the same structural unit but with the different linkages. Because cellulose does not have reactive groups to maltooligosaccharide, amino groups should be first introduced to cellulose Therefore, the synthesis of an amine-functionalized cellulose was first performed, which was successfully obtained by successive partial tosylation of the OH groups at C-6 positions, displacement of the tosylates by azido groups, and reduction to amino groups. Then, maltooligosaccharide was introduced onto the cellulose main-chain by reductive amination of the amine-functionalized cellulose with maltoheptaose (Glc_7) using $NaBH_3CN$. Subsequently, the amylose-grafted cellulose was synthesized by the phosphorylase-catalyzed polymerization of Glc-1-P from the maltooligosaccharide chains on the cellulose derivative.

Publication Date (Web): November 22, 2013 | doi: 10.1021/bk-2013-1144.ch011

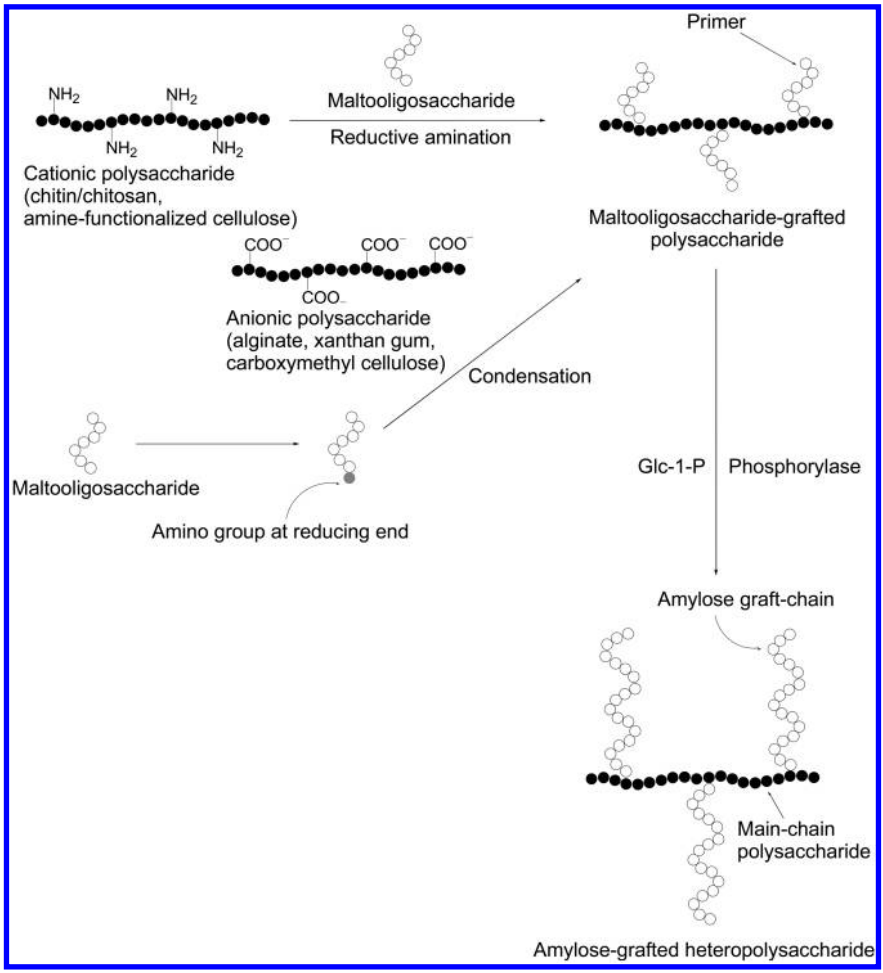

Figure 14. Chemoenzymatic synthesis of amylose-grafted heteropolysaccharides.

In Green Polymer Chemistry: Biocatalysis and Materials II; Cheng, H., et al.;
ACS Symposium Series; American Chemical Society: Washington, DC, 2013.

Publication Date (Web): November 22, 2013 | doi: 10.1021/bk-2013-1144.ch011

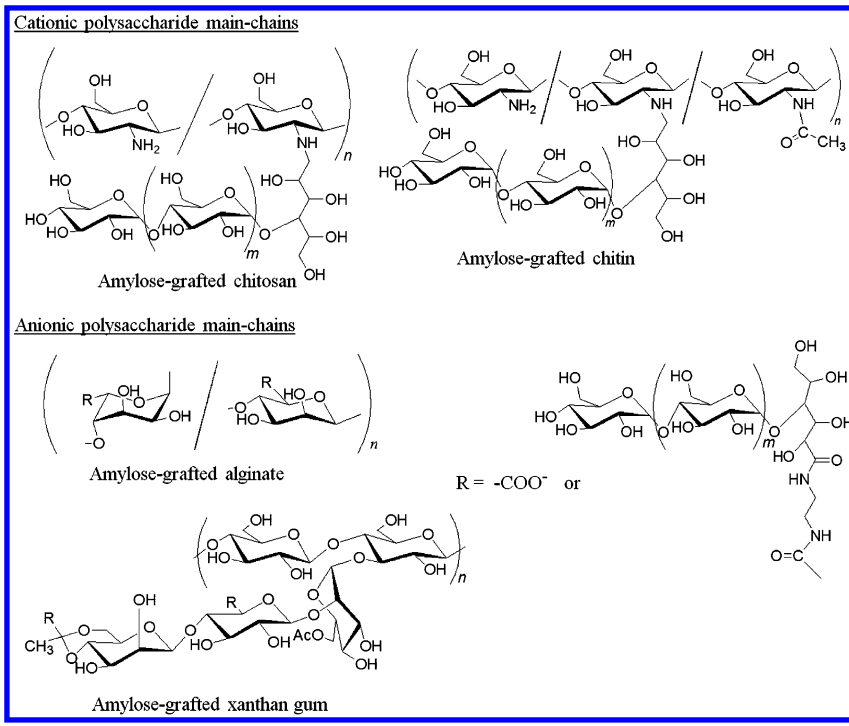

Figure 15. Structures of amylose-grafted chitin, chitosan, alginate, and xanthan gum.

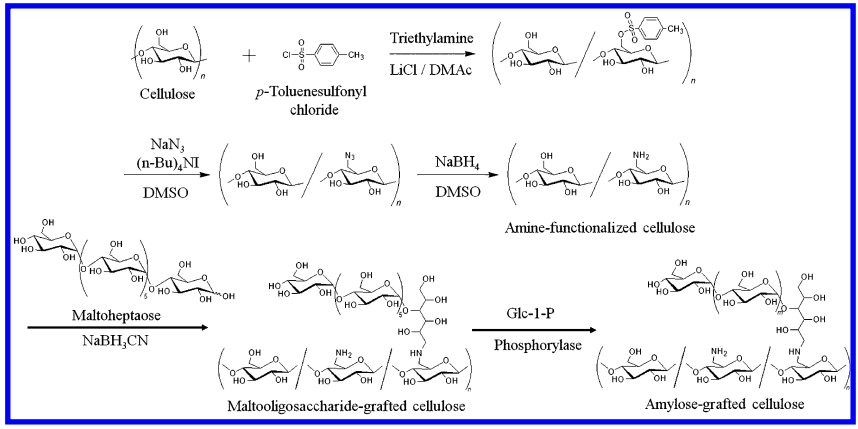

Figure 16. Chemoenzymatic synthesis of amylose-grafted cellulose.

In Green Polymer Chemistry: Biocatalysis and Materials II; Cheng, H., et al.;
ACS Symposium Series; American Chemical Society: Washington, DC, 2013.

Publication Date (Web): November 22, 2013 | doi: 10.1021/bk-2013-1144.ch011

Amylose-grafted sodium carboxymethyl cellulose (NaCMC) was also synthesized by the chemoenzymatic approach (*67*). NaCMC is an anionic water-soluble polysaccharide and one of the most widely used cellulose derivatives in various fields such as detergent, food, paper, and textile industries (*68*). The introduction of maltooligosaccharides onto NaCMC was first performed by condensation of the amine-functionalized maltooligosaccharide with carboxylates of NaCMC in the presence of WSC/NHS under the same conditions as those using alginate and xanthan gum to produce a maltooligosaccharide-grafted NaCMC (Figure 17).

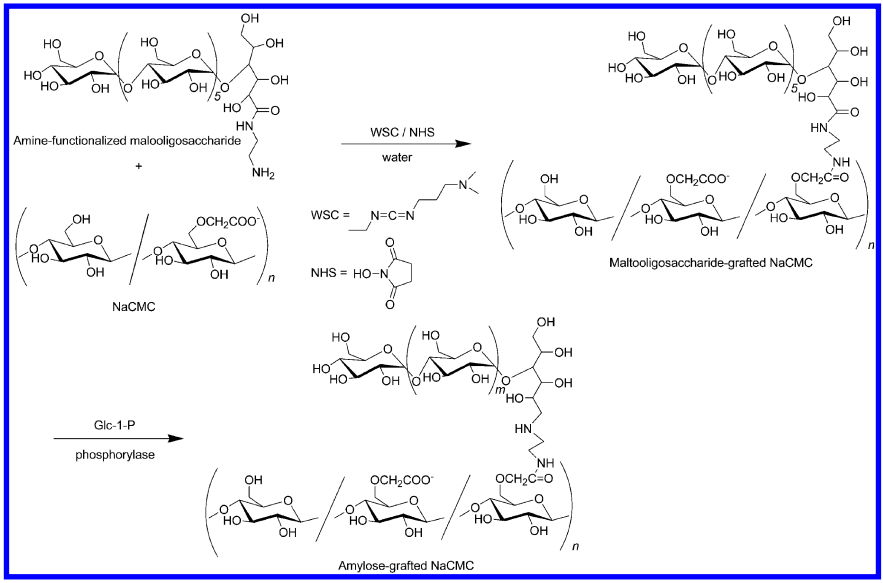

Figure 17. Chemoenzymatic synthesis of amylose-grafted sodium carboxymethyl cellulose (NaCMC).

When the phosphorylase-catalyzed polymerization of Glc-1-P using the maltooligosaccharide-grafted NaCMC with the functionality of 35.4% was carried out in the feed ratios of Glc-1-P/maltooligosaccharide = 300 and 500 in 0.20 mol/L sodium acetate buffer (pH 6.2) at 40 – 45 °C for 20 h, the resulting reaction mixtures turned into gel form. Therefore, the products were isolated by immersing the mixtures in water, followed by lyophilization to give the water-insoluble products. Average degrees of polymerization (DPs) of amylose graft chains in the products obtained by the above feed ratios were calculated on the basis of the elemental analysis data and the functionality of the maltooligosaccharide chain to be 140 and 214, respectively. The SEM image of the sample, which was prepared by drying a diluted alkaline solution of the product (1.0×10^{-4} mol/L) in 5.0×10^{-4} mol/L aqueous NaOH under ambient conditions showed morphologically controlled nanofibers as shown in Figure 18(a).

In Green Polymer Chemistry: Biocatalysis and Materials II; Cheng, H., et al.;
ACS Symposium Series; American Chemical Society: Washington, DC, 2013.

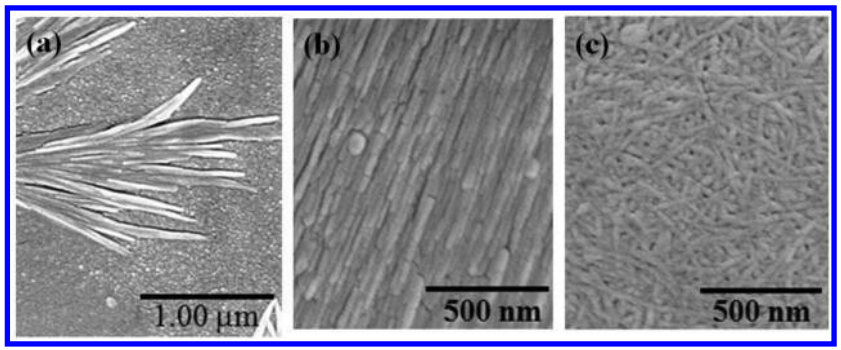

Figure 18. SEM images of sample prepared from alkaline solution (1.0 x 10^{-4} mol/L) of amylose-grafted NaCMC (a) and films prepared from alkaline solutions (0.040g in 0.50 mol/L aqueous NaOH (1.50 mL)) of amylose-grafted NaCMCs ((b) and (c); DPs of amylose chains = 140 and 214, respectively).

Publication Date (Web): November 22, 2013 | doi: 10.1021/bk-2013-1144.ch011

The films were obtained by drying the thinly spread alkaline solutions of the products with different amylose lengths in a higher concentration (0.040 g in 0.50 mol/L aqueous NaOH (1.50 mL)); the films still contained alkali. The SEM images of the films showed the morphologies of nanofibers. Furthermore, it was confirmed from the SEM images that the film of the amylose-grafted NaCMC with average DP = 140 was constructed from nanofibers arrayed in parallel (Figure 18(b)), whereas the film of the amylose-grafted NaCMC with average DP = 214 was constructed from highly entangled nanofibers (Figure 18(c)). These results indicated that DPs of graft chains on the CMC chains strongly affected the arrangements of nanofibers in the films. Then, alkali present in the films was removed by immersion in water. The SEM images of the resulting films without alkali showed that the nanofibers were merged each other at interfacial area with remaining the fiber arrangements as observed in the films before washing out alkali. Conventional approaches to the production of cellulose nanofibers are mainly performed upon top-down procedures that break down the starting bulk materials from native cellulose resources. The present method is the completely different approach from the above to produce the nanofibers of cellulose derivatives, that accords to self-assembling generative (bottom-up) route and provides the morphologically controlled self-assembly of heteropolysaccharides to produce new nanofibrillated materials.

Mechanical properties of the films after washing out alkali were evaluated by tensile testing. The film from the amylose-grafted NaCMC with average DP = 140 showed more elastic nature, while harder nature was significantly confirmed in the film from the amylose-grafted NaCMC with average DP = 214. These results suggested that the arrangements of nanofibers in the films strongly affected mechanical properties.

Conclusions

In this chapter, the synthesis of new polysaccharide materials by means of the phosphorylase-catalyzed enzymatic α-glycosylations using multifunctional polymeric glycosyl acceptors has been reviewed. Because the enzymatic α-glycosylations by the phosphorylase catalysis proceeds from the nonreducing ends of the maltooligosaccharide chains modified at the reducing ends by another polysaccharide chain, the complicated polysaccharide structures such as glycogen-based highly branched polysaccharides and amylose-grafted heteropolysaccharides can be obtained. Additionally, the motivation for the studies of the phosphorylase-catalyzed enzymatic synthesis of new polysaccharides has strongly been based on the viewpoints that the greener and sustainable processes should be developed in the fields not only of fundamental research, but also of practical applications of polymeric materials. Polysaccharides and the related compounds have been attracting much attention because of their potential applications as new functional materials in many research fields such as medicines, pharmaceutics, foods, and cosmetics. Therefore, the enzymatic synthesis of polysaccharide materials with the complicated structures by the phosphorylase catalysis, which are hardly produced by conventional chemical synthetic approaches, will be increasingly important and useful in the future.

Publication Date (Web): November 22, 2013 | doi: 10.1021/bk-2013-1144.ch011

References

1. Berg, J. M.; J. Tymoczko, L.; Stryer, L. *Biochemistry*, 6th International ed.; W. H. Freeman & Co.: New York, 2006; Chapter 11.
2. Schuerch, C. *Polysaccharides in Encyclopedia of Polymer Science and Engineering*, 2nd ed.; John Wiley & Sons: New York, 1986; Vol. 13, pp 87−162.
3. McMurry, J.; Castellion, M. E.; Ballantine, D. S.; Hoeger, C. A. *Fundamentals of General, Organic, and Biological Chemistry*, 6th ed.; Prentice Hall Inc.: New Jersey, 2009.
4. *Carbohydrates in Chemistry and Biology*; Ernst, B., Hart, G. W., Sinaÿ, P., Eds.; Wiley-VCH: Weinheim, Germany, 2000.
5. *Glycoscience*, 2nd ed.; Fraser-Reid, B. O., Tatsuta, K., Thiem, J., Coté, G. L., Flitsch, S., Ito, Y., Kondo, H., Nishimura, S.-I., Yu, B., Eds.; Springer: Berlin, 2008.
6. *Essentials of Glycobiology*, 2nd ed.; Varki, A., Cummings, R. D., Esko, J. D., Freeze, H. H., Stanley, P., Bertozzi, C. R., Hart, G. W., Etzler, M. E., Eds.; Cold Spring Harbor Laboratory Press: New York, 2009.
7. Paulsen, H. *Angew. Chem., Int. Ed. Engl.* **1982**, *21*, 155–173.
8. Schmidt, R. R. *Angew. Chem., Int. Ed. Engl.* **1986**, *25*, 212–235.
9. Toshima, K.; Tatsuta, K. *Chem. Rev.* **1993**, *93*, 1503–1531.
10. Klemm, D.; Heublein, B.; Fink, H.-P.; Bohn, A. *Angew. Chem., Int. Ed.* **2005**, *44*, 3358–3393.
11. Lenz, R. W. *Adv. Polym. Sci.* **1993**, *107*, 1–40.
12. Mydock, L. K.; Demchenko, A. V. *Org. Biomol. Chem.* **2010**, *8*, 497–510.

13. *Enzyme Nomenclature 1992, Recommendations of the NCIUBMB on the Nomenclature and Classification of Enzymes*, Webb, E. C., Ed.; International Union of Biochemistry and Molecular Biology, Academic Press: San Diego, 1992.
14. Kobayashi, S.; Uyama, H.; Kimura, S. *Chem. Rev.* **2001**, *101*, 3793–3818.
15. Kobayashi, S. *J. Polym. Sci., Part A: Polym. Chem.* **2005**, *43*, 693–710.
16. Kobayashi, S. *Proc. Jpn. Acad., Ser. B* **2007**, *83*, 215–247.
17. Kobayashi, S.; Makino, A. *Chem. Rev.* **2009**, *109*, 5288–5353.
18. Kadokawa, J.; Kobayashi, S. *Curr. Opin. Chem. Biol.* **2010**, *14*, 145–153.
19. Kadokawa, J. *Chem. Rev.* **2011**, *111*, 4308–4345.
20. Shoda, S.; Fujita, M.; Kobayashi, S. *Trends Glycosci. Glycotechnol.* **1998**, *10*, 279–289.
21. Shoda, S.; Izumi, R.; Fujita, M. *Bull. Chem. Soc. Jpn.* **2003**, *76*, 1–13.
22. *Handbook of Glycosyltransferases and Related Genes*; Taniguchi, N., Honke, K., Fukuda, M. Eds.; Springer: Tokyo, 2002.
23. Kitaoka, M.; Hayashi, K. *Trends Glycosci. Glycotechnol.* **2002**, *14*, 35–50.
24. Seibel, J.; Jördening, H.-J.; Buchholz, K. *Biocatal. Biotransform.* **2006**, *24*, 311–342.
25. Rupprath, C.; Schumacher, T.; Elling, L. *Curr. Med. Chem.* **2005**, *12*, 1637–1675.
26. Makino, A.; Kobayashi, S. *J. Polym. Sci., Part A: Polym. Chem.* **2010**, *48*, 1251–1270.
27. Kobayashi, S.; Kashiwa, K.; Kawasaki, T.; Shoda, S. *J. Am. Chem. Soc.* **1991**, *113*, 3079–3084.
28. Kobayashi, S.; Shimada, J.; Kashiwa, K.; Shoda, S. *Macromolecules* **1992**, *25*, 3237–3241.
29. Kobayashi, S.; Wen, X.; Shoda, S. *Macromolecules* **1996**, *29*, 2698–2700.
30. Kobayashi, S.; Kiyosada, T.; Shoda, S. *J. Am. Chem. Soc.* **1996**, *118*, 13113–13114.
31. Kobayashi, S.; Morii, H.; Itoh, R.; Kimura, S.; Ohmae, M. *J. Am. Chem. Soc.* **2001**, *123*, 11825–11826.
32. Kobayashi, S.; Fujikawa, S.; Ohmae, M. *J. Am. Chem. Soc.* **2003**, *125*, 14357–14369.
33. Ohmae, M.; Fujikawa, S.; Ochiai, H.; Kobayashi, S. *J. Polym. Sci., Part A: Polym. Chem.* **2006**, *44*, 5014–5027.
34. Kobayashi, S.; Ohmae, M.; Ochiai, H.; Fujikawa, S. *Chem.—Eur. J.* **2006**, *12*, 5962–5971.
35. Ohmae, M.; Makino, A.; Kobayashi, S. *Macromol. Chem. Phys.* **2007**, *208*, 1447–1457.
36. Ziegast, G.; Pfannemüller, B. *Carbohydr. Res.* **1987**, *160*, 185–204.
37. Fujii, K.; Takata, H.; Yanase, M.; Terada, Y.; Ohdan, K.; Takaha, T.; Okada, S.; Kuriki, T. *Biocatal. Biotransform.* **2003**, *21*, 167–172.
38. Yanase, M.; Takaha, T.; Kuriki, T. *J. Food Agric.* **2006**, *86*, 1631–1635.
39. Ohdan, K.; Fujii, K.; Yanase, M.; Takaha, T.; Kuriki, T. *Biocatal. Biotransform.* **2006**, *24*, 77–81.
40. Boeck, B.; Schinzel, R. *Eur. J. Biochem.* **1996**, *239*, 150–155.

Publication Date (Web): November 22, 2013 | doi: 10.1021/bk-2013-1144.ch011

41. Yanase, M.; Takata, H.; Fujii, K.; Takaha, T.; Kuriki, T. *Appl. Environ. Microbiol.* **2005**, *71*, 5433–5439.
42. Withers, S. G. *Carbohydr. Res.* **1990**, *197*, 61–73.
43. Kadokawa, J. In *Oligosaccharides: Sources, Properties and Applications*; Gordon, N. S., Ed.; Nova Science Publishers, Inc.: Hauppauge, NY, 2011; Chapter 10, pp 269−281.
44. Evers, B.; Mischnick, P.; Thiem, J. *Carbohydr. Res.* **1994**, *262*, 335–341.
45. Evers, B.; Thiem, J. *Starch* **1995**, *47*, 434–439.
46. Evers, B.; Thiem, J. *Bioorg. Med. Chem.* **1997**, *5*, 857–863.
47. Nawaji, M.; Izawa, H.; Kaneko, Y.; Kadokawa, J.-i. *J. Carbohydr. Chem.* **2008**, *27*, 214–222.
48. Nawaji, M.; Izawa, H.; Kaneko, Y.; Kadokawa, J. *Carbohydr. Res.* **2008**, *343*, 2692–2696.
49. Kawazoe, S.; Izawa, H.; Nawaji, M.; Kaneko, Y.; Kadokawa, J. *Carbohydr. Res.* **2010**, *345*, 631–636.
50. Bhuiyan, S. H.; Rus'd, A. A.; Kitaoka, M.; Hayashi, K. *J. Mol. Catal. B: Enzym.* **2003**, *22*, 173–180.
51. Umegatani, Y.; Izawa, H.; Nawaji, M.; Yamamoto, K.; Kubo, A.; Yanase, M.; Takaha, T.; Kadokawa, J. *Carbohydr. Res.* **2012**, *350*, 81–85.
52. Takata, H.; Takaha, T.; Okada, S.; Takagi, M.; Imanaka, T. *J. Ferment. Bioeng.* **1998**, *85*, 156–161.
53. Kitamura, S.; Yunokawa, H.; Mitsuie, S.; Kuge, T. *Polym. J.* **1982**, *14*, 93–99.
54. Kaneko, Y.; Kadokawa, J. In *Handobook of Carbohydrate Polymers*; Ito, R., Matsuo, Y., Eds.; Nova Science Publishers, Inc.: Hauppauge, NY, 2009; Chapter 23, pp 671−691.
55. Omagari, Y.; Kadokawa, J. *Kobunshi Ronbunshu* **2011**, *68*, 242–249.
56. Calder, P. C. *Int. J. Biochem.* **1991**, *23*, 1335–1352.
57. Manners, D. J. *Carbohydr. Polym.* **1991**, *16*, 37–82.
58. Izawa, H.; Nawaji, M.; Kaneko, Y.; Kadokawa, J. *Macromol. Biosci.* **2009**, *9*, 1098–1104.
59. Putaux, J. –L.; Potocki-Véronèse, G.; Remaud-Simeon, M.; Buleon, A. *Biomacromolecules* **2006**, *7*, 1720–1728.
60. Bernfield, M.; Götte, M.; Park, W. P.; Reizes, O.; Fitzgerald, M. L.; Lincecum, J.; Zako, M. *Annu. Rev. Biochem.* **1999**, *68*, 729–777.
61. Stern, R.; Jedrzejas, M. J. *Chem. Rev.* **2008**, *108*, 5061–5085.
62. Matsuda, S.; Kaneko, Y.; Kadokawa, J. *Macromol. Rapid Commun.* **2007**, *28*, 863–867.
63. Kaneko, Y.; Matsuda, S.; Kadokawa, J. *Biomacromolecules* **2007**, *8*, 3959–3964.
64. Omagari, Y.; Kaneko, Y.; Kadokawa, J. *Carbohydr. Polym.* **2010**, *82*, 394–400.
65. Arimura, T.; Omagari, Y.; Yamamoto, K.; Kadokawa, J. *Int. J. Biol. Macromol.* **2011**, *49*, 498–503.
66. Omagari, Y.; Matsuda, S.; Kaneko, Y.; Kadokawa, J. *Macromol. Biosci.* **2009**, *9*, 450–455.

67. Kadokawa, J.; Arimura, T.; Takemoto, Y.; Yamamoto, K. *Carbohydr. Polym.* **2012**, *90*, 1371–1377.
68. Stephen, A. M.; Philips, G. O.; Williams, P. A. *Food Polysaccharides and Their Applications*; Taylor & Francis: London, 1995.

Publication Date (Web): November 22, 2013 | doi: 10.1021/bk-2013-1144.ch011

Publication Date (Web): November 22, 2013 | doi: 10.1021/bk-2013-1144.ch012

Chapter 12

Biocatalytic ATRP: Controlled Radical Polymerizations Mediated by Enzymes

Kasper Renggli, Mariana Spulber, Jonas Pollard, Martin Rother, and Nico Bruns*

Department of Chemistry, University of Basel, Klingelbergstrasse 80, CH-4056 Basel, Switzerland
***E-mail: nico.bruns@unibas.ch**

The advent of controlled radical polymerizations has made polymer science a key discipline for the preparation of nano-, biomedical-, and high tech-materials. Atom transfer radical polymerization (ATRP) is one of the most widely applied controlled radical polymerization. However, an ongoing quest is to develop ATRP reaction conditions that allow reducing the amount of catalyst needed, or to replace the currently used transition metal complex catalysts with less toxic ones. Using enzymes as catalysts is a classic strategy in the green chemistry approach, and many enzymatic polymerizations are known. However, controlled radical polymerizations that are catalyzed by enzymes or proteins were not known until our discovery that the metalloproteins horseradish peroxidase and hemoglobin can polymerize vinyl-monomers under conditions of activators regenerated by electron transfer (ARGET) ATRP. In this book chapter, we review the emerging field of biocatalytic ATRP.

In Green Polymer Chemistry: Biocatalysis and Materials II; Cheng, H., et al.;
ACS Symposium Series; American Chemical Society: Washington, DC, 2013.

Publication Date (Web): November 22, 2013 | doi: 10.1021/bk-2013-1144.ch012

Introduction

Radical polymerization is one of the most widely employed reactions to synthesize polymers on an industrial scale or in academic labs, due to its simplicity and tolerance of functional groups. Products like polystyrene (e.g. Styrofoam), polymethylmethacrylate (Plexiglass), and polyvinylchloride (PVC) are all synthesized on a scale of millions of tons worldwide by free radical polymerization, i.e. a chain growth polymerization in which the active, propagating species are radicals. These radicals are highly reactive and readily undergo termination and side reactions that interrupt the growth of a polymer chain (*1*). Due to the short life-span of the growing chains, they are active for about 1 s, chemical control of these reactions is poor, giving rise to ill-defined molecular weights and preventing end-group-functionalization of polymer chains (*1*). Poor control represents the main drawback of the method, especially when well-defined molecular weights, architectures, sequences of monomers, and functional chain end groups are desired. For example, block copolymers of a specific design can be used as emulsifiers, as drug-delivery systems, as building blocks for nanostructures, and as materials in solar cells and batteries (*2–7*). The formation of conjugates of polymers and proteins, e.g. for therapeutic applications, relies on the well-defined end-group chemistry of polymers (*8*, *9*). If control of radical polymerization is achieved, some materials' applications, e.g. self-healing plastics, can be implemented (*10*). Over the last two decades, synthesis techniques have been developed that allow controlling radical polymerization, such as atom transfer radical polymerization (ATRP), reversible addition-fragmentation chain transfer (RAFT) polymerization, and nitroxide-mediated radical polymerization (NMP) (*1*, *11*). Each of these methods has its specific strengths and drawbacks. ATRP is one of the most popular, controlled radical polymerizations because of its great versatility: It is applicable to most vinyl and styrene monomers, tolerates most functional groups, is compatible with proteins and other biomolecules and it results in halide-terminated polymer chains that can be easily converted into a multitude of other functional end-groups (*1*, *11–14*). ATRP relies on the reversible deactivation of propagating radicals by transition metal complex catalysts, most often copper(I)-copper(II) redox couples, thus lowering the radical concentration in a reaction and therefore the chances of chain termination, while still producing reactive chain ends (*1*). Without a doubt, ATRP and other controlled radical polymerizations are amongst the most important recent developments in the field of polymer chemistry and have spurred thousands of scientific publications and several industrial processes (*11*). Polymers prepared by ATRP can be used, e.g., as sealants, lubricants, oil additives, wetting agents, blend compatibilizers, surfactants and pigment stabilizers (*11*). However, ATRP also suffers some limitations. The catalysts are tedious to remove from a polymer product, causing unwanted coloration, toxicity and environmental issues (*12*, *15*). The problem of residual traces of transition metal or amine ligands in final products can hinder biomedical, food-grade, and electronic applications of the polymers. Several recent developments aim to make ATRP environmentally friendlier and the resulting polymers more compatible with biomedical, food grade and electronic requirements. Less toxic iron catalysts are investigated

In Green Polymer Chemistry: Biocatalysis and Materials II; Cheng, H., et al.;
ACS Symposium Series; American Chemical Society: Washington, DC, 2013.

as alternative to copper-based catalysts (*13*)(*16*), the ATRP catalyst can be scavenged during work-up of the polymerization (*12*, *15*) and variations of the experimental protocol of ATRP, such as Activators ReGenerated by Electron Transfer (ARGET) and Initiators for Continuous Activator Regeneration (ICAR) ATRP lead to a significant reduction in concentration of catalysts required for this polymerization (*11*, *12*).

Radical polymerizations are not limited to man-made processes. Nature uses radical polymerization to produce a variety of biopolymers (*17*). The prime example is the synthesis of lignin by an enzyme-catalyzed coupling between aromatic compounds (*18*). Lignin's key function is to strengthen wood, and it is the second most abundant polymer on earth (*19*). However, the manner in which Nature controls this polymerization is not fully elucidated and is a topic of ongoing scientific debate (*18–20*). Enzymes are environmentally friendly, sustainable, and non-toxic catalysts (*21*). They are derived from natural resources, are completely biodegradable (and even edible), and work under mild conditions such as ambient temperature, ambient pressure and in aqueous solution. Moreover, they are highly selective, allowing for desired regio-, stereo-, or chemo-selective transformations. Not surprisingly, enzymes have been extensively used *in vitro* to the benefit of synthetic chemists, and are often considered as "green" alternatives for conventional catalysts (*21–25*). Indeed, many enzymatic reactions have been exploited for the synthesis of polymers, including polycondensation, ring-opening polymerizations, free radical polymerizations of vinyl-type monomers and the polymerization of aromatic compounds by radical-induced oxidative coupling (*22–25*). However, controlled radical polymerizations catalyzed by enzymes remained unknown. Recently our group (*26*, *27*) and di Lena and coworkers (*28*) discovered concurrently and independently that some metalloproteins can mediate ATRP. These findings represent the first reports of biocatalytic, controlled radical polymerization.

Publication Date (Web): November 22, 2013 | doi: 10.1021/bk-2013-1144.ch012

ATRPases

While investigating conjugates of proteins and copper complexes as ATRP catalysts to confine radical polymerization into the cavity of the protein cage thermosome (*29*, *30*), we discovered that the heme proteins horseradish peroxidase (HRP) and bovine hemoglobin (Hb) can catalyze the polymerizations of N-isopropylacrylamide (NIPAAm), polyethyleneglycol methylether acrylate (PEGA) and polyethyleneglycol methylether methacrylate (PEGMA) in aqueous solutions under ARGET ATRP conditions, i.e. in the presence of an excess of ascorbic acid or sodium ascorbate as reducing agents (Figure 1) (*26*, *31*). The polmyerizations were not only catalyzed by pure enzymes, but also by fresh red blood cells.

Investigation of PNIPAAm polymers with ^{1}H COSY NMR and neutron activation analysis (NAA) revealed that the polymer chains carried the ATRP initiator and that the chains were bromine terminated (*26*). Thus, the activity of the enzymes in these reactions encompasses radical formation due to a homolytic cleavage of a C-Br bond of an organohalogen initiator, and reversible halogen

In Green Polymer Chemistry: Biocatalysis and Materials II; Cheng, H., et al.;
ACS Symposium Series; American Chemical Society: Washington, DC, 2013.

atom transfer from the initator to the enzyme and back to the polymer chain, giving rise to the same type of radical control as in conventional, transition-metal catalyzed ATRP. We therefore named this novel activity of enzymes and proteins ATRPase activity.

While HRP can be used without further modification as a catalyst in these reactions, native Hb formed protein-polymer conjugates, due to radical chain transfer to a free cysteine residue on the surface of the protein. Blocking the cysteine with *N*-(2-hydroxyethyl) maleimide prior to polymerization (yielding Cys-blocked Hb) suppressed this side reaction.

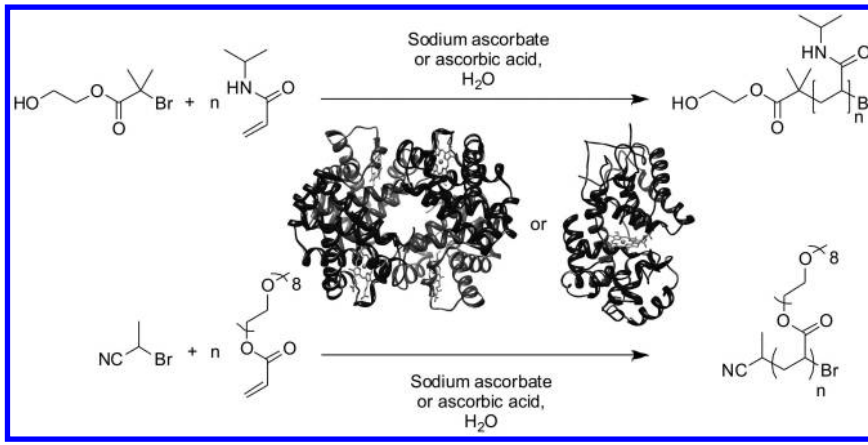

Figure 1. Examples of ATRP catalyzed by hemoglobin (Cys-blocked Hb) or horseradish peroxidase (HRP).

The polymerizations with HRP and Cys-blocked Hb followed first order kinetics at room temperature and yielded polymers with relatively low molecular weight distributions. Using 2-hydroxyethyl-2-bromoisobutyrate (HEBIB) as the initiator, HRP catalyzed the polymerization of NIPAAm to polyNIPAAm with a polydispersity index (PDI) down to 1.44 (*26*). With the same initiator, Cys-blocked Hb produced polyPEGA with PDIs between 1.14 – 1.42 and polyPEGMA with PDIs below 1.2 (*31*). As an example, the kinetics of the polymerization of PEGA using 2-bromopropionitrile (BPN) as the initiator are shown in Figure 2. After an induction period of approx. 30 min in which presuamably small conformational changes occured within the protein (see below), the reaction followed first order kinetics and the molecular weight increased linearly with conversion. The PDI was around 1.1.

Taken together, these findings show that biocatalytic ATRP can result in controlled radical polymerizations and that biocatalysts have potential as environmentally benign catalysts for the synthesis of well-defined polymers. However, the degree of control, especially of NIPAAM polymerizations, was not perfect. Thus, there is still a need to optimize reaction parameters, to identify and suppress possible side reactions and to tailor the ratio of activation and deactivation rates in the ATRP equilibrium.

In Green Polymer Chemistry: Biocatalysis and Materials II; Cheng, H., et al.;
ACS Symposium Series; American Chemical Society: Washington, DC, 2013.

Publication Date (Web): November 22, 2013 | doi: 10.1021/bk-2013-1144.ch012

Publication Date (Web): November 22, 2013 | doi: 10.1021/bk-2013-1144.ch012

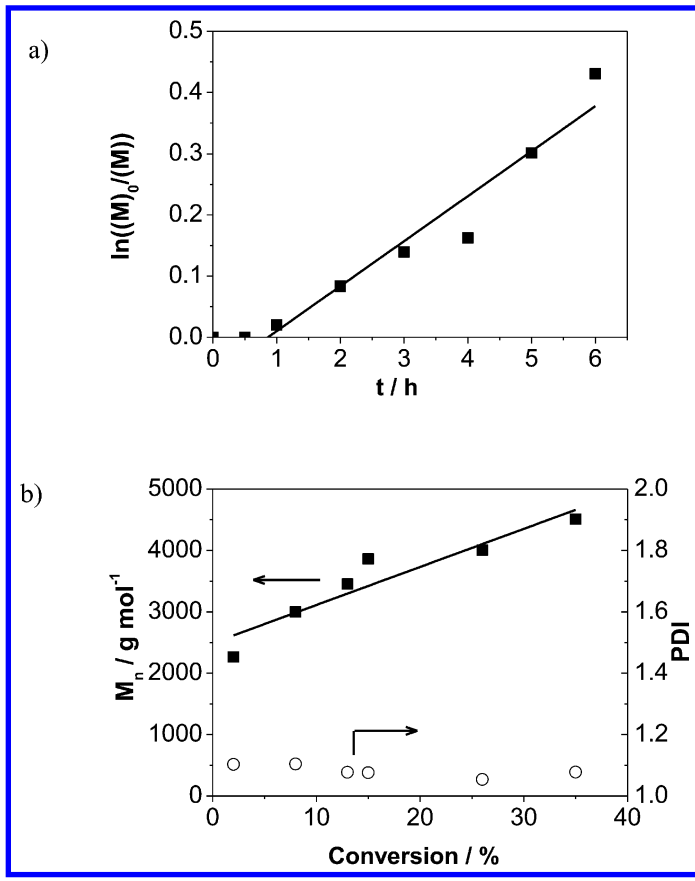

Figure 2. (a) Kinetic plot and (b) evolution of molecular weight (■) and polydispersity index (○) with conversion in an ARGET ATRP of PEGA catalyzed by Cys-blocked Hb using BPN as initiator. (Reaction conditions: Molar ratio of BPN:PEGA:ascorbic acid:Hb 1:77:1:0.007; water, room temperature). (Data from reference (31)).

Enzymes are much more complex catalysts than the simple transition metal complexes usually used for ATRP. The performance of the biomolecules depends not only on the properties of the metal center, but is also a function of the whole macromolecular structure of the biomolecules. Therefore, our studies on ATRPase activity were flanked by extensive characterization of the biomolecules before, during and after the polymerizations with methods including gel electrophoresis, circular dichroism (CD) spectroscopy, UV/Vis spectroscopy and mass spectrometry. HRP and Cys-blocked Hb were stable under the reaction conditions and did not precipitate. Neither did they form conjugates (as revealed by size exclusion chromatography and mass spectrometry; see Figure 3 for the data of HRP). Moreover, the CD spectrum of HRP proved that the protein's

In Green Polymer Chemistry: Biocatalysis and Materials II; Cheng, H., et al.;
ACS Symposium Series; American Chemical Society: Washington, DC, 2013.

structure was not altered during the reaction. Cys-blocked Hb showed some minor changes in the CD spectrum, indicating that it underwent slight conformational changes.

Hb is a tetrameric protein consisiting of two α- and two β-subunits. UV/Vis measurements during the polymerization revealed that, under the chosen reaction conditions with ascorbate as the reducing agent, only the β-subunits participated in the redox reactions involved in ATRP.

These results exemplify that it is essential to study the fundamentals of ATRPase activity, both from a polymer chemistry perspective and from a biochemistry perspective, in order to understand the role of the biomolecules in these reactions.

Publication Date (Web): November 22, 2013 | doi: 10.1021/bk-2013-1144.ch012

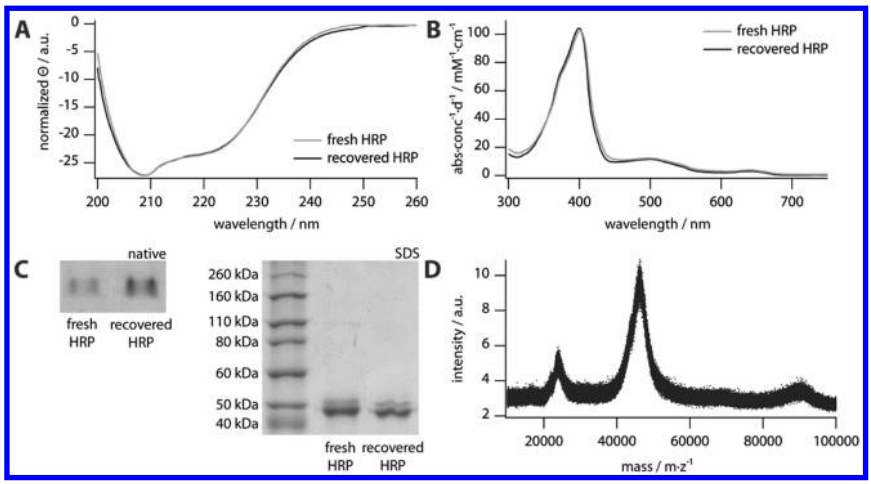

Figure 3. Characterization of HRP before and after polymerization of NIPAAm under ARGET ATRP conditions at pH 6.0 for 16 h. (a) circular dichroism spectra, (b) UV/Vis spectra, (c) native and SDS gel electrophoresis. (d) MALDI-TOF mass spectrum of recycled HRP shows the molecular ion peak of HRP^{+} at m/z 44000, HRP^{2+} at m/z 22000, HRP $dimer^{+}$ at m/z 88000 and HRP $trimer^{2+}$ weak at m/z 66000. (Reproduced with permission from reference (26). Copyright 2011 Wiley-VCH Verlag GmbH & Co. KGaA).

Independent of our results, Di Lena and coworkers reported free radical polymerizations that were initiated from an alkylbromide initiator by the copper enzyme laccase under reductive conditions (*32*). Polymerization of PEGMA was performed in homogeneous aqueous solution. Emulsion polymerization was used for the water-insoluble monomers methylmethacrylate, styrene and hydroxyethyl methacrylate. The reactions were free radical polymerizations with no control over the molecular weight. They yielded polymers of high molecular weight that were often insoluble. The addition of chain transfer agents and of RAFT

agents allowed controlling the reactions. In their next paper, the authors turned to the heme enzyme catalase and the monomer PEGA (*28*). Controlled radical polymerizations were achieved under aqueous ARGET ATRP conditions at 60 °C. The reactions resulted in polymers with low molecular weight distributions (polydispersity indices (PDI) between 1.2 and 1.7), and bromine-terminated chain ends. The molecular weight increased with conversion and the reaction followed first order kinetics. A limited set of reactions was also performed with the enzymes HRP and laccase, with similar results. In these two papers the ezymes were not characterized with biochemical methods during or after the polymerizations. Nevertheless, these reports underscore the fact that enzymes can catalyze ATRP, and therefore the reports from the two groups complement each other nicely.

Publication Date (Web): November 22, 2013 | doi: 10.1021/bk-2013-1144.ch012

Conclusion and Outlook

In conclusion, the first examples of biocatalytic ATRP are promising approaches to alleviating environmental and toxicity issues that hamper conventional ATRP. The investigated enzymes are non-toxic and environmentally friendly catalysts. Moreover, enzymes are easy to remove from a polymerization mixture by methods well-established in biochemistry, such as precipitation with ammonium sulfate or affinity binding to microbeads. Some of the investigated enzymes, especially Hb, are cheap and abundantly available (Hb is a waste product of meat production), scale-up with these enzymes is thus feasible. In order to be able to compete with conventional ATRP catalysts in terms of performance, the biocatalysts will need to improve. Fortunately, a whole range of methods exist in biotechnology to enhance the catalytic performance of biocatalysts. The optimization of simple parameters such as pH, temperature, addition of cosolvents, or the concentration of salts is one possibility. More sophisticated methods include the use of enzymes in organic solvents, or genetic engineering methods.

Enzymes potentially offer opportunities that cannot be realized with conventional ATRP catalysts. For example, some monomers are difficult to polymerize in ATRP. These include amine-containing monomers, as they tend to complex copper non-specifically, and acrylic acid, which protonates the amine-ligands of ATRP catalysts. These problems are unlikely to be encountered with enzymes, as the metal ions are firmly bound within the protein structure and the protonation of coordinating residues and cofactors within the active site is controlled (and therefore buffered) by the overall electrostatic potential of the enzyme. Thus, it is expected that the use of ATRPases can complement the monomer range of ATRP.

Many interesting questions regarding the biochemical mechanism, the scope of monomers and accessible polymers, as well as applications of ATRPases in material and nano sciences, remain yet to be elucidated and will be the scope of future work.

In Green Polymer Chemistry: Biocatalysis and Materials II; Cheng, H., et al.;
ACS Symposium Series; American Chemical Society: Washington, DC, 2013.

Publication Date (Web): November 22, 2013 | doi: 10.1021/bk-2013-1144.ch012

Acknowledgments

Generous financial support by the Swiss National Science Foundation, by the Holcim Stiftung Wissen, by the NCCR Nanosciences, by a Marie Curie Intra European Fellowship and a Marie Curie European Reintegration Grant within the 7th European Community Framework Programme is gratefully acknowledged. We thank Mark Inglin for editing and proofreading the manuscript.

References

1. Braunecker, W. A.; Matyjaszewski, K. *Prog. Polym. Sci.* **2007**, *32*, 93–146.
2. Lazzari, M.; Liu, G.; Lecommandoux, S. *Block Copolymers in Nanoscience*; Wiley-VCH Verlag GmbH & Co. KGaA: Weinheim, Germany, 2008.
3. Kita-Tokarczyk, K.; Grumelard, J.; Haefele, T.; Meier, W. *Polymer* **2005**, *46*, 3540–3563.
4. Onaca, O.; Enea, R.; Hughes, D. W.; Meier, W. *Macromol. Biosci.* **2009**, *9*, 129–139.
5. Renggli, K.; Baumann, P.; Langowska, K.; Onaca, O.; Bruns, N.; Meier, W. *Adv. Funct. Mater.* **2011**, *21*, 1241–1259.
6. Egli, S.; Nussbaumer, M. G.; Balasubramanian, V.; Chami, M.; Bruns, N.; Palivan, C.; Meier, W. *J. Am. Chem. Soc.* **2011**, *133*, 4476–4483.
7. Topham, P. D.; Parnell, A. J.; Hiorns, R. C. *J. Polym. Sci., Part B: Polym. Phys.* **2011**, *49*, 1131–1156.
8. Klok, H. A. *Macromolecules* **2009**, *42*, 7990–8000.
9. Heredia, K. L.; Maynard, H. D. *Org. Biomol. Chem.* **2007**, *5*, 45–53.
10. Wang, H. P.; Yuan, Y. C.; Rong, M. Z.; Zhang, M. Q. *Macromolecules* **2010**, *43*, 595–598.
11. Matyjaszewski, K. *Macromolecules* **2012**, *45*, 4015–4039.
12. Tsarevsky, N. V.; Matyjaszewski, K. *Chem. Rev.* **2007**, *107*, 2270–2299.
13. Ouchi, M.; Terashima, T.; Sawamoto, M. *Chem. Rev.* **2009**, *109*, 4963–5050.
14. Matyjaszewski, K.; Tsarevsky, N. V. *Nat. Chem.* **2009**, *1*, 276–288.
15. Mueller, L.; Matyjaszewski, K. *Macromol. React. Eng.* **2010**, *4*, 180–185.
16. di Lena, F.; Matyjaszewski, K. *Prog. Polym. Sci.* **2010**, *35*, 959–1021.
17. Williams, R. J. P.; Baughan, E. C.; Willson, R. L. *Phil. Trans. R. Soc., B* **1985**, *311*, 593–603.
18. Hatfield, R.; Vermerris, W. *Plant Physiol.* **2001**, *126*, 1351–1357.
19. Boerjan, W.; Ralph, J.; Baucher, M. *Annu. Rev. Plant Biol.* **2003**, *54*, 519–546.
20. Pickel, B.; Constantin, M.-A.; Pfannstiel, J.; Conrad, J.; Beifuss, U.; Schaller, A. *Angew. Chem., Int. Ed.* **2010**, *49*, 202–204.
21. Faber, K. *Biotransformations in Organic Chemistry: A Textbook*; Springer-Verlag: Berlin, 2011.
22. Kobayashi, S.; Makino, A. *Chem. Rev.* **2009**, *109*, 5288–5353.
23. Hollmann, F.; Arends, I. W. C. E. *Polymers* **2012**, *4*, 759–793.
24. Loos, K. *Biocatalysis in Polymer Chemistry*; Wiley-VCH: Weinheim, Germany, 2010.
25. Walde, P.; Guo, Z. *Soft Matter* **2011**, *7*, 316–331.

26. Sigg, S. J.; Seidi, F.; Renggli, K.; Silva, T. B.; Kali, G.; Bruns, N. *Macromol. Rapid Commun.* **2011**, *32*, 1710–1715.
27. Kali, G.; Silva, T. B.; Sigg, S. J.; Seidi, F.; Renggli, K.; Bruns, N. ATRPases: Using Nature's Catalysts in Atom Transfer Radical Polymerizations. In *Progress in Controlled Radical Polymerization: Mechanisms and Techniques*; Matyjaszewski, K., Sumerlin, B. S., Tsarevsky, N. V., Eds.; ACS Symposium Series 1100; American Chemical Society: Washington, DC, 2012; pp 171-181.
28. Ng, Y.-H.; di Lena, F.; Chai, C. L. L. *Chem. Commun.* **2011**, *47*, 6464–6466.
29. Bruns, N.; Renggli, K.; Seidi, F.; Kali, G. *Polym. Prepr. (Am. Chem. Soc., Div. Polym. Chem.)* **2011**, *52*, 521–522.
30. Bruns, N.; Pustelny, K.; Bergeron, L. M.; Whitehead, T. A.; Clark, D. S. *Angew. Chem., Int. Ed.* **2009**, *48*, 5666–5669.
31. Silva, T. B.; Spulber, M.; Kocik, M. K.; Seidi, F.; Charan, H.; Sigg, S. J.; Rother, M.; Renggli, K.; Kali, G.; Bruns, N. *Biomacromolecules* **2013**, DOI: 10.1021/bm400556x.
32. Ng, Y.-H.; di Lena, F.; Chai, C. L. L. *Polym. Chem.* **2011**, *2*, 589–594.

Publication Date (Web): November 22, 2013 | doi: 10.1021/bk-2013-1144.ch012

Publication Date (Web): November 22, 2013 | doi: 10.1021/bk-2013-1144.ch013

Chapter 13

Microbial Plastic Factory: Synthesis and Properties of the New Lactate-Based Biopolymers

John Masani Nduko, Ken'ichiro Matsumoto, and Seiichi Taguchi*

Division of Biotechnology and Macromolecular Chemistry, Graduate School of Engineering, Hokkaido University, N13W8, Kita-ku, Sapporo 060-8628, Japan
***Tel./Fax: +81-11-706-6610. E-mail: staguchi@eng.hokudai.ac.jp.**

The dwindling nature of petroleum resources and increased emission of greenhouse gases into the atmosphere have accelerated efforts towards the finding of alternatives to the extensively used petroleum-derived plastics, with a 'green agenda'. Polylactic acids (PLAs), which are produced from renewable biomass, have gained enormous attention as replacements for the conventional synthetic petroleum-derived plastics due to their biodegradability and bioresorbability. However, the current system of PLA synthesis involves a two-step bio-chemo process, where fermentative lactic acid is polymerized using heavy metal catalysts. The remnants of metal catalysts hinder the PLA application for medical devices and food handling packages. To circumvent these challenges, bacteria have been engineered to produce lactate (LA)-based polyesters in a single-step metal-free system, which is the focus of this review. First, the discovery of a lactate-polymerizing enzyme (LPE) that facilitated the creation of a microbial plastic factory (MPF) for the synthesis of LA-based polyesters will be discussed in detail. Then, approaches for the enrichment of LA fraction in LA-based polyesters including the change of

In Green Polymer Chemistry: Biocatalysis and Materials II; Cheng, H., et al.;
ACS Symposium Series; American Chemical Society: Washington, DC, 2013.

culture conditions, the use of metabolically engineered bacteria and further evolution of LPE are described. Furthermore, the expansion of monomers that could be copolymerized with LA, the properties of LA-based polyesters, the transfer of the LA-based production system into other bacteria resulting into the synthesis of PLA-like polyesters and the engineering of new LPEs, will be highlighted. Finally, the future perspectives of the MPF for the synthesis of LA-based polyesters are discussed.

Publication Date (Web): November 22, 2013 | doi: 10.1021/bk-2013-1144.ch013

Introduction

Global concerns pertaining to the depletion of fossil resources, increased energy demands and elevated levels of atmospheric CO_2 have accelerated the search of substitutes for the petrochemical-derived fuels and materials (*1*, *2*). Polylactic acids (PLAs) are biodegradable aliphatic polyesters produced from renewable resources as alternatives to the conventional synthetic petrochemical-derived polymers such as polypropylene and polystyrene etc (*3*, *4*). PLAs have good mechanical properties, light weight, and processability and have a low environmental impact. In addition, their biodegradability and biocompatibility renders them attractive for applications in the medical and agricultural fields (*5–9*). The unprecedented momentum on PLAs research has not only been on their synthesis, but also on their modification through blending, stereocomplexation, and copolymerization among others so as to enhance their properties and biodegradability (*6*, *10–12*). PLAs are thus potential materials as replacements of the petrochemical-derived plastics for a myriad of applications.

The current standard route of PLA synthesis involves the oligomerization of lactic acid into lactides and the polymerization of the lactides into PLA by the ring-opening polymerization method using heavy metal catalysts such as tin (*6*, *8*, *13–16*). Most of the lactic acid used for the synthesis of PLA is sourced from fermentation processes. Typically, strains of *Lactobacillus* that give high yields are used to convert carbohydrates into lactic acid (*17*). The lactic acid produced is then recovered from the fermentation broth, whereby calcium hydroxide is used to precipitate lactic acid as calcium lactate. Lactic acid is then recovered by the addition of sulfuric acid followed by purification (*16*). The purified lactic acid is transformed into a cyclic dimer, lactide, which can exist in three different forms i.e. D, D lactide, L, L-lactide and D, L-lactide (*meso*-lactide). The stereochemical composition of the lactides influences the properties of the resulting PLA. The two-step process for PLA synthesis is complicated, rendering this polymer more costly compared to the petrochemical-derived polyesters and the use of heavy metal catalysts limits the application of PLA in the medical and food handling fields due to potential toxicity of the heavy metal remnants (*16*, *18*, *19*).

To decipher these bottlenecks, efforts have been made to establish a microbial system; the microbial plastic factory (MPF) for a metal-free single-step process for the synthesis of PLA (*20*). To establish such a microbial system, the simple approach could have been the discovery of microbes with inherent capability

In Green Polymer Chemistry: Biocatalysis and Materials II; Cheng, H., et al.;
ACS Symposium Series; American Chemical Society: Washington, DC, 2013.

to polymerize lactic acid into PLA. Nonetheless, natural pathways for the synthesis of PLA have not been elucidated. Therefore, the establishment of an MPF for the LA-based polymer production through lactic acid polymerization is a daunting task. On the other hand, some bacteria are known to accumulate polyhydroxyalkanoates (PHAs) as carbon and energy reserves when carbon resources are in excess in the environment (*21*, *22*). The PHAs are biocompatible polyesters with similar properties as petrochemical-derived plastics such as polypropylene and rubber (*22*). The most commonly characterized PHA is polyhydroxybutyrate [P(3HB)], which is synthesized in a two step process involving monomer supply and polymerization (*23*). Polymerization is the key step where the polymerizing enzymes (PHA synthases) play a significant role in polymerizing various monomers dependent on the substrate specificity of the PHA synthase (*24*). Lactic acid (2-hydroxypropionic acid) shares structural similarity with PHA monomers hence, it could potentially be polymerized in a similar way as PHA monomers. However, the pioneering works of Valentin et al. (*20*) and Yuan et al. (*25*), which attempted to exploit the PHA biosynthetic system to polymerize lactic acid, were unsuccessful in finding a native PHA synthase capable of polymerizing lactic acid. Nevertheless, working on similar lines, Taguchi et al. (*26*) resorted to the PHA biosynthetic system for the establishment of an MPF for the production of LA-based polymers but, on the premise that; since PHA synthases have been engineered to expand their substrate specificity (*27–31*), artificially evolved enzymes could polymerize LA. In the study, representative native PHA synthases and some mutant PHA synthases were screened in an *in vitro* chemoenzymatic system (*26*, *32*). Serendipitously, a PHA synthase mutant was found that incorporated lactic acid to form P(LA-*co*-3HB) copolymer. After the discovery of this enzyme designated as lactate-polymerizing enzyme (LPE), the establishment of an MPF for the synthesis of LA-based polymers was envisioned (Figure 1).

Subsequently, in a landmark experiment reported by Taguchi et al. in 2008, an MPF for the single-step synthesis of LA-based polyesters in microorganisms was reported for the first time (*26*). The system was assembled by expressing the requisite LA and 3HB monomer supplying enzymes in tandem with LPE in *Escherichia coli*. The first MPF for LA-based polymers was thus established with the production of P(LA-*co*-3HB) having 6 mol% of LA (*26*). These studies laid the foundation upon which subsequent studies related to enhancement of the LA fraction in the copolymer were conducted (*33–38*).

This chapter will give a synopsis into the discovery of LPE and the application of LPE for the production of LA-based polymers with varying LA fractions. Advancement of the MPF into the polymerization of other 3HAs will be highlighted. Furthermore, the transfer of the P(LA-*co*-3HB) production system into *Corynebacterium glutamicum* for the synthesis of PLA-like polyesters will be discussed, and the engineering of a PHA synthase from *Ralstonia eutropha* into LPE status will be mentioned. Polymer properties resulting thereof and future perspectives regarding the MPF for the synthesis of advanced polymers will be highlighted in detail.

In Green Polymer Chemistry: Biocatalysis and Materials II; Cheng, H., et al.;
ACS Symposium Series; American Chemical Society: Washington, DC, 2013.

Publication Date (Web): November 22, 2013 | doi: 10.1021/bk-2013-1144.ch013

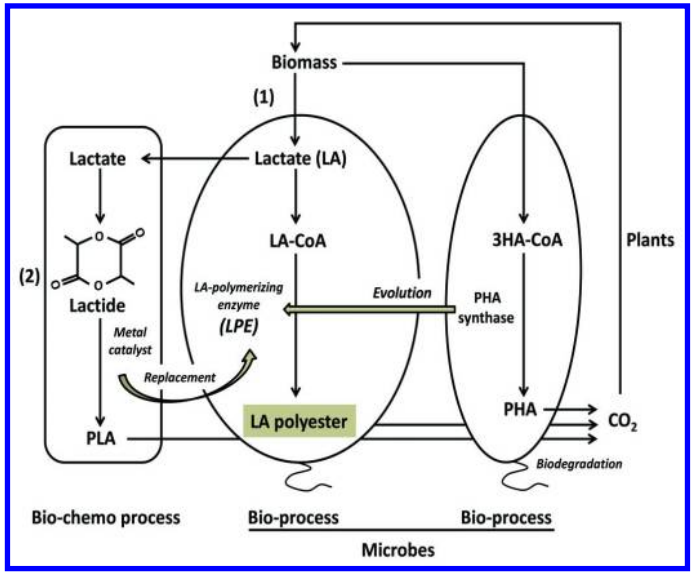

Figure 1. Process conversion for the production of lactate (LA)-based polyesters from the two-step bio-chemo process, which involves fermentation (1) and chemical polymerization (2) into a single-step metal free bio-process using microbes. The lactate-polymerizing enzyme (LPE) is the key to the process conversion. Figure adapted from Nduko et al. (39).

Establishment of a Microbial Plastic Factory for the Synthesis of LA-Based Polymers in Bacteria

Studies That Facilitated the Discovery of a Lactate-Polymerizing Enzyme (LPE)

The major impediment towards the establishment of an MPF for the synthesis of LA-based polymers had been the lack of naturally occurring LPEs and pathways resulting into the formation of LA-based polymers. However, due to the structural similarity of PLA and PHAs, the PHA biosynthetic system could be manipulated to polymerize LA. Such successful manipulation will allow the microbial accumulation of LA-based polymers analogous to PHAs, thus overcoming the need for lactic acid purification and polymerization using heavy metal catalysts associated with PLA production (*19*). In the PHA biosynthetic system, PHA synthases are the key enzymes that play the ultimate role of monomer polymerization (*24*). PHA synthases are categorized into four classes (Class I - IV) on the basis of their primary structures and substrate specificity (*40*). The PHA synthases dictate the polymer composition, molecular weights and have a significant effect on the efficiency of PHA synthesis (*30*, *31*). Therefore, the approach of engineering PHA synthases into LPEs requires the alteration of their

In Green Polymer Chemistry: Biocatalysis and Materials II; Cheng, H., et al.;
ACS Symposium Series; American Chemical Society: Washington, DC, 2013.

substrate specificity. Prior to the discovery of the LPE, several excellent studies related to enhanced enzyme activity and substrate specificity of PHA synthases had been undertaken, revealing that the PHA biosynthetic system is amenable to change so as to expand the repertoire of substrates that can be polymerized (*27*, *41–43*). Of the four classes of PHA synthases (*39*, *44*), the PHA synthase ($PhaC1_{Ps}$) from *Pseudomonas* sp. 61-3 has been a target of directed evolution due to its innate broad substrate specificity. This enzyme polymerizes both short-chain-length (SCL) and medium-chain-length (MCL) hydroxyacyl-CoAs however; its activity towards SCL hydroxyacyl-CoAs is weak (*29*). Despite the lack of structural models of any PHA synthase, directed evolution has been employed to increase the activity of $PhaC1_{Ps}$ towards SCL. For instance, the amino acid residues at positions 130, 325, 477 and 481 of $PhaC1_{Ps}$ were found to be influential towards enzyme activity and substrate specificity of the enzyme (*41*, *45*). These mutations were evolved in different directions and the double mutant, Ser325Thr/Gln481Lys ($PhaC1_{Ps}$STQK) exhibited high *in vitro* and *in vivo* activity (*29*, *46*). Eventually, this mutant was discovered to be an LPE as discussed in the following text.

Publication Date (Web): November 22, 2013 | doi: 10.1021/bk-2013-1144.ch013

Discovery of LPE To Drive the MPF

The pioneering work of screening the PHA synthases for LA polymerization was reported by Valentin et al. (*20*). PHA synthases polymerizes the hydroxyacyl-CoA thioesters releasing CoA in the process (*47*, *48*). In the study, several native PHA synthases were analyzed for LA polymerization and only the class III PHA synthase from *Allochromatium vinosum* exhibited a weak CoA releasing activity but LA polymerization did not occur (*20*). In a similar attempt, Yuan et al. characterized in detail the activity of the PHA synthase from *A. vinosum* towards (*R*) LA-CoA, however LA was not polymerized either (*25*). Towards the discovery of LPE, Taguchi et al. (*26*) concentrated on artificially evolved PHA synthases since evolved PHA synthases have been shown to exhibit a broader substrate specificity spectra (*27–29*) and could potentially polymerize LA. To test this hypothesis, an *in vitro* screening experiment (for details, see references (*26*); and (*32*)) was preferred to the use of microbes due to the overwhelming complexity of the living cells. The screening system was set to include representative native enzymes from each of the four classes of PHA synthases and some mutants from the class II of the PHA synthases; single mutants Ser325Thr(ST) and Gln481Lys(QK), and a double mutant carrying the two mutations (STQK) (*26*). The LA polymerization activity was judged by the formation of a white polymer-like precipitate in a test tube. However, using this system, when LA-CoA was supplied, PLA was not formed by all the representative PHA synthases and the mutants (*26*). Considering the previous reports where a PHA synthase was demonstrated to polymerize a less preferred substrate in the presence of a preferred one, 3-hydroxybutyryl-CoA (3HB-CoA) was supplied as the preferred substrate together with LA-CoA. Notably, one PHA synthase mutant, [$PhaC1_{Ps}$STQK] with a Ser325Thr and Lys481Gln mutations exhibited a polymer-like precipitation when LA-CoA coexisted with a small amount of 3HB-CoA. GC/MS and NMR analysis of the polymer-like precipitate

In Green Polymer Chemistry: Biocatalysis and Materials II; Cheng, H., et al.;
ACS Symposium Series; American Chemical Society: Washington, DC, 2013.

confirmed the formation of a copolymer, [P(LA-*co*-3HB)] containing 36 mol% LA; hence this was the first discovery of an LPE (*26*). From this experiment, the intrinsic character of LPE was revealed; its dependence on 3HB-CoA to exhibit LA-polymerizing activity. The discovery of LPE from PHA synthase mutants was a classical demonstration of the power of evolutionary engineering in generating artificial enzymes with tailor-made properties (*30*). The success of the *in vitro* LA polymerization inspired the desire for rewiring native bacteria to synthesize the LA-based polymers in a similar way as the PHAs. It could be assumed that the heterologous expression of LPE [$PhaC1_{Ps}$(STQK)] could result into the creation of an MPF for the production of LA-based polymers, and this is discussed in the next section.

Publication Date (Web): November 22, 2013 | doi: 10.1021/bk-2013-1144.ch013

Microbial Plastic Factory for Synthesis of LA-Based Polymers

The discovery of LPE was the major breakthrough in the efforts to create an MPF for the synthesis of LA-based polyesters in an environmentally friendly manner from renewable biomass using a single-step process in microbes (*26*, *39*, *49*). The use of microbes could overcome the challenge of using heavy metal catalysts and the costly multi-step processes of producing PLA. *E. coli* was recruited as a host for the synthesis of P(LA-*co*-3HB) due to its genetic tractability, it indigenously produces lactic acid thus it could allow the interfacing of the indigenous and heterologous metabolic pathways, and it has already been used to produce P(3HB) and several other PHAs (*50–52*). *E. coli* does not naturally produce PHAs (*53*), thus in the experimental setup for the production of P(LA-*co*-3HB), the requisite monomer supplying enzymes were expressed alongside LPE (*26*). To create a metabolic link between lactic acid and LA-CoA, a propionyl CoA transferase (PCT) from *Megasphaera elsdenii* that was selected on the basis of its superior LA-CoA formation ability was heterologously expressed and the 3HB-CoA was supplied by the β-ketothiolase (PhaA) and acetoacetyl-CoA reductase (PhaB) from the native P(3HB) producer, *R. eutropha* (*54*). The enzymes were expressed from a vector in *E. coli* JM109 (Figure 2). The recombinant cells were then cultivated in a medium supplemented with glucose for polymer production.

To confirm the *in vivo* polymer synthesis, the cells were analyzed by GC/MS and NMR after cultivation. GC/MS analysis detected ethyl-LA, the ethanolysis product of LA, suggesting the *in vivo* polymerization of LA to form P(LA-*co*-3HB) with 6 mol% LA. To further confirm the incorporation of LA to form P(LA-*co*-3HB), other analyzes were necessary. NMR techniques have been excellent in polymer analysis and the ^{1}H NMR spectra allows the determination of polymer composition (*23*, *55*). When the polymer sample extracted from the bacteria was applied to ^{1}H NMR, the sample exhibited signals characteristic of P(LA-*co*-3HB) copolymer hence, this was the first MPF for the synthesis of LA-based polymers (*26*). In agreement with the *in vitro* experiments, there was no polymer formation in the absence of 3HB-CoA supplying pathway, further confirming the dependence of the LPE on 3HB-CoA for LA polymerization in *E. coli*.

In Green Polymer Chemistry: Biocatalysis and Materials II; Cheng, H., et al.;
ACS Symposium Series; American Chemical Society: Washington, DC, 2013.

Publication Date (Web): November 22, 2013 | doi: 10.1021/bk-2013-1144.ch013

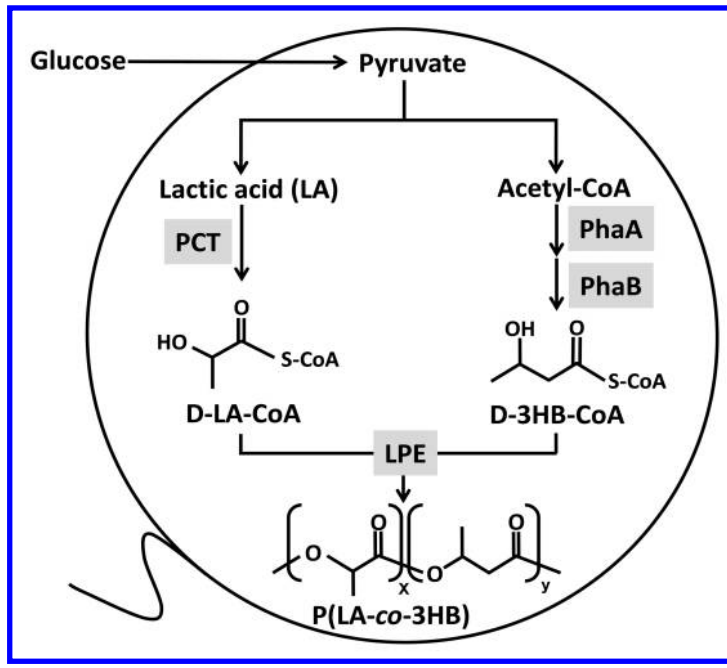

Figure 2. The microbial plastic factory (MPF), E. coli expressing propionyl-CoA transferase (PCT) from Megasphaera elsdenii, β-ketothiolase (PhaA) and acetoacetyl-CoA reductase (PhaB) from R. eutropha and LPE [PhaC1$_{Ps}$(STQK)], mutant of PHA synthase from Pseudomonas sp. 61-3 for the production of P(LA-co-3HB). Lactic acid is intrinsically produced by E. coli.

Enrichment of LA Units in P(LA-*co*-3HB) Polymers

The monomeric constituents affect the polymer properties due to the altered crystallinity and melting temperatures (T_m) (*23*). As demonstrated, the incorporation of 6 mol% of LA into P(LA-*co*-3HB) reduced the T_m of the copolymer compared to that of P(3HB) (*26*). This result suggests that novel materials could be obtained by varying the LA fraction in the copolymers. As a result, strategies such as metabolic engineering, different culture conditions and enzyme evolutionary engineering to regulate monomer composition of the copolymers were applied to enhance incorporation of LA into the copolymers as discussed in the following text.

Use of Metabolically Engineered *E. coli* and Anaerobic Culture Conditions Enhanced LA Units in P(LA-*co*-3HB)

In the *in vitro* chemo enzymatic system for the production of P(LA-*co*-3HB), the LA fraction in the copolymer was 36 mol% when LA-CoA and 3HB-CoA were supplied in a ratio of 1:1 (*26*). This LA fraction was significantly higher than the 6

In Green Polymer Chemistry: Biocatalysis and Materials II; Cheng, H., et al.;
ACS Symposium Series; American Chemical Society: Washington, DC, 2013.

mol% of LA fraction in the copolymer intracellularly accumulated by recombinant *E. coli*. The discrepancy between the *in vivo* and the *in vitro* LA fractions in the copolymers suggested that lactic acid supply in the cells was presumably low. To effectively improve the lactic acid concentrations, a metabolically engineered *E. coli* JW0885 (*pflA*$^-$) strain (*56*, *57*), which had been shown to overproduce lactic acid was employed as a host for P(LA-*co*-3HB) production. By using the recombinant *E. coli* JW0885 expressing the same set of enzymes for P(LA-*co*-3HB) production under the same culture conditions as JM109, *E. coli* JW0885 synthesized P(LA-*co*-3HB) with 26 mol% of LA (*58*). These results suggested that the metabolic engineering strategy for lactic acid overproduction was effective for the enrichment of LA units in the copolymers.

Generally, glucose is metabolized to pyruvate, which is sequentially converted into acetyl-CoA under aerobic conditions. In contrast, pyruvate is converted into lactic acid under anaerobic conditions. This is so since the *ldhA* gene, which encodes lactate dehydrogenase that converts pyruvate into LA, has high activity under anaerobic and acidic conditions (*59*). Further, the lactic acid generated is activated into LA-CoA by the PCT-mediated reaction. Therefore, the cultivation of *E. coli* cells under anaerobic conditions could channel much of the carbon flux towards lactic acid, which in turn could enrich LA fraction in the copolymers. This was demonstrated to be true when recombinant *E. coli* JW0885 cells cultivated under anaerobic conditions resulted into improved lactic acid yields, consequently increasing the LA fraction in P(LA-*co*-3HB) to 47 mol% (*38*). The results suggested that high lactic acid production under anaerobic culture conditions was effective in improving LA fractions in the copolymers. Although, the LA fraction in the copolymers was enhanced under anaerobic conditions, polymer content was reduced (2 wt%), thus strategies enhancing LA units while maintaining high polymer yields are deemed necessary (*33*).

Publication Date (Web): November 22, 2013 | doi: 10.1021/bk-2013-1144.ch013

Enrichment of LA Units in P(LA-*co*-3HB) via Further Engineering of LPE

The discovery of the ancestral LPE laid the foundation for the microbial synthesis of LA-based polymers. To boost the capacity of the LPE to polymerize LA, an engineering strategy was recruited. The engineering was based on the enhanced enzyme activity of a class I PHA synthase ($PhaC_{Re}$) from *R. eutropha* upon the substitution of phenylalanine amino acid at position 420 to serine (*42*). Through homology modelling, an amino acid corresponding to position 420 of $PhaC_{Re}$ was identified as the phenylalanine residue at position 392 on the $PhaC1_{Ps}$(STQK). Thus, site-directed saturation mutagenesis was carried out at this position and the mutants were used for P(LA-*co*-3HB) production using *E. coli* JW0885. The analysis of cells cultivated for polymer production indicated that some of the mutants significantly enhanced the LA fractions in the copolymers (*38*). In particular, a mutant with serine at position 392 of the $PhaC1_{Ps}$(STQK) led to the production of P(LA-*co*-3HB) with 47 mol% LA and polymer contents of 62% under aerobic conditions (*38*). Upon using this mutant, termed as $PhaC1_{Ps}$(STFSQK) under anaerobic conditions, copolymers having 62 mol% LA were obtained. This suggested that position 392 of $PhaC1_{Ps}$(STQK) has a critical role on enzyme activity and/or substrate specificity. Overall, this

In Green Polymer Chemistry: Biocatalysis and Materials II; Cheng, H., et al.;
ACS Symposium Series; American Chemical Society: Washington, DC, 2013.

strategy of enzyme evolutionary engineering played a key role in finding suitable mutants with enhanced LA-polymerization capability.

Copolymerization of Other Monomers with LA

Although PLA is transparent, it lacks flexibility with less than 10% elongation at break (*60*). This property narrows its range of uses with limitations on applications requiring plastic deformation at high stress levels (*61*). In response to these problems, several studies have applied techniques such as blending, copolymerization and addition of plasticizers to improve the properties of PLA (*5*, *17*). However, for the biological systems, monomer composition can be fine-tuned in order to attain the desired properties. For example, the brittle P(3HB) has been copolymerized with 3-hydroxyvalerate (3HV) and 3-hydroxyhexanoate (3HHx) to give copolymers with altered thermal and physical properties (*62*, *63*). In particular, copolymers of 3HV and 3HHx with 3HB are more flexible than P(3HB). In a similar version, the introduction of 3HV or 3HHx monomers into LA-based polymers could render these polymers more flexible.

To incorporate 3HV monomer into P(LA-*co*-3HB), Shozui et al. (*58*) established the metabolic pathway for the supply of 3HV. The 3HV-CoA monomer that could potentially be polymerized was supplied from extraneously supplemented propionate. Once in the cells, propionate could be converted to propionyl-CoA by the inherent *E. coli* acetyl-CoA synthases or propionyl-CoA synthetases and subsequently be converted into 3HV-CoA by PhaA and PhaB (*62*, *64*). The recombinant cells were cultivated on a medium supplemented with glucose and varying concentrations of propionate. The polymers extracted from the cells were terpolymers, [P(LA-*co*-3HB-*co*-3HV)] having 3HV fractions up to 7.2 mol%, which were dependent on the concentrations of the added propionate (*35*). To further investigate the incorporation of 3HV, the authors subjected the terpolymer to NMR analysis. The polymers exhibited ^{13}C signals that were assigned to LA, 3HB and 3HV units in reference to those reported for P(LA-*co*-3HB) and P(3HB-*co*-3HV) (*26*, *65*). Moreover, ^{1}H NMR spectrum revealed chemical shifts of 3HB and LA which were identical to those of P(6 mol% LA-*co*-3HB) reported by Taguchi et al. (*26*). The 3HV signals were in good agreement with those of 3HV reported elsewhere (*65*). These analyses confirmed the presence of 3HV, LA and 3HB units in the polymers. The proton peaks around 0.9 ppm for 3HV in the terpolymer included some peaks slightly shifted to low field. Similar peak shifts were observed on the proton peak of 3HB. However, such peak shifts were not detected on the blends of P(LA-*co*-3HB) and P(3HB-*co*-3HV), suggesting that the signal shift were due to the presence 3HV unit in proximity with LA unit in the same polymer chain. All these results confirmed the formation of P(LA-*co*-3HB-*co*-3HV) in *E. coli*.

To synthesize LA-based polymers containing 3HHx, a new metabolic pathway was designed (*66*). The 3HHx is an MCL monomer of PHA that can be supplied from fatty acids via the β-oxidation pathway. The *R*-specific enoyl-CoA hydratase (PhaJ4) channels the intermediates of the β-oxidation pathway to PHA synthesis (*67*). The attempt to incorporate 3HHx into LA-based polyesters was

In Green Polymer Chemistry: Biocatalysis and Materials II; Cheng, H., et al.;
ACS Symposium Series; American Chemical Society: Washington, DC, 2013.

Publication Date (Web): November 22, 2013 | doi: 10.1021/bk-2013-1144.ch013

made by feeding *E. coli* cells with hexanoate. Unfortunately, hexanoate was found to be toxic and the cells supplied with hexanoate did not grow. To overcome this obstacle, the authors supplied butyrate instead of hexanoate and the cells grew normally and produced polymers (*66*). Surprisingly, analysis of the monomer composition of the synthesized polymers revealed the presence of 3HHx with its molar ratio varying with the concentration of butyrate added into the medium. The highest 3HHx fraction recorded was 38 mol% when the amount of butyrate added was 1.25 mg/mL (*66*). This result implied the activation of the β-oxidation pathway however, working in a reverse manner. In that case, butyrate will be transformed into butyryl-CoA in the cells. The butyryl-CoA will then react with acetyl-CoA to eventually form hexenoyl-CoA. Subsequently, PhaJ4 will channel hexenoyl-CoA into PHAs as illustrated in Figure 3.

Publication Date (Web): November 22, 2013 | doi: 10.1021/bk-2013-1144.ch013

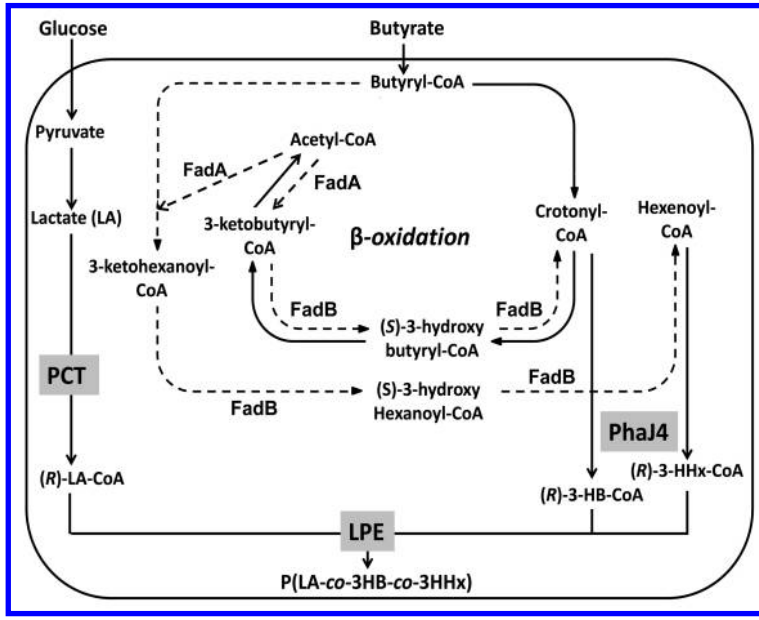

Figure 3. The proposed pathway for the synthesis of P(LA-co-3HB-co-3HHx) in recombinant E. coli LS5218. Dashed arrows represent the reverse reaction of the β-oxidation pathway and the highlighted enzymes were heterologously expressed. PCT, propionyl-CoA transferase from Megasphaera elsdenii; LPE, LA-polymerizing enzyme; PhaJ4, (R)-specific enoyl-CoA hydratase 4 from Pseudomonas aeruginosa. FadA (3-ketoacyl-CoA thiolase) and FadB (3-hydroxyacyl-CoA dehydrogenase/(S)-specific enoyl-CoA hydratase are native to E. coli LS5218.

In Green Polymer Chemistry: Biocatalysis and Materials II; Cheng, H., et al.;
ACS Symposium Series; American Chemical Society: Washington, DC, 2013.

Since the linkage of LA to 3HV in the copolymers had been characterized (*58*), the authors carried out NMR analyses to confirm whether 3HHx could also be polymerized next to LA (*66*). The presence of LA-3HHx in P(LA-*co*-3HB-*co*-3HHx) was confirmed by 2D-NMR analysis, demonstrating that LPE could link LA next to HHx hence it has no limitations regarding the incorporation of monomers next to LA. This property of LPE is advantageous in consideration of the fact that due to its broad substrate specificity; it has potential of synthesizing LA-based polymers with different monomers thus, resulting into materials with novel properties. The potential monomers that could be polymerized by LPE are illustrated elsewhere (*68*).

Publication Date (Web): November 22, 2013 | doi: 10.1021/bk-2013-1144.ch013

Synthesis of P(96 mol% LA-*co*-3HB-3HV)

In the initial reports when P(6 mol% LA-*co*-3HB) was synthesized, it had been observed that there was no LA-based polymer synthesis in the absence of 3HB-CoA supply (*26*). These results suggested that 3HB was essential for the polymerization of LA. In subsequent studies attempting to enrich the LA fractions in the polymers, the use of anaerobic culture conditions, engineering of LPE and metabolic engineering strategies were demonstrated to be effective in enhancing LA fractions, attaining up to 63 mol% LA in the polymers (*33*, *38*, *58*). Furthermore, NMR analysis had indicated the presence of the LA-LA-LA triad sequence in the polymers suggesting the possibility of synthesizing higher LA-containing polymers (*33*). To synthesize LA-enriched polyesters, Shozui et al. eliminated the 3HB-CoA supplying pathway from the P(LA-*co*-3HB) production system and instead introduced PhaJ4 to supply 3HV from extraneously added valerate (*36*). Surprisingly, when valerate was supplied at 0.5 g l^{-1}, the cells accumulated P(LA-*co*-3HB-*co*-3HV) with 96 mol% of LA, which was designated LA96. With valerate concentrations below 0.5 g l^{-1}, the cells grew normally however concentrations higher than that were detrimental to the cells.

To increase the LA units in the copolymers, one strategy is to reduce the 3HB supply. In this study, the authors replaced the 3HB supply pathway with 3HV supply. This strategy proved effective as nearly PLA was synthesized. However, 3HB was also detected in the polymers presumably supplied from the β-oxidation pathway as illustrated in Figure 4. Therefore, the ability of LPE to form P(LA-*co*-3HV) only i.e. the dependence of LPE on 3HV to polymerize LA could not be verified. Nevertheless, these results demonstrated that PLA-like polymers could be produced in bacteria in a single-step process; however the process needs to be optimized to improve polymer yields.

Publication Date (Web): November 22, 2013 | doi: 10.1021/bk-2013-1144.ch013

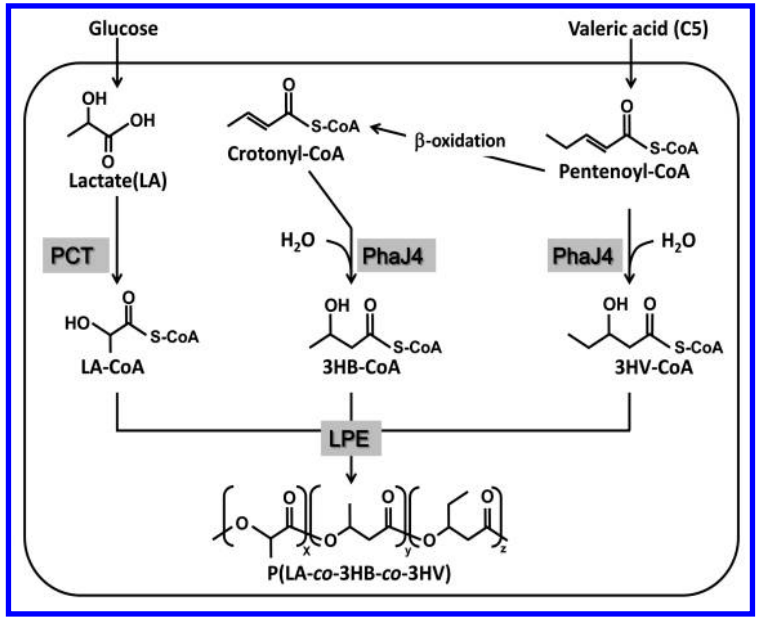

Figure 4. The proposed pathway for the synthesis of P(96 mol% LA-co-3HB-co-3HV) in recombinant E. coli from glucose and valerate. PCT, LPE and PhaJ4 were heterologously expressed.

LA-Based Polymer Properties

Enantiomeric Purity of LA in P(LA-*co*-3HB)

The enantiopurity of PLA affects the crystallinity of the polymer which in turn influences the melting point (T_m) of the polymers. Homopolymers of each LA enantiomer are crystalline polymers with a T_m of approximately 180°C (*16*). The stereocomplex of PDLA and PLLA has been developed and its T_m greatly increases (220 - 230°C) (*68*). The regulation of the enantiopurity is therefore important in determining polymer properties. The enantiopurity of P(LA-*co*-3HB) can be linked to the enantioselectivity of the LPE, which carries out polymerization. Yamada et al. subjected the alkaline hydrolyzate of the P(LA-*co*-3HB) synthesized by bacteria to chiral HPLC analysis (*33*). It was then realized that the microbially synthesized P(LA-*co*-3HB) polymers were all of the *R*(D) forms of LA and 3HB. The native PHA synthases are known to be specific towards *R*-form of the monomers, 3HB inclusive (*24*). Furthermore, Tajima et al. had demonstrated in an *in vitro* chemo-enzymatic polymerization system that only P(*R*-3HB) was synthesized when (*S*)-LA-CoA was fed together with (*R*)-3HB-CoA (*32*). The engineered LPE thus retained its enantioselectivity towards the (*R*)-form of LA. The enantioselectivity of LA in *E. coli* should also

In Green Polymer Chemistry: Biocatalysis and Materials II; Cheng, H., et al.;
ACS Symposium Series; American Chemical Society: Washington, DC, 2013.

be considered in the monomer supplying enzymes; lactate dehydrogenase (LdhA) and PCT. *E. coli* intrinsically possess LdhA that generates D-LA (*69*). PCT on the other hand has no strict selectivity towards either enantiomers, hence in terms of enantioselectivity of P(LA-*co*-3HB) copolymers, LdhA and LPE are the main determinants. The chemical synthesis of P(LA-*co*-3HB) with 100% e.e. has not been achieved, therefore the enantioselectivity of the bio-process has the advantage of producing optically pure P(LA-*co*-3HB)s with desired properties.

Thermal Properties and Transparency of the Copolymers

The interest for polymer modification stems from the ability to alter the properties of polymers, thereby creating a range of designer materials with a plethora of applications. Thermal properties have an effect on the quality of polymeric materials since they are related to thermal resistance and crystallization (*16*). Polymers such as PLA and P(3HB) are crystalline at temperatures above their glass transition temperatures (T_g) (*16*, *23*). The T_g values of PLA and P(3HB) determine their respective properties. PLAs have T_g values above room temperatures (about 55°C) hence PLA films do not crystallize at room temperature and they remain transparent (*16*). On the other hand, P(3HB) has T_g values lower than room temperature (*23*). This makes P(3HB)s to crystallize at room temperature, in the process increasing their brittleness, which limits their use for multiple applications. To address the limitations of P(3HB), copolymerization with MCL monomers, 3HV or 3HHx has been applied to acquire polymers with lower melting temperatures (T_m), lower crystallinity and flexible properties compared to P(3HB) (*70*).

The incorporation of LA to form P(LA-*co*-3HB) could be expected to alter the thermal properties of the copolymers in respect to PLA and P(3HB) homopolymers. As demonstrated by Yamada et al., the T_g and the T_m values of the copolymers ranged between those of PLA and P(3HB) (Table I) (*37*). It was also observed that, with increases in LA fractions in the polymers, the T_g of the copolymer rose significantly with the T_g of LA96 (49.3°C) being compatible with that of chemically synthesized PLA (*36*, *37*). Moreover, the T_m of LA96 (153.3°C) was shown to be similar to that of PLAs (*36*). The slight differences between the biologically produced and chemically synthesized copolymers were attributed to the different enantiomeric configuration of the monomers where; D-LA was polymerized by microorganisms while L-LA is commonly used in chemical copolymer synthesis for the reported cases (*13*, *33*).

The biologically synthesized copolymers with 47 mol% LA were shown to be semi-transparent compared to P(3HB) (Figure 5) (*37*). In general, the transparency of the films prepared had a positive correlation of the LA fraction in the copolymers (see details in reference number (*37*)). Taken together, these findings suggested that copolymers had thermal properties and transparency comparable to the chemically synthesized PLAs hence; they have potential applications in place of the chemically synthesized PLA with respect to thermal properties and transparency.

In Green Polymer Chemistry: Biocatalysis and Materials II; Cheng, H., et al.;
ACS Symposium Series; American Chemical Society: Washington, DC, 2013.

Publication Date (Web): November 22, 2013 | doi: 10.1021/bk-2013-1144.ch013

Publication Date (Web): November 22, 2013 | doi: 10.1021/bk-2013-1144.ch013

Table I. Thermal and mechanical properties of microbially synthesized LA-based polymers. Data from references (*36*), (*37*), and (*71*)

Monomer composition (mol%)		*Molecular weights*		*Mechanical properties*			*Thermal properties*		
LA	*3HB*	M_w (x10^4)	M_w/M_n	*Tensile strength (Mpa)*	*Young's modulus (Mpa)*	*Elongation at break (%)*	T_g (°C)	T_m (°C)	ΔH_m (cal g^{-1})
100	0	20		52±2	1020	2	60	153	2.2
LA96		1.3	1.7	ND	ND	ND	49.3	153.3	9.5
47	53	7	2.3	7±2	153±15	84±20	-8, 34	140, 157	0.4, 1.9
40	60	7	3.5	6±0	148±10	64±7	-8, 30	140, 156	0.3, 1.4
29	71	9	2.2	7±7	154±5	156±34	-8, 25	141,158	0.2, 0.9
15	85	82	2.4	10±0	194±5	75±2	-9, 19	149, 167	0.6, 3.2
4	96	74	4.6	30±4	905±136	7±1	-6	160, 174	1.8, 5.4
0	100	70	2.3	19±1	1079±215	9±1	-7	159, 176	1.6, 9.9

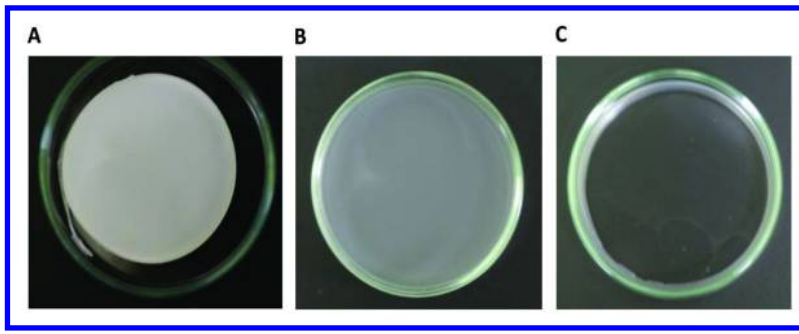

*Figure 5. Solvent-cast films of P(LA-co-3HB) with 47 mol% LA (**B**) compared to P(3HB) film, **A** and PLA film, **C**. Transparency of P(LA-co-3HB) film improved compared to P(3HB) homopolymer.*

Publication Date (Web): November 22, 2013 | doi: 10.1021/bk-2013-1144.ch013

Polymer Sequence and Molecular Weight

The copolymer architecture, either block or random affects polymer properties. One method used to analyze the microstructure nature of the polymers is NMR (*55*, *56*). For the analysis of the monomer sequence of P(LA-*co*-3HB), the LA unit signals in NMR analysis are affected by both the neighboring monomer units. As such, a triplet sequence can be distinguished and especially the methane group can be a good 'fingerprint' (*26*). For the P(LA-*co*-3HB)s, the possible triplet sequences are; LA-LA-LA, LA-LA-3HB, 3HB-LA-LA and 3HB-LA-3HB. The ^{1}H - ^{13}C COSY - NMR profile indicated the clustering sequences of LA-LA-LA and LA-LA, implying that LPE can link two LA units sequentially. Moreover, all the possible triad sequences were detected in the copolymers, indicating that the polymers were random copolymers (*33*).

The molecular weights of polymers affect polymer properties such as tensile strength (*23*). The molecular weights of P(LA-*co*-3HB)s were found to vary inversely with the ratio of LA fractions in the copolymers (Table I) (*36*, *37*). This was thought to be accounted by the fact that although LPE can polymerize LA, the LA-CoA monomer was still not the preferred substrate to achieve the synthesis of high-molecular weight polymers. However, clarification of this issue could be important in facilitating the fine-tuning of the molecular weights of the polymers.

Mechanical Properties of P(LA-*co*-3HB)s

Semicrystalline PLA has an approximate tensile strength of 50 - 70 MPa and an elongation at break of about 4% (*16*). Similarly, P(3HB) has a tensile strength of about 40 MPa and an elongation at break of about 9% (*21*). These properties make these materials brittle and rigid. Copolymerization of P(3HB) with 3HV has been shown to increase the elongation at break, reduce young modulus and tensile strength (*21*). The incorporation of LA into the copolymer could definitely alter the mechanical properties of the polymers. Table I shows the mechanical properties of P(LA-*co*-3HB)s synthesized by microbes (*37*). From the analysis of P(LA-*co*-3HB)s, it was found out that the young modulus of the copolymers

(ranging between 148 - 905 MPa) was lower than those of the PLA and P(3HB) homopolymers, and it had an inverse relationship with the LA fraction in the copolymers. Likewise, the tensile strength had the same tendency. Moreover, the elongation at break of the copolymers was higher than that of the homopolymers. For instance, the elongation at break of copolymers with 29 mol% LA was 150%. These results demonstrated that the P(LA-*co*-3HB) are more pliable and stretchy compared to their respective homopolymers. The results were in good agreement with their thermal properties, which imply reduced crystallinity of the copolymers.

The stretchy and pliable characteristics of P(LA-*co*-3HB)s compares favorably with those of P(3HB-*co*-3HA) previously reported by Matsusaki et al. (*72*). However, P(LA-*co*-3HB)s have a higher T_g that could afford them semi-transparency and long-term stability unlike their counterparts, P(3HB-*co*-HA)s. The chemically synthesized PLAs and P(3HB) lack impact resistance, which is considered an impediment in their applications (*9*, *23*), hence the P(LA-*co*-3HB)s offers an alternative as potent materials covering a broader range of applications.

Publication Date (Web): November 22, 2013 | doi: 10.1021/bk-2013-1144.ch013

Production of P(LA-*co*-3HB) in *Corynebacterium glutamicum*

Thus far, the synthesis of P(LA-*co*-3HB) had been done in the model microbe, *E. coli* (*26*, *36*, *38*). However, to upgrade this prototype system to the practical scale, the Gram-positive *C. glutamicum* which has GRAS status, is endotoxin-free and widely used industrially for the production of amino acids could rank highly as a potential chassis for the production of LA-based polymers (*73*). The consideration of this bacterium stems from its excellent capacity to consume crude sugars such as molasses, it has high cell density and its applications for the production of P(3HB) and other PHAs had already been demonstrated, thus indicating the potential to accumulate LA-based polyesters (*74–76*).

For the synthesis of P(LA-*co*-3HB) in *C. glutamicum*, the necessary pathways were assembled (*34*). The supply of D-lactic acid was achieved by heterologously expressing the D-LdhA from *E. coli* since *C. glutamicum* mainly produces L-lactic acid (*77*). The expression of PCT was confirmed by western blotting and the functional expression of PhaA and PhaB had already been profiled (*76*), hence 3HB-CoA and LA-CoA could be generated in *C. glutamicum*. With the expression of the monomer supplying pathways, LPE was introduced, thus the requisite pathways for the production of P(LA-*co*-3HB) in *C. glutamicum* were assembled (Same as Figure 2 with additional expression of D-LdhA from *E. coli*) (*34*). The recombinant cells cultivated on glucose were analyzed, and the result obtained was a stark contrast of those obtained in *E. coli*. Whereas, *E. coli* cells harboring the same set of genes could produce P(LA-*co*-3HB) with up to 47 mol% of LA (*37*), *C. glutamicum* synthesized copolymers with 97 mol% LA (*34*). The high LA fractions of LA-based polymers synthesized by *C. glutamicum* was attributed to the weak 3HB supply in *C. glutamicum* supported by the fact that the P(3HB) yield when the D-LA-CoA supplying enzyme, PCT was eliminated was lower compared to the P(LA-*co*-3HB) yield.

In Green Polymer Chemistry: Biocatalysis and Materials II; Cheng, H., et al.;
ACS Symposium Series; American Chemical Society: Washington, DC, 2013.

The low 3HB fraction in the copolymers synthesized in *C. glutamicum* led to the investigation of the necessity of the 3HB-CoA supplying enzymes. It was then found that unlike *E. coli*, with the elimination of PhaA and PhaB from the system, *C. glutamicum* could still produce P(LA-*co*-3HB)s with almost 100% LA fraction (*34*). This result gave an impression that PhaA and PhaB are not necessary for the production of P(LA-*co*-3HB)s in *C. glutamicum*. Since there were minute 3HB units in the PLA-like polyester, an endogenous 3HB-CoA supplying pathway could be predicted to exist in *C. glutamicum*. The polymer yield and the molecular weights of the PLA-like copolymer were found to be lower compared to the polymers synthesized with the presence of PhaA and PhaB. This phenomenon was consistent with that previously observed in *E. coli* (*36*, *37*). The PLA-like polymer produced in *C. glutamicum* exhibited strong resonances of LA in the ^{1}H NMR analysis which is characteristic of chemically synthesized PLA but with weak 3HB signals (*34*). This study demonstrated the ability of *C. glutamicum* to produce PLA-like polymers, suggesting that the bacterium milieu and/or genetic diversity could play a critical role in regulating the monomer ratio of P(LA-*co*-3HB). The production of PLA-like copolymers in *C. glutamicum* was an exemplary case, which eliminates the need of the additional costly co-substrates that were employed in synthesizing LA96 in *E. coli* (*36*). However, the system was characterized by low polymer yields, which calls for further engineering of the metabolic circuitry of the bacterium for the realization of an economically viable system with precise control of monomer composition of the polymers. Furthermore, the use of other bacteria might prove useful in expanding the spectra of microbially producing LA-based polymers with novel character and monomer composition efficiently.

Engineering of Other PHA Synthases To Acquire LA-Polymerizing Activity

The ancestral LPE [PhaC1$_{Ps}$(STQK)] was a double mutant of the class II PHA synthase from *Pseudomonas* sp. 61-3 (*26*, *29*). Since the discovery of this LPE in 2008 by Taguchi et al. (*26*), several LPEs have been reported (*78*, *79*), but all these are members of the class II of the PHA synthases rationally engineered on the basis on the PhaC1$_{Ps}$(STQK) with similar property. To expand the LPE character, it is useful to consider the engineering of the PHA synthases of other classes to obtain LPEs with diverse substrate specificity and activity. The engineering of the class I PHA synthase representative (PhaC$_{Re}$) from *R. eutropha* to attain LPE status is therefore an attractive target since this enzyme intrinsically has high productivity and synthesizes high-molecular weight polymers (*31*). The best strategy to implement this is to apply the accumulated knowledge that led to the finding of LPE [PhaC1$_{Ps}$(STQK)] where positions S325 and Q481 of PhaC1$_{Ps}$ had been identified as essential for the LA-polymerizing activity (*26*). Predictably, the alteration of the amino acids of PhaC$_{Re}$ (positions 348 and 510), which corresponds to S325T and Q481K mutations of PhaC1$_{Ps}$(STQK), respectively could confer PhaC$_{Re}$ with LPE status. The residue, Thr348 in PhaC$_{Re}$ is identical to the corresponding mutation in PhaC1$_{Ps}$(STQK). However, the

In Green Polymer Chemistry: Biocatalysis and Materials II; Cheng, H., et al.;
ACS Symposium Series; American Chemical Society: Washington, DC, 2013.

Publication Date (Web): November 22, 2013 | doi: 10.1021/bk-2013-1144.ch013

residue at position 510 of $PhaC_{Re}$, which corresponds to the residue at position 481 in $PhaC1_{Ps}$(STQK), is Ala. As was reported by Ochi et al., saturation mutagenesis of $PhaC_{Re}$ at position 510 resulted to 15 mutants with LA-polymerizing activity. The P(LA-*co*-3HB)s synthesized by the mutants had LA molar fractions of up to 40% (*80*), hence this was the first report of a class I PHA synthase mutant to polymerize LA.

The P(8 mol% LA-*co*-3HB) synthesized by A510S mutant of $PhaC_{Re}$ that gave stable molar ratios in the copolymer and high productivity had a weight average molecular weight (M_w) of 3.2×10^5, suggesting that $PhaC_{Re}$ mutants could synthesize high molecular weight copolymers (*80*). The ^{1}H NMR analysis of the major fraction of P(LA-*co*-3HB) synthesized by A510S mutant, which was fractionated by GPC gave resonances indicating the presence of LA unit in the copolymer. Interestingly, the sequence of the copolymer indicated unusually high LA-LA-LA triad sequences. The sequence of the polymer was predicted to have LA rich regions, suggesting the block nature of the copolymer (*80*). The synthesis of block copolymers is of particular interest since their microstructure where two or more polymer regions/blocks are covalently linked provides the polymers with properties of each block, thus achieving new properties that could not be provided by either blending or random copolymerization (*81*). The synthesis of LA-based copolymers using $PhaC_{Re}$ mutants was therefore a milestone that should contribute to the controlled synthesis of an array of LA-based polymers. With improvements in yield, these $PhaC_{Re}$ mutants could complement the $PhaC1_{Ps}$(STFSQK) in generating new materials, which could offer alternatives to the petroleum-based plastics.

Conclusions and Future Perspectives

As the results discussed here show, the successful establishment of an MPF for the production of LA-based polyesters was facilitated by the discovery of an engineered enzyme that was integrated into a synthetic pathway. Initially, the first copolymers to be synthesized in bacteria had low LA fractions (6 mol% LA) (*26*). However, through the interaction of enzyme evolutionary engineering and metabolic engineering strategies together with the modification of culture conditions, the LA fractions in the copolymers have been significantly improved (*33*, *36*, *38*). In particular, the use of an advanced version of LPE in metabolically engineered *E. coli* gave about 50 mol% of LA units in the copolymers with relatively high polymer yields from glucose (*38*). Substitution of the 3HB-CoA monomer supply pathway by extraneously adding valerate as the 3HV precursor saw the synthesis of LA96, which was demonstrated to exhibit properties similar to chemically synthesized PLA (*36*). Furthermore, the broad substrate specificity character of LPE was exploited in the copolymerization of 3HV and 3HHx, thereby expanding the properties of materials synthesized (*58*, *66*). With the transfer of the P(LA-*co*-3HB) synthesis system into *C. glutamicum,* PLA-like polyesters were synthesized (*34*), indicating that further exploration of bacterial hosts might not only enhance the LA fractions, but also improve polymer yields. The engineering of the class I PHA synthase ($PhaC_{Re}$) into LPE status was a

In Green Polymer Chemistry: Biocatalysis and Materials II; Cheng, H., et al.;
ACS Symposium Series; American Chemical Society: Washington, DC, 2013.

Publication Date (Web): November 22, 2013 | doi: 10.1021/bk-2013-1144.ch013

significant effort towards finding polymerases with unique LA polymerizing properties (*80*). Moreover, recently the use of xylose as a carbon source has been shown to be superior to glucose in giving high-yield LA-enriched copolymers in *E. coli* (*82*). All these successes related to the LA-based polymer production in *E. coli* and *C. glutamicum* described above offers great promises in accelerating the commercial production although optimization processes remains to be accomplished.

Then what are the remaining challenges for the full commercialization of LA-based polyesters? First, it was observed that the synthesis of high LA-containing copolymers led to a drop in polymer yields and molecular weights (*34*, *36*, *37*). These are obstacles, which calls for multifaceted approaches such as metabolic engineering, enzyme evolutionary engineering and synthetic biology among others to tackle. The low polymer yield/molecular weights could be as a result of LA not being a suitable substrate therefore; continued pursuit of LPEs with superior properties should be undertaken. For instance, the attempts to create new LPEs such as $PhaC_{Re}$ mutants (*80*), and the thermotolerant LPE reported by Tajima et al. (*79*) gives promising results and indicates that a superior LPE could be engineered that will allow the high-yield synthesis of LA-based polymers with high molecular weights and unique properties. In addition, efforts should also be directed towards the understanding of copolymer synthesis mechanism as this will allow the reengineering of the MPF with reconstructed metabolic and gene regulatory networks for optimum channeling of carbon fluxes towards the desired polymer products with minimum by-product formation, efficient biotransformation of sugars into polymers and overall high productivity. As already demonstrated by other groups (*83–87*), the use of the inexpensive carbon sources such as molasses, starch, whey and lignocellulosic biomass for the production of LA-based polyesters could contribute towards the reduction of the cost of producing these attractive polymers. This will enhance the competitiveness of LA-based polymers against their petrochemical-derived counterparts and thus contribute to the creation of a sustainable 'bioeconomy'.

Publication Date (Web): November 22, 2013 | doi: 10.1021/bk-2013-1144.ch013

Abbreviations

LA: Lactic acid/lactate
PLA: polylactic acid/polylactate
LPE: Lactate-polymerizing enzyme
MPF: Microbial plastic factory
HAs: Hydroxyalkanoates
PHAs: Polyhydroxyalkanoates
3HB: 3-hydroxybutyrate
P(3HB): Poly(3-hydroxybutyrate)
P(LA-*co*-3HB): Poly(lactate-*co*-3-hydroxybutyrate)
LA-CoA: Lactyl-CoA
3HB-CoA: 3-hydroxybutyryl-CoA
PCT: Propionyl-CoA transferase
PhaA: β-ketothiolase

In Green Polymer Chemistry: Biocatalysis and Materials II; Cheng, H., et al.;
ACS Symposium Series; American Chemical Society: Washington, DC, 2013.

PhaB: Acetoacetyl-CoA reductase

PflA: Pyruvate formate-lyase activating enzyme

$PhaC_{Re}$: Polyhydroxyalkanoate synthase from *Ralstonia eutropha*

$PhaC1_{Ps}$: Polyhydroxyalkanoate synthase from *Pseudomonas* sp. 61-3

3HV: 3-hydroxyvalerate

3HV-CoA: 3-hydroxyvaleryl-CoA

3HHx: 3-hydroxyhexanoate

P(LA-*co*-3HB-*co*-3HV): Poly(lactic acid-*co*-3-hydroxybutyrate-*co*-3-hydroxyvalerate)

LA96: P(LA-*co*-3HB-*co*-3HV) with 96 mol% LA

P(LA-*co*-3HB-*co*-3HHx): Poly(lactic acid-*co*-3-hydroxybutyrate-*co*-3-hydroxyhexanoate)

SCL: Short-chain-length

MCL: Medium-chain-length

$PhaC1_{Ps}$(STQK): $PhaC1_{Ps}$ with two mutations; Ser325Thr and Gln481Lys

$PhaC1_{Ps}$(STFSQK): PhaC1Ps with three mutations; Ser325Thr, Phe392Ser and Gln481Lys

PhaJ4: R-specific enoyl-CoA hydratase

FadA: 3-ketoacyl-CoA thiolase

FadB: 3-hydroxyacyl-CoA/(*S*)-specific enoyl-CoA hydratase

LdhA: Lactate dehydrogenase

References

1. Fortman, J. L.; Chhabra, S.; Mukhopadhyay, A.; Chou, H.; Lee, T. S.; Steen, E.; Keasling, J. D. *Trends Biotechnol.* **2008**, *26*, 375–381.
2. Mecking, S. *Angew. Chem., Int. Ed. Engl.* **2004**, *43*, 1078–1085.
3. Carrasco, F.; Pages, P.; Gamez-Perez, J.; Santana, O. O.; Maspoch, M. L. *Polym. Degrad. Stab.* **2010**, *95*, 116–125.
4. Lim, L. T.; Auras, R.; Rubino, M. *Prog. Polym. Sci.* **2008**, *33*, 820–852.
5. Nampoothiri, K. M.; Nair, N. R.; John, R. P. *Bioresour. Technol.* **2010**, *101*, 8493–8501.
6. Rasal, R. M.; Janorkar, A. V.; Hirt, D. E. *Prog. Polym. Sci.* **2010**, *35*, 338–356.
7. Lunt, J. *Polym. Degrad. Stab.* **1998**, *59*, 145–152.
8. Drumright, R. E.; Gruber, P. R.; Henton, D. E. *Adv. Mater.* **2000**, *12*, 1841–1846.
9. Kricheldorf, H. R. *Chemosphere* **2001**, *43*, 49–54.
10. Saulnier, B.; Ponsart, S.; Coudane, J.; Garreau, H.; Vert, M. *Macromol. Biosci.* **2004**, *4*, 232–237.
11. Tsuji, H. *Macromol. Biosci.* **2007**, *7*, 1299–1299.
12. Zhang, M.; Thomas, N. L. *Adv. Polym. Technol.* **2011**, *30*, 67–79.
13. Vink, E. T. H.; Rabago, K. R.; Glassner, D. A.; Gruber, P. R. *Polym. Degrad. Stab.* **2003**, *80*, 403–419.
14. Jacobsen, S.; Fritz, H. G.; Degee, P.; Dubois, P.; Jerome, R. *Ind. Crops Prod.* **2000**, *11*, 265–275.

Publication Date (Web): November 22, 2013 | doi: 10.1021/bk-2013-1144.ch013

15. Chisholm, M. H. *Pure Appl. Chem.* **2010**, *82*, 1647–1662.
16. Sodergard, A.; Stolt, M. *Prog. Polym. Sci.* **2002**, *27*, 1123–1163.
17. Lasprilla, A. J. R.; Martinez, G. A. R.; Lunelli, B. H.; Jardini, A. L.; Maciel, R. *Biotechnol. Adv.* **2012**, *30*, 321–328.
18. Tanzi, M. C.; Verderio, P.; Lampugnani, M. G.; Resnati, M.; Dejana, E.; Sturani, E. *J. Mater. Sci: Mater. Med.* **1994**, *5*, 393–396.
19. Corma, A.; Iborra, S.; Velty, A. *Chem. Rev.* **2007**, *107*, 2411–2502.
20. Valentin, H. E.; Steinbüchel, A. *Appl. Microbiol. Biotechnol.* **1994**, *40*, 699–709.
21. Sudesh, K.; Abe, H.; Doi, Y. *Prog. Polym. Sci.* **2000**, *25*, 1503–1555.
22. Steinbüchel, A.; Füchtenbusch, B. *Trends Biotechnol.* **1998**, *16*, 419–427.
23. Anderson, A. J.; Dawes, E. A. *Microbiol. Rev.* **1990**, *54*, 450–472.
24. Rehm, B. H. A. *Biochem. J.* **2003**, *376*, 15–33.
25. Yuan, W.; Jia, Y.; Tian, J. M.; Snell, K. D.; Muh, U.; Sinskey, A. J.; Lambalot, R. H.; Walsh, C. T.; Stubbe, J. *Arch. Biochem. Biophys.* **2001**, *394*, 87–98.
26. Taguchi, S.; Yamada, M.; Matsumoto, K.; Tajima, K.; Satoh, Y.; Munekata, M.; Ohno, K.; Kohda, K.; Shimamura, T.; Kambe, H.; Obata, S. *Proc. Natl. Acad. Sci. U.S.A.* **2008**, *105*, 17323–17327.
27. Taguchi, S.; Nakamura, H.; Hiraishi, T.; Yamato, I.; Doi, Y. *J. Biochem.* **2002**, *131*, 801–806.
28. Tsuge, T.; Saito, Y.; Narike, M.; Muneta, K.; Normi, Y. M.; Kikkawa, Y.; Hiraishi, T.; Doi, Y. *Macromol. Biosci.* **2004**, *4*, 963–970.
29. Takase, K.; Matsumoto, K.; Taguchi, S.; Doi, Y. *Biomacromolecules* **2004**, *5*, 480–485.
30. Taguchi, S.; Doi, Y. *Macromol. Biosci.* **2004**, *4*, 146–156.
31. Nomura, C. T.; Taguchi, S. *Appl. Microbiol. Biotechnol.* **2007**, *73*, 969–979.
32. Tajima, K.; Satoh, Y.; Satoh, T.; Itoh, R.; Han, X. R.; Taguchi, S.; Kakuchi, T.; Munekata, M. *Macromolecules* **2009**, *42*, 1985–1989.
33. Yamada, M.; Matsumoto, K.; Nakai, T.; Taguchi, S. *Biomacromolecules* **2009**, *10*, 677–681.
34. Song, Y. Y.; Matsumoto, K.; Yamada, M.; Gohda, A.; Brigham, C. J.; Sinskey, A. J.; Taguchi, S. *Appl. Microbiol. Biotechnol.* **2012**, *93*, 1917–1925.
35. Shozui, F.; Matsumoto, K.; Nakai, T.; Yamada, M.; Taguchi, S. *Appl. Microbiol. Biotechnol.* **2010**, *85*, 949–954.
36. Shozui, F.; Matsumoto, K.; Motohashi, R.; Sun, J. A.; Satoh, T.; Kakuchi, T.; Taguchi, S. *Polym. Degrad. Stab.* **2011**, *96*, 499–504.
37. Yamada, M.; Matsumoto, K.; Uramoto, S.; Motohashi, R.; Abe, H.; Taguchi, S. *J. Biotechnol.* **2011**, *154*, 255–260.
38. Yamada, M.; Matsumoto, K.; Shimizu, K.; Uramoto, S.; Nakai, T.; Shozui, F.; Taguchi, S. *Biomacromolecules* **2010**, *11*, 815–819.
39. Nduko, J. M.; Matsumoto, K.; Taguchi, S. Biological Lactate-Polymers Synthesized by One-Pot Microbial Factory: Enzyme and Metabolic Engineering. In *Biobased Monomers, Polymers, and Materials*; Smith, B. S., Gross, R. A., Eds.; ACS Symposium Series 1105; American Chemical Society: Washington, DC, 2012; pp 213−235.

Publication Date (Web): November 22, 2013 | doi: 10.1021/bk-2013-1144.ch013

40. Rehm, B. H. A. *Curr. Issues Mol. Biol.* **2007**, *9*, 41–62.
41. Matsumoto, K.; Aoki, E.; Takase, K.; Doi, Y.; Taguchi, S. *Biomacromolecules* **2006**, *7*, 2436–2442.
42. Normi, Y. M.; Hiraishi, T.; Taguchi, S.; Sudesh, K.; Najimudin, N.; Doi, Y. *Biotechnol. Lett.* **2005**, *27*, 705–712.
43. Normi, Y. M.; Hiraishi, T.; Taguchi, S.; Abe, H.; Sudesh, K.; Najimudin, N.; Doi, Y. *Macromol. Biosci.* **2005**, *5*, 197–206.
44. Rehm, B. H. *Curr. Issues Mol. Biol.* **2007**, *9*, 41–62.
45. Matsumoto, K.; Takase, K.; Aoki, E.; Doi, Y.; Taguchi, S. *Biomacromolecules* **2005**, *6*, 99–104.
46. Takase, K.; Taguchi, S.; Doi, Y. *J. Biochem.* **2003**, *133*, 139–145.
47. Stubbe, J.; Tian, J. *Nat. Prod. Rep.* **2003**, *20*, 445–457.
48. Rehm, B. H.; Steinbuchel, A. *Int. J. Biol. Macromol.* **1999**, *25*, 3–19.
49. Matsumoto, K.; Taguchi, S. *Appl. Microbiol. Biotechnol.* **2010**, *85*, 921–932.
50. Bunch, P. K.; Mat-Jan, F.; Lee, N.; Clark, D. P. *Microbiology* **1997**, *143* (Pt 1), 187–195.
51. Shi, H. D.; Nikawa, J.; Shimizu, K. *J. Biosci. Bioeng.* **1999**, *87*, 666–677.
52. Tyo, K. E. J.; Fischer, C. R.; Simeon, F.; Stephanopoulos, G. *Metab. Eng.* **2010**, *12*, 187–195.
53. Li, R.; Zhang, H. X.; Qi, Q. S. *Bioresour. Technol.* **2007**, *98*, 2313–2320.
54. Peoples, O. P.; Sinskey, A. J. *J. Biol. Chem.* **1989**, *264*, 15298–15303.
55. Inkinen, S.; Hakkarainen, M.; Albertsson, A. C.; Sodergard, A. *Biomacromolecules* **2011**, *12*, 523–532.
56. Baba, T.; Ara, T.; Hasegawa, M.; Takai, Y.; Okumura, Y.; Baba, M.; Datsenko, K. A.; Tomita, M.; Wanner, B. L.; Mori, H. *Mol. Syst. Biol.* **2006**, *2*.
57. Zhu, J.; Shimizu, K. *Appl. Microbiol. Biotechnol.* **2004**, *64*, 367–375.
58. Shozui, F.; Matsumoto, K.; Nakai, T.; Yamada, M.; Taguchi, S. *Appl Microbiol. Biotechnol.* **2010**, *85*, 949–954.
59. Zhu, J. F.; Shimizu, K. *Metab. Eng.* **2005**, *7*, 104–115.
60. HiljanenVainio, M.; Varpomaa, P.; Seppala, J.; Tormala, P. *Macromol. Chem. Phys.* **1996**, *197*, 1503–1523.
61. Auras, R.; Harte, B.; Selke, S. *Macromol. Biosci.* **2004**, *4*, 835–864.
62. Slater, S.; Gallaher, T.; Dennis, D. *Appl. Environ. Microbiol.* **1992**, *58*, 1089–1094.
63. Doi, Y.; Kitamura, S.; Abe, H. *Macromolecules* **1995**, *28*, 4822–4828.
64. Wong, M. S.; Causey, T. B.; Mantzaris, N.; Bennett, G. N.; San, K. Y. *Biotechnol. Bioeng.* **2008**, *99*, 919–928.
65. Doi, Y.; Kunioka, M.; Nakamura, Y.; Soga, K. *Macromolecules* **1986**, *19*, 2860–2864.
66. Shozui, F.; Matsumoto, K.; Motohashi, R.; Yamada, M.; Taguchi, S. *Polym. Degrad. Stab.* **2010**, *95*, 1340–1344.
67. Tsuge, T.; Taguchi, K.; Taguchi, S.; Doi, Y. *Int. J. Biol. Macromol.* **2003**, *31*, 195–205.
68. Tsuji, H. *Macromol. Biosci.* **2005**, *5*, 569–597.

Publication Date (Web): November 22, 2013 | doi: 10.1021/bk-2013-1144.ch013

69. Zhou, S. D.; Shanmugam, K. T.; Ingram, L. O. *Appl. Environ. Microbiol.* **2003**, *69*, 2237–2244.
70. Kim, Y. B.; Lenz, R. W. *Adv. Biochem. Eng. Biotechnol.* **2001**, *71*, 51–79.
71. Zaman, H. U.; Song, J. C.; Park, L. S.; Kang, I. K.; Park, S. Y.; Kwak, G.; Park, B. S.; Yoon, K. B. *Polym. Bull.* **2011**, *67*, 187–198.
72. Matsusaki, H.; Abe, H.; Taguchi, K.; Fukui, T.; Doi, Y. *Appl. Microbiol. Biotechnol.* **2000**, *53*, 401–409.
73. Takors, R.; Bathe, B.; Rieping, M.; Hans, S.; Kelle, R.; Huthmacher, K. *J. Biotechnol.* **2007**, *129*, 181–190.
74. Tateno, T.; Hatada, K.; Tanaka, T.; Fukuda, H.; Kondo, A. *Appl. Microbiol. Biotechnol.* **2009**, *84*, 733–739.
75. Jo, S. J.; Matsumoto, K.; Leong, C. R.; Ooi, T.; Taguchi, S. *J. Biosci. Bioeng.* **2007**, *104*, 457–463.
76. Jo, S. J.; Maeda, M.; Ooi, T.; Taguchi, S. *J. Biosci. Bioeng.* **2006**, *102*, 233–236.
77. Toyoda, K.; Teramoto, H.; Inui, M.; Yukawa, H. *J Bacteriol* **2009**, *191*, 4251–4258.
78. Yang, T. H.; Jung, Y. K.; Kang, H. O.; Kim, T. W.; Park, S. J.; Lee, S. Y. *Appl. Microbiol. Biotechnol.* **2011**, *90*, 603–614.
79. Tajima, K.; Han, X. R.; Satoh, Y.; Ishii, A.; Araki, Y.; Munekata, M.; Taguchi, S. *Appl. Microbiol. Biotechnol.* **2012**, *94*, 365–376.
80. Ochi, A.; Matsumoto, K.; Ooba, T.; Sakai, K.; Tsuge, T.; Taguchi, S. *Appl. Microbiol. Biotechnol.* **2012**DOI: 10.1007/s00253-012-4231-9.
81. Pederson, E. N.; McChalicher, C. W. J.; Srienc, F. *Biomacromolecules* **2006**, *7*, 1904–1911.
82. Nduko, J. M.; Matsumoto, K. I.; Ooi, T.; Taguchi, S. *Metab. Eng.* **2013**, *15*, 159–166.
83. Song, Y.; Matsumoto, K.; Tanaka, T.; Kondo, A.; Taguchi, S. *J. Biosci. Bioeng.* **2012**, *115*, 12–14.
84. Silva, L. F.; Taciro, M. K.; Ramos, M. E. M.; Carter, J. M.; Pradella, J. G. C.; Gomez, J. G. C. *J. Ind. Microbiol. Biotechnol.* **2004**, *31*, 245–254.
85. Yu, J.; Stahl, H. *Bioresour. Technol.* **2008**, *99*, 8042–8048.
86. Matsumoto, K.; Kobayashi, H.; Ikeda, K.; Komanoya, T.; Fukuoka, A.; Taguchi, S. *Bioresour. Technol.* **2011**, *102*, 3564–3567.
87. Nduko, J. M.; Suzuki, W.; Matsumoto, K.; Kobayashi, H.; Ooi, T.; Fukuoka, A.; Taguchi, S. *J. Biosci. Bioeng.* **2012**, *113*, 70–72.

Publication Date (Web): November 22, 2013 | doi: 10.1021/bk-2013-1144.ch013

Publication Date (Web): November 22, 2013 | doi: 10.1021/bk-2013-1144.ch014

Chapter 14

Synthesis of Poly-(R)-3 Hydroxyoctanoate (PHO) and Its Graphene Nanocomposites

Ahmed Abdala,[*,1] John Barrett,[2] and Friedrich Srienc[2]

[1]Department of Chemical Engineering, The Petroleum Institute, Abu Dhabi, United Arab Emirates
Permanent Address: Department of Chemical Engineering and Petroleum Refining, Faculty of Petroleum and Mining Engineering, Suez University, Suez, Egypt
[2]Department of Chemical Engineering and Materials Science, University of Minnesota, Minneapolis, Minnesota 55455 and BioTechnology Institute, University of Minnesota, St. Paul, Minnesota 55108
[*]E-mail: aabdala@pi.ac.ae

Polyhydroxyalkanoates are a popular class of bioplastics valued for their rapid biodegradadion, biocompatibility, and renewable feedstocks. While there are already a few commercial applications for these biopolymers, a greater diversity of properties is needed to compete with petroleum based polymers. In this chapter, we report the synthesis and characterization of polyhydroxyoctanoate and its nanocomposite with thermally reduced graphene. The results indicate the incorporation of graphene into the PHO matrix leads to a small upshift in the glass transition, enhance the thermal stability, and ~600% increase in modulus. Electrical percolation between 0.5 and 1 vol.% TRG was obtained.

In Green Polymer Chemistry: Biocatalysis and Materials II; Cheng, H., et al.;
ACS Symposium Series; American Chemical Society: Washington, DC, 2013.

Publication Date (Web): November 22, 2013 | doi: 10.1021/bk-2013-1144.ch014

Introduction

Polyhydrxyalkanotes (PHAs) are polyesters that can be biologically synthesized by microbial cultivation or in other biological systems (*1*). They become an important class of biopolymers due to their renewable sources, biodegradation and applications in tissue engineering because of their biocompatbility (*2*). Structurally, the PHA backbone is comprised of 3-carbon repeat units with oxo-ester linkages. The attachment of various aliphatic and aromatic moieties stemming from the 3-carbon postion of each monomer imparts a range of material properties. Polyhydroxybutyrate (PHB), which possesses a single methyl group at the 3-carbon postion, is a stiff thermoplastic with a high melting temperature and is by far the most commonly used form of PHA. In contrast, medium chain-length PHA, (PHA_{mcl}) contains longer aliphatic appendages (3-11 carbons) at the 3-carbon position which enhance elasticity but reduce polymer strength and melting temperature (*3*). Among PHA_{mcl}, poly(3-hydroxyoctanoate) (PHO), which is a heteropolymer composed of C_6, C_8, and C_{10} monomers, is significantly more amorphous and flexible than PHB (*4*, *5*). Thus, new methods to increase the strength and melting temperature of PHA_{mcl} have significant potential for stimulating commercial proliferation of these materials and encouraging development of the larger natural products industry. Therefore, Nanocomposites of biopolymers with nano-fillers such as carbon nanotubes or clay, offer a significant potential for their increased utilization, as a result of the improvements in mechanical and thermal properties. There are a few publications that reports the production and characterization nanocomposites of PHB with nanofillers such as clay/layered silicate (*6*, *7*) and carbon nanotubes (*8*, *9*).

Two new carbon allotropes, carbon nanotubes (*10*) and graphene (*11*), have received much attention as nanofillers because of their extraordinary mechanical, thermal, and electrical properties. With Young's modulus of 1 TPa and ultimate strength of 130 GPa, graphene is the stiffest and strongest material ever measured (*12*). The incorporation of graphene into polymer matrices is expected to result in significant enhancement of the thermal, mechanical, electrical, and barrier properties (*13*).

In this study, we develop a series of PHO-graphene nanocomposites with different graphene loading using solvent mixing in chloroform. Graphene dispersion in the PHO matrix is examined using TEM and the effect of graphene loading on the mechanical, thermal, and electrical properties are discussed.

Experimental

PHO Synthesis

PHO was produced via a fed-batch biosynthesis using the wild-type organism, Pseudomonas oleovorans . Initially, one fresh colony was selected and inoculated into a test tube containing 5-mL of LB medium (10 g Tryptone, 5 g Yeast Extract Powder, and 5 g NaCl in 1L of water) and grown overnight at 30°C. The culture was then transferred into a 2-L baffled flask with 500-mL of LB medium + 1% (v/v)

In Green Polymer Chemistry: Biocatalysis and Materials II; Cheng, H., et al.;
ACS Symposium Series; American Chemical Society: Washington, DC, 2013.

alkane for an additional 16 hours at 30°C with shaking at 250 RPM. This 500-mL culture was used to inoculate a 10-L bioreactor containing 5-L of E medium + 2% (v/v) alkane. E medium consisted of 1.1 g $(NH_4)_2HPO_4$, 5.8 g K_2HPO_4, 3.7 g $KHPO_4$, 0.25 g $MgSO_4 \cdot 7H_2O$, and 1mL of trace metals in 1 L of water. Trace metals consisted of 2.78 g $FeSO_4 \cdot 7H_2O$, 1.98 g $MnCl_2 \cdot 4H_2O$, 2.81 g $CoSO_4 \cdot 7H_2O$, 0.17 g $CuCl_2 \cdot 2H_2O$, 0.29 g ZnSO4$\cdot 7H_2O$, 1.67 g $CaCl_2 \cdot 2H_2O$, 1M 1 mL in 1 L of water. Airflow and agitation were adjusted to maintain dissolved oxygen in the culture above 40%. During biosynthesis carbon dioxide evolution rate (CER) of the culture was monitored via mass spectroscopy. A sharp decline in CER indicated depletion of the carbon source, at which time more alkane was added to maintain growth. Batches were harvested at 50 hrs. The resulting cell pellet was lyophilized to dry the cells. PHO within the pellet was extracted in boiling chloroform using a Soxhlet apparatus for 16 hrs. Dissolved polymer was then precipitated with excess methanol, 8:1 v/v. The solvent mixture was decanted and residual solvent was evaporated under ambient conditions until the polymer is dry.

Purified PHO were analyzed via gas chromatography fitted with a flame ionization detector (GC-17A, Shimadzu) using a DB-WAX column (ID 0.32 mm, 0.5 μm film thickness) (Agilent Technologies). Prior to injection, polyhydroxyalkanoic acids were converted to 3-hydroxyalkanoic propyl esters by the method of propanolyis (*14*). Quantitative determination the of different PHAs was made by comparison to standards synthesized from purified 3-hydroxyalkanoic acids (Sigma)

Graphene Production and Characterization

Thermally reduced graphene (TRG) is produced following the thermal exfoliation method (*15*, *16*). In this method, natural flake graphite (-10 mesh, 99.9%, Alfa Aesar) is oxidized using Staudenmaier method (*17*) using a mixture of H_2SO_4 (95-97%, J.T. Bakers) and HNO_3 (68%, J.T. Bakers), and Potassium chlorate (Fisher Scientific). The produced graphite oxide (GO) is washed with 5% HCl (37%, Reidel-de Haen), until no sulfate ions are detected then it repeatedly washed with water till no chloride ions are detected and dried in a vacuum overnight. GO was exfoliated by rapid heating at 1000 °C in a tube furnace (Barnstead Thermolyne) under flow of nitrogen for 30 s.

XRD (X'Pert PRO MPD diffractometer, PANalytical) was used to test the oxidation of graphite and the complete exfoliation of graphite oxide. XRD scan between 5-35° was conducted at a scan rate of 0.02°/sec with instrument parameters of 40 kV voltage, 20 A intensity and 1.5406 Å CuKα radiation. TEM images were obtained using FEI Tecnai G20 TEM.

Fabrication and Characterization of the Nanocomposites

PHO/graphene nanocomposites with 1, 2, 5 wt.% (0.5, 1, and 2.5 vol.%) graphene were prepared by the following procedure. First, 1 g of polymer was dissolved in 20 mL of chloroform using a vortex tube mixer. Periodic incubation of the mixture in an 80° water bath was used to promote dissolution. Second, graphene powder was dispersed in chloroform at a concentration of 0.5 mg/L. To

In Green Polymer Chemistry: Biocatalysis and Materials II; Cheng, H., et al.;
ACS Symposium Series; American Chemical Society: Washington, DC, 2013.

Publication Date (Web): November 22, 2013 | doi: 10.1021/bk-2013-1144.ch014

promote the dispersion of graphene sheets, sonication was applied to the mixture using a electrode sonicator (Misonix 3000) at a power density of 1.5-3 W/mL. The graphene dispersion was added to PHO solution and stirrer for 1 hr. This mixture was then poured into a petri dish and evaporated on a hotplate at 55°C. Films were dried overnight to remove excess chloroform. For mechanical, rheological, and surface resistance measurements specimens were prepared from the dry composite samples by hot press (Tetrahedron, MTP-10) at 100°C and 1.0 MPa for 5 minutes. 5 cm x 5 cm square with a thickness of 0.5 mm was prepared and cut into rectangles (5 cm x 5 cm x 0.5 mm) for (1.25 cm x 0.5 mm) disks for electrical conductivity. All samples were aged at room temperature for more than 72 hrs prior to testing.

Differential scanning calorimeter (DSC) (Netzsch 204 F1 Phoenix) and thermogravimetric analyzer (TGA) (Netzsch STA 409 PC) were employed to investigate thermal properties of PHO and its graphene nanocomposite. The mechanical properties of the pure and composite samples were measured using dynamic mechanical analyzer (TA Instruments, RSAIII) operating in a tension mode at an extension rate of 5 mm/min. Surface resistance measurements were taken from circular disks, 10 x 0.5 mm, using an 11-point probe (Prostat Corp., PRF-914B probe with PRS-801 meter). For each sample, 4 readings were collected, two from each side of the film. Graphene morphology and graphene dispersion into the PHO matrix is analyzed with TEM (FEI Tecnai G20 TEM). 80-100 nm thick composite films for TEM imaging were prepared at -80°C using an ultramicrotome (Leica, EM UC6).

Publication Date (Web): November 22, 2013 | doi: 10.1021/bk-2013-1144.ch014

Results and Discussion

Preparation of Purified PHO

The biosynthesis route for PHO in Pseudomonas oleovorans is shown in Figure 1. Briefly, octane in the media is consumed by the microorganism while undergoing a string of enzymatic conversions to produce a biologically active fatty acyl-CoA molecule.

This intermediate molecule is degraded via successive fatty acid β-oxidation cycle in which two carbons are removed to produce the central metabolite, acetyl-CoA, and the corresponding n-2 fatty acyl-CoA. In Pseudomonas oleovorans, one of the intermediates of β -oxidation, trans-2-enoyl-CoA is converted via a 3-R-enoyl-CoA hydratase, PhaJ, to the monomer species, 3-hydoxyalkanoyl-CoA. The cyclical nature of β-oxidation results in a distribution of different monomers. This variation in the monomer pool combined with the promiscuous nature of the PhaC polymerase results in a random co-polymer comprised of several unique but structurally similar monomers. The synthesized sample is a random polymer of 3-hydroxyoctanoate (3HB), 3-hydroxyhexanoate (3HH), 3-hydroxydecanoate (3HD), and 3-hydroxybutyrate (3HB) with composition of 91.4, 7, 1.2, and 0.4 mol%, respectively.

In Green Polymer Chemistry: Biocatalysis and Materials II; Cheng, H., et al.;
ACS Symposium Series; American Chemical Society: Washington, DC, 2013.

Publication Date (Web): November 22, 2013 | doi: 10.1021/bk-2013-1144.ch014

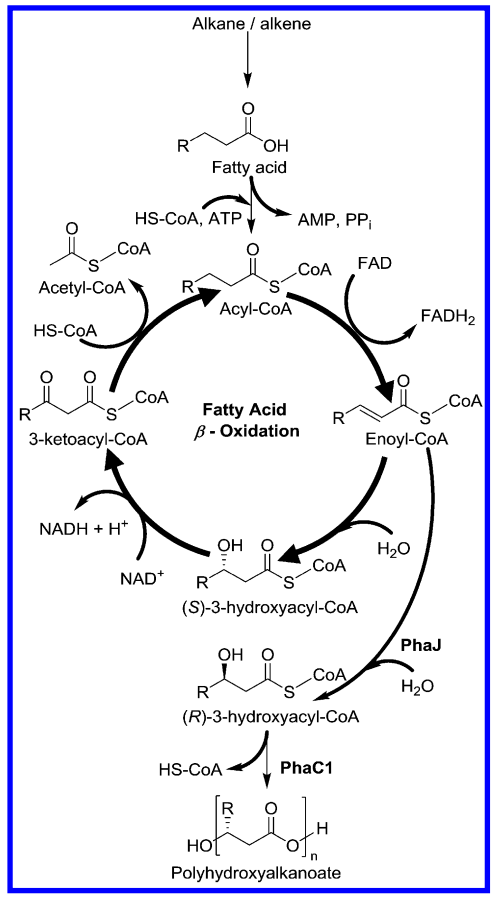

Figure 1. Metabolic pathway for PHO synthesis in Pseudomonas oleovorans.

Production and Characterization of TRG

Oxidation of graphite leads to the introduction of polar oxygen functionalities on the surface of GO and change in carbon hyperdization to a mixture of sp^2 and sp^3 carbon. This leads to the expansion of the interlayer inter spacing from the graphite 3.35 Å (002 peak at $2\theta = 26.5$) to 7.8 Å ($2\theta = 11.4$) as indicated by the XRD patterns for graphite and GO, Figure 2-a. In contrast, TRG diffraction pattern shows no noticeable diffraction peaks confirming the complete exfoliation of GO and production of TRG. TEM image of TRG (Figure 1-b) shows very thin and large (micron size) graphene sheets with wrinkled structure. The dark areas on the TEM micrograph represent the edges of folded or overlapped sheets.

In Green Polymer Chemistry: Biocatalysis and Materials II; Cheng, H., et al.;
ACS Symposium Series; American Chemical Society: Washington, DC, 2013.

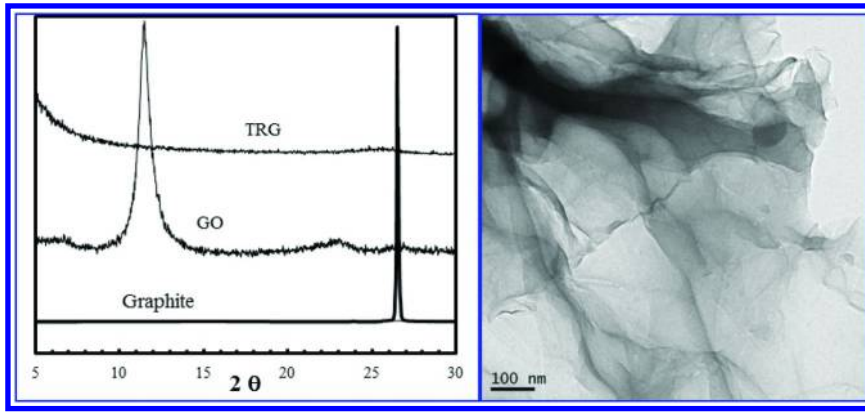

Figure 2. a) XRD patterns of pure graphite, GO and TRG. b) TEM of TRG.

Morphology PHO-TRG Nanocomposites

The dispersion of TRG in PHO is examined using TEM. As shown in Figure 3, although TRG is homogeneously distributed in the PHO matrix, it is not very well dispersed into the matrix as evidence by the presence of dark areas that represent the edges of stacked graphene layers. The high resolution image in the right indicates that TRG maintained its wrinkled structure while imbedded into the matrix.

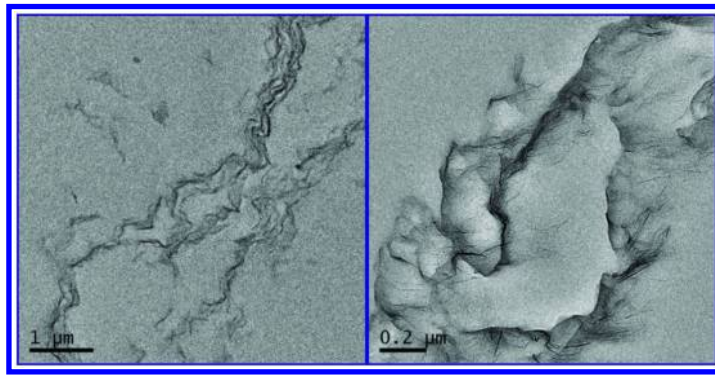

Figure 3. TEM images of PHO-TRG composite with 1% TRG.

Thermal Properties

The nonoxidative thermal degradation of PHO and its TRG nanocomposites is studied using TGA and the results are shown in Figure 4. The pure and composite samples are stable up to 275°C as they show no significant weight loss below that temperature. Above 275°C, the pure and composite sample undergoes a slow degradation up to 295°C. Above 295°C , the pure samples rapidly degrade to

In Green Polymer Chemistry: Biocatalysis and Materials II; Cheng, H., et al.;
ACS Symposium Series; American Chemical Society: Washington, DC, 2013.

almost zero weight over a narrow range of about 30°C . The degradation rate of the composite samples is lower than that of the pure sample suggesting TRG inhibits the nonoxidative thermal degradation of PHO.

Table 1. Effect of TRG loading on thermal transitions of PHO

TRG (vol%)	T_g *(°C)*	T_m *(°C)*	ΔH_m *(J/g)*	$T_{90\%}$ *(°C)*	$T_{50\%}$ *(°C)*
0	-41.9	53.7	15.5	297.1	309.8
0.5	-38.1	55.7	13.9	299.3	311.7
1	-38.6	55.5	9.0	300.5	315.6
2.5	-39.0	54.1	12.2	299.5	314.5

The effects of TRG loading on the thermal transitions of PHO are also provided in Table 1. The addition of TRG increases the glass transition of PHO by a few degrees. The increase in the glass transition can be attributed to restraining the motion of PHO chains by the TRG sheets.

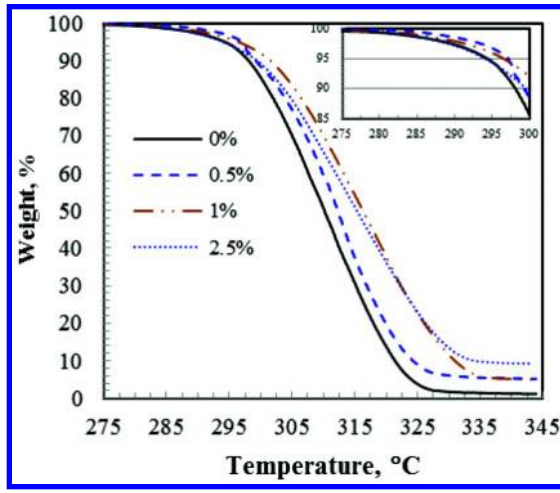

Figure 4. TGA thermograms of PHO and its TRG nanocomposites with 0, 0.5, 1, and 2.5 vol.% TRG.

The crystallization behavior of biodegradable polymers is an important parameter because it significantly affects not only the crystalline structure and morphology but also the final physical properties and biodegradability of the polymer. Table 1 provides the melt temperature and heat of melting for the pure PHO and the composite samples. The melt temperature increases by 2°C with the addition of 0.5 vol.% TRG. A further increase in the TRG loading does not increase the melt temperature. In contrary, the melt temperature decreases when TRG loading increases from 1 to 2.5 vol.%. This behavior could be attributed to

In Green Polymer Chemistry: Biocatalysis and Materials II; Cheng, H., et al.;
ACS Symposium Series; American Chemical Society: Washington, DC, 2013.

Publication Date (Web): November 22, 2013 | doi: 10.1021/bk-2013-1144.ch014

the agglomeration of TRG sheets at higher loading. On the other hand, the heat of melting and consequently the %crystallinity decreases with the addition of TRG. This decrease in crystallinity suggests that the incorporation of TRG decreases the nucleation rate of PHO.

Mechanical Properties

The mechanical properties of pure PHO and its TRG nanocomposite have been studied using DMA. The addition of TRG significantly increases the stiffness of PHO, reduces the elongation at break, and have no significant effect of the ultimate strength as shown in Figure 5 and table 2.

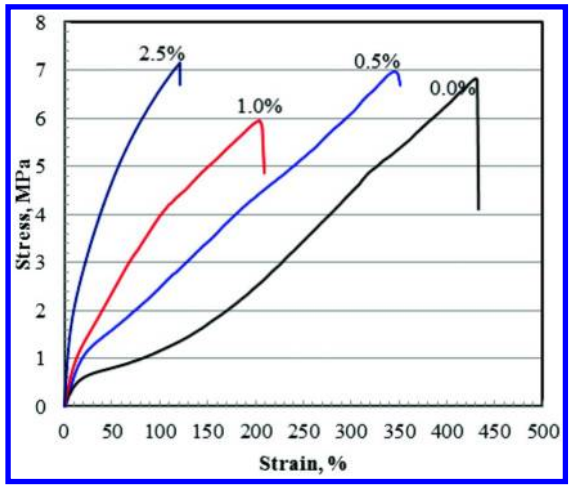

Figure 5. Stress-strain curves of PHO and its TRG nanocomposites with different TRG loading, vol.%.

Table 2. Mechanical properties of PHO-TRG nanocomposites

TRG (vol%)	*Modulus (MPa)*	*Strength (MPa)*	*Elongation at break (%)*
0	4.5	6.4	425
0.5	7.2	7.0	346
1	10.9	5.6	205
2.5	31.0	6.7	105

Publication Date (Web): November 22, 2013 | doi: 10.1021/bk-2013-1144.ch014

The addition of TRG resulted in a very significant increase in the modulus (600% at 2.5 vol.%). This is even more impressive if we recall that the composite samples has a lower crystallinity compared to the pure sample as discussed earlier. This level of enhancement is significantly higher than the reported for graphene and graphene oxide composite with glassy polymers such as PA (*18*), PMMA (*19*), and PCL (*20*) but similar to that of elastomeric polymers such as natural rubber (*21*), PDMS (*21*), and TPU (*22*). Although, Figure 5 shows no appreciable change in the ultimate strength, we claim that TRG enhances the strength of PHO just enough to overcome the decrease in strength due to the lower crystallinity of the composite samples. The main drawback of the addition of TRG is the reduction in the elongation at break. Nevertheless, the composite samples remain highly flexible with a minimum elongation at break of over 100%.

Publication Date (Web): November 22, 2013 | doi: 10.1021/bk-2013-1144.ch014

Electrical Properties

The greatest advantage of carbon nanofillers and graphene in particular versus other nanofillers is the ability to increase the electrical conductivity of nonconductive polymers and the measured electrical resistivity of PHO and the nanocomposite samples provides an example of such ability. The required TRG loading to produce electrically conductive PHO, the electrical percolation, is slightly above 0.5 vol.%. This low percolation limit is an indication of a good dispersion of TRG into the matrix. The observed percolation limit is similar to that solution processed polyethylene-TRG (*23*) but lower than that of polar polymer-TRG composites (*22*). A further increase in the loading of TRG greatly increases the electrical conductivity (decreases resistivity) as shown in Figure 6. Compared to the resistivity of the pure polymer of 1.3×10^3 MΩ.m, a resistivity of less than 5 Ω.m is obtained with 2.5 vol.% loading of TRG.

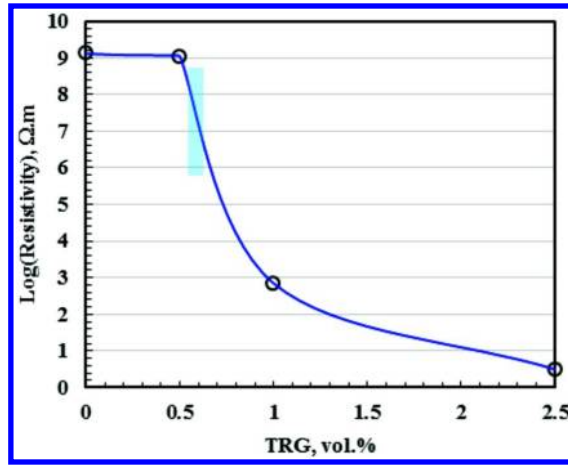

Figure 6. Effect of TRG loading on the electrical resistance of PHO-TRG nanocomposites.

In Green Polymer Chemistry: Biocatalysis and Materials II; Cheng, H., et al.;
ACS Symposium Series; American Chemical Society: Washington, DC, 2013.

Conclusions

We have successfully produced PHO, TRG, and their nanocomposites. The solvent blended PHO-TRG nanocomposite with TRG loading of 0.5, 1, and 2.5 vol.% exhibited enhanced thermal, mechanical, and electrical properties compared to the pure PHO. The addition of TRG resulted in a slight upshift in the glass transition, increase in the melt temperature, and decrease in crystallinty. Regardless of this decrease in crystallinity, the mechanical properties of the composite sample revealed a striking 600% increase in modulus with 2.5 vol.% TRG while maintaining elongation at break above 100%. Electrically conductive PHO samples can be made with the addition of slightly more than 0.5 vol% TRG and a very low resistivity of less than 5 Ω.m is obtained with 2.5 vol.% TRG. These promising results would increase the applications of medium chain PHAs.

Publication Date (Web): November 22, 2013 | doi: 10.1021/bk-2013-1144.ch014

Acknowledgments

Financial support from the Abu Dhabi-Minnesota Institute for Research Excellence (ADMIRE) is acknowledged. The authors also thank Dr. Marios Katsiotis at the Department of Chemical Engineering, the Petroleum Institute for the TEM work and Mr. Daniel Rouse, the university of Minnesota, for his role in the synthesis of PHO.

References

1. Jackson, J. K.; Srienc, F. Effects of recombinant modulation of the phbCAB operon copy number on PHB synthesis rates in Ralstonia eutropha. *J. Biotechnol.* **1999**, *68* (1), 49–60.
2. Chen, G. Q.; Wu, Q. The application of polyhydroxyalkanoates as tissue engineering materials. *Biomaterials* **2005**, *26* (33), 6565–6578.
3. Barrett, J. S. F.; Srienc, F. *Green Chemistry for the Production of Biodegradable, Biorenewable, Biocompatible, and Polymers*; John Wiley & Sons, Inc.: New York, 2011.
4. Foster, L. J. R.; et al. Biosynthesis and characterization of deuterated polyhydroxyoctanoate. *Biomacromolecules* **2006**, *7* (4), 1344–1349.
5. Sanguanchaipaiwong, V.; et al. Biosynthesis of natural-synthetic hybrid copolymers: polyhydroxyoctanoate-diethylene glycol. *Biomacromolecules* **2004**, *5* (2), 643–649.
6. Botana, A.; et al. Effect of modified montmorillonite on biodegradable PHB nanocomposites. *Appl. Clay Sci.* **2010**, *47* (3−4), 263–270.
7. Maiti, P.; Batt, C. A.; Giannelis, E. P. New biodegradable polyhydroxybutyrate/layered silicate nanocomposites. *Biomacromolecules* **2007**, *8* (11), 3393–3400.
8. Xu, C.; Qiu, Z. Crystallization behavior and thermal property of biodegradable poly (3-hydroxybutyrate)/multi-walled carbon nanotubes nanocomposite. *Polym. Adv. Technol.* **2011**, *22* (5), 538–544.

9. Yun, S. I.; et al. Mechanical properties of biodegradable polyhydroxyalkanoates/single wall carbon nanotube nanocomposite films. *Polym. Bull.* **2008**, *61* (2), 267–275.
10. Byrne, M. T.; Gun'ko, Y. K. Recent advances in research on carbon nanotube–polymer composites. *Adv. Mater.* **2010**, *22* (15), 1672–1688.
11. Verdejo, R.; et al. Graphene filled polymer nanocomposites. *J. Mater. Chem.* **2011**, *21* (10), 3301–3310.
12. Lee, C.; et al. Measurement of the elastic properties and intrinsic strength of monolayer graphene. *Science* **2008**, *321* (5887), 385–388.
13. Kim, H.; Abdala, A. A.; Macosko, C. W. Graphene/polymer nanocomposites. *Macromolecules* **2010**, *43* (16), 6515–-6530.
14. Riis, V.; Mai, W. Gas chromatographic determination of poly- beta-hydroxybutyric acid in microbial biomass after hydrochloric acid propanolysis. *J. Chromatogr., A* **1988**, *445* (1), 285–289.
15. Prud'homme, R. K.; et al. *Thermally Exfoliated Graphite Oxide*; Trustees of Princeton University: Princeton, NJ, 2010; p 65.
16. McAllister, M. J.; et al. Single sheet functionalized graphene by oxidation and thermal expansion of graphite. *Chem. Mater.* **2007**, *19* (18), 4396–4404.
17. Staudenmaier, L. Method for the preparation of graphitic acid. *Ber. Dtsch. Chem. Ges.* **1898**, *31*, 1481–1487.
18. Steurer, P.; et al. Functionalized graphenes and thermoplastic nanocomposites based upon expanded graphite oxide. *Macromol. Rapid Commun.* **2009**, *30* (4−5), 316–327.
19. Ramanathan, T.; et al. Functionalized graphene sheets for polymer nanocomposites. *Nat. Nanotechnol.* **2008**, *3* (6), 327–331.
20. Hua, L.; et al. A new poly (L-lactide)-grafted graphite oxide composite: facile synthesis, electrical properties and crystallization behaviors. *Polym. Degrad. Stab.* **2010**, *95* (12), 2619–2627.
21. Ponnamma, D.; et al. Rubber Nanocomposites: Latest Trends and Concepts. In *Advances in Elastomers II*; Springer: New York, 2013; pp 69−107.
22. Kim, H.; Miura, Y.; Macosko, C. W. Graphene/polyurethane nanocomposites for improved gas barrier and electrical conductivity. *Chem. Mater.* **2010**, *22* (11), 3441–3450.
23. Kim, H.; et al. Graphene/polyethylene nanocomposites: Effect of polyethylene functionalization and blending methods. *Polymer* **2011**, *52* (8), 1837–1846.

Publication Date (Web): November 22, 2013 | doi: 10.1021/bk-2013-1144.ch014

Publication Date (Web): November 22, 2013 | doi: 10.1021/bk-2013-1144.ch015

Chapter 15

Biosynthesis of Polyhydroxyalkanoate by a Marine Bacterium *Vibrio* sp. Strain Using Sugars, Plant Oil, and Unsaturated Fatty Acids as Sole Carbon Sources

Satoshi Tomizawa,[1] Jo-Ann Chuah,[1] Misato Ohtani,[2] Taku Demura,[2] and Keiji Numata*,[1]

[1]Enzyme Research Team, Biomass Engineering Program, RIKEN, Hirosawa, Wako-shi, Saitama 351-0198, Japan
[2]Cellulose Production Research Team, Biomass Engineering Program, RIKEN, Suehiro-cho, Tsurumi-ku, Yokohama City, Kanagawa 230-0045, Japan
***E-mail: keiji.numata@riken.jp**

This is a mini review of our recent work and update on polyhydroxyalkanoate (PHA) production by marine bacteria using sugars, plant oils and three types of unsaturated fatty acids as sole carbon sources. Marine bacteria have recently attracted attention as potentially useful candidates for the production of practical materials from marine ecosystems, including the oceanic carbon dioxide cycle. A newly-identified marine bacterium, *Vibrio* sp. strain KN01, was characterized with respect to PHA productivity using various carbon sources under aerobic and aerobic-anaerobic marine conditions. The produced PHA was further analyzed with respect to its monomer composition. The influence of unsaturated fatty acids as sole carbon sources as well as aerobic-anaerobic conditions on PHA compositions is summarized and discussed in this chapter.

In Green Polymer Chemistry: Biocatalysis and Materials II; Cheng, H., et al.;
ACS Symposium Series; American Chemical Society: Washington, DC, 2013.

Publication Date (Web): November 22, 2013 | doi: 10.1021/bk-2013-1144.ch015

Introduction

Polyhydroxyalkanoate (PHA), one of the eco-friendly, bio-based and biodegradable plastics, is produced by various bacteria as an intracellular storage material of carbon and energy. PHA also shows excellent biodegradability and biocompatibility, and diverse mechanical properties related to the chemistry of secondary monomer units (*1–3*). In the PHA biosynthetic pathway of microbial cells, the provision and polymerization of the hydroxyalkanoate (HA) monomers are performed by various enzymes. Typical PHA synthesis genes such as the genes from *Ralstonia eutropha* (also known as *Cupriavidus necator*) within an operon including a beta-ketothiolase (*phaA*), an acetoacetyl-coenzyme A (CoA) reductase (*phaB*) and a synthase (*phaC*) (*4*). The thiolase and reductase synthesize a monomer substrate, 3-hydroxybutyryl CoA (3HBCoA), and the synthase polymerizes the monomers to PHA (*4*). Also, the other proteins related to PHA synthesis are an intracellular PHA depolymerase, a phasin protein, and a regulatory protein, which are often encoded near *phaA*, *phaB*, and *phaC*. With respect to PHA synthesis via the beta-oxidation pathway, the *phaJ* and *fabG* genes encoding (*R*)-specific 2-enoyl-CoA hydratase and 3-ketoacyl-acyl carrier protein (ACP) reductase are also known to be responsible for converting 3-enoyl-CoA and 3-ketoacyl-CoA into (*R*)-3-hydroxyacyl-CoA, respectively (*5*, *6*). The substrate specificity differs depending on the species of PHA synthase, PhaC, thus, the monomeric compositions of the resultant PHA copolymers are influenced by the PhaC activities and/or combination of these related proteins (*7*).

Poly[(*R*)-3-hydroxybutyrate] [P(3HB)], the most ubiquitous of PHAs, is one of the most studied bio-based and biodegradable plastics. P(3HB) was first isolated as a microbial reserve polyester from *Bacillus megaterium* (*8*). Following the discovery of P(3HB), many types of bacteria, such as *Bacillus* spp., *Pseudomonas* spp., *Cupriavidus* spp. and *Aeromonas* spp., have been investigated for their potential use in producing PHA more efficiently for industrial use (Table 1) (*9–12*). A few kinds of marine bacteria have also been investigated for the production of PHA under marine conditions, but the resultant PHAs have not been characterized in detail (*13–15*). The advantages of biosynthesizing PHA under marine conditions include avoiding contamination with bacteria that lack salt-water resistance, and the ability to use filtered seawater as a culture medium, which would enable large-scale industrial production of PHA. Further, marine bacteria have recently attracted attention as candidates for the production of practical materials from marine ecosystems, including the oceanic carbon dioxide cycle (*16–18*). These make it attractive to find or construct other marine bacteria that are able to produce PHA efficiently enough to be used for the industrial production of PHA.

Research on the medical, environmental and taxonomic aspects of *Vibrio* species, which are typical marine bacteria, has expanded in the last several decades, because several species of *Vibrio*, i.e., *V. cholerae*, *V. parahaemolyticus* and *V. vulnificus*, are clinically important human pathogens. On the other hand, some species of *Vibrio*, such as *V. fischeri*, have not been shown to be pathogens. With respect to PHA productivity, *V. harveyi* was shown to form PHA granules at a high cell density during its development of luminescence (*19*). Recently, a novel

In Green Polymer Chemistry: Biocatalysis and Materials II; Cheng, H., et al.;
ACS Symposium Series; American Chemical Society: Washington, DC, 2013.

type of marine bacterium, *Vibrio* sp. strain KN01 (Figure 1), was isolated and characterized with respect to its PHA productivity using various carbon sources under aerobic and aerobic-anaerobic marine conditions (*20*). In this minireview, we provide our recent works of PHA production by marine bacteria, based on the results of feeding experiments on the strain KN01, using sugars, plant oils and unsaturated fatty acids as sole carbon sources.

Table 1. Types of PHA production

Carbon source	Strains	Monomer unit
Plant oil Sugar	*Ralstonia eutropha* *Delftia acidovorans* *Bacillus megaterium*	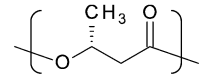 3-hydroxybutyrate (3HB)
Plant oil Organic acid (Octanoic acid)	*Aeromonas caviae* *Pseudomonas* sp. 61-3	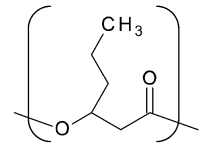 3-hydroxyhexanoate (3HHx)
Organic acid 5-hydroxyvaleric acid Lactone ω-Pentadecanolactone	*Ralstonia eutropha*	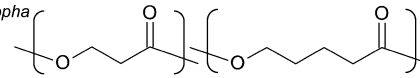 3-hydroxypropionate (3HP) 5-hydroxyvalerate (5HV)

Figure 1. Atomic force microscopy amplitude image of Vibrio sp. strain KN01 cast on mica in air at 25°C (A). Vibrio sp. strain KN01 shows a flagellum. The strain was isolated from seawater of Hizushi beach (B).

PHA Production Using Sugars and Organic Acid

The isolated strain, *Vibrio* sp. KN01, was investigated with respect to PHA productivity from well-known carbon sources, namely, glucose, fructose or gluconate at 30°C for 48 h under an aerobic condition (Table 2) (*20*). The strain exhibited cell growth ranging from approximately 1.4 to 1.7 g/L. PHA accumulation was observed with all three carbon sources, and PHA contents (wt%) were determined by the weight of the produced PHA. The ^{1}H-NMR

In Green Polymer Chemistry: Biocatalysis and Materials II; Cheng, H., et al.;
ACS Symposium Series; American Chemical Society: Washington, DC, 2013.

Publication Date (Web): November 22, 2013 | doi: 10.1021/bk-2013-1144.ch015

spectrum revealed that all of these products were composed of 3HB without any major second monomer units, such as medium chain-length hydroxyalkanoates (HA).

The PHA productivity of *Vibrio* sp. KN01 under an aerobic-anaerobic condition was also examined, because *Vibrio* spp. are known as facultative anaerobes that can grow under both aerobic and anaerobic conditions. Lee and coworkers reported that the reduction in dissolved oxygen concentration from 40% to 5% inhibited cell growth of recombinant *Escherichia coli* harboring PHA-synthesis genes and enhanced PHA contents from 10 to 27 wt% (*21*), demonstrating that PHA production could be enhanced under conditions similar to the aerobic-anaerobic ones used here. In our study, the strain cultured under the aerobic-anaerobic condition demonstrated constant cell growth irrespective of whether glucose, fructose or gluconate was used as the sole carbon source (Table 2) (*20*). Here, an aerobic–anaerobic condition denotes that the strain was prepared and sealed under nitrogen atmosphere and cultured. PHA accumulation was observed under the aerobic-anaerobic condition with each of the three kinds of carbon sources, and the average PHA content of the isolate cultured with fructose and gluconate was over 10%. Also, the PHA contents of the isolate cultured with glucose and fructose were significantly higher compared with the PHA contents from the isolate cultured under an aerobic condition. The number-average molecular weights of the PHAs synthesized by *Vibrio* sp. KN01 under the aerobic condition ranged from 110×10^3 to 140×10^3 g/mol. On the other hand, the number-average molecular weights of the PHAs synthesized under the aerobic-anaerobic condition ranged from 86×10^3 to 100×10^3 g/mol, which were lower in comparison to the PHA produced under the aerobic condition (*20*).

Table 2. PHA accumulations using different carbon sources under aerobic and aerobic-anaerobic conditions. Data from Numata and Doi, 2012 (*20*)

Culture Condition	*Carbon Source*	*Dry Cell Weight, g/L*	*PHA Content, wt%*	*PHA Composition, mol%* [a]
				3HB
Aerobic	Glucose	1.7 ± 0.2	0.06 ± 0.01	100
	Fructose	1.6 ± 0.1	0.3 ± 0.1	100
	Gluconate	1.4 ± 0.1	14 ± 2	100
Aerobic-Anaerobic	Glucose	1.6 ± 0.2	5 ± 2	100
	Fructose	1.3 ± 0.2	17 ± 3	100
	Gluconate	1.1 ± 0.2	15 ± 2	100

[a] PHA composition determined by ^{1}H NMR. The data of dry cell weight and PHA content denote averages of three replicates and their standard deviations.

Publication Date (Web): November 22, 2013 | doi: 10.1021/bk-2013-1144.ch015

PHA Production Using Plant Oil

Plant oil is also one of the most important carbon sources in nature. Here, we focused on soybean oil, a typical industrial plant oil, and Jatropha oil, which is getting much attentions as next-generation material for bio-diesel. The fatty acid compositions of these oils have been described by several groups as shown in Table 3 (*22*, *23*) .Many types of bacteria have been reported to use soybean oil as a sole carbon source via the beta oxidation pathway to produce PHA containing medium-chain length units such as 3-hydroxyhexanoate (*24–27*). P(3HB) homopolymer production with plant oils such as soybean oil is a rare characteristic among PHA-producing bacteria, including *Pseudomonas* spp. and *Cupriavidus* spp. (*Cupriavidus necator* was formally known as *Ralstonia eutropha*). The composition of plant oil has been investigated and described by several groups (Table 3) (*22*, *23*). The PHA productivity of the isolated strain, *Vibrio* sp. KN01, was characterized using soybean oil and jatropha oil, respectively, as sole carbon sources at 30°C for 48 h under aerobic and aerobic-anaerobic conditions (Table 4) (*20*). The cell growth when soybean oil was used as the sole carbon source was relatively low and its dry cell weight was approximately 0.4 g/L. PHA accumulation was observed with both plant oils, however the PHA content (wt%) of the culture using jatropha oil was significantly lower. Under the aerobic-anaerobic condition, the average PHA content of the isolate cultured with soybean oil was over 40%, which is a high level of PHA productivity in comparison to the other native bacteria (*1*, *3*). The PHA contents of all the samples under the aerobic-anaerobic condition were enhanced by limiting the amount of dissolved oxygen, especially when soybean oil was used as the sole carbon source, under which condition the limitation of dissolved oxygen increased the PHA contents from 8 ± 2% to 40 ± 6%. The ^{1}H-NMR spectrum revealed that only the PHA obtained from the isolate cultured with soybean oil under the aerobic-anaerobic condition contained 3-hydroxypropionate (3HP) and 5-hydroxyvalerate (5HV) as monomer units (Figure 2A). Furthermore, gas chromatography measurement using methylated 5-hydroxyvalerate as a standard confirmed the presence of the 5HV unit. PHA containing 5HV units was recently reported to show lipase-mediated degradation and supported cell viability better than the other PHAs (*28*).

The PHA synthesized from soybean oil under the aerobic-anaerobic condition was composed of 3HP and 5HV, in addition to 3HB, according to the assignment based on the ^{1}H-NMR spectrum and gas chromatography data (Figure 2A). The additional monomer units (3HP and 5HV) have odd-numbered carbon atoms, even though the major fatty acids in soybean oil have even-numbered carbon atoms. These fatty acids might be metabolized inefficiently under the aerobic-anaerobic condition and converted into 3HPCoA and 5HVCoA from acetyl-CoA and acyl-CoA via the beta-oxidation pathway or another pathway by carboxylase, based on findings in the literature (*29*). The chromosomes of *Vibrio* sp. Ex25, which shows over 99% identity to *Vibrio* sp. KN01 in the 16S rDNA sequence, have been revealed to contain genes encoding acetyl-CoA carboxylase, 3-polyprenyl-4-hydroxybenzoate carboxylase, succinylbenzoate-CoA synthase, and 2,4-dienoyl-CoA reductase, in addition to FabG, PhaJ, PhaA, PhaB and PhaC. Furthermore,

Publication Date (Web): November 22, 2013 | doi: 10.1021/bk-2013-1144.ch015

In Green Polymer Chemistry: Biocatalysis and Materials II; Cheng, H., et al.;
ACS Symposium Series; American Chemical Society: Washington, DC, 2013.

the substrate specificities of the carboxylases, CoA synthase and CoA reductase are not known and might be broad enough to process C5 substrates. Although the pathways to produce 3HPCoA and 5HVCoA were not confirmed in the present study, a possible pathway for production of these monomers is the conversion from acetyl-CoA and acyl-CoA by carboxylase.

Table 3. Fatty acids compositions of plant oil

Fatty acid (wt%)	*Saturated acid*			*Unsaturated acid*			
	C14:0 (Myristic acid)	*C16:0 (Palmitic acid)*	*C18:0 (Stearic acid)*	*C16:1 (Palmitoleic acid)*	*C18:1 (Oleic acid)*	*C18:2 (Linoleic acid)*	*C18:3 (Linolenic acid)*
Soybean oil [a]	-	10	5	-	23	51	11
Jatropha oil [b]	0.1	17.1	4.3	1.2	42	34.8	0.1

[a] Liu et al. Catalysis Commu 2007 (*22*). [b] Ng et al. Polym. Degrad. Stab. 2010 (*23*).

Table 4. PHA accumulations in *Vibrio* sp. KN01 using plant oils as sole carbon sources. The data are partially from Numata and Doi, 2012 (*20*)

Culture Condition	*Carbon Source*	*Dry Cell Weight, g/L*	*PHA Content, wt%*	*PHA Composition, mol%* [a]	
				3HB	*HA*
Aerobic	Soybean oil	2.4	8	100	- [b]
	Jatropha oil	1.2	0.3	100	- [b]
Aerobic-Anaerobic	Soybean oil	0.4	40	83	3HP: 14 5HV: 3
	Jatropha oil	0.8	0.1	100	- [b]

[a] PHA composition determined by ^{1}H NMR. [b] Not detected. The data of dry cell weight and PHA content denote averages of three replicates and their standard deviations.

Publication Date (Web): November 22, 2013 | doi: 10.1021/bk-2013-1144.ch015

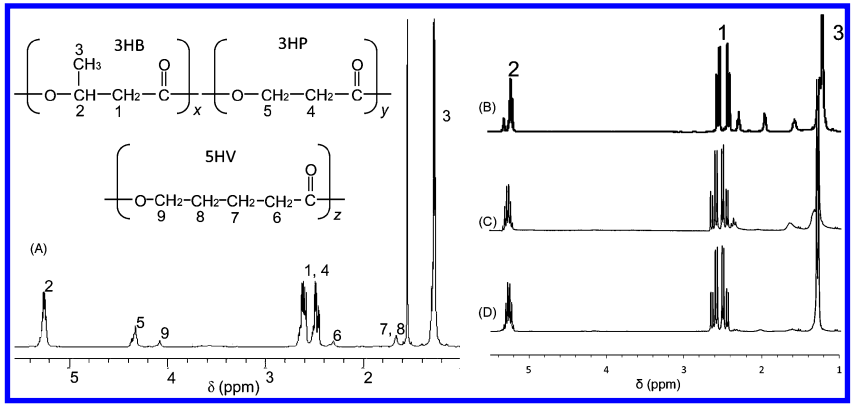

Figure 2. [1]H-NMR spectrum of PHA produced by the isolate under the aerobic–anaerobic condition using soybean oil (A), oleic acid (B), linoleic acid (C) and jatropha oil (D) as sole carbon sources. The data are partially from Numata and Doi, 2012 (20).

PHA Production Using Unsaturated Fatty Acids

Plant oils, such as soybean oil and jatropha oil, contain several saturated and unsaturated fatty acids (Table 3) (*22*, *23*). To clarify the influence of unsaturated acids as carbon sources in PHA production, PHA synthesis from three types of unsaturated fatty acids by *Vibrio* sp. KN01 was performed at 30°C for 48 h under aerobic and aerobic-anaerobic conditions (Table 5). The cell growth under the aerobic condition when unsaturated fatty acids were used as sole carbon sources was significantly lower than when soybean oil was used. PHA accumulation was also detected with three of the unsaturated fatty acids, and the PHA contents (wt%) were relatively low (0.1-3.2 wt%). Under the aerobic-anaerobic condition, the average PHA content of the isolate cultured with oleic acid was slightly higher than that under the aerobic condition. The [1]H-NMR spectra revealed that the polymers from the isolate cultured with the unsaturated fatty acids were P(3HB) homopolymers (Figure 2B, C and D). Based on the present results, the pure unsaturated fatty acids are not good candidates to produce a novel type of PHA, which suggests that another biomass such as lignin and seaweed, containing chemicals other than fatty acids, would be a more promising carbon source than fatty acids from animals and plants.

Publication Date (Web): November 22, 2013 | doi: 10.1021/bk-2013-1144.ch015

Table 5. PHA accumulations using three types of unsaturated fatty acids as a sole carbon source under aerobic and aerobic-anaerobic conditions

Culture Condition	*Carbon Source*	*Dry Cell Weight, g/L*	*PHA Content, wt%*	*PHA Composition, mol%* [a]	
				3HB	*HA* [b]
Aerobic	Oleic acid	0.7	0.3	100	- [c]
	Linoleic acid	0.6	0.4	100	- [c]
	Linolenic acid	1.5	0.2	100	- [c]
Aerobic-Anaerobic	Oleic acid	0.9	3.2	100	- [c]
	Linoleic acid	0.3	0.2	100	- [c]
	Linolenic acid	0.2	0.1	100	- [c]

[a] PHA composition determined by ^{1}H NMR. [b] HA denotes hydroxyalkanoate units. [c] Not detected.

Publication Date (Web): November 22, 2013 | doi: 10.1021/bk-2013-1144.ch015

PHA Synthase from Marine Bacteria

Our results presented here indicate that PHA production is dependent on the culture conditions, i.e. carbon sources and aerobic/anaenobic condition, in *Vibrio* sp. KN01. The data concerning the PHA produced with soybean oil suggest critical roles of metabolic regulation in the endogenous production of monomer units, to response with the level of environmental oxygen. In other words, one of key targets for engineering should be the supply of unique monomer units, which are provided endogenously and/or exogenously, to produce novel types of PHA (*20*).

As the other important target, PHA synthase, the key enzyme for biosynthesis of PHA, has been classified into 4 classes with respect to their primary structures (*7*). The relationship between the structure and function of PHA synthases has been discussed based on their primary structures, because the crystal structures of PHA synthases (i.e., PhaCs), are currently unavailable. *V. cholera*, *V. parahaemolyticus* and *V. harveyi* have been reported to possess the class I PHA synthases (*7*, *19*). Similarly, *Vibrio* sp. Ex25, which shows over 99% similarity to *Vibrio* sp. KN01 in 16S rDNA sequence, was found to possess a PHA synthase belonging to the class I, according to the revealed chromosome sequences (*20*). Class I PhaC is composed of a single subunit with molecular weights between 61 and 68 kDa. The PhaCs from *R. eutropha* and *A. caviae* are known to be typical class I PhaCs that exhibit strict and broad substrate specificities, respectively (*7*, *30*, *31*). The PhaC from *A. caviae* is one of the exceptional PhaCs in Class I, because of its low similarity in amino acid sequence (approximately 45%) to the other Class I PHA synthases (*32*, *33*). Multiple alignments of the amino acid sequences of PhaC from *Vibrio* sp. Ex25, *R. eutropha* and *A. caviae* are shown in Figure 3. The amino acid sequence of the PhaC from *Vibrio sp*. Ex25 showed 31% and 54% identities to those from *R. eutropha* and *A. caviae*, respectively. Inspection of the protein model of PhaC from *R. eutropha* revealed that the active

In Green Polymer Chemistry: Biocatalysis and Materials II; Cheng, H., et al.;
ACS Symposium Series; American Chemical Society: Washington, DC, 2013.

site Cys-319, the conserved Asp-485 and His-513 are adjacent and conceivably form a catalytic triad (*7*, *34*) (see the arrows in Figure 3). The amino acid sequence of PhaC from *Vibrio* sp. Ex25 showed high identity to that from *A. caviae*, especially around those three amino acid residues, which could form the catalytic triad, in comparison to that from *R. eutropha*. This would suggest the potential of wide substrate specificity of PhaC from *Vibrio* sp. Ex25, much as in the case of the PhaC from *A. caviae*.

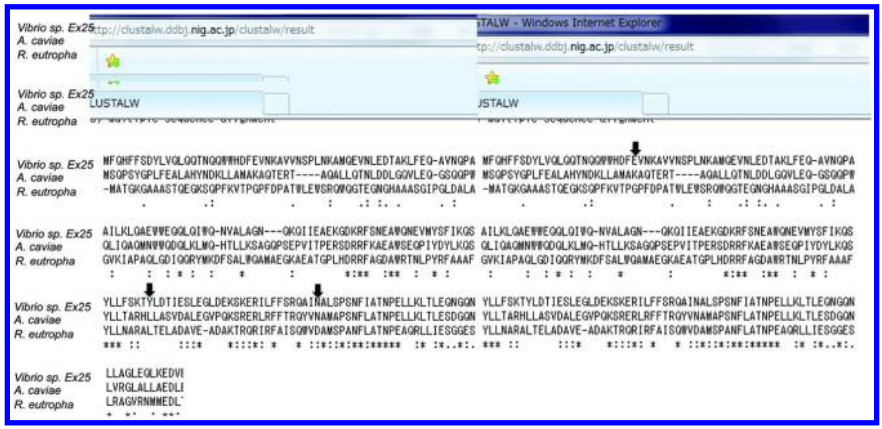

Figure 3. Multiple alignment of amino acid sequences of PHA synthases originating from the isolate Vibrio sp. Ex25, Ralstonia eutropha, and Aeromonas caviae. The arrows denote Cys-319, Asp-485 and His-513 for PhaC from R. eutropha. Modified data from Numata and Doi, 2012 (20).

Conclusion

The newly-identified marine facultative anaerobe *Vibrio* sp. KN01 produced PHA under aerobic and aerobic-anaerobic conditions when artificial seawater is used as the culture medium. The PHA production from plant oil and unsaturated fatty acids demonstrated no significant difference from that shown by some previously reported bacteria. However, the amino acid sequence of PHA synthase of the isolated strain seemed to be different from that of the typical soil bacteria. This new insight could lead to marine biotechnology for the production of various polymeric materials, including PHA, by marine bacteria to alleviate the problem of carbon dioxide emissions.

References

1. Doi, Y. *Microbial Polyesters*; VCH Publishers: New York, 1990.
2. Doi, Y.; Steinbüchel, A. *Biopolymers*; Wiley-VCH: Weinheim, Germany, 2001; Vol. 3.
3. Lenz, R. W.; Marchessault, R. H. *Biomacromolecules* **2005**, *6*, 1–8.
4. Pohlmann, A.; Fricke, W. F.; Reinecke, F.; Kusian, B.; Liesegang, H.; Cramm, R.; Eitinger, T.; Ewering, C.; Potter, M.; Schwartz, E.;

Publication Date (Web): November 22, 2013 | doi: 10.1021/bk-2013-1144.ch015

Strittmatter, A.; Voss, I.; Gottschalk, G.; Steinbüchel, A.; Friedrich, B.; Bowien, B. *Nat. Biotechnol.* **2006**, *24*, 1257–1262.
5. Fiedler, S.; Steinbüchel, A.; Rehm, B. H. *Arch. Microbiol.* **2002**, *178*, 149–160.
6. Tsuge, T.; Fukui, T.; Matsusaki, H.; Taguchi, S.; Kobayashi, G.; Ishizaki, A.; Doi, Y. *FEMS Microbiol. Lett.* **2000**, *184*, 193–198.
7. Rehm, B. H. *Biochem. J.* **2003**, *376*, 15–33.
8. Lemoignei, M. *Bull. Soc. Chim. Biol.* **1926**, *8*, 770–782.
9. Shimamura, E.; Kasuya, K.; Kobayashi, G.; Shiotani, T.; Shima, Y.; Doi, Y. *Macromolecules* **1994**, *27*, 878–880.
10. Abe, H.; Doi, Y.; Fukushima, T.; Eya, H. *Int. J. Biol. Macromol.* **1994**, *16*, 115–119.
11. Saito, Y.; Doi, Y. *Int. J. Biol. Macromol.* **1994**, *16*, 99–104.
12. Fuchtenbusch, B.; Wullbrandt, D.; Steinbüchel, A. *Appl. Microbiol. Biotechnol.* **2000**, *53*, 167–172.
13. Gonzalez-Garcia, Y.; Nungaray, J.; Cordova, J.; Gonzalez-Reynoso, O.; Koller, M.; Atlic, A.; Braunegg, G. *J. Ind. Microbiol. Biotechnol.* **2008**, *35*, 629–633.
14. Wang, Q.; Zhang, H. X.; Chen, Q.; Chen, X. L.; Zhang, Y. Z.; Qi, Q. S. *World J. Microbiol. Biotechnol.* **2010**, *26*, 1149–1153.
15. Lopez, N. I.; Pettinari, M. J.; Stackebrandt, E.; Tribelli, P. M.; Potter, M.; Steinbüchel, A.; Mendez, B. S. *Curr. Microbiol.* **2009**, *59*, 514–519.
16. Karl, D. M. *Nat. Rev. Microbiol.* **2007**, *5*, 759–769.
17. Moran, M. A.; Miller, W. L. *Nat. Rev. Microbiol.* **2007**, *5*, 792–800.
18. Umani, S. F.; Del Negro, P.; Larato, C.; De Vittor, C.; Cabrini, M.; Celio, M.; Falconi, C.; Tamberlich, F.; Azam, F. *Aquat. Microb. Ecol.* **2007**, *46*, 163–175.
19. Sun, W. Q.; Teng, K.; Meighen, E. *Can. J. Microbiol.* **1995**, *41*, 131–137.
20. Numata, K.; Doi, Y. *Mar. Biotechnol.* **2012**, *14*, 323–331.
21. Park, S. J.; Ahn, W. S.; Green, P. R.; Lee, S. Y. *Biomacromolecules* **2001**, *2*, 248–254.
22. Liu, X. J.; He, H. Y.; Wang, Y. J.; Zhu, S. L. *Catal. Commun.* **2007**, *8*, 1107–1111.
23. Ng, K. S.; Ooi, W. Y.; Goh, L. K.; Shenbagarathai, R.; Sudesh, K. *Polym. Degrad. Stab.* **2010**, *95*, 1365–1369.
24. de Smet, M. J.; Eggink, G.; Witholt, B.; Kingma, J.; Wynberg, H. *J. Bacteriol.* **1983**, *154*, 870–878.
25. Fukui, T.; Ohsawa, K.; Mifune, J.; Orita, I.; Nakamura, S. *Appl. Microbiol. Biotechnol.* **2011**, *89*, 1527–1536.
26. Timm, A.; Steinbüchel, A. *Appl. Environ. Microbiol.* **1990**, *56*, 3360–3367.
27. Tsuge, T.; Yamamoto, T.; Yano, K.; Abe, H.; Doi, Y.; Taguchi, S. *Macromol. Biosci.* **2009**, *9*, 71–78.
28. Chuah, J. A.; Yamada, M.; Taguchi, S.; Sudesh, K.; Doi, Y.; Numata, K. *Polym. Degrad. Stab.* **2013**, *98*, 331–338.
29. Fukui, T.; Suzuki, M.; Tsuge, T.; Nakamura, S. *Biomacromolecules* **2009**, *10*, 700–706.
30. Fukui, T.; Doi, Y. *J. Bacteriol.* **1997**, *179*, 4821–4830.

Publication Date (Web): November 22, 2013 | doi: 10.1021/bk-2013-1144.ch015

31. Fukui, T.; Yokomizo, S.; Kobayashi, G.; Doi, Y. *FEMS Microbiol. Lett.* **1999**, *170*, 69–75.
32. Steinbüchel, A.; Hustede, E.; Liebergesell, M.; Pieper, U.; Timm, A.; Valentin, H. *FEMS Microbiol. Rev.* **1993**, *10*, 347–350.
33. Liebergesell, M.; Steinbüchel, A. *Appl. Microbiol. Biotechnol.* **1993**, *38*, 493–501.
34. Qi, Q.; Rehm, B. H. *Microbiology* **2001**, *147*, 3353–3358.

Publication Date (Web): November 22, 2013 | doi: 10.1021/bk-2013-1144.ch015

Publication Date (Web): November 22, 2013 | doi: 10.1021/bk-2013-1144.ch016

Chapter 16

PEGylated Antibodies and DNA in Organic Media and Genetic PEGylation

Seiichi Tada, Hiroshi Abe, and Yoshihiro Ito*

Nano Medical Engineering Laboratory, RIKEN Advanced Science Institute, Wako, Saitama, 351-0198 Japan
***E-mail: y-ito@riken.jp**

Polyethylene glycol (PEG) is an amphiphilic polymer that is soluble in both water and organic media and can add many functions to biopolymers by conjugation. Here, PEG was coupled to antibodies or oligonucleotides for solubilization into organic media. The former interacted with antigens and the latter formed specific structures and had catalytic activity in organic media. In addition, we attempted to incorporate PEG genetically into a polypeptide. Although the PEG incorporation ratio decreased as the molecular weight of PEG was increased, PEG with a molecular weight of ≤1000 Da was incorporated successfully. The potential applications of PEGylated biopolymers and the methodology for gene PEGylation are discussed.

Introduction

Synthetic polymer–protein hybrids have been developed for use as therapeutic proteins or bioreactor enzymes (*1–10*). Polyethylene glycol (PEG), which is nontoxic, nonimmunogenic, highly soluble in water and approved by the United States Food and Drug Administration, is very useful in the preparation of therapeutic proteins (*11*, *12*). Some proteins trigger immune reactions and proteases, and other compounds inside the body can rapidly degrade them and remove them from the body. Many PEGylated protein drugs have been developed since the pioneering work of Abuchowsky et al. on the PEGylation of proteins (*13*, *14*). Thus, PEGylation has proven very valuable.

In Green Polymer Chemistry: Biocatalysis and Materials II; Cheng, H., et al.;
ACS Symposium Series; American Chemical Society: Washington, DC, 2013.

On the other hand, Inada et al. found that an enzyme modified with PEG was soluble in organic media (*15*) and that the PEG-modified enzyme catalyzed reactions reverse of those in aqueous solutions in organic media (*16*). Ito and colleagues modified the enzymes with other polymers and extended the usefulness of the modified enzymes (*1*, *2*, *17*–*19*).

Here, PEG was conjugated with an antibody and DNA and the conjugate's solubility and behavior in organic media were investigated (Figure 1). By using a catalytic antibody (abzyme) and a catalytic DNA (DNAzyme) as the targets of PEGylation, applications as biocatalysts are considered. In addition, a new PEGylation method, genetic PEGylation is discussed. The method provides site-specific modification using PEG chains.

Publication Date (Web): November 22, 2013 | doi: 10.1021/bk-2013-1144.ch016

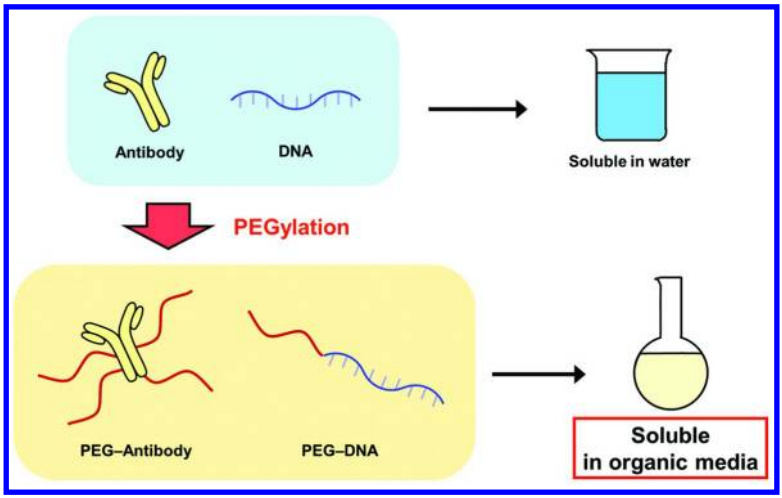

Figure 1. Polyethylene glycol (PEG) conjugation renders an antibody and DNA soluble both in organic solvents and in water.

PEGylated Antibody in Organic Media

The interaction of a PEGylated antiatrazine antibody with toluene was first investigated by Sasaki et al. (*20*). We prepared new PEG-modified antibodies and investigated their properties such as solubility, antigen affinity, and catalytic activity in aqueous and organic media (*21*). The antibodies 7B9 and 4S112 used are listed in Table 1; 7B9 is an abzyme developed by Fujii's group (*22*). PEGylated antibodies were synthesized by coupling with PEG–*N*-hydroxysuccinimide ester (10,000 Da). Mass spectroscopy indicated that both antibodies (7B9 and 4S112) were modified with eight chains of PEG.

Table 1. List of antibodies used

Antibody	*Antigen*	*Catalytic antibody*
7B9	p-nitrobenzyl ester	Hydrolysis of ester bonds
4S112	17β-estradiol	No activity

The solubility of modified and native antibodies in buffered aqueous and organic solvents including dichloromethane and acetone was examined (Table 2). The organic solvents were saturated with distilled water in advance. Both unmodified and PEG-modified antibodies were soluble in aqueous solution. The modified antibodies were soluble in dichloromethane and acetone. The solubility for PEGylated 7B9 and 4S112 in organic media was less than in aqueous solutions. After conjugation with PEG, no significant differences were observed in the circular dichroism (CD) spectra. When the catalytic activity of PEGylated 7B9 was examined, there were no significant differences in activity from unmodified 7B9. Thus, PEG chains did not affect the conformation and activity of these antibodies.

The interactions of unmodified and modified antibodies with antigens were compared (Table 3). Both of the unmodified antibodies (7B9 and 4S112) were insoluble in organic media. However, both of the PEGylated antibodies were organic solvents were similar to those in aqueous buffer solutions (Table 2). Therefore, we can conclude that an antigen–antibody reaction can occur in organic media using a PEGylated antibody. However, PEGylated 7B9 did not catalyze ester formation, which is the reverse of the hydrolysis observed in aqueous solutions and in PEGylated enzymes in organic media.

Publication Date (Web): November 22, 2013 | doi: 10.1021/bk-2013-1144.ch016

Table 2. Solubility of unmodified and PEGylated antibodies. Reproduced with permission from ref. (*21*). Copyright 2011 Elsevier

	7B9		*4S112*	
	Unmodified (μg/mL)	*PEGylated (μg/mL)*	*Unmodified (μg/mL)*	*PEGylated (μg/mL)*
Tris-HCl buffer	> 50.0	> 50.0	> 50.0	> 50.0
Dichloromethane	0	28.1 ± 1.9	0	30.0 ± 0.8
Acetone	0	22.0 ± 2.0	0	35.1 ± 2.2

In Green Polymer Chemistry: Biocatalysis and Materials II; Cheng, H., et al.;
ACS Symposium Series; American Chemical Society: Washington, DC, 2013.

Table 3. Interactions of unmodified and PEGylated antibodies to antigen-immobilized beads. Reproduced with permission from ref. (*21*). Copyright 2011 Elsevier

	7B9		*4S112*	
	Unmodified (%)	*PEGylated (%)*	*Unmodified (%)*	*PEGylated (%)*
Tris-HCl buffer	33.3 ± 4.2	24.0 ± 1.0	48.1 ± 1.2	38.0 ± 5.2
Dichloromethane	−	35.8 ± 3.2	−	47.6 ± 2.4
Acetone	−	22.6 ± 2.7	−	25.7 ± 8.2

Publication Date (Web): November 22, 2013 | doi: 10.1021/bk-2013-1144.ch016

PEGylated DNA in Organic Media

Although PEGylated proteins were found to be soluble in most organic solvents as well as in water and to maintain their enzymatic activity in organic solvents, PEGylated DNA with a biologically important structure and catalytic activity in organic solvents has not been investigated. Therefore, we attempted to prepare PEGylated DNA and investigated its properties (*23*).

A DNAzyme was utilized as a DNA to be coupled with PEG. To date, many DNAzymes have been discovered (*24*). However, one that works in organic solvents has never been reported. We chose a peroxidase DNAzyme because a structured DNA molecule—a G-quadruplex—is known to work as its component. G-quadruplex DNA with a G-rich sequence plays an important role as a telomere in biological processes (Figure 2a, b). Hence, we tested whether this DNAzyme chemically modified with PEG would form the required structure and show catalytic activity in organic solvents.

PEG–DNAs (Table 4) were synthesized by coupling a PEG–*N*-hydroxysuccinimide ester (10,000 Da) with 5′-amino-modified DNAs. In the first step, we performed a solubility test for PEG–DNA using HT21, which contains triple human telomeric motifs (TTAGGG). HT21 was dissolved in various organic solvents, including 1,4-dioxane, dichloroethane (DCE), chloroform, acetonitrile and methanol, at 0.1 mM, although unmodified DNA was not soluble in these solvents (Figure 2c).

The shorter PEG-DNA HT6 including a single human telomeric motif (TTAGGG) was then tested for the formation of a G-quadruplex structure in solvents (Figure 3). In aqueous solution, the 6-nucleotide telomeric sequence d(TTAGGG) forms an all-parallel G-quadruplex in the presence of K^+ ions (Figure 3a). HT6 exhibited CD spectra in organic solvents that differed from that in an aqueous buffer, with a relatively wide positive band between 260 and 295 nm (Figure 3b). However, the CD spectrum of CON6, which contains a control sequence of d(GTGTAG), showed no obvious CD band, either in aqueous buffer or in organic solvents (Figure 3c). This result suggests that PEG-modified d(TTAGGG) (HT6) formed G-tract-specific structures, which can be G-quadruplexes, in organic solvents as well in an aqueous buffer.

In Green Polymer Chemistry: Biocatalysis and Materials II; Cheng, H., et al.;
ACS Symposium Series; American Chemical Society: Washington, DC, 2013.

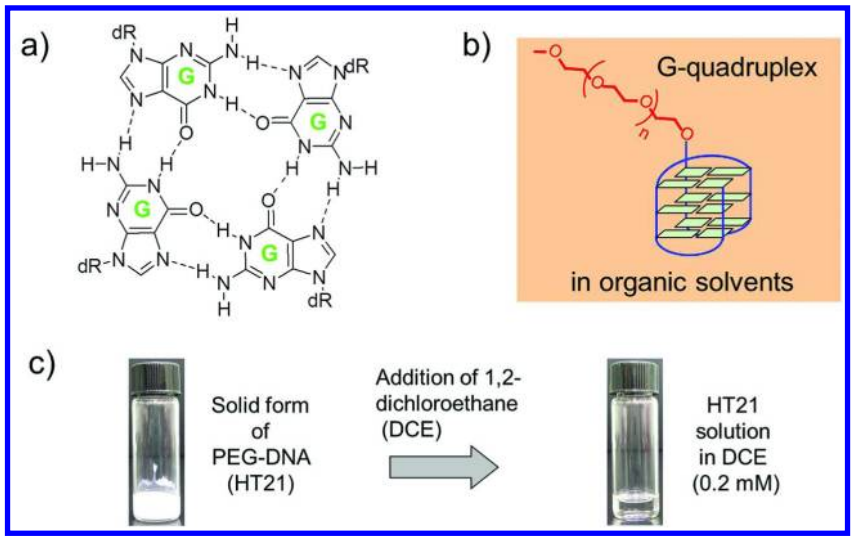

Figure 2. a) G-quartet structure. b) Structural model of a G-quadruplex formed by PEG–DNA with a human telomere motif (HT21) in 1,2-dichloroethane (DCE). c) PEG–DNA (HT21) is soluble in DCE. Reproduced with permission from ref. (23). Copyright 2012 John Wiley and Sons

Table 4. PEG-modified DNA sequences

Name	*Sequence*
HT21	5′ PEG-d(GGG TTA GGG TTA GGG TTA GGG) 3′
CON21	5′ PEG-d(GGA GTG TGT GTG AGG TGA GTG) 3′
HT6	5′ PEG-d(TTA GGG) 3′
CON6	5′ PEG-d(GTG TAG) 3′

The catalytic activity of HT6 was investigated after binding to hemin in organic solvents. In aqueous solution, the specific interaction of hemin with a G-quadruplex results in the formation of a DNAzyme that is capable of accelerating an oxidative reaction with peroxidase-like activity.

It uses 3-aminophthalic hydrazide (luminol) as a substrate to generate chemiluminescence in the presence of hydrogen peroxide in an aqueous environment. The peroxidase activities of various DNAs—HT6, CON6, d(TTAGGG), or d(GTGTAG)—in methanol were compared (Figure 4). Among them, HT6 exhibited the strongest luminescence. Only a weak luminescence was observed in reactions using other DNAs because of the low solubility of non-PEG-modified DNAs—d(TTAGGG) or d(GTGTAG)—or the absence of structure formation (CON6). Integrated photon counting revealed that the complex of HT6 with hemin was the most efficient catalyst, as it exhibited 4.5 and 9 times higher activity than that of CON6 and no DNA, respectively (Figure 4b).

This result demonstrated that the DNAzyme formed by the PEG–DNA–hemin complex exhibits oxidative activity in an organic solvent.

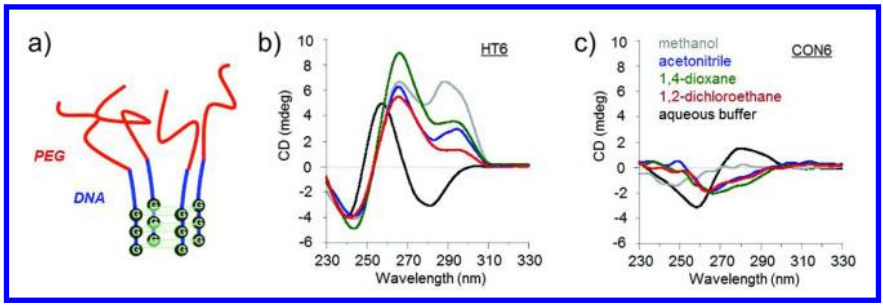

Figure 3. G-quadruplex formation by a hexameric DNA in organic solvents. a) Schematic model of the PEG–DNA G-quadruplex. CD spectra of b) HT6 or c) CON6 in various organic solvents (10 μM DNA, 20 °C). Samples were prepared by annealing the DNA at a concentration of 10 μM in aqueous buffer (50 mM K phosphate pH 7.0, 300 mM KCl), lyophilizing the sample and redissolving it in organic solvents or aqueous buffer. Reproduced with permission from ref. (23). Copyright 2012 John Wiley and Sons.

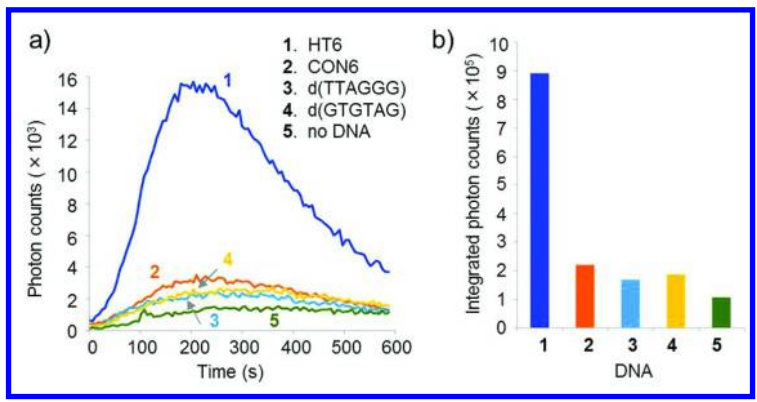

Figure 4. Peroxidase activity of the PEG–DNA–hemin complex in methanol. a) Time course of chemiluminescence to measure the peroxidase activity of DNA in methanol. The composition of the reaction mixture was: 1 mM DNA, 0.25 mM hemin, 1 mM luminol, and 12 mM H_2O_2 in methanol. b) Integrated photon counts of the chemiluminescence reaction. The bar numbering corresponds to (a). Reproduced with permission from ref. (23). Copyright 2012 John Wiley and Sons.

Thus, PEG–DNA–HT6 seemed to form an intermolecular G-quadruplex in various organic solvents (Figure 3). Furthermore, this G-quadruplex structure associated with hemin in methanol and formed a DNAzyme that was capable of performing catalytic oxidative reactions in methanol, an organic solvent (Figure 4).

In Green Polymer Chemistry: Biocatalysis and Materials II; Cheng, H., et al.;
ACS Symposium Series; American Chemical Society: Washington, DC, 2013.

Publication Date (Web): November 22, 2013 | doi: 10.1021/bk-2013-1144.ch016

Genetic PEGylation

A genetic-encoding approach was first reported in 1989 as an alternative method for the site-specific incorporation of nonnatural amino acids into peptides or proteins (*25*, *26*) and various amino acids have been incorporated in this way (*27–31*). The method utilizes the UAG codon (the amber nonsense stop codon)—which normally directs the termination of protein synthesis—to encode instead a nonnatural amino acid that is loaded onto the complementary tRNA. Deiters et al. (*32*) made 20 different versions of human growth factor, each of which had a nonnatural amino acid, p-acetylphenylalanine, inserted at a different site using the misacylated tRNA method. They linked a single PEG molecule to each keto group as a posttranslational modification. Johnson et al. (*33*) enhanced the efficiency of the ribosomal incorporation of nonnatural amino acids at multiple sites by release factor 1 (RF1) knockout in a live cell. However, it is difficult to insert more than two PEG chains of different lengths or two different nonnatural amino acids precisely into each desirable position in one protein molecule using this posttranslational modification method.

Sisido and colleagues developed a frameshift-suppression method, in which nonnatural amino acids are incorporated into proteins using four-base codon–anticodon pairs instead of the stop codon (*34*). Using the four-base codon method, Shozen et al. (*35*) recently attempted to incorporate a short PEG chain into a polypeptide, although its production was not confirmed directly by mass spectrometry and the incorporation of a long PEG chain was not attempted. Therefore, we attempted to add tRNAs recognizing a stop codon attached to PEGs of various molecular weights into a translation system (Figure 5) (*36*). Here, the incorporation of PEG with a molecular weight of 1000 Da using an *in vitro* translation system was confirmed directly by mass spectrometry.

A FLAG tag-labeled peptide was prepared by an in vitro translation reaction using PEG4 (ethylene glycol tetramer, M_w 170 Da), PEG12 (dodecamer, M_w 500 Da), PEG16 (16-mer, M_w 700 Da), PEG24 (24-mer, M_w 1000 Da) and PEG48 (48-mer, M_w 2000 Da). To enhance the efficiency of PEG chain incorporation, a peptide sequence containing the ProX tag was used (Figure 6). The sequence of the ProX tag was optimized for the effective incorporation of a nonnatural amino acid into a protein, with minimum irregular product (*37*).

The translation reactions were performed at 30 °C for 7 h and the products were confirmed using mass spectrum analysis (Figure 7). PEG4 or PEG12 were incorporated successfully in the presence of 8 μM PEG–AF–tRNA. However, PEG chains longer than PEG24 were not incorporated. Therefore, the amount of PEG–AF–tRNA in the translation system was increased. PEG16 or PEG24 were incorporated in the presence of 20 or 40 μM PEG–AF–tRNA, respectively. However, no incorporation of PEG with a molecular weight of >2000 Da was observed, even in the presence of 60 μM PEG–AF–tRNA.

The dependence of the translational incorporation of PEG on its molecular weight was estimated from the mass analysis. Each product peak was compared with a standard peak at a molecular weight of 4364 Da, attributed to ribosomal protein L36 in the cell-free translation system and the corresponding value was plotted (Figure 7b). The higher the molecular weight, the less translation product

Publication Date (Web): November 22, 2013 | doi: 10.1021/bk-2013-1144.ch016

In Green Polymer Chemistry: Biocatalysis and Materials II; Cheng, H., et al.;
ACS Symposium Series; American Chemical Society: Washington, DC, 2013.

was produced. We inferred that the longer PEG chains hindered the processing of the polypeptide sterically because the tunnel space in the ribosome is narrow. It is also possible that the PEG groups hinder the binding of elongation factor (EF)-Tu to acylated tRNA.

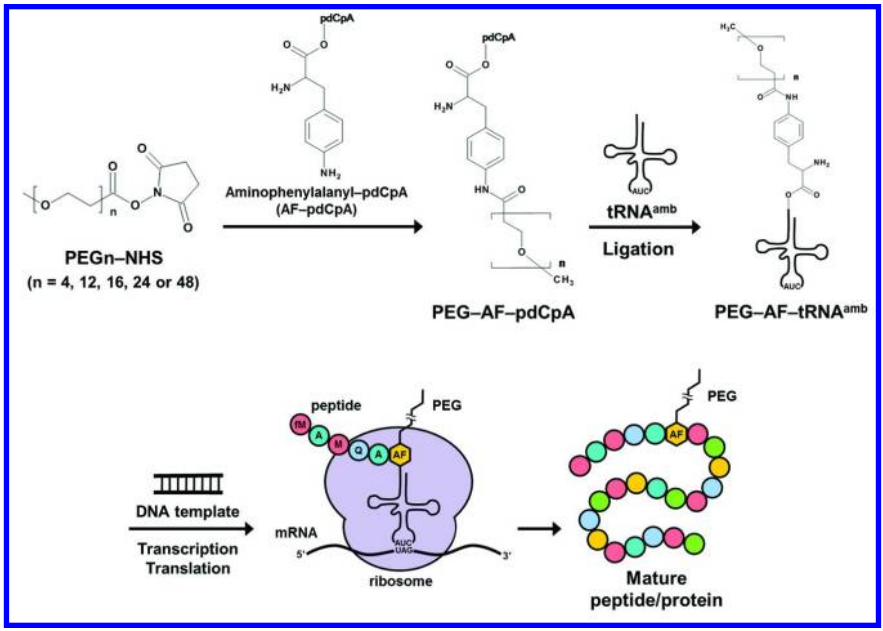

Figure 5. Illustration of the synthesis of a PEG-bound tRNA and the incorporation of PEG into a polypeptide by in vitro translation. Tada, S., et al. (2012) Genetic PEGylation. PLoS ONE 7(11): e49235.

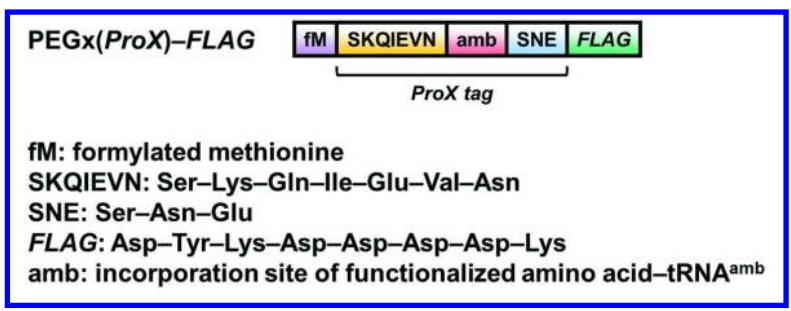

Figure 6. Prepared DNA templates. The ProX tag sequence (SKQIEVN–amber–SNE) was contained in PEGx(ProX)–FLAG. Tada, S., et al. (2012) Genetic PEGylation. PLoS ONE 7(11): e49235.

In Green Polymer Chemistry: Biocatalysis and Materials II; Cheng, H., et al.;
ACS Symposium Series; American Chemical Society: Washington, DC, 2013.

Publication Date (Web): November 22, 2013 | doi: 10.1021/bk-2013-1144.ch016

Publication Date (Web): November 22, 2013 | doi: 10.1021/bk-2013-1144.ch016

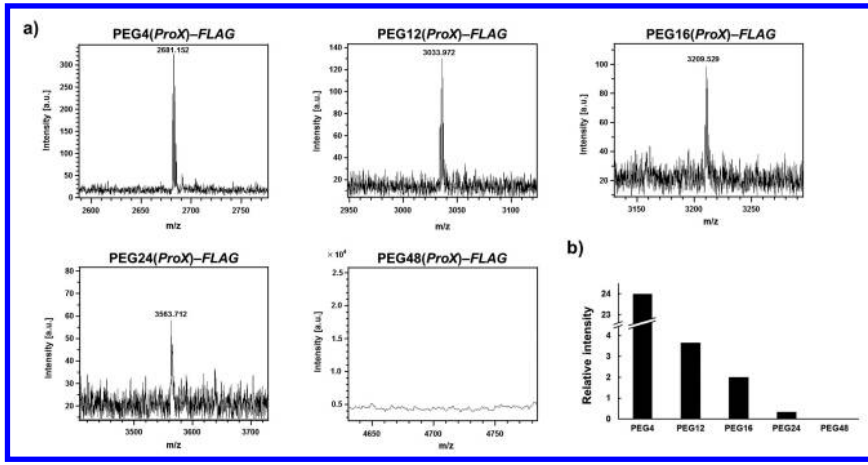

Figure 7. Mass spectrometry analysis of PEG-incorporated polypeptides in m/z units. a) PEG4–FLAG, calculated 2680.836 for $(M+H)^+$, found 2681.152; PEG12–FLAG, calculated 3033.252 for $(M+H)^+$, found 3033.972; PEG16–FLAG, calculated 3209.460 for $(M+H)^+$, found 3209.529; PEG24–FLAG, calculated 3561.876 for $(M+H)^+$, found 3563.712; PEG48–FLAG, calculated 4707.228 for $(M+H)^+$, not found. b) Molecular weight dependence of the coefficient of incorporation of PEG into polypeptides by in vitro translation. Tada, S., et al. (2012) Genetic PEGylation. PLoS ONE 7(11): e49235.

Concluding Remarks and Future Outlook

We have prepared PEG-modified antibodies and DNAzymes successfully and investigated their properties including solubility, antigen affinity, and catalytic activity in aqueous and organic media. Although PEGylated antibodies did not have catalytic activity in organic media, an antibody–antigen interaction was confirmed. Therefore, such PEGylated antibodies could be used for organic-phase immunosensors for the measurement of poorly water-soluble analytes in organic solvents.

On the other hand, a PEGylated DNAzyme was soluble in both water and organic solvents and catalyzed a reaction in organic media. DNAzymes can be designed by in vitro selection. Although the current molecular designs are inspired by known molecules that evolved in aqueous environments, in vitro selection should allow us to create novel structured and functional oligonucleotides that will evolve in organic solvents.

Site-specific PEGylation will be important for the preparation of defined protein drugs. Some modifications to the ribosome should be investigated, which would enlarge the entrance and exit spaces or increase the binding of EF-Tu to allow the incorporation of longer PEG chains or other macromolecules. Elaborate synthesis of (bio-)macromolecules will be developed by this methodology (*38*).

In Green Polymer Chemistry: Biocatalysis and Materials II; Cheng, H., et al.;
ACS Symposium Series; American Chemical Society: Washington, DC, 2013.

Publication Date (Web): November 22, 2013 | doi: 10.1021/bk-2013-1144.ch016

References

1. Ito, Y.; Sugimura, N.; Kwon, O. H.; Imanishi, Y. *Nat. Biotechnol.* **1999**, *17*, 73–75.
2. Kwon, O. H.; Imanishi, Y.; Ito, Y. *Biotechnol. Bioeng.* **1999**, *66*, 265–270.
3. Pennadam, S.; Firman, K.; Alexander, C.; Gorecki, D. *J. Nanotechnol.* **2004**, *2*, 1–7.
4. Elvira, C.; Gallardo, A.; Roman, J. S.; Cifuentes, A. *Molecules* **2005**, *10*, 114–125.
5. Hest, J. C. M. *J. Macromol. Sci. Polym. Rev.* **2005**, *47*, 63–92.
6. Broyer, R. M.; Grover, G. N.; Maynard, H. D. *Chem. Commun.* **2011**, *47*, 2212–2226.
7. Klok, H.-A. *Macromolecules* **2009**, *42*, 7990–8000.
8. de Graaf, A. J.; Kooijiman, M.; Hennink, W. E.; Mastrobattista, E. *Bioconjug. Chem.* **2009**, *20*, 1281–1295.
9. Krishna, O. D.; Kiick, K. L. *Biopolymers (Pep. Sci.)* **2010**, *94*, 32–48.
10. Velonia, K. *Polym. Chem.* **2010**, *1*, 944–952.
11. Veronese, F. M.; Mero, A. *Biodrugs* **2008**, *22*, 315–329.
12. Joralemon, M. J.; McRae, S.; Emrick, T. *Chem. Commun.* **2010**, *46*, 1377–1393.
13. Abuchowsky, A.; van Es, T.; Palczuk, N. C.; Davis, F. F. *J. Biol. Chem.* **1977**, *251*, 3578–3581.
14. Abuchowsky, A.; McCoy, T. J. R.; Palczuk, N. C.; van Es, T.; Davis, F. F. *J. Biol. Chem.* **1977**, *251*, 3582–3586.
15. Inada, Y.; Takahashi, K.; Yoshimoto, T.; Ajima, A.; Matsushima, A.; Saito, Y. *Trends Biotechnol.* **1986**, *4*, 190–194.
16. Takahashi, K.; Ajima, A.; Yoshimoto, T.; Okada, M.; Matsushima, A.; Tamaura, Y.; Inada, Y. *J. Org. Chem.* **1985**, *50*, 3414–3415.
17. Ito, Y. *J. Biomater. Sci. Polym. Ed.* **1999**, *10*, 1237–1249.
18. Ito, Y.; Kwon, O. H.; Ueda, M.; Tanaka, A.; Imanishi, Y. *J. Bioact. Comp. Polym.* **2000**, *15*, 376–395.
19. Kwon, O. H.; Ito, Y. *Biotechnol. Genet. Eng. Rev.* **2001**, *18*, 237–263.
20. Sasaki, S.; Tokitsu, Y.; Ikebukuro, K.; Yokoyama, K.; Masuda, Y.; Karube, I. *Anal. Lett.* **1997**, *30*, 429–443.
21. Liu, M.; Xu, M.; Loh, X. J.; Abe, H.; Tsumuraya, T.; Fujii, I.; Li, J.; Son, T. I.; Ito, Y. *J. Biosci. Bioeng.* **2011**, *111*, 564–568.
22. Kurihara, S.; Tsumuraya, T.; Suzuki, K.; Kuroda, M.; Liu, L.; Takaoka, Y.; Fujii, I. *Chemistry* **2000**, *6*, 1656–1662.
23. Abe, H.; Abe, N.; Shibata, A.; Ito, K.; Tanaka, Y.; Ito, M.; Saneyoshi, H.; Shuto, S.; Ito, Y. *Angew. Chem., Int. Ed. Engl.* **2012**, *51*, 6475–6479.
24. Joyce, G. F. *Angew. Chem., Int. Ed.* **2007**, *46*, 6420–6436.
25. Noren, C. J.; Anthony-Cahill, S. J.; Griffith, M. C.; Schultz, P. G. *Science* **1989**, *244*, 182–188.
26. Bain, J. D.; Glabe, C. G.; Dix, T. A.; Chamberlin, A. R.; Diala, E. S. *J. Am. Chem. Soc.* **1989**, *111*, 8013–8014.
27. Josephson, K.; Hartman, M. C.; Szostak, J. W. *J. Am. Chem. Soc.* **2005**, *127*, 11727–11735.

In Green Polymer Chemistry: Biocatalysis and Materials II; Cheng, H., et al.;
ACS Symposium Series; American Chemical Society: Washington, DC, 2013.

28. Wang, L.; Xie, J.; Schultz, P. G. *Annu. Rev. Biophys. Biomol. Struct.* **2006**, *35*, 225–249.
29. Liu, C. C.; Schultz, P. G. *Annu. Rev. Biochem.* **2010**, *79*, 413–444.
30. Young, T. S.; Schults, P. G. *J. Biol. Chem.* **2010**, *285*, 11039–11044.
31. Wang, F.; Robbins, S.; Guo, J.; Shen, W.; Schults, P. G. *PLoS ONE* **2010**, *5*, e9354.
32. Deiters, A.; Cropp, T. A.; Summerer, D.; Mukherji, M.; Schultz, P. G. *Bioorg. Med. Chem. Lett.* **2004**, *14*, 5743–5745.
33. Johnson, D. B.; Xu, J.; Shen, Z.; Takimoto, J. K.; Schultz, M. D.; Schmitz, R. J.; Xiang, Z.; Ecker, J. R.; Briggs, S. P.; Wang, L. *Nat. Chem. Biol.* **2011**, *7*, 779–786.
34. Hohsaka, T.; Ashizuka, Y.; Murakami, H.; Sisido, M. *J. Am. Chem. Soc.* **1996**, *118*, 9778–9779.
35. Shozen, N.; Iijima, I.; Hohsaka, T. *Bioorg. Med. Chem. Lett.* **2009**, *19*, 4909–4911.
36. Tada, S.; Andou, T.; Suzuki, T.; Dohmae, N.; Kobatake, E.; Ito, Y. *PLoS One* **2012**, *7*, e49235.
37. Kajihara, D.; Abe, R.; Iijima, I.; Komiyama, C.; Sisido, M.; Hohsaka, T. *Nat. Methods* **2006**, *3*, 923–929.
38. Ito, Y. *ChemBioChem* **2012**, *13*, 1100–1102.

Publication Date (Web): November 22, 2013 | doi: 10.1021/bk-2013-1144.ch016

Publication Date (Web): November 22, 2013 | doi: 10.1021/bk-2013-1144.ch017

Chapter 17

Effect of Polycondensation Conditions on Structure and Thermal Properties of Poly(caffeic acid)

Daisuke Ishii,[*,1,3] Hiroki Maeda,[1] Hisao Hayashi,[1] Tomohiko Mitani,[2] Naoki Shinohara,[2] Koichi Yoshioka,[2] and Takashi Watanabe[2]

[1]Department of Materials Chemistry, Graduate School of Science and Technology, Ryukoku University, Otsu, Shiga 520-2194, Japan
[2]Research Institute for Sustainable Humanosphere (RISH), Kyoto University, Uji, Kyoto 611-0011, Japan
[3]Current address: Department of Biomaterials Sciences, Graduate School of Agricultural and Life Science, The University of Tokyo, 1-1-1 Yayoi, Bunkyo-ku, Tokyo 113-8657, Japan
[*]E-mail: adishii@mail.ecc.u-tokyo.ac.jp

Effect of polycondensation conditions of caffeic acid (CA) on solubility and thermal properties of the resultant poly(caffeic acid) (PCA), a homopolyester of CA, was investigated. Polycondensation of CA was performed by transesterification after acetylation using sodium acetate and acetic anhydride. Acetylation and oligomerization of CA was performed by refluxing a mixture of CA, sodium acetate and acetic anhydride at 160 °C for 18 h or at 100 °C for 2 h under a nitrogen atmosphere. Polycondensation of the acetylated-oligomerated CAs was performed at 160 °C or 200 °C and under reduced pressure below 3 kPa. Characterization of PCAs was performed by FTIR, MALDI-TOF-MS, ^{1}H NMR, GPC, DSC, TG-DTA and hotstage-equipped polarized optical microscopy. Both the solubility and thermal properties of PCAs significantly depended on polycondensation conditions. In particular, PCAs polycondensed at 200 °C lost melt fusibility. However, the infusible PCAs showed glass transition at about 110 °C and were thermally processed by hotpress. The thermally processed PCA film retained its original form even after heated up to 300 °C.

In Green Polymer Chemistry: Biocatalysis and Materials II; Cheng, H., et al.;
ACS Symposium Series; American Chemical Society: Washington, DC, 2013.

Introduction

Recently, needs for 'biomass plastics' that is produced from natural biomasses (woods, agricultural wastes, and many other resources from plants, animals, and micrroorganisms) as starting materials or monomeric components have extensively been increased. Biopolyesters of microbial or synthetic origins, such as poly(hydroxyalkanoate)s and poly(lactide)s, are expected as most promising biomass plastics for commodity or specialty applications (*1*, *2*). These biological polyesters have improved mechanical properties, high processability into films (*3*, *4*), fibers (*5–10*), and other various forms. Furthermore, the polyesters show biodegradability under in vitro enzymatic (*11*, *12*), alkaline (*13*), physiological (*14*, *15*), and microbial (*16*) conditions under the hydrated state. Apart from these advantages, improvement of thermal stability at the elevated temperatures still remains as a major problem. While stereocomplex formation of enantiomeric poly(lactide)s has been proposed for the increment of melting point (*17*, *18*), improvement of thermal degradability should also be attained. One of the expected solutions to improve the thermal stability is the introduction of aromatic moieties as rigid component to polymer backbone. In this context, we intend to utilize lignin-related materials, that can be obtained from wooden or plant biomasses, as starting materials for biomass polymers.

Lignin is a natural phenylpropanoid polymer that is biosynthesized in wooden plants by dehydrogenative polymerization of *p*-hydroxycinnamyl alcohol precursors (*19*). These cinnamic alcohols originate from aromatic amino acids, i.e., phenylalanine and tyrosine, via shikimic acid pathway. The chemical structure is highly complex because many reaction intermediates are formed during the dehydrogenative polymerization of the cinnamyl alcohols. Although the lignin itself can be abundantly obtained as byproduct in papermaking industry (black liquor from pulping waste solutions) or as remnant of bioethanol production from agricultural resources (*20–27*), the utilization of lignin as material for functional polymers has been interfered by the inherent structural complexity. Therefore, utilization of low-molecular-weight substances produced by degradation of the lignins followed by selective extraction or separation has been performed to develop structurally-controlled functional materials from the lignins.

Plant-derived cinnamic acid derivatives, such as *p*-coumaric, caffeic and ferulic acids attract attention as precursors for novel heat-resistant bioplastics (*28–33*). These cinnamic acid derivatives, produced as a precursor of lignins, can be extracted from the plant/wooden biomasses by alkaline extraction or microbial degradation (*34*, *35*). These cinnamic acid derivatives possess rigid phenylpropanoid structure similar to conventional monomers of liquid crystalline polymers (LCPs). Therefore, development of bio-based LCP is expected by the polycondensation. In particular, because CA has two phenolic hydroxyl groups and one carboxyl group, polyesters containing CA as monomeric unit can form multibranched main-chain structure. Previously, several research groups have shown that copolyester of CA with *p*-coumaric acid possesses various functionalities such as thermotropic liquid crystallity, high heat resistance, adherence, and cell growth properties (*30–32*). On the other hand, poly(caffeic

In Green Polymer Chemistry: Biocatalysis and Materials II; Cheng, H., et al.;
ACS Symposium Series; American Chemical Society: Washington, DC, 2013.

Publication Date (Web): November 22, 2013 | doi: 10.1021/bk-2013-1144.ch017

acid) (PCA), a homopolyester of CA, has not been investigated in detail because of the limitation of molecular weight of the homopolyester obtained. In this paper, we report the preparation of high molecular weight PCA by the detailed investigation of polycondensation conditions of CA. Furthermore, thermal, mechanical, and optical properties as well as molecular characteristics of the PCAs are reported.

Experimental

Materials

Caffeic acid (98%), sodium acetate (97%) and acetic anhydride (93%) were purchased from Wako Pure Chemical Co., Japan. All reagents were used without further purification.

Synthesis of PCA

Polycondensation of CA was performed by transesterification after acetylation using sodium acetate and acetic anhydride (Figures 1 and 2). A mixture of CA, sodium acetate and acetic anhydride was refluxed at 160 °C for 18 h or at 100 °C for 2 h under a nitrogen atmosphere. Polycondensation under reduced pressure below 3 kPa was performed at 160 °C for 2 h or at 200 °C for 4 h or 22 h.

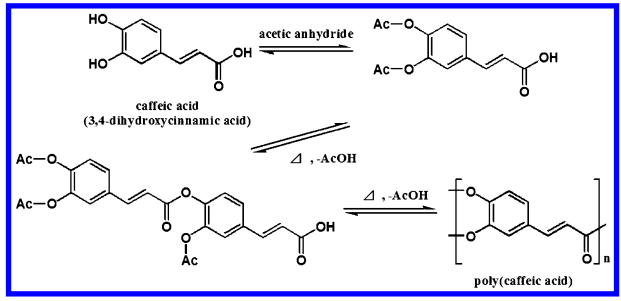

Figure 1. Schematic representation of polycondensation reaction of caffeic acid via acetylation followed by transesterification.

Publication Date (Web): November 22, 2013 | doi: 10.1021/bk-2013-1144.ch017

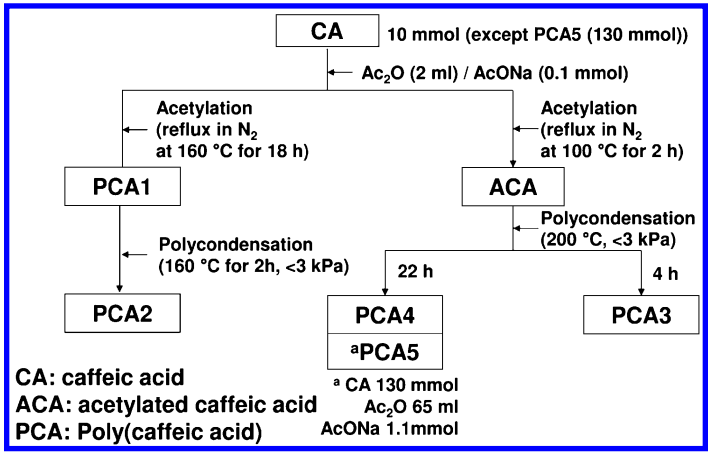

Figure 2. Scheme for synthesis of poly (caffeic acid).

Publication Date (Web): November 22, 2013 | doi: 10.1021/bk-2013-1144.ch017

Instrumentation

FT-IR spectra of CA and PCAs were obtained by KBr method on a HORIBA FT-720 spectrometer. Gel permeation chromatography (GPC) measurements were performed on a Tosoh HLC-8020 system in which TSKGel GMH_{HR}-M column was attached. Chloroform was used as the mobile phase. Injection port, column oven and RI detector were kept at 40 °C. Molecular weights of polymer samples were calibrated by using monodisperse polystyrene standards (Tosoh Corporation, Japan). ^{1}H NMR spectra of the PCAs were obtained on a JEOL Lambda 400 spectrometer at 50 °C using 5 mm o.d. tubes. Sample concentrations were about 10 % (w/v) in DMSO-d_6 (Cambridge Isotope Laboratories) containing 0.05 % (v/v) TMS. The chemical shifts of ^{1}H spectra were calibrated by signals at 2.50 ppm assigned to methyl proton of DMSO. Matrix-assisted laser desorption ionization / time-of-flight mass spectrometry (MALDI-TOF-MS) was also performed on a Bruker autoflex III spectrometer under positive ion detection mode. Matrix used was 2,5-dihydroxybenzoic acid. Mass numbers were calibrated by PEG standards. Differential scanning calorimetry (DSC) and thermogravimetry / differential thermal analysis (TG/DTA) were performed on a Rigaku DSC8230 calorimeter and TG8120 thermogravimeter, respectively. These thermal analyses were performed under air atmosphere with heating / cooling runs at 10 K/min. Polarized optical microscopy was performed on a Nikon ECLIPSE 50iPOL microscope equipped with Linkam 10013L hotstage. Optical transmittance of hot-pressed PCA film was measured on a Shimadzu UV3100 spectrophotometer. Dynamic mechanical analysis (DMA) was performed on a DVA-200 rheometer (itk Co. Ltd., Osaka, Japan).

In Green Polymer Chemistry: Biocatalysis and Materials II; Cheng, H., et al.;
ACS Symposium Series; American Chemical Society: Washington, DC, 2013.

Publication Date (Web): November 22, 2013 | doi: 10.1021/bk-2013-1144.ch017

Results and Discussion

Molecular Structure, Solubility, and Molecular Weight Distribution of PCAs

Figure 3 shows FT-IR spectra of CA and PCAs. The intense OH absorption at 3400 cm^{-1} in CA was rather broadened and diminished in PCAs. In addition, ester C=O (1725-1730 cm^{-1}) and C-O (1095 cm^{-1}) stretching bands were observed in the PCAs. These show that the esterification of CA, whether acetylation or polycondensation, proceeded by the reactions.

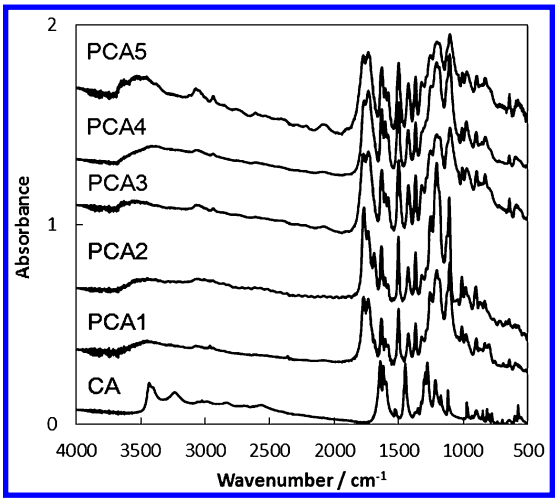

Figure 3. FT-IR spectra of CA and PCAs obtained by KBr method.

In order to perform molecular structural analysis of PCAs in the dissolved state, solubility of the PCAs to various solvents were investigated. The results are summarized in Table 1. While CA dissolved in methanol and ethanol, no PCAs were dissolved in these alcohols. Alternatively, the PCAs showed variant solubility dependent on the polymerization conditions. Namely, PCA1 and PCA2 showed similar solubility to chloroform and *N*,*N*-dimethylacetamide (DMAc) but showed different solubility to acetone. The PCAs polymerized at 200 °C were insoluble to the solvents investigated, except for PCA3 that only partially dissolved in DMAc. The following analyses were performed on the basis of these results.

Figure 4 shows ^{1}H NMR spectra and structural assignments of ACA, PCA1 and PCA2. Signals at 2.28, 6.53, 7.30, 7.63, and 7.65 ppm in ACA and PCA1 were assigned to methyl and caffeoyl protons in 3,4-diacetoxycaffeic acid. Apart from these signals, downfield signals of caffeoyl protons were observed at 6.93, 7.40, 7.84 and 7.88 ppm in all the spectra. These broadened signals are assigned to polymerized portion of CA. These results suggests that, while ACA and PCA1 are mainly composed of 3,4-diacetoxycaffeic acid (DCA) containing small amount of oligomeric CA, PCA2 is mainly composed of the polymerized CA.

In Green Polymer Chemistry: Biocatalysis and Materials II; Cheng, H., et al.;
ACS Symposium Series; American Chemical Society: Washington, DC, 2013.

Publication Date (Web): November 22, 2013 | doi: 10.1021/bk-2013-1144.ch017

Table 1. Solubility of CA and PCAs

	Methanol	*Ethanol*	*Acetone*	*Chloroform*	*DMAc*	*DMSO*
CA	○ [a]	○	○	× [b]	○	○
PCA1	×	×	○	○	○	○
PCA2	×	×	△ [c]	○	○	○
PCA3	×	×	×	×	※ [d]	– [e]
PCA4	×	×	×	×	×	– [e]
PCA5	×	×	×	×	×	– [e]

[a] Soluble. [b] Insoluble. [c] Swelling. [d] Partially soluble. [e] Not investigated.

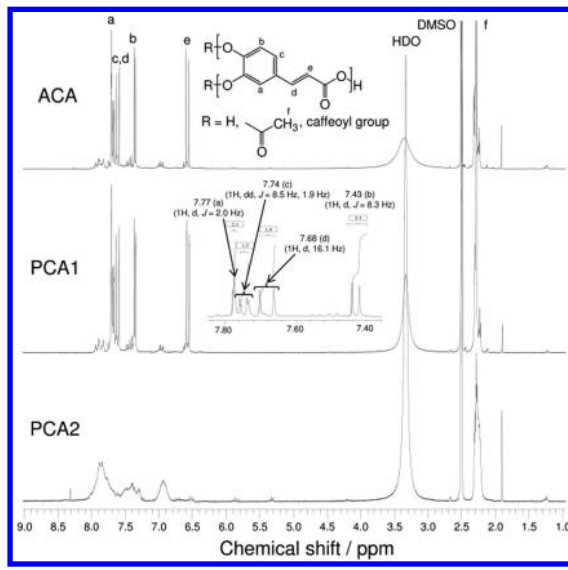

Figure 4. [1]H NMR spectra of ACA, PCA1 and PCA2 in DMSO-d_6.

The composition and molecular weight distribution of ACA, PCA1, and PCA2 were further analyzed by GPC. Figure 5(a) shows elution profiles of the three samples. ACA and PCA1 showed almost identical elution behavior, in which small amount of polymerized CA eluted first and DCA eluted later. The delayed elution of DCA is possibly caused by the strong interaction between DCA and column bed composed of crosslinked polystyrene gel. Molecular weight distribution (MWD) of these PCAs were estimated from the elution curves assigned to polymerized portion of CA, as shown in Figure 5(b). These profiles also indicate that ACA and PCA1 have almost the same MWD, while PCA2 has larger molecular weight than the two. The weight-averaged MW and polydispersity index of ACA, PCA1 and PCA2 are shown in Table 2.

In Green Polymer Chemistry: Biocatalysis and Materials II; Cheng, H., et al.;
ACS Symposium Series; American Chemical Society: Washington, DC, 2013.

Publication Date (Web): November 22, 2013 | doi: 10.1021/bk-2013-1144.ch017

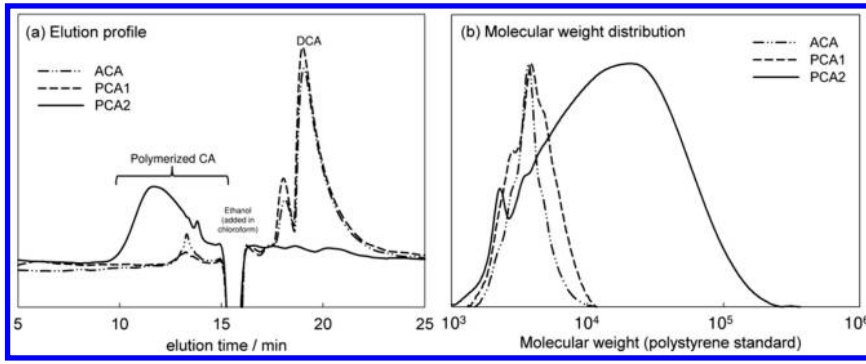

Figure 5. (a) GPC elution profiles and (b) molecular weight distribution profiles of ACA, PCA1, and PCA2.

Table 2. Weight-averaged molecular weight, M_w, and polydispersity index, PDI, of ACA, PCA1, and PCA2

	Mw $\times 10^3$	*PDI*
ACA [a]	3.8	1.1
PCA1 [a]	4.2	1.2
PCA2	25	2.9

[a] Estimated for polymerized portions of each samples.

The molecular structure of polymerized portion of ACA and PCA1 was further investigated by MALDI-TOF-MS, as shown in Figure 6. Arrays of ionization peaks were observed from m/z = 287 and 449 in PCA1 and 491 and 653 in ACA, with the regular period of 204.

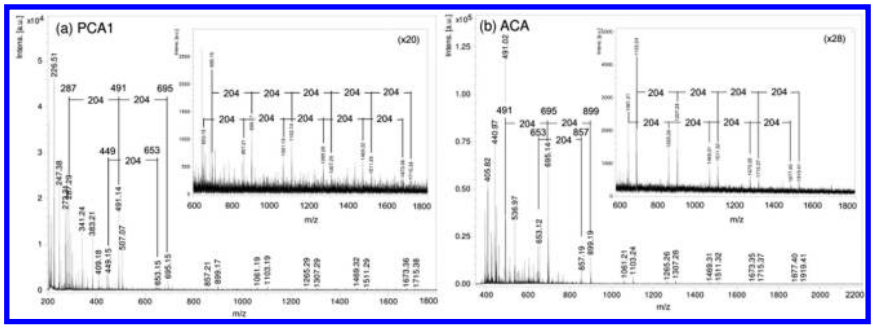

Figure 6. MALDI-TOF-MS spectra of (a)PCA1 and (b) ACA.

In Green Polymer Chemistry: Biocatalysis and Materials II; Cheng, H., et al.;
ACS Symposium Series; American Chemical Society: Washington, DC, 2013.

As shown in Figure 7, m/z = 287 and 449 corresponds to the sodium ion-added DCA and monohydroxy DCA dimer, respectively. The value of periodic peak distance corresponds the sum of the mass numbers of CA monomeric unit (m/z = 161) and acetyl group (m/z = 43). Therefore, the appearance of these periodic peaks suggests that the linear sequence of CA units is contained in the backbone of polymerized portions in ACA and PCA1. These linear CA oligomers may be formed by endwise ester exchange reaction of DCA.

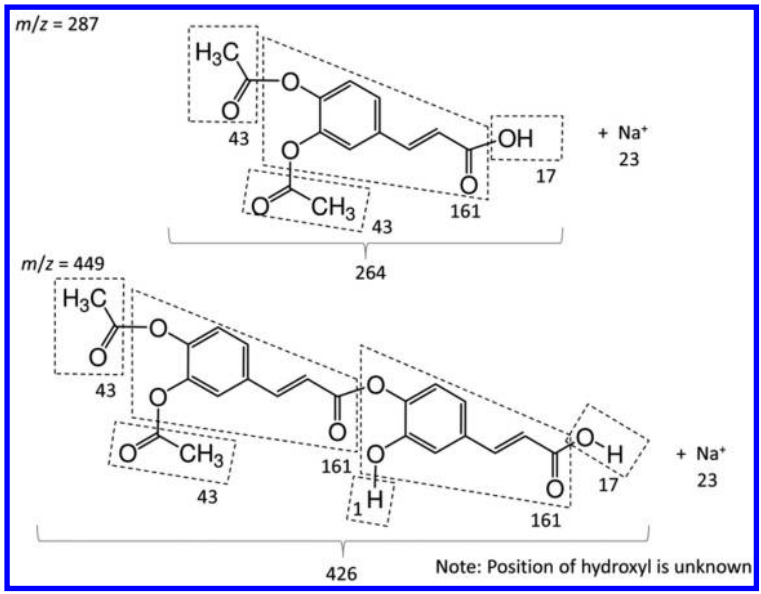

Figure 7. Molecular structure of sodium ion-added DCA (m/z = 287) and monohydroxy DCA dimer (m/z = 449).

Publication Date (Web): November 22, 2013 | doi: 10.1021/bk-2013-1144.ch017

Thermal and Mechanical Properties of PCA

Thermal properties of PCAs significantly depended on the polycondensation conditions. Firstly, thermal fusibility of PCAs was investigated by optical microscopy. Figure 8 shows the optical micrographs of PCAs at 25 °C and the elevated temperatures (135 °C for PCA1 and 250 °C for the other samples). While PCA1 and PCA2 showed melting transition at the elevated temperatures, PCA3, PCA4, and PCA5 did not show melting transition even when heated up to 250 °C.

Publication Date (Web): November 22, 2013 | doi: 10.1021/bk-2013-1144.ch017

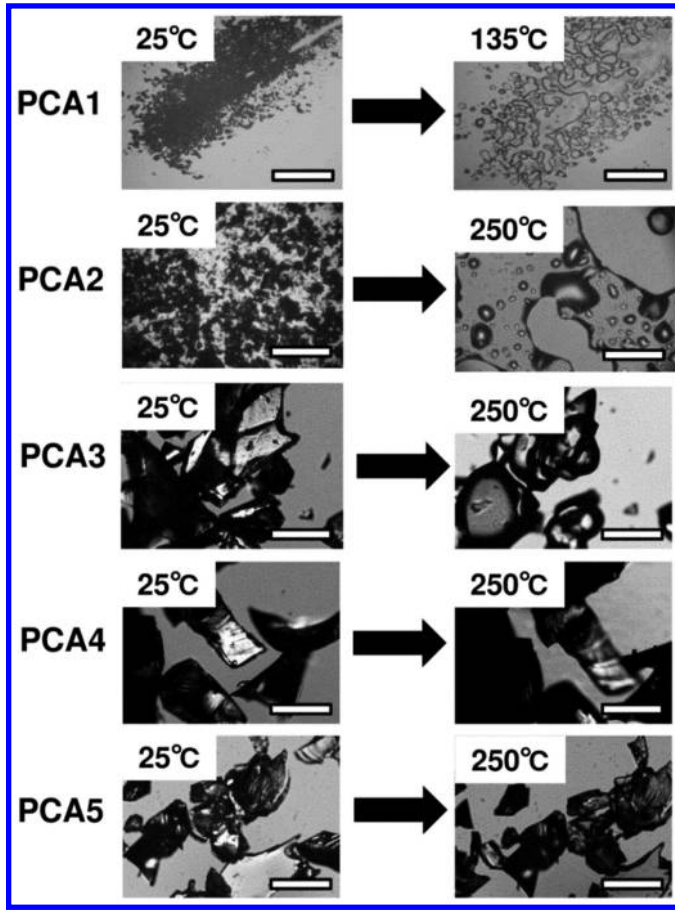

Figure 8. Optical micrographs of PCAs at 25, 135 (PCA1), and 250 °C.

The difference in fusibility is well correlated to the solubility as mentioned in the former section. Namely, PCA1 with the relatively low molecular weight and the high solubility in various solvents showed melting transition at relatively low temperature. In contrast to PCA1, PCA2 showed complex thermal behavior. Figure 9(a) shows DSC thermogram and polarized optical micrographs at different temperatures of PCA2. PCA2 showed glass transition at 62 °C and melting transition at 164 °C. Furthermore, PCA2 formed liquid crystalline mesophase at 172 °C under shear. Formation of mesophase was also observed under shear at the rubbery state above 200 °C (data not shown). This shows that the highly condensed PCAs act as thermotropic liquid crystalline polymer responsive to external field. The shear-induced mesophase formation of polycondensed PCAs makes marked contrast to other cinnamic acid detivative polyesters that spontaneously form mesophase at the elevated temperatures. The three PCAs

In Green Polymer Chemistry: Biocatalysis and Materials II; Cheng, H., et al.;
ACS Symposium Series; American Chemical Society: Washington, DC, 2013.

polycondensed at 200 °C with the poor or no solubility showed infusibility. The insolubility and infusibility imply that the permanent crosslinks in the molecular backbones are formed in these PCAs. However, as seen in DSC thermograms shown in Figure 9(b), these infusible PCAs shows glass transition and thus thermoplasticity.

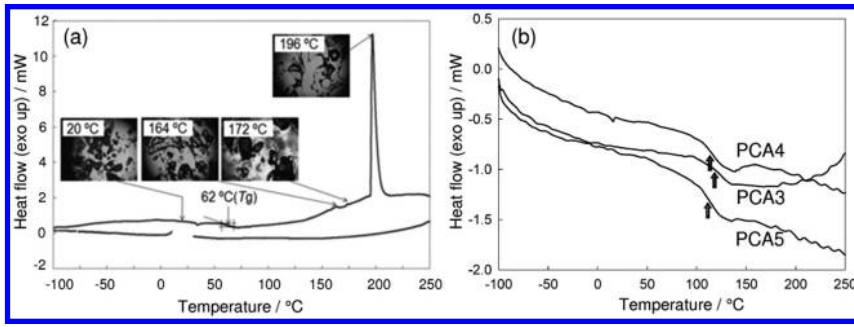

Figure 9. (a) DSC thermograms of PCA2 taken at first heating and cooling runs. Inset: polarized optical micrographs of PCA2 at 20 °C (glassy solid), 164 °C (melt), 172 °C (liquid crystalline mesophase formed under shear) and 196 °C (isotropic melt). Exothermic peak observed at 196 °C originates from the polycondensation reaction of residual functional groups (phenolic hydroxyl or acetyl and carboxyl groups) and vanishes in second heating. (b) DSC thermograms of PCA3, PCA4, and PCA5. Arrows indicate the glass transition points.

PCAs were processed into solid film by hot-press above their glass transition temperatures. The films were colored in reddish brown but showed moderate translucency, as shown in Figure 10(a). However, the films of PCAs polycondensed at relatively low temperatures, such as 160 °C, were too brittle to investigate the mechanical properties. On the other hand, the film of PCA5 hot-pressed at 250 °C showed sufficient mechanical strength that endures rubbing by sandpaper. Dynamic mechanical analysis was performed for the hot-pressed PCA5 film. PCA5 film retained the dynamic storage modulus above 10^6 Pa even at 300 °C. Furthermore, the sample almost retained its original shape, as shown in Figure 10(b). This indicates the high thermal durability of PCA5 possibly resulting from the chemical crosslinking.

The thermal durability of PCAs was semi-quantitatively evaluated by TG/DTA. For each PCAs, 5 % weight decrease temperature, $T_{5\%d}$, was estimated from TG chart shown in Figure 11. Similarly to the solubility and fusibility, $T_{5\%d}$ was correlated with the polycondensation conditions. Namely, PCA2 with the superior solubility and fusibility showed the lowest $T_{5\%d}$ of 232 °C. On the other hand, PCA4 and PCA5, that are infusible and insoluble, showed the highest $T_{5\%d}$ of 344 °C. All these results indicate that the properties of PCA are affected by the molecular mobility of main chain, as determined by the polycondensation conditions.

In Green Polymer Chemistry: Biocatalysis and Materials II; Cheng, H., et al.;
ACS Symposium Series; American Chemical Society: Washington, DC, 2013.

Publication Date (Web): November 22, 2013 | doi: 10.1021/bk-2013-1144.ch017

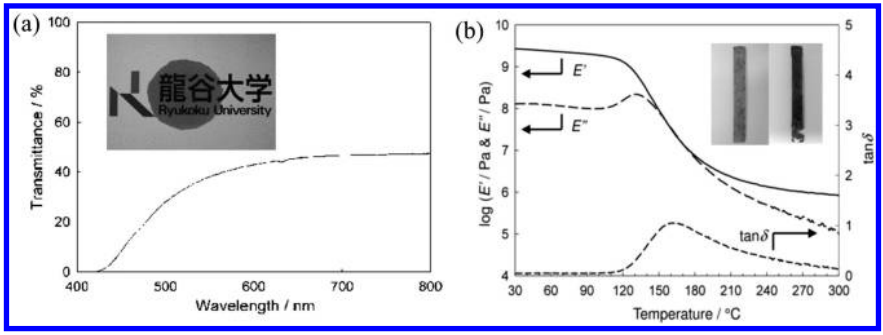

Figure 10. (a) Optical transmittance spectrum and appearance (inset) of hot-pressed film of PCA polycondensed at 160 °C for 22 h after acetylated at 160 °C for 18 h. The hot-press was performed at 140 °C. (b) Temperature dependence of dynamic storage, E′, and loss, E″, moduli and loss tangent, tanδ, of PCA5. Inset: PCA5 film before (left) and after (right) the dynamic mechanical analysis measurement. Sample size is 5 mm×40 mm.

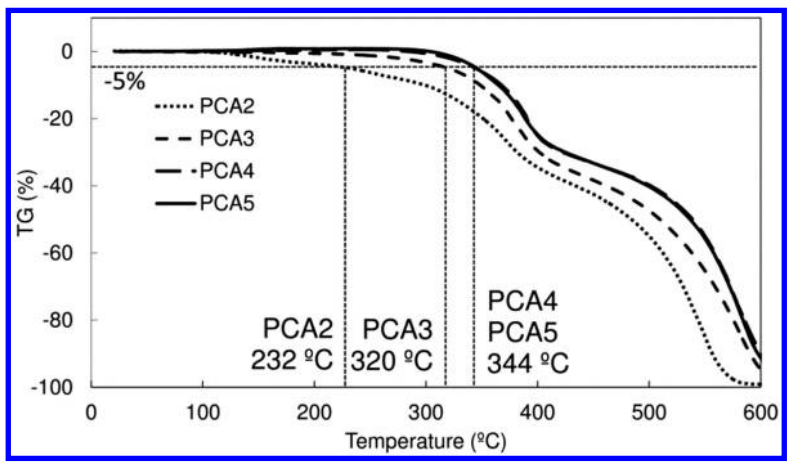

Figure 11. TG curves of PCA2, PCA3, PCA4, and PCA5.

Conclusions

PCA, a homopolyester of CA, was prepared by polycondensation via acetylation of CA followed by transesterification. The product of acetylation reaction was mainly diacetoxycaffeic acid (DCA), containing small amount of linearly polymerized DCA. Transesterification of the acetylated product yielded a thermoplastic PCA showing variant thermal behaviors depending on the reaction conditions. In particular, PCA2 retaining solubility and fusibility formed liquid crystalline mesophase under shear at the elevated temperatures. This suggests the thermotropic liquid crystalline nature of PCA. Thermally processed PCA5

showed dynamic viscoelastic behavior as a glassy polymer retaining its original shape even after heated up to 300 °C. Furthermore, PCA5 was thermally stable that showed 5% weight decrease at 344 °C. These results offer the potential of PCA as biomass-derived novel engineering plastics.

Acknowledgments

The present study was supported by Grant-in-Aid for Young Scientists (B) from Japan Society for the Promotion of Science (JSPS) (No. 22710084), Analysis and Development System for Advanced Materials (ADAM) from RISH, Kyoto University, and Innovative Materials and Processing Research Center, Ryukoku University.

Publication Date (Web): November 22, 2013 | doi: 10.1021/bk-2013-1144.ch017

References

1. Doi, Y. *Microbial Polyesters*; VCH Publishers: New York, 1990.
2. Ikada, Y.; Tsuji, H. *Macromol. Rapid Commun.* **2000**, *21*, 117–132.
3. Aoyagi, Y.; Doi, Y.; Iwata, T. *Polym. Degrad. Stab.* **2003**, *79*, 209–216.
4. Iwata, T.; Tsunoda, K.; Aoyagi, Y.; Kusaka, S.; Yonezawa, N.; Doi, Y. *Polym. Degrad. Stab.* **2003**, *79*, 217–224.
5. Iwata, T.; Aoyagi, Y.; Fujita, M.; Yamane, H.; Doi, Y.; Suzuki, Y.; Takeuchi, A.; Uesugi, K. *Macromol. Rapid Commun.* **2004**, *25*, 1100–1104.
6. Iwata, T. *Macromol. Biosci.* **2005**, *5*, 689–701.
7. Tanaka, T.; Fujita, M.; Takeuchi, A.; Suzuki, Y.; Uesugi, K.; Ito, K.; Fujisawa, T.; Doi, Y.; Iwata, T. *Macromolecules* **2006**, *39*, 2940–2946.
8. Tsuji, H.; Ikada, Y.; Hyon, S. H.; Kimura, Y.; Kitao, T. *J. Appl. Polym. Sci.* **1994**, *51*, 337–344.
9. Takasaki, M.; Ito, H.; Kikutani, T. *J. Macromol. Sci., Part B: Phys.* **2003**, *B42*, 57–73.
10. Furuhashi, Y.; Kimura, Y.; Yoshie, N.; Yamane, H. *Polymer* **2006**, *47*, 5965–5972.
11. Shirakura, Y.; Fukui, T.; Saito, T.; Okamoto, Y.; Narikawa, T.; Koide, K.; Tomita, K.; Takemasa, T.; Masamune, S. *Biochim. Biophys. Acta* **1986**, *880*, 46–53.
12. Iwata, T.; Aoyagi, Y.; Tanaka, T.; Fujita, M.; Takeuchi, A.; Suzuki, Y.; Uesugi, K. *Macromolecules* **2006**, *39*, 5789–5795.
13. Tsuji, H.; Miyauchi, S. *Biomacromolecules* **2001**, *2*, 597–604.
14. Hasirci, V.; Lewandrowski, K.; Gresser, J. D.; Wise, D. L.; Trantolo, D. J. *J. Biotechnol.* **2001**, *86*, 135–150.
15. Williams, S. F.; Martin, D. P. In *Biopolymers, Volume 4: Polyesters III - Applications and Commercial Products*; Doi, Y., Steinbüchel, A., Eds.; Wiley-VCH: Weinheim, Germany, 2002; pp 91−128.
16. Kasuya, K.; Mitomo, H.; Nakahara, M.; Akiba, A.; Kudo, T.; Doi, Y. *Biomacromolecules* **2000**, *1*, 194–201.
17. Ikada, Y.; Jamshidi, K.; Tsuji, H.; Hyon, S. H. *Macromolecules* **1987**, *20*, 904–906.

18. Tsuji, H. *Macromol. Biosci.* **2005**, *5*, 569–597.
19. Sakakibara, A.; Sano, Y. In *Wood and Cellulose Chemistry*; Hon, D. N. S, Shiraishi, N., Eds.; Mercel Dekker: New York, 2001; Chapter 4, pp 109−174.
20. Billa, E.; Koukios, E. G.; Monties, B. *Polym. Degrad. Stab.* **1998**, *59*, 71–75.
21. Sun, R. C.; Tomkinson, J.; Bolton, J. *Polym. Degrad. Stab.* **1999**, *63*, 195–200.
22. Sun, R. C.; Tomkinson, J.; Lloyd Jones, G. *Polym. Degrad. Stab.* **2000**, *68*, 111–119.
23. Sun, R. C.; Tomkinson, J.; Wang, S. Q.; Zhu, W. *Polym. Degrad. Stab.* **2000**, *67*, 101–109.
24. Xiao, B.; Sun, X. F.; Sun, R. C. *Polym. Degrad. Stab.* **2001**, *74*, 307–319.
25. Sun, R. C.; Lu, Q.; Sun, X. F. *Polym. Degrad. Stab.* **2001**, *72*, 229–238.
26. El Hage, R.; Brosse, N.; Chrusciel, L.; Sanchez, C.; Sannigrahi, P.; Ragauskas, A. *Polym. Degrad. Stab.* **2009**, *94*, 1632–1638.
27. Watanabe, T.; Mitani, T. In *The Role of Green Chemistry in Biomass Processing and Conversion*; Xie, H., Gathergood, N., Eds.; John Wiley & Sons, Inc.: New York, 2012; pp 281−291.
28. Du, J.; Fang, Y.; Zheng, Y. *Polym. Degrad. Stab.* **2008**, *93*, 838–845.
29. Fang, Y.; Zheng, Y.; Hu, F. *Polym. Degrad. Stab.* **2012**, *97*, 185–191.
30. Tran, H. T.; Matsusaki, M.; Shi, D. J.; Kaneko, T.; Akashi, M. *J. Biomater. Sci. Polym. Ed.* **2008**, *19*, 75–85.
31. Kaneko, T.; Kaneko, D.; Wang, S. *Plant Biotechnol.* **2010**, *27*, 243–250.
32. Thi, T. H.; Matsusaki, M.; Hirano, H.; Kawano, H.; Agari, Y.; Akashi, M. *J. Polym. Sci., Part A: Polym. Chem.* **2011**, *49*, 3152.
33. Xu, S.; Uyama, H.; Whitten, J. E.; Kobayashi, S.; Kaplan, D. L. *J. Am. Chem. Soc.* **2005**, *127*, 11745.
34. Matsushita, K.; Adachi, O. Patent Abst. Japan JPA2009-201473, 2009.
35. Tsukada, S.; Ikeda, K.; Yoshimoto, M.; Kurata, R.; Fujii, M.; Ko, N. Patent Abst. Japan JPA2009-100760, 2009.

Publication Date (Web): November 22, 2013 | doi: 10.1021/bk-2013-1144.ch017

Publication Date (Web): November 22, 2013 | doi: 10.1021/bk-2013-1144.ch018

Chapter 18

Biodegradable Films and Foam of Poly(3-Hydroxybutyrate-*co*-3-hydroxyvalerate) Blended with Silk Fibroin

Amy Tsui,[1] Xiao Hu,[2] David L. Kaplan,[3] and Curtis W. Frank*,[1]

[1]Department of Chemical Engineering, Stanford University, Stanford, California 94305-5025
[2]Department of Physics & Astronomy and Department of Biomedical Engineering and Sciences, Rowan University, Glassboro, New Jersey 08028
[3]Department of Biomedical Engineering, Tufts University, Medford, Massachusetts 02155
***E-mail: curt.frank@stanford.edu**

Solvent-cast films of poly(3-hydroxybutyrate-*co*-3-hydroxyvalerate) (PHBV) and silk fibroin (SF) blends were investigated to evaluate miscibility and mutual impacts on thermal properties and morphology to inform how SF may impact the cell microstructure of PHBV foam. It was determined through modulated differential scanning calorimetry (MDSC) and thermal gravimetric analysis (TGA) that the blends were immiscible at all compositions studied. Using attenuated total reflectance Fourier transform infrared spectroscopy (ATR-FTIR), we found that SF morphology changed from amorphous to 38.2-47.6% crystallinity in the presence of PHBV. Additionally, we observed that SF acts as a crystal nucleating agent for PHBV, but subsequently is excluded to the interspherulitc regions during PHBV crystal growth. After melting and fast cooling in the DSC, we found that SF reduces melting temperature and crystallinity of PHBV films, except for 1 and 40 wt% SF, which exhibited anomalous behavior. It is likely that SF nucleates new PHBV crystals, but in regions of higher SF content. The immobile SF causes

In Green Polymer Chemistry: Biocatalysis and Materials II; Cheng, H., et al.;
ACS Symposium Series; American Chemical Society: Washington, DC, 2013.

more disorder of PHBV crystals near the nuclei resulting in overall lower crystallinity. To produce SF powder for foam extrusion, three 1-day freeze-thaw cycles reproducibly yielded SF aerogels from tough hydrogels after drying in a vacuum oven. These aerogels were ground and added to PHBV and foamed with 0.5, 1, 2, 3, and 4 phr azodicarbonamide (AZ) for 1 wt% SF and 4 phr AZ for 5 wt% SF. Surprisingly, SF actually led to poorer cell density above 0.5 phr AZ, especially for 5 wt% SF due to cell coalescence and greater foam shrinkage during cooling.

Publication Date (Web): November 22, 2013 | doi: 10.1021/bk-2013-1144.ch018

Introduction

Over recent decades, there has been a resurgence of effort to develop more sustainable plastics to address environmental and political concerns over the use of fossil fuels and accumulation of alarming levels of plastic in the environment. A particularly attractive option is using a family of biorenewable polyesters called polyhydroxyalkanoates (PHAs). PHAs occur naturally in bacteria, serving as energy storage for times of nutrient limitation. This non-toxic, biodegradable polymer has properties similar to polypropylene (*1*), a ubiquitous plastic found in bottle caps, diapers, containers, and other products. Furthermore, because PHAs are readily found in the environment, anaerobic pathways already exist for their biodegradation. In contrast, poly(lactic acid) (PLA), a synthetic biodegradable polymer that is one of the most commercially prevalent biopolymers, only degrades in industrial composting facilities, not in landfill or marine environments.

Though PHAs are ideal for addressing needs for both renewable feedstocks and biodegradability at end-of-life, they are prone to brittleness and aging effects, and are relatively expensive (*2*, *3*). Additionally, their susceptibility to environmental degradation creates drawbacks during processing. They begin to thermally degrade at or above their melting temperature, reducing their already poor melt strength. This is particularly challenging for foam applications where high melt strength and elongational viscosity are important for stabilizing cell growth and achieving uniform, high density cell microstructure and low foam density. Poly(3-hydroxybutyrate-co-3-hydroxyvalerate) (PHBV) is one of the most commonly used PHAs because it has a lower melting temperature than poly(3-hydroxybutyrate) (PHB) and because it is more commercially available than other PHA copolymers. The ability to foam PHA can reduce costs by lowering the amount of polymer required and expand PHA application to packaging (e.g., foam packing), construction (e.g., insulation), and consumer products (e.g., serving ware). Development of PHBV foams for these areas of application has been studied (*4*, *5*).

Blending is a common strategy for imparting complementary beneficial properties on polymers in general and on PHAs in particular (*4*–*7*). Previously, we have shown that blending PHBV with cellulose acetate butyrate, a higher viscosity biodegradable polymer, can result in improved cell uniformity and

In Green Polymer Chemistry: Biocatalysis and Materials II; Cheng, H., et al.;
ACS Symposium Series; American Chemical Society: Washington, DC, 2013.

lower bulk density at high gas content; however, achievable bulk density was not significantly reduced (*4*). Cellulose acetate butyrate has been shown to be miscible or partially miscible with PHBV depending on the composition (*8*). Other blends that have been investigated include PLA/PHBV (*7*) and PHBV/hyperbranched polymer (*5*). Miscibility of blend components determines the final properties of the blend since the degree of compatibility will impact the domain size and morphology of the two phases. Because of intermolecular interaction, blend components can also impact the morphology and thermal properties of the other phase, such as by reducing or eliminating crystallinity and melting temperature (*8*), even in immiscible blends (*9*). For example, Thirtha et al. (*10*, *11*) documented changes in T_g for immiscible blends, noting that T_g should not change except in cases where there is a difference in thermal expansion coefficients of the components, in which case T_g would increase due to increased pressure at the interface. Reductions in T_g have been observed for non-adhering nanoparticle-filled systems due to the high amount of surface area introduced by the nanoparticles (*12*). The presence of non-bonded interfaces can increase mobility of chains at the interface and reduce the T_g (*10*).

A relatively unexplored potential additive for PHBV is silk fibroin (SF), which is the core protein in silk fibers that form silkworm cocoons. Two strands of SF are linked by the glue-like protein sericin, which is further surrounded by a protective protein layer. SF is known for its excellent mechanical properties, including an enhanced elongation-at-break over PHBV (*13*), and biocompatibility (*14*, *15*), which makes it an attractive candidate for improving the processability of PHBV. The unique mechanical properties originate from the random sequence of amorphous and crystalline regions, which are hydrophilic and hydrophobic, respectively, based on the amino acids that comprise those regions. The crystalline regions form β-sheet structures, also referred to as silk II, through hydrogen-bonding and van der Waals interactions (*16*, *17*). A metastable SF crystalline formation is an α-helix crystal structure, known as silk I (*18*). Though Sashina et al. (*19*) determined that SF is immiscible with PHB in films, they also hypothesized that there was some interaction below 20 wt% SF, though they did not probe this composition range. It was also demonstrated that SF could firmly coat a PHA scaffold or film via hydrogen bonding or surface modification (*14*, *20*). Though PHBV has a similar crystal structure as PHB (*21*), it has been shown that the chains are more flexible and have a lower crystallization ability than PHB (*22*). It would, therefore, be valuable to investigate the miscibility of PHBV and SF, especially at low concentrations of SF. If SF and PHBV were miscible, SF could potentially enhance the melt strength or subsequent solid mechanical properties. If they are immiscible, the SF phase could serve to nucleate crystal growth, resulting in earlier solidification of foams or to nucleate bubbles to produce higher cell density and more uniform microstructure. Significantly, SF powder has been shown to improve the microstructure of PLA foams with 7 wt% SF by significantly increasing cell density and reducing cell size using a batch foaming process and CO_2 blowing agent (*23*). Here, we investigate the miscibility of PHBV and SF in films and determine the impact of SF on PHBV foam microstructure to develop a low density, rigid biodegradable foam.

Publication Date (Web): November 22, 2013 | doi: 10.1021/bk-2013-1144.ch018

In Green Polymer Chemistry: Biocatalysis and Materials II; Cheng, H., et al.;
ACS Symposium Series; American Chemical Society: Washington, DC, 2013.

Publication Date (Web): November 22, 2013 | doi: 10.1021/bk-2013-1144.ch018

Experimental Materials and Methods

Silk Fibroin Aqueous Solutions

Bombyx mori silk fibroin (SF) aqueous solutions were prepared from silkworm cocoons (Tajima Shoji Co., LTD, Yokohama, Japan), as published previously (*24*, *25*), for film casting and shown in Figure 1. The cocoons were boiled for 30 minutes in 0.02 M sodium carbonate (Alfa Aesar) aqueous solution, then rinsed for 60 minutes in water to remove sericin proteins. The extracted silk was dried overnight, then placed in 9.3 M lithium bromide (Alfa Aesar) aqueous solution for 4-6 hours until all fibers were dissolved, yielding a 20 w/v% solution. This solution was dialyzed in water for three days using Slide-a-Lyzer dialysis cassettes (Pierce, 3500 MWCO) to remove the salt. The SF solution was removed and centrifuged at 13,000 rpm and 10°C for 40 min until impurities and insoluble SF were pelletized. The final concentration of the aqueous SF solution was ~7 wt% as determined by weighing the solution before and after drying. MilliQ water was used throughout the extraction process.

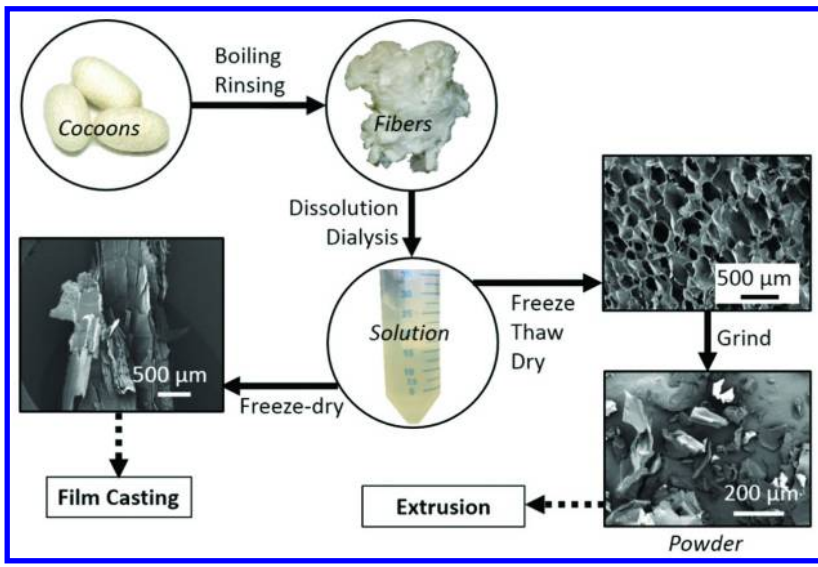

Figure 1. Silk fibroin extraction process to yield material for film casting and extrusion foaming.

Silk Gelation and Powder Preparation

Aqueous SF solutions were frozen at -15 °C, then thawed at 4 °C for a range of freeze-thaw cycles and time periods to form a hydrogel. The minimum total time for a single freeze-thaw cycle to form a gel was determined systematically using 1 mL aqueous SF solutions. When solutions had gelled, the color was white and there was no flow upon inversion. Multiple freeze-thaw cycles were applied to 10 mL samples to reduce overall time for gel formation and improve the toughness of the gels. 10 vol% methanol was also added to some SF solutions

In Green Polymer Chemistry: Biocatalysis and Materials II; Cheng, H., et al.;
ACS Symposium Series; American Chemical Society: Washington, DC, 2013.

to induce gelation earlier; these gels were translucent after gelation. However, the resulting gels were easily broken and yielded an extremely friable and yellowed dried structure. Therefore, methanol was not effective in forming SF powder in this process, so is not discussed further. After cycles where gel formation was observed, small samples were removed for drying to determine when the bulk could dry into grindable material. The tough gels were dried in a vacuum oven at 70°C for at least 24 hours. Dried gels that formed a low density solid were ground with mortar and pestle or a coffee bean grinder for a few seconds to a powder of heterogeneous diameter and shape, as shown in Figure 1. Large particles were removed using a sieve with 1 mm mesh size before extrusion.

Publication Date (Web): November 22, 2013 | doi: 10.1021/bk-2013-1144.ch018

PHBV/SF Film Preparation

Poly(3-hydroxybutyrate-co-3-hydroxyvalerate) (PHBV) with 5 mol% hydroxyvalerate content (trade name ENMAT Y1000) was obtained from Tianan Biologic Materials Company, Ningbo, China and appears as a white powder. The batch of PHBV used for films has a weight-average molecular weight (M_w) of 374k and polydispersity of 4.58, as determined from gel permeation chromatography (GPC). SF aqueous solutions were dried by first freezing the solution at -80 °C overnight, then lyophilizing in a Labconco FreeZone6L Freeze Dry System for 2-3 days until completely dried to achieve a relatively soft, solid material from which small flakes could be manually torn.

Hexafluoroisopropanol (HFIP, Sigma-Aldrich) was used as a common solvent for PHBV and SF. PHBV and SF were refluxed in HFIP for 24 hours at the following PHBV/SF compositions: 100/0 (PHBV), 99/1 (P99S1), 95/ 5 (P95S5), 90/10 (P90S10), 80/20 (P80S20), 60/40 (P60S40), 40/60 (P40S60) and 0/100 (SF). 90/10 PHBV/SF (P90S10) blend film was produced for observation of film morphology using SEM and for thermal transitions in DSC. The blended solution was poured into a shallow glass petri dish and covered loosely with aluminum foil for solvent casting. HFIP was allowed to evaporate from the solution for 24 hours in a fume hood, then further dried for 3 days in a vacuum desiccator to ensure complete removal of solvent.

Thermal Analysis of Films

Thermal transitions of PHBV/SF blended films were measured with a TA Instruments Q100 differential scanning calorimeter (DSC) at a nitrogen flow rate of 50 mL/min with temperature modulation. Small samples were encapsulated in aluminum pans and heated from -40 °C to 200 °C in the first heating cycle and from -45 °C to 300 °C in the second heating cycle with modulation of 0.32 °C every 60 seconds and at a rate of 2 °C/min throughout. Between heating cycles, samples were cooled quickly to -45 °C to retain maximum levels of amorphous regions in the films, thus accentuating T_g, which was taken to be the midpoint of the heat capacity change during this second heating cycle on the reversing heat flow curve. Other thermal transitions were taken from the total heat flow second heating cycle. The melting temperature, T_m, was measured from the endothermic peak and the crystallization temperature was taken as the peak temperature of the

In Green Polymer Chemistry: Biocatalysis and Materials II; Cheng, H., et al.;
ACS Symposium Series; American Chemical Society: Washington, DC, 2013.

exothermic peak. Decomposition endotherms of PHBV and SF were observed as separate peaks above 200 °C. However, the decomposition temperatures from DSC are not discussed due to potential mass loss causing possibility for error.

Instead, a TA Instruments Q500 thermal gravimetric analyzer (TGA) was used to accurately determine decomposition temperature. Small samples were heated from room temperature to 500 °C at 5 °C/min under a nitrogen atmosphere. The decomposition temperature at the maximum rate of degradation, $T_{d\,max}$, was taken as the peak of the differential TGA (DTGA) weight loss curves.

Film Morphology Characterization

Attenuated total reflectance Fourier transform infrared (ATR-FTIR) spectra of PHBV/SF blend films and SF materials were obtained using a Jasco 6200 FTIR spectrometer with ATR crystal accessory at 4 cm^{-1} resolution. The spectra for the blends were normalized to the 1340-1400 cm^{-1} region. The peaks were fitted using the multi-fit tool in the Origin 8 software (OriginLab, USA) applying a Lorentzian fitting. The number of peaks was determined in advance of fitting based on the observed and expected peaks in the spectrum.

Film morphology was observed with a scanning electron microscope (SEM, FEI XL30 Sirion with FEG source) after sputter-coating with Au60Pd40 alloy using a Gressington 108Auto sputter coater operated at 20 mA for 30 seconds. The average distance between spherulites, D_S, was measured using ImageJ image analysis software (available through the National Institutes of Health).

PHBV/SF Foam Processing

The pelletized form of PHBV with 5 mol% hydroxyvalerate content (trade name ENMAT Y1000P) (Tianan Biologic Materials Company, Ningbo, China) was blended with the powdered PHBV (ENMAT Y1000) for foam processing. ENMAT Y1000P had a M_w of 394K and polydispersity of 2.80, as determined from GPC. The batch of ENMAT Y1000 used for extrusion foaming had a M_w of 701K and polydispersity of 4.19, as determined from GPC. Powder and pellet PHBV were blended at a composition of 10/90 by weight in order to retain as much blowing agent as possible during material transfer to the extruder hopper.

The chemical blowing agent utilized in this study is activated azodicarbonamide (AZ) (trade name Actafoam 765A) from Chemtura. This blowing agent is a fine yellow powder that decomposes in the temperature range of 152 to 160 °C, generating approximately 180 cc of gas per gram of solid, most of which is nitrogen, according to the manufacturer.

PHBV was dried at 100 °C for at least 90 minutes before dry blending with 1 wt% SF powder and AZ. AZ content was 0, 0.5, 1, 2, 3, and 4 parts per hundred grams of polymer (phr). The dry blends were extruded through a 3/4 inch single-screw extruder (L/D ratio 25:1, compression ratio 3:1, C.W. Brabender) equipped with a 2-inch horizontal flex-lip ribbon die fixed at 1 mm thickness. The screw rotation speed was 80 rpm. The extruder temperature profile was set at 150 °C, 170 °C, 160 °C, and 150 °C, from the hopper to the die. The extruder was cleaned using Sample X purging compound kindly supplied by DynaPurge, NY.

Publication Date (Web): November 22, 2013 | doi: 10.1021/bk-2013-1144.ch018

Publication Date (Web): November 22, 2013 | doi: 10.1021/bk-2013-1144.ch018

Foam Characterization

Samples from foam produced after approximately four minutes of extrusion at a given composition were cryo-fractured to expose the cellular morphology along the direction of extrusion at the center point of the foam width. Samples were sputter-coated as described earlier for films, but for 90 seconds to completely coat the porous structure, then imaged using SEM. The outlines of each cell were manually drawn using a Bamboo Capture tablet (Wacom, USA) so that ImageJ software (NIH) could be used to analyze the cells to provide number of cells (N), sampling area (A), and cell area. For each foam composition, cells were counted within a sampling area of around 7 cm^2.

The cell density, n_b, was calculated as follows:

$$n_b = \left(\frac{N}{A}\right)^{3/2} m\, E$$

where m is the unit conversion to achieve cubic centimeter units. The exponent is for the conversion from an area to volume basis. The expansion ratio, E, is determined by:

$$E = \frac{\rho_u}{\rho_f}$$

Bulk density of foam samples, ρ_f, and unfoamed samples, ρ_u, is measured using the water displacement method.

Characterization of PHBV/SF Blend Films

Results

Glass Transition of PHBV/SF Blend Films

The total heat flow DSC thermograms from the second heating cycle are shown in Figure 2(a) and the thermal transitions observed in the second heating curves are summarized in Table I. In this study, a fast cooling cycle was utilized to kinetically trap the polymer chains in a more amorphous stage. As such, the T_g is only observable in the second DSC heating cycle after this fast cooling cycle and the reversing heat flow thermograms highlighting the PHBV T_g range are shown in Figure 2(b). T_gs of the PHBV/SF films were observed between -4.2—1.1 °C. T_g of SF was not observable in SF films along the entire thermogram, although it has been measured previously in references (*26*, *27*).

In Green Polymer Chemistry: Biocatalysis and Materials II; Cheng, H., et al.;
ACS Symposium Series; American Chemical Society: Washington, DC, 2013.

Publication Date (Web): November 22, 2013 | doi: 10.1021/bk-2013-1144.ch018

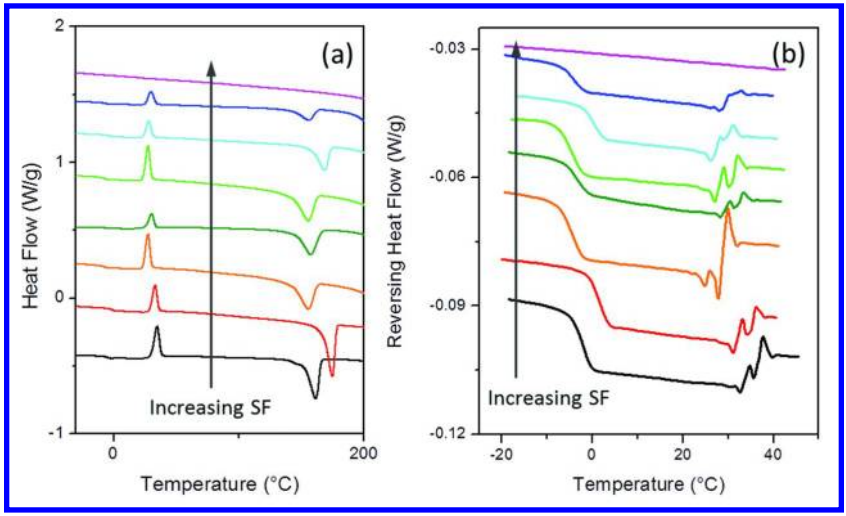

Figure 2. DSC thermograms from the second heating cycle of PHBV films with SF content ranging from 0 to 100 wt% showing the (a) total heat flow curve for the entire temperature range and (b) reversing heat flow curve of temperature range of the PHBV glass transition. From bottom: PHBV, P99S1, P95S5, P90S10, P80S20, P60S40, P40S60, and SF.

Complete miscibility of two polymers is typically expressed through the presence of a single thermal transition that is intermediate to those of the neat polymers. For example, T_g of a miscible blend may follow the Fox-Flory equation, which is given by:

$$\frac{1}{T_g} = \frac{w_1}{T_{g1}} + \frac{w_2}{T_{g2}}$$

where w_i and T_{gi} are the weight fraction and T_g, respectively, of each phase, *i*. In the case of the compositions studied here, T_g of a miscible SF-PHBV blend would be expected to range from -1.1 °C for P99S1 to 82.1°C for P40S60. Clearly, the blend T_gs do not follow these predicted T_g values, which indicates that SF and PHBV are immiscible at the compositions studied. Most of the blend compositions exhibit a lower T_g, which generally reflects a greater amount of free volume or disorder in the system such that the material requires less thermal energy to achieve the glass transition. For P99S1 and P60S40, the T_g is slightly greater than that of PHBV, particularly P99S1, whose T_g surpasses what would be predicted by Fox-Flory. The overall change is small, however, and may simply be within experimental error.

In Green Polymer Chemistry: Biocatalysis and Materials II; Cheng, H., et al.;
ACS Symposium Series; American Chemical Society: Washington, DC, 2013.

Table I. Thermal properties of PHBV/SF blends from the 2nd DSC heating cycle

Sample	T_g (°C)	T_m (°C)	T_c (°C)	ΔH_m (J/g)	χ_c (%)
PHBV	-2.2	161.3	30.2	84.4	57.8
P99S1	1.1	174.8	33.2	85.3	59.0
P95S5	-4.2	155.5	27.5	77.9	52.8
P90S10	-3.7	157.3	30.4	71.0	54.0
P80S20	-4.1	154.9	29.2	64.3	55.1
P60S40	0.1	168.6	28.1	50.7	57.9
P40S60	-4.1	155.9	29.9	29.8	51.0
SF	175-180[a]	NE[b]	NE	NE	NE

[a] Reference (*26*, *27*). [b] NE – Nonexistent.

Publication Date (Web): November 22, 2013 | doi: 10.1021/bk-2013-1144.ch018

Melting and Crystallization Properties of PHBV/SF Blend Films

In films containing PHBV, endotherms were present in the range of 130-185 °C corresponding to melting peaks of PHBV, as shown in Figure 2(a) and summarized in Table I. In general, melting temperature decreases with increasing SF content. Again, P99S1 and P60S40 samples appear anomalous.

From the melting endotherm, a relative degree of crystallinity, x_c, can also be calculated. The degree of crystallinity of the PHBV phase was determined by

$$x_c = \frac{(\Delta H_m)/n}{\Delta H^\circ_m} \times 100\%$$

where ΔH_m is the heat of enthalpy of melting and n is the weight fraction of PHBV. ΔH°_m is the heat of melting of 100% crystalline PHB and was taken to be 146 J/g (*28*). We do not subtract the heat of enthalpy of crystallization, and thus the crystallization upon heating is included in the final crystallinity. From this calculation, as shown in Table I, it is observed that the degree of crystallinity generally decreases with SF content in the second heating cycle.

The presence of a crystallization peak between 27.5 and 33.2 °C in the second heating cycle, as shown in Figure 2(a), is expected to be due to crystallization of amorphous PHBV after devitrification. The crystallization peak coincides with fluctuations and then increase in the baseline heat flow observed in Figure 2(b). Though reorganization is typically expressed in the non-reversing heat flow (*29*), the increase in the heat flow baseline suggests a more ordered structure. Additionally, the crystallization peak only appears in the second heating cycle, so it must be associated with the presence of a higher amorphous content after fast cooling.

In Green Polymer Chemistry: Biocatalysis and Materials II; Cheng, H., et al.;
ACS Symposium Series; American Chemical Society: Washington, DC, 2013.

The degradation temperatures were determined using TGA and DTGA, as shown in Figures 3(a) and 3(b), respectively, and summarized in Table II. The SF phase was too small to exhibit a decomposition curve for P99S1. The heating curves in Figures 3(a) and 3(b) both exhibit two distinct degradation behaviors corresponding to PHBV, then SF degradation. These two phases of degradation support the conclusion that PHBV and SF are immiscible. However, the PHBV and SF phases do affect the thermal properties of the other phase, suggesting that there is some degree of interaction.

Publication Date (Web): November 22, 2013 | doi: 10.1021/bk-2013-1144.ch018

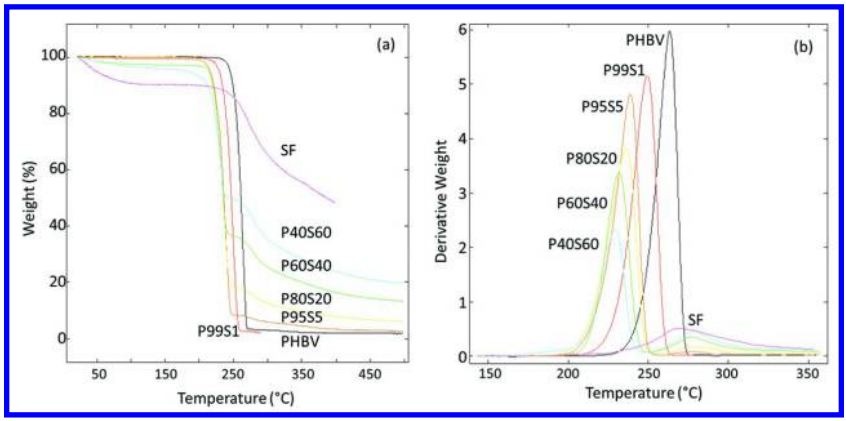

Figure 3. (a) TGA weight loss curves of SF and PHBV blends, and (b) DTGA weight loss curves of SF and PHBV blends.

Table II. Degradation temperatures determined from TGA

Sample	*PHBV $T_{d\ max\ DTGA}$ (°C)*	*SF $T_{d\ max\ DTGA}$ (°C)*
PHBV	263.38	--
P99S1	249.33	N.D.[a]
P95S5	238.72	277.55
P80S20	235.91	278.69
P60S40	231.59	276.96
P40S60	229.36	277.98
SF	--	268.48

[a] N.D. – not determined.

In Green Polymer Chemistry: Biocatalysis and Materials II; Cheng, H., et al.;
ACS Symposium Series; American Chemical Society: Washington, DC, 2013.

The initial plateau present in Figure 3(a) at higher silk contents is associated with loss of bound water (*19*), and shows a proportional increase in water content with SF content. It is also apparent from the DTGA curves in Figure 3(b) that the temperature at maximum degradation rate, $T_{d\ max}$, of the PHBV phase decreases monotonically with increasing SF content. Because PHBV is susceptible to hydrolysis (*30*), especially at elevated temperatures, the reduction in T_d of PHBV is likely due to the presence of bound water associated with the SF. Additionally, PHBV chain ends at the interface of the two polymer phases would be more mobile, which could allow for easier chain backbiting to form the six-membered ring intermediate in the PHBV thermal degradation mechanism (*31*). This could be potentially detrimental to the PHBV processability. In contrast, $T_{d\ max}$ of the silk phase increases almost 10 °C with presence of PHBV.

Publication Date (Web): November 22, 2013 | doi: 10.1021/bk-2013-1144.ch018

Morphology of SF/PHBV Blend Films

Figure 4 shows the SEM images of the different film compositions. With up to 10% SF, the interspherulitic boundaries remain distinct and even show some detachment between spherulites, which could result in brittleness. With increased SF content, the interspherulitc boundaries become less distinct and no detachment is observed. In the PHBV phases, the average distances between the PHBV nuclei, D_S, can be measured and are listed in Table III. With inclusion of silk, D_S more than doubles suggesting that there are fewer crystal nucleating sites, so crystals can grow much larger before impingement. Additionally, the standard deviation, σ, of D_S increases as well, reflecting a higher distribution of spherulite sizes. It is possible that SF is nonuniformly distributed in the film or that homogeneous nucleation occurs as well after additional cooling.

ATR-FTIR can provide more insights into the morphological changes occurring in both phases. FTIR has been applied widely to quantitatively study polymer crystallinity and crystallization (*32–34*). In SF, the absorbance spectrum is divided into the amide I (1700-1600 cm^{-1}), amide II (1600-1500 cm^{-1}), and amide III (1350-1200 cm^{-1}) regions (*35*). The amide I region is most often used to quantitatively evaluate secondary SF structure (*35*, *36*). Within this region, the C=O stretching vibration will shift from around 1646 to 1624 cm^{-1} corresponding to the amorphous and crystalline regions, respectively, with the formation of β-sheet crystals (*35*, *37*). The amide II region is mostly associated with C-N stretching and N-H in-plane bending vibrations where there is a shift from 1537-1545 to 1526 cm^{-1} corresponding to crystalline or amorphous phases, respectively (*35*, *37*). The region of C=O stretching vibration for amorphous and crystalline PHBV is around 1740 and 1720 cm^{-1}, respectively (*32*, *33*, *38*). Figure 5 shows the absorption spectra from 1800 to 1550 $cm^{-1}$of the blend compositions.

In Green Polymer Chemistry: Biocatalysis and Materials II; Cheng, H., et al.;
ACS Symposium Series; American Chemical Society: Washington, DC, 2013.

Publication Date (Web): November 22, 2013 | doi: 10.1021/bk-2013-1144.ch018

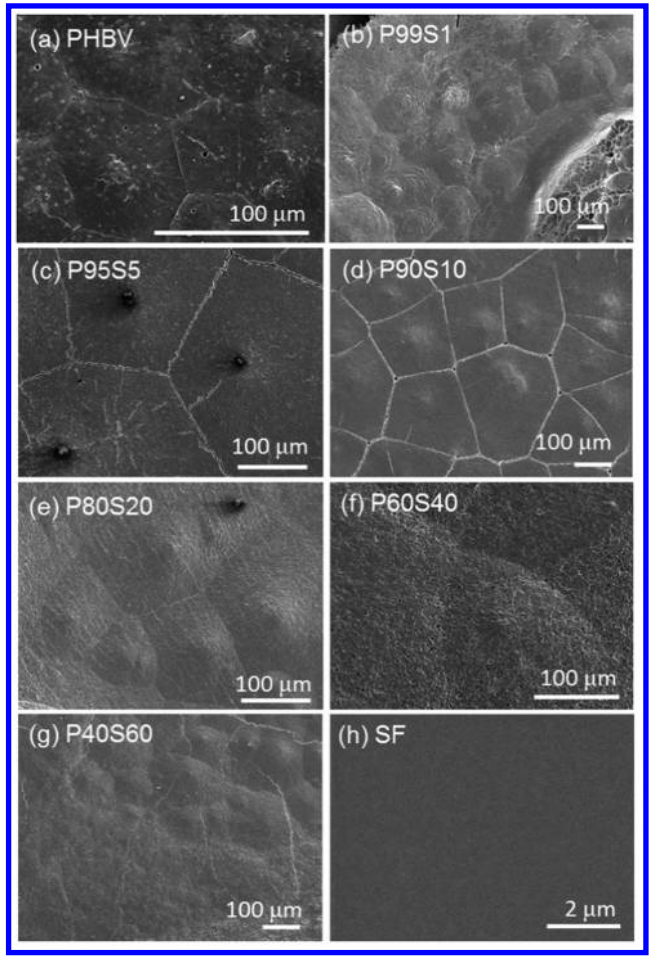

Figure 4. SEM images showing spherulitic formation in (a) PHBV, (b) P99S1, (c) P95S5, (d) P90S10, (e) P80S20, (f) P60S40, (g) P40S60, and (h) SF films.

Publication Date (Web): November 22, 2013 | doi: 10.1021/bk-2013-1144.ch018

Table III. Average distance between PHBV nuclei

Sample	*D_s (μm)*	*σ (μm)*
PHBV	60.9	13.9
P99S1	179.4	49.2
P95S5	252.6	80.2
P90S10	174.7	62.3
P80S20	156.4	64.2
P60S40	256.1	74.8
P40S60	130.7	38.7

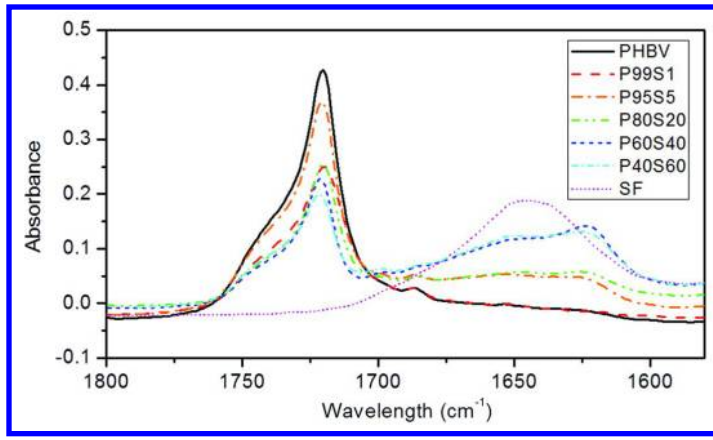

Figure 5. FTIR absorbance spectra of PHBV/SF blends from 1580-1800 cm-1.

There is a clear shift in the SF carbonyl-stretching region (1700-1600 cm^{-1}) from amorphous to increasing crystalline structure in SF. Any shift in the PHBV carbonyl-stretching region (1750-1700 cm^{-1}) is less obvious, but the crystallinity of SF and PHBV can be calculated from the FTIR data using the following equations:

$$\text{PHBV: } x = \frac{A_{1724}}{A_{1724}+A_{1740}} \times 100\%$$

$$\text{SF: } x = \frac{A_{1624}}{A_{1624}+A_{1646}} \times 100\%$$

where $A_{\text{wavenumber}}$ is the absorbance peak intensity, which is determined using a multi-peak fitting. To produce the best fitting, a broader region of wavenumbers was selected, from 1400-1800 cm^{-1}. This included the peak at 1515 cm^{-1} associated with vibrations in tyrosine in SF (*35*) and C=O and O-H interaction in PHBV crystals (1686-1690 cm^{-1}) (*33*) and CH2 scissoring in PHBV (1453 cm^{-1}) (*32*). Representative peak fittings are shown in Figures 6(a)-(c), and all had R-squared values above 99.6%.

In Green Polymer Chemistry: Biocatalysis and Materials II; Cheng, H., et al.;
ACS Symposium Series; American Chemical Society: Washington, DC, 2013.

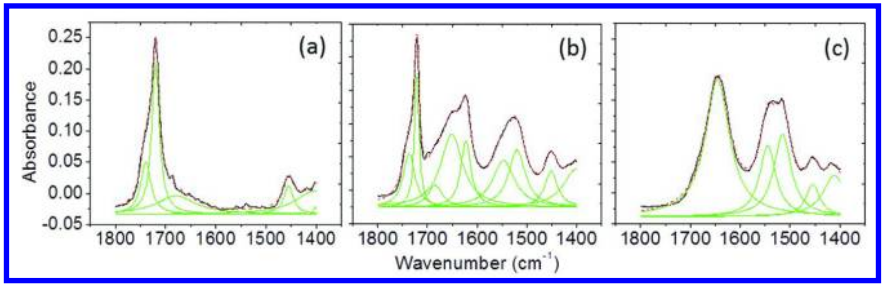

Figure 6. Representative FTIR absorbance spectra with deconvoluted peaks for (a) PHBV, (b) P60S40, and (c) SF. Black line is original data, dashed line is total fit, and lighter peaks are the deconvoluted peaks.

Figure 7 compares the crystallinities calculated from DSC and FTIR for PHBV and SF. SF appears to remain amorphous from 0-1 wt% SF, but it is likely that the crystalline portion in SF is difficult to detect in FTIR for P99S1. At 5 wt% SF, there is a marked jump to 38% crystallinity. PHBV crystallinity calculated from FTIR is higher than that calculated from the second heat cycle of DSC by 15.5 percentage points on average.

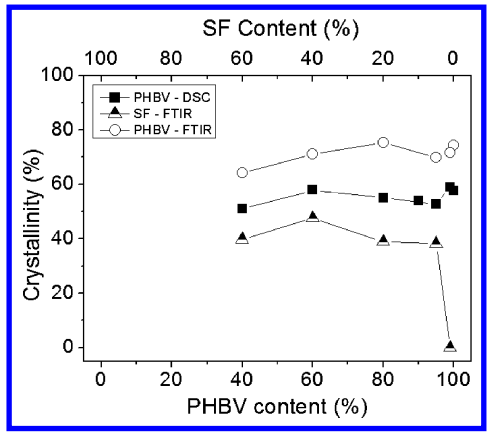

Figure 7. Crystallinity of PHBV and SF versus blend composition from DSC and FTIR.

The difference in crystallinity values determined by FTIR and DSC is primarily due to the pre-measurement processing. The crystallinity from DSC was taken after a fast cooling cycle that hinders crystallization. Thermal degradation of PHBV during slow heating in MDSC may also contribute to lower crystallinity as well as the fact that crystallinity from DSC is calculated with respect to a purely crystalline PHB rather than PHBV. From both FTIR and DSC, crystallinity appears to decrease at P95S5 by about 5% before returning to the maximum at P80S20 for FTIR or P60S40 for DSC. P40S60 has the lowest PHBV crystallinity in both cases.

Publication Date (Web): November 22, 2013 | doi: 10.1021/bk-2013-1144.ch018

Publication Date (Web): November 22, 2013 | doi: 10.1021/bk-2013-1144.ch018

Discussion

Structure and Property Development of PHBV/SF Due to Film Casting

In the case of neat PHBV, crystallization of the film can proceed without hindrance as solvent evaporates. As such, the film produced is highly crystalline (74.4% by FTIR) with more uniformly dispersed spherulites. Assuming no impurities, nucleation of the crystals is a homogeneous process where the nuclei are formed spontaneously when enough energy is introduced to the system, e.g., through solvent evaporation and cooling, as diagrammed in Figure 8(a).

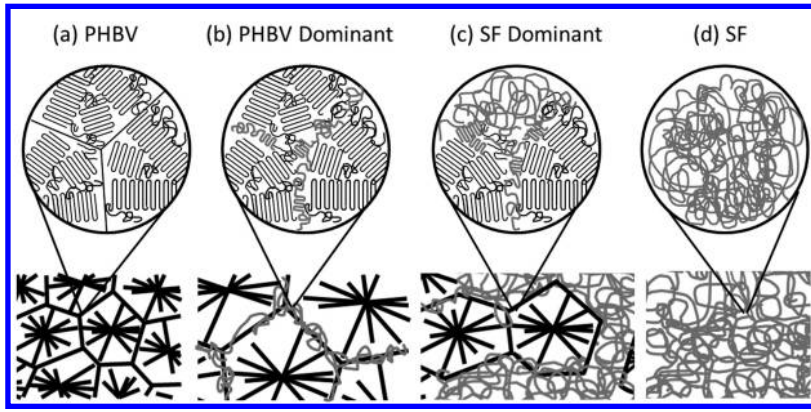

Figure 8. Proposed morphology of PHBV/SF films, where PHBV is black and SF is gray. (a) 100% PHBV is highly crystalline with distinct spherulites formed from homogeneous nucleation. (b) Up to 40 wt% SF, SF acts as a nucleating agent for PHBV and is also excluded to the interspherulitic regions where SF may form β-sheet crystals. (c) At 60% SF, SF continues to reduce PHBV crystallinity while the PHBV nucleates SF β-sheet crystals. (d) SF films are completely amorphous.

For SF and PHBV dissolved in solution, the two phases are initially mixed due to a common solvent. As the solvent evaporates, the SF must associate with itself or with PHBV. At the interfaces between SF and PHBV, there may be some interaction between hydrophobic PHBV and the hydrophobic regions of SF. This may promote some agglomeration and then crystallization of the SF hydrophobic regions, expressed in Figures 8(b)-8(c). During degradation, β-sheet crystals are known to be very resistant to thermal decomposition, and more resistant than amorphous SF (*36*, *37*, *39*, *40*). The shift of SF to becoming a semi-crystalline material, as shown using FTIR, is thus consistent with the shift of SF to higher degradation temperatures observed using TGA. As the SF crystallizes, it may also then simultaneously serve as a heterogeneous nucleating agent for PHBV crystals. Heterogeneous nucleation requires less activation energy to generate crystal nuclei so can occur earlier. Since SF is not miscible in PHBV, the dispersion is poor so there are fewer nucleation sites that are not uniformly distributed. This is reflected in the increased D_s and large standard deviation of spherulite size observed in SEM.

In Green Polymer Chemistry: Biocatalysis and Materials II; Cheng, H., et al.;
ACS Symposium Series; American Chemical Society: Washington, DC, 2013.

Over time, the two phases will phase separate in solution since they were shown earlier to be immiscible without solvent. The competition between crystallization and phase separation for a blend of semicrystalline and amorphous polymers was investigated by Tanaka and Nishi (*41*) who found that the amorphous polymer acts as an impurity and is excluded to the interlamellar regions. Di Lorenzo (*42*) stated that not all particles will be pushed to the boundaries; this will depend on the balance of energy required for incorporating, removing, and deforming the particle. Therefore, as the crystallization of PHBV proceeds and solvent continues to evaporate during film casting, some SF may become trapped in the interlamellar regions of a growing spherulite while other SF may be excluded and segregated to the interspherulitic regions. Considering that the interspherulitic boundaries observed in SEM become less distinct with increasing SF content, it is likely that SF is becoming constrained to these regions and the constraint as well as hydrophobic surroundings may induce a restructuring of the chain to form β-sheet crystals, which will occupy less volume and are hydrophobic. This proposed change in morphology is expressed in Figure 8(b). Additionally, since crystallization was allowed to occur over several days, the presence of residual solvent during this time could lead to improved crystalline morphology. Genovese and Shanks (*43*) observed a similar phenomenon when blending immiscible isotactic polypropylene and poly(ethylene-co-methyl acylate) (EMA), both semicrystalline polymers. They found that EMA reduced the nucleation density of PP spherulites, though did not decrease the crystallization rate and crystallinity. They also proposed that the EMA was pushed to the interspherulitic regions.

In the unique case where SF is less than 20 wt% SF, the degree of crystallinity of PHBV showed a local minimum at 5 wt% SF according to FTIR. In this range, it appears that there is increased interaction between PHBV and SF. For example, 1 wt% SF achieves the same decrease in crystallinity of the PHBV phase as 40 wt% SF. If the 1 wt% SF is more dispersed in the PHBV phase due to higher interaction, more interfaces are present that generate greater mobility of adjacent PHBV chains. This would also explain the much larger rate of degradation decrease of PHBV T_d of P99S1 and P95S5. At larger SF concentrations, there may be a greater driving force for phase separation to reduce interfacial regions.

Where SF is the major phase, as shown in Figure 8(c), the crystalline regions of PHBV may serve as heterogeneous nucleation sites for crystal formation or phase separation may have also contributed to β-sheet formation. In this case, the PHBV phase was slightly less crystalline. PHBV may be more disperse and not able to crystallize to completion. Films of SF remain amorphous, as depicted in Figure 8(d).

Structure and Property Development of PHBV/SF Due to Fast Cooling From Melt

After the fast cooling cycle in DSC, there was an overall reduction in crystallinity and some reduction of T_g of the SF/PHBV blends with 5 wt% SF or greater compared to PHBV. Sashina et al. (*19*) proposed that SF had a plasticizing effect for compositions with less than 20 wt% SF content. Another explanation is

In Green Polymer Chemistry: Biocatalysis and Materials II; Cheng, H., et al.;
ACS Symposium Series; American Chemical Society: Washington, DC, 2013.

Publication Date (Web): November 22, 2013 | doi: 10.1021/bk-2013-1144.ch018

that because the SF phase does not melt during the first heating cycle it remains a solid during subsequent cooling and heating steps. The presence of this solid particle can act as a nucleating agent for PHBV crystallization, as diagrammed in Figure 9. The new site of the PHBV crystal nuclei would be located near regions of higher SF content and may already be entangled in the SF phase so crystallization will be hindered in these vicinities. Therefore, the presence of SF as a nucleating agent and source of crystal imperfections is important in the increased amorphous fraction in PHBV/SF blended films after quenching in the DSC.

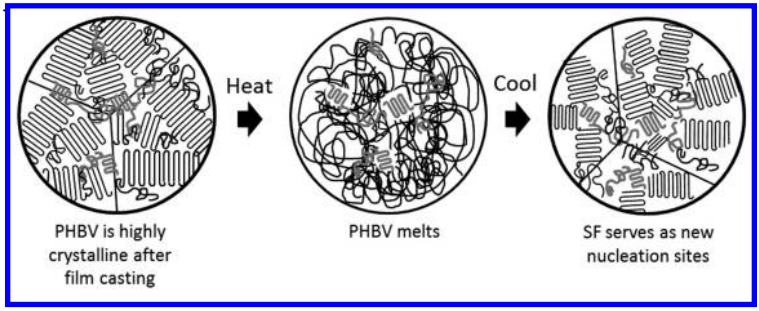

Figure 9. Structure development of PHBV morphology from PHBV/SF blends in the DSC. The PHBV phase is highly crystalline after film casting with SF primarily constrained to interlamellar regions. Upon heating, the PHBV melts while the SF remains a solid. On fast quenching, SF acts as a nucleating agent for new PHBV spherulites. However, the local area is more highly concentrated with SF which leads to more disordered and less crystal formation.

Because the structure is forming from the melt stage, the properties here more reflect phenomena that could occur during extrusion. For extrusion foaming, higher crystallinity is more important for stabilizing the foams in a solid structure, preferably before cell coalescence can happen. To take advantage of the nucleating behavior of SF while minimizing additional thermal degradation, SF powder was blended with PHBV at low concentrations for foam extrusion.

Development of Silk Gelation Process for Powder Production

Results

Silk fibroin powder is not readily available through chemical manufacturers in the US, although it is used commercially in a degraded form by the cosmetics industry (*44*). The freeze-dried SF produced for use in films is not able to be ground into powder. Water evacuation from SF during lyophilization and lack of a tough physical gel network causes a collapsed layered sheet structure, as shown in Figure 10. Instead, a silk aerogel must be made. An aerogel is a dry gel with high porosity where the liquid has been replaced by a gas without collapsing the wet gel structure (*45*). Kim et al. (*24*) prepared silk hydrogels at room temperature and higher, and the resulting freeze-dried structure was highly porous. While silk hydrogels have been studied extensively, it has been in the context of biomaterials for cell scaffolds (*25*) and drug delivery (*24*, *46*).

Publication Date (Web): November 22, 2013 | doi: 10.1021/bk-2013-1144.ch018

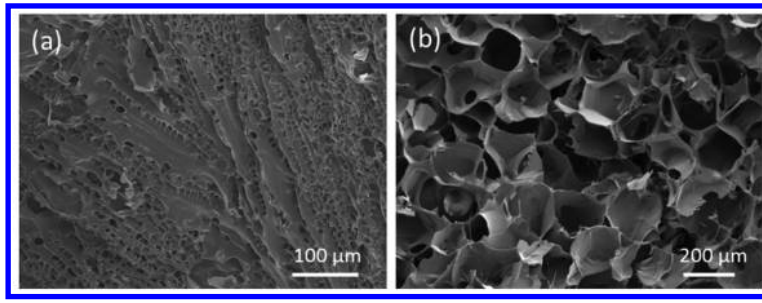

Figure 10. Microstructure of dried SF when (a) freeze-dried from aqueous solution and (b) dried in an oven after freeze-thawing to form a gel.

Publication Date (Web): November 22, 2013 | doi: 10.1021/bk-2013-1144.ch018

We have developed a simple process that can lead to a brittle porous material for grinding into powder. This process is outlined in Figure 1 and involves freezing the aqueous SF solution at -15 °C to form a solid, then thawing at 4 °C. Over time, gelation will occur and the resulting gel is vacuum-dried at 70 °C to reveal a brittle, dry solid that can be ground with a mortar and pestle to powder, as shown in Figure 1. As expected, the processing procedure of the SF solutions has a significant impact on the final bulk morphology, as shown in Figure 10(a)-(b). In the freeze-drying process used in this work, any pores left by water collapse to form sheets (Figure 10(a)), while the pores will remain open when freeze-thawed to form a gel and then dried in a vacuum oven at 70 °C (Figure 10(b)).

Single Freeze−Thaw Cycle for SF Gelation

A time study to determine the minimum overall time required to produce a silk hydrogel was carried out using 1 mL samples, and the results are shown in Figure 11(a). These gels were not dried following gelation. With increasing days at -15 °C, the time to gelation at 4 °C decreased. After 12 days in the freezer, gelation would reach completion in the -15 °C environment such that it would already be a gel upon thawing. It appeared that the minimum time required was 6 days of freezing at -15 °C and 2 days of thawing at 4 °C or 8 days total. Faster gelation upon thawing occurred for all samples with greater than 6 days of freezing. When using room temperature for the thawing stage, the time to gelation was generally longer, as shown in Figure 11(b). The shortest time to achieve a gel was 19 days or 14 days of freezing and 5 days of thawing. Therefore, subsequent SF gelation experiments were performed using at 4 °C thawing temperature.

Multiple Freeze−Thaw Cycling for SF Gelation

The effect of freeze-thaw cycling on SF was investigated to determine whether the gelation process could be improved in terms of reproducibility and length of time; the various freeze-thaw cycling schemes are summarized in Table IV. In this study, 10 mL samples were used to reduce any surface effects from the container

and evaluate a bulk state; each scheme used 4 samples. The results of the total cycles and days required to produce a tough hydrogel that could be potentially ground are shown in Figure 12. Scheme 24 resulted in grindable foams for all four samples after 4 cycles or 8 days. This scheme was chosen to produce more aerogels using 30 mL samples. The result was 8 of 9 large samples yielding grindable foams with an average of 3.1 ± 1.1 cycles and 7.9 ± 3.2 days. Some of the foams showed some shrinkage after drying, with very large pores, but could still be ground. The schemes with longer cycles required many more days before gelation and resulted in solids that were yellowed and collapsed so were unable to be ground. Scheme 72 yielded gels that were very difficult to dry for the conditions used; after many days of drying, the gels remained mostly hydrated. In all cases, at least three cycles were required before gel formation occurred. Foams that could be ground had large pores after drying, as shown in Figure 10(b).

Publication Date (Web): November 22, 2013 | doi: 10.1021/bk-2013-1144.ch018

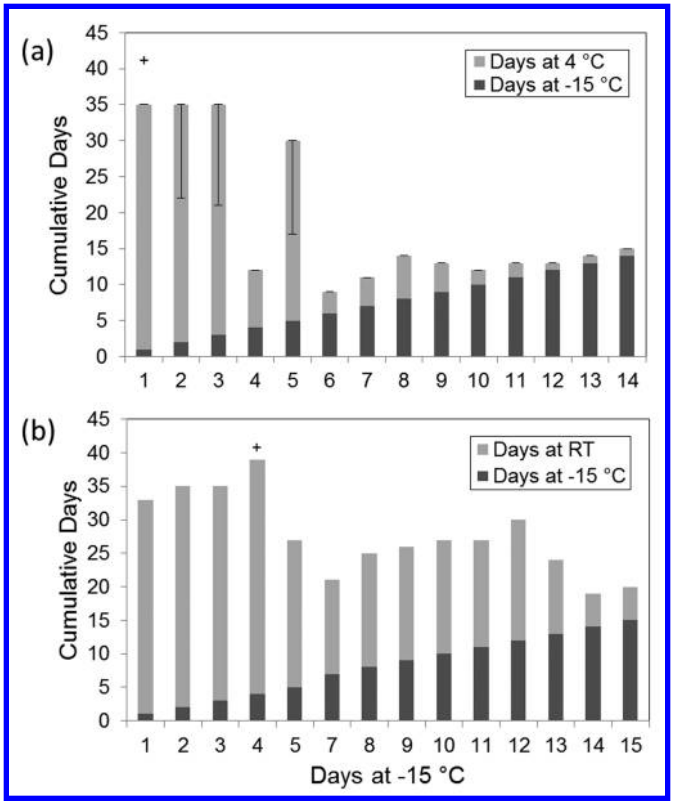

Figure 11. The total number of days to achieve a gel through one cycle of freezing the SF aqueous solution at -15 °C for 1-14 days then thawing at (a) 4 °C and (b) room temperature (RT) until a gel is formed. + indicates that the sample did not achieve gelation within the experimental time frame.

In Green Polymer Chemistry: Biocatalysis and Materials II; Cheng, H., et al.;
ACS Symposium Series; American Chemical Society: Washington, DC, 2013.

Publication Date (Web): November 22, 2013 | doi: 10.1021/bk-2013-1144.ch018

Table IV. Freeze−thaw cycling schemes for achieving silk gelation

Scheme Abbreviation	*Freeze Time at -15 °C (days)*	*Thaw Time at 4 °C (days)*
Q	Shortest time to freeze (average 0.45 ± 0.22)	Shortest time to thaw (average 0.59 ± 0.20)
12	0.5	1
24	1	1
48	2	2
72	3	3
321	Cycle 1: 3 days Cycle 2: 2 days Cycle 3+: 1 day	Cycle 1: 3 days Cycle 2: 2 days Cycle 3+: 1 day

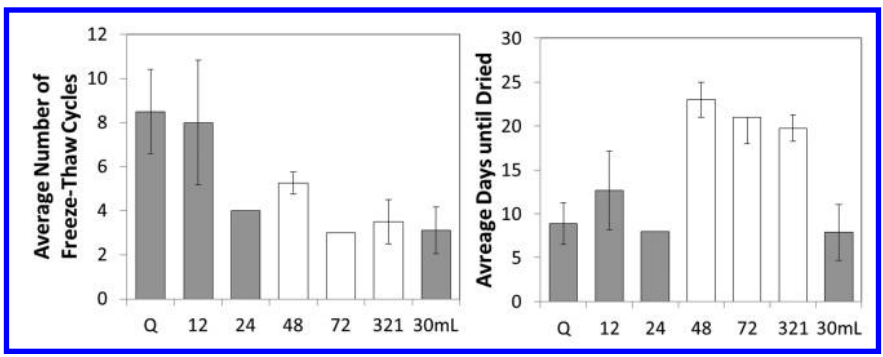

Figure 12. Results of freeze-thaw cycling. (a) Average number of freeze-thaw cycles and (b) average number of days until gel could be dried. Gray bars yielded foams that could be ground into powder while white bars did not. Error bars are the standard deviation of four samples except for Scheme 72 in (b) which reflects drying that could have occurred earlier.

Discussion: Impact of Temperature, Time, and Cycling on Gelation of SF

If the aqueous SF solution does not undergo freezing, storage of the solution at higher temperatures will lead to faster gelation compared to storage at low temperature. Jin and Kaplan (*47*) found that storing an 8% SF solution at room temperature will lead to hydrogelation in about 5 days compared to about 40 days at 7 °C. It has been shown that silk gelation at room temperature and physiological temperature occurs over two stages. The first stage is association of chains through weaker interchain interactions such as hydrogen bonding, hydrophobic interactions, and electrostatic interactions. After more time, β-sheets form and these physical crosslinks are to be considered irreversible (*48*). However, gels formed without a freeze step likely have poor mechanical properties not conducive to maintaining a porous structure during drying. We found that gels

In Green Polymer Chemistry: Biocatalysis and Materials II; Cheng, H., et al.;
ACS Symposium Series; American Chemical Society: Washington, DC, 2013.

formed at 4 °C for more than one year had very poor tear strength and would dry to a yellowed, non-porous solid. Similarly, poly(vinyl alcohol) (PVA) will gel over time at room temperature, but the resulting toughness is poor (*49*). In fact, highly elastic PVA gels can only be formed after repeated freeze-thaw cycles (*49*).

Once the SF solution has been frozen, we observed that gelation occurred more quickly when thawing SF at 4 °C rather than room temperature. It has been hypothesized that the freezing of the water molecules in a PVA solution leads to exclusion of PVA from the ice crystals and then gel formation (*50*). A similar mechanism may be occurring in SF solution. In aqueous solution, the water interacts with the hydrophilic regions of the SF chain, which stabilizes the amorphous conformation and prevents crystallization in solution (*47*). Exclusion of the polymer from the water will promote interchain interactions and formation of β-sheet crystals and thus reduce the time required to form a tough, irreversible network. As the hydrophobic β-sheet crystals form, water will also be excluded from the SF phase forming a larger water phase. By thawing at cooler temperatures, the melting of ice is delayed, which could allow more time for the silk to form β-sheets from the amorphous regions before they may reassociate with water molecules.

Nazarov et al. (*25*) found that freezing of aqueous SF solution at particular temperatures would impact the pore size of the resulting dried gel. If the freezing temperature was within the T_g of aqueous silk (-20 to -34 °C (*51*)), pore sizes from ice crystallization were large. Freezing below this range resulted in small pores due to fast ice crystallization. Peppas and Stauffer (*50*) attributed larger pore size of PVA gels to the continued perfection of ice crystals. This perfection was also promoted through repeated PVA freeze-thaw cycling, which could explain why all freeze-thaw cycling schemes investigated in this work required at least 3 cycles on average before forming an appropriate gel for grinding. The fastest gel formation scheme when performing multiple freeze-thaw cycling required 4 total days of freezing as opposed to a single freeze-thaw cycle which required 6 continuous days of freezing, though both methods led to gels in 8 total days.

Furthermore, Li et al. (*51*) reported that the freezing temperature affected the SF chain morphology. Freezing above -20 °C led to SF that was composed significantly of α-helices, while below -20 °C would lead to primarily amorphous SF and some β-sheets. These foams were immediately freeze-dried and the resulting foams were described as "spongey," which may imply that they would be too soft for grinding. In the present study, freezing of SF was performed at -15 °C, yet the resulting gel and dried foam did have β-sheet formation according to FTIR. Because α-helices are metastable, the thawing period may have provided sufficient time for the change to β-sheets. These considerations also suggest that the lyophilization process used in this study may not have been conducive to porous foam formation. The short freezing time at -80 °C followed by immediate freeze-drying did not allow time for SF to self-associate enough to form a tough gel structure to support the porous structure when water was removed.

The need for sufficient freezing time is reflected in Schemes Q and 12-24, which both required many more cycles and more days until tough gel formation than Scheme 24. The primary difference was Schemes Q and 12-24 had freezing cycle times of around 0.5 days instead of 1 day. However, schemes that had

Publication Date (Web): November 22, 2013 | doi: 10.1021/bk-2013-1144.ch018

longer cycling times than 1 day required many more days until gel formation. When dried, many of those gels collapsed to solid material when dried. While it is not clear why that occurs, it may be that these gels require more aggressive drying such as using supercritical methods (*52*) or freeze-drying to avoid a liquid state capable of collapsing pores through high surface tension (*53*). When much smaller samples were dried, the resulting solid was often white and appeared grindable. Any grindable foams produced were ground into powder of heterogeneous dimensions ranging from 10 to 1000 μm, as shown in Figure 1.

Characterization of PHBV:SF Foams

Results

Impact of SF on PHBV Foam Density and Cell Density

The SF powder was used as an additive in PHBV foaming at 1 (P99S1) and 5 wt% (P95S5) SF. Figures 13 and 14 show the resulting foams for neat PHBV and SF/PHBV, respectively, at AZ content from 0.5 to 4 phr. In general, with increasing blowing agent content, bulk density decreased and cell density increased. The differences between the foams are not drastic. As shown in Figure 15(a), the SF powder is less dense and is able to reduce the bulk density of unfoamed PHBV from 1.43 g/mL to 1.22 g/mL. This continues to reduce the density of 0.5 phr and 4 phr AZ foams. The bulk density of 1, 2, and 3 phr AZ foams were mostly unchanged though the cell densities at these AZ contents were lower for P99S1 than PHBV. Cell density only improved for 0.5 phr AZ.

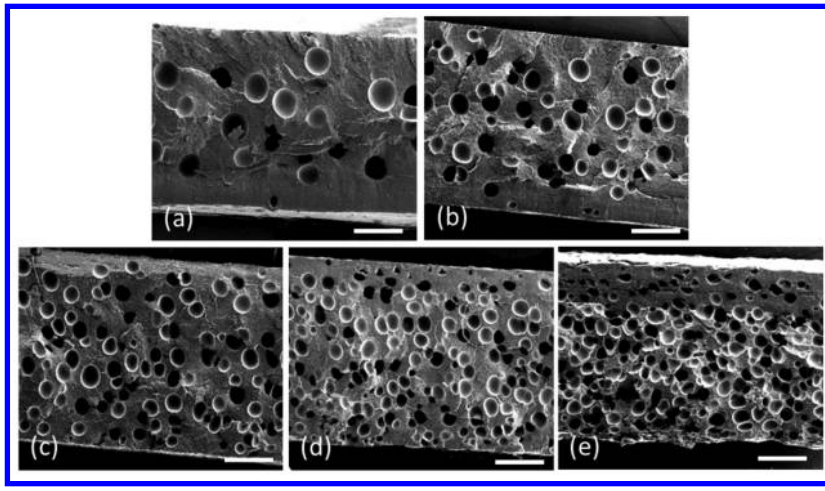

Figure 13. SEM images of PHBV foams blown with (a) 0.5, (b) 1, (c) 2, (d) 3, (e) 4 phr AZ at 80 rpm screw speed. Scale bars are 500 μm.

Publication Date (Web): November 22, 2013 | doi: 10.1021/bk-2013-1144.ch018

Publication Date (Web): November 22, 2013 | doi: 10.1021/bk-2013-1144.ch018

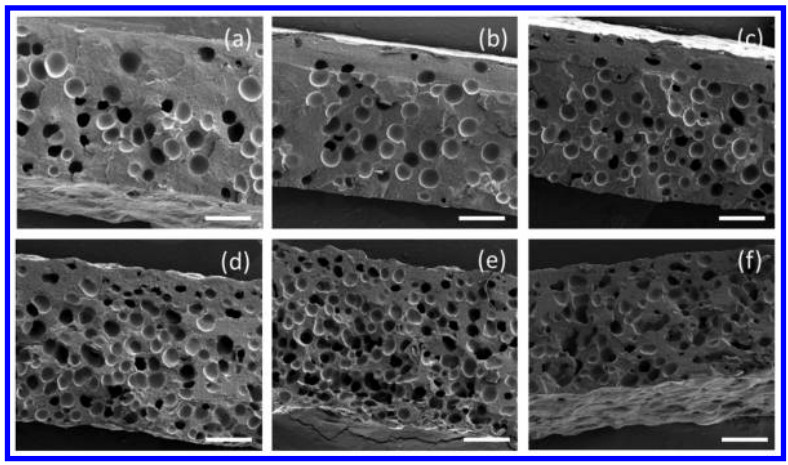

Figure 14. SEM images of PHBV foams with 1 wt% SF blown with (a) 0.5, (b) 1, (c) 2, (d) 3, (e) 4 phr AZ at 80 rpm screw speed, and (f) PHBV foam with 5 wt% SF blown with 4 phr AZ. Scale bars are 500 μm.

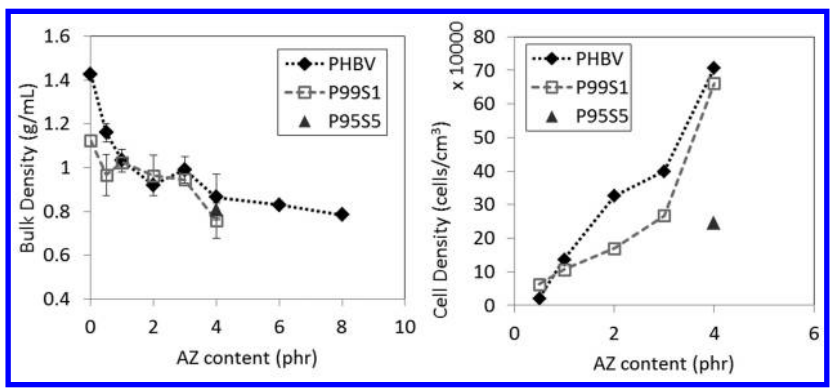

Figure 15. (a) Bulk density and (b) cell density of PHBV foams and PHBV/SF foams with a range of blowing agent contents.

In Green Polymer Chemistry: Biocatalysis and Materials II; Cheng, H., et al.;
ACS Symposium Series; American Chemical Society: Washington, DC, 2013.

Publication Date (Web): November 22, 2013 | doi: 10.1021/bk-2013-1144.ch018

Shrinkage in PHBV/SF Foams

During extrusion, the SF foams exhibited significant shrinkage during the cooling process after initial expansion upon exiting the extruder. From the SEM images in Figure 14(a)-(f), the upper and lower surfaces of the foam appear more rough due to shrinkage of the foams, especially compared to the surfaces of foams in Figure 13(a)-(e). Shrinkage occurs due to cooling of the gas and diffusion of the gas out faster than air can diffuse in (*54*). To evaluate the degree of shrinkage of foams during cooling, surface roughness of the foams was determined by drawing over the upper and lower surface lines in ImageJ to measure the actual rough surface length, l_R, and measuring the end-to-end distance of the upper and lower surface as a line, l_s. The roughness ratio, R, was determined as

$$R = \frac{l_R}{l_S}$$

Figure 16 shows the average roughness ratio of the top and bottom surfaces for the various AZ contents. P99S1 shows increasingly more shrinkage at contents above 0.5 phr AZ. In contrast, neat PHBV does not exhibit shrinkage until 4 phr AZ. Table V lists the calculated bulk density of foams pre-shrinkage depending on whether shrinkage is assumed to uniformly occur only in 1D (i.e., the width) or up to 3D (i.e., length, width, and height of the foam). With this adjustment, the bulk density of P99S1 foam with 4 phr AZ could be as low as 0.66 g/mL.

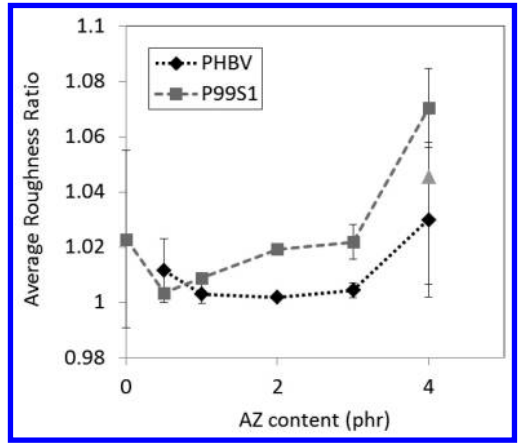

Figure 16. Average roughness ratio of PHBV/SF foams.

In Green Polymer Chemistry: Biocatalysis and Materials II; Cheng, H., et al.;
ACS Symposium Series; American Chemical Society: Washington, DC, 2013.

Table V. Adjusted foam bulk density based on shrinkage of P99S1 foams

AZ content (phr)	*Roughness ratio*	*Non-adjusted bulk density (g/mL)*	*1D adjusted bulk density (g/mL)*	*3D adjusted bulk density (g/mL)*
0	1.023	1.12	1.10	1.07
0.5	1.003	0.97	0.96	0.96
1	1.009	1.03	1.02	1.01
2	1.019	0.96	0.95	0.93
3	1.022	0.95	0.93	0.91
4	1.070	0.76	0.71	0.66

Publication Date (Web): November 22, 2013 | doi: 10.1021/bk-2013-1144.ch018

Discussion: Overall Impact of SF Content on PHBV/SF Foams

Because 1 wt% SF decreased bulk density of the PHBV matrix, and reduced the overall foam density achievable, it was possible that increasing the SF content may further improve on these areas as well as have a greater impact on cell density. However, the higher SF content of P95S5 foams did not improve bulk density beyond that of P99S1 because there was extremely low cell density in Figure 15(b). From the SEM images, significant cell coalescence can be observed in P99S5. To accentuate the cell coalescence, binary images of the foam structure from SEM were drawn using ImageJ software and are compared in Figure 17. The large, irregularly shaped features in Figure 17(c) suggest the coalescence of multiple neighboring cells, which reduces the observed cell density multifold. Additionally, the height of the foam clearly decreases with increasing SF content as shown by the diminished dimensions occupied by cells. This indicates that there was also significant gas loss and shrinkage. From Figure 14(f), the bottom surface of the foam can be observed and there are many holes where gas escaped. Though the roughness ratio was determined to be intermediate to PHBV and P99S1, the variability was very high due to differences in the top and bottom surface roughness, so that shrinkage is expected to be more significant than was calculated.

The increased content of SF appears to promote cell coalescence. If the SF is nucleating more cells, the sudden diffusion of gas to these lower pressure areas may result in cell coalescence if melt strength of PHBV is insufficient to withstand the expansion at the cell wall. Because more shrinkage also occurs in neat PHBV foams at 4 phr AZ, this is likely a major contribution. Another explanation could be that the presence of more SF particles on the cell walls may promote bursting of cell walls since the SF and PHBV are immiscible. If the cell wall is thinner than a particle embedded in the cell wall, the interfacial energy between the particle and the liquid will determine whether the wall will drain more quickly or slowly (*54*). In the case of SF and PHBV, which are not miscible, the SF particle will likely cause faster drainage of the wall leading to coalescence.

In Green Polymer Chemistry: Biocatalysis and Materials II; Cheng, H., et al.;
ACS Symposium Series; American Chemical Society: Washington, DC, 2013.

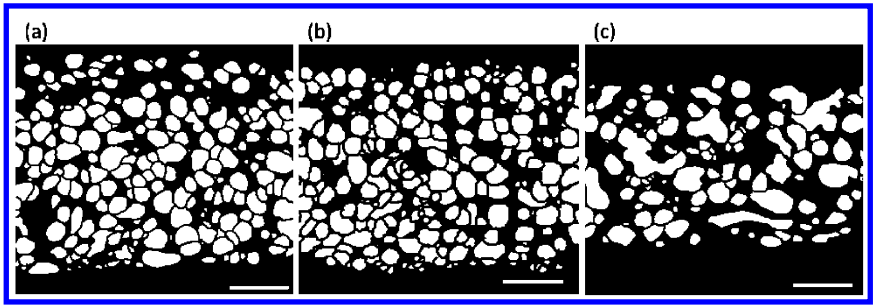

Figure 17. Binary images traced from SEM micrographs comparing the cell coalescence in (a) PHBV, (b) P99S1, and (c) P95S5 foams with 4 phr AZ. Scale bar is 500 μm.

Publication Date (Web): November 22, 2013 | doi: 10.1021/bk-2013-1144.ch018

Conclusions

It was determined that PHBV and SF were immiscible across the range of compositions studied. However, the two phases still had mutual influence on thermal properties and morphology. The hydrophobic nature of PHBV promotes crystallization of the hydrophobic SF regions to form β-sheets that result in high crystallinity and higher thermal stability of the SF phase. SF also acts as a crystal nucleating agent for PHBV, but is excluded to the interspherulitc regions during PHBV crystal growth. Below 20 wt% SF, crystallinity decreased and degradation temperature more rapidly decreased suggesting more interaction between the phases in this range.

Following melting and fast cooling in the DSC, PHBV melting temperature and crystallinity were generally reduced below that of neat PHBV films processed in the same way. The new PHBV crystals are likely nucleated in regions of higher SF content hindering the already shortened crystallization process. At 1 wt% SF, melting temperature and crystallinity are higher because of less SF to hinder growth. Unfortunately, PHBV degradation temperatures were monotonically reduced with increasing SF content. The addition of water bound to SF can promote hydrolysis and more mobile chain ends at the SF/PHBV interface can lead to more chain backbiting as part of thermal degradation. Subsequently, low contents of SF should be used for foaming to minimize potential for hydrothermal degradation while utilizing the nucleating properties.

To produce SF powder for foam extrusion, it was found that 3 cycles of 1-day freeze-thaw cycles were able to reproducibly yield SF aerogels from tough hydrogels after drying in a vacuum oven. Shorter cycles required many more periods and were less reproducible. Hydrogels formed with longer cycles required significantly more days to yield a tough hydrogel, and were more difficult to dry completely or collapsed to a solid. The freezing step was important in forming the porous structure and driving the SF to self-associate and form a tough gel.

Though SF powder was found to be lighter than PHBV and thus reduced the bulk density of unfoamed PHBV, it only improved foam density for 0.5 and 4 phr AZ at 1 wt% SF. For the intermediate AZ contents, cell density was more significantly below that of neat PHBV so bulk density was not enhanced. When

5 wt% SF was added with 4 phr AZ, there was substantial cell coalescence so cell density was drastically reduced. Using the roughness ratio, it was shown there there is greater foam shrinkage in foams with SF. SF may be promoting gas diffusion out of the matrix and may destablilize cell walls due to immiscibility. The poor PHBV melt strength must be improved before SF can have a significant impact.

Acknowledgments

This material is based upon work supported by the National Science Foundation Graduate Research Fellowship under Grant No. DGE-1147470. Any opinion, findings, and conclusions or recommendations expressed in this material are those of the authors and do not necessarily reflect the views of the National Science Foundation. The authors would also like to thank Dr. Carmen Preda for support in producing silk fibroin and Dr. Yilin Chung for help with GPC measurements. A portion of this work was performed at the Stanford Nanocharacterization Laboratory (SNL) part of the Stanford Nano Shared Facilities and the NIH P41 resource center on Tissue Engineering (EB002520).

Publication Date (Web): November 22, 2013 | doi: 10.1021/bk-2013-1144.ch018

References

1. Maier, C.; Calafut, T. *Polypropylene: The Definitive User's Guide and Databook*; Plastics Design Library: Norwich, NY, 1999.
2. Doi, Y. *Microbial Polyesters*; VCH Publsihers: New York, 1990.
3. Srubary, W. V.; Wright, Z. C.; Tsui, A.; Michel, A. T.; Billington, S. L.; Frank, C. W. *Polym. Degrad. Stab.* **2012**, *97*, 1922–1929.
4. Liao, Q.; Tsui, A.; Billington, S. L.; Frank, C. W. *Polym. Eng. Sci.* **2012**, *52*, 1495–1508.
5. Javadi, A.; Srithep, T.; Pilla, S.; Clemons, C.; Turng, L. S.; Gong, S. *Soc. Plast. Eng., Plast. Res. Online* **2011**, 1–4.
6. Verhoogt, H.; Ramsay, B. A.; Favis, B. D. *Polymer* **1994**, *35*, 5155–5169.
7. Richards, E.; Rizvi, R.; Chow, A.; Naguib, H. *J. Polym. Environ.* **2008**, *16*, 258–266.
8. Buchanan, C. M.; Gedon, S. C.; White, A. W.; Wood, M. D. *Macromolecules* **1992**, *25*, 7371–7381.
9. Kubo, S.; Kadla, J. F. *Biomacromolecules* **2003**, *4*, 561–567.
10. Thirtha, V.; Lehman, R.; Nosker, T. *Polymer* **2006**, *47*, 5392–5401.
11. Thirtha, V.; Lehman, R.; Nosker, T. *Polym. Eng. Sci.* **2005**, *45*, 1187–1193.
12. Ash, B. J.; Siegel, R. W.; Schadler, L. S. *J. Polym. Sci., Part B.: Polym. Physics* **2004**, *42*, 4371–4383.
13. Fu, C.; Shao, Z.; Fritz, V. *Chem. Commun. (Cambridge, U.K.)* **2009**, 6515–6529.
14. Sun, M.; Zhou, P.; Pan, L.-F.; Liu, S.; Yang, H.-X. *J. Mater. Sci.: Mater. Med.* **2009**, *20*, 1743–1751.
15. Vepari, C.; Kaplan, D. L. *Prog. Polym. Sci.* **2007**, *32*, 991–1007.
16. Numata, K.; Cebe, P.; Kaplan, D. L. *Biomaterials* **2010**, *31*, 2926–2933.

17. Breslauer, D. N.; Kaplan, D. L. In *Polymer Science: A Comprehensive Review*; Matyjaszewski, K., Möller, M., Eds.; Elsevier B.V.: Waltham, MA, 2012; Vol. 9, pp 57−69.
18. He, S. J.; Valluzzi, R.; Gido, S. P. *Int. J. Biol. Macromol.* **1999**, *24*, 187–195.
19. Sashina, E. S.; Novoselov, N. P.; Heinemann, K. *Russ. J. Appl. Chem.* **2005**, *78*, 153–158.
20. Yang, H. *J. Biomed. Sci. Eng.* **2010**, *3*, 1146–1155.
21. Sudesh, K.; Hideki, A. *Practical Guide to Microbial Polyhydroxyalkanoates*; Smithers Rapra Technology: Shawbury, U.K., 2010; pp 25−50.
22. Peng, S. *Eur. Polym. J.* **2003**, *39*, 1475–1480.
23. Kang, D. J.; Xu, D.; Zhang, Z. X.; Pal, K.; Bang, D. S.; Kim, J. K. *Macromol. Mater. Eng.* **2009**, *294*, 620–624.
24. Kim, U. –J.; Park, J.; Li, C.; Jin, H. –J.; Valluzzi, R.; Kaplan, D. L. *Biomacromolecules* **2004**, *5*, 786–792.
25. Nazarov, R.; Jin, H. –J.; Kaplan, D. L. *Biomacromolcules* **2004**, *5*, 718–726.
26. Motta, A.; Fambri, L.; Migliaresi, C. *Macromol. Chem. Phys.* **2002**, *203*, 1658–1665.
27. Nakamura, S.; Magoshi, J.; Magoshi, Y. In *Silk Polymers: Materials Science and Biotechnology*; Kaplan, D. L., Adams, W. W., Farmer, B., Viney, C., Eds.; ACS Symposium Series 544; American Chemical Society: Washington, DC, 1993; pp 211−221.
28. Barham, P. J.; Keller, A.; Otun, E. *J. Mater. Sci.* **1984**, *19*, 2781–2794.
29. Shanks, R. A.; Amarasinghe, G. In *Polymer Characterization Techniques and the Application to Blends*; Simon, G. P., Ed.; Oxford University Press: New York, 2003; pp 22−67.
30. Renard, E.; Walls, M.; Guérin, P.; Langlois, V. *Polym. Degrad. Stab.* **2004**, *85*, 779–787.
31. Liu, Q.-S.; Zhu, M.-F.; Wu, W.-H.; Qin, Z.-Y. *Polym. Degrad. Stab.* **2009**, *94*, 18–24.
32. Cheng, M.-L.; Sun, Y.-M.; Chen, H.; Jean, Y. C. *Polymer* **2009**, *50*, 1957–1964.
33. Reis, K.; Pereira, J.; Smith, A.; Carvalho, C.; Weller, N.; Yakimets, I. *J. Food Eng.* **2008**, *89*, 361–369.
34. Tian, G.; Wu, Q.; Sun, S.; Noda, I.; Chen, G.-Q. *Appl. Spectrosc.* **2001**, *55*, 888–893.
35. Hu, X.; Kaplan, D. L.; Cebe, P. *Macromolecules* **2008**, *41*, 3939–3948.
36. Hu, X.; Kaplan, D. L.; Cebe, P. *Macromolecules* **2006**, *39*, 6161–6170.
37. Gil, E. S.; Frankowski, D. J.; Bowman, M. K.; Gozen, A. O.; Hudson, S. M.; Spontak, R. J. *Biomacromolecules* **2006**, *7*, 728–735.
38. Buzarovska, A.; Grozdanov, A. *J. Mater. Sci.* **2009**, *44*, 1844–1850.
39. Glišović, A.; Salditt, T. *Appl. Phys. A: Mater. Sci. Process.* **2007**, *87*, 63–69.
40. Magoshi, J.; Nakamura, S. *J. Appl. Polym. Sci.* **1975**, *19*, 1013–1015.
41. Tanaka, H.; Nishi, T. *Phys. Rev. Lett.* **1985**, *55*, 1102–1105.
42. Di Lorenzo, M. L. *Prog. Polym. Sci.* **2003**, *28*, 663–689.
43. Genovese, A.; Shanks, R. A. *J. Appl. Polym. Sci.* **2003**, *90*, 175–185.
44. Nam, J.; Park, Y. H. *J. Appl. Polym. Sci.* **2001**, *81*, 3008–3021.

Publication Date (Web): November 22, 2013 | doi: 10.1021/bk-2013-1144.ch018

45. Pierre, A. C. In *Aerogels Handbook*; Aegerter, M. A., Leventis, N., Koebel, M. M., Eds.; Springer: New York, 2011; pp 3−18.
46. Nagarkar, S.; Nicolai, T.; Chassenieux, C.; Lele, A. *Phys. Chem. Chem. Phys.* **2010**, *12*, 3834–3844.
47. Jin, H.-J.; Kaplan, D. L. *Nature* **2003**, *424*, 1057–1061.
48. Matsumoto, A.; Chen, J.; Collette, A. L.; Kim, U. –J.; Altman, G. H.; Cebe, P.; Kaplan, D. L. *J. Phys. Chem. B* **2006**, *110*, 21630–21638.
49. Stauffer, S. R.; Peppas, N. A. *Polymer* **1992**, *33*, 3932–3936.
50. Peppas, N. A.; Stauffer, S. R. *J. Controlled Release* **1991**, *16*, 305–310.
51. Li, M.; Lu, S.; Wu, Z.; Yan, H.; Mo, J.; Wang, L. *J. Appl. Polym. Sci.* **2001**, *79*, 2185–2191.
52. Kistler, S. S. *Nature* **1931**, *127*, 741–741.
53. Fricke, J.; Tillotson, T. *Thin Solid Films* **1997**, *297*, 212–223.
54. Zhang, X. D.; Neff, R. A.; Macosko, C. W. In *Polymer Foams: Mechanisms and Materials*; Lee, S. T., Ramesh, N. S., Eds.; CRC Press: Boca Raton, FL, 2004.

Publication Date (Web): November 22, 2013 | doi: 10.1021/bk-2013-1144.ch018

Publication Date (Web): November 22, 2013 | doi: 10.1021/bk-2013-1144.ch019

Chapter 19

Synthesis and NMR Characterization of Hyperbranched Polyesters from Trimethylolpropane and Adipic Acid

Tracy Zhang,[1,2] Bobby A. Howell,[2] Paul K. Martin,[1] Steven J. Martin,[1] and Patrick B. Smith*,[1]

[1]Michigan Molecular Institute, 1910 West St., Andrews Road, Midland, Michigan 48640
[2]Central Michigan University, Department of Chemistry, Dow Science Complex 263, Mount Pleasant, Michigan 48859
***E-mail: smith@mmi.org**

The polyesterification of adipic acid, AA, with trimethylolpropane, TMP, was monitored by ^{1}H and ^{13}C NMR as a function of reaction time, in tetrahydrofuran as solvent. The reaction was catalyzed by p-toluenesulfonic acid, pTSA. NMR assignments of the mono, di and triester of TMP were determined and these reaction products were monitored as a function of time by both ^{1}H and ^{13}C NMR spectroscopy to determine the reaction kinetics. The reaction was first order in AA and TMP concentration and the reaction rate was found to significantly increase with increasing pTSA level up to a concentration of 2.5 mole% based on acid functionality.

Introduction

Hyperbranched polyesters, HBPE, are attracting much interest because many of their monomeric building blocks can be obtained from biobased sources and are biodegradable, opening many new areas of application. HBPEs have been synthesized from a number of different monomeric building blocks, including those from multifunctional aliphatic alcohols and diacids

In Green Polymer Chemistry: Biocatalysis and Materials II; Cheng, H., et al.;
ACS Symposium Series; American Chemical Society: Washington, DC, 2013.

(*1–7*), from 2,2-bis(hydroxymethyl)propionic acid (*8*), from glycolide and 2,2-bis(hydroxymethyl)butyric acid (*9*), aconitic acid and diethylene glycol (*10*) and several from glycerol and difunctional acids (*11–17*). Many of the applications targeted for these HBPEs from biobased sources include the administration of pharmaceuticals, pesticides and antimicrobials (*18–27*). They are synthesized from mutually reactive multifunctional monomers, A_x and B_y, where x and y are the functionality of the molecule.

The simplest of these multifunctional monomers is the $A_2 + B_3$ reaction system, such as adipic acid with trimethylolpropane, which is the system described in this investigation. This $A_2 + B_3$ system forms a hyperbranched polyester by a step-growth polymerization reaction, which if performed in equimolar quantities of functional groups, forms an insoluble gel at high conversions. However, by proper choice of monomer stoichiometry, one can produce soluble materials and even have some control over the molecular weight of the resulting HBPE (*28*). This is the basis of bimolecular nonlinear polymerization (BMNLP) methodology (see Scheme 1). The use of BMNLP to control the molecular weight of HBPEs will be described in more detail in a future publication. The endgroup composition for BMNLP is also determined by the monomer stoichiometry. The endgroup functionality is primarily that of the excess component at high conversion as shown in Scheme 1.

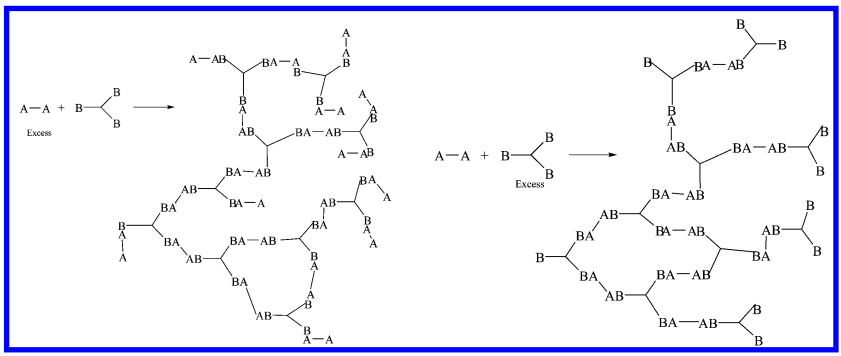

Scheme 1

This reaction strategy can lead to either HBPs with B or A endgroups. The ability to easily control endgroup functionality is a valuable attribute for HB systems since so many polymer properties depend on it including solubility, solution and melt viscosity and thermal properties. The endgroups are capable of further reaction with the addition of the other reactive components. This property may be exploited to covalently attach active agents or for crosslinking into 3D networks. Scheme 2 shows the structure of an HBPE from glycerol and a diprotic acid such as adipic acid with glycerol in excess such that the endgroups are alcohols. The molecular interiors of these polymers contain polar ester groups which facilitate host-guest interactions with various active agents for encapsulation, which after delivering them to the application site, release them by diffusion. Finally, it should also be noted that the versatility and the simplicity of the BMNLP approach enables the use of biobased polyfunctional

Publication Date (Web): November 22, 2013 | doi: 10.1021/bk-2013-1144.ch019

alcohols and acids for the preparation of HBPEs which possess the ability to degrade to the starting monomers either by hydrolysis or enzymatic degradation, providing a benign process for the HBP carrier to assimilate into the environment after delivering the active agent. These HBPEs provide a versatile platform for achieving a variety of material properties.

HBPEs from trimethylolpropane, TMP, and adipic acid, AA, an $A_2 + B_3$ system was synthesized in this investigation. TMP was used as a model for synthesis of biobased polyesters since all three alcohol groups are primary and have equivalent reactivity. The polycondensation reaction was monitored by NMR spectroscopy in order to assist in the assignment of the spectra as well as to understand the rate dependence on catalyst level, side reactions and the time required for complete conversion.

Publication Date (Web): November 22, 2013 | doi: 10.1021/bk-2013-1144.ch019

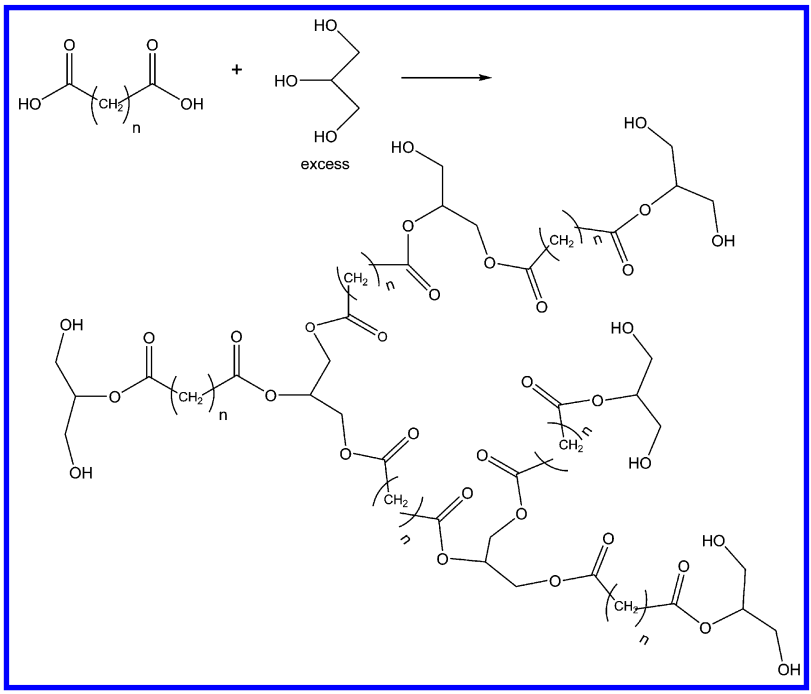

Scheme 2

Materials and Methods

Trimethylolpropane, TMP, adipic acid, AA, p-toluenesulfonic acid, p-TSA, and tetrahydrofuran, THF, were obtained from Sigma Aldrich and used without further purification.

The polyester was synthesized using p-TSA as catalyst and driven to completion by stripping water using a soxhlet extraction apparatus with 4Å molecular sieves. A typical reaction used a stoichiometry of [OH] / [COOH] equal to 1.0. In one example, 10.0 g of TMP, 2.5 mole% p-TSA (based on acid functionality) or 1.06 g, and 16.34 g of AA were added to 109.6 g of THF (20

In Green Polymer Chemistry: Biocatalysis and Materials II; Cheng, H., et al.;
ACS Symposium Series; American Chemical Society: Washington, DC, 2013.

weight% solids). These reactants were added to a 250 ml three neck round bottom flask and brought to reflux conditions, about 66°C, using an oil bath. The reaction was blanketed with N_2. The concentration of reactants and the temperature cycled as the solvent and water cycled through the soxhlet extractor. The reaction mixture flask was sampled periodically through one of the necks equipped with a septum. Roughly 1 ml samples were taken with a syringe throughout the reaction. The samples were cooled in a freezer to quench the reaction for analysis by NMR. The samples were always taken directly after the siphon dumped. NMR spectra were used to determine the extent of reaction, as will be discussed later.

^{1}H NMR spectra of neat reaction mixtures (without deuterated solvent) were obtained using a Varian Inova 500 NMR spectrometer operating at 499.7 MHz for ^{1}H observe. The pulse width was 8°, the pulse repetition time was 5 seconds, sweep width 8,000 Hz, number of points 65536, 0.1 Hz line broadening, 16 scans. The analysis was performed without an internal lock but no significant line broadening was observed due to field drift over the 2 minute acquisition time.

^{13}C NMR spectra of neat reaction mixtures were obtained using the same instrument at 125.7 MHz. A 90° pulse width was used, the pulse repetition time was 5 seconds with complete decoupling, the sweep width was 31 KHz, number of points 131,072, 3.0 Hz line broadening, 256 scans. No significant line broadening due to field drift was observed over the 21 minute acquisition time. These conditions were not strictly quantitative but carbons of the same type, e.g., the carbonyl carbon resonances of adipic acid and the quaternary carbon resonances of TMP, were expected to have very similar NOEs and relaxation times such that quantitative data could be obtained from the ratio of their areas. In fact, the conversion values calculated from the ^{1}H NMR spectra and the carbonyl carbons of adipic acid or the quaternary carbon of TMP gave very consistent conversion values.

Publication Date (Web): November 22, 2013 | doi: 10.1021/bk-2013-1144.ch019

Results

NMR Assignments

The esterification of TMP with AA was expected to provide a simple model for hyperbranched polyesterification reactions since each TMP hydroxyl is an equivalent primary hydroxyl unit, having equal reactivity towards esterification. The expected reactions are given in Scheme 3, which incorporates some simplifying assumptions, namely that the reactivity of one acid group of adipic acid is not affected by whether the other is acid or ester. This reaction is ignored in Scheme 3. The substitution of one hydroxyl unit of TMP might also affect the reactivity of the other hydroxyl units on the TMP molecule. Therefore, k_1, k_2 and k_3 might each be different. The model used to fit the reaction profile, which is described later in this work, assumes that $k_1 = k_2 = k_3$. This model fits the observed kinetics quite well.

Each of the structures given in Scheme 3 possesses distinct NMR signatures, both in their ^{1}H and ^{13}C NMR spectra. Therefore, NMR was able to monitor the progress of the esterification reactions.

Publication Date (Web): November 22, 2013 | doi: 10.1021/bk-2013-1144.ch019

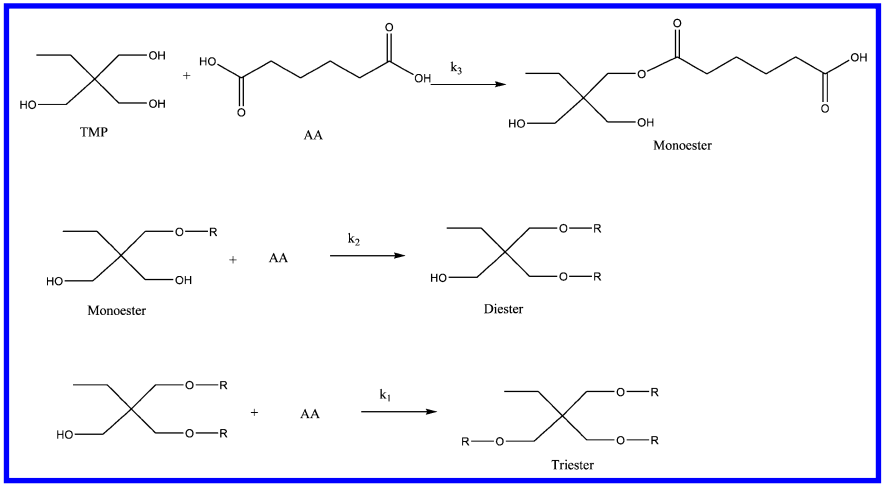

Scheme 3

Figure 1 gives the ^{1}H NMR spectrum of a reaction mixture of TMP and adipic acid of stoichiometry 2.1:1, [OH]:[COOH]. The assignments are given on the spectrum. The methyl resonance of TMP is a multiplet located at about 0.8 ppm, the methylene resonances are located between 1.0 and 1.5 ppm, the origin of the multiplicity is very complex, being due to both coupling and substituent effects, as will be discussed later. The adipic acid methylenes are located at 1.58 and 2.28 ppm. Resonances from residual THF are also noted in the spectrum. The resonances from 3.3 to about 4.0 ppm are those of the -OCH_2 protons of TMP as well as a resonance from THF and water which are labeled on the spectrum.

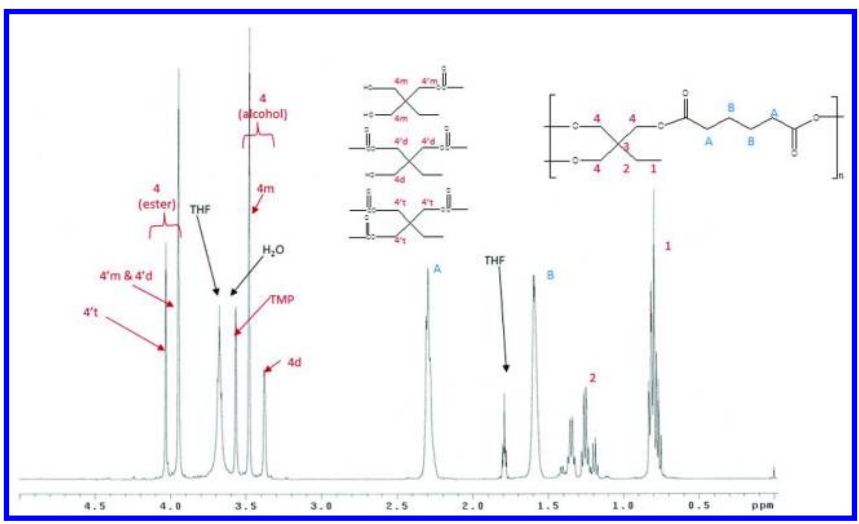

Figure 1. The ^{1}H NMR Spectrum of a Copolymer of TMP and AA with Stoichiometry of 2.1:1, [OH]:[COOH], with Assignments.

In Green Polymer Chemistry: Biocatalysis and Materials II; Cheng, H., et al.;
ACS Symposium Series; American Chemical Society: Washington, DC, 2013.

The -OCH_2 proton resonances of TMP, labeled 4 on the figure are separated into 2 distinct regions, one group located between 3.3 and 3.7 ppm and a second group at 3.9 to 4.1 ppm. The upfield group of resonances, from 3.3 to 3.7 ppm, are those of the TMP methylene with alcohol functional groups, –CH_2-OH, and the downfield group are those of the -OCH_2s of TMP which are esters. These groups are further split due to substituent effects. Unreacted TMP is observed at 3.55 ppm and water at 3.60 ppm. Within the alcohol group of resonances, the monoester, labeled 4m, is located at 3.45 ppm and the diester, 4d, is observed at 3.35 ppm. The -OCH_2 proton resonances of the TMP esters are observed between 3.9 and 4.5 ppm. The resonance of the triester, 4′t, is located at about 4.02 ppm and that of the diester, 4′d, is located with the monoester, 4′m, at about 3.92 ppm. The assignments were determined from the kinetic sequence of the reaction, knowing that the TMP substitution would proceed from mono ester to di and tri. These assignments are also consistent with the ^{13}C NMR spectra, which are much easier to assign.

Figure 2 gives the ^{13}C NMR spectrum of a TMP, AA reaction product in $CDCl_3$ as solvent, with assignments. An expansion of the quaternary carbon region of the spectrum, between 40 and 44 ppm, is given in Figure 3. The assignments of the quaternary carbons of TMP as a function of substitution were determined from kinetic runs like the one given in Figure 3 and are consistent with those described elsewhere[1]. At early reaction times only TMP and the monoester are observed. As the reaction proceeds, these resonances diminish and the di and triester resonances grow in. The same trends can be followed with the carbonyl resonances of adipic acid. These ^{13}C NMR assignments, which are straightforward, were used to assist in assigning the ^{1}H NMR spectra such that all the spectra were self-consistent.

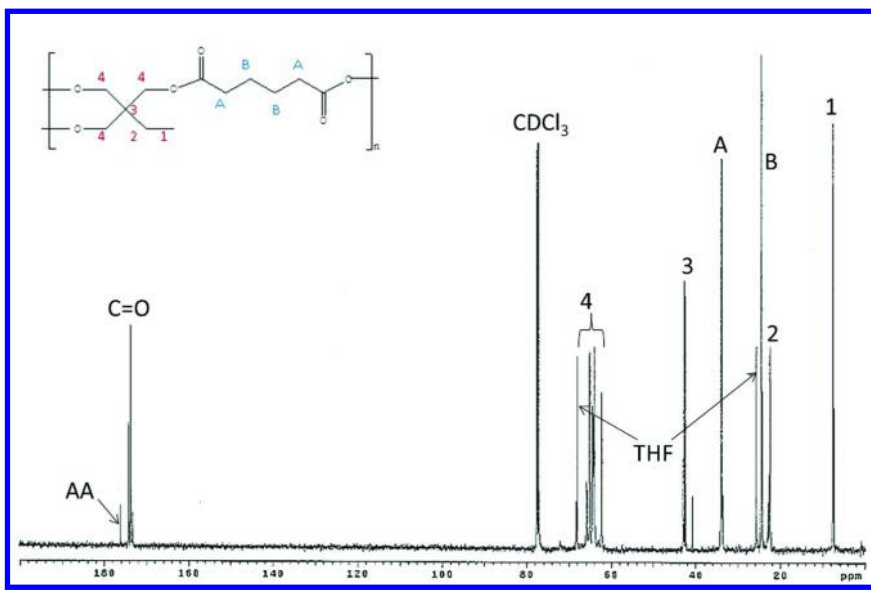

Figure 2. The ^{13}C NMR Spectrum of the Hyperbranched Copolymer of TMP and AA in $CDCl_3$ with assignments.

In Green Polymer Chemistry: Biocatalysis and Materials II; Cheng, H., et al.;
ACS Symposium Series; American Chemical Society: Washington, DC, 2013.

Publication Date (Web): November 22, 2013 | doi: 10.1021/bk-2013-1144.ch019

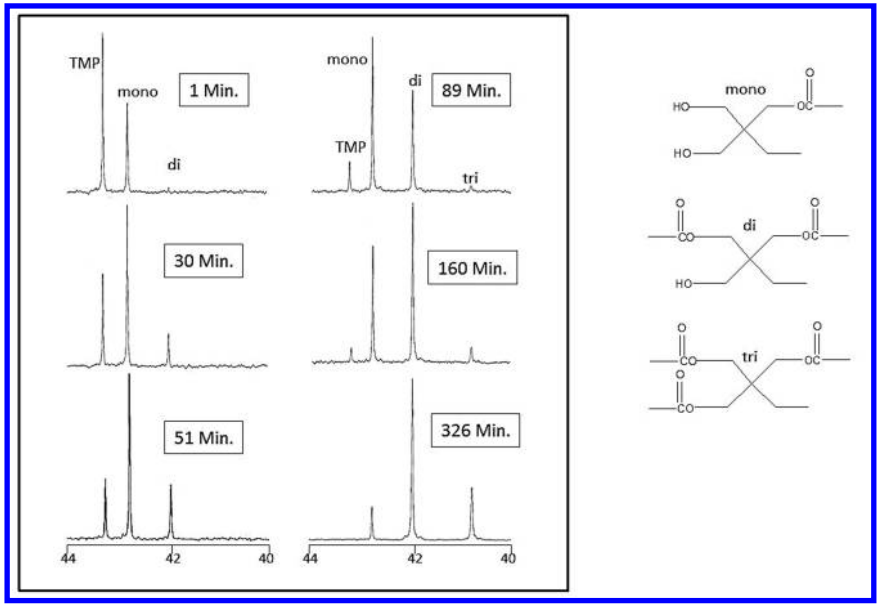

Figure 3. The ^{13}C NMR Spectra of the Quaternary Carbon Resonances of TMP for a Reaction Mixture of TMP and AA of Stoichiometry [OH]:[COOH] Equal to 1:1.

Publication Date (Web): November 22, 2013 | doi: 10.1021/bk-2013-1144.ch019

Kinetic Analysis

The esterification reaction between trimethylolpropane, TMP, and adipic acid, AA, was modeled as:

$$ROH + R'COOH \xrightarrow{k} R'COOR + H_2O$$

This expression assumes equal reactivity of the three hydroxyl groups of TMP and that the carboxylic acid functionality of adipic acid has equal reactivity regardless of whether the other carboxylate group in the molecule is acid or ester. A second assumption is that the esterification only proceeds to the right which is usually not the case because acid catalyzed esterifications are equilibrium reactions. However, since water is being removed throughout the reaction to drive the equilibrium to the right, this expression represents a good approximation of the process. The rate equation for this reaction is the following:

$$\frac{d[ROH]}{dt} = -k\,[ROH][R'COOH]$$

In Green Polymer Chemistry: Biocatalysis and Materials II; Cheng, H., et al.;
ACS Symposium Series; American Chemical Society: Washington, DC, 2013.

If the reaction is run at 1:1 [OH]:[COOH] stoichiometry such that:

$$[ROH] = [R'COOH] = [R]$$

$$\frac{d[R]}{dt} = -k\,[R]^2$$

Integrating:

$$\frac{1}{[R]_t} = \frac{1}{[R]_o} + kt$$

The extent of reaction, P, is defined as:

$$P = \frac{[R]_0 - [R]_t}{[R]_0}$$

$$\frac{1}{1-P} = 1 + k[R]_0$$

If one plots 1/(1-P) as a function of time, one should get a straight line of slope k $[R]_0$ with an intercept of 1.0. Figure 4 shows a typical plot of 1/(1-P) as a function of time for the 1:1, [OH]:[COOH] stoichiometry TMP, AA reaction with 2.5 mole% p-TSA as catalyst. The plot behaves as one would expect, a straight line behavior with an intercept of 1.0. (Time zero on these plots is shifted 10 to 20 minutes because there is a finite time for the reactor to come to temperature.) The three overlayed plots on the graph of Figure 4 were taken from the ^{1}H NMR spectra of the reaction as a function of time as well as the quaternary carbon and the carbonyl carbon from the ^{13}C NMR spectra, validating the assumption that carbons of the same type (e.g., the quaternary carbon of TMP and that of the mono, di and triester) have very similar NOE and T_1 values and therefore, give kinetic data consistent with the quantitative ^{1}H NMR spectra. The rate constant values from the three sets of data, 4.2, 4.4 and 3.5 x 10^{-3} l/mol-min are equivalent within the precision of the experiment (10% relative). Therefore, the assumption that $k_1 = k_2 = k_3$ and that each carboxylic acid functional group of adipic acid has equal reactivity is valid within the precision of the measurement.

The reaction was run as a function of catalyst level, varying from 0.5 mole% to 5 mole% based on TMP hydroxyl functionality. The rates for these catalyst concentrations are given in Table 1. The rates showed a significant increase in rate as the catalyst level is increased, leveling off above 2.5 mole%.

Publication Date (Web): November 22, 2013 | doi: 10.1021/bk-2013-1144.ch019

In Green Polymer Chemistry: Biocatalysis and Materials II; Cheng, H., et al.;
ACS Symposium Series; American Chemical Society: Washington, DC, 2013.

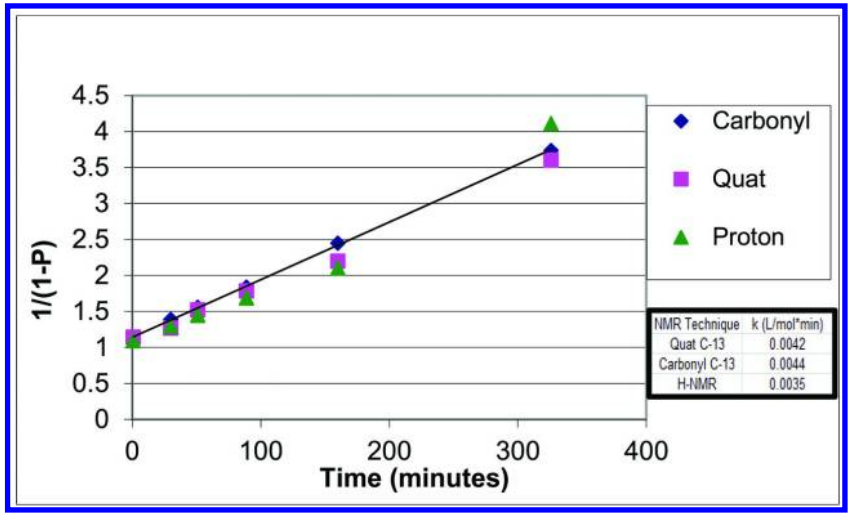

Figure 4. The Reaction Profile for TMP, AA 1:1, [OH]:[COOH] Stoichiometry, 2.5 mole% p-TSA.

Table 1. The Dependence of the Reaction Rate Constant, *k*, on Catalyst Concentration

Catalyst Level (Mole%)	*Reaction Rate [l/mol-min]*
0.0	0.08×10^{-3}
0.5	1.6×10^{-3}
1.0	1.7×10^{-3}
2.5	4.2×10^{-3}
5.0	4.7×10^{-3}

Conclusions

The kinetics of the esterification reaction of TMP and AA yielding a hyperbranched polyester were characterized by NMR spectroscopy. The reaction kinetics are approximations only, due to the process by which water was removed from the reaction with a soxhlet extraction. This process caused the concentration of the reactants to cycle as well as the reaction temperature, due to the fact that the temperature was controlled by reflux conditions. Even so, the analysis is instructive since it provided assurance that the NMR assignments of these copolymers are correct. It also documented that the rate of the reaction increases as the level of p-TSA is increased from 0.5 mole% to 5 mole%. Most syntheses of this type in the literature use very low levels of p-TSA catalyst. This study indicates that higher levels of p-TSA promote faster esterification rates.

In Green Polymer Chemistry: Biocatalysis and Materials II; Cheng, H., et al.;
ACS Symposium Series; American Chemical Society: Washington, DC, 2013.

Publication Date (Web): November 22, 2013 | doi: 10.1021/bk-2013-1144.ch019

References

1. Kulshrestha, A. S.; Gao, W.; Fu, H.; Gross, R. A. *Biomacromolecules* **2007**, *8*, 1794–1801.
2. Kricheldorf, H. R.; Behnken, G. *Macromolecules* **2008**, *41*, 5651–5657.
3. Kricheldorf, H. R.; Behnken, G. *J. Polym. Sci., Part A: Polym. Chem.* **2009**, *47*, 231–238.
4. Malmstrom, E.; Johansson, M.; Hult, A. *Macromolecules* **1995**, *28*, 1698–1703.
5. Bruggeman, J. P.; Bettinger, C. J.; Nijst, C. L. E.; Kohane, D. S.; Langer, R. *Adv. Mater.* **2008**, *20*, 1922–927.
6. Barret, D. G.; Luo, W.; Yousaf, M. N. *Polym. Chem.* **2010**, *1*, 296–302.
7. Kricheldorf, H. R.; Behnken, G. *Macromolecules* **2008**, *41*, 5651–5657.
8. Magnusson, H.; Malmstrom, E.; Hult, A. *Macromolecules* **2000**, *33*, 3099–3104.
9. Fischer, A. M.; Frey, H. *Macromolecules* **2010**, *43*, 8539–85448.
10. Cao, H.; Zheng, Y.; Zhou, J.; Wang, W.; Pandit, A. *Polym. Int.* **2011**, *60*, 630–634.
11. Yang, Y.; Lu, W.; Cai, J.; Hou, Y.; Ouyang, S.; Xie, W.; Gross, R. A. *Macromolecules* **2011**, *44*, 1977–1985.
12. Kulshrestha, A. S.; Gao, W.; Gross, R. A. *Macromolecules* **2005**, *38*, 3193–3204.
13. Carnahan, M. A.; Grinstaff, M. W. *Macromolecules* **2001**, *34*, 7648–7655.
14. Stumbe, J.-F.; Bruchmann, B. *Macromol. Rapid Commun.* **2004**, *25*, 921–924.
15. Wyatt, V. T.; Strahan, G. D. *Polymers* **2012**, *4*, 396–407.
16. Carnahan, M. A.; Grinstaff, M. W. *J. Amer. Chem. Soc.* **2001**, *123*, 2905–2906.
17. Brioude, M. d. M.; Guimaraes, D. H.; Fiuza, R. d. P.; Prado, L. A. S. d. A.; Boaventura, J. S.; Jose, N. M. *Mat. Res.* **2007**, *10*, 335–339.
18. Coneski, P. N.; Rao, K. S.; Schoenfisch, M. H. *Biomacromolecules* **2010**, *11*, 3208–3215.
19. Cao, W.; Zhou, Z.; Wang, Y.; Zhu, L. *Biomacromolecules* **2010**, *11*, 3680–3687.
20. Ifran, M.; Seiler, M. *Ind. Eng. Chem. Res.* **2010**, *49*, 1169–1196.
21. Lin, C.; Gitsov, I. *Macromolecules* **2010**, *43*, 10017–10030.
22. Shi, X.; Wang, S. H.; Lee, I.; Shen, M.; Baker, J. R., Jr. *Biopolymers* **2009**, *91*, 936–942.
23. Ye, L.; Letchford, K.; Heller, M.; Liggins, R.; Guan, D.; Kizhakkedathu, J. N.; Brooks, D. E.; Jackson, J. K.; Burt, H. M. *Biomacromolecules* **2011**, *12*, 145–155.
24. Chaterjee, S.; Ramakrishnan, S. *Macromolecules* **2011**, *44*, 4658–4664.
25. Gao, C.; Yan, D. *Prog. Polym. Sci.* **2004**, *29*, 183–275.
26. Mishra, M. K.; Kobayashi, S. *Star and Hyperbranched Polymers*; Mercel Dekker, Inc.: New York, 1999; p 53.
27. Coullerez, G.; Lundmark, S.; Malmstrom, E.; Hult, A.; Mathieu, H. J. *Surf. Interface Anal.* **2003**, *35*, 693–708.
28. Dvornic, P. U.S. Patent 6,812,298, 2004.

Publication Date (Web): November 22, 2013 | doi: 10.1021/bk-2013-1144.ch019

Publication Date (Web): November 22, 2013 | doi: 10.1021/bk-2013-1144.ch020

Chapter 20

Direct Fluorination of Poly(3-hydroxybutyrate-co)-hydroxyhexanoate

Samsuddin F. Mahmood, Benjamin R. Lund, Sriram Yagneswaran, Shant Aghyarian, and Dennis W. Smith, Jr.*

Department of Chemistry and the Alan G. MacDiarmid NanoTech Institute, The University of Texas at Dallas, Richardson, Texas 75080, U.S.A.
***E-mail: dwsmith@utdallas.edu**

Polyhydroxyalkanoates (PHAs) are a class of polymers synthesized by bacteria as intracellular carbon and energy storage granules. PHAs are biodegradable with tailorable physical properties; however, often their properties are not ideal for many applications. The incorporation of fluorine containing substituents within these polymers or direct surface modification to enhance the fluorine content of these polymers, and thus their surface properties, should greatly enhance their utility and speed their adoption for a range of applications. Direct fluorination of poly(3-hydroxybutyrate-co)-hydroxyhexanoate (hereafter P3HB-co-HH) was carried out at elevated pressure with elemental F_2/N_2 gas mixture. Fluorination of P3HB-co-HH showed marked changes in both thermal and chemical characteristics. Fluorination was demonstrated by X-Ray Photoelectron Spectroscopy (XPS), Attenuated Total Reflectance – Fourier Transform Infrared Spectroscopy (ATR-FTIR), and Nuclear Magnetic Resonance Spectroscopy (^{19}F NMR). The effect of fluorination on the physical properties of F-P3HB-co-HH was probed by Gel Permeation Chromatography (GPC), Thermo Gravimetric Analysis (TGA) and Differential Scanning Calorimetry (DSC).

In Green Polymer Chemistry: Biocatalysis and Materials II; Cheng, H., et al.;
ACS Symposium Series; American Chemical Society: Washington, DC, 2013.

Publication Date (Web): November 22, 2013 | doi: 10.1021/bk-2013-1144.ch020

Introduction and Background

Interest in biorenewable polymers among the scientific and industrial communities has grown substantially in recent years. Production from biorenewable feedstocks, degradation into biofriendly components, and (often) compatibility within the human body have made biorenewable polymers an excellent alternative to traditional petroleum based polymeric materials for specific applications. Among these, aliphatic polyesters (poly(lactic acid) PLA and poly(hydroxyalkanoates) PHA) have gained preeminence due to their facile synthesis and good physical properties (Figure 1) (*1*, *2*). By far, the greatest share of academic and industrial research has targeted PLA, however, PHAs are making inroads due to their unique plastic like properties (similar to polypropylene in some cases) and degradation under both aerobic and anaerobic conditions.

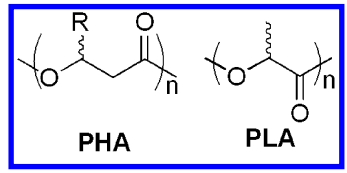

*Figure 1. General structures for poly(hydroxy alkanoate) (**PHA**) and poly(lactic acid) (**PLA**).*

Traditionally, synthesis of PLA polymers has been achieved by oligomerization of lactic acid, cyclization to lactide, and polymerization to high molecular weight polymers *via* ring opening polymerization with a tin catalyst (*3*). Lactide exists in two isomeric forms (D and L) can be polymerized as homo- or copolymers comprising various ratios of the two stereoisomers (Figure 2). Controlling monomer feed ratios allows for control over the properties of the resultant material in terms of crystallinity, thermal stability, rate of degradation, etc. (*4*). Additionally, blends of PLA with other polymers as well as copolymerization with other monomers (caprolactone for example) have worked to further expand the breadth of physical properties of known PLA polymers.

PLAs have been explored for a range of applications, with special interest paid by biomedical device community, due to its low cost and biocompatibility (*5*). In biological environments PLA degrades back to its monomeric form, lactic acid, which is a natural byproduct of the human body. This degradation is generally slow (being effected by surface area and crystallinity of the sample) and non-toxic due to the low amounts of biomimetic waste formed. Many PLA based devices have been approved by the FDA for applications ranging from bone plates to drug eluting stents (*6*).

In Green Polymer Chemistry: Biocatalysis and Materials II; Cheng, H., et al.;
ACS Symposium Series; American Chemical Society: Washington, DC, 2013.

Publication Date (Web): November 22, 2013 | doi: 10.1021/bk-2013-1144.ch020

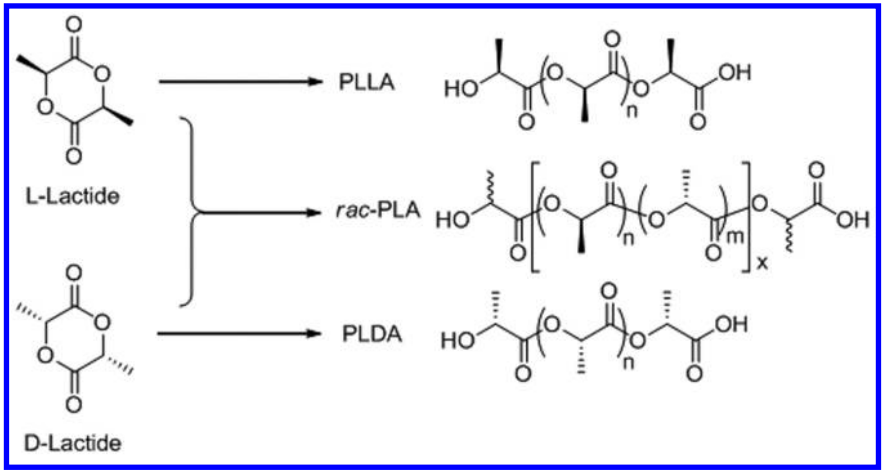

Figure 2. Ring opening polymerization (ROP) of lactide (L or D). Homopolymers of L and D lactide form PLLA and PLDA as well as random copolymer of L and D lactide to form D,L-PLA or racemic PLA if molar ration of L to D is 50:50.

PHA polymers are synthesized by an entirely different route from PLA polymers. Bacteria form PHA macromolecules as intracellular carbon and energy storage granules (*7*). These bacteria can be encouraged to synthesize PHA polymers in bioreactors by culturing them, allowing them to grow, stimulating them to produce PHA polymers (via changing the environment of the culture, decreasing nutrient levels, lowering oxygen levels, changing trace element concentrations, etc.) and then harvesting the PHA polymers from the bacteria (via centrifugation, extraction, and precipitation) (Figure 3). The resultant properties of the PHA polymer can be tailored by the feedstock (monomer) given to the bacteria (*8*).

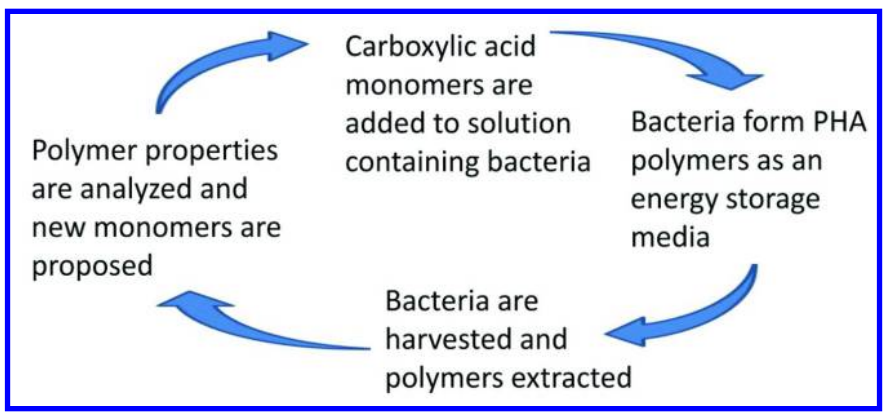

Figure 3. General lifecycle of PHA synthesis and development.

In Green Polymer Chemistry: Biocatalysis and Materials II; Cheng, H., et al.;
ACS Symposium Series; American Chemical Society: Washington, DC, 2013.

Publication Date (Web): November 22, 2013 | doi: 10.1021/bk-2013-1144.ch020

Fluorine Containing PLAs and PHAs

Fluoropolymers possess many desirable properties such as excellent thermal stability, chemical inertia, solvent resistance, excellent barrier properties, low coefficient of friction and low surface energy, to name a few (*9*). Many of these properties are of particular interest to applications where surface interactions are important such as paints, adhesives, biomaterials, coatings, etc. Fluoropolymers, however are often difficult to process, lacking solubility in many common solvents, and phase separate when blended with many engineering thermoplastics. Alternative techniques including the formation of block copolymers, end capping and surface functionalization through physical and chemical means have been employed to enable the interaction of fluorinated and non-fluorinated materials.

PLAs and PHAs possess many useful qualities, as previously discussed; however, their physical properties are not ideal for many applications. The incorporation of fluorine containing substituents within these polymers or direct surface modification to enhance the fluorine content of these polymers, and thus their surface properties, should greatly enhance their utility and speed their adoption for a range of applications.

One such application, explored by Lee *et al*, was the controlled functionalization of a fluorine endcapped poly(lactide-co-glycolide) surface by plasma treatment (*10*). Due to the favorable interactions of fluorine at the air polymer interface the fluorocarbon segments bloomed to the surface, displacing proximal hydrophilic hydroxyl functionalities. Subsequent plasma treatment was utilized to predictably control the hydroxyl functionalization of the fluorocarbon surface for anchoring of a range of biomolecules. Endcapping of the poly(lactide-co-glycolide) polymers was achieved utilizing a hydroxyl terminated fluorocarbon (Figure 4). This approach produced polymers with molecular weights (M_n) varying from 14 KDa to 74.3 KDa (PDI ~2) and T_gs ranging between 35 and 53 °C with T_ms between 156 and 174 °C.

Alternately, work on diblock copolymers of poly(lactic acid-co-perfluoropropylene oxide) (PLA-FPO) was used to explore the formation of micelles in supercritical CO_2 (*11*). Fluoropolymers exhibit excellent solubility in supercritical CO_2 whereas PLA does not. The formation of amphiphilic PLA-FPO copolymers allowed for the preferential segregation of these polymers into micelles in supercritical CO_2.

The formation of fluorocarbon enchained triblock copolymers with PLA was initially performed to enhance the processability of caprolactone triblock copolymers with enchained Fomblin™ Z-DOL TX (*12*). Due to the selective chiral nature of PLA (L, D, or rac) the incorporation of PLA was utilized to decrease the crystallinity of the caprolactone triblock copolymer and enhance the processability of the system. The PLA copolymers exhibited glass transitions (T_g) ranging from -60 to 15 °C with increasing PLA content and melting temperatures from 35 to 47 °C with increasing caprolactone content.

In a similar fashion, our group explored the formation of segmented copolymers with PLA and fluorocarbon segments. Specifically, triblock copolymers of PLA-Fomblin-PLA were formed with a range of fluorine loading levels (1-20 wt%) (*13*). It was found that the optimum loading of fluorine

In Green Polymer Chemistry: Biocatalysis and Materials II; Cheng, H., et al.;
ACS Symposium Series; American Chemical Society: Washington, DC, 2013.

occurred at 5 wt% whereas higher fluorine loading levels produced little change in the polymer's properties. Further work done by our group explored the scalability of these systems to understand their potential for industrial applications (*14*). It was found that batches on the liter scale were attainable with excellent reproducibility. Specific applications of this system have been researched for historical preservation applications (*15*, *16*).

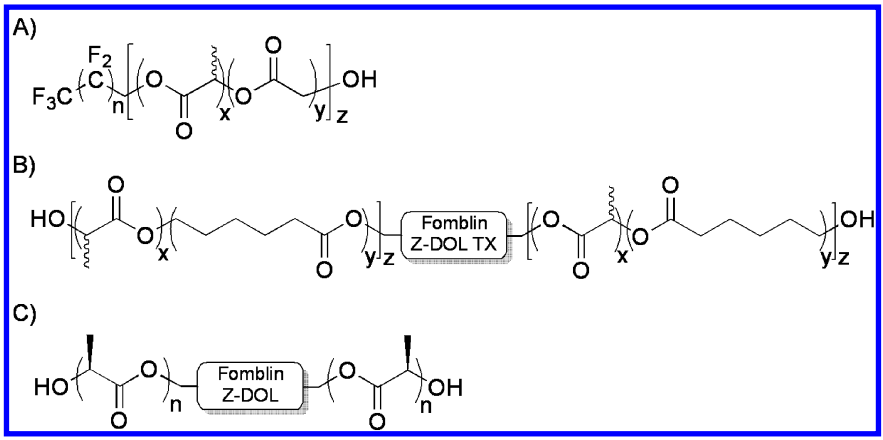

Figure 4. PLA endcapped and enchained fluoropolymers. (A) Fluorocarbon endcapped poly(lactide-co-glycolide). (B) Segmented triblock copolymer with Fomblin Z-DOL TX core and flanking random poly(caprolactone/D,L-lactide) copolymer segments. (C) Segmented triblock copolymers with Fomblin Z-DOL core and flanking PLLA homopolymer segments.

Alternately, early work on fluorinated PHA polymers was achieved through microbe synthesis, feeding *pseudomonas putida* fluorophenoxy alkanoic acids and stimulating the bacteria grown the fluorinated PHA polymer (Figure 5). Molecular weights (M_n) of ~10,000 Da were achieved with reasonable polydispersities (PDI ~2-3) (*8*). Uniquely, melting temperatures of >100 °C were attained for these fluoro PHA polymers.

More recent work on poly(3-hydroxybutyric acid-co-3-hydroxyvaleric acid) (PHBV) utilized plasma polymerization to form fluoropolymer films on the surface of PHA polymers to enhance barrier properties and retard degradation. Plasma fluorination was achieved by utilizing a plasma source (14.56 Hz rf generator) and a fluorocarbon feedstock. The fluorocarbon was introduced to the plasma where it began to dimerize, oligomerize and polymerize in the gas phase. The reactive fluorocarbon material condensed onto the PHA surface, reacting with it and each other to form a dense, often crosslinked, fluoropolymer layer on top of the PHA. The process enhanced the contact angle of the PHA polymers from 74° to 98° and dramatically extended its degradation from 5 days to 8-14 days (depending on fluorination conditions) (*17*). Indeed, this technique has been extended to PLA polymers where it has shown to increase the contact angle from 54° to 80° and

Publication Date (Web): November 22, 2013 | doi: 10.1021/bk-2013-1144.ch020

to impart antimicrobial properties to the PLA films (*18*). An obvious, but to date untested extension of this work would be to extend these methodologies to the direct fluorination of PLA and PHA polymeric materials.

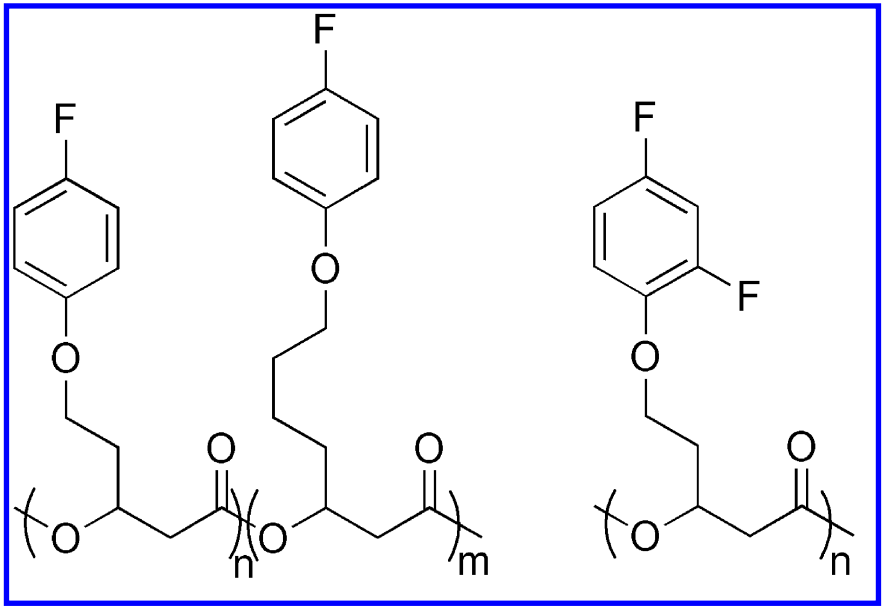

Figure 5. Bacterially synthesized fluoro-functionalized PHA polymers.

Direct fluorination, a process whereby gaseous fluorine (F_2) is utilized to functionalize a surface, exchanges C-H bonds for C-F bonds, producing HF as a byproduct. Direct fluorination is a surface technique, functionalizing to a depth of 0.01 to 10 μm, while leaving the bulk unchanged. This process often results in enhanced chemical resistance, and improved barrier properties, however as fluorine is an aggressive oxidant, it may also result in lower molecular weight (*19*) due to oxidative degradation of the polymer chains.

Direct Fluorination

General Procedure for Direct Fluorination Using 5% F_2 in a N_2 Gas Mixture

Direct fluorination was carried out at room temperature in a stainless steel flow reactor designed and built in our lab. A picture of the reactor (top) as well as a schematic diagram (bottom) of the reactor are shown in the Figure 6. The reactor is composed of a stainless steel vessel equipped with a pressure gauge (up to 60 psi) and removable lid mounted on shaker and connected via flexible tubing to the reactive (5% F_2/N_2) and purge (N_2) gases. N_2 and 5% F_2/N_2 gas are connected upstream to the reactor with a scrubber (equipped with soda lime pellets), vacuum and bubbler (filled with fluorinated oil) downstream. This set-up facilitates the evacuation, loading and purging of the system with minimal opportunity for leakage of F_2.

Publication Date (Web): November 22, 2013 | doi: 10.1021/bk-2013-1144.ch020

Publication Date (Web): November 22, 2013 | doi: 10.1021/bk-2013-1144.ch020

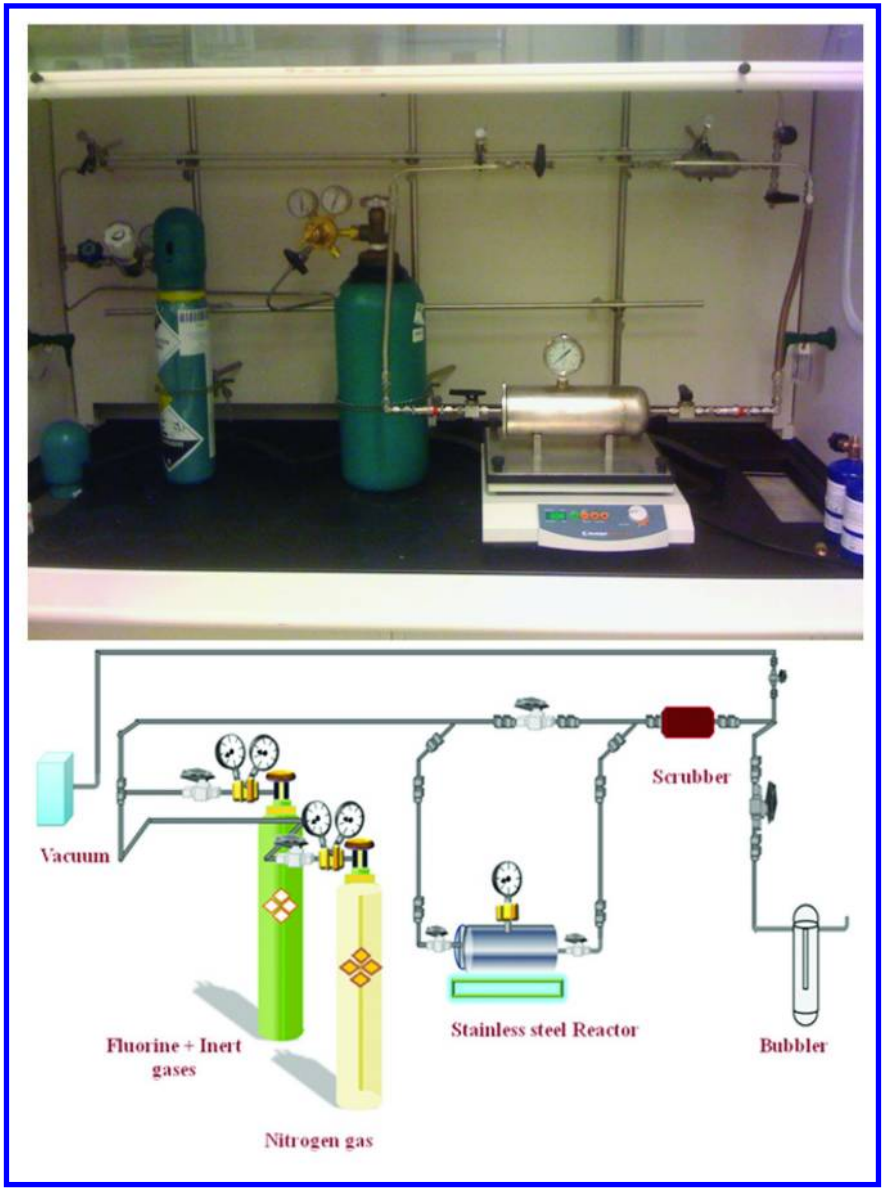

Figure 6. Picture (top) and schematic diagram (bottom) of the direct fluorination reactor at The University of Texas at Dallas.

A Typical Procedure

Samples to be fluorinated are dried (often in a vacuum oven or vacuum dessicator for 24 h) and then transferred into the stainless steel fluorination reactor which is sealed with the aid of a fluorinated lubricant (applied around the door of the reactor). The system is then evacuated, purged with nitrogen (until positive pressure is observed in the reactor gauge), evacuated again, and finally charged with fluorine to the desired pressure. The system is then sealed and set to agitate for the allotted time of the reaction. Once complete, the reaction is pacified by slowly venting the remaining F_2 and evolved HF through a scrubber and testing the effluent for excess corrosive gas (with KI paper). The system is finally purged with a steady flow of nitrogen after which the reaction vessel is opened and the reactants removed.

Fluorination of PHA Polymers

Fluorination was performed using dilute F_2 gas at room temperature in the described reactor utilizing the general procedure previously described (*vide supra*). Specific details are as follows: PHA = Poly(3-hydroxybutyrate-co)-hydroxyhexanoate, F_2 gas was at a concentration of 3-5% diluted in N_2. The reaction was performed at 20 psi for 24 h.

Evidence of Fluorination

While fluorination is generally considered a surface modification technique, visible changes were observed in the bulk of the PHA sample. Whereas the starting material was white and powdery in appearance, the fluorinated product appeared creamy yellow in color with a sticky, almost gummy, consistency. Solubilization in chloroform, an excellent solvent for PHA, was attempted and insoluble material was removed. FTIR of the insoluble material was complex and was set aside. The following discussion pertains to the soluble component of the reaction product.

Spectroscopic analyses of the fluorinated PHA (F-PHA) was attempted by both XPS (atomic analysis) as well as FTIR and NMR spectroscopies (functional group analysis). XPS analysis of the neat PHA versus F-PHA shows a new peak at 700 eV corresponding to the F1s electron in the F-PHA sample (Figure 7A). Analysis of this peak reveals a 5 % fluorine composition of F-PHA compared to its complete absence in neat PHA. Further, ATR-FTIR of the F-PHA revealed the formation of new peaks around 1300 cm^{-1}, 700 cm^{-1} and 1180 cm^{-1}. These absorbances correspond to vibrational modes of $-CF_3$ and $-CF_2-$ moieties, suggesting the fluorination of PHA. An overlay of neat PHA and F-PHA is shown in Figure 7B. It is worth noting that these results are in good agreement with the aforementioned study performed by Guerrouani *et al* (2007) (*17*). Finally, ^{19}F-NMR shows clear peaks at -75, -83, -114, -123 and -127 ppm corresponding to terminal and methylene perfluorinated and fluorinated alkanes, no such absorbances are observed in the neat PHA. These analyses clearly indicate the

In Green Polymer Chemistry: Biocatalysis and Materials II; Cheng, H., et al.;
ACS Symposium Series; American Chemical Society: Washington, DC, 2013.

Publication Date (Web): November 22, 2013 | doi: 10.1021/bk-2013-1144.ch020

presence of fluorine into a variety of chemical environments within the F-PHA structure. Analysis into the specific mechanism of the fluorination of PHA is currently ongoing.

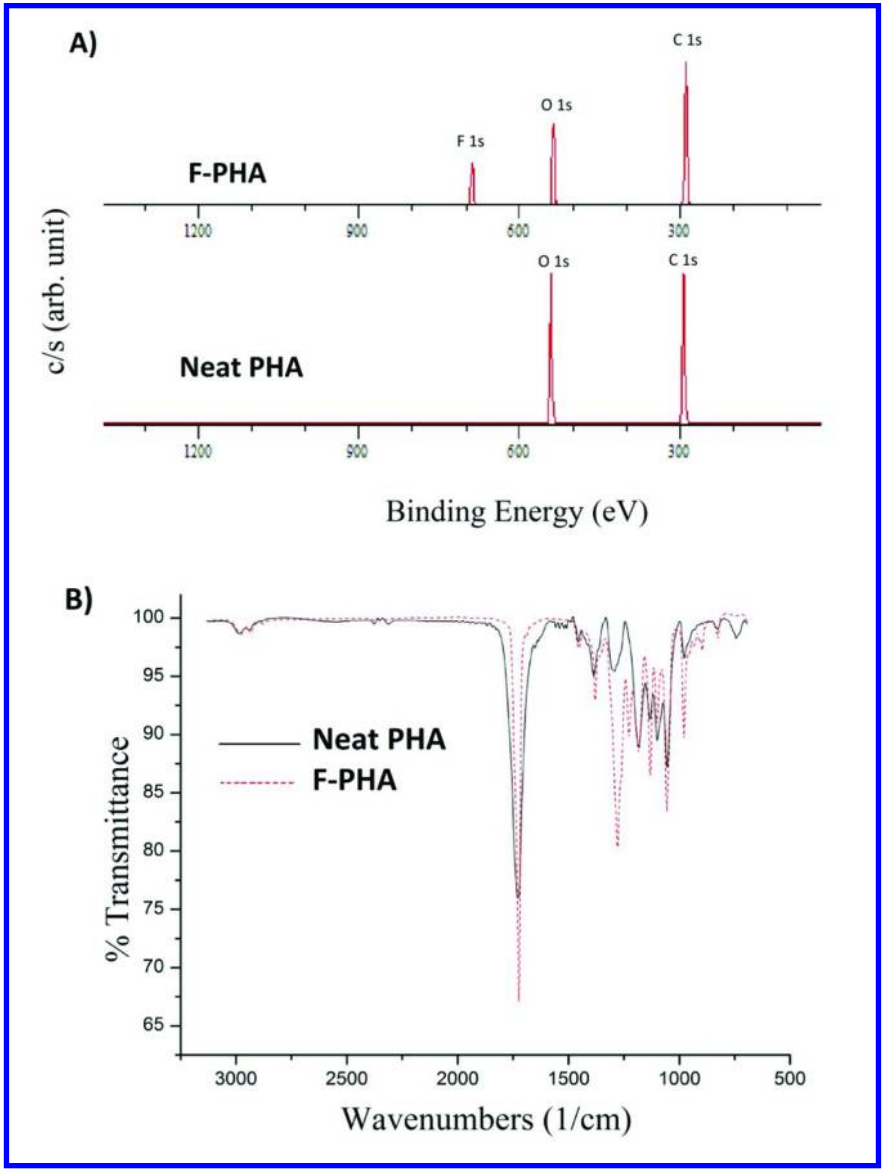

Figure 7. XPS (A) and ATR-FTIR (B) spectra of neat PHA and F-PHA.

Publication Date (Web): November 22, 2013 | doi: 10.1021/bk-2013-1144.ch020

Effect of Fluorination

Substantial changes in the physical and thermal properties of PHA were observed post fluorination. A dramatic decrease in the molecular weight of F-PHA was observed from an initial M_n = ~126 KDa (neat PHA) to a M_n = ~13 KDa. The reason for this decrease is still under investigation, however the prevailing theories focus around F_2 mediated chain scission or HF catalyzed hydrolysis of the ester functionalities along the PHA backbone (*17*, *20*). The effect of this decreased molecular weight can be observed in the TGA where the thermal stability of the F-PHA is decreased substantially. While ultimate degradation remained near 300 °C, the onset of degradation began much sooner around 120 °C (N_2) or 50 °C (Air) (Figure 8). Indeed, the DSC analysis of this material shows a complete loss of thermal properties. Whereas neat PHA possesses transitions at -1 °C (T_g), 62 °C (T_c) and, 126 and 145 °C (T_m), F-PHA shows no discernible thermal transitions. These changes in the thermal properties of the F-PHA can be attributed to the tenfold decrease in its molecular weight and are potentially useful for applications which require enhanced degradation at lower temperatures.

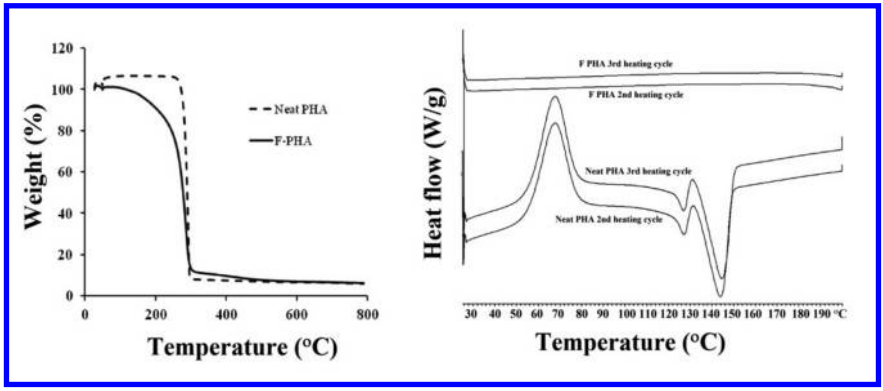

Figure 8. TGA (left) and DSC (right) of PHA and F-PHA in nitrogen.

Future Prospective

F-PHA materials are of much current interest as compatibilizing agents for fluoropolymers with aliphatic polyester (PLA, PHA) polymers, especially for biomedical devices. Successful fluorination of PHA polymers using fluorine gas was achieved forming low molecular F-PHA. Exploration of the specific mechanism of fluorination and chain scission is currently ongoing as well as studies on the efficacy of F-PHA as a compatibilizing agent in blended systems and degradation studies including hydrolysis (in neutral and acid/base conditions).

In Green Polymer Chemistry: Biocatalysis and Materials II; Cheng, H., et al.;
ACS Symposium Series; American Chemical Society: Washington, DC, 2013.

Publication Date (Web): November 22, 2013 | doi: 10.1021/bk-2013-1144.ch020

Publication Date (Web): November 22, 2013 | doi: 10.1021/bk-2013-1144.ch020

Acknowledgments

The authors would like to thank the Robert A. Welch Foundation (Grant AT-0041), the Alan G. MacDiarmid NanoTech Institute, the Center for Energy Harvesting Materials and Systems (NSF-I/UCRC, Grant 1035024) and the University of Texas at Dallas for their generous support. We would also like to thank Proctor and Gamble Co. for kindly supplying PHA samples under the trade name, NODAX.

References

1. Garlotta, D. *J. Polym. Environ.* **2001**, *9*, 63.
2. Chen, G. Q.; Wu, Q. *Biomaterials* **2005**, *26*, 6565.
3. Drumright, R. E.; Gruber, P. R.; Henton, D. E. *Adv. Mater.* **2000**, *12*, 1841.
4. Perego, G.; Cella, G. D.; Bastioli, C. *J. Appl. Polym. Sci.* **1996**, *59*, 37.
5. Lasprilla, A. J. R.; Martinez, G. A. R.; Lunelli, B. H.; Jardini, A. L. *Biotechnol. Adv.* **2012**, *30*, 321.
6. Wu, M.; Kleiner, L.; Tang, F. W.; Hossainy, S.; Davies, M. C.; Roberts, C. J. *Drug Delivery* **2010**, *17*, 376.
7. Anderson, A. J.; Dawes, E. A. *Microbiol. Rev.* **1990**, *54*, 450.
8. Takagi, Y.; Yasuda, R.; Maehara, A.; Yamane, T. *Eur. Polym. J.* **2004**, *40*, 1551.
9. Scheirs, J. *Modern Fluoropolymers: High Performance Polymers for Diverse Applications*; Wiley: New York, 1997.
10. Lee, W. K.; Losito, I.; Gardella, J. A., Jr; Hicks, W. L., Jr. *Macromolecules* **2001**, *34*, 3000.
11. Edmonds, W. F.; Hillmyer, M. A.; Lodge, T. P. *Macromolecules* **2007**, *40*, 4917.
12. Bongiovanni, R.; Malucelli, G.; Messori, M.; Pilati, F.; Priola, A.; Tonelli, C.; Toselli, M. *J. Polym. Sci., Part A: Polym. Chem.* **2005**, *43*, 3588.
13. Haynes, D.; Naskar, A. K.; Singh, A.; Yang, C. C.; Burg, K. J.; Drews, M.; Harrison, G.; Smith, D. W., Jr. *Macromolecules* **2007**, *40*, 9354.
14. Singh, A.; Naskar, A. K.; Haynes, D.; Drews, M. J.; Smith, D. W., Jr. *Polym. Int.* **2011**, *60*, 507.
15. Frediani, M.; Rosi, L.; Camaiti, M.; Berti, D.; Mariotti, A.; Comucci, A.; Vannucci, C.; Malesci, I. *Macromol. Chem. Phys.* **2010**, *211*, 988.
16. Giuntoli, G.; Rosi, L.; Frediani, M.; Sacchi, B.; Frediani, P. *J. Appl. Poly. Sci.* **2012**, *125*, 3125.
17. Guerrouani, N.; Baldo, A.; Maarouf, T.; Belu, A. M.; Kassis, C. M.; Mas, A. *J. Fluorine Chem.* **2007**, *128*, 925.
18. Boonyawan, D.; Sarapirom, S.; Tunma, S.; Chaiwong, C.; Rachtanapun, P.; Auras, R. *Surf. Coat. Technol.* **2011**, *205*, S552.
19. Rand, A. A.; Mabury, S. A. *Environ. Sci. Technol.* **2011**, *45*, 8053.
20. Lagow, R.; Wei, H.-C. In *Fluoropolymers 1: Synthesis*; Hougham, G., Cassidy, P., Johns, K., Davidson, T., Eds.; Springer New York: 2002; p 209.

Publication Date (Web): November 22, 2013 | doi: 10.1021/bk-2013-1144.ch021

Chapter 21

Biobased Industrial Products from Soybean Biorefinery

E. Hablot, D. Graiver, and R. Narayan*

Department of Chemical Engineering and Materials Science, Michigan State University, East Lansing, Michigan 48824, U.S.A.
***E-mail: narayan@msu.edu**

The use of biomass as raw materials for the production of fuels and chemicals to displace fossil resources has been the focus of many research activities in recent years. These activities are motivated by the desire for a sustainable resource supply, enhanced national security, and macroeconomic benefits for rural communities and the society at large. The use of plastic materials in the modern world has been increasing rapidly due to the relatively low cost of production and specific set of properties that can be derived from them. Until recently crude oil was the major source of these basic chemicals and value-added polymeric materials. Sustainable economics requires a similar wide range of processes that can utilize every component of these renewable resources. In our work with soybeans, we have used all parts of the bean (meal, oil and hulls) as a source of materials that can be converted economically to value-added products. The focus of this paper is to provide a few examples of this biorefinery concept that includes a catalyzed ozonation process of oil triglycerides to produce polyols, the conversion process of proteins in the meal to rigid polyurethane foams and the production of isocyanate-free polyurethanes from dimer acids. We will also review a novel silylation process that yields moisture activated RTV coatings from vegetable oils.

In Green Polymer Chemistry: Biocatalysis and Materials II; Cheng, H., et al.;
ACS Symposium Series; American Chemical Society: Washington, DC, 2013.

Publication Date (Web): November 22, 2013 | doi: 10.1021/bk-2013-1144.ch021

Introduction

The use of biomass as raw materials for production of fuels and chemicals to displace fossil resources has been the focus of many research activities in recent years. These activities are motivated by the possibility of positive contributions to a sustainable resource supply and macroeconomic benefits for local communities and the society at large. Much of these activities are directed following the biorefinery concept which integrates biomass conversion and equipment to produce fuels, energy and chemicals. Industrial biorefineries have been identified as the most promising route to the creation of a new domestic biobased industry. By producing a large range of products, a biorefinery can take advantage of the diversity in biomass components and intermediates to increase the value derived from the biomass feedstock. Furthermore, a viable biorefinery should produce low-volume but high-value chemicals with high profit margins as well as high-volume but low-value products such as biofuel and commodity products. The biofuel can be used to meet the national energy needs as well as providing energy for in-house use to reduce process costs and minimize CO_2 emission from fossil fuel.

Soybean is an attractive candidate for such biorefinery transformation since it is readily available and its relatively low price ($430/T in the USA in 2010 (*1*)). The soybean is primarily an industrial crop cultivated for its oil and proteins and both can be used as raw materials for industrial products and intermediates. A typical soybean composition is presented in Figure 1. Although the exact composition of the bean depends on many variables including trait, climate, soil, geographical location, maturity, the extraction process, etc. it is apparent that the protein content in the bean is almost twice the content of the oil (about 38% compared with only 18% oil).

Despite the relatively low oil content in the bean, soybeans are the largest single source of edible oil and account for 52% of the total oil seed production of the world. According to FAO estimates over 260 million tonnes of soybean was produced worldwide in the year 2010 (*1*). Soybeans are grown predominantly in North and South America (Brazil and Argentina) where 34% and 47%, respectively, of the 2010/11 world's supply of beans was harvested (*2*).

The recovery of oil from the bean has been done for many years but both the process and the equipment have undergone continuous evolution through this time. Currently, the most common methods are hydraulic pressing, expeller pressing and solvent extraction. Presently, the solvent extraction process is the most common process using hexane as the solvent. The oil is found as triglycerides, which are tri-esters of glycerol with the fatty acids that are listed in Table I. It should be noted that the concentration of these fatty acids in the bean varies depending on the trait of the soy, the season and the growing conditions (humidity, light, soil, etc.) (*3*). In general, the soybean oil contains a significant amount of unsaturation on the order of 4.6 double bonds per triglyceride. These double bonds can be used as a starting point for various chemical modifications to modify the oil and produce new derivatives and chemicals.

In Green Polymer Chemistry: Biocatalysis and Materials II; Cheng, H., et al.;
ACS Symposium Series; American Chemical Society: Washington, DC, 2013.

Publication Date (Web): November 22, 2013 | doi: 10.1021/bk-2013-1144.ch021

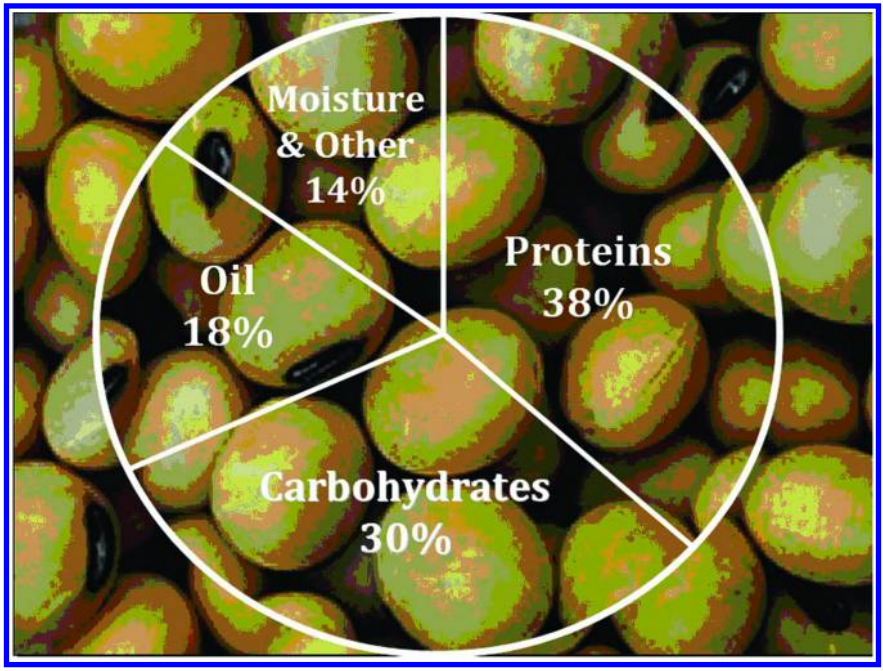

Figure 1. Typical soybean composition.

Table I. Typical soybean oil fatty acid composition

Fatty acid	Structure	%
Palmitic	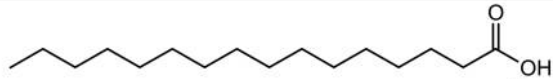	7-11
Stearic	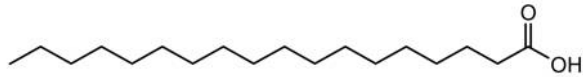	2-6
Oleic	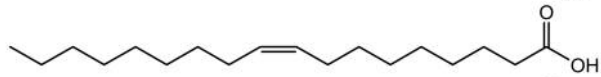	22-34
Linoleic	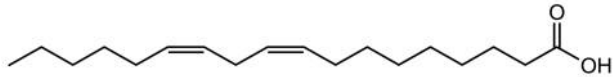	43-56
Linolenic	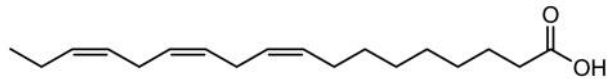	5-11
Myristic	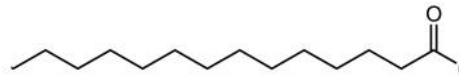	trace

In Green Polymer Chemistry: Biocatalysis and Materials II; Cheng, H., et al.;
ACS Symposium Series; American Chemical Society: Washington, DC, 2013.

Publication Date (Web): November 22, 2013 | doi: 10.1021/bk-2013-1144.ch021

Traditionally, soybean oil has been considered as a major agricultural crop of great importance for the food and feed market. Nowadays however, it is increasingly used as a feedstock for a wide variety of industrial products including lubricants, candles, cleaning products, hydraulic fluids, paint strippers, dust suppressants, solvents and printing inks (*4–6*). Recently, an increasing amount of soybean oil is also being used for biodiesel (*7*), which has led to increase soybean oil production and consequently a need to define new applications for the soymeal.

The left-over product from the oil extraction process is known as soymeal and is composed of proteins (44%), carbohydrates (36.5%), moisture (12%), fiber (7%) and fat (0.5%) (*8*). Most of the soymeal is processed toward animal feed primarily for poultry, swine, cattle, and aquaculture as soy flour, soy concentrates, or soy isolates. A relatively small portion is also processed for human consumption and even a smaller portion (about 0.5%) is used for industrial applications, primarily as adhesives for plywood and particle board. Some other minor applications also include additives in textured paints, insecticides, dry-wall tape compounds, linoleum backing, paper coatings, fire-fighting foams, fire-resistant coatings, asphalt emulsions, cosmetics and printing inks (*9*).

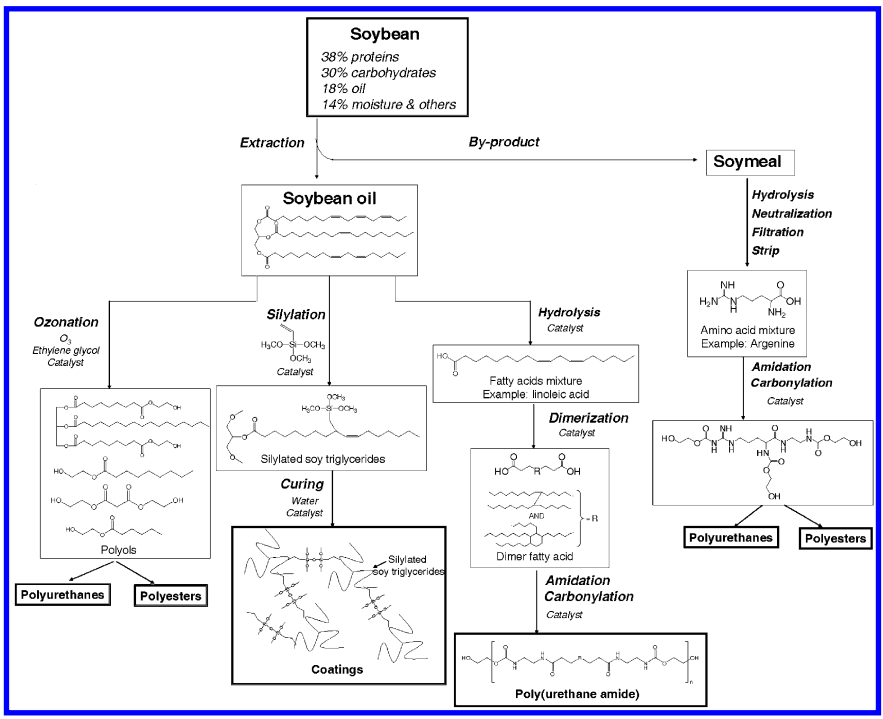

Figure 2. Technology platform for value-added industrial products from a soybean refinery.

In Green Polymer Chemistry: Biocatalysis and Materials II; Cheng, H., et al.;
ACS Symposium Series; American Chemical Society: Washington, DC, 2013.

In our work, we developed a multiple biorefinery processes that utilized both the oil and the meal of the soybean as the starting materials for various intermediates and industrial products. The general technology platforms are shown schematically in Figure 2. Special attention was directed toward complying with the 'green chemistry' principles for all the synthetic strategies that we employed. These include the use of non-hazardous reagents, solvent-less processes, and safe operating procedures. A brief description of some of these processes is described below.

Polyols by Ozonation of Soybean Oil

Publication Date (Web): November 22, 2013 | doi: 10.1021/bk-2013-1144.ch021

Polyols suitable for polymerization into polyurethane resins have been prepared in the past directly from hydroxyl containing castor oil (*10*, *11*). These early open cell foams were later improved by DuPont (*12*) and were made over a wide density range (2-20 lb./ft^3). However, castor oil contains secondary alcohol groups and a fairly low hydroxyl number. Consequently, polyurethane resins prepared from castor oil tend to be rubbery with inferior properties and are relatively expensive due to the relatively high cost of the oil.

Several methods are described in the literature that have been used to prepare polyols from soy oil. Alcoholysis of triglycerides with glycerol (*13*), α-methylglucoside or pentaerytol (*14*) has been used in the past. In this process the hydroxyl number of the product is determined by the ratio of the reagents. However, usually, this process requires an elevated temperature (250°C) and base catalysis such as sodium hydroxide (which must be carefully neutralized before adding the isocyanate to prepare the polyurethane). Problems due to premature degradation limit the use of the process.

Vegetable oil polyols are commonly prepared by epoxidation (*15*) whereby the oil is first reacted with peroxyacid acid (e.g. peracetic acid) for several hours and then hydroxylated (*16*). Although significant improvements have been realized since these reactions were first proposed, side-reactions including cyclization, transesterification, polymerization and undesirable by-products also occur. More importantly, secondary alcohols are obtained by this process which are inherently less reactive than primary alcohols and can adversely impact the polymerization process. Hydroformylation of vegetable oils leads to primary polyols. Here, an aldehyde functional oil is first obtained which is then hydrogenated to yield primary alcohols (*17*). Polyurethanes prepared from such polyols had different mechanical properties depending on the hydroformylation catalyst that was used. Thus, rigid materials at room temperature were obtained with a rhodium catalyst while cobalt catalyzed hydroformylation led to rubbery materials.

Various oxidation methods are available and all lead to primary alcohols. These methods utilize air at elevated temperatures, molecular oxygen (*18*), organic hydroperoxide in the presence of OsO_4 and a NaBr cocatalyst (*19*) or ozonation followed by decomposing ozonides to alcohols using $NaBH_4$ or similar reducing agents. Ozonation is most effective method due to the high reactivity of the ozone toward double bonds. In the past it was used to

In Green Polymer Chemistry: Biocatalysis and Materials II; Cheng, H., et al.;
ACS Symposium Series; American Chemical Society: Washington, DC, 2013.

determine the structure of olefins and identify the position of the double-bond. These analyses were based on the generally agreed mechanism (*20*) that the reaction occurs in several steps (Figure 3) starting with the formation of a 1,3-dipolar cycloaddition product from the insertion of ozone to the double bond. This cycloaddition product eventually decomposes into a mixture of aldehydes and carbonyl oxides which can be reduced to alcohols. Currently, it is used commercially by Emery-Oleochimicals group which produces around 10,000 tons per year of azelaic acid (nonane-1,9-dioic acid) along with pelargonic acid (nonanoic acid) by ozonolysis of oleic acid (*21*). Industrial scale ozonolysis is carried out in pelargonic acid run countercurrent to ozone at 25-45°C followed by decomposition at 60-100°C in excess oxygen (*22*, *23*).

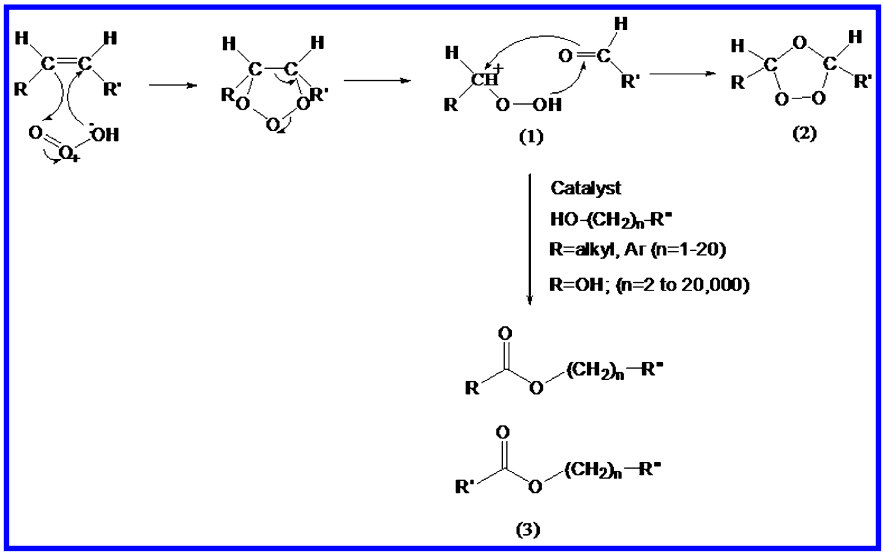

Figure 3. Generalized ozonolysis reaction where carbonyl oxide and aldehyde (structure 1) recombine to yield an ozonide intermediate (structure 2) which further reacts with an alcohol to yield an ester (structure 3).

Ozone, as an oxidation agent, has several distinct advantages over other oxidation agents. Since ozone is produced and used on-site, issues related to safe storage and transportation are avoided. Unreacted ozone is simply decomposed back to oxygen and no separation or removal of by products is needed as is the case with other oxidation agents. Production of ozone is fairly simple and involves passing an oxygen containing atmosphere through an ozone generator. Modern ozone generators are readily available; they are relatively inexpensive and are much more efficient than old models. However, care must be used since ozone is highly reactive and the ozonide intermediate can decompose violently. Thus, previous ozonation reactions were conducted at low temperatures (-78 °C) in dilute solutions usually with a chlorinated solvent and in small batches.

We investigated this reaction and devised a continuous process that can be run safely close to room temperature to produce vegetable oil polyols (*24–27*). In this process, the chain-ends that are formed by the cleavage of the double

In Green Polymer Chemistry: Biocatalysis and Materials II; Cheng, H., et al.;
ACS Symposium Series; American Chemical Society: Washington, DC, 2013.

Publication Date (Web): November 22, 2013 | doi: 10.1021/bk-2013-1144.ch021

bonds are coupled with low molecular weight alcohols containing multiple hydroxyl groups (e.g. ethylene glycol, glycerol, etc.). As shown in Figure 4, the cleavage of the double bonds and the subsequent esterification reaction to yield the new chain-ends hydroxyl groups lead to a product distribution containing hydroxyl terminated short molecular weight triglycerides and linear mono- and difunctional hydroxylated species. Thus, oleic acid would be cleaved at the double bond in the 9th carbon leaving 2-hydroxy nonanoate residue on the triglyceride and 2-hydroxyethyl nonanoate (Figure 4A). Similarly, linoleic acid would be cleaved at the double bonds to yield 2-hydroxy nonanoate residue on the triglyceride, 2-hydroxyethyl hexanoate and bis(2-hydroxyethyl) malonate (Figure 4B). Linolenic acid, which contains multiple unsaturations at the 9th, 12th, and 15th positions would yield the same 2-hydroxy nonanoate residue on the triglyceride, 2-hydroxyethyl propionoate and bis(2-hydroxyethyl) malonate (Figure 4C). The saturated fatty acids (e.g. palmitic and stearic) are not cleaved by the ozone and remain intact. The statistical distribution of these polyols is shown in Figure 5 whereby 2-hydroxy nonanoate is designated as N, palmitate as P, stearate as S, bis(2-hydroxyethyl) malonate as EE, (2-hydroxyethyl) nonanoate as E1, (2-hydroxyethyl) hexanoate as E2 and (2-hydroxyethyl) propionoate as E3.

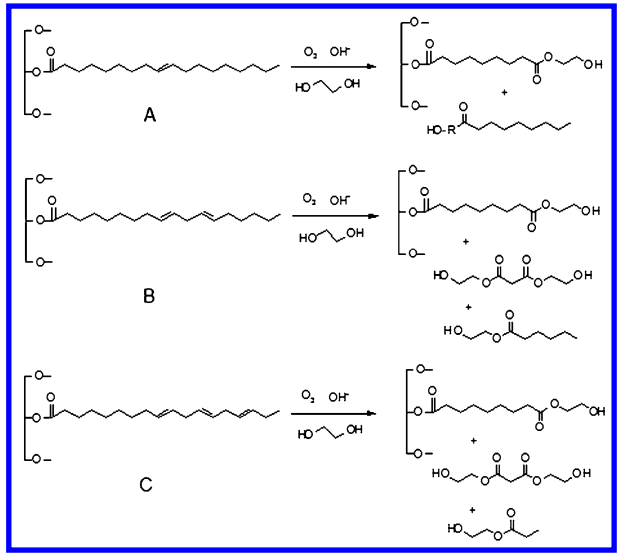

Figure 4. Polyols composition of triglycerides containing (A) oleic acid, (B) linoleic acid, and (C) linolenic acid by catalyzed ozonolysis of soy oil with ethylene glycol.

Several important conclusions are apparent from this statistical analysis: (1). Overall, the polyol triglyceride mixture is much more uniform than the original soy triglyceride composition since the double bonds of all the unsaturated fatty acid in the 9th position leading to a significant concentration of NNN polyol. (2). About 24 wt% of the product mixture contains triols (NNN), 13 wt.% contains diols (NNP and NNS), less than 3 wt.% contains mono functional alcohols (NPS, PPN and SSN) and only a very small component (less than 0.2 wt.%) of unreactive

In Green Polymer Chemistry: Biocatalysis and Materials II; Cheng, H., et al.;
ACS Symposium Series; American Chemical Society: Washington, DC, 2013.

Publication Date (Web): November 22, 2013 | doi: 10.1021/bk-2013-1144.ch021

triglycerides having no hydroxyl groups is present in the mixture. The very small quantity of unreactive components is very important since upon polymerization it is not reactive and thus could diffuse out of the polymer over time resulting in undesirable changes in its properties. (3). About half of the polyols product mixture is composed of triglycerides. The other half is composed of the low molecular weight diol (EE) and mono functional alcohols (E1, E2 and E3). If needed, these low molecular weight species can be removed and separated from the polyol triglycerides. However, in most cases this is not necessary as these polyols are reactive and will participate in the polymerization. It is also important to note that all these polyols are composed of primary hydroxyls, which are more desirable than secondary alcohols in the preparation of polyurethanes and polyesters.

Publication Date (Web): November 22, 2013 | doi: 10.1021/bk-2013-1144.ch021

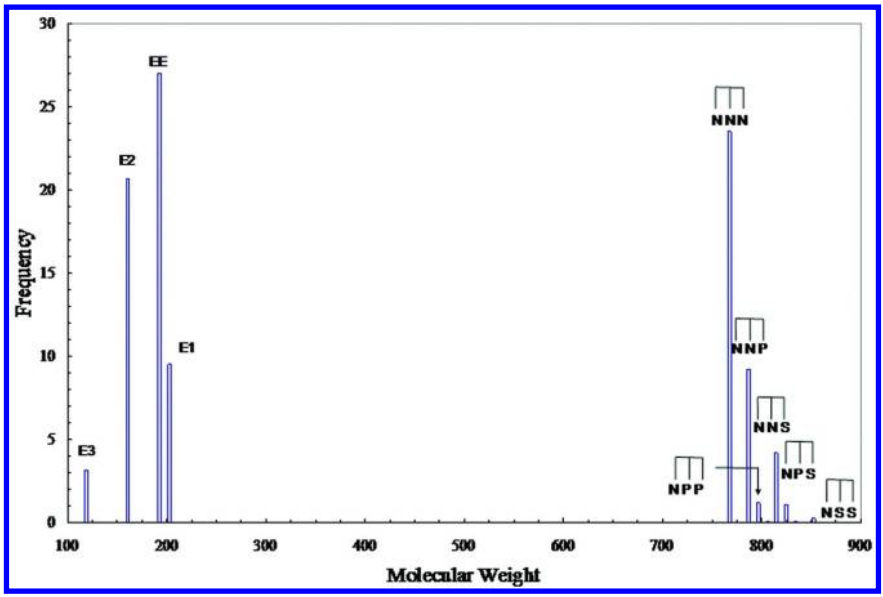

Figure 5. Statistical distribution of soy polyols obtained by alkaline catalytic ozonolysis of soy oil with ethylene glycol.

As expected, the FTIR spectrum of the soy polyol mixture is characterized by a broad hydroxyl stretching peak around 3500 cm^{-1}, the complete disappearance of the C=C band at 3005 cm^{-1}, and the C=C stretch at 1650 cm^{-1}. The FTIR spectrum further indicates that at the end of the ozonolysis reaction the carbonyl stretch at 1743 cm^{-1} is broad, suggesting the formation of new carbonyl compounds. No absorptions around 2900–2700 cm^{-1} were noted indicating the absence of aldehyde groups. Further confirmation of the soy polyol structure was obtained from ^{13}C-NMR (Figure 6). The characteristic double peak of double bonds at 130 ppm, related to the unsaturated fatty acids in the soybean oil, didn't appear in the soybean polyol spectrum, indicating complete cleavage of the double bonds. The carbonyl ester peaks (177 ppm) and the various methylene peaks (between 25 and 36 ppm) remained unchanged as did the glycerol carbons (64 and 69 ppm). Additionally, new resonance peaks appeared at 66 ppm, which were related to ethylene oxide

carbons, as well as peaks at 60 ppm, related to the new C–OH functional groups. It was apparent from the NMR data that the hydroxylation of soybean oil progressed as expected to yield the desired polyols.

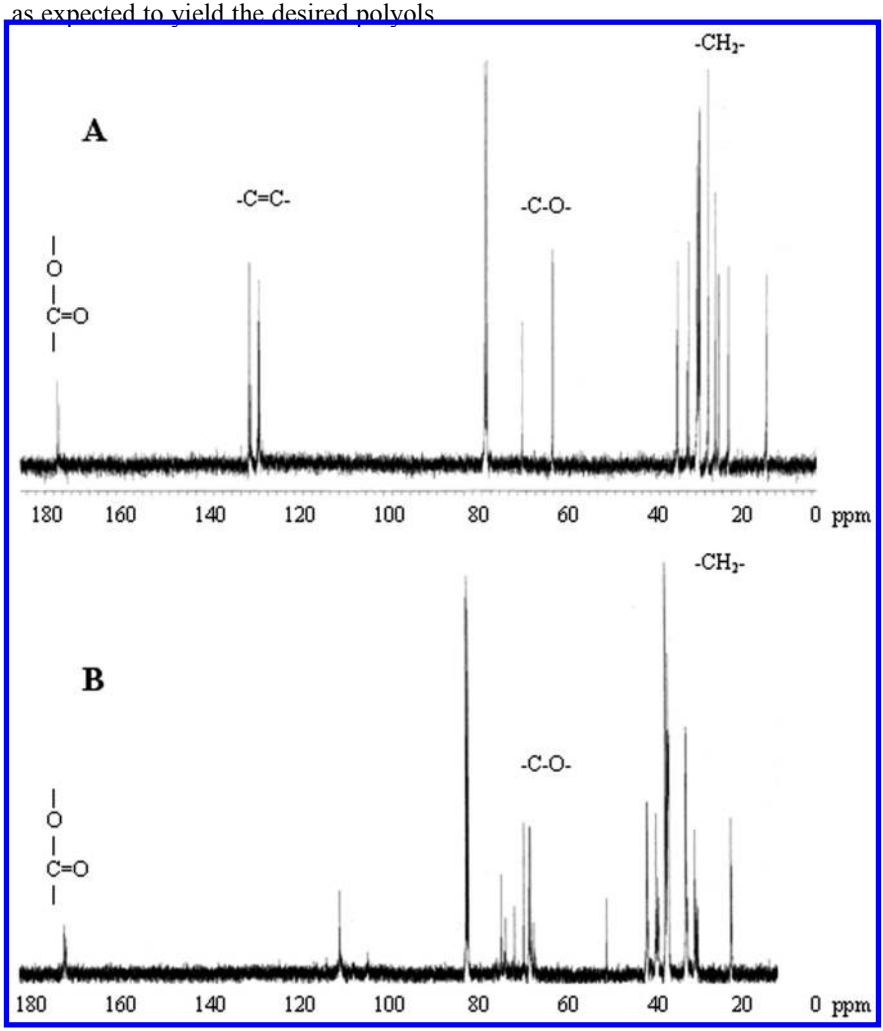

Figure 6. ^{13}C-NMR of soy oil (A) and soy polyol obtained by catalyzed ozonolysis of soy oil with ethylene glycol (B).

Polyols from Soymeal

Only limited effort has been directed toward using the protein biomass to produce value added industrial products due to difficulties associated with processing the meal and the high sensitivity of the proteins to moisture. We avoided these problems by first hydrolyzing the meal to its individual amino acids and then protecting the carboxylic acid and converting the amines to hydroxyl terminated urethanes (*28*, *29*). Our approach is shown in Figure 7 for L-Arginine that was used as a model compound and includes protecting the carboxylic acid by

Publication Date (Web): November 22, 2013 | doi: 10.1021/bk-2013-1144.ch021

reacting it with ethylene diamine to form an amido-amine terminated intermediate followed by reaction of the terminal amines with ethylene carbonate (*30–36*) to yield hydroxy-terminated urethane prepolymers. These urethane polyols can be further polycondensed to high molecular weight poly(amide-urethane)s. The use of ethylene diamine and ethylene carbonate has several advantages: these reactants are relatively inexpensive compounds, their respective reactions are well known and proceed smoothly to high yields and both reactants are readily available. The preparation process was studied and optimized using glycine and L-Arginine as model compounds. Glycine was chosen as it is the simplest amino acid composed of one amine and one carboxylic acid. L-Arginine was chosen since it is present in the soy meal at relatively high concentrations and its structure is relatively complex (e.g. it contains two primary amines, one secondary amine and one imine group). Both of these amino acids exist as zwitterions, which limit their reactivity.

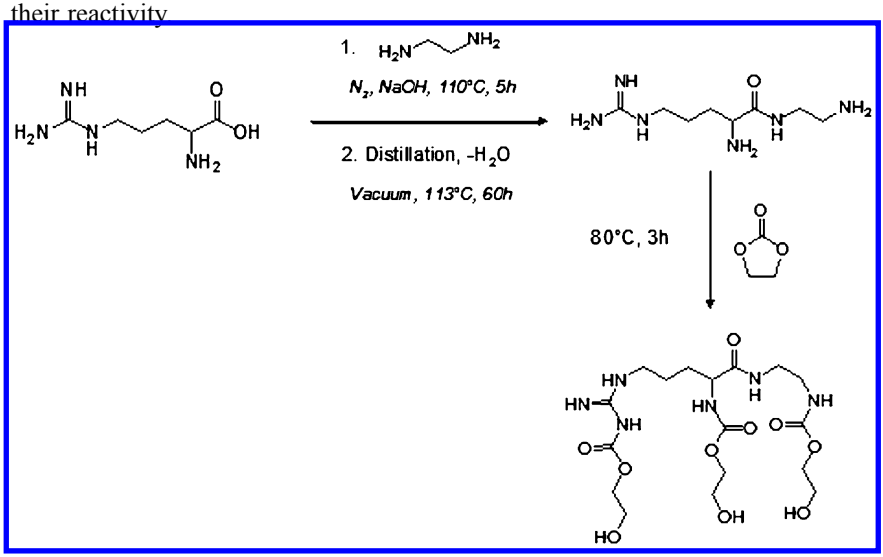

Figure 7. Preparation of hydroxyl-terminated urethane pre-polymers.

In the first step, a large excess of ethylene diamine was used to react with the carboxylic acid in order to minimize possible dimerization reactions and ensure the formation of amine terminated products. NMR and FTIR were used to identify the structure of these products and provided clear indication that the amidation reaction proceeded as desired. Furthermore, end-group analyses (Table II) provided additional evidence and showed a significant increase in the amine value after the conversion of the carboxylic acid groups in the amino acid to the diamine derivative. A subsequent reaction with ethylene carbonate led to the formation of the desired hydroxyl terminated urethane prepolymers (Arg-ED-EC) as indicated by the significant decrease in the amine value and the high hydroxyl value. The reaction of amines with ethylene carbonate to yield hydroxyl terminated urethanes is well known (*30–38*). It should be noted here that the amine value did not decrease to zero due to the presence of the less reactive secondary amines and imine groups.

In Green Polymer Chemistry: Biocatalysis and Materials II; Cheng, H., et al.;
ACS Symposium Series; American Chemical Society: Washington, DC, 2013.

Publication Date (Web): November 22, 2013 | doi: 10.1021/bk-2013-1144.ch021

Publication Date (Web): November 22, 2013 | doi: 10.1021/bk-2013-1144.ch021

Table II. End-group analysis

Sample	*Amine value [mg KOH/g]*		*Acid value [mg KOH/g]*		*OH value [mg KOH/g]*	
	Calc.	*Exp.*	*Calc.*	*Exp.*	*Calc.*	*Exp.*
Arg	644.1	336.6	322.0	-	0.0	-
Arg-ED	778.1	665.1	0.0	0.0	0.0	-
Arg-ED-EC	0.0	103.1	0.0	0.0	480.5	448.2
Arg-ED-EC-PO	0.0	74.7	0.0	0.0	-	533.0
SMS	483.7	33.7	549.4	64.9	0.0	-
SMS-ED	726.7	650.4	0.0	0.0	0.0	-
SMS-ED-EC	0.0	58.9	0.0	0.0	456.2	454.4
SMS-ED-EC-PO	0.0	49.3	0.0	0.0	-	623.0

Similar polyols were then synthesized from the soymeal following the same procedure after acid hydrolysis of the proteins to the corresponding amino acids. The composition of the amino acids in the soy proteins is well known and does not vary much (*37*). In order to minimize any degradation of the amino acids, a relatively weak HCl solution (3N) was used in the hydrolysis step. The final hydrolyzate was filtered to remove unreacted humin, treated with activated carbon to remove some of the dark brown color, neutralized with NaOH and then vacuum distilled to remove water. The amino acid mixture thus obtained was reacted with ethylene diamine and ethylene carbonate as described before to yield hydroxyl terminated pre-polyurethanes. It should be noted that instead of separating the carbohydrates already present in the meal, they were converted to reactive polyols by reacting them with propylene oxide. This propoxylation reaction is fairly fast and provided better economics since it eliminated the separation step and allowed higher yield polyols. The hydrolyzed mixture of amino acids from the soy meal (SMS) showed a marked increase in the amine value after the reaction with ethylene diamine (SMS-ED) followed by high hydroxyl value after the reaction with ethylene carbonate (SMS-ED-EC). The propoxylation reaction led to a significant increase in the hydroxyl value and a notable decrease in the viscosity making these polyols particularly suitable for rigid polyurethane foams. Indeed, water-blown pour-in-place rigid foams were prepared from these soymeal polyols by reacting them with polymeric methylene diphenyl diisocyanate (Rubinate M, eq. wt. = 135.5) targeting a foam density of 2 pcf (Table III). The foams were then evaluated against similar foams prepared with a commercial sucrose-based polyol.

It was noted that the reaction of the soymeal polyols with polymeric methylene diphenyl diisocyanate (MDI) was noticeably faster than the reaction of sucrose-based polyols with MDI most likely because the tertiary amines and imines in the soymeal polyols catalyzed this reaction. The reaction profile of these foams is listed in Table IV and clearly shows that the cream time, gel time, rise time and tack-free time were all significantly shorter than the control polyol. It was noted that due to this self-catalytic reaction and the high reactivity of the soymeal polyols, no amine-based catalysts were needed to produce foams.

Typical properties of rigid foams prepared from soymeal polyols with water as the blowing agent as well as with 1,1,1,3,3-Pentafluoropropane (HFC-245fa) blowing agent are listed in Table IV and compared with a control foam prepared with a sucrose/glycerin-based polyol. It was noted that the two polyols were completely miscible allowing us to prepare a series of foams with various concentrations of these polyols. However, it was noted that the physical properties (e.g. density, compressive strength, compressive strain and friability) of foams prepared with various blends of these polyols were comparable. Similarly, results of the dimensional stability in aging tests at -30°C and 70°C up to 2 weeks and flammability measured as burning rate (with no flame retardant additives) were essentially identical to the control foams.

Publication Date (Web): November 22, 2013 | doi: 10.1021/bk-2013-1144.ch021

Table III. Typical formulation of rigid foams derived from L-arginine-polyol

Sample	*Eq. Wt.*	*Control*	*Foam 1*	*Foam 2*	*Foam 3*
Polyol system*					
Jeffol SG-360	155.40	100	50	50	50
Argenine-based polyol	114.48	0	50	50	50
Water	9.00	4.5	4.5	4.5	4.5
Dabco DC193		2.0	2.0	2.0	2.0
Dabco 33LV		1.8	0	0.8	0
Niax A-1		0.1	0	0	0
Dabco T-12		0	0	0	0.05
Isocyanate System					
Rubinate M	135.50	165.55	179.41	180.49	179.41
Isocyanate Index		105	105	105	105
Reaction Profile					
Mix time, sec.		10	10	5	5
Cream time, sec.		13	6	5	6
Gel time, sec.		60	-	-	-
Rise time, sec.		95	-	45	55
Tack-free time, sec.		105	120	50	50

Publication Date (Web): November 22, 2013 | doi: 10.1021/bk-2013-1144.ch021

Publication Date (Web): November 22, 2013 | doi: 10.1021/bk-2013-1144.ch021

Table IV. Properties of rigid PU foams prepared from soymeal urethanep olyols

Sample designation	*Control polyol**	*Soymeal polyol*	*Control polyol**	*Soymeal polyol*
Type of blowing agent	*H_2O*	*H_2O*	*H_2O+HFC245fa*	*H_2O+HFC245fa*
Soy meal polyol [%]	*0*	*25*	*0*	*50*
Density, pcf	2.13 ± 0.19	1.62 ± 0.01	2.32 ± 0.03	2.03 ± 0.07
Compressive Strength, psi	23.98 ± 2.11	17.84 ± 2.06	27.65 ± 2.1	23.40 ± 2.5
Compressive Strain, [%]	6.06 ± 0.38	5.44 ± 0.31	5.83 ± 0.34	4.93 ± 0.71
Friability, mass loss [%]	5.28 ± 0.03	12.99 ± 1.88	4.41 ± 0.73	8.02 ± 0.26
Mass and Volume Change [%] with Aging and Water Immersion Tests				
	Mass	*Vol.*	*Mass*	*Vol.*	*Mass*	*Vol.*	*Mass*	*Vol.*
Aging Test @ -30°C								
after 1 day (24h)	0.61	0.66	-0.19	0.60	-0.42	0.43	-0.43	0.72
after 1 week (168 h)	1.69	0.88	0.93	0.17	0.98	0.11	-0.14	0.49
after 2 weeks (336 h)	1.53	-0.55	1.12	0.24	1.41	0.10	-0.14	-0.30
Aging Test @ 70°C								
after 1 day (24h)	-0.31	0.78	0.19	-0.29	-1.23	0.09	-1.04	-0.33
after 1 week (168 h)	-0.31	0.78	0.19	-0.29	-1.23	-0.29	-1.04	-0.32
after 2 weeks (336 h)	0.47	0.92	-0.19	-0.83	0.14	1.58	-1.19	-1.51
Water Absorption @ 25°C								
after 4 days (96 h)	217.5	0.39	304.5	2.17	165.4	-0.2	252.0	6.5

Publication Date (Web): November 22, 2013 | doi: 10.1021/bk-2013-1144.ch021

Mass and Volume Change [%] with Aging and Water Immersion Tests								
	Mass	*Vol.*	*Mass*	*Vol.*	*Mass*	*Vol.*	*Mass*	*Vol.*
after 1 week (168 h)	229.73	0.73	325.84	2.14	162.04	0.14	300.15	2.44
Burning rate, mm/min	387 ± 55		380 ± 47		377 ± 35		242 ± 15	
K-factor, BTUs	-		-		0.170		-	
Density K-factor, pcf	-		-		2.62		-	
*** Control polyol:** Poly-G 74-376, Sucrose/glycerine-based polyol; Hydroxyl value=361 from Arch Chemical								

Isocyanate-Free Poly(amide-urethane)s from Dimer Fatty Acids

Dimer fatty acids (also known as dimerized acids) are obtained from fatty acids by a condensation reaction of unsaturated fatty acids using a combination of pressure, temperature and catalysis. These dimer acids are suitable for preparation of linear polymers by polycondensation since they are composed of two functional carboxylic acids. We have used these dimer acids to develop isocyanate-free polyurethane resins (*29*, *39*).

Polyurethanes are an important class of polymers having widespread industrial applications in automotive, construction, packaging, furniture, medicine and many other markets (*40*). Traditionally they are synthesized by a condensation of polyols with isocyanates. However, the use of isocyanate is problematic due to its high toxicity as well as its preparation method from the corrosive and toxic phosgene gas (*41*, *42*). Consequently, much attention has been focused on developing procedures to synthesize polyurethanes by safer and environmentally friendlier methods that do not involve isocyanates, phosgenation or carbamates. One such method involves the reaction of cycloalkyl carbonates with aliphatic amines to yield hydroxyalkylurethanes (*43–55*). It is expected that avoiding isocyanate in the preparation of polyurethanes and using renewable resources in the process would offer a safe and environmentally responsible synthetic strategy which could dramatically improve the LCA profile (*56*) of the process. It has been shown that under certain conditions high molecular weight polyurethanes can be prepared by a urethane-exchange reaction with no need for isocyanate in the process. However, only few studies have been published in the literature dealing with polycondensation by such urethane-exchange reactions from renewable resources. One notable example is the preparation of poly(trimethylene carbonate hydroxyl-urethane)s from glycerol carbonate (*57*). Our work was focused on a solvent-free process to obtain poly (urethane amides) from dimer acids following the three steps described in Figure 8. In the first step the dimer fatty acid (DA) is condensed with ethylene diamine (ED) to produce amine terminated oligomers intermediates (P1). In the second step these intermediates are reacted with ethylene carbonate (EC) to yield hydroxyl terminated di-urethanes (P2). The third step involves urethane-exchange polycondensation reaction where terminal ethylene glycols ares removed and the molecular weight is increased (P3) (*29*, *39*). The final polymer was a transparent, flexible material at ambient temperature and contained 88 wt% renewable carbon.

The conversion of the carboxylic acid to amide in P1 was studied by monitoring the amine and the acid values as a function of the reaction time. It was observed that 71% of the amine groups and 95% of the acid groups were consumed after 3 hrs indicating a calculated degree of polymerization DP_n=4.3 and a number average molecular weight (M_n) = 2640 g/mol (Table V). These results were confirmed by FTIR (Figure 9) where the C=O peak (carboxylic acid) at 1710 cm^{-1} of the dimer acid disappeared and new peaks appeared at 1640 and 1560 cm^{-1} corresponding to C=O deformation of amide groups and N-H deformation of amine groups, respectively. FTIR spectroscopy was also used to monitor the reaction of P1 with ethylene carbonate to yield P2 in the 2nd step of this synthesis. It is apparent from the data in Figure 9 that ethylene carbonate

Publication Date (Web): November 22, 2013 | doi: 10.1021/bk-2013-1144.ch021

In Green Polymer Chemistry: Biocatalysis and Materials II; Cheng, H., et al.;
ACS Symposium Series; American Chemical Society: Washington, DC, 2013.

was consumed as indicated by the disappearance of the peak at 1800 cm^{-1} and a new peak at 1695 cm^{-1} appeared corresponding to the C=O deformation of the urethane groups. The completion of this reaction was further confirmed by a significant decrease in the amine value to 4.0 mg KOH/g and a corresponding increase in the hydroxyl value to 32.5 mg KOH/g, suggesting that 90% of P1 chain-ends were reacted with EC in this step. The calculated M_n was 2570 g/mol, which was in good agreement with the experimental value determined by GPC.

Publication Date (Web): November 22, 2013 | doi: 10.1021/bk-2013-1144.ch021

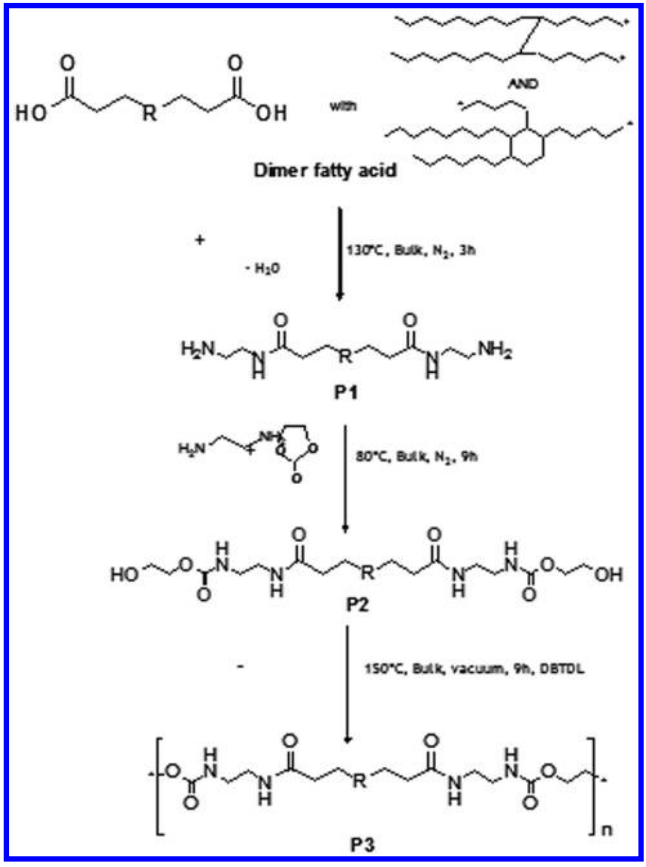

Figure 8. Representation of the general approach for the synthesis of poly(amide urethane)s from dimer fatty acids.

In Green Polymer Chemistry: Biocatalysis and Materials II; Cheng, H., et al.;
ACS Symposium Series; American Chemical Society: Washington, DC, 2013.

Finally, P2 was polymerized in the bulk by the urethane exchange reaction and the molecular weight increased as ethylene glycol was removed and the hydroxyl value decreased. The final hydroxyl value was 12.7 mg KOH/g corresponding to calculated Mn = 8330 g/mol in fairly good agreement with the GPC results (Mn = 7700 g/mol, M_w = 14000 g/mol). The polyurethane P3 exhibited a T_g at -10 °C and a melting point at +73 °C with a corresponding melting enthalpy at 0.04 W/g. TGA under nitrogen atmosphere showed the onset of degradation at 288 °C followed by a main degradation at 465 °C. These new poly (amide urethane)s contain high biomass content, yet, they can be formulated and used as coatings, adhesives and elastomers similarly to conventional polyurethanes prepared from fossil resources.

Publication Date (Web): November 22, 2013 | doi: 10.1021/bk-2013-1144.ch021

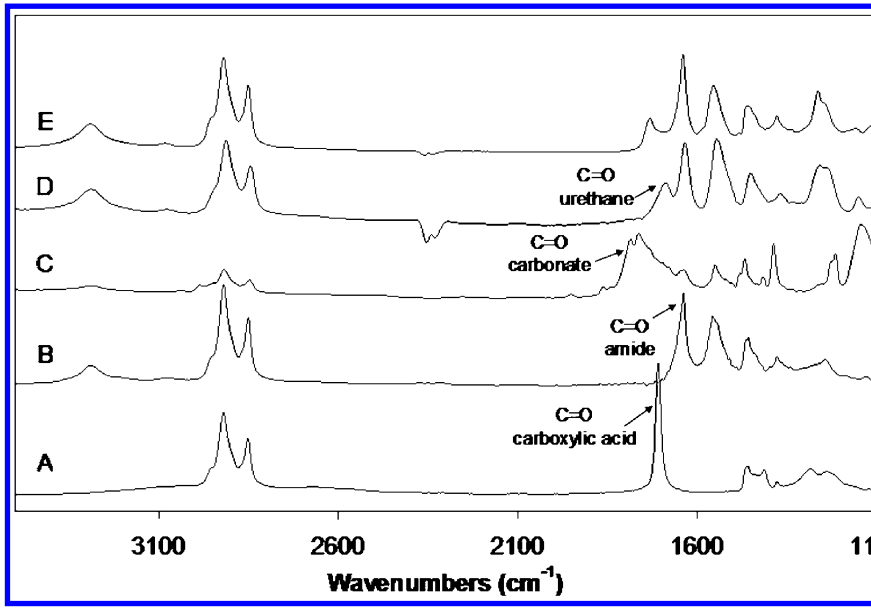

Figure 9. FTIR spectra of dimer acid (A), P1 (B), ethylene carbonate (C), P2 (D) and P3 (E).

In Green Polymer Chemistry: Biocatalysis and Materials II; Cheng, H., et al.;
ACS Symposium Series; American Chemical Society: Washington, DC, 2013.

Table V. Molecular parameters of P1, P2 and P3

	Calc. DP_n	*Calc. M_n (g/mol)*	*Exp M_n (g/mol)*	*Exp M_w (g/mol)*	*PD*
P1	4.3	2640	1) 720	1) 880	1) 1.22
			2) 2810	2) 3370	2) 1.20
P2	0.9	2570	1) 1660	1) 1770	1) 1.06
			2) 4220	2) 4890	2) 1.16
P3	3.3	8330	7700	14000	1.80

Publication Date (Web): November 22, 2013 | doi: 10.1021/bk-2013-1144.ch021

Coatings from Silylated Soybean Oil

It is well know that vegetable oils have been used as important components in alkyd resins. The cured coatings obtained from such resins were noted for their anticorrosion properties, excellent water barrier, enhanced chemical protection and high wear and UV resistance. The "drying" character of these oils is achieved by air oxidation when the double bonds in the fatty acids undergo cross linking upon exposure to oxygen. The presences of certain metal salts in trace, such as cobalt naphteneate, are used as a catalyst to accelerate the cure time. Similarly, linseed oil is known as a fast drying oil due to the high unsaturation content and is widely used in coatings but its use is limited due to high costs and limited availability. In practice, curable oils must be diluted in an organic solvent or emulsified in water. If solvents are used as diluents, they are considered as volatile organic content (VOC) and will evaporate upon application to pollute the air. When the oil is dispersed in water as a suspension, the use of surfactant stabilizing agents is required. These surfactants remain in the finished coatings and tend to degrade the physical properties of the coating as well as its aesthetic appearance (*58*).

A more convenient approach, that we have developed in our work as part of the soybean refinery concept is a *one-component* moisture activated cure. This cure strategy is based on a well known limited hydrolytic stability of alkoxy silanes that is widely used in various silicone sealants (*27*, *59–62*). Our work was based on grafting vinyltrimethoxysilane (VTMS) onto the unsaturation sites of the fatty acids in the triglycerides of the oil by the well known as 'Ene-reaction' as shown in Figure 10 (*62*). This reaction is catalyzed by peroxides and is based on the fact that VTMS does not undergo free radical polymerized like other vinyl monomers due to the stabilization of the free radicals by the silicon atom. Furthermore, this one-step addition reaction does not require a solvent and no by-products are produced that require neutralization or purification at the end of the reaction. Since only small concentrations of VTMS are needed for crosslinking, the physical properties of the modified oil remains unchanged. Most notably, the product is a low viscosity oil that requires no solvent or diluent and it can be applied by any common technique such as brushing, spraying, dip-coating or casting using conventional equipment.

The success of the grafting reaction and the structure of the silane modified oil were determined by FTIR, GC and NMR. Representative ^{1}H-NMR spectrum (Figure 11) clearly shows that the grafting reaction was successful. Figure 11

In Green Polymer Chemistry: Biocatalysis and Materials II; Cheng, H., et al.;
ACS Symposium Series; American Chemical Society: Washington, DC, 2013.

(A) represents the partial ^{1}H-NMR spectrum of soybean oil. The resonance peaks with a chemical shift near 5.25 ppm are associated with the proton atoms located in the unsaturation linkages of soybean oil. Figure 11 (B) shows the ^{1}H NMR spectrum of the intermediate product soybean oil-VTMOS reaction product. It is clear that the proton atoms located in unsaturation linkages in VTMOS exhbitis a group of resonance peaks near 6.0 ppm. We can also notice that the shape of the resonance peak changed because of the reaction proceeding. The final consumption of unsaturations present in VTMOS by ene reaction was supported by the partial ^{1}H-NMR presented in Figure 11 (C). It clearly showed the disappearance of 6.0 ppm resonance peak associated with the proton atoms located in the unsaturation linkages in VTMOS. Further confirmation of the structure was obtained by ^{13}C-NMR and iodine number titration. Moreover, the extent of the grafting reaction was found to directly proportional to the reaction time and the reaction temperature (*11*, *58*, *62*).

Publication Date (Web): November 22, 2013 | doi: 10.1021/bk-2013-1144.ch021

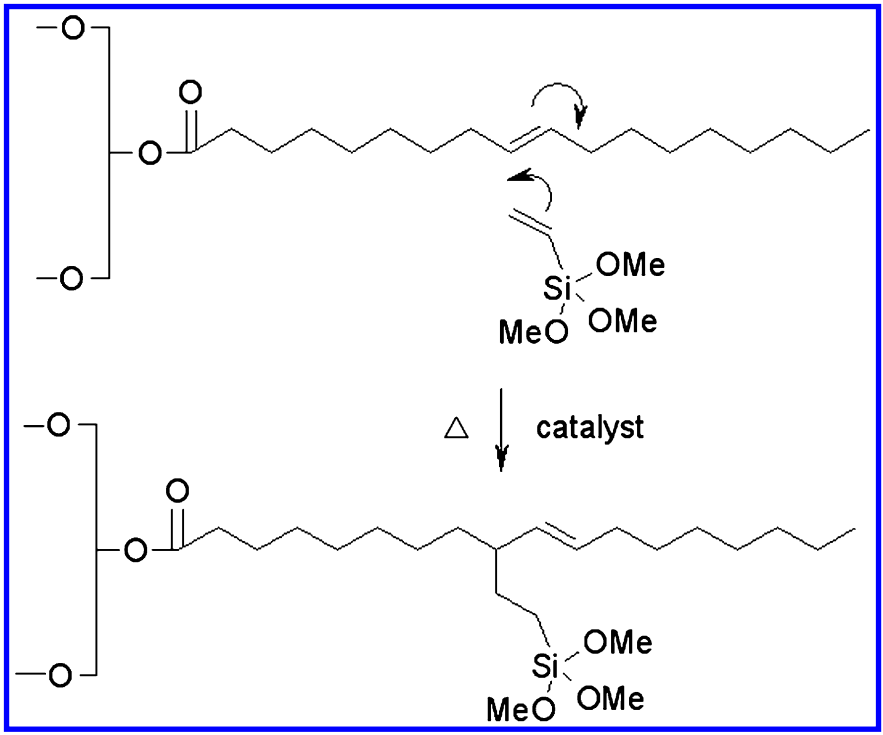

Figure 10. Grafting VTMS onto soy oil.

In Green Polymer Chemistry: Biocatalysis and Materials II; Cheng, H., et al.;
ACS Symposium Series; American Chemical Society: Washington, DC, 2013.

Publication Date (Web): November 22, 2013 | doi: 10.1021/bk-2013-1144.ch021

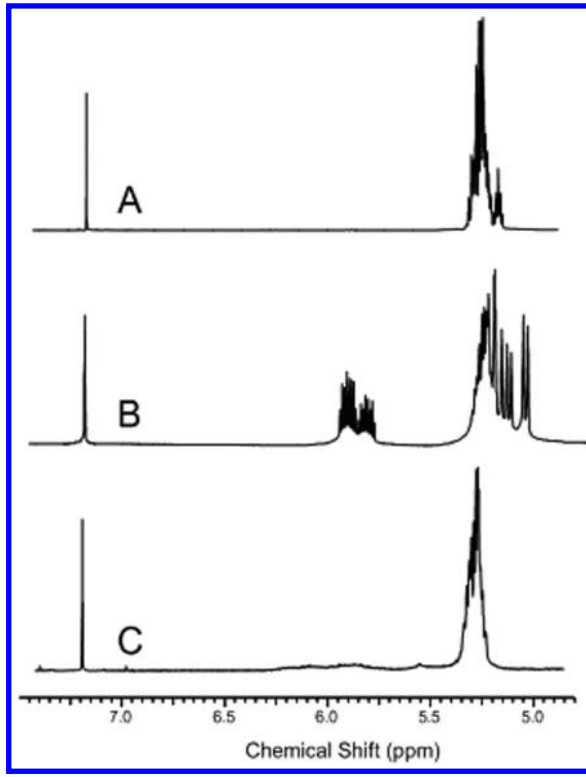

Figure 11. [1]H-NMR of (A) soybean oil, (B) the intermediate soybean oil-VTMOS reaction product, (C) the final silylated soybean oil.

Upon exposure of moisture, hydrolysis of the alkoxysilanes readily takes place to yield silanols which are condensed to form stable siloxane crosslinks as shown in Figure 12. The rate of cure is proportional to the relative humidity, the temperature and the presence of any cure accelerators (for example, dibutyltin diacetate). exhibits the partial spectrum of final cured product. The properties of the protective coating is largely controlled by the crosslink density and the type of silane used. This cure system is very convenient as it does not require mixing different components prior to curing and, essentially, has an infinite shelf life as long as it is stored away from moisture. The major drawback of this system is the fact that the cure is controlled by diffusion of moisture into the bulk and diffusion of the by-product alcohol out of the bulk. Thus, the thickness of the sample is critical, making this system particularly suitable for coatings or adhesives that require only thin layers.

In Green Polymer Chemistry: Biocatalysis and Materials II; Cheng, H., et al.;
ACS Symposium Series; American Chemical Society: Washington, DC, 2013.

Publication Date (Web): November 22, 2013 | doi: 10.1021/bk-2013-1144.ch021

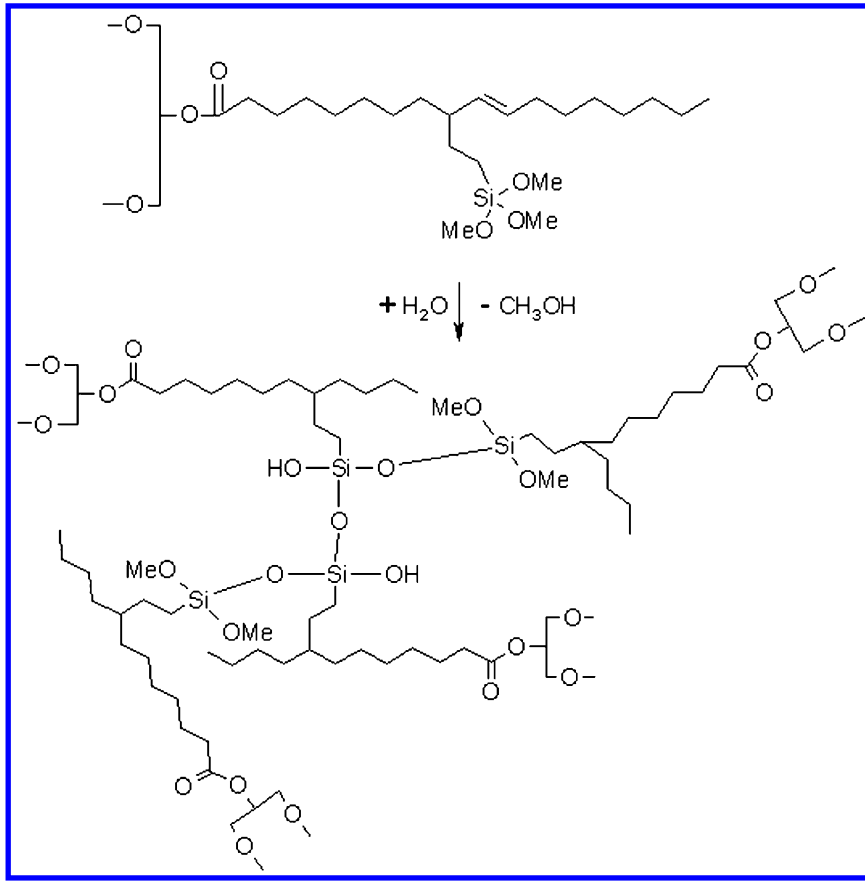

Figure 12. Moisture activated cure mechanism of soybean oil grafted with VTMS.

These coatings exhibited excellent adhesion to steel, concrete, wood, paper and glass. The hardness of the coating was greatly enhanced when the oil was formulated with fine particle size silica. Formulation with silica is particularly affective since good interface is obtained between the filler particles and the matrix through silanol interactions between the surface of the silica and the oil grafted silanes. It was shown that these coatings can be used as a moisture barrier to protect substrates such as wood, paper and concrete against water.

Conclusions

This work provides a few examples of our biorefinery concept where the oil and the meal of soybeans were used to produce useful intermediates for industrial products. In all cases safe processes were used following the 'green chemistry' principles. These examples include:

- New polyols from soy oil prepared by continuous ozonation process that can be further used in the synthesis of polyesters and polyurethanes.
- New hydroxyl terminated urethane prepolymers prepared from soymeal that were obtained by converting the amine in amino acids to urethanes. These high hydroxyl value polyols were further used in rigid polyurethane foams.
- A new class of poly(amide urethane)s were prepared from dimer fatty acid by isocyanate-free polymerization. The properties of these polymers make them suitable for coating and adhesive applications.
- We have also successfully demonstrated a novel moisture activated cure of soy oil by grafting onto the oil reactive silanes. Upon exposure to moisture the low viscosity oil is cured into a transparent film that provides excellent protective coating over a wide range of substrates.

Publication Date (Web): November 22, 2013 | doi: 10.1021/bk-2013-1144.ch021

References

1. Food and Agricultural Organization of the United Nations, FAO. www.fao.org.
2. Commodity Oils and Fats: Soybean Oil, The AOCS Lipid Library. http://lipidlibrary.aocs.org/market/soybean.htm.
3. Gunstone, F. D. In *The Lipid Handbook*; Taylor & Francis Ltd.: Oxford, U.K., 2004.
4. Carlsson, A. S. *Biochimie* **2009**, *91*, 665.
5. Erhan, S. Z.; Sharma, B. K.; Liu, Z. S.; Adhvaryu, A. *J. Agric. Food Chem.* **2008**, *56*, 8919.
6. Sharma, B. K.; Adhvaryu, A.; Perez, J. A.; Erhan, S. Z. *J. Agric. Food Chem.* **2005**, *53*, 2961.
7. Durrett, T. P.; Benning, C.; Ohlrogge, J. *Plant J.* **2008**, *54*, 593.
8. Soymeal Info Center. http://www.soymeal.org/.
9. Johnson, L. A.; Myers, D. J.; Burden, D. J. *Inform* **1992**, *3*, 429.
10. Heiss, H. L.; Saunders, J. H.; Morrris, M. R.; Davis, B. R.; Hardy, E. E. *Ind. Eng. Chem. Res.* **1954**, *46*, 1498.
11. Saunders, J. H.; Frisch, K. C. *Polyurethanes Chemistry and Technology*; Interscience Publishers, John Wiley & Sons: New York, 1964.
12. Detrick, S. R.; Barthel, E. U.S. Patent 2,787,601, 1957.
13. Wells, E. R.; Hixenbaugh, J. C. *Am. Paint J.* **1962**, *46*, 88.
14. Stanton, J. M. *J. Am. Oil Chem. Soc.* **1959**, *36*, 503.
15. Findley, T. W.; Swern, D.; Scanlan, J. T. *J. Am. Chem. Soc.* **1945**, *67*, 413.
16. Mefferet, A.; Kluth, H. U.S. Patent 4,886,893, 1989.
17. Frankel, E. N.; Pryde, E. H. *J. Am. Oil Chem. Soc.* **1977**, *54*, 873.
18. Takahara, J.; Setoyama, T. W.O. Application Patent 2,002,049,999, 2002.
19. Michaelson, R. G.; Austin, R. C. U.S. Patent 4,314,088, 1982.
20. Brinksma Schmieder, J.; Schmieder, L.; Van Vliet, G.; Boaron, R.; Hage, R.; DeVos, D. E.; Alsters, P. L. *Tetrahedron Lett.* **2002**, *43*, 2619.
21. Vannozzi, G. P. *HELIA* **2006**, *29*, 1.
22. Rebrovic, L.; Gunstone, F. D. *Lipid Technol.* **1996**, *8*, 135.

23. Von Gunten, U. *Water Res.* **2003**, *37*, 1443.
24. Graiver, D.; Patil, M.; Narayan, R. *Recent Pat. Mater. Sci.* **2010**, *3*, 203.
25. Narayan, R.; Graiver, D.; Farminer, K. W.; Srinivasan, M. U.S. Patent 8,110,036, 2012.
26. Tran, P.; Daniel, D.; Narayan, R. *J. Am. Oil Chem. Soc.* **2005**, *82*, 653.
27. Narayan, R.; Graiver, D.; Farminer, K. W.; Tran, P. T. U.S. Patent 7,589,222, 2009.
28. Chalasani , S. R. K.; Heric, S.; Amin, P.; Sendijarevic, V.; Hablot, E.; Graiver, D.; Narayan, R. *Polyurethanes Technical Conference*, Atlanta, GA, September 24−26, 2012.
29. Hablot, E.; Graiver, D.; Narayan, R. *Polym. Prep. (Am. Chem. Soc., Div. Polym. Chem.)* **2012**, *53*, 269.
30. Rokicki, G.; Piotrowska, A. *Polymer* **2002**, *43*, 2927.
31. Guan, J.; Song, Y.; Lin, Y.; Yin, X.; Zuo, M.; Zhao, Y.; Tao, X.; Zheng, Q. *Ind. Eng. Chem. Res.* **2011**, *50*, 6517.
32. Rokicki, G.; Lazinski, R. *Angew. Makromol. Chem.* **1989**, *170*, 211.
33. Kihara, N.; Kushida, Y.; Endo, T. *J. Polym. Sci., Part A: Polym. Chem.* **1996**, *34*, 2173.
34. Kihara, N.; Endo, T. *J. Polym. Sci., Part A: Polym. Chem.* **1993**, *31*, 2765.
35. Tomita, H.; Sanda, F.; Endo, T. *J. Polym. Sci., Part A: Polym. Chem.* **2001**, *39*, 4091.
36. Tomita, H.; Sanda, F.; Endo, T. *J. Polym. Sci., Part A: Polym. Chem.* **2001**, *39*, 3678.
37. Tomita, H.; Sanda, F.; Endo, T. *Macromol.* **2001**, *34*, 7601.
38. Tomita, H.; Sanda, F.; Endo, T. *J.Polym. Sci., Part A: Polym. Chem.* **2001**, *39*, 860.
39. Hablot, E.; Graiver, D.; Narayan, R. *PU Magazine*, Vol. 9, August/ September 2012.
40. Szycher, M. *Handbook of Polyurethanes*; CRC Press: Boca Raton, FL, 1999.
41. Bernstein, I. L. *J. Allergy Clin. Immunol.* **1982**, *70*, 24.
42. Pauluhn, J. *Arch. Toxicol.* **2000**, *74*, 257.
43. Assumption, H. J.; Mathias, L. J. *Polymer* **2003**, *44*, 5131.
44. Clark, A. J.; Echenique, J.; Haddleton, D. M.; Straw, T. A.; Taylor, P. C. *J. Org. Chem.* **2001**, *66*, 8687.
45. Clements, J. H. *Ind. Eng. Chem. Res.* **2003**, *42*, 663.
46. Deepa, P.; Jayakannan, M. *J. Polym. Sci., Part A: Polym. Chem.* **2008**, *46*, 2445.
47. Helou, M.; Carpentier, J. F.; Guillaume, S. M. *Green Chem.* **2011**, *13*, 266.
48. Javni, I.; Doo, P. H.; Petrovik, Z. S. *J. Appl. Polym. Sci.* **2008**, *108*, 3867.
49. Li, Z.; Zhao, Y.; Yan, S.; Wang, X.; Kang, M.; Wang, J.; Xiang, H. *Catal. Lett.* **2008**, *123*, 246.
50. Matsumura, S.; Soeda, Y.; Toshima, K. *Appl. Microbiol. Biotechnol.* **2006**, *70*, 12.
51. Ochiai, B.; Inoue, S.; Endo, T. *J. Polym. Sci., Part A: Polym. Chem.* **2005**, *43*, 6613.
52. Oestreich, S.; Struck, S. *Macromol. Symp.* **2002**, *187*, 325.
53. Rokicki, G.; Piotrowska, A. *Polymer* **2002**, *43*, 2927.

Publication Date (Web): November 22, 2013 | doi: 10.1021/bk-2013-1144.ch021

54. Tamami, B.; Sohn, S.; Wilkes, G. L. *J. Appl. Polym. Sci.* **2004**, *92*, 883.
55. Yokoe, M.; Keigo, A. O. I.; Okada, M. *J. Polym. Sci., Part A: Polym. Chem.* **2003**, *41*, 2312.
56. Lonescu, M. *Chemistry and Technology of Polyols for Polyurethanes*; Smithers Rapra Publishing: Shropshire, U.K., 2005.
57. Helou, M.; Carpentier, J. F.; Guillaume, S. M. *Green Chem.* **2011**, *13*, 266.
58. Nabuurs, T.; Baijards, R. A.; German, A. L. *Prog. Org. Coating* **1996**, *27*, 163.
59. Graiver, D.; Dacomba, R.; Khawaji, M.; Jaros, A.; Berglund, K.; Narayan, R. *J. Am. Oil Chem. Soc.* **2012**, *89*, 1895.
60. Zhuang, Y. M.S. Thesis, Chemical Engineering Department, Michigan State University, 2011.
61. Srinivasan, M. Ph.D. Thesis, Chemical Engineering Deartment, Michigan State University, 2010.
62. Dubac, J; Laporterie, A. *Chem. Rev.* **1987**, *87*, 319.

Publication Date (Web): November 22, 2013 | doi: 10.1021/bk-2013-1144.ch021

Publication Date (Web): November 22, 2013 | doi: 10.1021/bk-2013-1144.ch022

Chapter 22

Applications of Common Beans in Food and Biobased Materials

Atanu Biswas,[*,1] William C. Lesch,[2] and H. N. Cheng[3,*]

[1]National Center for Agricultural Utilization Research, Agricultural Research Services, U.S. Department of Agriculture, 1815 N. University Street, Peoria, Illinois 61604
[2]Department of Marketing, University of North Dakota, Grand Forks, North Dakota 58202
[3]Southern Regional Research Center, Agricultural Research Service, U.S. Department of Agriculture, 1100 Robert E. Lee Blvd., New Orleans, Louisiana 70124
[*]E-mail: atanu.biswas@ars.usda.gov (A.B.); hn.cheng@ars.usda.gov (H.N.C.)

One of the research trends in recent years is to use natural renewable materials as "green" raw materials for industrial applications. Common beans (*Phaseolus vulgaris L.*) are well known, widely available, and relatively cheap. They contain polysaccharides, proteins, triglyceride oils, minerals, vitamins, and phenolic antioxidants. Many of these compounds seem to be attractive components for food and biobased products. A review is given here of the more promising approaches for these applications, emphasizing in particular the work done by the authors in the past several years. These include 1) extrusion cooking of whole beans as food products, 2) use of beans as fillers in polymeric blends and composites, 3) extraction of triglyceride oils from whole beans, 4) extraction of phenolic phytochemicals from beans, and 5) conversion of starch in beans to ethanol. These examples illustrate the range of applications possible and the potential value of non-conventional uses of common beans.

In Green Polymer Chemistry: Biocatalysis and Materials II; Cheng, H., et al.; ACS Symposium Series; American Chemical Society: Washington, DC, 2013.

Publication Date (Web): November 22, 2013 | doi: 10.1021/bk-2013-1144.ch022

Introduction

Common beans (*Phaseolus vulgaris L.*) are significant raw materials for food and are good sources of carbohydrates, proteins, fiber, and micronutrients (*1*). They are also appreciated for their long storage life, ease of storage and relatively simple preparation as food. The health benefits of beans are well recognized. The U.S. produces about 2.5 billion pounds of dry common beans per year, with a price of about 20 cents per pound (*2*). The states with the most bean production are North Dakota, Michigan, Nebraska, Colorado, California, and Idaho. Thus far, the leading varieties are pinto beans (42%), navy beans (17%), black beans (11%), and Great Northern beans (5%) (*2*, *3*).

Typically common beans (like pinto beans) contain about 64% carbohydrates, 23% proteins, 2% fat, and lower levels of minerals (e.g., iron, potassium, selenium, and molybdenum), vitamins (such as thiamine, vitamin B_6, and folic acid), and other bioactive compounds, including flavonoids, polyphenols and phenolics (*4*). Most of the common beans are currently consumed as food. However, there have been some efforts to find non-food industrial uses for them. Such applications are attractive to the consumers because common beans are natural renewable raw materials that are non-toxic and environmentally friendly and beneficial to the bean growers because they provide added value to the products.

Since 2009 there has been a fair amount of work done at USDA to explore new applications of common beans in food and biobased products (*5–11*). In this article, we aim to review many of these developments. Examples are shown particularly to illustrate the versatility of common beans in different applications. These include the extrusion cooking of beans, the conversion of bean starch to ethanol, the incorporation of beans as fillers in polymer composites, and the possible use of triglyceride oils and phenolic antioxidants as functional additives.

Extrusion Cooking of Common Beans

The effects of extrusion cooking on the functional, physiological and nutritional properties of common beans had been reported before (*12–20*). However, relatively few investigations had been done on whole seed extrudates of common beans (*13*, *21*, *22*). It was useful therefore to determine the physicochemical and functional properties of extruded products of four whole common beans including dark red kidney, black, pinto and great northern beans as affected by process variables such as extrusion temperature, feed moisture and screw speed (*5*).

The four common beans were obtained from the Northarvest Bean Growers Association (Frazee, MN). The whole beans were separately ground to particle size less than 0.6 mm using a Retsch mill and defatted using Soxhlet extraction with hexane for 6 h. The % moisture content of defatted ground beans was adjusted by hydrating them with distilled water (to 24% and 28% moisture content) using an electric mixer. The ground beans were fed manually into a single screw Brabender extruder (Brabender Instruments, Inc., South Hackensack, NJ) at constant speed (10 g/min). The process variables included feed moisture (24% and 28%), die end temperature (125, 135, and 160 °C) and screw speed (40, 90 rpm). Bean extrudates

In Green Polymer Chemistry: Biocatalysis and Materials II; Cheng, H., et al.;
ACS Symposium Series; American Chemical Society: Washington, DC, 2013.

were chopped into pieces and ground to pass through 2-mm sieve using a Thomas mill (*5*).

The results showed that bean type and feed moisture had no significant effect on moisture content of extruded beans, but increasing extrusion temperature led to lower moisture content (*5*). Bulk density of bean extrudates was not significantly affected by screw speed, bean type, and extrusion temperature. There was, however, a slight trend of decreased bulk density of bean extrudate with increased feed moisture (*5*).

The oil absorption capacity (OAC) showed decreases in three beans (dark red kidney, black, and pinto) after extrusion cooking relative to bean control prior to extrusion (*5*). Other variables, such as screw speed, bean type, feed moisture and extrusion temperature, did not contribute significantly to change in OAC. Changes in color were also noted after extrusion (*5*). The bean extrudates were darker and had more redness and yellowness in comparison to the ground beans prior to extrusion.

Publication Date (Web): November 22, 2013 | doi: 10.1021/bk-2013-1144.ch022

Table 1. Water absorption index (WAI) of bean extrudates under four extrusion conditions at two different moistures compared to defatted ground bean control

Bean	*FM %*[b]	*WAI (g absorbed water/g dry weight)*[a]				
		Control bean	*125°C/ 40 rpm*	*125°C/ 90 rpm*	*135°C/ 90 rpm*	*165°C/ 90 rpm*
DK	24	2.62±0.00	2.53±0.01	3.19±0.11	2.81±0.21	3.44±0.07
	28		2.47±0.01	2.88±0.07	2.87±0.04	3.77±0.06
GN	24	2.35±0.01	2.69±0.01	3.17±0.04	3.37±0.07	4.15±0.01
	28		2.89±0.04	2.85±0.02	2.86±0.03	3.02±0.04
BL	24	2.40±0.03	2.91±0.06	2.97±0.21	2.81±0.26	4.01±0.01
	28		2.94±0.04	2.34±0.00	2.35±0.10	3.32±0.03
PT	24	2.21±0.02	2.90±0.06	2.66±0.18	2.99±0.18	4.13±0.02
	28		2.72±0.02	2.60±0.07	2.84±0.00	3.71±0.03

[a] Data adapted from ref. (*5*). Values expressed in mean ± standard deviation, DK=Dark red kidney, GN=Great northern, BL=Black, PT=Pinto. [b] FM= Feed Moisture.

Extrusion strongly influenced the water absorption index (WAI) of bean extrudates. As shown in the data given in Table 1, most WAI values increased upon extrusion. WAI was not significantly affected (at statistical p-value < 0.05) by both screw speed and bean type, but extrusion temperatures and feed moistures had strong influences on WAI. The effect of temperature might be the result of denaturation of protein during extrusion, separation of amylose and amylopectin chains, and swelling of crude fiber in beans. A decrease in WAI was observed when feed moisture went from 24 to 28%. A study of the water solubility

In Green Polymer Chemistry: Biocatalysis and Materials II; Cheng, H., et al.;
ACS Symposium Series; American Chemical Society: Washington, DC, 2013.

index (WSI) indicated that it was significantly affected by all process variables, including screw speed, extrusion temperature, and feed moisture (*5*).

It appeared that feed moisture was the most critical factor affecting the extrudate properties including water absorption, water solubility, and color. Screw speed only influenced the moisture and water solubility of final extrudates. Changing extrusion temperature resulted in extrudates that showed differences in moisture, water absorption and solubility (*5*). The data reported in this work may be useful in process design and product optimization to people who contemplate making commercial products from extruded beans.

Common Bean as Filler in Polymers

Whole pinto beans were used as fillers in poly(lactic acid) (PLA) (*6*), low density polyethylene (LDPE) (*4*), and poly(vinyl alcohol) (PVOH) (*7*). For these applications, the pinto beans were first ground into a powder. The scanning electron microscopy (SEM) photomicrographs of pinto bean powder are shown in Figure 1. Elliptically shaped starch granules and irregular particles of protein and other bean components can be observed.

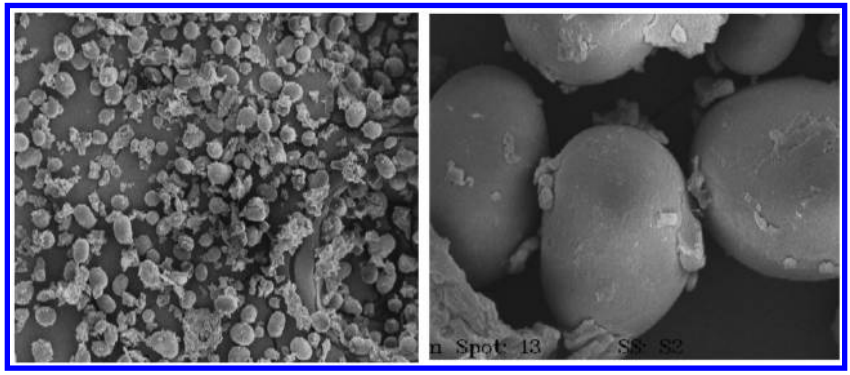

Figure 1. SEM photomicrographs of pinto bean powder. Left image 190X, right image 1700X.

PLA Filler

For composite formation, pinto bean powder was mixed with PLA and extruded into ribbons (*6*). The SEM photomicrographs of the fracture surfaces of PLA and PLA composites are shown in Figure 2. PLA itself had a relatively smooth fracture surface, but the surface of the PLA-bean powder composite was rough and clearly showed the presence of starch granules.

The mechanical properties of PLA and PLA-filler composites were reduced by the addition of the filler (*6*) (Table 2, where TS = tensile strength, E = elongation at breakage, and YM = Young's modulus). The addition of maleic anhydride (MA) and Lupersol 101 peroxide (L101) caused further reductions in mechanical properties. The main advantage of using bean filler in PLA is to

In Green Polymer Chemistry: Biocatalysis and Materials II; Cheng, H., et al.;
ACS Symposium Series; American Chemical Society: Washington, DC, 2013.

Publication Date (Web): November 22, 2013 | doi: 10.1021/bk-2013-1144.ch022

decrease cost. The filler perhaps can be used in PLA applications where cost reduction is important and reduced mechanical properties are acceptable. Possible examples are biodegradable and compostable plastics, such as agricultural mulch films, compost bags, and perhaps disposable dinnerware.

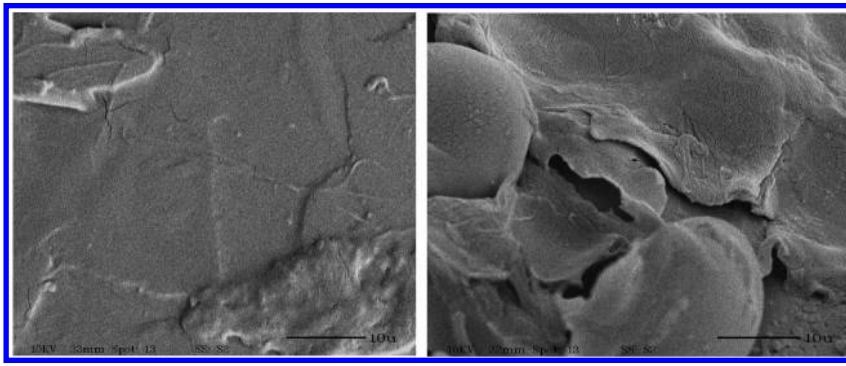

Figure 2. SEM photomicrographs of PLA (left) and PLA-pinto bean powder composite, both at 1700X.

Table 2. Mechanical properties of pre-dried PLA and PLA-filler composites formed with pinto bean powder [a]. Data adapted from ref. (*6*)

PLA:filler:MA:L101	*Thickness (mm)*	*TS (N/mm^2)*	*E (%)*	*YM (N/mm^2)*
100:0	1.83±0.08	58.6±0.8	16.7±1.2	493±14
90:10	1.75±0.16	31.5±2.6	9.5±1.8	448±26
80:20	1.72±0.06	23.2±2.3	6.9±0.8	412±42
90:10:2:0.5	1.86±0.15	17.9±3.6	7.8±0.9	314±12
90:10:4:0.5	1.89±0.21	16.3±2.2	8.2±1.1	285±14
80: 20:2:0.5	1.96±0.07	12.0±1.6	5.7±0.9	288±21
80:20:4:0.5	1.93±0.05	14.1±1.3	6.2±1.3	322±30

[a] PLA and filler were preheated and dried at 50°C for 3 days in an oven. Standard deviations are shown after ± signs.

LDPE Filler

Powdered pinto bean was mixed with LDPE in an extruder, and the resulting composite was cut into ribbons (*6*). The SEM photomicrographs of the fracture surfaces of PLA and PLA-bean composite are shown in Figure 3. LPDE had a wrinkled and partly torn surface; the surface of the LDPE-bean composite appeared even more torn, with starch particles clearly evident that gave signs of incompatibility with LDPE.

In Green Polymer Chemistry: Biocatalysis and Materials II; Cheng, H., et al.;
ACS Symposium Series; American Chemical Society: Washington, DC, 2013.

Publication Date (Web): November 22, 2013 | doi: 10.1021/bk-2013-1144.ch022

Publication Date (Web): November 22, 2013 | doi: 10.1021/bk-2013-1144.ch022

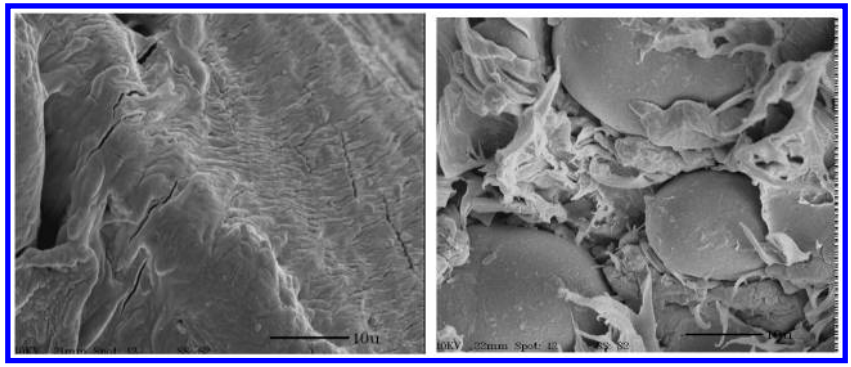

Figure 3. SEM photomicrographs of LDPE (left) and LDPE-pinto bean powder composite, both at 1700X.

The addition of bean powder filler to LDPE had a negative effect on tensile strength and elongation of the composite materials (*6*) (Table 3). However, the Young's modulus was enhanced. The addition of MA and L101 negatively impacted tensile strength and elongation, but further enhanced Young's modulus. Thus, for applications needing a stiffer polyethylene at reduced cost, the use of bean filler might be beneficial.

Table 3. Mechanical properties of pre-dried LDPE and LDPE-filler composites formed with pinto bean powder [a]. Data adapted from ref. (*6*)

LDPE:filler:MA:L101	*Thickness (mm)*	*TS (N/mm^2)*	*E (%)*	*YM (N/mm^2)*
100:0	2.12±0.32	12.4±0.7	241.3±13.2	78±2.1
90:10	2.27±0.21	9.5±0.6	35.2±4.2	83±3.5
80:20	2.28±0.25	7.1±0.6	22.4±2.3	87±4.9
90:10:2:0.5	2.35±0.10	8.7±0.4	20.9±1.6	87±5.8
90:10:4:0.5	2.32±0.29	7.4±0.6	16.8±1.0	86±2.3
80:20:2:0.5	2.27±0.15	6.5±0.5	11.6±1.4	99±5.4
80:20:4:0.5	2.27±0.08	7.0±0.9	12.4±1.8	97±6.8

[a] PLA and filler were preheated and dried at 50°C for 3 days in an oven. Standard deviations are shown after ± signs.

PVOH Filler

The pinto bean was defatted (fat < 0.01%), milled into powder, and passed through a 30-mesh screen (sieve size 0.6 mm) to give the pinto bean flour (PBF) (*7*). The pinto bean high starch fraction (PBHSF) was obtained from the bean flour through repeated extractions in dilute alkali according to a procedure in the literature (*23*).

In Green Polymer Chemistry: Biocatalysis and Materials II; Cheng, H., et al.;
ACS Symposium Series; American Chemical Society: Washington, DC, 2013.

Cold gelatinization (*24*, *25*) was used to make films of PBF and PBHSF with PVA. Initial mechanical testing showed PVOH/PBF film to have better properties than PVOH/PBHSF film; thus, more work was done with the PVA/PBF composite (*7*). Different amounts of PBF in the composite were used, and mechanical testing carried out along (parallel) and perpendicular (nonparallel) to the direction of film formation. The results obtained for both directions were the same within the limits of experimental error, indicating no strong directional dependence (Table 4). The tensile strength was reduced when PBF was added to PVA, but the elongation actually increased when 20-40% PBF was added to PVA and then decreased at 60% PBF. The Young's modulus first decreased in the films containing 20-40% PBF but then increased in the film containing 60% PBF.

Publication Date (Web): November 22, 2013 | doi: 10.1021/bk-2013-1144.ch022

Table 4. Mechanical properties of films from PVA and PVA/PBF composites at different PBF levels [a]

sample	*% PBF*	*thickness (mm)*	*TS (N/mm^2)*	*E (%)*	*YM (N/mm^2)*
parallel-1	0	0.083	49±3	336±62	652±121
parallel-2	20	0.140	31±1	757±75	31±8
parallel-3	40	0.125	23±0	530±27	55±12
parallel-4	60	0.152	13±1	44±7	184±24
nonparallel-1	0	0.076	57±7	315±59	865±74
nonparallel-2	20	0.131	28±1	706±52	31±5
nonparallel-3	40	0.088	23±1	539±99	66±9
nonparallel-4	60	0.164	13±1	36±12	177±34

[a] Data from ref. (*7*). Standard deviations are shown after ± signs.

Thus, pinto bean appears to be a potentially low-cost filler for PVA with enhanced elongation up to 40% PBF level. Currently PVA-starch composites are being considered for use in agriculture for transportation of plants (*26*), as film to cover the surface of cultivated fields (*26*), as fertilizer encapsulant (*27*), and as water-soluble packaging material (*28*). Perhaps the PVA/edible bean composites can also be considered for these same applications in the future.

Triglyceride Oils in Common Beans

Four common beans (black, kidney, Great Northern, and pinto) were extracted with hexane and found to contain about 2% triacylglycerols (*8*). The fatty acids in these bean oils were mainly linolenic (41.7–46 wt%), linoleic (24.1–33.4 wt%), palmitic (10.7–12.7 wt%) and oleic (5.2–9.5 wt%). Although the levels of polyunsaturated fatty acids in the bean oils were higher than those in soybean oil, the bean oils exhibited high oxidative stability because of the high amounts of tocopherols present (2,670–2,970 ppm) (*8*).

In Green Polymer Chemistry: Biocatalysis and Materials II; Cheng, H., et al.;
ACS Symposium Series; American Chemical Society: Washington, DC, 2013.

Triglycerides are known to be viable alternatives to mineral oils in lubricants. It was reported that the oil extracted from the navy bean hull could be a potential natural antioxidant for use in vegetable oils such as soybean and sunflower oils (*29*). Since triglycerides are compatible with mineral oils, the bean oils may also be used as antioxidants for other lubricants. In addition, triglycerides have been converted to epoxides, polyols, and dimer products and used as polymer components or additives (such as stabilizers, plasticizers, and surfactants) (*30*, *31*). The bean oils should be able to serve in the same capacities and with improved oxidative stability.

Phenolic Phytochemicals in Common Beans

Common beans are known to contain a significant amount of flavonoids, polyphenols, and phenolics. The levels were found to be higher in seed hull than in cotyledon, and higher in dark-colored beans versus light colored beans (*9*, *32*, *33*). Recently microwave-assisted extraction at 150°C and 50% ethanol in water was found to be particularly effective in extracting phenolics out of common beans, producing 2-3 times more phenolics than conventional heat extractions (*9*). The phenolic level ranged from 3 to 11 mg per g bean hull and from 8 to 70 mg per g bean cotyledon (in gallic acid equivalents). Somewhat similar results were obtained from antioxidant assays (*10*). In view of the high phenolic content and the ease of extraction, the phenolic antioxidants from common beans may perhaps be potential natural additives for use in food polymers or in food-contact packaging materials.

Conversion of Bean Starch to Ethanol

Eight common beans, from Northarvest Bean Growers Association, were evaluated for potential conversion of starch to ethanol (*11*). Enzymes were supplied by Genencor International (Beloit, WI). The beans were assayed in a laboratory-scaled process based upon the commercial corn dry grind fermentation process (*34*, *35*). The beans were ground and added to 100 mL distilled water in 500 mL Corning bottles and adjusted to pH 6.0-6.5 with $Ca(OH)_2$. α-Amylase (8 units/g beans) was added, and the mixtures heated to 90°C and then autoclaved for 15 min. Additional α-amylase (16 units/g beans) was added, and the mixture was incubated at 95°C for 60 min. They were cooled on ice, and the pH of mixtures adjusted to 4.0-4.5 with phosphoric acid. Glucoamylase (0.4 units/g), 0.03% (w/v) $(NH_4)_2SO_4$ and 4×10^{-4}% Antifoam 289 (Sigma, St. Louis, MO) were added, followed by inoculation with an overnight preculture of *S. cerevisiae* Y-2034 to OD 550 = 1.0 (1-cm path-length; DU640 spectro-photometer, Beckman Coulter, Fullerton, CA). Fermentations were carried out at 32°C and mixed by shaking at 100 rpm (Innova 4230 incubator shaker, New Brunswick Scientific, Edison, NJ). At 72 h, fermentation supernatants were sampled for product analysis. More details were given in the original reference (*11*).

The starch content of the beans used was around 40% (Table 5). Ethanol yield was 0.43–0.51 g ethanol/g glucose (0.19–0.23 g ethanol/g beans). The average

In Green Polymer Chemistry: Biocatalysis and Materials II; Cheng, H., et al.;
ACS Symposium Series; American Chemical Society: Washington, DC, 2013.

Publication Date (Web): November 22, 2013 | doi: 10.1021/bk-2013-1144.ch022

ethanol yield for the eight bean types was 92% of maximum theoretical yield, demonstrating that starch from beans could be efficiently converted to ethanol. Ethanol concentration obtained from 20% (w/w) solids loading was 3.5–4.4% (w/v). The residual fermentation solids contained, on a dry basis, 37.1–43.6% crude protein, 10.8–15.1% acid detergent fiber and 19.1–31.3% neutral detergent fiber. Thus, this work showed that bean starch could be readily converted to ethanol, using the same process and enzymes applied to corn.

Table 5. Starch present in beans and ethanol[a] derived from fermentation. Data adapted from ref. (*11*)

Bean type	*Starch (% db)*	*Final ethanol (% w/v)*	*Ethanol yield (g g−1 glucose)*	*Efficiency (% of theoretical)*
Black	40.9	4.09 ± 0.33	0.46 ± 0.04	88.3
Pinto	42.2	4.39 ± 0.44	0.48 ± 0.04	94.0
Dark red kidney	39.5	3.54 ± 0.45	0.48 ± 0.01	92.6
Light red kidney	42.1	3.92 ± 0.12	0.46 ± 0.01	90.3
Pink	40.8	3.67 ± 0.02	0.43 ± 0.01	83.5
Navy	40.0	4.22 ± 0.06	0.50 ± 0.01	97.6
Great northern	39.8	4.29 ± 0.24	0.51 ± 0.04	100
Small red	44.0	4.22 ± 0.55	0.46 ± 0.06	90.4

[a] Average values reported ± standard deviation; each experiment was carried out at least twice, in triplicate.

Publication Date (Web): November 22, 2013 | doi: 10.1021/bk-2013-1144.ch022

Conclusions

In this work, several examples from the authors' work are given to illustrate the potential applications of common beans in food and biobased products. The use of common beans as fillers in polymers is perhaps unconventional, but in all three polymers (PLA, LDPE, and PVOH) the bean fillers seem to be useful; at the very least the bean fillers reduce the cost of the polymeric composites. The rather extensive data on extrusion cooking of beans may be of use to food technologists interested in the product development of extruded beans. The results of triglycerides and phenolic phytochemicals demonstrate the ease of extraction and the potential value of these materials. The ethanol yield obtained from bean starch suggests that the ethanol may be considered a coproduct, and together with bean triglycerides and phytochemicals they may provide added value to the common beans.

In Green Polymer Chemistry: Biocatalysis and Materials II; Cheng, H., et al.;
ACS Symposium Series; American Chemical Society: Washington, DC, 2013.

Publication Date (Web): November 22, 2013 | doi: 10.1021/bk-2013-1144.ch022

Acknowledgments

The USDA work cited in this review was supported by a grant from Northarvest Bean Growers Association. The authors thank N. Sutivisedsak, M.A. Cotta, B.S. Dien, R.L. Evangelista, V. L. Finkenstadt, C. Hall, S. Liu, B. R. Moser, N. N. Nichols, B. K. Sharma, M. Singh and J. L. Willett for fruitful collaborations. Mention of trade names or commercial products in this publication is solely for the purpose of providing specific information and does not imply recommendation or endorsement by the U.S. Department of Agriculture. USDA is an equal opportunity provider and employer.

References

1. Sathe, S. K.; Deshpande, S. S.; Salunkhe, D. K. *Crit. Rev. Food Sci. Nutr.* **1984**, *20*, 1–46.
2. Data from U.S. Department of Agriculture, Economics, Statistics and Market Information System (ESMIS). http://usda.mannlib.cornell.edu/MannUsda/viewDocumentInfo.do?documentID=1394.
3. U.S. Department of Agriculture, Economic Research Service, Briefing Room: Dry Beans. http://www.ers.usda.gov/Briefing/Drybeans/background.htm.
4. Ensminger, A. H. *Food and Nutrition Encyclopedia*, 2nd ed.; CRC Press: Boca Raton, FL, 1993; Vol. 1, p 170.
5. Sutivisedsak, N.; Singh, M.; Liu, S.; Hall, C.; Biswas, A. *J. Food Process. Preserv.* **2012**, DOI: 10.1111/j.1745-4549.2012.00692.x.
6. Sutivisedsak, N.; Cheng, H. N.; Liu, S.; Lesch, W. C.; Finkenstadt, V. L.; Biswas, A. *J. Biobased Mater. Bioenergy* **2012**, *6*, 1–10.
7. Sutivisedsak, N.; Biswas, A.; Finkenstadt, V. L.; Cheng, H. N. *ACS Polym. Prepr.* **2011**, *52* (2), 256–257.
8. Sutivisedsak, N.; Moser, B. R.; Sharma, B. K.; Evangelista, R. L.; Cheng, H. N.; Lesch, W. C.; Tangsrud, R. R.; Biswas, A. *J. Am. Oil Chem. Soc.* **2011**, *88*, 193–200.
9. Sutivisedsak, N.; Cheng, H. N.; Willett, J. L.; Lesch, W. C.; Biswas, A. *Food Res. Int.* **2010**, *43*, 516–519.
10. Biswas, A.; Sutivisedsak, N.; Cheng, H. N.; Willett, J. L.; Lesch, W. C.; Tangsrud, R. R. *J. Food Agric. Environ.* **2012**, *10* (1), 89–96.
11. Nichols, N. N.; Sutivisedsak, N.; Dien, B. S.; Biswas, A.; Lesch, W. C.; Cotta, M. A. *Ind. Crops Prod.* **2011**, *33*, 644–647.
12. Camire, M. E.; Camire, A.; Krumhar, K. *Crit. Rev. Food Sci. Nutr.* **1990**, *29*, 35–571990.
13. Avin, D.; Chin-Hong, K.; Maga, J. A. *J. Food Process. Preserv.* **1992**, *16*, 327–335.
14. Steel, C. J.; Sgarbieri, V. C.; Jackix, M. H. *J. Agric. Food Chem.* **1995**, *43*, 2487–2492.
15. Berrios, J. D. J.; Camara, M.; Torija, M. E.; Alonso, M. *J. Food Process. Preserv.* **2002**, *26* (2), 113–128.

16. Gomes, J. C.; Oliveira da Silva, C.; Costa, N. M. B.; Pirozi, M. R. *Rev. Ceres* **2006**, *53* (309), 548–558.
17. Rocha-Guzman, N. E.; Gallegos-Infante, J. A.; Gonzalez-Laredo, R. F.; Castillo-Antonio, P. A.; Delgado-Licon, E.; Ibarra-Perez, F. *LWT – Food Sci. Technol.* **2006**, *39* (1), 6–10.
18. Drago, S. R.; Velasco-Gonzalez, O. H.; Torres, R. L.; Gonzalez, R. J.; Valencia, M. E. *Plant Foods Hum. Nutr.* **2007**, *62* (2), 43–48.
19. Korus, J. *Zywnosc* **2007**, *14* (6), 149–1582007.
20. Korus, J.; Gumul, D.; Czechowska, K. *Food Technol. Biotechnol.* **2007**, *45* (2), 139–146.
21. Balandran-Quintana, R. R.; Barbosa-Canovas, G. V.; Zazueta-Morales, J. J.; Anzaldua-Morales, A.; Quintero-Ramos, A. *J. Food Sci.* **1998**, *63* (1), 113–116.
22. Matin-Cabrejas, M. A.; Jaime, L.; Karanja, C.; Downie, A. J.; Parker, M. L.; Lopez-Andreu, F. J.; Maina, G.; Esteban, R. M.; Smith, A. C.; Waldron, K. W. *J. Agric. Food Chem.* **1999**, *47*, 1174–1182.
23. Sathe, S. K.; Salunkhe, D. K. *J. Food Sci.* **1981**, *46*, 617–621.
24. Wootton, M.; Ho, P. *Starch/Starke* **1989**, *41*, 261–265.
25. Romero-Bastida, C. A.; Bello-Perez, L. A.; Garcia, M. A.; Martino, M. N.; Solorza-Feria, J.; Zaritzky, N. E. *Carbohydr. Polym.* **2005**, *60*, 235–244.
26. Maruhashi, M.; Tokonami, H. U.S. Patent 5,106,890, April 21, 1992.
27. Han, X. Z.; Chen, S. S.; Hu, X. G. *Desalination* **2009**, *240*, 21–26.
28. BDP Green Technology Co. www.bdpplastics.com.
29. Onyeneho, S. N.; Hettiarachchy, N. S. *J. Agric. Food Chem.* **1991**, *39*, 1701–1704.
30. Hill, K. *Pure Appl. Chem.* **2000**, *72*, 1255–1264.
31. Biswas, A.; Sharma, B. K.; Willett, J. L.; Erhan, S. Z.; Cheng, H. N. *Energy Environ. Sci.* **2008**, *1*, 639–644.
32. Xu, B. J.; Yuan, S. H.; Chang, S. K. C. *J. Food Sci.* **2007**, *72*, 167–177.
33. Hassimoto, N. M. A.; Genovese, M. I.; Lajolo, F. M. *J. Agric. Food Chem.* **2005**, *53*, 2928–2935.
34. Nichols, N. N.; Dien, B. S.; Wu, Y. V.; Cotta, M. A. *Cereal Chem.* **2005**, *82*, 554–558.
35. Wilhelmi, A. J.; Wiesenborn, D. P.; Gustafson, C. R.; Pryor, S. W. *Appl. Eng. Agric.* **2009**, *25*, 709–717.

Publication Date (Web): November 22, 2013 | doi: 10.1021/bk-2013-1144.ch022

Publication Date (Web): November 22, 2013 | doi: 10.1021/bk-2013-1144.ch023

Chapter 23

Preparation and Characterization of Protein Isolate from Glandless and Glanded Cottonseed

Michael K. Dowd*,[1] and Milagros P. Hojilla-Evangelista[2]

[1]Southern Regional Research Center, U.S. Department of Agriculture, 1100 Robert E. Lee Blvd., New Orleans, Louisiana 70124
[2]National Center for Agriculture Utilization Research, U.S. Department of Agriculture, 1815 N. University Ave., Peoria, Illinois 61604
***E-mail:michael.dowd@ars.usda.gov**

Protein isolates were prepared from meals recovered from both glandless and glanded cottonseed. Isolate yield was 2.5-fold greater from the glandless meal than from the glanded meal, indicating that the gossypol in the glanded meal was likely promoting the formation of protein aggregates that were more difficult to extract. Both isolate preparations were very high in protein (>96%). Electrophoresis showed essentially identical band patterns in the meals and isolates, although some bands appeared to be preferentially concentrated in the isolates. Small shifts in the amino acid distributions were apparent—the most notable being a decrease in the lysine and an increase in the arginine levels in the isolates compared with the meals. Cottonseed isolates demonstrated considerable solubility in both acidic and alkaline environments. Functional properties were largely within the range of typical values for protein preparations. The composition and functional properties of the glandless isolates suggest that cottonseed proteins should be useful in food formulation.

In Green Polymer Chemistry: Biocatalysis and Materials II; Cheng, H., et al.;
ACS Symposium Series; American Chemical Society: Washington, DC, 2013.

Publication Date (Web): November 22, 2013 | doi: 10.1021/bk-2013-1144.ch023

Introduction

Defatted cottonseed meal is used mainly as a protein ingredient in ruminant animal feed. Unlike other oilseed meals, the development of alternative uses for cottonseed protein has been limited by the presence of gossypol, a polyphenolic secondary product of the cotton plant that exhibits some toxicity. This toxicity keeps cottonseed protein from being used in non-ruminant feeds or developed into food ingredients. In part because of its chemistry and the steps used to prepare seed for oil extraction, most gossypol remains with the meal after separation of the oil.

In the late 1950s, McMichael identified a "glandless" trait in Hopi cotton varieties (*1*). Cotton plants with this recessive trait do not contain the lysigenous glands that the plant uses to sequester gossypol, and consequently, gossypol accumulation in these plants is greatly limited. For a period of time in the late 1960s and early 1970s, it was thought these varieties might become commercial, and efforts were made to study the proteins from varieties with this trait (*2*). Unfortunately, questions regarding reduced crop yield and lower fiber quality due to increased insect susceptibility kept these varieties from becoming commercial, and most of the efforts focused on new uses for cottonseed proteins were abandoned. Over time, the idea developed to modify the plant to suppress gossypol production in the seed but maintain its presence in other tissues. Rathore and coworkers (*3*) recently achieved this goal by employing RNAi techniques with a seed specific promoter. Although many hurdles need to be overcome before these plants can become commercial, this development has reinitiated interest into the processing and product benefits that might be derived from a "gossypol-free" cottonseed. Because it is not yet possible to work with quantities of these new seed lines, glandless varieties are being grown for the purpose of getting a head start on the benefits that might be expected from this development.

In this work, cottonseed protein isolates were prepared to study their compositional and functional properties. Isolates were derived from defatted meals prepared from both "glandless" and "glanded" seed types. Defatted meals were produced under conditions typically used for commercial cottonseed oil extraction. Isolates were prepared by alkaline extraction, similar to methods used for preparation of isolates from other plant seeds (*4–6*). This procedure differs from the sequential fractionation approach proposed for cottonseed by Berardi et al. (*7*) and Martinez et al. (*8*) but the process is simpler, and it provides a good indication of the yields, purities, and basic protein compositional and functional properties that can be obtained from currently available meals.

Methods

Materials

The two cottonseed meals used for this work were provided by Cotton, Inc. (Cary, NC, USA). One meal (referred to as glanded meal) was prepared from glanded cottonseed and was produced under typical expander-solvent extraction conditions, except that the usual addition of hulls back to the meal was reduced

In Green Polymer Chemistry: Biocatalysis and Materials II; Cheng, H., et al.;
ACS Symposium Series; American Chemical Society: Washington, DC, 2013.

in order to elevate the meal's protein level above that of commercial meal. This meal was ground to pass a 20-mesh sieve and was used essentially as is. The second meal (referred to as glandless meal) was produced by the same process from glandless cottonseed. Due to processing problems at the time, however, this meal contained around 6% lipid, which was too high for good isolate preparation. Consequently, this meal was ground to pass a 20-mesh sieve and was re-extracted with hexane (commercial grade, 4:1 v/w) for 2 hr at 50 °C in a 20-L rotary evaporator with condensate recycling. After extraction, the meal was separated by vacuum filtration, washed with additional hexane, then allowed to off-gas solvent vapors first under a hood and then under vacuum. This process reduced the amount of oil in the meal to a level suitable for isolate preparation.

Publication Date (Web): November 22, 2013 | doi: 10.1021/bk-2013-1144.ch023

Isolate Preparation

Isolates were prepared from both meal samples by alkali solubilization and acid precipitation. Fifty gram batches of each meal were extracted with a 0.027 M NaOH solution (pH 11) (1:15 w/v) for 30 min at room temperature. After extraction, the slurries were centrifuged at 10,000 x g for 10 min to pellet meal debris and the supernatants were recovered. These solutions were acidified to pH 5 with 1 M HCl, resulting in precipitation of a significant portion of the solubilized protein. The recovered slurries were allowed to stand overnight at 4 °C, which facilitated settling of the protein solids. Most of the liquid fraction was decanted, and the wet solids were centrifuged to separate more liquid. The recovered protein was washed twice with water and centrifuged at 10,000 x g for 5 min to remove salt. The isolates were freeze-dried, weighed, and stored at –20 °C until used. Each sample was prepared in triplicate. Yield and basic compositional properties were determined from these samples.

A second set of extractions was then conducted at the same scale with the same procedures. The products from these extractions were pooled to provide sufficient sample (~100 g of each isolate) to conduct electrophoresis, amino acid and functional property testing.

Isolate and Meal Characterization

The meals and isolates were characterized for moisture, protein, crude oil, gossypol and color. Crude oil was determined by extraction with a Soxtec HT6 solvent extractor (Foss North America, Eden Prairie, MN, USA). Three-gram samples were extracted with 40 mL of petroleum ether. The extraction period was 30 min followed by a 2 hr oil recovery cycle, a 30 min solvent evaporation step, and a 30 min oven drying step to remove traces of solvent. Extracted oil was measured gravimetrically. Protein was measured with a LECO (St. Joseph, MI, USA) TrueSpec nitrogen analyzer on 150 mg samples. The nitrogen-to-protein conversion ratio used was 5.9, which is recommended for cottonseed meal products based on reported amino acid distributions (*9*). Gossypol was measured by forming a Schiff's base adduct with *R*-(–)-2-amino-1-propanol, which was detected and quantified by reverse-phase HPLC as described in AOCS Recommended Practice Ba 8a-99 (*10*). These procedures were conducted in

In Green Polymer Chemistry: Biocatalysis and Materials II; Cheng, H., et al.;
ACS Symposium Series; American Chemical Society: Washington, DC, 2013.

duplicate, and the results were averaged for each sample. Meal and isolate color was determined with a HunterLabs (Reston, VA, USA) Colorflex EZ colorimeter and recorded on the Hunter *L*, *a*, *b* scale. Each sample was analyzed four times and the results averaged.

Amino acid analysis of the meal and pooled isolate sample was determined by Eurofins Nutrition Analysis Center (Des Moines, IA, USA) employing typical acid hydrolysis and HPLC separation techniques. Electrophoretic separation of the peptides/proteins was also conducted. For this, samples were weighed into micro centrifuge tubes to provide 5 mg of protein, and each sample was mixed with 1 mL of sample buffer containing 42 mM Tris-HCl (pH 6.8), 2% SDS, 7% glycerol, 4.4% β-mercaptoethanol and 5 M urea. The tubes were heated briefly in a 100 °C dry bath with periodic vortex mixing to maximize protein solubilization. These samples (5 µL) with 0.5 µL of NuPage sample buffer (4X) were loaded onto lanes of a 4–12% Bis-Tris NuPage gradient polyacryamide gel (Life Technologies, Grand Island, NY, USA). One lane was loaded with 10 to 250 kDa protein standards (Bio-Rad Life Science, Hercules, CA, USA). Electrophoresis was conducted in a Novex XCell II mini electrophoresis system with NuPage MES-SDS running buffer. After electrophoresis, the gel was heated with water in a microwave oven for 90 sec, the water changed, and the process repeated with 1 min of additional heating, and then the samples were slowly agitated on a rocker table for 5 min. The gel was stained with SimplyBlue SafeStain (Life Technologies), heated in the microwave oven for 30 sec and again allowed to sit on the rocker table for 5 min. The gel was destained in water with gentle agitation on the rocker table for 20 min, the water was changed, and the gel was left on the rocker table overnight. Peptide/protein bands were observed with the Odyssey CLx gel imaging system (LI-COR Biosciences, Lincoln, NE, USA).

Publication Date (Web): November 22, 2013 | doi: 10.1021/bk-2013-1144.ch023

Functional Characterization of Isolates

Solubility Profiles

Solubility profiles were generated as described by Myers et al. (*11*). Aqueous dispersions containing 10 mg protein/mL were prepared, and their pH was adjusted to 2.0, 4.0, 5.5, 7.0, 8.5 or 10.0 by adding 1 M HCl or 1 M NaOH. The samples were mixed vigorously on a platform shaker for 5 min, and then centrifuged at 10,000 x g for 15 min. The amount of soluble protein in the supernatants was determined spectrophotometrically by the Biuret method with bovine serum albumin used for the standard curve.

Surface Hydrophobicity Index (S_o)

The method of Hojilla-Evangelista et al. (*12*), a modification of the method reported by Sorgentini et al. (*4*), was used to determine the surface hydrophobicity of the soluble proteins. Protein dispersions with 2 mg protein/mL were prepared, and their pH values were adjusted to provide the greatest amounts of soluble protein (i.e., pH 2 or 10) by adding 1 M HCl or 1 M NaOH.

In Green Polymer Chemistry: Biocatalysis and Materials II; Cheng, H., et al.;
ACS Symposium Series; American Chemical Society: Washington, DC, 2013.

Supernatants were diluted with appropriate buffer to produce 1/2, 1/5, 1/10, and 1/100 concentrations of the starting protein content. The fluorescence probe was 8-anilino-1-naphthalene sulfonate (8.0 mM). Fluorescence intensities were measured with a Varian (Walnut Creek, CA, USA) Cary Eclipse Fluorescence Spectrophotometer with a slit opening of 2.5 nm (pH 2) or 5 nm (pH 10) and wavelengths of 350 nm (excitation) and 525 nm (emission). Intensities were plotted against protein concentration, and the initial slope of the graph was taken as S_o.

Foaming Properties

Foaming capacity (mL) and foam stability (%) were determined according to the method described by Myers et al. (*11*) at pH 2.0 and 10.0. Twenty-five milliliters of aqueous dispersions containing 10 mg protein/mL were prepared, and their pH was adjusted to the desired level as described above. A calibrated pipette containing 20 mL of supernatant was lowered carefully, avoiding contact with the sides, towards the fritted disc at the bottom of a graduated foaming column, where its contents were dispensed. Air was introduced into the bottom stem (below the fritted disc) at a flow rate of 100 mL/min. Time was started at the first appearance of bubbles, and foaming proceeded for 1 min at which time the air valve was closed. The volume of foam produced at 1 min was taken as the foaming capacity, while the percentage of foam volume remaining in the column after 15 min was taken as the foam stability.

Emulsification Properties

Emulsification activity index (m^2/g), which measures the area of an oil-water emulsion interface stabilized per unit weight of protein, and emulsion stability index (min) were determined according to the method of Wu et al. (*13*). Samples providing 1 mg protein/mL were dispersed in water, and small amounts of 1 M NaOH or HCl were added to attain the desired final sample pH. Mixtures were allowed to stand for 15 min. Sample supernatants (6 mL) and corn oil (2 mL) were combined in a beaker and then homogenized by a hand-held homogenizer operated at 20,000 rpm for 1 min. Aliquots (50 μL) were pipetted from the bottom of the mixture immediately after homogenization and after standing for 10 min. Each sample was diluted with 5 mL of a 0.1% SDS solution, and its absorbance was read at 500 nm. Emulsification activity and stability indices were calculated as described by Wu et al. (*13*).

Water-Holding Capacity

Water holding capacity (g/g) was determined by adapting the method of Balmaceda et al. (*14*) for partly-soluble materials. In a pre-weighed centrifuge tube, 1.0 g of sample was added followed by 30 mL distilled water. The tube

Publication Date (Web): November 22, 2013 | doi: 10.1021/bk-2013-1144.ch023

was capped tightly, secured on a platform shaker, and then mixed vigorously for 15 min. The supernatant pH was measured and adjusted to the desired value by adding 1 M HCl or NaOH. The tube containing the sample was heated for 30 min in a water-bath set at 60 °C, cooled for 30 min in tap water, and centrifuged at 10,000 x g for 15 min at 25 °C. The supernatant was decanted and the tube with spent solids was weighed. The water holding capacity was calculated as described in the original report (*14*).

Results

As expected, the glanded and glandless meals were considerably different in gossypol composition, with the glanded meal containing 1.18% gossypol (dwb) and the glandless containing 0.02% gossypol (dwb) (Table 1). The protein levels of the meals were higher than in commercial cottonseed meal (~41%), primarily because of the limited amount of hull material added back to the kernels during oil extraction. Crude oil level in the glanded meal was typical of commercial operations (1–2%). The additional hexane extraction of the glandless sample resulted in a very low oil level of 0.14% (dwb). Commercial cottonseed meals are typically yellow to reddish-brown in color. The glandless meal was lighter in color (higher Hunter *L* value) and contained less "redness" (lower *a* value) compared with the glanded meal. This difference is partly related to the difference in gossypol levels, as gossypol itself is pigmented (yellow) and often darkens cottonseed products, e.g., the color-set problems that can occur when refining some crude cottonseed oils that have been exposed to the compound for prolonged periods.

Initial experiments were conducted to determine isolate yield and composition (Table 1). The yield of isolate from the glandless meal was 23.6%, compared with only 10.6% from the glanded meal. This difference is likely due to the presence of gossypol in the glanded meal. Gossypol has two aldehyde groups that readily form Schiff's base adducts with primary amines, and the compound is well-known to bind to cottonseed proteins (*15*, *16*). In cottonseed meal, most gossypol (generally greater than 70%) is present in bound form (*17*). Because gossypol has a pair of aldehyde groups, it has the potential to cross-link protein, which would promote protein aggregation and make the protein less soluble. Evidence that this has occurred in the glanded sample comes from the gossypol level in the glanded isolate, which was only 0.17% compared with the 1.18% level in the original meal. Because most of the gossypol in the meal is bound to protein and it is not extracted into the isolate, it must be retained within the nonextractable fraction of the meal protein.

Protein levels were very high in both cottonseed isolates (97–99% dwb) compared with typical soy protein isolates, which would have ~90% protein. These protein values (Table 1) are based on a nitrogen-to-protein conversion factor of 5.9 derived from reported amino acid analyses for cottonseed meals (*9*). Use of the more conventional 6.25 conversion factor would have resulted in protein levels greater than 100%. Given the pureness of the protein and the 26% product yield, recovery of meal protein as isolate was ~40% for the glandless

Publication Date (Web): November 22, 2013 | doi: 10.1021/bk-2013-1144.ch023

In Green Polymer Chemistry: Biocatalysis and Materials II; Cheng, H., et al.;
ACS Symposium Series; American Chemical Society: Washington, DC, 2013.

sample but only 20% for the glanded preparation. The isolates were darker in color than their parental meals, as indicated by the lower Hunter *L* values (Table 1). In appearance, the glandless isolates were a light-brown color, whereas the glanded isolates were more of a medium-to-dark brown color.

Table 1. Isolate yield and the composition and color of cottonseed meals and isolates[a]

	Glandless meal	*Glandless isolate*	*Glanded meal*	*Glanded isolate*
Yield,[b] %	-	23.6 ± 0.4	-	10.6 ± 0.2
Composition[b]				
Protein,[c] %	61.9 ± 0.1	99.3 ± 0.3	53.7 ± 0.1	96.7 ± 0.5
Lipid, %	0.14 ± 0.03	0.02 ± 0.02	1.67 ± 0.04	0.09 ± 0.04
Gossypol, %	0.02 ± 0.00	0.01 ± 0.00	1.18 ± 0.01	0.17 ± 0.01
Color				
L	76.5 ± 0.3	54.0 ± 4.9	47.9 ± 0.2	32.5 ± 1.2
a	2.0 ± 0.1	5.9 ± 0.8	10.8 ± 0.1	10.3 ± 0.0
b	21.9 ± 0.2	24.6 ± 0.3	29.8 ± 0.1	19.8 ± 0.7

[a] Values reported as mean±standard deviation. Standard deviations for the meals represent measurement variance. Standard deviations for the isolate data represent replicate variance (n=3). [b] Yield and compositional data are reported on dry weight basis. [c] Protein = measured nitrogen x 5.9.

Amino acid analysis, electrophoresis, and functionality testing were performed on the meals and pooled isolate samples. The amino acid analyses (Table 2) showed that there were only minor differences in the distributions between the glanded and glandless meals and between the glanded and glandless isolates. There appeared to be some shift in the amino acid distributions between the meal and isolate samples for each type of seed, suggesting preferential extraction of individual protein components. For example, the lysine content of the glanded meal was reduced from 4.2 g per 100 g protein to 2.7 g per 100 g of protein in the glanded isolate (Table 2) and a similar reduction was apparent in the glandless meal and isolate samples. Gossypol Schiff's base cross-linking of proteins with lysine moieties might reduce the extractability of these proteins and result in this kind of shift, but the same effect does not account for the shift in the glandless preparation, which suggests that these shifts are more likely related to general extractability of individual components. Cystine, threonine, and methionine levels also appeared to be reduced in the isolates compared with the original meals. The opposite trend was apparent for phenylalanine and arginine, which were present in greater proportions in the isolates than in the meals.

Publication Date (Web): November 22, 2013 | doi: 10.1021/bk-2013-1144.ch023

Electrophoresis separation of the proteins from the meals and isolates was conducted under reducing conditions (Figure 1). The electrophoretograms showed that the isolates contained individual components largely reflective of the peptides and proteins in the original meals. Some preferential extraction of the 10, 22, 48, 52, and 100 kDa components was apparent, as these bands appeared more prominent in the isolates than in the meals. This occurred regardless of whether the samples were derived from glanded or glandless cottonseed. A faint band of ~150 kDa molecular weight was present in both isolates, suggesting modest aggregation of lower molecular weight components. Alternatively, given the diffuse staining of the meal lanes toward the top of the gel (Figure 1), this might also represent a specific component that was preferentially extracted into the isolates. Otherwise, the exposure to alkali during extraction did not appear to alter the basic structure of the meal protein.

Publication Date (Web): November 22, 2013 | doi: 10.1021/bk-2013-1144.ch023

Table 2. Amino acid composition (g/100 g protein) of the cottonseed meals used for isolate preparation and the recovered isolates

Amino acid	*Glandless meal*	*Glandless isolate*	*Glanded meal*	*Glanded isolate*
Cystine	1.63	0.94	1.67	1.05
Methionine	1.59	1.18	1.71	1.16
Aspartic acid	9.62	9.89	9.38	9.64
Threonine	3.34	2.95	3.43	2.78
Serine	4.71	5.02	4.67	4.92
Glutamic acid	21.04	21.63	20.06	21.98
Proline	3.89	3.88	3.75	3.71
Glycine	4.36	4.17	4.40	4.21
Alanine	4.05	3.83	4.22	3.59
Valine	4.58	5.02	4.49	4.83
Isoleucine	3.31	3.48	3.34	3.32
Leucine	6.14	6.29	6.22	5.97
Tyrosine	2.92	2.91	2.90	2.88
Phenylalanine	5.68	7.12	5.46	7.01
Lysine	4.00	2.87	4.22	2.72
Histidine	2.92	3.19	2.83	3.20
Arginine	11.69	12.62	10.87	12.74

In Green Polymer Chemistry: Biocatalysis and Materials II; Cheng, H., et al.;
ACS Symposium Series; American Chemical Society: Washington, DC, 2013.

Solubility of the isolate protein was determined from aqueous dispersions at different pH levels (Table 3). As the isolates were made by solubilizing the protein at pH 11 then precipitating it at pH 5, it was expected that the protein would be highly soluble at pH 10 and essentially insoluble at pH 5. This was observed. At pH 4 for example, the protein was essentially insoluble. As the pH was further reduced, solubility increased, and most of the protein was soluble at pH 2 (75–85%). With soy proteins this trend also occurs, but it is less pronounced (*11*); hence, cottonseed proteins appear to be more soluble than soy proteins in acidic environments.

Publication Date (Web): November 22, 2013 | doi: 10.1021/bk-2013-1144.ch023

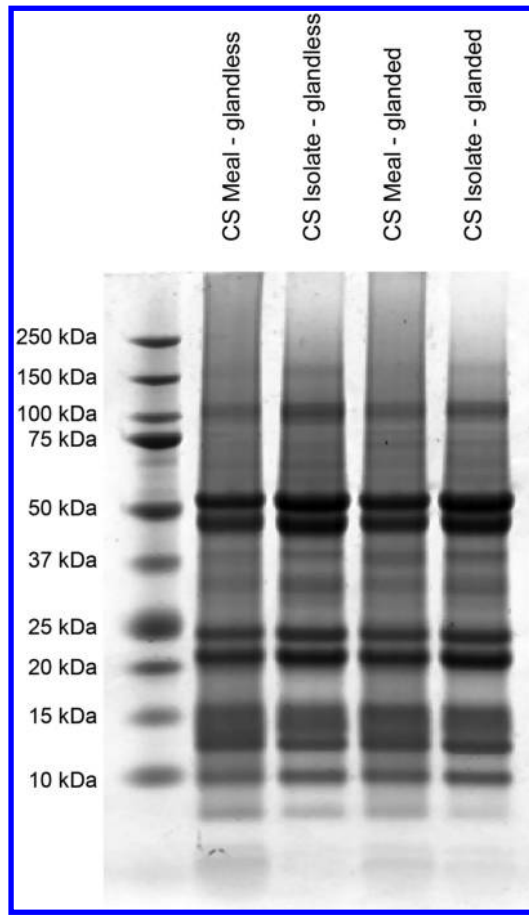

Figure 1. Separation of the individual peptides/proteins from glandless and glanded cottonseed meals and isolates.

In Green Polymer Chemistry: Biocatalysis and Materials II; Cheng, H., et al.;
ACS Symposium Series; American Chemical Society: Washington, DC, 2013.

Because of the solubility patterns, most functionality testing was conducted at pH 2.0 and 10.0. The foaming capacities of the cottonseed isolates were between 95–110 mL (Table 4), which is roughly comparable to the foaming capacity reported for soy protein isolate at pH 7 (*11*). Good foam stability (>88%) was obtained at pH 2.0 for the glandless isolate. In contrast, the foam stability was only 9% for the glanded isolate at the same pH level. At pH 10, foam stability was about 60% regardless of the isolate form.

Table 3. Solubility (% soluble protein) of isolates prepared from glanded and glandless cottonseed meals

pH	*Glandless isolate*	*Glanded isolate*
2.0	73.7 ± 3.8	85.6 ± 1.3
4.0	0.5 ± 0.0	0.7 ± 0.4
5.5	2.1 ± 0.2	1.7 ± 0.3
7.0	8.6 ± 0.3	15.6 ± 5.8
8.5	24.5 ± 4.1	35.8 ± 1.1
10.0	42.0 ± 0.9	59.6 ± 5.6

Publication Date (Web): November 22, 2013 | doi: 10.1021/bk-2013-1144.ch023

To gauge the ability of the protein to support the formation of an oil-in-water emulsion, each isolate was dispersed in water and adjusted to pH 2.0 or 10.0. Supernatants of these solutions (that is containing the protein that was soluble at these conditions) were mixed with corn oil and homogenized. The ability of the cottonseed isolate protein to emulsify oil was noticeably improved at pH 10 compared with pH 2 (Table 4). These values are greater than those reported for soy protein isolates at pH 7 of around 100 m^2/g (*13*). However, stability of the emulsion was quite low at 14 min in acidic conditions and 19–23 min in alkaline conditions. In comparison, oil-in-water emulsion stability of soy isolate is around 37 min (*13*).

Water holding capacity is the amount of water that the protein sample can hold. It is measured by mixing the protein in water then heating the sample under specific conditions. The water holding capacity of the cottonseed isolates was greater at pH 7.0 and 10.0 than at pH 2.0 (Table 4). Water holding capacity did appear to be greater for the glandless isolates compared with the glanded isolates in neutral and alkaline conditions.

Surface hydrophobicity is a measure of how dispersed or unaggregated the protein is, and it may be related to the number of hydrophobic sites exposed on the protein surface. Both cottonseed isolates had lower surface hydrophobicities than reported for soybean isolate at neutral pH (*11*). The glandless isolate had considerably greater surface hydrophobicity compared with that of the glanded isolate (Table 4). This difference seems related to the binding and likely cross-linking that gossypol may cause in the glanded preparation. Reduced surface

In Green Polymer Chemistry: Biocatalysis and Materials II; Cheng, H., et al.;
ACS Symposium Series; American Chemical Society: Washington, DC, 2013.

hydrophobicities have also been observed after enzymatic cross-linking of wheat, barley, and soy proteins (*18*). Alternatively, the presence of gossypol on the protein surface may reduce the number of sites available to interact with the hydrophobic fluorescence probe.

Table 4. Functional properties of cottonseed protein isolates from glandless and glanded meals

Property	*pH*	*Glandless isolate*	*Glanded isolate*
Foaming capacity, mL	2.0	111 ± 5	95 ± 9
	10.0	97 ± 1	111 ± 1
Foam stability, % remaining	2.0	87.8 ± 1.4	8.8 ± 4.4
	10.0	57.0 ± 7.7	57.2 ±8.2
Emulsion activity index, m^2/g	2.0	129.4 ± 11.5	120.7 ± 16.4
	10.0	282.8 ± 16.3	277.4 ± 3.7
Emulsion stability index, min	2.0	14.4 ±0.2	14.3 ± 1.1
	10.0	18.6 ± 0.1	22.9 ± 1.0
Water holding capacity, g/g	2.0	0.40 ±0.07	0.52 ± 0.16
	7.0	1.51 ± 0.11	1.32 ± 0.04
	10.0	1.72 ± 0.15	0.99 ± 0.04
Surface hydrophobicity	2.0	111.0 ± 5.1	60.0 ± 1.7
	10.0	182.7 ± 0.3	40.9 ± 1.0

Publication Date (Web): November 22, 2013 | doi: 10.1021/bk-2013-1144.ch023

Discussion

Isolate Preparation

While several researchers have reported on methods to recover cottonseed protein, the techniques used were not always compatible with techniques commercially used for extracting oil. Consequently, considerable differences exist in the compositional and functional properties of these preparations. Our focus was to determine the properties of isolates from meals generated under typical oil extraction conditions. Hence, the meals used in this work had been through various heat treatments. It was clear that these steps negatively influenced some aspects of isolate recovery, and it was not surprising to see differences in protein solubility and in some functional properties.

The presence of gossypol in cottonseed meal has a pronounced influence on the preparation of the isolate. Isolate yield is significantly reduced when gossypol is present (Table 1), suggesting that the likely cross-linking of the protein results in polymeric structures that are harder to extract. Damaty and Hudson have also proposed such structures in their studies on gossypol-protein interactions (*19*).

In Green Polymer Chemistry: Biocatalysis and Materials II; Cheng, H., et al.;
ACS Symposium Series; American Chemical Society: Washington, DC, 2013.

Because cross-linked protein is less extractable, the recovered glanded isolate had much lower gossypol levels than might have been expected. Despite its reduced concentration in the isolate compared with the glanded meal, the small amount of gossypol present still appeared to influence the functionality of the preparation.

Berardi, Martinez and their coworkers (*7*, *8*) reported considerable work on cottonseed protein recovery and recommended a two-step extraction procedure. This procedure first extracted meal with water to recover an initial fraction (non-storage proteins) then extracted the meal with dilute sodium hydroxide to recover a second fraction (storage proteins). Combined, the amount of protein extracted was modestly higher than obtained by a more traditional single-step process, and the properties of the two separate protein fractions were considerably different. However, the concentration of protein in the first fraction was significantly below what would normally be considered for an isolate. Based on their control single-step extraction trials (that are closest to the isolate extraction conditions used here), a yield of 39% and a recovery of 63% were obtained, which are both greater than achieved in this work. This difference appears to be related to the conditions used to generate the defatted meals, as their glandless seed was dehulled, flaked, hexane extracted, and then air and vacuum desolventized all at room temperature. In contrast, the meals used in this work were exposed to elevated temperatures during the seed cooking, extrusion, oil extraction, and meal desolventization steps. While less total protein was recovered in this work, the protein levels in the isolates were notable greater than those reported by Berardi et al. (*7*) and Martinez et al. (*8*), suggesting that some non-protein components were also more extractable when the meals were not exposed to heat.

Liadakis and coworkers (*20*) prepared isolates from glanded cottonseed meals generated by screw-pressing of cooked ground seed, which would be closer to the initial seed treatments used in this work. As their primary concern was to reduce isolate gossypol levels, they pre-extracted the meals with alcohols before protein recovery. After acid precipitation, the isolate proteins were washed first with a 50% solution of 2-propanol and then with water, before being freeze-dried. Their initial alcohol extraction was only mildly effective, removing about a third of the gossypol, i.e., most of the free or unbound compound. Hence, the amount of gossypol in their defatted meals was between the levels in the glanded and glandless meals used in this work, and their isolate yields (7.6–16.7%) are accordingly between those reported here for the glanded and glandless samples. The protein contents of their isolates were considerably lower (83–86%) than those obtained here. We have no clear explanation for this difference.

Isolate Properties

Isolate color can be an important factor for some processed food uses. Prior work on cottonseed isolate color has been confusing because of different opinions about what constitutes a light or dark color and because different color systems have been used to report color. Regardless, prior authors have noted the tendency of cottonseed proteins to be relatively dark (*21*, *22*). The association of gossypol with protein is one factor (but not the only factor) that influences this attribute. This was apparent in this work, as both meals and isolates were darker when

Publication Date (Web): November 22, 2013 | doi: 10.1021/bk-2013-1144.ch023

In Green Polymer Chemistry: Biocatalysis and Materials II; Cheng, H., et al.;
ACS Symposium Series; American Chemical Society: Washington, DC, 2013.

prepared from glanded cottonseed than they were when prepared from glandless cottonseed (Table 1). In this work, upon precipitation of the protein at pH 5, the isolates appeared a creamy white or light yellow color, but darkened to light brown upon freezing in preparation for freeze-drying. Drying the preparations with heat darkened the isolates to a much greater degree (observed during preliminary testing). Although no color measurements were reported by Berardi et al. (*7*) and Martinez et al. (*8*), their isolates were described as being a "light yellow-tan" color. This was reported even for isolates prepared from glanded meal with normal levels of gossypol. This result may have stemmed from the low temperatures used to prepare the starting meals. The Liadakis et al. isolates were described as being "light-colored" and Lovibond color level were reported (*20*). No difference was found between their untreated and alcohol-treated preparations, somewhat surprising as the gossypol levels were partially reduced by the alcohol treatment. However, they suggest that their washing of the isolates with 2-propanol contributed to the light color, as alcohols can weaken hydrogen bonding interactions between proteins and phenolic compounds and help solubilize these components. Kim et al. (*21*) have focused on this point, noting that washing with 2-propanol does improve the color of glandless cottonseed isolate. They were, however, not convinced that the extraction of polyphenolic compounds (including gossypol) was responsible for the improvement, as the inclusion of reducing agents that would be expected to inhibit polyphenolic oxidation were not effective at reducing color. As in the Berardi et al. (*7*) and Martinez et al. (*8*) reports, these results were obtained for isolate prepared from a cottonseed meal produced by low temperature processing. Whether or not an alcohol wash would improve the color of isolates prepared from meals exposed to heat remains an open question.

Cottonseed isolate solubility profiles show promise for potential food use. Of particular interest is the high solubility found at low pH values, as the isolate solubility appears greater than reported for soy protein isolates, e.g., the 30% solubility reported by Wu et al. at pH 3 (*13*). Solubility patterns were similar for the glanded and glandless preparations and were similar to those reported for the one-step isolate preparation by Berardi et al. (*7*) and Martinez et al. (*8*). However, their isolate appeared to be fully soluble at pH 2, while the preparations studied in this work were 75–85% soluble at this pH. This difference is again likely associated with the different conditions used to defat the starting material. The water holding capacities of the glanded and glandless isolates from this work were improved at pH 10 compared with pH 2. They were, however, lower than those reported by Liadakis et al. (*20*), which ranged between 3.5 and 6.2 g/g.

Other protein functional tests produced results that were similar between the glanded and glandless isolates (Table 4) and were within the range of values reported for other vegetable proteins. One exception to this was for foam stability at pH 2, where stability was 10-fold better for the glandless isolate than for the glanded isolate. This difference is perhaps related to the stability of gossypol-bound protein in acid conditions. As acid promotes hydrolysis of Schiff's bases, these conditions would be expected to release gossypol from the protein. As the compound has a rigid binaphthylene structure and each naphthalene ring has a polar and nonpolar side, freed gossypol may be able

In Green Polymer Chemistry: Biocatalysis and Materials II; Cheng, H., et al.;
ACS Symposium Series; American Chemical Society: Washington, DC, 2013.

Publication Date (Web): November 22, 2013 | doi: 10.1021/bk-2013-1144.ch023

to associate with the protein in ways that interfere with the protein's ability to stabilize the water-air interface. If free gossypol does promote bubble collapse, then even low levels of gossypol appear effective, as the total gossypol level in the glanded isolate was only 0.17%. This suggests that gossypol may be useful as a defoaming agent, although further work on this point is needed to fully understand the effect.

Application and Potential Use of Cottonseed Proteins

Development of uses for cottonseed proteins has been hampered by the presence of gossypol. At present, cottonseed proteins are used as a feed ingredient for ruminant animals, which are able to tolerate some gossypol in their diets. Even potential industrial uses have largely been ignored, although some effort to look at these proteins as wood adhesives is currently underway (*23*). Among the advantages of developing a gossypol-free cottonseed would be expanded use of the seed protein into higher-valued applications. These applications would potentially include use as a replacement for fish meal in aquaculture diets and use as ingredients in food processing. For this latter application, protein solubility and functionality is critical. That isolates prepared from meals derived under current oil recovery methods have reasonable functionality argues that there is potential for these components in food formulations. As many modifications have been reported to improve protein functionality (e.g., chemical, physical and enzymatic treatments), there is also considerable opportunity for further development of this underutilized cottonseed fraction.

In addition, processing changes also seem possible that might increase the value of cottonseed protein. Current oil extraction practice uses cooking and extraction conditions that are designed in part to bind gossypol to the protein. These conditions also tend to reduce the feed value of the meal (*17*), and it is apparent that they also reduce protein extractability, solubility and some functionality. The development of gossypol-free seed should allow for reoptimization of these preparation steps without the need to be concerned about the presence of gossypol, which may allow for additional improvement in protein quality and value.

Publication Date (Web): November 22, 2013 | doi: 10.1021/bk-2013-1144.ch023

Acknowledgments

The authors thank Cotton, Inc. for supplying the meals used in the work and for funding under projects 12-217 and 13-707. The authors are also indebted to Chris Mattison (USDA) for allowing access to the electrophoresis equipment and gel scanner used in this work.

References

1. McMichael, S. C. *Agron. J.* **1959**, *51*, 630.
2. Lusas, E. W.; Jividen, G. M. In *Proceedings of the World Conferences on Emerging Technologies in the Fats and Oils Industry*; AOCS Press: Urbana, IL, 1986; pp 221–231.
3. Sunilkumar, G.; Campbell, L. M.; Puckhaber, L.; Stipanovic, R. D.; Rathore, K. S. *Proc. Nat. Acad. Sci.* **2006**, *103*, 18054–18059.
4. Sorgentini, D. A.; Wagner, J. R.; Añon, M. C. *J. Agric. Food Chem.* **1995**, *43*, 2471–2479.
5. Karayannidou, A.; Makri, E.; Papalamprou, E.; Doxastakis, G.; Vaintraub, I.; Lapteva, N.; Articov, G. *Food Chem.* **2007**, *104*, 1728–1733.
6. Mohamed, A.; Hojilla-Evangelista, M. P.; Peterson, S. C.; Biresaw, G. *J. Am. Oil Chem. Soc.* **2007**, *84*, 281–288.
7. Berardi, L. C.; Martinez, W. H.; Fernandez, C. J. *Food Technol.* **1969**, *23*, 75–82.
8. Martinez, W. H.; Berardi, L. C.; Goldblatt, L. A. *J. Agric. Food Chem.* **1970**, *18*, 961–968.
9. Dowd, M. K.; Wakelyn, P. A. In *Cotton: Technology for the 21st Century*; Wakelyn, P. J., Chaudhry, M. R., Eds.; International Cotton Advisory Committee: Washington, DC, 2010; pp 437−460.
10. Method Ba 8a-99. In *Official Methods and Recommended Practices of the AOCS*, 5th ed.; Firestone, D., Ed.; AOCS Press: Champaign, IL, 1998.
11. Myers, D. J.; Hojilla-Evangelista, M. P.; Johnson, L. A. *J. Am. Oil Chem. Soc.* **1994**, *71*, 1201–1204.
12. Hojilla-Evangelista, M. P.; Sessa, D. J; Mohamed, A. *J. Am. Oil Chem. Soc.* **2004**, *81*, 1153–1157.
13. Wu, W. U.; Hettiarachchy, N. S.; Qi, M. *J. Am. Oil Chem. Soc.* **1998**, *75*, 845–850.
14. Balmaceda, E. A.; Kim, M. K.; Franzen, R.; Mardones, B.; Lugay, J. C. In *Food Protein Chemistry*; Regenstein J. M., Regenstein, C. E., Eds.; Academic Press: New York, 1984; pp 278–291.
15. King, W. H.; Frampton, V. L.; Altschul, A. M. *J. Am. Oil Chem. Soc.* **1958**, *35*, 358–360.
16. Conkerton, E. J.; Frampton, V. L. *Arch. Biochem. Biophys.* **1959**, *81*, 130–134.
17. Altschul, A. M.; Lyman, C. M.; Thurber, F. H. In *Processed Plant Protein Foodstuffs*; Altschul, A. M., Ed.; Academic Press, Inc.: New York, 1958; pp 469–534.
18. Ahn, H. J.; Kim, J. H.; Ng, P. K. W. *J. Food Sci.* **2005**, *70*, c380–c386.
19. Damaty, S. M.; Hudson, B. J. F. *J. Sci. Food Agric.* **1979**, *30*, 1050–1056.
20. Liadakis, G. N.; Floridis, A.; Tzia, C.; Orepoulou, V. *J. Agric. Food Chem.* **1993**, *41*, 918–922.
21. Kim, M. K.; Colvin, B. M.; Lawhon, J. T. *Cereal Sci. Today* **1971**, *16*, 216–217, 227.
22. Choi, Y. R.; Lusas, E. W.; Rhee, K. C. *J. Food Sci.* **1982**, *47*, 1032–1033, 1035.
23. Cheng, H. N.; Dowd, M. K.; He, Z. *Ind. Crop Prod.* **2013**, *46*, 399–403.

Publication Date (Web): November 22, 2013 | doi: 10.1021/bk-2013-1144.ch023

In Green Polymer Chemistry: Biocatalysis and Materials II; Cheng, H., et al.;
ACS Symposium Series; American Chemical Society: Washington, DC, 2013.

Publication Date (Web): November 22, 2013 | doi: 10.1021/bk-2013-1144.ch024

Chapter 24

Hydrogenated Cottonseed Oil as Raw Material for Biobased Materials

H. N. Cheng,* Mason Rau, Michael K. Dowd, Michael W. Easson, and Brian D. Condon

Southern Regional Research Center, USDA Agricultural Research Service, 1100 Robert E. Lee Blvd., New Orleans, Louisiana 70124, U.S.A.
***E-mail: hn.cheng@ars.usda.gov**

There has been a lot of recent interest in using vegetable oils as biodegradable and renewable raw materials for the syntheses of various biobased materials. Although most of the attention has been paid to soybean oil thus far, cottonseed oil is a viable alternative. An advantage of cottonseed oil is that the reactive groups consist primarily of oleic and linoleic moieties, and their amounts can be varied with appropriate hydrogenation. In this work a detailed hydrogenation study is carried out using three commercially available Ni, Pt and Pd catalysts under different hydrogenation conditions. Kinetic modeling of the observed data has also been done. With cottonseed oil and selective use of hydrogenation, oleic acid content up to 40% and linoleic acid content up to 53% can be produced, and these functionalities can be derivatized to produce specific biobased products. In addition, relative to the hydrogenated soybean oil, hydrogenated cottonseed oil exhibits lower trans fatty acid, and this feature may be beneficial in the context of food use.

In Green Polymer Chemistry: Biocatalysis and Materials II; Cheng, H., et al.;
ACS Symposium Series; American Chemical Society: Washington, DC, 2013.

Publication Date (Web): November 22, 2013 | doi: 10.1021/bk-2013-1144.ch024

Introduction

Recently vegetable oils have attracted renewed interest as raw materials for industrial products because of environmental concerns and increased interest in sustainability (*1–3*). A popular approach is to convert soybean oil to polymers, and several recent reviews on this topic are available (*4–6*). For example, soybean oil has been directly polymerized with "heat-bodying" reactions typically at temperatures of 290-330 °C with or without catalysts (*7–10*), with "air blown polymerization" involving air passing through soybean oil at 100-110 °C for 30-50 hours (*11*, *12*), with permanganate oxidation (*13*), and with cationic polymerization using BF_3 (*14*, *15*), BF_3-etherate (*16*, *17*), or superacids (*18*) under various reaction conditions. Copolymerization of triglyceride oils with vinyl comonomers has also been achieved through cationic means via BF_3-etherate (*19*). Epoxidized soybean oil has been polymerized using BF_3-etherate (*20*) or superacids (*21*). A number of chemically modified oils have also been prepared through polymerization with free radical initiators (*22*, *23*).

Another popular area of research and development is to produce polyurethanes from soybean oil. For such reactions, hydroxyl groups need to be generated from the oil and then reacted with diisocyanates to form the polyurethanes. Several methods have been devised, and many papers have appeared (*3*, *4*, *6*). Other methods to produce polymers from soybean oil include the use of diethyl azodicarboxylate (DEAD) (*24*) and 4-phenyl-1,2,4-triazoline-3,5-dione (PTAD) (*25*).

In many of these applications the amounts of oleic, linoleic, and linolenic functionalities in a vegetable oil have a major role in the reactivities of the oil, the speed of the reactions, and the nature of the polymer products. For example, linseed and tung oils have numerous olefinic bonds and are the preferred materials to use in drying oils (*26*, *27*). In superacid-catalyzed polymerization, it is known that oleic functionality alone cannot bring about polymerization; linoleic and linolenic functionalities are needed (*18*). In polymerizations with DEAD and PTAD (*24*, *25*), higher levels of linoleic and linolenic functionalities are known to increase the rate of polymerization, and linolenic functionality produces more complex polymer structures. It seems to us that if the starting oil can be customized to have specific amounts of oleic, linoleic and linolenic functionalities, the polymerization reaction and the polymer structures can be better controlled. In our view, a commercially viable and cost-effective method to achieve such control is through customized hydrogenation of vegetable oils, and (if needed) appropriate blending of different oils.

In this work, we have concentrated our efforts on cottonseed oil. In the literature most of the polymerization efforts thus far have been made on soybean oil. Only occasionally has cottonseed oil been included for comparison (*8*). Yet, cottonseed oil is one of the major edible oils, is readily available, and relatively cheap. An additional advantage of cottonseed oil is the low linolenic content (0.5%). Thus, polymerization of cottonseed oil only involves mostly oleic and linoleic, thereby simplifying the polymerization kinetics and the resulting polymer structures.

In Green Polymer Chemistry: Biocatalysis and Materials II; Cheng, H., et al.;
ACS Symposium Series; American Chemical Society: Washington, DC, 2013.

In order to obtain hydrogenated cottonseed oil with specific compositions of oleic and linoleic moieties, a detailed kinetic study of hydrogenation is desirable. Previously we have shown that cottonseed oil can be hydrogenated under high-agitation, ambient pressure environments, using 11 hydrogenation catalysts (*28*). In this work we have used three commercially available Ni, Pt, and Pd catalysts and carried out detailed hydrogenation studies. A range of concentration values for oleic and linoleic functionalities has been obtained. With the choice of different hydrogenated oils as starting materials, different polymeric products may potentially be obtained.

Experimental

Cottonseed oil (Admiration Foods, Englewood, NJ) was purchased from a local store in Kenner, LA. Catalyst samples were supplied by BASF (Iselin, NJ) and Johnson Matthey (West Deptford, NJ). High purity hydrogen was obtained from Airgas, Inc. (The Woodlands, TX). Other reagents were acquired from Sigma Aldrich (Milwaukee, WI) and used without further purification.

For hydrogenation, cottonseed oil and catalyst (total weight 10g) were weighed into a 100-mL round bottom flask that contained a magnetic stir bar. The flask was sealed with a rubber stopper, purged with argon, and then with hydrogen. The flask was immersed in a silicone oil bath at 80-130 °C. The stir bar was turned on at a rate of 1200 rpm. A balloon containing high purity hydrogen was attached to the flask for hydrogenation. At the end of the desired hydrogenation time (55 min.), the balloon was removed, and the flask removed from the bath. Chloroform (10-25 mL) was mixed into the reaction mixture, which was then filtered twice through Whatman medium filter paper into a 50-mL Erlenmeyer flask. Chloroform was removed through a combination of rotary evaporation, vacuum pumping and 80 °C heating. After chloroform removal, the sample was transferred to a 10-mL vial for analysis and storage.

The iodine value (IV) is defined as the weight of iodine absorbed by 100 g of an oil or fat and was determined via the Wijs method (*29*). It entailed dissolving an oil sample at 70 °C in 15 mL CCl_4, adding 25 mL Wijs solution, keeping the reaction mixture in the dark for approximately 30 minutes at room temperature to complete the reaction, and adding 20 mL KI and 100 mL distilled water. The excess iodine was then titrated with 0.1N sodium thiosulfate. In this work the standardized Wijs solution was purchased from Sigma Aldrich; it contained 0.1 mole/L of iodine monochloride.

^{1}H NMR analysis of the oil samples was carried out on a Varian Unity 400 spectrometer at the University of New Orleans. Typical instrument settings included 399.939 MHz spectral frequency, 30° pulses, 1-s pulse delay, and ambient probe temperature. Chemical shifts were referenced to tetramethylsilane at 0 ppm. For each spectrum the peak areas at 5.0–5.6 ppm and 2.6–2.9 ppm were determined while setting the area of glycerol peaks (4.0–4.5 ppm) to 1.00. Because the 5.0–5.6 ppm area contained the olefins and the methine from glycerol, the "NMR olefin content" was obtained by subtracting 0.25 (for the glycerol methine) from the 5.0–5.6 ppm area. It has been shown previously (*28*)

Publication Date (Web): November 22, 2013 | doi: 10.1021/bk-2013-1144.ch024

In Green Polymer Chemistry: Biocatalysis and Materials II; Cheng, H., et al.;
ACS Symposium Series; American Chemical Society: Washington, DC, 2013.

that the "NMR olefin content" determined in this way correlated very well with IV, and a linear relationship was obtained. Since "NMR olefin content" was faster to determine and incurred less experimental error, all the samples in this work were subjected to NMR analysis, and the IV values calculated from the NMR data. Occasionally IV was also determined to double check the accuracy of the NMR olefin content.

For gas chromatography (GC), an oil sample was first converted to fatty acid methyl esters. In this procedure, 200 μL of 0.5 N methanolic base (Supelco, Inc., Bellefonte, PA) was added to the cottonseed oil, and the tube was capped and heated to 70 °C for 10 min with periodic vortex mixing. Upon cooling, 1 mL of brine and 1 mL of hexane were added, and the contents were vortex mixed again. After allowing the phases to separate, 1 mL of the organic phase containing the methyl esters was transferred to a gas chromatography autoinjector vial. GC analysis was conducted with an Agilent (Santa Clara, CA) model 7890A gas chromatograph, fitted with a split/splitless injector, a flame-ionization detector (FID), and a Supelco SP-2380 capillary column (0.25 mm i.d. x 30 m x 0.2mm film thickness). Injectors were operated in split mode with a split ratio of 1:100. Injector and detector temperatures were set at 240 °C. Helium was used as carrier gas and was controlled in constant flow mode at a linear velocity of 20 cm/sec. The oven was programmed to start at 170 °C, which was held for 3 min; the temperature was ramped at 1 °C/min to 180 °C; then the temperature was ramped at 4 °C/min to 240 °C, which was held for an additional 5 min. Injection volumes were 1 μL. The fatty acids were identified by their retention volumes. The trans fatty acids (TFA) consisted of a series of peaks that include trans-mono-enoic acids (such as elaidic acid) and trans-dienoic acids (including conjugated linoleic acids).

All calculations were done on Excel. The kinetic data were analyzed with the "Coupled ODE Solver" from www.engineers-excel.com. This software uses fourth order Runge-Kutta method to solve up to 10 coupled ordinary differential equations. Boundary values were built into the software and were entered into the spreadsheet prior to calculations.

Publication Date (Web): November 22, 2013 | doi: 10.1021/bk-2013-1144.ch024

Results and Discussions

The fatty acid composition of cottonseed oil is typically 25% palmitic, 3% stearic, 18% oleic, 53% linoleic, and 0.5% linolenic. In contrast, soybean oil has the following composition: 10% palmitic, 4% stearic, 24% oleic, 54% linoleic, and 7% linolenic. Thus, relative to soybean oil, cottonseed oil is higher in palmitic content and lower in linolenic content.

Hydrogenation of Cottonseed Oil

Hydrogenation is a well-known process used for vegetable oils (*30–32*), with the purpose of decreasing unsaturation, improving melting characteristics and oxidative stability. Most commercial processes employ Ni catalysts. In this work, three commercially available catalysts were used: Nysosel® 820 (Ni catalyst

In Green Polymer Chemistry: Biocatalysis and Materials II; Cheng, H., et al.;
ACS Symposium Series; American Chemical Society: Washington, DC, 2013.

Publication Date (Web): November 22, 2013 | doi: 10.1021/bk-2013-1144.ch024

from BASF), Pt catalyst Lot C-9616 B103032-5 (5% on carbon, from Johnson Matthey), and Pd catalyst Lot SE09756C (5% on carbon, from BASF). These are considered by the suppliers as appropriate catalysts for hydrogenation of vegetable oils. In the experimental design, we studied two parameters: catalyst level and reaction temperature. The three reaction temperatures were 80 °C, 105 °C, and 130 °C. Because Ni catalyst is less reactive than Pt and Pd catalysts, different catalysts levels were used. For Ni catalysts, six catalyst levels were selected: 0.25%, 0.5%, 1.0%, 1.5%, 2.0% and 2.5%. For Pt catalysts, seven catalyst levels were selected: 0.02%, 0.05%, 0.1%, 0.2%, 0.3%, 0.4%, and 0.5%. For Pd catalysts, nine catalyst levels were used: 0.0025%, 0.005%, 0.01%, 0.05%, 0.1%, 0.2%, 0.3%, 0.4%, and 0.5%. Hydrogenation was done on each sample using the same procedure as given in the Experimental Section. Each product was analyzed by ^{1}H NMR and GC.

For the Ni catalyst, the amounts of stearic, oleic, linoleic, and TFA as a function of IV are given in Figure 1. The data points came from GC analysis, and the curves are trend-lines from the Excel spreadsheet. Not surprisingly, at the initial stage of hydrogenation linoleic acid decreases whereas oleic acid, TFA, and stearic acid increase in amount. Initially oleic show a higher rate of hydrogenation (higher slope) than TFA; however, oleic slows down with further hydrogenation and reaches its maximum at about 36% and 75 IV. TFA reaches its maximum at 25% and ca. 50 IV. With further hydrogenation, both oleic and TFA decrease in concentration, generating the stearic functionality.

Analogous data for the Pd catalyst are shown in Figure 2, and similar trends are observed. Hydrogenation causes a steady decrease in linoleic and a steady increase in stearic content. Oleic and TFA contents increase first and then decrease. For Pd the hydrogenation rate of linoleic is higher than for Ni; also the maximum TFA level achieved for Pd (30%) is higher than for Ni (25%).

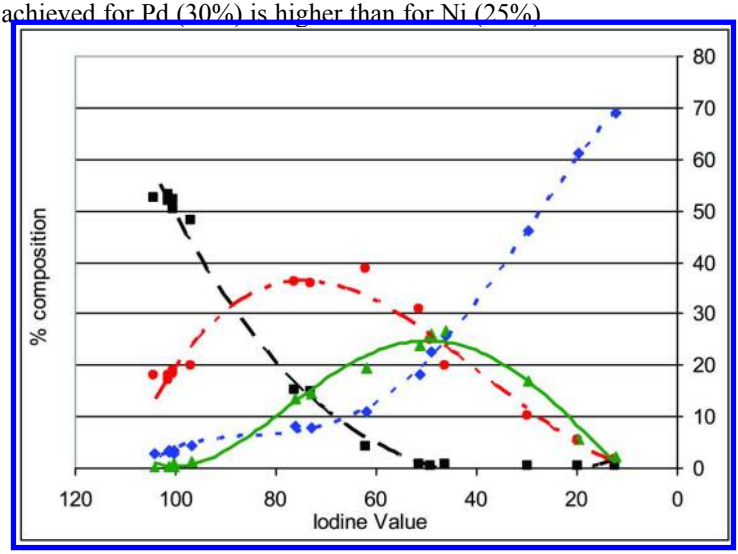

Figure 1. Composition of stearic, oleic, TFA, and linoleic (from GC) as a function of IV for Ni-catalyzed hydrogenation. Stearic is shown as blue diamonds, oleic as red spheres, 18:2 as black squares, and TFA as green triangles.

In Green Polymer Chemistry: Biocatalysis and Materials II; Cheng, H., et al.;
ACS Symposium Series; American Chemical Society: Washington, DC, 2013.

Publication Date (Web): November 22, 2013 | doi: 10.1021/bk-2013-1144.ch024

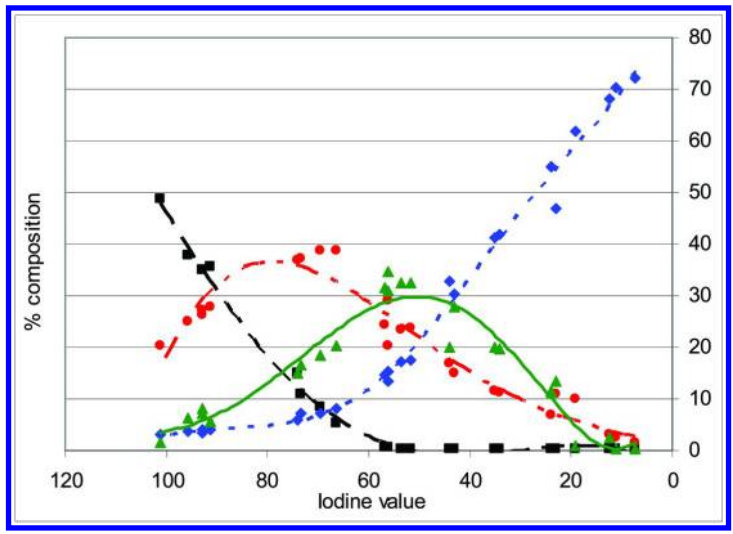

Figure 2. Composition of stearic, oleic, TFA, and linoleic (from GC) as a function of IV for Pd-catalyzed hydrogenation. Stearic is shown as blue diamonds, oleic as red spheres, 18:2 as black squares, and TFA as green triangles.

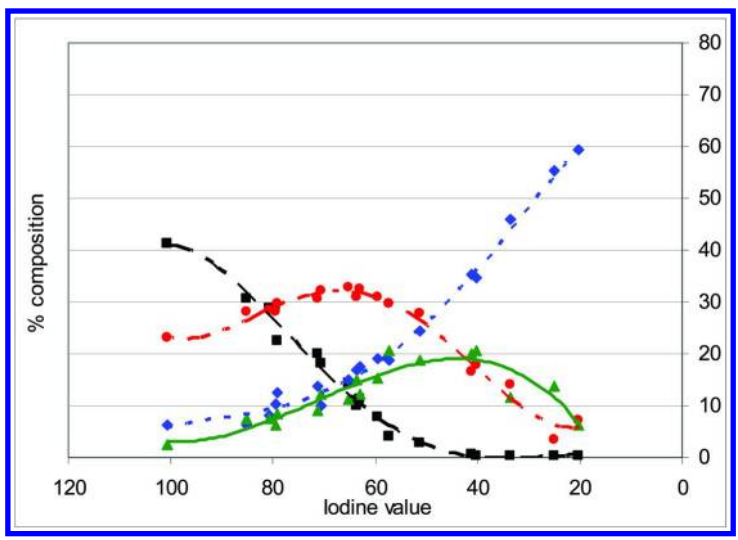

Figure 3. Composition of stearic, oleic, TFA, and linoleic (from GC) as a function of IV for Pt-catalyzed hydrogenation. Stearic is shown as blue diamonds, oleic as red spheres, 18:2 as black squares, and TFA as green triangles.

The situation is different with the Pt catalyst (Figure 3). In this case, the amount of linoleic acid decreases more slowly at initial hydrogenation, and the amounts of oleic acid and TFA also increase slowly. In contrast, the amount of stearic acid increases at about the same rate as the other catalysts. Thus, oleic reaches a lower maximum point at 32% and 65 IV, and TFA reaches its maximum relatively late, at 40 IV and 18%.

In Green Polymer Chemistry: Biocatalysis and Materials II; Cheng, H., et al.;
ACS Symposium Series; American Chemical Society: Washington, DC, 2013.

Publication Date (Web): November 22, 2013 | doi: 10.1021/bk-2013-1144.ch024

Modeling of the Hydrogenation Kinetics

An attempt has been made to approximately model the data. Following the literature (*33–38*), we use the following simplified reaction scheme to simulate the hydrogenation process:

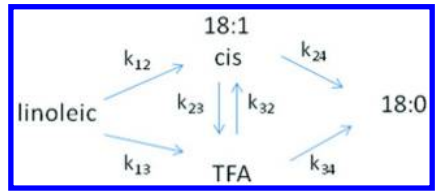

Since the rate expressions involve time, but our data involve IV, a proportional relationship between IV and time was assumed, and the IV scaled to fit the data. The term "18:1 cis" includes both 18:1 (n-9) and 18:1 (n-6); TFA represents both trans-mono-enoic and trans di-enoic acids. Analysis was carried out using four coupled differential equations (Eqs. 1-4) using the fourth order Runge-Kutta method, where f_x = fraction of species x. The initial levels of the four species are: $f^0_{\text{linoleic}} = 0.53$; $f^0_{18:1\ cis} = 0.18$; $f^0_{TFA} = 0$; and $f^0_{18:0} = 0.03$. The curves that resulted from model fitting are given in Figures 4-6.

$$\frac{df_{\text{linoleic}}}{dt} = -(k_{12} + k_{13})\, f_{\text{linoleic}} \tag{1}$$

$$\frac{df_{18:1\ cis}}{dt} = k_{12}\, f_{\text{linoleic}} - k_{23}\, f_{18:1\ cis} + k_{32}\, f_{TFA} - k_{24}\, f_{18:1\ cis} \tag{2}$$

$$\frac{df_{TFA}}{dt} = k_{13}\, f_{\text{linoleic}} - k_{32}\, f_{TFA} + k_{23}\, f_{18:1\ cis} - k_{34}\, f_{TFA} \tag{3}$$

$$\frac{df_{18:0}}{dt} = k_{24}\, f_{18:1\ cis} + k_{34}\, f_{TFA} \tag{4}$$

The kinetic parameters from model fitting are summarized in Table 1. For all catalysts, k_{12} is the largest k value, converting linoleic to 18:1 cis. Moreover, $k_{12} > k_{13}$, indicating that the direct conversion of linoleic to TFA is less favored than the conversion to 18:1 cis. Note that $k_{23} > k_{32}$ in all three cases; thus the conversion of cis to trans 18:1 contributes to the accumulation of TFA. k_{24} and k_{34} represent the rates of the hydrogenation of the 18:1 cis and TFA to 18:0, respectively. In all three cases, $k_{24} \approx k_{34}$, showing no preference in the hydrogenation of the olefins.

In Green Polymer Chemistry: Biocatalysis and Materials II; Cheng, H., et al.;
ACS Symposium Series; American Chemical Society: Washington, DC, 2013.

Publication Date (Web): November 22, 2013 | doi: 10.1021/bk-2013-1144.ch024

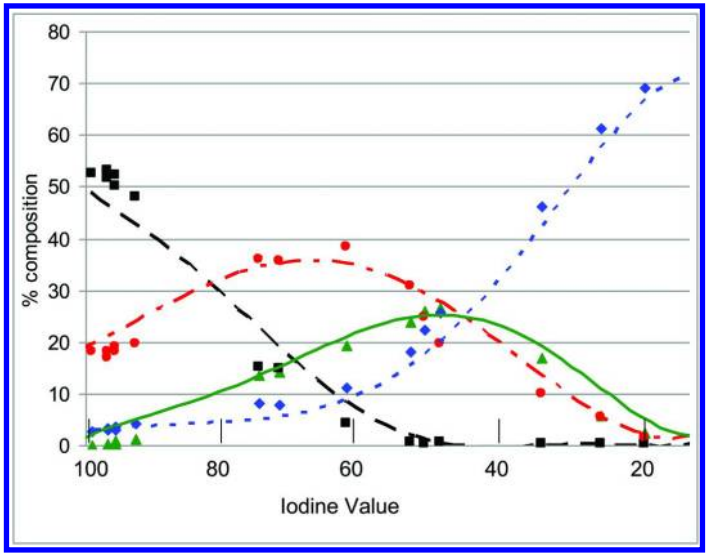

Figure 4. Kinetic modeling of hydrogenation data of Ni-catalyzed hydrogenation of cottonseed oil. Stearic is shown as blue diamonds, oleic as red spheres, 18:2 as black squares, and TFA as green triangles. Curves with corresponding colors are calculated from the kinetic model.

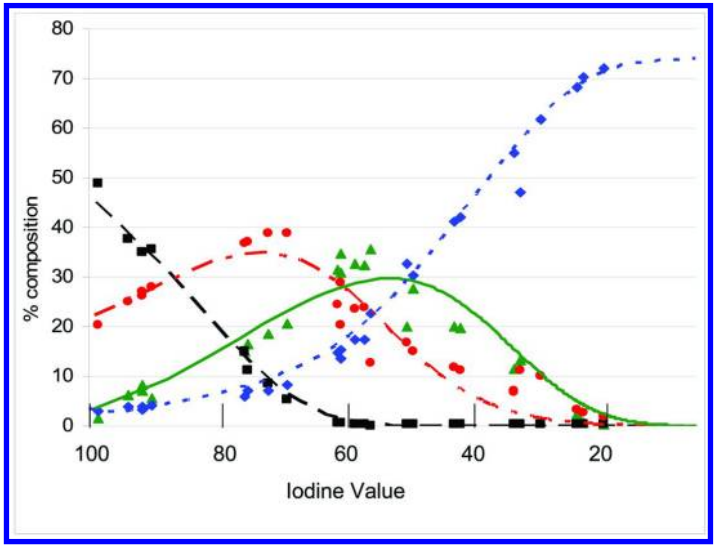

Figure 5. Kinetic modeling of hydrogenation data of Pd-catalyzed hydrogenation of cottonseed oil. Stearic is shown as blue diamonds, oleic as red spheres, 18:2 as black squares, and TFA as green triangles. Curves with corresponding colors are calculated from the kinetic model.

In Green Polymer Chemistry: Biocatalysis and Materials II; Cheng, H., et al.;
ACS Symposium Series; American Chemical Society: Washington, DC, 2013.

Publication Date (Web): November 22, 2013 | doi: 10.1021/bk-2013-1144.ch024

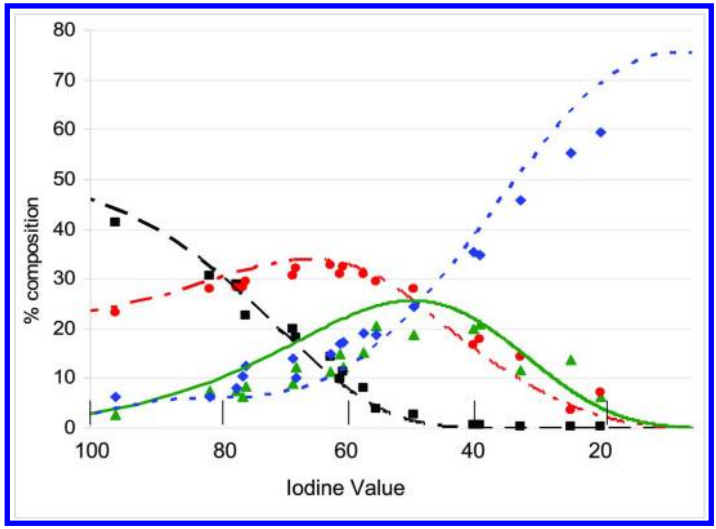

Figure 6. Kinetic modeling of hydrogenation data of Pt-catalyzed hydrogenation of cottonseed oil. Stearic is shown as blue diamonds, oleic as red spheres, 18:2 as black squares, and TFA as green triangles. Curves with corresponding colors are calculated from the kinetic model.

A closer look can be made of the exact k values in the three catalysts. For k_{12} and k_{13} Pd has the largest values relative to Ni and Pt; therefore, the rates of hydrogenation and the formation of TFA are fastest for Pd. Yet for Pd and Pt, k_{24} and k_{34} are also larger; thus, both 18:1 and TFA are more quickly depleted by hydrogenation. Note that relative to Pd, Pt has smaller k_{23} but larger k_{32}. These factors contribute towards the relatively low TFA level observed in Pt catalysis.

Table 1. k values obtained by modeling of hydrogenation kinetics

k value	*Ni*	*Pt*	*Pd*
k_{12}	0.0300	0.0350	0.0700
k_{13}	0.0200	0.0175	0.0400
k_{23}	0.0050	0.0125	0.0150
k_{32}	0.0025	0.0075	0.0020
k_{24}	0.0035	0.0060	0.0080
k_{34}	0.0035	0.0060	0.0080

In Green Polymer Chemistry: Biocatalysis and Materials II; Cheng, H., et al.;
ACS Symposium Series; American Chemical Society: Washington, DC, 2013.

Utility of Hydrogenated Cottonseed Oil

From the curves shown in Figures 1-3, and the kinetic analysis, it is clear that a wide range of values can be obtained for oleic and linoleic functionalities in the cottonseed oil and hydrogenated cottonseed oil. Table 2 shows the compositions obtainable under some selected experimental conditions.

Table 2. Selected compositions (in %) of hydrogenated cottonseed oil (CSO)

fatty acid	*CSO, starting*	*Pd, 70 IV*	*Pt, 80 IV*	*Ni, 47 IV*
palmitic 16:0	25	25	25	25
stearic 18:0	3	8	9	25
oleic 18:1	18	40	30	25
TFA	0	20	7	25
linoleic 18:2	53	8	28	0
linolenic 18:3	0.5	0	0	0

Publication Date (Web): November 22, 2013 | doi: 10.1021/bk-2013-1144.ch024

Thus, with cottonseed oil and selected hydrogenation conditions, linoleic acid content up to 53% and oleic acid content up to 40% can be produced. Note that according to GC data TFA consists mostly of trans mono-enic acid moieties. Thus, both TFA and oleic count as mono-enic acids, whereas linoleic is a di-enic acid. In view of the different amounts of mono-enic and dienic moieties available, different biobased materials can potentially be made from cottonseed oil and its hydrogenated derivatives. A preliminary study of the thermal polymerization of soybean oil, cottonseed oil, and hydrogenated cottonseed oil (carried out at 330 °C for 6 hours in nitrogen) produced polymers with viscosities in decreasing order: soybean oil polymer > cottonseed oil polymer > polymer derived from cottonseed oil that had been hydrogenated to IV 97. These viscosity results for the polymers are consistent with the amounts of unsaturation present in the starting oils.

For food use, prior research has shown that diets high in saturated fats increase low density lipoproteins, which tend to promote the deposition of cholesterol on blood vessels (*39*, *40*). Furthermore, dietary consumption of foods high in TFA has also been linked to increased serum cholesterol content (*41*). For hydrogenated cottonseed oil under the present hydrogenation conditions used, all three catalysts used in this study produce less than 6% TFA with 95 IV. At 70 IV, Pt catalyst produces 12% TFA, Ni 17% TFA, and Pd 23% TFA. Moreover, under the same hydrogenation conditions, at IV 95 all three catalysts produce no more than 6% stearic acid. At IV 70, Pt catalyst yields about 14% stearic acid in the hydrogenated cottonseed oil, whereas Ni and Pd catalysts yield less than 10% stearic acid. Note that these results are lower than the TFA and stearic acid levels reported for soybean, canola and sunflower oils in the recent literature (*42–46*). Similar results have been shown earlier in a survey study of 11 hydrogenation catalysts (*28*); the present results confirm the earlier findings.

In Green Polymer Chemistry: Biocatalysis and Materials II; Cheng, H., et al.;
ACS Symposium Series; American Chemical Society: Washington, DC, 2013.

Thus, for applications as edible oil, cottonseed oil offers a distinct advantage as the starting oil for hydrogenation relative to soybean, canola, and sunflower oils with respect to TFA and stearic acid levels.

Conclusions

Cottonseed oil has a compositional profile that is different from soybean oil and may be a viable alternative raw material for polymerization. More importantly, the use of hydrogenation makes available a much wider range of oleic/linoleic compositions. In this work, we have used commercially available Ni, Pd, and Pt catalysts and produced hydrogenated cottonseed oil with different compositional profiles from unmodified vegetable oils. Thus, cottonseed oil and hydrogenated cottonseed oil appear to be promising starting materials for the synthesis of biobased polymeric materials.

It may be noted that although this work is concentrated only on cottonseed oil, the same hydrogenation approach can be applied to other triglyceride oils as raw materials for biobased products. In addition, appropriate blending may also be used, involving hydrogenated and/or unhydrogenated triglyceride oils in order to optimize the properties of the resulting products.

Publication Date (Web): November 22, 2013 | doi: 10.1021/bk-2013-1144.ch024

Acknowledgments

Thanks are due to Catrina Ford for her assistance with hydrogenation and polymerization, Melina Farve for GC analysis, and Deborah Boykin for experimental design. The authors also thank Robert Duffin at BASF, and Joe Ferrer, Marta K. Roth, and Bart Zwijnenburg at Johnson Matthey for providing the catalyst samples used in this investigation and for helpful information relating to the catalysts. Mention of trade names or commercial products in this publication is solely for the purpose of providing specific information and does not imply recommendation or endorsement by the U.S. Department of Agriculture. USDA is an equal opportunity provider and employer.

References

1. Biermann, U.; Friedt, W.; Lang, S.; Lühs, W.; Machmuller, G.; Metzher, J. O.; Klaas, M. R.; Schafer, H. J.; Schneider, M. P. *Angew. Chem., Int. Ed.* **2000**, *39*, 2206.
2. Crandall, L. *Inform* **2002**, *13*, 626.
3. Biswas, A.; Sharma, B. K.; Willett, J. L.; Erhan, S. Z.; Cheng, H. N. *Energy Environ. Sci.* **2008**, *1*, 639.
4. Guner, F. S.; Yagci, Y.; Erciyes, A. T. *Prog. Polym. Sci.* **2006**, *31*, 633.
5. Sharma, V.; Kundu, P. P. *Prog. Polym. Sci.* **2006**, *31*, 983.
6. Sharma, V.; Kundu, P. P. *Prog. Polym. Sci.* **2008**, *33*, 1199.
7. Powers, P. O. *J. Am. Oil Chem. Soc.* **1950**, *27*, 468.
8. Erhan, S. Z.; Bagby, M. O. *J. Am. Oil Chem. Soc.* **1994**, *71*, 1223.

9. Lozada, Z.; Suppes, G. J.; Hsieh, F.; Lubguban, A.; Tu, Y. *J. Appl. Polym. Sci.* **2009**, *112*, 2127.
10. Arca, M.; Sharma, B. K.; Price, N. P. J.; Perez, J. M.; Doll, K. M. *J. Am. Oil Chem. Soc.* **2012**, *89*, 987.
11. Christianson, R.; Noble, M.; Rourke, A.; Geiger, E.; Mahlum, L. U.S. Patent 7262311, August 28, 2007.
12. Geiger, E. J.; Becker, N. M.; Armbruster, L. A. U.S. Patent 7989647, August 2, 2011.
13. Mercangoz, M.; Kusefoglu, S.; Akman, U.; Hortacsu, O. *Chem. Eng. Processing* **2004**, *43*, 1015.
14. Eichvald, E. U.S. Patent 2160572, 1939.
15. Uloth, M. U.S. Patent 2365919, 1944.
16. Li, F.; Hanson, M. V.; Larock, R. C. *Polymer* **2001**, *42*, 1567 and references cited therein.
17. Liu, Z.; Sharma, B. K.; Erhan, S. Z. *Biomacromolecules* **2006**, *8*, 233.
18. Ionescu, M.; Petrovic, Z. U.S. Patent 7501479, 2009.
19. Li, F.; Larock, R. C. *J. Appl. Polym. Sci.* **2001**, *80*, 658.
20. Liu, Z. S.; Erhan, S. Z. *J. Am. Oil Chem. Soc.* **2010**, *87*, 437.
21. Liu, Z. S. Ring Opening Polymerization of Epoxidized Soybean Oil Catalyzed by Superacid. In *Proceedings of the 41st Annual Meeting United States–Japan Cooperative Program in Natural Resources (UJNR), Food and Agriculture Panel*, December 8−12, 2012, New Orleans, Louisiana.
22. Wool, R. P. *ChemTech* **1999**, *29*, 44.
23. Khot, S. N.; Lascala, J. J.; Can, E.; Morye, S. S.; Williams, G. I.; Palmese, G. R.; Kusefoglu, S. H.; Wool, R. P. *J. Appl. Polym. Sci.* **2001**, *82*, 703.
24. Biswas, A.; Sharma, B. K.; Willett, J. L.; Erhan, S. Z.; Cheng, H. N. *Green Chem.* **2008**, *10*, 298.
25. Biswas, A.; Cheng, H. N.; Kim, S.; Liu, Z. *J. Am. Oil Chem. Soc.* **2013**, submitted.
26. Derksen, J. T. P.; Cuperus, F. P.; Kolster, P. *Ind. Crops Prod.* **1995**, *3*, 225.
27. Lazzari, M.; Chiantore, O. *Polym. Degrad. Stab.* **1999**, *65*, 303.
28. Cheng, H. N.; Dowd, M. K.; Easson, M. W.; Condon, B. D. *J. Am. Oil Chem. Soc.* **2012**, *89*, 1557.
29. *AOAC Official Method*; AOAC Press: Gaithersburg, MD, 1984; Chapter 28.023.
30. Patterson, H. B. W. *Hydrogenation of Fats and Oils: Theory and Practice*; AOCS Press: Champaign, IL, 1994.
31. Jang, E. S.; Jung, M. Y.; Min, D. B. *Compr. Rev. Food Sci. Food Saf.* **2005**, *1*, 22.
32. Beers, A. E. W.; Mangnus, G. *Inform* **2004**, *15*, 404.
33. Eldib, I. A.; Albright, L. F. *Ind. Eng. Chem.* **1957**, *49* (5), 825.
34. Wisniak, J.; Albright, L. F. *Ind. Eng. Chem.* **1961**, *53* (5), 375.
35. Hashimoto, K.; Muroyama, K.; Nagata, S. *J. Am. Oil Chem. Soc.* **1971**, *498*, 291.
36. Marangozis, J.; Keramidas, O. B.; Paparisvas, G. *Ind. Eng. Chem. Process Des. Dev.* **1977**, *16* (3), 361.
37. Krishnaiah, D.; Sarkar, S. *J. Am. Oil Chem. Soc.* **1990**, *67* (4), 233.

In Green Polymer Chemistry: Biocatalysis and Materials II; Cheng, H., et al.;
ACS Symposium Series; American Chemical Society: Washington, DC, 2013.

Publication Date (Web): November 22, 2013 | doi: 10.1021/bk-2013-1144.ch024

38. Fillion, B.; Morsi, B. I.; Heier, K. R.; Machado, R. M. *Ind. Eng. Chem. Res.* **2002**, *41*, 697.
39. Willett, W. C. *Science* **1994**, *264* (5158), 532.
40. Hu, F. B.; Stampfer, M. J.; Manson, J. E.; Ascherio, A.; Colditz, G. A.; Speizer, F. E.; Hennekens, C. H.; Willett, W. C. *Am. J. Clin. Nutrition* **1999**, *70* (6), 1001.
41. Mensick, R. P.; Katan, M. B. *New England J. Med.* **1990**, *323* (7), 435.
42. Hsu, N.; Diosady, L. L.; Graydon, W. F.; Rubin, L. J. *J. Am. Oil Chem. Soc.* **1988**, *65*, 608.
43. Eller, F. J.; List, G. R.; Teel, J. A.; Steidley, K. R.; Adlof, R. O. *J. Agric. Food Chem.*, *53*, 5982**205**.
44. Beers, A. E. W. *Lipid Technol.* **2007**, *19*, 56.
45. List, G. R.; Jackson, M.; Eller, F.; Adlof, R. O. *J. Am. Oil Chem. Soc.* **2007**, *84*, 497.
46. Fernandez, M. B.; Tonetto, G. M.; Crapiste, G. H.; Damiani, D. E. *J. Food Eng.* **2007**, *82*, 199.

Publication Date (Web): November 22, 2013 | doi: 10.1021/bk-2013-1144.ch024

Publication Date (Web): November 22, 2013 | doi: 10.1021/bk-2013-1144.ch025

Chapter 25

Lignin-Based Graft Copolymers *via* ATRP and Click Chemistry

Hoyong Chung,[1,3] Amer Al-Khouja, and Newell R. Washburn[*,1,2]

[1]Department of Chemistry, Carnegie Mellon University, 4400 Fifth Avenue, Pittsburgh, Pennsylvania 15213
[2]Department of Biomedical Engineering, Carnegie Mellon University, 4400 Fifth Avenue, Pittsburgh, Pennsylvania 15213
[3]Current address: Division of Chemistry and Chemical Engineering, California Institute of Technology, Pasadena, California 91125
[*]E-mail: washburn@andrew.cmu.edu

New lignin-based graft copolymers have been developed by atom transfer radical polymerization (ATRP) and click chemistry. These hybrid materials have a lignin center and poly(*n*-butyl acrylate) or polystyrene grafts. Poly(*n*-butyl acrylate) represents a typical elastomeric polymer, and polystyrene is used as a representative glassy polymer, and grafting these onto lignin was pursued as a method to integrate a renewable resource into polymers commonly used in a broad range of applications. Two different graft copolymerization methods were used: "graft from" and "graft onto". The "graft from" method utilized ATRP to polymerize vinyl monomers from a lignin-based macroinitiator. Kinetic data showed that the ATRP graft copolymerization occurred in controlled manner for both polystyrene and poly(*n*-butyl acrylate) with a conversion up to 25%. In "graft onto" method, the backbone lignin was linked to polystyrene graft via click chemistry. In the "graft onto" method, a polystyrene homopolymer was prepared by ATRP followed by end-group functionalization to obtain azide functionality at polymer chain terminals. As a counterpart of azide group, lignin hydroxyl groups were functionalized to alkyne groups for the click reaction, copper-catalyzed Huisgen cycloaddition. The click chemistry was conducted with high efficiency to form lignin-*graft*-polystyrene under

In Green Polymer Chemistry: Biocatalysis and Materials II; Cheng, H., et al.;
ACS Symposium Series; American Chemical Society: Washington, DC, 2013.

mild conditions. Grafting efficiency was monitored by ^{1}H NMR and GPC. The ^{1}H NMR data demonstrated a complete functionalization of polystyrene terminal groups and following successful click reaction without remaining lignin or polystyrene fragments. In these experiments, GPC characterization indicated that click coupling completed within 5 hours. Unlike fully crosslinked lignin-based network polymers such as lignin-based polyurethane, these lignin-based graft copolymers may show high flexibility in processing as a thermoplastic polymer.

Keywords: lignin; polystyrene; poly(*n*-butyl acrylate); ATRP; click chemistry; graft copolymerization

Publication Date (Web): November 22, 2013 | doi: 10.1021/bk-2013-1144.ch025

Introduction

Lignin is abundant in nature but is not used extensively in commercial polymers due to its chemical complexity, low reactivity, and poor processibility (*1–4*). Many approaches have been investigated to overcome these problems, one being the integration of lignin with a synthetic polymer (*5–9*). Various thermosetting lignin-based polymers have been developed, such as lignin-based polyurethane (*10–17*) and lignin-based phenol formaldehyde resin (*18–26*). Thermoset materials, such as lignin-based polyurethane, cannot be reprocessed due to their crosslinked nature. Unlike thermoset polymers, thermoplastic polymers can be reprocessed multiple times by heating to form a polymer melt (*27*). In order to produce useful commodity materials, synthesis efficiency and production costs need to be considered. Lignin-based thermoplastics can be prepared satisfying the above listed important thermoplastic conditions. To design a high quality lignin-based thermoplastic, robust linking is needed between lignin and synthetic polymers, and also a defined architecture is needed with narrow molecular weight distribution. Graft copolymerization is a very effective approach to integrate lignin and commercial polymers. This report presents two graft copolymerization methods: a "graft from" method via atom transfer radical polymerization (ATRP) from a lignin macroinitiator, and a "graft onto" method via ATRP and click chemistry.

ATRP is one of the most widely used controlled radical polymerization methods. ATRP synthesis requires a transition metal catalyst (commonly copper with nitrogen-containing ligands) and alkyl halide initiators together with vinyl monomers. Due to the character of controlled radical polymerization, products from ATRP differ from conventional radical polymerization. These stem from the living character of polymer chains from the halogen-containing dormant species, which allow controlled architecture and compositions, controlled functionality and tolerance of various experimental conditions than other living polymerization methods. Details of ATRP are well described in elsewhere (*28*, *29*). In the first part of this report, lignin was copolymerized via a "graft from" method of ATRP. Briefly, the "graft from" method is polymerization from macroinitiators

In Green Polymer Chemistry: Biocatalysis and Materials II; Cheng, H., et al.;
ACS Symposium Series; American Chemical Society: Washington, DC, 2013.

Publication Date (Web): November 22, 2013 | doi: 10.1021/bk-2013-1144.ch025

which contains multiple initiating functional groups on macromolecules (*30*, *31*). This method is compatibile with ATRP to synthesize a well-defined graft copolymer structure with relatively high grafting density compare to other graft copolymerization methods such as grafting onto and grafting through (*30*, *31*). Two polymers, polystyrene, a common glassy polymer, and poly(*n*-butyl acrylate), a common rubbery polymer, were investigated for lignin graft-copolymerization. Polystyrene is an important thermoplastic polymer that has a wide range of applications with large production capacity (11.5×10^6 tons worldwide in 2004) (*32*). Generally, polystyrene demonstrates stronger mechanical properties due to high glass transition temperature compared to poly(*n*-butyl acrylate). Normally atactic polystyrene has a T_g of 100 °C and typical tensile strength of approximately 50 MPa (*32*). Conversely, poly(*n*-butyl acrylate) is an important commercial elastomer which widely used for rubbers, adhesives, coatings and other various applications. Poly(*n*-butyl acrylate) is much weaker polymer than polystyrene; poly(*n*-butyl acrylate) has T_g value of approximately -55 °C and therefore, it is viscoelastic liquid at room temperature (*33*, *34*). In the first part of this report, a lignin-based macroinitiator was synthesized from lignin using the hydroxyl groups on lignin. Subsequently, well-defined graft copolymer of lignin and polystyrene/ poly(*n*-butyl acrylate) were prepared via grafting from method using ATRP.

The second graft copolymerization method is "graft onto" copolymerization of lignin and polystyrene using click chemistry. Click chemistry was first discussed by Sharpless et al. in 2001 to cover a range of coupling reactions that share common aspects (*35*). Important features of click chemistry include high selectivity, efficiency, moderate experimental conditions, and high tolerance of functionality. Common types of click reaction are copper(I)-catalyzed 1,3-dipolar cycloaddition of azides and alkynes (*36–38*), thiol-ene click chemistry (*39*), Diels-Alder cycloadditions (*40*, *41*) and epoxide ring-opening reactions (*42–45*). Recently, copper(I)-catalyzed 1,3-dipolar cycloaddition of azides and alkynes has received the significant attention because the reaction is readily applicable for biological conditions in aqueous media with no-significant side reactions and high yield (*46–48*). In addition, click reactions have been using for modification of polymer and copolymerization to introduce various architectures and functionalities (*49–52*). This report presents the synthesis of alkyne group functionalized lignin and synthesis of azide group functionalized polystyrene via ATRP followed by click reaction between azide and alkyne groups. This click reaction was used as an efficient "graft onto" copolymerization method of polystyrene branch on lignin. Overall, the present report describes both "graft from" and "graft onto" methods to produce lignin-based graft copolymers.

Experimental Section

Materials

Lignin was purchased from TCI America (TCI product number: L0082, softwood lignin). Prior to the experiment, lignin was washed with 2 M aqueous HCl solution and dried in vacuum oven for overnight. Hydroxyl group

In Green Polymer Chemistry: Biocatalysis and Materials II; Cheng, H., et al.;
ACS Symposium Series; American Chemical Society: Washington, DC, 2013.

concentration of lignin was determined by acetylation of hydroxyl group followed by ^{1}H NMR characterization. Acetylation of lignin hydroxyl groups is described elsewhere (*10*, *53*). Briefly, lignin (200 mg) was dissolved in 4 ml of pyridine and then 4 ml of acetic anhydride was added to the lignin - pyridine solution. The reaction mixture was stirred for 48 hours at room temperature. After 24 hours, the resulting solution was slowly added to the deionized (DI) water to precipitate acetylated lignin product. The precipitate was recovered by vacuum filtration and then dried in vacuo for overnight. The obtained solid was characterized by ^{1}H NMR in $CDCl_3$ with internal standard, pentafluorobenzaldehyde. All other chemicals were purchased from Aldrich Chemical Co. (Milwaukee, WI) and used as received.

Publication Date (Web): November 22, 2013 | doi: 10.1021/bk-2013-1144.ch025

Preparation of Lignin-Based Macroinitiator

Lignin (1 g) and pyridine (20 g) were mixed and stirred until they become homogeneous solution. The resulting solution mixture was placed in an ice bath while *2*-bromoisobutyryl bromide (11.69 g) solution in dry THF was added slowly. The reaction mixture was then stirred for 24 hours at room temperature. Next, DI water (10 mL) was added under vigorous stirring to quench the unreacted reagent, *2*-bromoisobutyryl bromide. After 15 minutes, the solution was dried using a rotary evaporator to remove remaining solvents and liquid reagents. The resulting dark yellow viscous solution was dissolved in 1,4-dioxane (15 mL) for the second precipitation. The solution was very slowly added to the saturated aqueous $NaHCO_3$ solution. Note that if the solution is added too fast the mixed solution generates large bubbles with strong heat. The precipitate was recovered by vacuum filtration. The product was dried in vacuum for 3 hours at 40 °C and then purified over diethyl ether once more. The final product was dried *in vacuo* overnight at 40 °C.

Graft Copolymerization (ATRP) of Styrene and *n*-Butyl Acrylate from Lignin-Based Macroinitiator

In a Schlenk flask, CuBr (22.2 mg), bipyridine (70 mg) and lignin-based macroinitiator (50 mg) were placed. Next, a Schlenk flask with the solid reagents was repeatedly vacuumed and backfilled with dry nitrogen for three times. Degased styrene (2.33 g) and dimethylformamide (DMF) (2 ml) were transferred to the solid reagent containing Schlenk flask. The first kinetic sample was taken prior to place the reaction mixture in the 100 °C oil bath. Kinetic samples were taken at designated times for ^{1}H NMR characterization and DMF eluent GPC characterization. The polymerization was stopped by removing heat followed by exposure the reaction solution in the air. The polymer solution was filtered through neutral alumina filled column to remove copper. The resulting filtrate polymer solution was added slowly into methanol to precipitate final lignin-*graft*-polystyrene product. The polymer was dried in vacuum overnight at room temperature. Then *n*-butyl acrylate was graft copolymerized via ATRP onto lignin with the same synthetic method used in polystyrene grafting, CuBr/PMDETA and reaction temperature, 70 °C.

In Green Polymer Chemistry: Biocatalysis and Materials II; Cheng, H., et al.;
ACS Symposium Series; American Chemical Society: Washington, DC, 2013.

Publication Date (Web): November 22, 2013 | doi: 10.1021/bk-2013-1144.ch025

Preparation of Alkyne Functionalized Lignin

Lignin (1 g), *N*,*N*′-dicychlohexylcarbodiimide (DCC, 4.73 g) and 4-pentynoic acid (2.25 g) were mixed in DMF (25 mL). The reaction mixture was cooled in ice bath and then 4-dimethylaminopyridine (DMAP, 140 mg) in 2 mL of DMF was added slowly to the cooled solution. This mixture was stirred for 40 hours at room temperature. The resulting heterogeneous solution was vacuum-filtered to separate the white solid part from the dark brown solution part. The filtrate solution part was then added dropwise in aqueous HCl solution (pH 1.0) to precipitate light brown pulp-like solid. The solid was isolated from the liquid by vacuum filtration and dried in vacuum oven at room temperature for 3 hours. The dry product was dissolved in methylene chloride again and then precipitated over hexane. The solid precipitate was stirred vigorously under ultrasonication for an hour in the hexane. Final product was recovered by vacuum filtration followed by drying in the vacuum oven overnight at room temperature. The synthesized alkyne functionalized lignin was characterized by ^{1}H NMR in DMSO-d_6 solvent with internal standard (pentafluorobenzaldehyde, 10 uL) to determine the concentration of alkyne group.

Preparation of Azide Functionalized Polystyrene

Azide-functionalized polystyrene was synthesized in two steps. First, bromine-terminated polystyrene was prepared by ATRP of styrene. Then, the bromine end group was converted to azide group by a substitution reaction. To prepare bromine end group containing polystyrene, CuBr (175 mg) was placed in Schlenk flask and then the vacuum / nitrogen backfill cycle was repeated three times. Next, degased styrene (5 g), *N*,*N*,*N*′,*N*′,*N*″-pentamethyldiethylenetriamine (PMDETA, 250 μL), anisole (1 mL) and ethyl *2*-bromoisobutyrate (EBiB, 352 μL) were added in order to the Schlenk flask using a nitrogen-purged syringe. Next the solution was exposed to air and then filtered through neutral alumina packed column to remove copper. The filtrate was slowly added to methanol to precipitate the product. A white, pulp-like solid product was isolated from solution by vacuum filtration. The product was dried in vacuum overnight at room temperature. Polystyrene was dissolved in THF for GPC analysis to determine number average molecular weight (M_n, 1,200) and polydispersity index (M_w/M_n, 1.23). The bromine end-group of polystyrene was verified by ^{1}H NMR, as shown in Figure 7.

The bromine-terminated polystyrene (2 g) was dissolved in DMF (13 mL) and mixed with sodium azide (221 mg). The heterogeneous reaction mixture was stirred for 14 hours at room temperature. The resulting solution was added slowly to the methanol (300 mL) and water (60 mL) mixture to form a precipitate of azide end group functionalized polystyrene. The final product was isolated by vacuum filtration and dried in vacuum oven at room temperature. The M_n and M_w/M_n of azide end group functionalized polystyrene was characterized by THF eluent GPC. There was no change of M_n and M_w/M_n values of azide-functionalized polystyrene compare to bromine-functionalized polystyrene. The functionalized

azide end-group of polystyrene was determined by ^{1}H NMR in $CDCl_3$ as shown in Figure 7.

Preparation of Lignin-*Graft*-Polystyrene via Click Chemistry

Previously synthesized azide-functionalized polystyrene (92 mg), alkyne-functionalized lignin (35 mg) and CuBr (5.6 mg) were placed in Schlenk flask. The solid reagent containing Schlenk flask was vacuumed and then back filled with nitrogen for three times to generate inert atmosphere inside. Next, DMF (1.5 mL), toluene (50 μL), and PMDETA (8.1 μL) were added in order to the Schlenk flask using the nitrogen purged syringes. After initial samples were taken for a kinetic study, the reaction mixture was stirred for 10 hours at room temperature. Reaction progress was checked at 5 hour and 10 hours of reaction time by DMF eluent GPC as shown in Figure 8. After the designated reaction time, the resulting solution was exposed to the air and filtered through neutral alumina packed column to remove copper. Then the solution was added dropwise to methanol in order to precipitate lignin-*graft*-polystyrene. The final product was dried in vacuum oven for overnight at room temperature. Chemical structure was determined by ^{1}H NMR in $CDCl_3$ as shown in Figure 7.

^{1}H NMR Characterization

Lignin, lignin-based macroinitiator, lignin-*graft*-polystyrene *via* ATRP, alkyne functionalized lignin, polystyrene, azide functionalized polystyrene and lignin-*graft*-polystyrene *via* click chemistry were characterized by ^{1}H NMR (Bruker Avance 300). Deuterated chloroform ($CDCl_3$) and deuterated dimethyl sulfoxide (DMSO-d_6) were used as a solvent to dissolve synthesized materials. ^{1}H NMR spectra are shown in Figure 1, 3, 5, 6 and 7.

GPC Characterization

Molecular weight and polydispersity index of polymer samples were analyzed by Waters GPC (Polymer Standards Services (PSS) columns (guard, 105, 103, and 102 Å)) using THF and DMF as an eluent with differential refractive index (RI) detector (Waters 2410). For THF eluent GPC flow rate was 1.0 mL/min at 25 °C and DMF eluent GPC's flow rate was 0.8 mL/min at 50 °C. The apparent molecular weights (M_n) and polydispersities (M_w/M_n) were determined with a calibration based on linear polystyrene standards using WinGPC 7.0 software from PSS. GPC traces are shown in Figure 8.

Publication Date (Web): November 22, 2013 | doi: 10.1021/bk-2013-1144.ch025

In Green Polymer Chemistry: Biocatalysis and Materials II; Cheng, H., et al.;
ACS Symposium Series; American Chemical Society: Washington, DC, 2013.

Publication Date (Web): November 22, 2013 | doi: 10.1021/bk-2013-1144.ch025

Results and Discussion

Preparation of Lignin ATRP Macroinitiator and Lignin-*Graft*-Polystyrene *via* "Graft From" Method

To prepare ATRP macroinitiator, lignin was reacted with 2-bromoisobutyryl bromide in the presence of pyridine as shown in Scheme 1. Previously, chemoselective phenolic hydroxyl group esterification was reported depending on base catalyst, triethylamine, from the mixed reagent's functionality of phenolic hydroxyl groups and aliphatic hydroxyl groups (*54*, *55*). In this report the base catalyst, pyridine, was used with 2-bromoisobutyryl bromide to convert both phenolic and aliphatic hydroxyl groups in lignin to ATRP initiation sites. The lignin ATRP macroinitiator was characterized by ^{1}H NMR in $CDCl_3$ as presented in Figure 1. Native lignin is soluble in DMSO. Lignin underwent esterification with 2-bromoisobutyryl bromide, and the product was found to be soluble in chloroform. The solubility change after esterification was consistent with successful modification of lignin functionality. Two methyl groups from bromoisobutyrate groups were appeared at 2.0 ppm in the ^{1}H NMR spectrum as shown in Figure 1. Also a broad signal is observed near 7 ppm and 3.7 ppm corresponding to lignin aromatic protons and lignin methoxy groups, respectively. The concentration of initiator sites (bromoisobutyrate groups) on unit weight of lignin was calculated by addition of the internal standard pentafluorobenzaldehyde (PFB) in ^{1}H NMR solution. The synthesized lignin-macroinitiator had 4.48×10^{-3} mmol of initiator sites per milligram of material. This corresponds to 112 initiators per lignin chain assuming a lignin molecular weight of 25,000 g/mole.

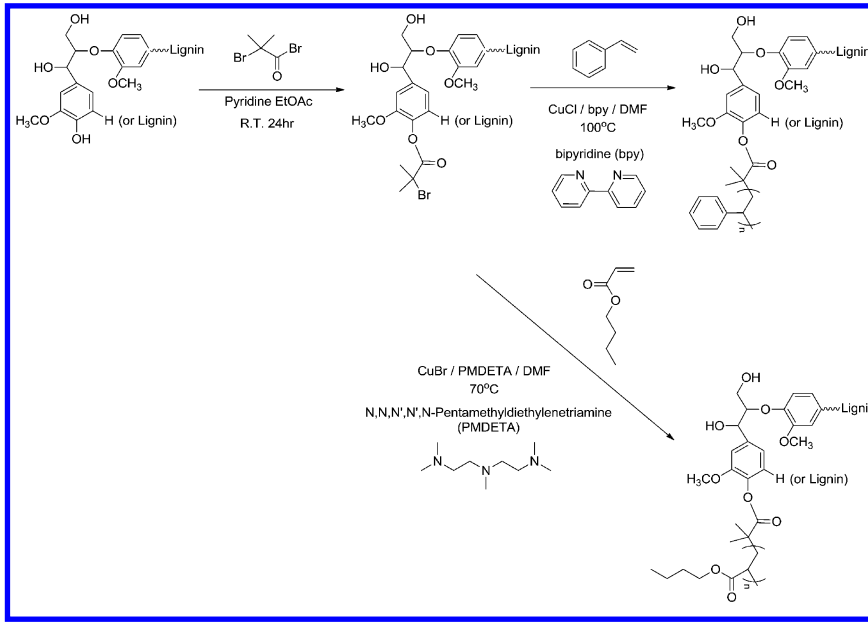

Scheme 1. Schematic illustration of preparation of lignin and styrene/n-butyl acrylate graft copolymer using "grafting from" method of ATRP.

In Green Polymer Chemistry: Biocatalysis and Materials II; Cheng, H., et al.;
ACS Symposium Series; American Chemical Society: Washington, DC, 2013.

Publication Date (Web): November 22, 2013 | doi: 10.1021/bk-2013-1144.ch025

Grafting from ATRP of styrene was initiated from the bromoisobutyrate groups on lignin-based macroinitiator. The polymerization was performed in the presence of copper (I) chloride and bypridine in DMF at 100 °C. Styrene was added at 100/1 ratio to moles of initiator to have a target degree of polymerization (DP) 100. The molar ratio of the polymerization was 1:2:1:100 ([CuCl]:[bypridine]:[initiator]:[styrene]). The catalyst complex CuCl/bypridine was found to offer the most efficient control of ATRP. Although CuBr/*N*,*N*,*N*′,*N*′,*N*″-pentamethyldiethylenetriamine (PMDETA) complex was tested (*56*), the polymerization reaction resulted in gel formation in minutes. Finally, CuCl complex with less active ligand (*56*), bipyridine, demonstrated well-controlled polymerization with moderate polymerization rate. Also a halogen exchange between CuCl catalyst and bromo initiator contribute to a better control in polymerization (*57*–*59*). For the best control, polymerization was tuned to occur at 100 °C. The lower temperature 70 °C was also examined, but the polymerization was too slow. All reagents were dissolved in DMF to keep a reaction mixture homogeneous.

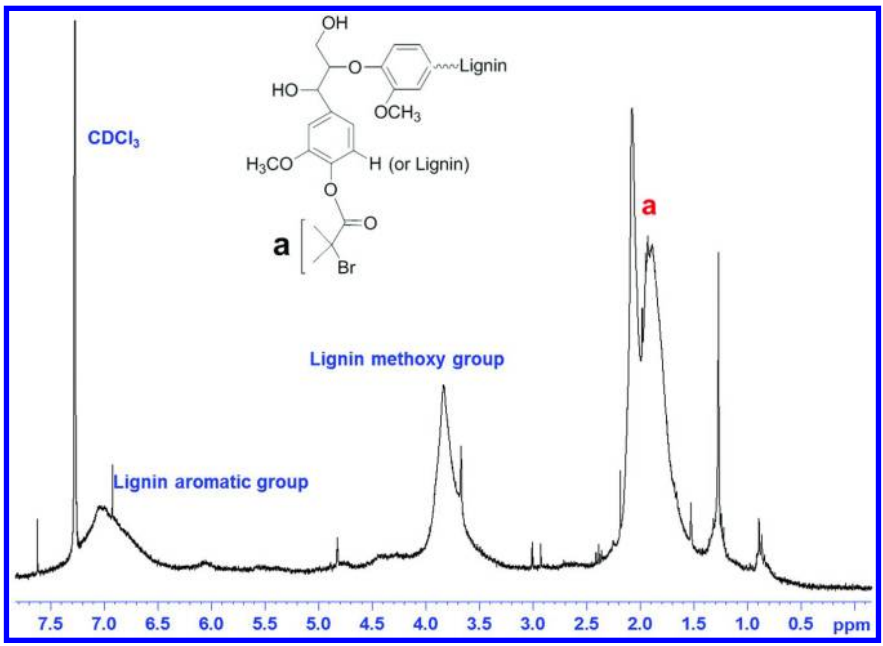

Figure 1. [1]H NMR spectrum of lignin-based macroinitiator for ATRP.

Aliquots of each polymerization were taken regularly from the reaction vessel to monitor the polymerization kinetics. The aliquots were analyzed by ^{1}H NMR and GPC to characterize decreases in vinyl group concentration of monomers and increases in number average molecular weight (M_n) of polymers, respectively. The conversion and the monomer concentration were derived from vinyl group concentration decrease compare to solvent as an internal standard in ^{1}H NMR analysis.

In Green Polymer Chemistry: Biocatalysis and Materials II; Cheng, H., et al.;
ACS Symposium Series; American Chemical Society: Washington, DC, 2013.

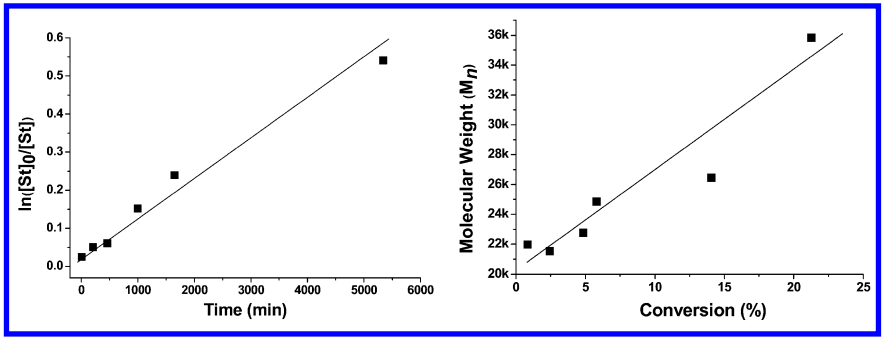

Figure 2. Kinetic results of ATRP graft-copolymerization of polystyrene from lignin.

Publication Date (Web): November 22, 2013 | doi: 10.1021/bk-2013-1144.ch025

The kinetic data in Figure 2 revealed that the polymerization of styrene on lignin-based macroinitiator occurred in controlled manner up to 23% conversion. Molecular weight of graft copolymer increased linearly with conversion (Figure 2, left). The kinetic plot (Figure 2, right) in semi-logarithmic coordinate demonstrated a first-order dependence of $\ln([st]_0/[st])$ over reaction time. This behavior indicates that the active species concentration kept constant during the polymerization. From these observations, we can conclude the polymerization occurred by controlled living polymerization without significant propagation chain terminations such as chain coupling termination, chain transfer reaction or other side reactions (*28*). The styrene ATRP from the lignin-based macroinitiator reached 23% conversion in 91 hours. The 23% conversion indicates that 2,400 g/mole of styrene were grafted onto lignin. Because apparent molecular weight (M_n) of native lignin is 25,000 g/mole (Table 1), the weight % of polystyrene in lignin-*graft*-polystyrene is 8.7%. Also the kinetic data of $\ln([st]_0/[st])$ revealed that $\ln([st]_0/[st])$ value at 91 hours deviated below that predicted from the assumption of living polymerization, which means active radical species start to terminate slowly. Our preliminary explanation of the low conversion is that there is stronger steric hindrance due to extended polystyrene branches; therefore, the accessibility of monomer to active species could be limited. Also active chain terminal radical species can be terminated by coupling or rarely by disproportionation. The reactivity of the used catalyst system may be not efficient enough to continue the polymerization in a highly polar solvent such as DMF. Considering the moderate conversion and decrease in active species concentration, we suggest that the appropriate ATRP target DP would be up to 25 at this high grafting density. This would still result in a final material that contains a significant fraction of lignin, consistent with the goal of reducing reliance on petroleum-based monomers in thermoplastics.

Figure 3 demonstrates a ^{1}H NMR spectrum of lignin-*graft*-polystyrene. Both lignin and polystyrene are qualitively confirmed by ^{1}H NMR. Lignin methoxy group protons are shown near 3.6 ppm and lignin aromatic group are invisible due to overlap with styrenic signals. Proton signals from polystyrene are assigned in Figure 3 at a, b and c. Two methyl groups from macroinitiator, bromoisobutyrate groups, are appeared at 2.0 ppm. The lignin copolymer was analyzed in $CDCl_3$

In Green Polymer Chemistry: Biocatalysis and Materials II; Cheng, H., et al.;
ACS Symposium Series; American Chemical Society: Washington, DC, 2013.

that is poor solvent for the lignin segment. The poor solubility of lignin segment in $CDCl_3$ caused very low noise-to-signal ratio in a ^1H NMR characterization. Because of the solubility difference in $CDCl_3$ between lignin segments and polystyrene segments, proton signal from styrene appears much bigger than lignin's proton signal in Figure 3. Figure 5 also displays small proton signals from lignin segments due to poor solubility of lignin segments in $CDCl_3$.

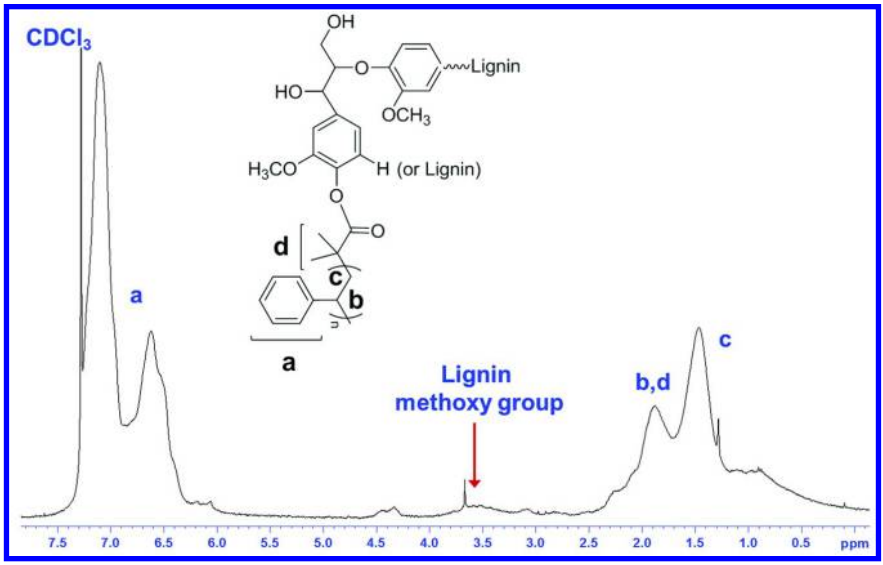

Figure 3. ^1H NMR spectrum of lignin-graft-polystyrene in $CDCl_3$.

Preparation of Lignin-*Graft*-Poly(*n*-butyl acrylate) *via* "Graft From" Method

Lignin-*graft*-poly(*n*-butyl acrylate) was synthesized in the presence of a CuBr/PMDETA catalyst complex in DMF as shown in Scheme 1. The CuBr/PMDETA is more active catalyst complex than above used CuCl/bypridine in styrene-lignin copolymerization. ATRP of lignin-*graft*-poly(*n*-butyl acrylate) with the CuBr/PMDETA was poorly active and therefore polymer's DP was very low (*56*). Other ATRP conditions were determined according to previous reports of *n*-butyl acrylate ATRP (*60–62*). The products were characterized using the same analytical tools and methods were used as lignin-*graft*-polystyrene synthesis for lignin-*graft*-poly(*n*-butyl acrylate).

Kinetic data in Figure 4 shows molecular weight as a function of extent of reaction having constant active species concentration until the polymerization was stopped at 21 hours with a conversion of 17%. At 17% conversion of *n*-butyl acrylate, the lignin-*graft*-poly(*n*-butyl acrylate) contained 8 weight % of poly(*n*-butyl acrylate) segments (Table 1). The number average molecular weight increased linearly with conversion, which is a typical character of controlled living polymerization (*28*, *29*, *63*, *64*). Lignin-*graft*-poly(*n*-butyl acrylate)

Publication Date (Web): November 22, 2013 | doi: 10.1021/bk-2013-1144.ch025

showed fairly low conversion under the given experimental conditions similar to the lignin-*graft*-polystyrene system. The kinetic results demonstrated that "graft from" methods using lignin-based macroinitiator is a suitable technique to produce short synthetic polymer graft chains on lignin.

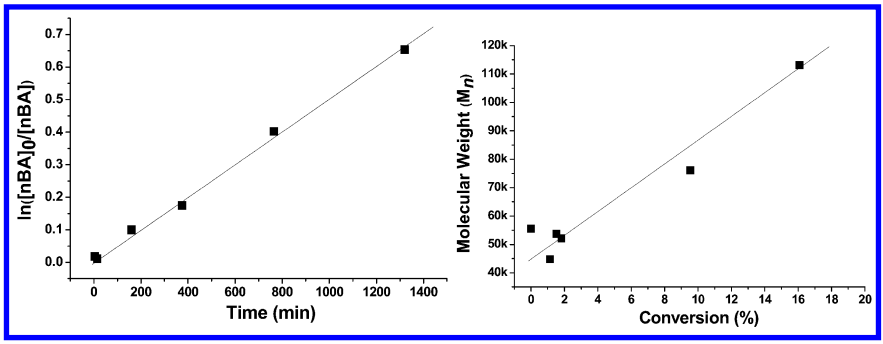

Figure 4. Kinetic results of ATRP graft-copolymerization of poly(n-butyl acrylate) from lignin.

The native lignin had a molecular weight of 25,000 g/mole with a polydispersity index (PDI) of 2.4 (Table 1). The lignin-based macroinitiator has slightly smaller molecular weight with a narrower PDI than native lignin's (Table 1). After the "graft from" polymerization, lignin-*graft*-polystyrene showed a smaller molecular weight than native lignin and macroinitiator at 10 minutes reaction time (see Table 1 and Figure 2 and 4). Lignin-*graft*-poly(*n*-butyl acrylate), however, demonstrates a much larger molecular weight at 15 minutes reaction than native lignin and this trend continues to the end of the polymerization. This result suggests that non-covalent interactions in lignin-*graft*-polystyrene cause the hydrodynamic volume of the copolymer to become smaller compared to the narrow molecular weight standard polymer (PS) used for GPC calibration (*65–68*). Because of the non-covalent interactions in lignin, the native lignin molecular weight in GPC is much smaller than copolymerized lignin, as shown in Table 1. The similar discrepancy in GPC analysis has been commonly observed by many other researchers as well (*65–68*). Therefore any changes of copolymer, eluent solvents, GPC columns and other additives may cause significant variation of results in GPC analysis of lignin-based copolymer. Although the undesirable non-covalent interaction limits exact measurement of molecular weight of lignin-based copolymer, the obtained GPC results are still useful for relative comparison between samples conducted under the same conditions during kinetic studies.

As shown in Table 1, there was significant decrease in polydispersity after graft copolymerization. Lignin-*graft*-polystyrene had a narrow PDI of 1.5 following 27.5 h of polymerization compare to that of native lignin, which was 2.4. Lignin-*graft*-poly(*n*-butyl acrylate) also showed a narrow PDI of 1.92 following 22 h of polymerization. Overall, ATRP of styrene and *n*-butyl acrylate from lignin was occurred in controlled manner with showing low PDI value after graft copolymerization.

Publication Date (Web): November 22, 2013 | doi: 10.1021/bk-2013-1144.ch025

Publication Date (Web): November 22, 2013 | doi: 10.1021/bk-2013-1144.ch025

Table 1. GPC data of lignin-*graft*-polystyrene and lignin-*graft*-poly(*n*-butyl acrylate) synthesized by "graft from" method

	Reaction time	M_n[a] *(g / mole)*	*PDI*[b]
Native Lignin	-	25,000	2.4
Macroinitiator	-	24,200	1.5
Lignin-*graft*-polystyrene	10 min	21,500	1.80
	27 hr 30min	35,800	1.50
Lignin-*graft*-poly(*n*-butyl acrylate)	15 min	44,700	2.04
	22 hr	86,400	1.92

[a] Apparent number average molecular weight. [b] Apparent polydispersity index (M_w/M_n).

The synthesized lignin-*graft*-poly(*n*-butyl acrylate) was analyzed by ^{1}H NMR in $CDCl_3$ (Figure 5). Poly(*n*-butyl acrylate) segment of the graft copolymer were confirmed by multiple proton signals assigned in Figure 5 a-f. Proton signals from lignin aromatic group and methoxy group were observed at 7 ppm and 3.7 ppm respectively. It confirms the presence of lignin in the graft copolymer.

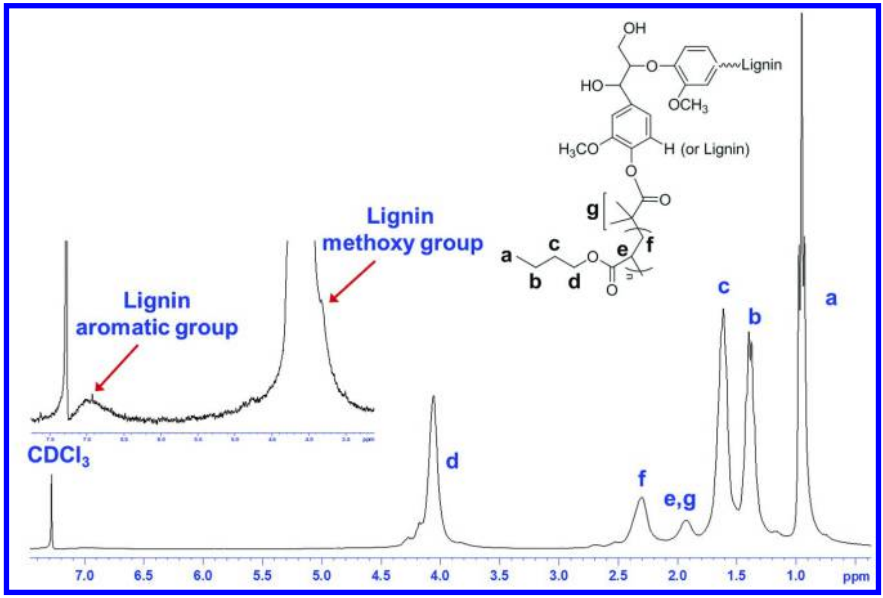

Figure 5. ^{1}H NMR spectrum of lignin-graft-poly(n-butyl acrylate) in $CDCl_3$.

Preparation of Alkyne Functionalized Lignin for "Graft Onto" Method

As another graft copolymerization method of lignin onto petroleum-based synthetic polymer, highly effective click chemistry was occurred between alkyne group functionalized lignin and azide end-group functionalized polystyrene. In order to introduce alkyne groups to lignin, lignin was reacted with

In Green Polymer Chemistry: Biocatalysis and Materials II; Cheng, H., et al.;
ACS Symposium Series; American Chemical Society: Washington, DC, 2013.

4-pentynoic acid in the presence of *N*,*N*′-dicychlohexylcarbodiimide (DCC) and 4-dimethylaminopyridine (DMAP) in DMF. The hydroxyl groups on lignin were converted to alkyne groups with ester linkages as shown in Scheme 2. The alkyne-functionalized lignin was characterized by ^{1}H NMR in DMSO-d_6 (Figure 6). Compare to non-modified lignin, newly introduced ester groups adjacent to the -CH_2CH_2- were observed at 2.7 ppm (Figure 6 (a)). Also protons from the alkyne group were identified at 1.7 ppm as shown in Figure 6 (a). The alkyne group concentration in unit weight of lignin was calculated by addition of ^{1}H NMR internal standard PFB; the PFB signal at 10.1 ppm is not shown in Figure 6. The resulting concentration of alkyne group was 2.22×10^{-3} mmol/mg.

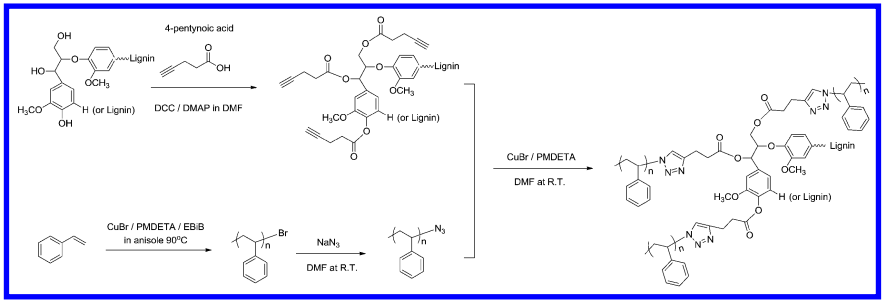

Scheme 2. Preparation of lignin-graft-polystyrene through click chemistry of graft onto method.

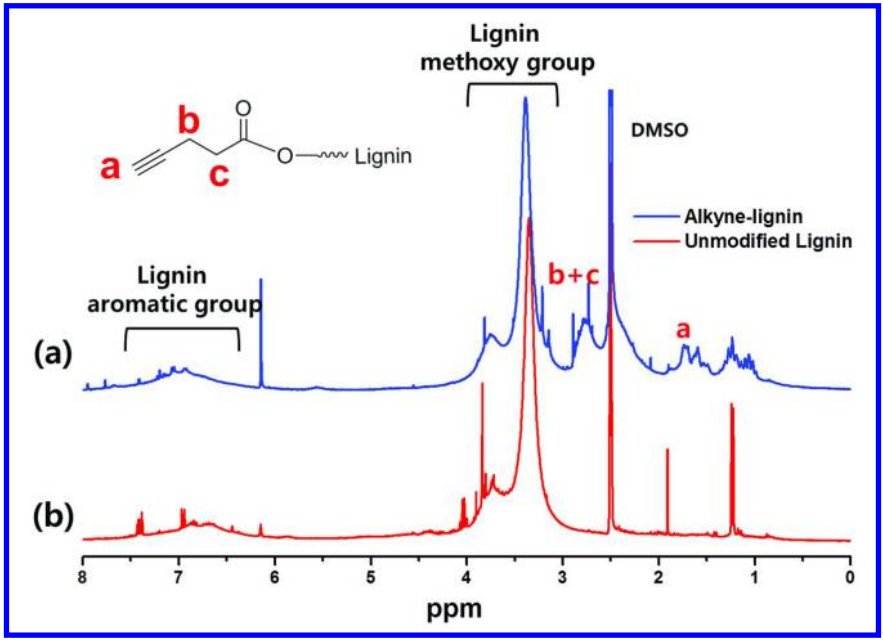

Figure 6. ^{1}H NMR of (a) alkyne functionalized lignin and (b) unmodified native lignin in DMSO-d_6.

In Green Polymer Chemistry: Biocatalysis and Materials II; Cheng, H., et al.;
ACS Symposium Series; American Chemical Society: Washington, DC, 2013.

Publication Date (Web): November 22, 2013 | doi: 10.1021/bk-2013-1144.ch025

Publication Date (Web): November 22, 2013 | doi: 10.1021/bk-2013-1144.ch025

Preparation of Azide Functionalized Polystyrene for "Graft Onto" Method

Azide-functionalized polystyrene was prepared in two steps. The first step was ATRP homopolymerization of styrene in the presence of CuBr/PMDETA and initiator ethyl 2-bromoisobutyrate (EBiB) in anisole. Because CuBr and bromo initiator were used for polymerization, the final polystyrene contains a bromine end group. The bromine end group underwent substitution reaction with sodium azide to introduce azide group at the end of each polystyrene chain as shown in Scheme 2. The polystyrene homopolymer had molecular weight of 1,200 g/mole with PDI of 1.2 by THF eluent GPC. The molecular weight and polydispersity of homopolystyrene was not changed after azide functionalization. End group functionality was characterized by ^{1}H NMR analysis (Figure 7). ^{1}H NMR spectrum of homopolystyrenes revealed typical polystyrene signals, however, the end group of polystyrene showed difference depending on functionality. Protons located adjacent to bromine had a signal at 4.5 ppm in Figure 7 (a). Azide adjacent proton has a signal at 4.0 ppm, which is upfield from the bromine terminal group due to shielding from the presence of the azide group (Figure 7 (b). After click reaction (cycloaddition between azide group of polystyrene and alkyne group of lignin), signal at 4.0 ppm, which represents azide terminal groups of homopolystyrene, disappeared from the NMR spectrum (Figure 7 (c)). The proton next to the triazole appeared at 5.1 ppm instead.

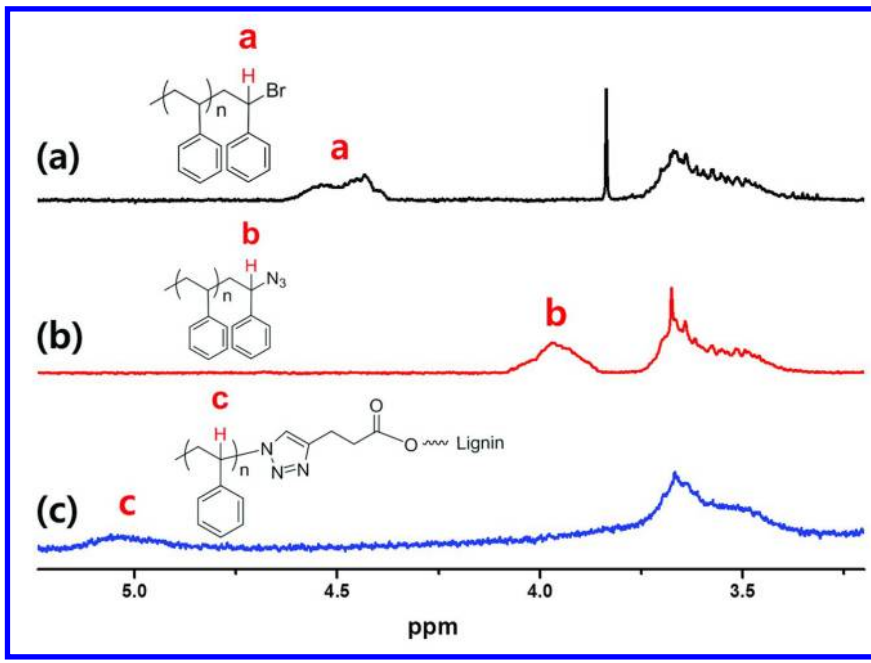

Figure 7. (a) Polystyrene prepared through ATRP (b) azide end group functionalized polystyrene and (c) lignin-graft-polystyrene after azide-alkyne cycloaddition reaction. Polystyrene proton adjacent to functional group is assigned in the ^{1}H NMR spectra. All products were analyzed in $CDCl_3$.

In Green Polymer Chemistry: Biocatalysis and Materials II; Cheng, H., et al.;
ACS Symposium Series; American Chemical Society: Washington, DC, 2013.

Graft Copolymerization of Lignin and Polystyrene *via* Click Chemistry

An equimolar ratio of alkyne groups at lignin and azide groups at polystyrene was used to graft polystyrene onto lignin. As shown in Scheme 2, the reaction was occurred in the presence of copper catalyst in DMF. Toluene was added as an inert internal standard for GPC analysis. The progress of cycloaddtiion between alkyne and azide was monitored by GPC analysis with a DMF eluent. Figure 8 shows GPC traces with three different reaction times: 0 hours, 5 hours and 10 hours. At 0 hours, the alkyne-functionalized lignin and azide functionalized homopolystyrene shows trace peaks at elution volume 25 mL and 32 mL, respectively. Based upon these two separated traces, it is clear that alkyne functionalized lignin and azide functionalized homopolystyrene exist in the solution as a mixture without chemical reactions as shown in blue at Figure 8. At 5 hours, the intensity of alkyne functionalized lignin trace was significantly increased whereas azide functionalized homopolystyrene trace was decreased. The GPC trace was not changed significantly at 10 hours. This result suggests that azide group functionalized homopolystyrene and alkyne functionalized lignin underwent cycloaddtion reaction to form a graft copolymer via "graft onto" method. Also most of the azide polystyrene was consumed in the reaction according to the GPC trace. If all azide groups and alkyne group reacted each other, the lignin-*graft*-polystyrene contained 72 weight % of polystyrene.

The GPC analysis of the lignin-*graft*-polystyrene showed M_n of 28,000 g/mole and PDI 2.0. Although there is fundamental technical limit of GPC analysis in lignin studies as above mentioned, increased M_n of the lignin-*graft*-polystyrene compare to native lignin's M_n proves the existence of grafted polystyrene on lignin. The graft copolymerization of well-defined homopolystyrene (i.e. low PDI homopolystyrene) onto lignin yielded lower PDI lignin-*graft*-polystyrene than native lignin's PDI, 2.4.

The graft copolymer formation via click reaction was confirmed once more with ^{1}H NMR characterization as well as GPC traces study. In Figure 7, it is observed that consecutive changes of the same terminal proton's signal on the ^{1}H NMR spectra. The clear change of polystyrene's terminal proton signal demonstrates that the completion of reactions for each step without no remaining starting reagents.

Overall, "graft onto" polymerization was successfully performed using click chemistry. All prepared azide terminated homopolystyrene grafts were reacted onto lignin with high efficiency. The prepared homopolystyrene had a DP of 11. The success of following click reaction suggested that the used length of polystyrene allowed facile coupling. In general, long grafts can interfere the efficient reaction in "graft onto" method due to steric hindrance (*30*, *31*). Also using lengthy chain for graft copolymerization will decrease the final fraction of lignin in lignin-synthetic copolymer which is not desirable for basic purpose of lignin-based polymer development.

Publication Date (Web): November 22, 2013 | doi: 10.1021/bk-2013-1144.ch025

In Green Polymer Chemistry: Biocatalysis and Materials II; Cheng, H., et al.;
ACS Symposium Series; American Chemical Society: Washington, DC, 2013.

Publication Date (Web): November 22, 2013 | doi: 10.1021/bk-2013-1144.ch025

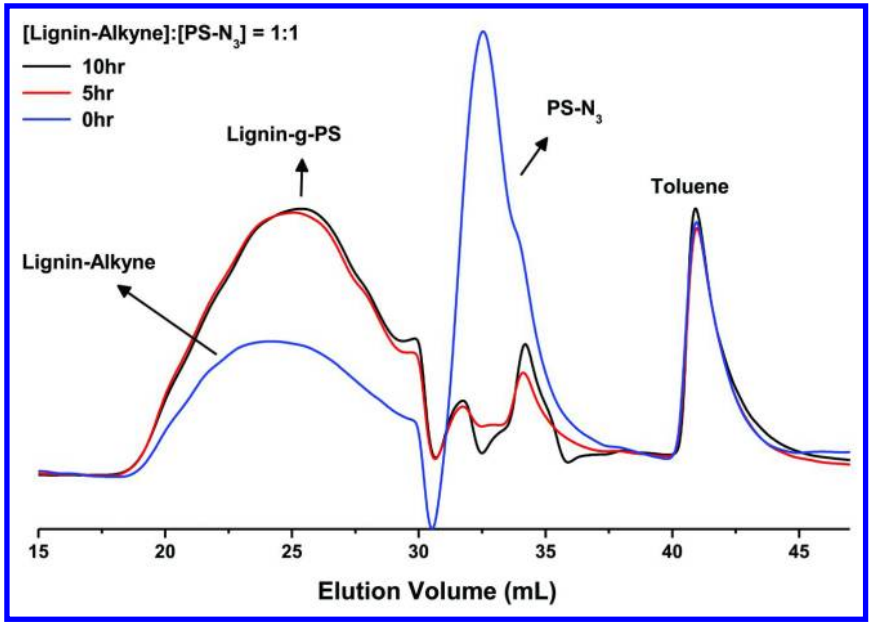

Figure 8. GPC traces of lignin-graft-polystyrene during the progress of the grafting. [Lignin-Alkyne]:[PS-N3] = 1:1. The reaction progress was monitored at 0 hour (blue), 5 hours (red) and 10 hours (black).

Conclusion

Two important commercial commodity polymers, polystyrene and poly(*n*-butyl acrylate), were successfully graft copolymerized to lignin. "Graft from" polymerization and "graft onto" polymerization methods were used for graft copolymerization. Lignin-synthetic graft copolymers displaying well-defined grafts with low PDI can be prepared using both methods. The "graft from" polymerizations demonstrated typical controlled living polymerization characters resulting moderate conversion of 23% (styrene) and 17% (*n*-butyl acrylate) according to the kinetic study. The prepared lignin-*graft*-polystyrene contains 8.7 weight % of polystyrene segment, and lignin-*graft*-poly(*n*-butyl acrylate) has 8.0 weight % of poly(*n*-butyl acrylate) segment. GPC study demonstrated that the lignin-based graft copolymers have much lower PDIs than native lignin, i.e. the graft copolymerization offered better controls in polymerization. For "graft onto" method, click chemistry was used to link alkyne functionalized lignin and azide functionalized homopolystyrene of DP 11. The copper catalyzed cycloaddition, click reaction, was occurred very efficiently; and the reaction consumed all polystyrene branches without significant side reactions and/or unreacted starting materials. The application of those two techniques, ATRP and click chemistry, presents that the successful chemistry to integrate the synthetic petroleum-based polymers to natural biopolymer lignin.

Publication Date (Web): November 22, 2013 | doi: 10.1021/bk-2013-1144.ch025

Acknowledgments

The authors would like to thank Prof. Krzysztof Matyjaszewski for allowing use of GPC.

References

1. Glasser, W. G.; Northey, R. A.; Schultz, T. P., Eds.; *Lignin: Historical, Biological, and Materials Perspectives*; ACS Symposium Series 742; American Chemical Society: Washington, DC, 1999.
2. Heitner, C.; Dimmel, D. R.; Schmidt, J. A. *Lignin and Lignins: Advances in Chemistry*; CRC Press: Boca Raton, FL, 2010.
3. Chakar, F. S.; Ragauskas, A. J. *Ind. Crops Prod.* **2004**, *20*, 131–141.
4. Saake, B.; Lehnen, R. In *Ullmann's Encyclopedia of Industrial Chemistry*; Wiley-VCH Verlag GmbH & Co. KGaA: Weinheim, Germany, 2000.
5. Meister, J. J. *J. Macromol. Sci., Polym. Rev.* **2002**, *C42*, 235–289.
6. Meister, J. J. In *Polymer Modification: Principles, Techniques, and Applications*; Meister, J. J., Ed.; Marcel Dekker: New York, 2000, pp 67−144.
7. Mohanty, A. K.; Kumar, M. N. S.; Erickson, L.; Misra, M. *J. Biobased Mater. Bioenergy* **2009**, *3*, 1–24.
8. Doherty, W. O. S.; Mousavioun, P.; Fellows, C. M. *Ind. Crops Prod.* **2011**, *33*, 259–276.
9. Calvo-Flores, F. G.; Dobado, J. A. *ChemSusChem* **2010**, *3*, 1227–1235.
10. Chung, H. Y.; Washburn, N. R. *ACS Appl. Mater. Interfaces* **2012**, *4*, 2840–2846.
11. Wang, J. S.; Manley, R. S.; Feldman, D. *Prog. Polym. Sci.* **1992**, *17*, 611–646.
12. Saraf, V. P.; Glasser, W. G. *J. Appl. Polym. Sci.* **1984**, *29*, 1831–1841.
13. Saraf, V. P.; Glasser, W. G.; Wilkes, G. L.; Mcgrath, J. E. *J. Appl. Polym. Sci.* **1985**, *30*, 2207–2224.
14. Saraf, V. P.; Glasser, W. G.; Wilkes, G. L. *J. Appl. Polym. Sci.* **1985**, *30*, 3809–3823.
15. Hatakeyama, H.; Nakayachi, A.; Hatakeyama, T. *Composites, Part A* **2005**, *36*, 698–704.
16. Bonini, C.; D'Auria, M.; Ernanuele, L.; Ferri, R.; Pucciariello, R.; Sabia, A. R. *J. Appl. Polym. Sci.* **2005**, *98*, 1451–1456.
17. Hatakeyama, T.; Asano, Y.; Hatakeyama, H. *Macromol. Symp.* **2003**, *197*, 171–180.
18. Pizzi, A. In *Handbook of Adhesive Technology*; Pizzi, A., Mittal, K. L., Eds.; Marcel Dekker: New York, 1994, pp 359−368.
19. Peng, W. L.; Riedl, B. *Polymer* **1994**, *35*, 1280–1286.
20. Park, Y.; Doherty, W.; Halley, P. J. *Ind. Crops Prod.* **2008**, *27*, 163–167.
21. Mondragon, I.; Tejado, A.; Kortaberria, G.; Pena, C.; Labidi, J.; Echeverria, J. M. *J. Appl. Polym. Sci.* **2007**, *106*, 2313–2319.
22. Alonso, M.; Oliet, M.; Domínguez, J.; Rojo, E.; Rodríguez, F. *J. Therm. Anal. Calorim.* **2011**, *105*, 349–356.

Publication Date (Web): November 22, 2013 | doi: 10.1021/bk-2013-1144.ch025

23. Pérez, J. M.; Rodríguez, F.; Alonso, M. V.; Oliet, M. *J. Appl. Polym. Sci.* **2011**, *119*, 2275–2282.
24. Kadla, J. F.; Kubo, S.; Gilbert, R. D.; Venditti, R. A. In *Chemical Modification, Properties, and Usage of Lignin*; Hu, T. Q., Ed.; Marcel Dekker: New York, 2002, pp 121−137.
25. Shen, Q.; Zhong, L. *Mater. Sci. Eng., A* **2007**, *445−446*, 731–735.
26. Shen, Q.; Zhang, T.; Zhang, W. X.; Chen, S. A.; Mezgebe, M. *J. Appl. Polym. Sci.* **2011**, *121*, 989–994.
27. Elias, H.-G. In *Ullmann's Encyclopedia of Industrial Chemistry*; Wiley-VCH Verlag GmbH & Co. KGaA: Weinheim, Germany, 2000.
28. Matyjaszewski, K.; Xia, J. H. *Chem. Rev.* **2001**, *101*, 2921–2990.
29. Braunecker, W. A.; Matyjaszewski, K. *Prog. Polym. Sci.* **2007**, *32*, 93–146.
30. Feng, C.; Li, Y.; Yang, D.; Hu, J.; Zhang, X.; Huang, X. *Chem. Soc. Rev.* **2011**, *40*, 1282–1295.
31. Hadjichristidis, N.; Iatrou, H.; Pitsikalis, M.; Mays, J. *Prog. Polym. Sci.* **2006**, *31*, 1068–1132.
32. Maul, J.; Frushour, B. G.; Kontoff, J. R.; Eichenauer, H.; Ott, K.-H.; Schade, C. In *Ullmann's Encyclopedia of Industrial Chemistry*; Wiley-VCH Verlag GmbH & Co. KGaA: Weinheim, Germany, 2000.
33. Penzel, E. In *Ullmann's Encyclopedia of Industrial Chemistry*; Wiley-VCH Verlag GmbH & Co. KGaA: Weinheim, Germany, 2000.
34. Stickler, M.; Rhein, T. In *Ullmann's Encyclopedia of Industrial Chemistry*; Wiley-VCH Verlag GmbH & Co. KGaA: Weinheim, Germany, 2000.
35. Sharpless, K. B.; Kolb, H. C.; Finn, M. G. *Angew. Chem,. Int. Ed.* **2001**, *40*, 2004–2021.
36. Binder, W. H.; Kluger, C. *Curr. Org. Chem.* **2006**, *10*, 1791–1815.
37. Johnson, J. A.; Finn, M. G.; Koberstein, J. T.; Turro, N. J. *Macromol. Rapid Commun.* **2008**, *29*, 1052–1072.
38. Lundberg, P.; Hawker, C. J.; Hult, A.; Malkoch, M. *Macromol. Rapid Commun.* **2008**, *29*, 998–1015.
39. Hoyle, C. E.; Bowman, C. N. *Angew. Chem., Int. Ed.* **2010**, *49*, 1540–1573.
40. Jen, A. K. Y.; Kim, T. D.; Luo, J. D.; Tian, Y. Q.; Ka, J. W.; Tucker, N. M.; Haller, M.; Kang, J. W. *Macromolecules* **2006**, *39*, 1676–1680.
41. Hizal, G.; Durmaz, H.; Dag, A.; Altintas, O.; Erdogan, T.; Tunca, U. *Macromolecules* **2007**, *40*, 191–198.
42. Pale, P.; Boningari, T.; Olmos, A.; Reddy, B. M.; Sommer, J. *Eur. J. Org. Chem.* **2010**, 6338–6347.
43. Matyjaszewski, K.; Tsarevsky, N. V.; Bencherif, S. A. *Macromolecules* **2007**, *40*, 4439–4445.
44. Parker, R. E.; Isaacs, N. S. *Chem. Rev.* **1959**, *59*, 737–799.
45. Petrova, S.; Riva, R.; Jérôme, C.; Lecomte, P.; Mateva, R. *Eur. Polym. J.* **2009**, *45*, 3442–3450.
46. Rostovtsev, V. V.; Green, L. G.; Fokin, V. V.; Sharpless, K. B. *Angew. Chem., Int. Ed.* **2002**, *41*, 2596–2599.
47. Bertozzi, C. R.; Saxon, E. *Science* **2000**, *287*, 2007–2010.
48. Tirrell, D. A.; Kiick, K. L.; Saxon, E.; Bertozzi, C. R. *Proc. Natl. Acad. Sci. U.S.A.* **2002**, *99*, 19–24.

49. Binder, W. H.; Sachsenhofer, R. *Macromol. Rapid Commun.* **2007**, *28*, 15–54.
50. Binder, W. H.; Sachsenhofer, R. *Macromol. Rapid Commun.* **2008**, *29*, 952–981.
51. Matyjaszewski, K.; Golas, P. L. *QSAR Comb. Sci.* **2007**, *26*, 1116–1134.
52. Matyjaszewski, K.; Golas, P. L. *Chem. Soc. Rev.* **2010**, *39*, 1338–1354.
53. Lundquist, K. *Acta Chem. Scand., Ser. B* **1979**, *33*, 27–30.
54. Melman, A.; Nahmany, M. *Org. Biomol. Chem.* **2004**, *2*, 1563–1572.
55. Kim, Y. S.; Kadla, J. F. *Biomacromolecules* **2010**, *11*, 981–988.
56. Matyjaszewski, K.; Tang, W.; Kwak, Y.; Braunecker, W.; Tsarevsky, N. V.; Coote, M. L. *J. Am. Chem. Soc.* **2008**, *130*, 10702–10713.
57. Matyjaszewski, K.; Shipp, D. A.; Wang, J. L. *Macromolecules* **1998**, *31*, 8005–8008.
58. Matyjaszewski, K.; Shipp, D. A.; Wang, J. L.; Grimaud, T.; Patten, T. E. *Macromolecules* **1998**, *31*, 6836–6840.
59. Matyjaszewski, K.; Qin, S. H.; Boyce, J. R.; Shirvanyants, D.; Sheiko, S. S. *Macromolecules* **2003**, *36*, 1843–1849.
60. Matyjaszewski, K.; Nakagawa, Y.; Jasieczek, C. B. *Macromolecules* **1998**, *31*, 1535–1541.
61. Muhlebach, A.; Gaynor, S. G.; Matyjaszewski, K. *Macromolecules* **1998**, *31*, 6046–6052.
62. Matyjaszewski, K.; Borner, H. G.; Beers, K.; Sheiko, S. S.; Moller, M. *Macromolecules* **2001**, *34*, 4375–4383.
63. Matyjaszewski, K. In *Controlled and Living Polymerization*; Matyjaszewski, K., Muller, H. E., Eds.; Wiley-VCH Verlag GmbH & Co.: Weinheim, Germany, 2009; pp 103−166.
64. Matyjaszewski, K.; Tsarevsky, N. V. *Chem. Rev.* **2007**, *107*, 2270–2299.
65. Dutta, S.; Garver Theodore, M.; Sarkanen, S. In *Lignin: Properties and Materials*; Glasser, W. G., Sarkanen, S., Eds.; ACS Symposium Series 397; American Chemical Society: Washington, DC, 1989; pp 155−176.
66. *Size Exclusion Chromatography of Lignin Derivatives*; Himmel, M. E., Mlynar, J., Sarkanen, S., Eds.; Marcel Dekker, Inc.: New York, 1995.
67. *Molar Mass and Size Distribution of Lignins*; Hortling, B., Turunen, E., Kokkonen, P., Eds.; Marcel Dekker, Inc.: New York, 1995.
68. Lage, L. E. C.; Sant'Anna, G. L.; Nobrega, R. *Bioresour. Technol.* **1999**, *68*, 63–70.

Publication Date (Web): November 22, 2013 | doi: 10.1021/bk-2013-1144.ch025

Publication Date (Web): November 22, 2013 | doi: 10.1021/bk-2013-1144.ch026

Chapter 26

Esterification of Xylan and Its Application

Noreen G. V. Fundador,[1,2] Yukiko Enomoto-Rogers,[1] and Tadahisa Iwata[*,1]

[1]Science of Polymeric Materials, Department of Biomaterial Sciences, Graduate School of Agricultural and Life Sciences, The University of Tokyo, 1-1-1 Yayoi, Bunkyo-ku, Tokyo 113-8657, Japan
[2]College of Science and Mathematics, University of the Philippines Mindanao, Mintal, Tugbok District, Davao City 8022, Philippines
[*]E-mail: atiwata@mail.ecc.u-tokyo.ac.jp

Xylan esters having different alkyl chain lengths (C2-C12) were prepared in homogeneous and heterogeneous systems. Analysis of the structure of the products was done by NMR. DSC results confirm that the xylan esters are amorphous. However, WAXD analysis suggests the presence of an ordered structure. Hence, a structural model for xylan esters was proposed. The mechanical properties of the xylan ester films were dependent on the length of the alkyl chain. Maximum values for tensile strength and elongation at break of the xylan esters were 29 MPa and 44%, respectively. Among the xylan esters, only XylPr and XylBu exhibited a nucleating effect on PLLA during non-isothermal and isothermal crystallization conditions. These xylan esters decreased the T_c of PLLA by almost 30 °C. Enhanced rate of crystallization, higher crystallinity and generation of smaller spherulites were observed in the PLLA blends containing the xylan esters compared to PLLA.

In Green Polymer Chemistry: Biocatalysis and Materials II; Cheng, H., et al.;
ACS Symposium Series; American Chemical Society: Washington, DC, 2013.

Publication Date (Web): November 22, 2013 | doi: 10.1021/bk-2013-1144.ch026

Introduction

Hemicelluloses represent one of the most abundant renewable polysaccharides found in nature. They comprise about one-fourth to one-third of the plant's material (*1*). Xylan is the major polysaccharide belonging to this class. Its main chain consists of D-xyl*p* (D-xylopyranose) units linked by β-(1→4) glycosidic bonds. Variation in the composition of xylan is dependent on the plant source. For example xylans in hardwood plants (e.g. eucalyptus, maple, birch are branched with 4-*O*-methylglucuronic acid (MeGlcA) and acetyl groups. Those in softwood plants (e.g. spruce, pine cedar) have MeGlcA and arabinose residues attached to the main chain. Recently, xylan is gaining importance for the basis of new biopolymeric materials and functional biopolymers by chemical modification. Several studies on the derivatization of arabinoxylan have already been published (*2–4*).

Poly(L-lactic acid) (PLLA) is a biodegradable thermoplastic polyester and can be synthesized either by the polycondensation of lactic acid or the ring opening polymerization of lactide. It is used in food packaging (e.g. bottles, cups and food wraps) and in the biomedical field (e.g. sutures, prosthetics). The processing of PLLA produces amorphous materials because of its slow rate of crystallization. Hence, the resulting materials are easily deformed when heated near their glass transition temperature (T_g) (*5*). One approach to address this problem is to add nucleating agents.

This chapter is a mini-review of our works done on xylan esters. Here, we describe the syntheses of xylan esters of different alkyl chain lengths (C2-C12) in homogeneous and heterogeneous reactions. Characterizations based on their structure, thermal and mechanical properties are presented. A preview of our recent findings on the use of xylan esters as bio-based nucleating agents for enhancing the crystallization of PLLA is discussed.

Experimental Methods

Materials

PLLA (M_w = 2.7 x 10^5, M_n = 1.6 x 10^5, M_w/M_n = 1.8) was purchased from Shimadzu, Japan. Trifluoroacetic anhydride (TFAA) and N,N- dimethylacetamide (DMAc) and other reagents were purchased from Wako. Xylan used was isolated from eucalyptus hardwood pulp based on the procedure described in our previous paper (*6*).

Syntheses of Xylan Ester

Xylan esters of different alkyl chain lengths (C2-C12) were prepared under homogeneous (DMAc/LiCl) and heterogeneous (TFAA/acid) conditions based the procedure described in our previous paper (*7*).

In Green Polymer Chemistry: Biocatalysis and Materials II; Cheng, H., et al.;
ACS Symposium Series; American Chemical Society: Washington, DC, 2013.

Publication Date (Web): November 22, 2013 | doi: 10.1021/bk-2013-1144.ch026

Stress-Strain Test

Films were prepared by solution casting using $CHCl_3$ as solvent. The mechanical properties of xylan ester films (20 mm x 1.5 mm) were carried out at room temperature using Shimadzu EZ test with a load cell of 10N. A crosshead speed of 20 mm/min and a 10 mm distance between grips were the parameters used. Five trials were done for each sample.

Wide-Angle X-ray Diffraction (WAXD)

X-ray diffractograms of the samples were obtained using a Rigaku RINT 2000 system operating at 40 kV and 200 mA. Measurements were performed with a Bragg-Bretano type 2 θ/θ goniometer in reflection mode. Ni-filtered Cu-Kα radiation (α = 0.15418 nm) was collimated in a 1/2 deg divergence slit, 1/6 deg scatter slit and 0.15 mm receiving slit. Scans were performed twice in the 2θ range at 5-40° with a scan rate of 0.5° min^{-1} and a step size of 0.1°.

Non-Isothermal Crystallization

Solutions of the xylan ester/PLLA blends (1% w/w) were prepared in $CHCl_3$ (10 mL) to obtain films by solution casting. The crystallization temperature (T_c) of the film samples during the heating process were obtained by differential scanning calorimetry (DSC) using a Perkin Elmer DSC 8500. For each DSC run, a small sample (1-2 mg) was heated from 50 to 200 °C at a rate of 20 °C/min. The sample was then cooled to -20 °C at a rate of 200 °C/min and heated back to 200 °C at rate of 20 °C/min. The T_c was determined from the second heating scan.

Isothermal Crystallization

Amorphous PLLA films were isothermally crystallized at 100 °C inside an oven for 10 min. The films were immediately quenched in an iced water bath and pat-dried prior to WAXD analysis.

Polarized Optical Microscopy (POM)

The spherulite morphology of the films was observed using a Nikon E600 POL polarized microscope equipped with a hot stage. The sample was initially melted at 200 °C for 1 min on stage A and then immediately transferred to stage B, which was preheated at a desired crystallization temperature (80, 90, 100, 110, 120 or 130 °C). The images were captured using Motic Image Plus 2.2S software.

Haze Measurement

The haze values of the film samples (4 × 4 cm) with a thickness of 0.1 mm were measured using a HZ-V3 haze meter (Suga Test Instruments Inc., Japan).

In Green Polymer Chemistry: Biocatalysis and Materials II; Cheng, H., et al.;
ACS Symposium Series; American Chemical Society: Washington, DC, 2013.

Publication Date (Web): November 22, 2013 | doi: 10.1021/bk-2013-1144.ch026

Results and Discussion

Syntheses, Molecular Weight, and Structure Analyses

Hardwood paper grade pulp is a suitable material for the extraction of xylan due to the presence minor lignin impurities. Extraction of xylan with different alkaline solutions such as nitren, DMSO, NaOH and KOH have been been investigated (*8*, *9*). In our study, xylan was isolated from eucalyptus hardwood kraft pulp using 10% NaOH. A yield of 6-8% was obtained (*6*).

Esterification of the isolated xylan with acyl groups of different alkyl chain lengths (C2-C12) were carried out under heterogeneous and homogeneous reaction conditions at 50 °C. Figure 1 shows the scheme for the esterification of xylan. Each xylose unit of xylan contains two hydroxyl groups which are potential sites for chemical modification. Heterogeneous reaction provides a simple and direct method of esterification. It uses TFAA which functions as a promoter for the rapid conversion of xylan to xylan esters. During the reaction, TFFA is converted to trifluoroacetic acid which makes the reaction medium acidic. Homogeneous reaction, on the other hand, requires the preswelling of xylan prior to esterification. Pyridine is used as a base-catalyst which also neutralizes any acid by-products. Accordingly, this method provides a milder reaction condition for the synthesis of xylan esters. Hence, the products obtained possessed higher molecular weights as compared to those synthesized from heterogeneous reaction. Table I shows the data obtained from GPC analysis of the xylan esters. The M_w and DP_n values of the xylan esters obtained by heterogeneous reaction ranged from 27 to 56 KDa and 77 to 96, respectively. In the case of those produced by homogeneous reaction, the M_w and DP_n values were higher ranging from 70 to 111 KDa and 139 to 189, respectively. The DP values of the xylan esters synthesized from homogeneous reaction are close to that of the literature value of hardwood xylan (DP=150-200) (*10*). In this article, the xylan esters synthesized in heterogeneous and homogeneous conditions are denoted as low-molecular weight (LMW) and high-molecular weight (HMW) xylan esters, respectively.

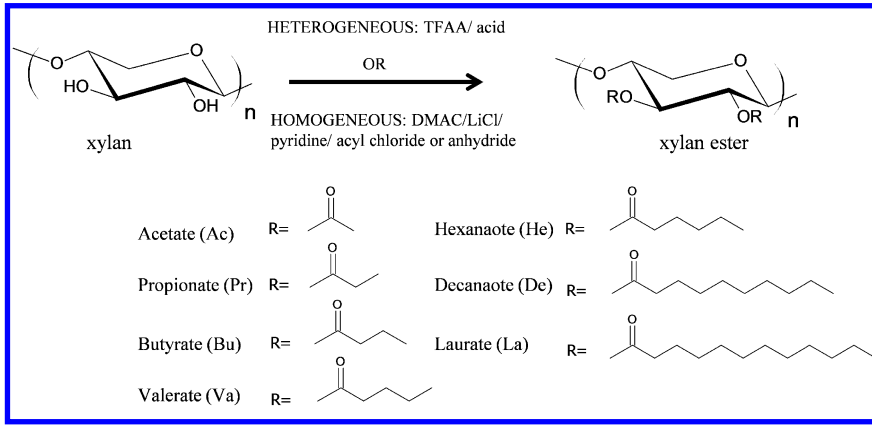

Figure 1. Scheme for the esterification of xylan.

In Green Polymer Chemistry: Biocatalysis and Materials II; Cheng, H., et al.;
ACS Symposium Series; American Chemical Society: Washington, DC, 2013.

Table I. GPC data of xylan esters obtained from different esterification reactions. SOURCE: Reproduced with permission from reference (*7*). Copyright 2012 Elsevier

*Xylan ester**	*# of carbons*	*Heterogeneous reaction*			*Homogeneous reaction*		
		M_w (x 10^3)	M_w/M_n	DP_n	M_w (x 10^3)	M_w/M_n	DP_n
XylAc	2	27	1.6	80	70	1.5	189
XylPr	3	33	1.4	96	62	1.5	168
XylBu	4	34	1.6	79	73	1.6	170
XylVa	5	37	1.5	82	77	1.7	156
XylHe	6	38	1.5	77	85	1.6	162
XylDe	10	53	1.3	92	100	1.7	126
XylLa	12	56	1.3	88	111	1.6	139

* DS=2.0.

Publication Date (Web): November 22, 2013 | doi: 10.1021/bk-2013-1144.ch026

Structure elucidation of xylan and xylan esters by NMR analyses have been discussed in detail in our previous studies (*6*, *7*). The ^{1}H-NMR spectra of xylan and xylan acetate are displayed in Figure 2. In spectrum of xylan (Figure 2a), the signals appearing at δ 3.0, 3.2, 3.3, 3.5, 3.9 and 4.3 correspond to H-2, H-5_a, H-3, H-4, H-5_e and H-1, respectively. The absence of the signals corresponding to the uronic acids indicates that only traces of these substances are present; hence, could not be detected by NMR. In comparison with the spectrum of XylAc (Figure 2b), the signals at δ 3.3, 3.7, 3.9, 4.5, 4.7 and 5.0 ppm are assigned to H-2, H-5_a, H-3, H-4, H-5_e and H-1, respectively. The intense signal at δ 2.0 ppm is assigned to the methyl protons (-CH_3) indicating that the hydroxyl groups were acetylated. We also reported that the acetylation of xylan is a non-selective reaction (*6*). Similar DS values were observed at the C-2 and C-3 positions of XylAc indicating uniform acetyl distribution. The DS was calculated based on the area of the carbonyl peaks in the ^{13}C-NMR spectra of the perpionylated XylAc. Furthermore, the DS can be controlled by varying the reaction times. Acetylation of xylan by homogeneous reaction proceeded rapidly wherein a DS= 2.0 was achieved within 6h. A longer reaction time was required for the complete esterification of xylan with longer acyl groups.

In Green Polymer Chemistry: Biocatalysis and Materials II; Cheng, H., et al.;
ACS Symposium Series; American Chemical Society: Washington, DC, 2013.

Publication Date (Web): November 22, 2013 | doi: 10.1021/bk-2013-1144.ch026

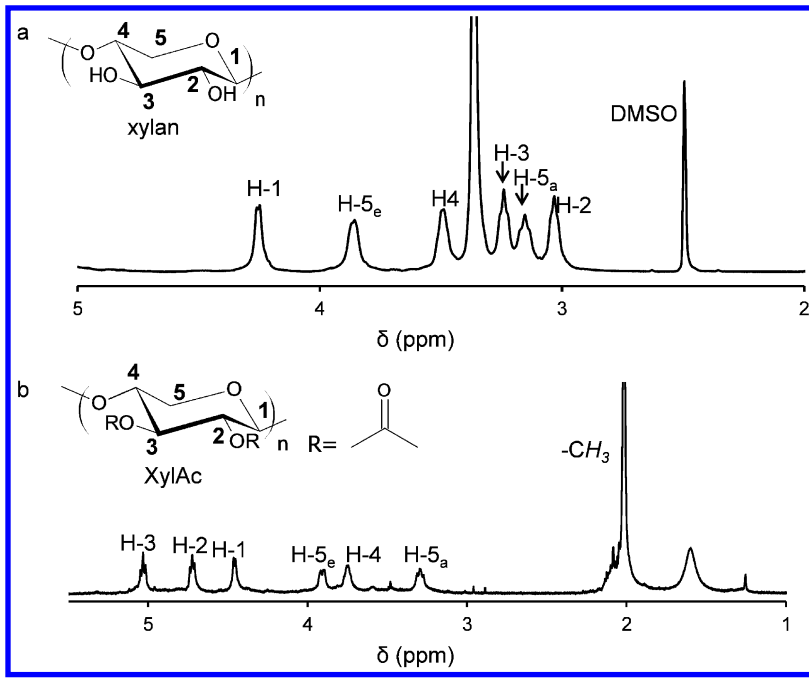

Figure 2. [1]H-NMR spectra of (a) xylan and (b) XylAc (DS= 2.0).

Mechanical Properties

Xylan esters with varying DS exhibited different solubilities in $CHCl_3$. In the case of HMW XylAc, its solubility increased with increase in DS. HMW XylAc with DS=2.0 still remained partially soluble (ca. 58%) (*6*). HMW xylan esters (DS=2.0) having longer alkyl chain lengths were completely soluble except for XylPr which was only 54% soluble.

The characteristic of xylan esters to be dissolved in $CHCl_3$ makes it possible for them to be fabricated into films. Studies on cellulose ester and starch ester films are already found in literature (*11*, *12*). HMW xylan esters with alkyl chain length ranging from C4 to C12 could form continuous films by solvent casting method. The stress-strain curves of the HMW xylan ester films are presented in Figure 3. The mechanical properties of the xylan ester films were dependent on the nature of the alkyl chain. The tensile strength of the film decreased with increase in alkyl chain length. Highest tensile strength was observed with XylBu having a value of 29 MPa. On the other hand, the elongation at break increased with increase in alkyl chain length. XylDe and XylLa were noted to have an elongation at break of 46 and 44%, respectively. These values were higher compared to the xylan esters with shorter alkyl chain length. Longer alkyl chains exhibit a plasticizing effect which permit the film to be further stretched. LMW xylan ester films can also be obtained, however these films were too weak to undergo mechanical testing.

In Green Polymer Chemistry: Biocatalysis and Materials II; Cheng, H., et al.;
ACS Symposium Series; American Chemical Society: Washington, DC, 2013.

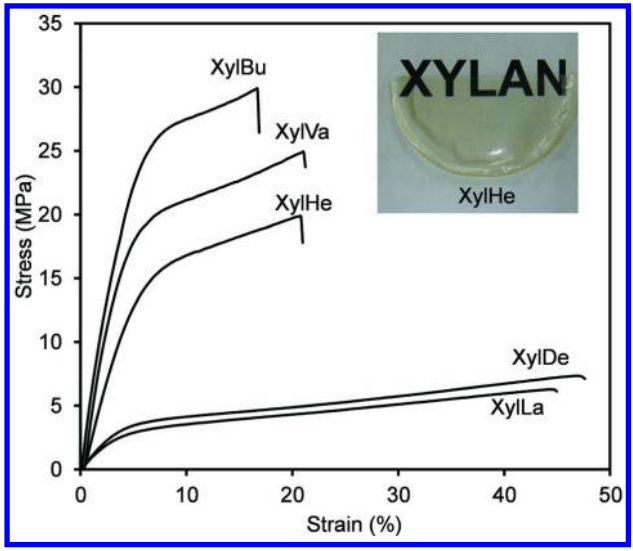

Figure 3. Stress-strain curves of HMW xylan ester films. Photograph of HMW XylHe film (embedded picture).

Thermal and WAXD Analyses

The thermal behaviors of xylan and xylan esters have been investigated by DSC analysis (*7*). Melting peaks (T_m) were not observed in all samples for the first and second heating scans. This result suggests that xylan and xylan esters are amorphous. Although the side chains of a certain polysaccharide are capable of undergoing side chain crystallization, xylan esters did not manifest any side chain melting probably due to the presence of shorter alkyl chains. This is because the movement of these alkyl chains is restricted by the immobile base polymer.

Contrary to the findings obtained from WAXD analysis, the xylan ester films reveal the presence of strong diffraction peaks in the low angle region as shown in Figure 4. This is indicative of the presence of an ordered structure. Diffraction peaks of xylans esters with longer alkyl chains appeared at higher angles. We calculated the alkyl chain length of the xylan esters and compared it with their *d*-spacing to understand the discrepancies between the DSC and WAXD results. The calculations for the alkyl chain length were based on the values of the C-C bond length and bond angle. Table II presents the WAXD data of the HMW xylan ester films. The *d*-spacing values of the xylan esters are larger as compared to the calculated alkyl chain lengths. Based on this, we propose that the main chains are arranged parallel to each other with the alkyl chains fully extended. Furthermore, it is assumed that no interdigitation has taken place. Accordingly, longer chain xylan esters would tend to possess larger *d*-spacing. This is in good agreement with the results obtained from the WAXD analysis. The diffraction peaks seen in the diffractograms arises from the alignment of the main chains causing the alkyl chains to assume a certain degree of order. However, due to the lack of interaction

In Green Polymer Chemistry: Biocatalysis and Materials II; Cheng, H., et al.;
ACS Symposium Series; American Chemical Society: Washington, DC, 2013.

of the alkyl chains it is impossible for side chain crystallization to occur. As a consequence, melting peaks were not detected in the DSC curves. The *d*-spacing of the xylan esters did not vary in the wide angle region.

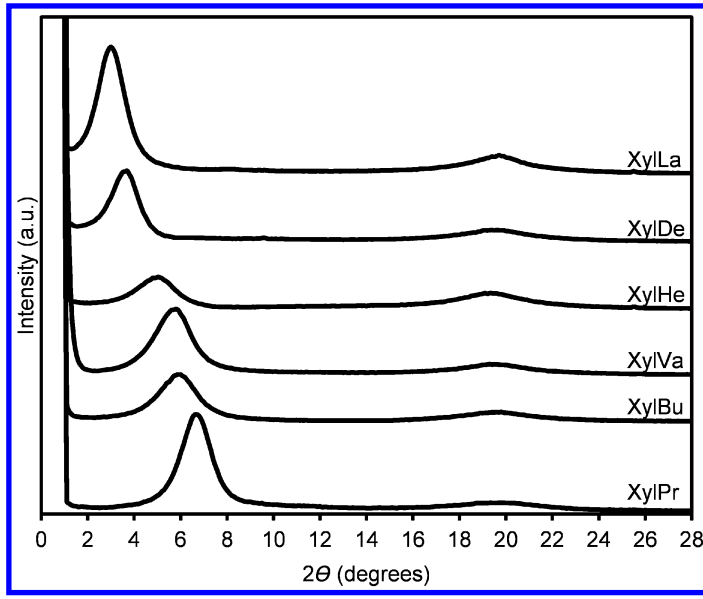

Figure 4. X-ray diffractograms of HMW xylan esters films. Reproduced with permission from reference (7). Copyright 2012 Elsevier.

Table II. WAXD data of xylan ester films. SOURCE: Reproduced with permission from reference (*7*). Copyright 2012 Elsevier

Xylan ester	*# of carbons*	*Low angle region*			*Wide angle region*	
		2θ (°)	*d-spacing[a] (Å)*	*Alkyl chain length[b] (Å)*	*2θ (°)*	*d-spacing (Å)*
XylPr	3	6.9	12.8	2.52	19.9	4.4
XylBu	4	6.0	14.8	3.75	20.0	4.5
XylVa	5	5.7	15.4	5.00	19.7	4.5
XylHe	6	5.0	18.0	6.25	19.3	4.6
XylDe	10	3.6	25.0	11.3	19.6	4.5
XylLa	12	2.9	30.0	13.8	19.7	4.5

[a] obtained from WAXD analysis [b] calculated based on the established values of C-C bond length (1.54 Å) and bond angle (109.5°). The sum of the distance between every other carbon within the alkyl chain would account for the alkyl chain length.

In Green Polymer Chemistry: Biocatalysis and Materials II; Cheng, H., et al.;
ACS Symposium Series; American Chemical Society: Washington, DC, 2013.

Publication Date (Web): November 22, 2013 | doi: 10.1021/bk-2013-1144.ch026

Crystallization Studies

Polymer crystallization is a physical reaction initiated either by homogeneous or heterogeneous nucleation and is subsequently proceeded by the growth of the nuclei. Homogenous nucleation takes place in uniform solution and requires the creation of a phase interface resulting in the formation of nucleating sites. In heterogeneous nucleation, the presence of foreign particles (e.g such as nucleating agents, dust) provides a surface on which a crystal can go thereby inducing crystal growth. This process proceeds more rapidly. Here, we present the effect of different types of xylan esters on the crystallization behavior of PLLA. A complete discussion of our results are presented in our recent paper (*13*) .

Publication Date (Web): November 22, 2013 | doi: 10.1021/bk-2013-1144.ch026

Non-Isothermal Crystallization

The LMW xylan ester series (C2-C12) were screened for their nucleating effect on PLLA. Figure 5 shows the DSC profiles of PLLA and PLLA blends containing 1% xylan ester observed in the second heating scan. PLLA showed a broad exothermic peak at 125 °C which corresponds to the crystallization temperature (T_c). Among the LMW xylan esters used, only XylPr and XylBu decreased the T_c of PLLA. The T_c values of XylPr/PLLA and XylBu/PLLA were 96 and 97°C, respectively. Sharper exothermic peaks were observed at lower temperature in these blends as compared to neat PLLA. A small exothermic peak prior to melting was also seen in the DSC curves of the blends. As for the PLLA blends containing the other xylan esters (XylAc/PLLA, XylHe/PLLA, XylDe/PLLA, and XylLa/PLLA), their T_c values were either almost the same or higher than that of neat PLLA. Similar to neat PLLA, these blends showed broad exothermic peaks. The double melting peaks observed in PLLA and in some blends (XylAc/PLLA, XylHe/PLLA, XylDe/PLLA, and XylLa/PLLA) is a result of the possible recrystallization of the samples during melting. This behavior was also observed in other studies (*14*, *15*). Table III gives a summary of the thermal data of PLLA and the PLLA blends. The values for the heat of crystallization (ΔH_c) of XylPr/PLLA and XylBu/PLLA were 16 and 19 J/g, respectively. The exact ΔH_c of PLLA and the other blends could not be obtained due the broadness of their peaks. No significant changes were observed in the T_g and T_m of PLLA following the addition of the xylan esters. XylPr/PLLA and XylBu/PLLA blends indicated higher ΔH_m as compared the rest of the samples. Comparable results were obtained when HMW xylan esters were used. A study on the crystallization of PLLA containing BTA (1,3,5-benzenetricarboxylamide) derivatives has been reported (*16*). It was observed that the T_c values of the PLLA blends containing BTA-nBu (BTA-n-butyl) and BTA-nHe (BTA-n-hexyl) during heating were reported to be 102, and 101 °C, respectively. In the presence of talc, the T_c of PLLA was reduced to 107 °C (*17*).

In Green Polymer Chemistry: Biocatalysis and Materials II; Cheng, H., et al.;
ACS Symposium Series; American Chemical Society: Washington, DC, 2013.

Publication Date (Web): November 22, 2013 | doi: 10.1021/bk-2013-1144.ch026

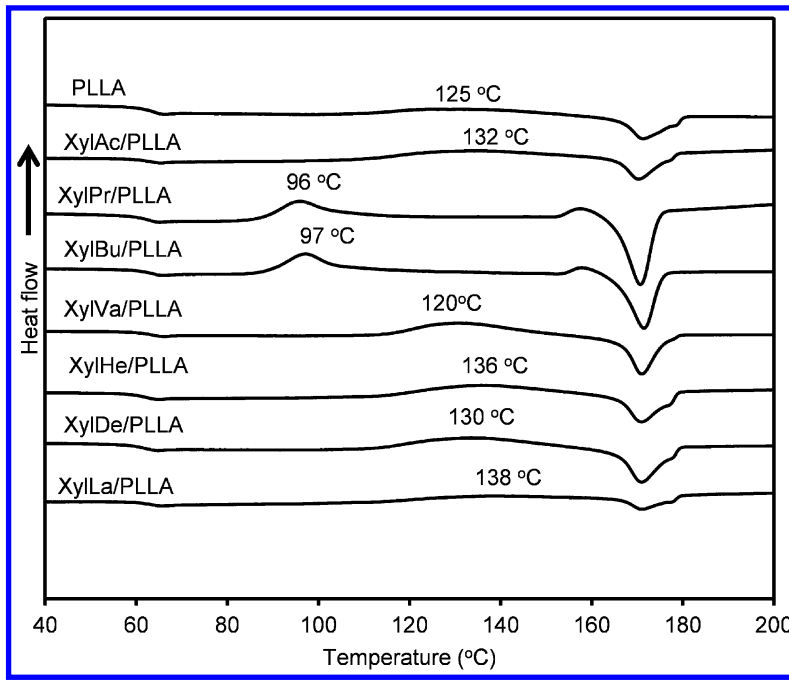

Figure 5. DSC traces of PLLA and the PLLA blends containing 1% xylan esters. Reproduced with permission from reference (13). Copyright 2013 Elsevier.

Table III. Thermal data obtained from DSC analysis of PLLA and the PLLA blends[a]. SOURCE: Reproduced with permission from reference (*13*). Copyright 2013 Elsevier

Sample	T_g *(°C)*	T_c *(°C)*	ΔH_c *(J/g)*	T_m *(°C)*	ΔH_m *(J/g)*
PLLA	62	125	-	171, 176	17
XylAc/PLLA	62	132	-	171	25
XylPr/PLLA	62	96	16	171	33
XylBu/PLLA	62	97	19	171	34
XylVa/PLLA	62	120	-	171	29
XylHe/PLLA	61	136	-	171,176	21
XylDe/PLLA	61	130	-	171,176	23
XylLa/PLLA	62	138	-	171, 176	12

[a] PLLA blends contain 1% xylan ester. The thermal values were obtained from the second heating cycle. - cannot be determined

In Green Polymer Chemistry: Biocatalysis and Materials II; Cheng, H., et al.;
ACS Symposium Series; American Chemical Society: Washington, DC, 2013.

An investigation on the crystallization behavior of PLLA, XyPr/PLLA and XylBu/PLLA from the melt at different cooling rates was also conducted. PLLA blends showed early appearance of the crystallization peaks as compared to PLLA (*6*). Furthermore, the ΔHc of the PLLA blends were larger as compared to PLLA suggesting that more crystals were formed. When faster cooling rates (≥ 10 °C/min) were employed, the crystallization peak was not detected for PLLA indicating that the sample remained amorphous after cooling. However, in the case of the blends the crystallization peaks were still observed. This indicates the effectiveness of XylPr and XylBu to induce crystallization even at higher cooling rates.

Publication Date (Web): November 22, 2013 | doi: 10.1021/bk-2013-1144.ch026

Isothermal Crystallization

PLLA and the PLLA blends were melted at 200 °C followed by isothermal crystallization at various temperatures (80, 90, 100, 110, 120 and 130 °C). Figure 6 shows the dependence of the crystallization half-time ($t_{1/2}$) on the T_c. The $t_{1/2}$ value is defined as the time required to achieve 50% of the final crystallinity of the sample. The $t_{1/2}$ values of the samples were observed to decrease when they were isothermally crystallized from 80 to 100 °C but increased when crystallized above 100 °C. It was noted, however, that the $t_{1/2}$ values of XylPr/PLLA and XylBu/PLLA were lower than that of neat PLLA. At 100°C, the crystallization rate of the samples was observed to be at its maximum. The $t_{1/2}$ values of XylPr/PLLA and XylBu/PLLA isothermally crystallized at 100 °C were 1.0 and 0.8 min, respectively. In the case of neat PLLA, however, its $t_{1/2}$ value was twice higher (1.8 min). Hence, this result indicated that the crystallization of PLLA was effectively enhanced by the addition XylPr or XylBu.

The $t_{1/2}$ values of the XylPr/PLLA blends isothermally crystallized from 90 to 120 °C were almost the same. In contrast to XylBu/PLLA, the $t_{1/2}$ value of this blend increased significantly above 100°C, indicating that the use of XylPr provides a wide processing range for PLLA.

Spherulite Morpholgy, Crystallinity, and Haze

Amorphous PLLA and PLLA blends annealed at 100 °C produced different spherulite morphologies. Figure 7a shows the POM images of the fully crystallized samples. Each samples showed different spherulite morphology and density. The spherulites of the XylPr/PLLA and XylBu/PLLA appeared smaller and denser as compared to PLLA. This indicates the ability of XylPr and XylBu to effectively nucleate PLLA which is also supported by their smaller $t_{1/2}$ values. Similar results have been were also reported when cellulose nanocrystals (*18*), multiamide compounds (*19*) and carbon nanotubes (*20*, *21*) were explored as the nucleating agents.

The difference in the size of the spherulites has an effect on the transparency of the samples. Larger spherulites causes light to scatter resulting in a decrease in the transparency of the material. The transparency of the samples can be assessed in terms of haze. The haze values of XylPr/PLLA and XylBu/PLLA annealed at 100 °C for 10 min were 13 and 9%, respectively. These values are significantly lower

In Green Polymer Chemistry: Biocatalysis and Materials II; Cheng, H., et al.;
ACS Symposium Series; American Chemical Society: Washington, DC, 2013.

compared to PLLA (45%). This indicates that the PLLA blends exhibit higher film transparency. Figure 7b shows that the images taken through the PLLA blend films are clearer while that captured through the PLLA film was faded and cloudy.

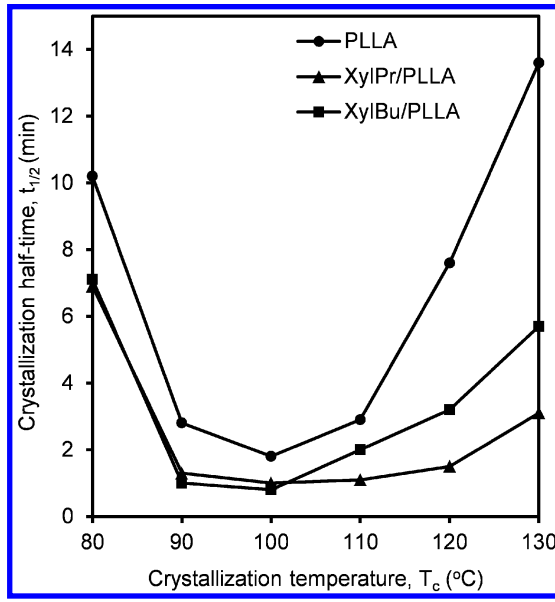

Figure 6. Effect of varying the T_c values on the $t_{1/2}$ values of PLLA and the PLLA blends. (PLLA blends contain 1% xylan ester). Reproduced with permission from reference (13). Copyright 2013 Elsevier.

To assess the effectiveness of XylPr and XylBu for enhancing the overall rate of crystallization of PLLA, the crystallinity of the samples annealed at 100 °C at different times were obtained based from the WAXD experiment. Our recent findings (*13*) indicate that the PLLA blends (XylPr/PLLA and XylBu/PLLA) already started to crystallized when annealed for 1 min. The crystallinity of the PLLA blends was 1%. In the case of PLLA, the sample remained amorphous. When the samples were annealed at a longer time (10 min), the crystallinity of the PLLA blends was more than 40%. However, for PLLA only 32% crystallinity was achieved. It was observed in the diffractograms (Figure 7c) that the position of the peaks were the same for PLLA and the PLLA blends suggesting that the xylan esters are excluded from the lattice during crystallization. The use of xylan esters as nucleating agents for PLLA results in obtaining a high crystalline material while retaining its transparency.

In Green Polymer Chemistry: Biocatalysis and Materials II; Cheng, H., et al.;
ACS Symposium Series; American Chemical Society: Washington, DC, 2013.

Publication Date (Web): November 22, 2013 | doi: 10.1021/bk-2013-1144.ch026

Publication Date (Web): November 22, 2013 | doi: 10.1021/bk-2013-1144.ch026

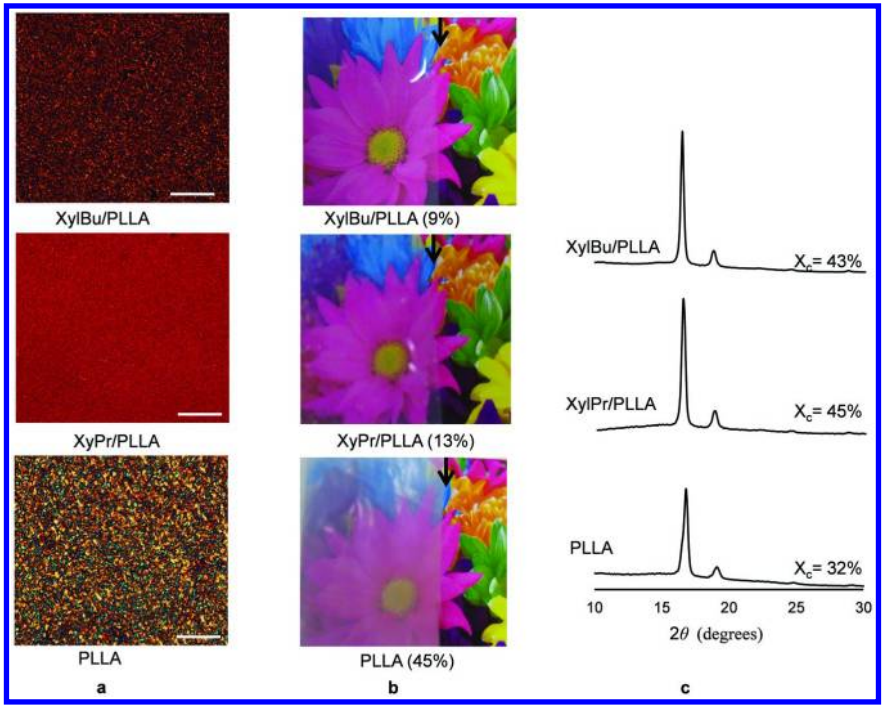

Figure 7. POM images of PLLA and the PLLA blends showing the impinged spherulites isothermally grown at 100 °C (Scale bar = 100 μm) (a), pictures taken through the PLLA and PLLA blend films annealed at 100 °C for 10 min (the arrows indicate the demarcation of the films) (b), and their corresponding X-ray diffractograms (c).

Conclusion

Xylan esters with varying alkyl chain lengths (C2-C12) were prepared by heterogeneous and homogeneous reactions, respectively. Xylan and xylan esters are amorphous based on the DSC analysis. A structural model for the xylan esters was proposed based from the WAXD results. Mechanical test on the xylan ester films indicate that the tensile strength of the xylan ester decreases with increase in alkyl chain length. However, the value for elongation at break increases. The tensile strength and elongation at break of the xylan esters ranged from 8 to 29 MPa and from 19 to 44% , respectively

Results on the crystallization studies indicate that among the xylan esters, only XylPr and XylBu showed a nucleating effect on PLLA during non-isothermal and isothermal crystallization. Blending of XylPr or XylBu with PLLA reduced its T_c from 125 °C to 96 and 97 °C, respectively. In addition the $t_{1/2}$ value of PLLA was also shortened indicating faster rate of crystallization. As a result, PLLA blends produced smaller spherullites as compared to PLLA. Consequently, the latter showed a higher degree of haze. The blending of the xylan esters with PLLA resulted in a high crystalline material with good transparency.

In Green Polymer Chemistry: Biocatalysis and Materials II; Cheng, H., et al.;
ACS Symposium Series; American Chemical Society: Washington, DC, 2013.

Publication Date (Web): November 22, 2013 | doi: 10.1021/bk-2013-1144.ch026

Acknowledgments

This work was supported by the Japan Society for the Promotion of Science (JSPS), Grant-Aid for Scientific Research (A) (No. 22245026) and Japan Science and Technology Agency, CREST.

References

1. Fang, J. M.; Sun, R. C.; Fowler, P.; Tomkinson, J.; Hill, C. A. S. *J. Appl. Polym. Sci.* **1999**, *74*, 2301–2311.
2. Sun, X. F.; Sun, R. C.; Sun, J. X. *J. Sci. Food Agric.* **2004**, *84*, 800–810.
3. Peng, F.; Ren, J. L.; Peng, B.; Xu, F.; Sun, R. C.; Sun, J. X. *Carbohydr. Res.* **2008**, *343*, 2956–2962.
4. Ren, J. L.; Sun, R. C.; Liu, C. F.; Cao, Z. N.; Luo, W. *Carbohydr. Polym.* **2007**, *70*, 406–414.
5. Bai, H.; Zhang, W.; Deng, H.; Zhang, Q.; Fu, Q. *Macromolecules* **2011**, *44*, 1233–1237.
6. Fundador, N. G. V.; Enomoto-Rogers, Y.; Takemura, A.; Iwata, T. *Carbohydr. Polym.* **2012**, *87*, 170–176.
7. Fundador, N. G. V.; Enomoto-Rogers, Y.; Takemura, A.; Iwata, T. *Polymer* **2012**, *53*, 3885–3893.
8. Janzon, R.; Saake, B.; Puls, J. *Cellulose* **2008**, *15*, 161–175.
9. Janzon, R.; Puls, J.; Bohn, A.; Potthast, A.; Saake, B. *Cellulose* **2008**, *15*, 739–750.
10. Saha, B. C. *J. Ind. Microbiol. Biotechnol.* **2003**, *30*, 279–291.
11. Yang, B. Y.; Montgomery, R. *Starch-Starke* **2008**, *60*, 146–158.
12. Crépy, L.; Chaveriat, L.; Banoub, J.; Martin, P.; Joly, N. *ChemSusChem* **2009**, *2*, 165–170.
13. Fundador, N. G. V.; Enomoto-Rogers, Y.; Takemura, A.; Iwata, T. *Polym. Degrad. Stab.* **2013**, *98*, 1064–1071.
14. Yasuniwa, M.; Tsubakihara, S.; Sugimoto, Y.; Nakafuku, C. *J. Polym. Sci., Part B: Polym. Phys.* **2004**, *42*, 25–32.
15. Pan, P.; Kai, W.; Zhu, B.; Dong, T.; Inoue, Y. *Macromolecules* **2007**, *40*, 6898–6905.
16. Nakajima, H.; Takahashi, M.; Kimura, Y. *Macromol. Mater. Eng.* **2010**, *295*, 460–468.
17. Battegazzore, D.; Bocchini, S.; Frache, A. *Express Polym. Lett.* **2011**, *5*, 849–858.
18. Pei, A.; Zhou, Q.; Berglund, L. A. *Compos. Sci. Technol.* **2010**, *70*, 815–821.
19. Song, P.; Wei, Z.; Liang, J.; Chen, G.; Zhang, W. *Polym. Eng. Sci.* **2012**, *52*, 1058–1068.
20. Wu, D.; Wu, L.; Zhou, W.; Zhang, M.; Yang, T. *Polym. Eng. Sci.* **2010**, *50*, 1721–1733.
21. Kim, S. Y.; Shin, K. S.; Lee, S. H.; Kim, K. W.; Youn, J. R. *Fibers Polym.* **2010**, *11*, 1018–1023.

Publication Date (Web): November 22, 2013 | doi: 10.1021/bk-2013-1144.ch027

Chapter 27

Converting Polysaccharides into High-Value Thermoplastic Materials

James H. Wang* and Bo Shi

Kimberly-Clark Corporation, Corporate Research and Engineering, 2100 County Road II, Neenah, Wisconsin 54956, U.S.A.
***E-mail: jhwang@kcc.com**

Modified starches including starch esters, pregelatinized Tapioca dextrin, and hydroxyalkylated starch were converted into thermoplastic materials. It was found that the rheology of thermoplastic modified starch (TPMS) was dependent on the type of modified starch, the type of plasticizers, and the amount of plasticizers present in TPMS. For the same modified starch, glycerol was a more effective plasticizer than sorbitol. The melt viscosity decreased as the amount of plasticizer amount increased. Binary polymer blends of TPMS and a biodegradable aliphatic-aromatic copolyester exhibited good film-forming properties and good water dispersibility, however, the mechanical properties of the films were poor. The binary polymer blend films had a laminar, layered microstructure. It was found that tertiary polymer blends comprising a majority of TPMS, a polyvinyl alcohol, and a biodegradable copolyester had good and balanced mechanical properties, film processability, and water dispersibility. The resulting water-soluble films had a high renewable content and properties needed for high-value, water-dispersible films.

Introduction

Water-soluble and water-dispersible polymers are an important class of specialty functional polymers. Due to the unique application properties, such polymers command a high price on the market than commodity polymers (*1*). Among the water-soluble polymers, thermoplastic water-soluble polymers are of

In Green Polymer Chemistry: Biocatalysis and Materials II; Cheng, H., et al.;
ACS Symposium Series; American Chemical Society: Washington, DC, 2013.

great industrial value due to the low process cost in making various articles such as films and fibers. The commonly practiced solution film casting and spinning processes have high operating costs and also high environmental footprint, primarily due to high energy requirements dealing with solution processing. Technical innovations are critically important to make water-soluble thermoplastic materials, for example, grafting-enabled thermoplastic polyethylene oxide (*2–7*) and rheologically engineered thermoplastic polyvinyl alcohol without use of a plasticizer (*8–10*).

Although synthetic water-soluble polymers possess the desirable properties for water-dispersible applications, these polymers are often very expensive for large volume applications. From another perspective, these polymers are synthesized from 100% non-renewable monomers made from fossil resources (*11*), it is therefore highly desirable to improve the sustainability of existing water-soluble polymers.

Since polysaccharides are the most abundant natural biopolymers in the world. Cellulose, hemicellulose, starch, chitins, alginates are the most common polysaccharides. Native starch can be extracted from a variety of plants including corn, cassava, potato, rice, wheat, etc. Both native and modified starches were utilized for many industrial applications including paper-making, adhesives, textiles, etc. However, starch is not thermoplastic and cannot be extruded; several technical approaches were developed to transform starch into thermoplastic starch (TPS). Although thermoplastic starch made from native starch is water sensitive, it is not water dispersible (*12*, *13*). It was previously found that water-dispersible TPS can be made from certain modified starch (*14*, *15*).

This paper describes the conversion of non-thermoplastic modified starch into thermoplastic materials and the development of water-sensitive films with improved processability and mechanical properties.

Experimental

Materials

GlucoSol® 800 material is a hydroxypropyl starch supplied by Chemstar (Minneapolis, MN), its weight averaged molecular weight, as determined by GPC, is 2,900,000 with a polydispersity estimated at 28. The modified starch has a bulk density of 0.48~0.64 g/cm^3, its particle sizes pass 98% minimum through 140 meshes, and it is supplied as off-white powders. Sorbitol was supplied by Archer-Daniel-Midland Co. (Decatur, IL), glycerol was from Cognis Corporation (Cincinnati, OH). Mono-diglyceride, Excel P-40S (Kao Corporation, Tokyo, Japan), was used as a surfactant. Aliphatic-aromatic copolyester, Ecoflex® F BX 7011 was purchased from BASF (Ludwigshafen, Germany). Polyvinyl alcohol, Elvanol® 51-05, was purchased from DuPont; it has a viscosity of 5.0 to 6.0 mPa.s (cP) as measured for a 4% solids aqueous solution at 20°C.

Publication Date (Web): November 22, 2013 | doi: 10.1021/bk-2013-1144.ch027

In Green Polymer Chemistry: Biocatalysis and Materials II; Cheng, H., et al.;
ACS Symposium Series; American Chemical Society: Washington, DC, 2013.

Converting Modified Starch into Thermoplastic Modified Starch

A mixture of the modified starch, sorbitol, and Excel P-40S was fed by a gravimetric feeder (K-Tron America, Pitman, NJ) at the feed throat of a ZSK-30 twin screw extruder (Werner and Pfleiderer Corporation, Ramsey, NJ). ZSK-30 extruder is a co-rotating, twin screw extruder. The extruder diameter is 30 mm with the length of the screws up to 1328 mm. The extruder has 14 barrels, numbered consecutively 1 to14 from the feed hopper to the die. The first barrel No. 1 received the mixture of starch and plasticizer at 19 lbs/hr. The temperature profile on the extruder was 100, 110, 124, 124, 124, 110, 105, 115oC, respectively, for the 7 heating zones and polymer melt. The melt pressure ranged from 2.76 to 3.45 MPa. The torque ranged from 50 to 60%. The screw speed was 160 rpm.

Publication Date (Web): November 22, 2013 | doi: 10.1021/bk-2013-1144.ch027

Melt Rheology

The rheological properties of polymers were determined using a Göttfert Rheograph 2003 capillary rheometer with WinRHEO version 2.31 analysis software. The setup included a 2000-bar pressure transducer and a 30/1 L/D round capillary die. Sample loading was done by alternating between sample addition and packing with a ramrod. A 2-minute melt time preceded each test to allow the polymer to completely melt at the test temperature (usually 150°C to 220°C). The capillary rheometer determined the apparent viscosity (Pa·s) at various shear rates, such as 100, 200, 500, 1000, 2000, and 4000 s^{-1}. The resultant rheology curve of apparent shear rate versus apparent viscosity gave an indication of how the polymer would run at that temperature in an extrusion process.

Tensile Properties

The strip tensile strength values were determined in accordance with ASTM Standard D638-99. A constant-rate-of-extension type of tensile tester was employed. The tensile testing system was a Sintech 1/D tensile tester, which is available from Sintech Corp. (Cary, NC). The tensile tester was equipped with TESTWORKS 4.08B software from MTS Corporation to support the testing. An appropriate load cell was selected so that the tested value fell within the range of 10-90% of the full scale load. The film samples were initially cut into dog-bone shapes with a center width of 3.0 mm before testing. The samples were held between grips having a front and back face measuring 25.4 millimeters x 76 millimeters. The grip faces were rubberized, and the longer dimension of the grip was perpendicular to the direction of pull. The grip pressure was pneumatically maintained at a pressure of 0.275 MPa. The tensile test was run using a gauge length of 18.0 millimeters and a break sensitivity of 40%. Five samples were tested by applying the test load along the machine-direction and five samples were tested by applying the test load along the cross direction. During the test, samples were stretched at a crosshead speed of about 127 millimeters per minute until breakage occurred. The modulus, peak stress, and strain at break (peak elongation) were measured in the machine direction (“MD”) and cross-machine directions (“CD”).

In Green Polymer Chemistry: Biocatalysis and Materials II; Cheng, H., et al.;
ACS Symposium Series; American Chemical Society: Washington, DC, 2013.

Water Disintegration

The rate of film disintegration in tap water was tested using a "slosh box", which has a physical dimension of a 35.6 cm x 45.7 cm x 30.5 cm plastic box on a hinged platform. The one end of the platform is attached to a reciprocating cam. The typical amplitude is 5.1 cm (10.2 cm range), with sloshing occurring at 0.5 ~1.5 sloshes per second. The preferred action is 0.9~1.3 sloshes per second.

During a test, the slosh box rocks up and down with the water inside, "sloshing" back and forth. This action produces a wave front and intermittent motion on a sample susceptible to dispersing in water. To quantify a measurement of sample film disintegration in water, without image analysis, simply timing is sufficient. Three liters of tap water were added into the slosh box and resulted in ~ 14.0 cm water depth in the box. A frequency of 3.5 was selected for the testing. Each film sample was cut into 2.5 cm x 7.6 cm size. Three pieces were dropped into the slosh box. The time to disintegrate the sample under the defined conditions was recorded twice for each sample. The average of the time to the sample disintegration is then reported.

Publication Date (Web): November 22, 2013 | doi: 10.1021/bk-2013-1144.ch027

Results and Discussion

Water-Dispersible Thermoplastic Materials from Modified Starch

Even though native starch is not water-soluble or water-dispersible, some chemically modified starches through etherification or esterification are water-dispersible. In this study, three modified starches: Tapon ND (a starch ester); INSTANT N-OIL® (a pregelatinized Tapioca dextrin), and GlucoSol® 800 (a hydroxypropyl starch, a starch ether) were investigated for developing water-dispersible polymer applications.

Since the modified starches are not thermoplastic, the first step of this study was to convert the "non-thermoplastic" modified starches into "thermoplastic" materials. This was accomplished by plasticization inside a twin screw extruder. Two types of plasticizers, glycerol and sorbitol, were used in this study.

The effects of plasticizer type and level on the melt rheological properties of thermoplastic modified starches (TPMS) were investigated. It was found that melt rheology of TPMS was highly dependent upon the type of modified starch. At the same level of plasticizer, the melt viscosity of the three types of modified starches was: Tapon ND < INSTANT N-OIL® < GlucoSol® 800 (*16*).

For the same modified starch, the melt rheology was determined by the type and amount of plasticizer present. As shown in Figure 1, thermoplastic hydroxypropyl starch (GlucoSol® 800) had a much lower melt viscosity with glycerol as the plasticizer than with sorbitol at the level of 30% of plasticizer. For the TPMS with different amount of sorbitol, the melt viscosity decreased as the amount of sorbitol increased from 30% to 40%.

Although thermoplastic modified starch is extrudable in a manner similar to typical thermoplastic synthetic polymer, the resulting materials had poor mechanical properties as exhibited by its highly brittle nature, the material was also weak and hygroscopic to be useful for any practical applications.

In Green Polymer Chemistry: Biocatalysis and Materials II; Cheng, H., et al.;
ACS Symposium Series; American Chemical Society: Washington, DC, 2013.

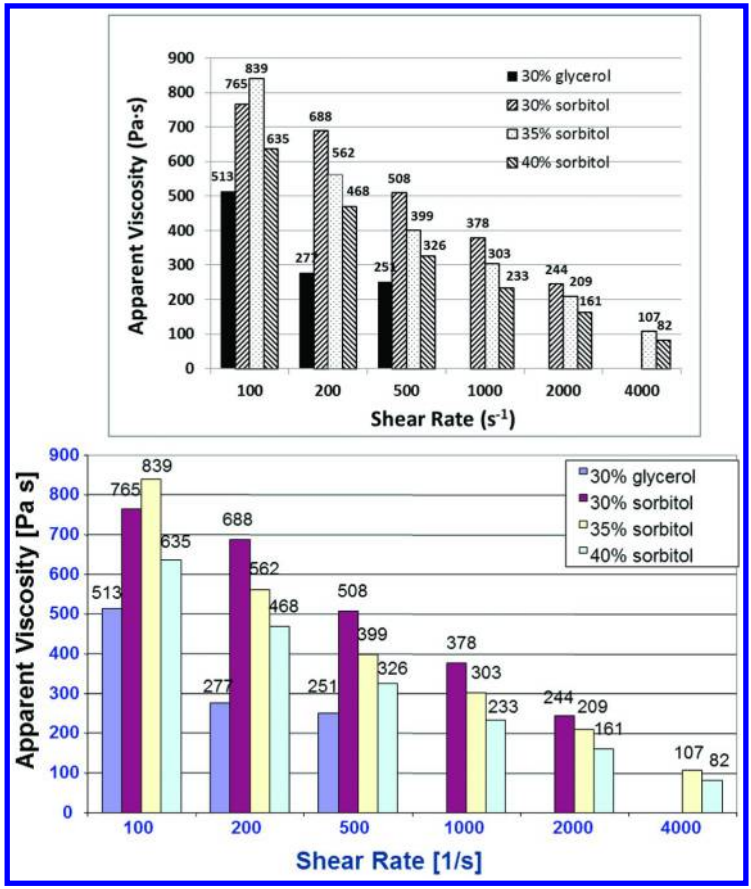

Figure 1. Melt rheology of thermoplastic hydroxypropylstarch.

Improving the Properties of Thermoplastic Modified Starch by Creating Binary Polymer Blends

To improve the mechanical properties of TPMS, a polymer blending approach with a biodegradable polymer having good mechanical properties was pursued. There are many of such biopolymers suitable for blending with TPMS, including polyalkylene alkanoate such as polybutylene succinate and aliphatic-aromatic copolyester. In this paper, the results on using an aliphatic-aromatic copolyester-polybutylene adipate terephthalate (PBAT) are discussed. The specific PBAT used was Ecoflex™ copolyester from BASF. PBAT had excellent tensile strength and ductility similar to polyethylene.

It was well known that good films could be made from polymer blends of thermoplastic starch and PBAT when TPS is a minority component, typically less than 45% by weight. However, this study was focused on making water-dispersible films, TPMS has to be the majority component in order to retain water-sensitivity. A number of binary polymer blends containing from 60% to 90% of TPMS and from 10 to 30% PBAT copolyester were prepared.

In Green Polymer Chemistry: Biocatalysis and Materials II; Cheng, H., et al.;
ACS Symposium Series; American Chemical Society: Washington, DC, 2013.

Publication Date (Web): November 22, 2013 | doi: 10.1021/bk-2013-1144.ch027

In contrast to the lack of processability of TPMS for making thin films, the polymer blends of TPMS and PBAT had excellent processability, thin films were made from these blends even though TPMS was the majority component, this showed significantly improved melt strength of the blends in the presence of PBAT.

The mechanical properties of binary blends containing a thermoplastic starch ester (Tapon ND) and PBAT copolyester were determined. The peak stress as a function of the blend composition is shown in Figure 2. The thin films had good tensile strength in the machine direction (MD), ranging from about 26 MPa to about 47 MPa, this is comparable to typical polyethylene films. The peak stress increased as the amount of PBAT copolyester increased, this is expected based on high peak stress of PBAT copolyester. However, the peak stress in the cross direction (CD) was quite low, showing a strong anisotropy between MD and CD.

The ductility of the thermoplastic starch ester at different compositions is illustrated in Figure 3. In the machine direction, the ductility increased with the amount of PBAT copolyester in the blends. In general, these films were quite brittle with only 2 to 6% of strain-at-break in MD. The low ductility resulted from the majority of TPMS in the blends. There was no trend in the cross direction (CD).

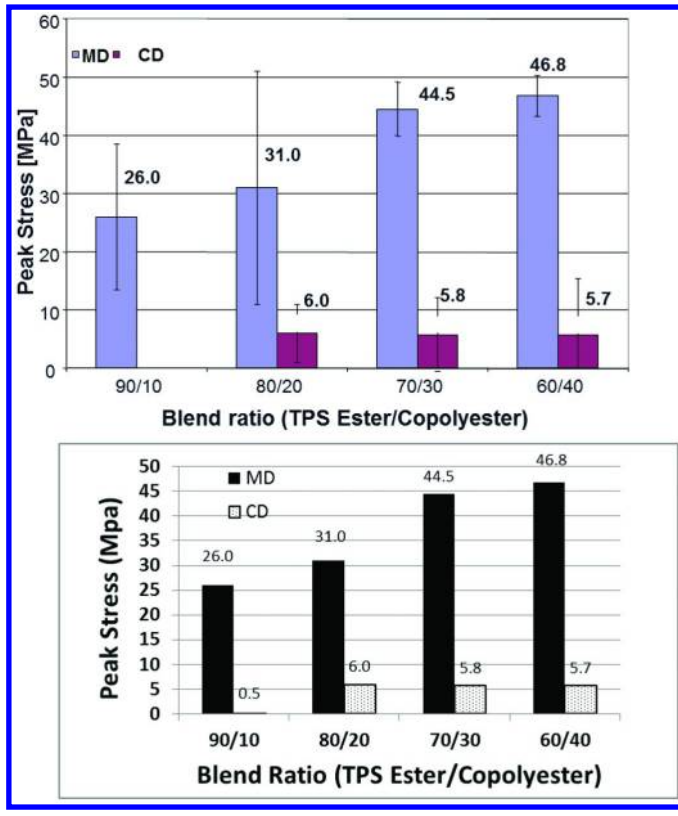

Figure 2. Peak stress of thermoplastic modified starch blends.

In Green Polymer Chemistry: Biocatalysis and Materials II; Cheng, H., et al.;
ACS Symposium Series; American Chemical Society: Washington, DC, 2013.

Publication Date (Web): November 22, 2013 | doi: 10.1021/bk-2013-1144.ch027

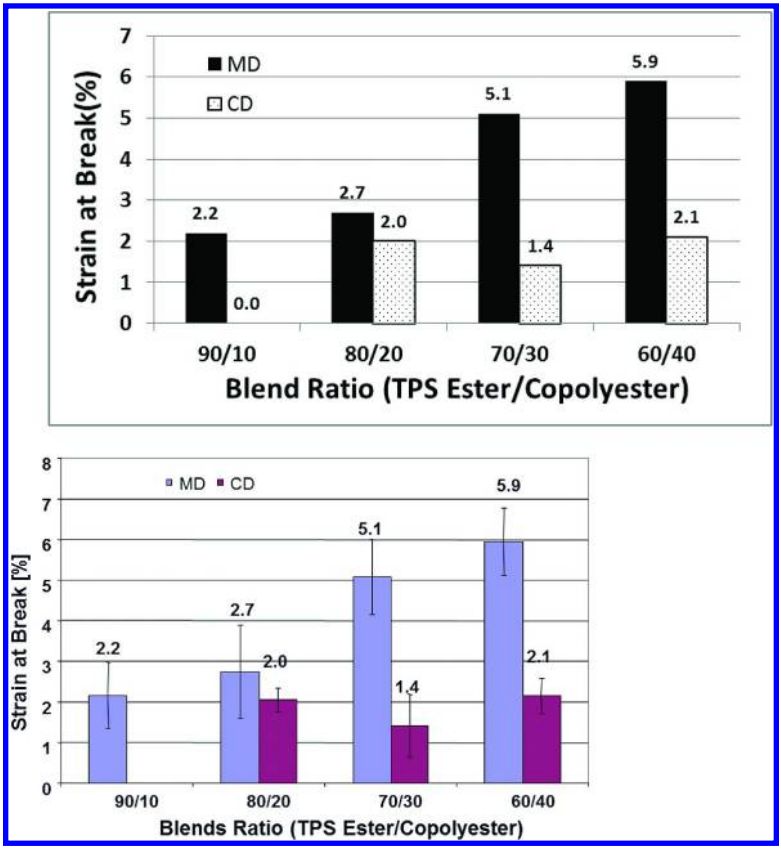

Figure 3. Ductility of thermoplastic modified starch ester blends.

The mechanical properties of thermoplastic starch ether (Glucosol 800) and PBAT copolyester were also characterized. The ductility of the blends is shown in Figure 4. As compared to the ductility of TPMS ester in Figure 3, the TMPS ether had much better ductility in MD, ranging from about 31% to about 95% in strain-to-break. The ductility was higher at a higher PBAT level, except from 10% to 20% of PBAT. But the ductility in CD was also very low, exhibiting a strong anisotropy between MD and CD.

The morphology of the binary TPMS/PBAT was studied by scanning electron microscopy (SEM). The microimage of 70/30 TPMS ether/PBAT blend film in machine direction is shown in Figure 5. The blend film had a laminar, layered structure.

In Green Polymer Chemistry: Biocatalysis and Materials II; Cheng, H., et al.;
ACS Symposium Series; American Chemical Society: Washington, DC, 2013.

Publication Date (Web): November 22, 2013 | doi: 10.1021/bk-2013-1144.ch027

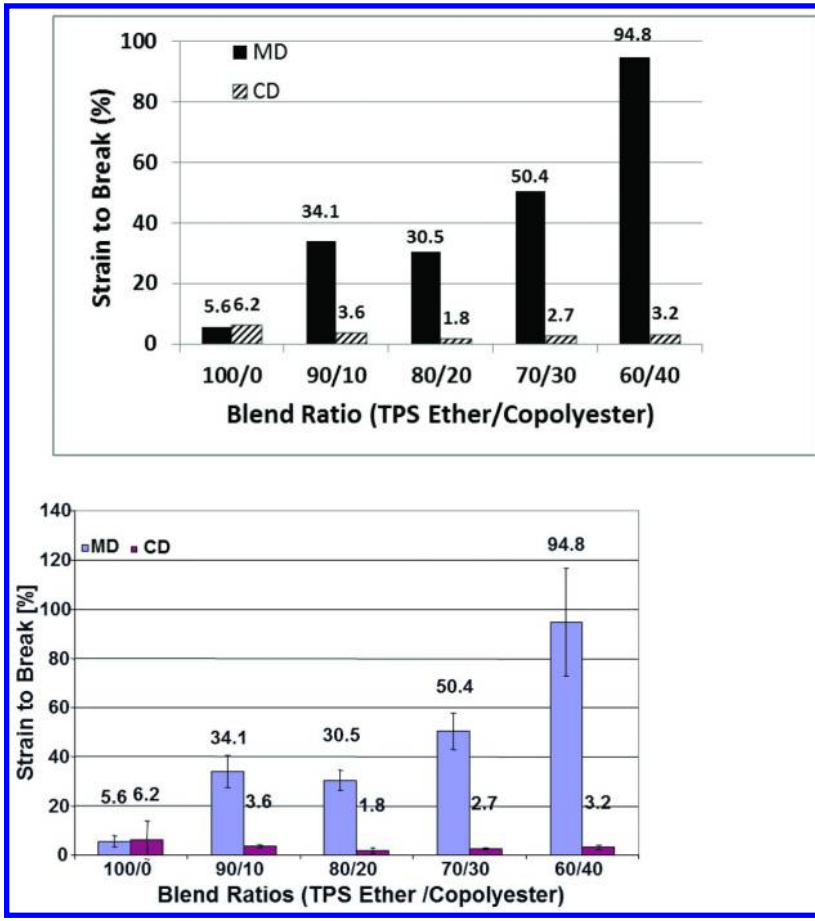

Figure 4. Ductility of thermoplastic modified starch ether (TPSE)/copolyester blends.

In Green Polymer Chemistry: Biocatalysis and Materials II; Cheng, H., et al.;
ACS Symposium Series; American Chemical Society: Washington, DC, 2013.

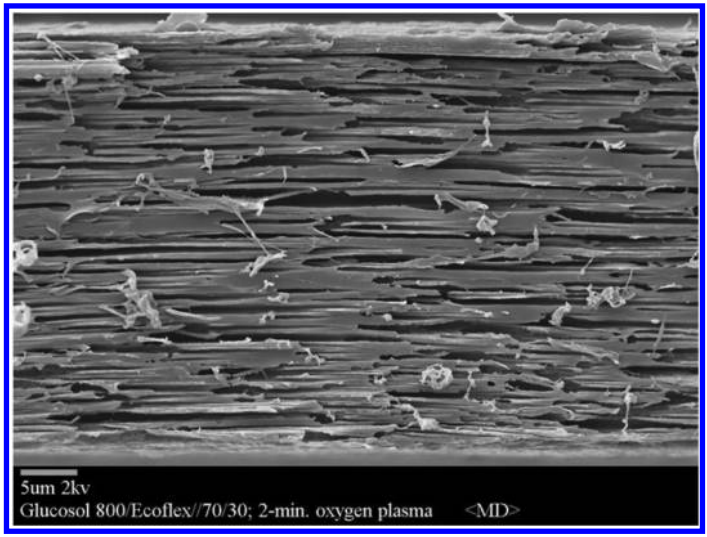

Figure 5. SEM image of TPSE/PBAT 70/30 film.

Publication Date (Web): November 22, 2013 | doi: 10.1021/bk-2013-1144.ch027

Water-Dispersible Films with Balanced Mechanical Properties

It was clear the mechanical properties of the binary thin films were deficient, especially the weak properties in cross directions. To overcome this issue, it was discovered that adding another component-thermoplastic polyvinyl alcohol, was critical to achieve the desired balance between MD and CD properties.

Polyvinyl alcohol (PVOH) is a water-soluble polymer, but most commercial polyvinyl alcohol is not thermoplastic, previous work by Wang, et. al. invented thermoplastic polyvinyl alcohol having certain compositions and molecular weights (*8–10*). In this study, the previously identified thermoplastic polyvinyl alcohol was used, 20% sorbitol plasticizer was added to the PVOH to further achieve high ductility and improved thermoplastic processability.

Water-Dispersible Tertiary Blend Films

A number of the tertiary polymer blends of the water-dispersible polymers were prepared and compared with the control water-dispersible films. The Young's moduli of these materials are shown in Figure 6. The pure thermoplastic modified starch ether (Material No. 1, TPSE) and plasticized PVOH (Material No. 2, p-PVOH) both had high moduli. The moduli in MD are significantly higher than those in CD. This shows that both the control materials are fairly stiff. However, the tertiary blends, Material 3 (TPSE/p-PVOH/copolyester 60/30/10) and Material 4 (TPSE/p-PVOH/copolyester 70/20/10) both had significantly lower moduli; therefore, the tertiary blend films were very soft.

In Green Polymer Chemistry: Biocatalysis and Materials II; Cheng, H., et al.;
ACS Symposium Series; American Chemical Society: Washington, DC, 2013.

Publication Date (Web): November 22, 2013 | doi: 10.1021/bk-2013-1144.ch027

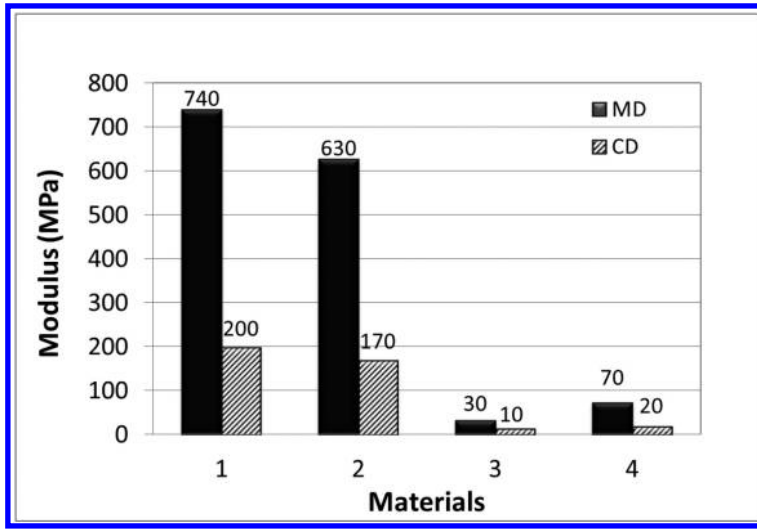

Figure 6. Modulus of water-dispersible tertiary blend films: 1. thermoplastic modified starch ether (TPSE: Glucosol 800/sorbitol 70/30), 2. plasticized PVOH/sorbitol 80/20 (p-PVOH), 3. TPSE/p-PVOH/copolyester 60/30/10, 4. TPSE/p-PVOH/copolyester 70/20/10.

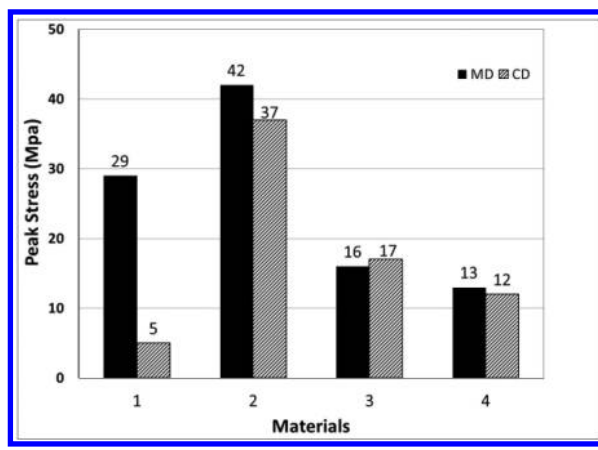

Figure 7. Peak stress of water-dispersible tertiary blend films: 1. TMSE, 2. p-PVOH, 3. TPSE/p-PVOH/copolyester 60/30/10, 4. TPSE/p-PVOH/copolyester 70/20/10.

In Green Polymer Chemistry: Biocatalysis and Materials II; Cheng, H., et al.;
ACS Symposium Series; American Chemical Society: Washington, DC, 2013.

The peak stress of the water-dispersible tertiary blend films are shown in Figure 7. The pure TPSE film (Material 1) had decent tensile strength in MD, but its peak stress in CD was unusually low. The plasticized PVOH (Material 2) film was strong with high peak stress values in both MD and CD (42 MPa and 37 MPa respectively). The films from the tertiary blends (Materials 3 and 4) both had balanced peak stresses in MD and CD. This is quite different from the anisotropic MD and CD tensile properties found on the binary blend films as discussed previously.

The ductility of these films is plotted in Figure 8. Pure TPSE films were very brittle. The plasticized PVOH films had strain to break values of 180% and 130% in MD and CD, respectively. However, the water-dispersible tertiary blend films were significantly higher, at 250% and 220% for Material 3 and 240% and 210% for Material 4, respectively. Therefore, the tertiary blends of TPSE, p-PVOH, and copolyester had good ductility, this is critically important for practical applications.

Publication Date (Web): November 22, 2013 | doi: 10.1021/bk-2013-1144.ch027

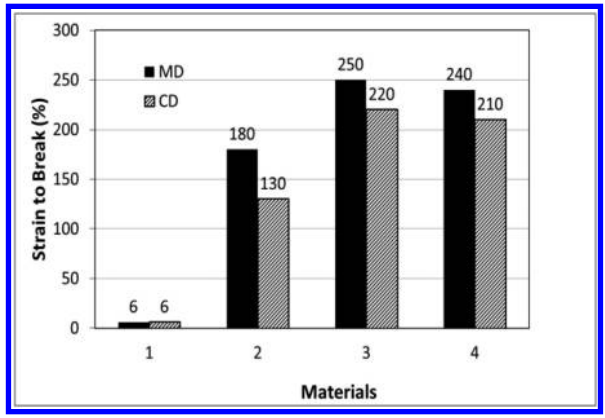

Figure 8. Ductility of water-dispersible tertiary blend films: 1. TMSE, 2. P-PVOH, 3. TPSE/p-PVOH/copolyester 60/30/10, 4. TPSE/p-PVOH/Copolyester 70/20/10.

Effects of Copolyester Level

To determine the impact of the composition of the tertiary blend films, three tertiary blends at 10%, 20%, and 30% of copolyester levels were prepared and processed into melt extruded films. These blends had excellent processability for cast film processing.

The relationship between the peak stresses of these films with compositions are shown in Figure 9. All the three films had very close tensile strength. In MD, the peak stress ranged from 16 to 19 MPa, while the peak stress varied from 17 to 21 MPa in CD. The material with the highest level of copolyester (Material 3) had the highest tensile strength.

Publication Date (Web): November 22, 2013 | doi: 10.1021/bk-2013-1144.ch027

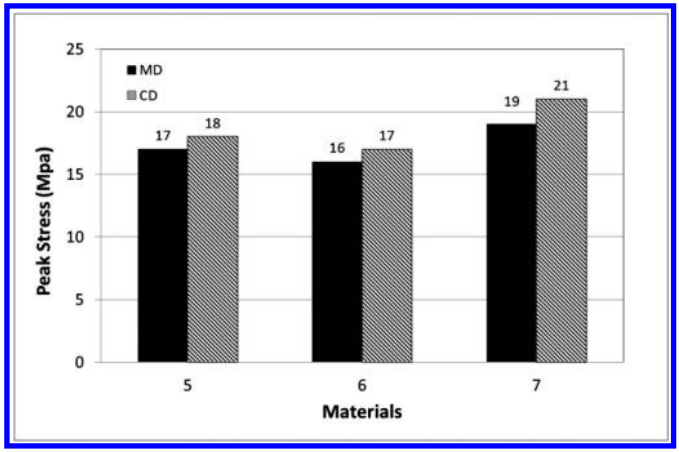

Figure 9. Peak stress of water-dispersible tertiary blend films: 5. TPSE/p-PVOH/copolyester 63/27/10, 6. TPSE/p-PVOH/copolyester 56/24/20, 7. TPSE/p-PVOH/copolyester 49/21/30.

The ductility of these films is illustrated in Figure 10. In general, these films had comparable ductility. With the film at 20% of copolyester (Material 6) had slightly higher strain-to-break value than the other two materials, all around 200%. For these mostly thermoplastic modified starch based films, the ductility values are fairly impressive, considering the fact that pure TPSE had strain to break of less than 10%. Therefore, the objective to develop highly ductile thermoplastic films from renewable starch based materials was achieved.

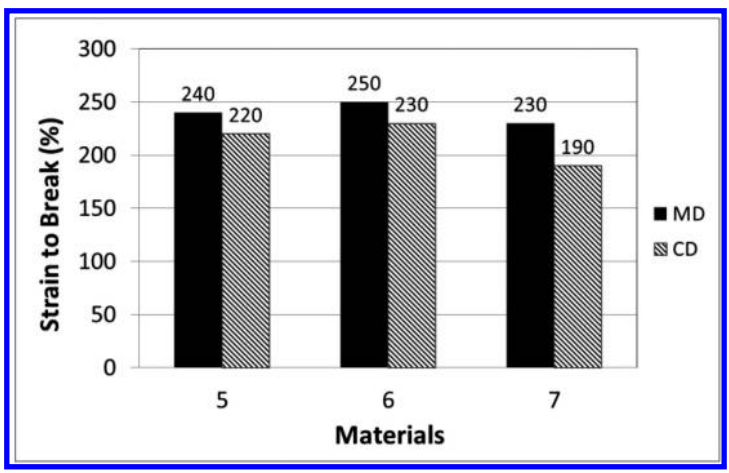

Figure 10. Ductility of water-dispersible tertiary blend films: 5. TPSE/p-PVOH/copolyester 63/27/10, 6. TPSE/p-PVOH/copolyester 56/24/20, 7. TPSE/p-PVOH/copolyester 49/21/30.

In Green Polymer Chemistry: Biocatalysis and Materials II; Cheng, H., et al.;
ACS Symposium Series; American Chemical Society: Washington, DC, 2013.

A water disintegration test was used to evaluate the water dispersibility of the films developed. Figure 11 shows the picture of the TPSE/p-PVOH/copolyester 60/30/10 (Material 3) film after placing in water for 30 seconds. The film was disintegrated and dispersed into small pieces. The image of the film in water at 60 seconds is showed in Figure 12, more finely dispersed film residues were formed after the extended exposure in water.

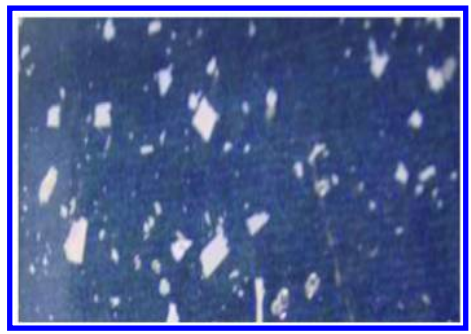

Figure 11. Water disintegration of TPSE/p-PVOH/copolyester 60/30/10 (Material 3), 30 seconds in water.

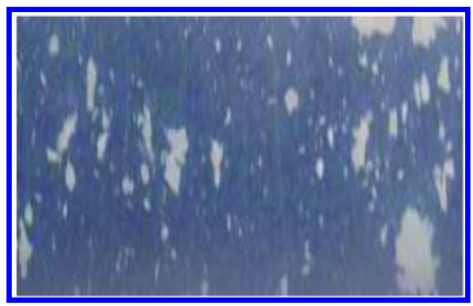

Figure 12. Water disintegration of TPSE/p-PVOH/copolyester 60/30/10 (Material 3), 60 seconds in water.

In the water-dispersible tertiary blends, there is a water-insoluble copolyester component, the concentration of the copolyester could substantially influence the water dispersibility of the resulting films. The results on the effects of copolyester on water-dispersibility are summarized in Table 1. Thermoplastic modified starch ether (Material 1) was the most water-dispersible materials; it had a water dispersion time of only 10 seconds. Thermoplastic PVOH had slightly longer water dispersion time of 20 seconds.

The tertiary blend films had water dispersion time dependent upon the amount of insoluble copolyester, when copolyester content was 10 and 20%, the water-dispersion times ranged from 30 to 60 seconds. However, when

In Green Polymer Chemistry: Biocatalysis and Materials II; Cheng, H., et al.;
ACS Symposium Series; American Chemical Society: Washington, DC, 2013.

Publication Date (Web): November 22, 2013 | doi: 10.1021/bk-2013-1144.ch027

copolyester content increased to 30% of the composition, the water dispersion time significantly increased to more than 1 hr. This indicated that the increased amount of copolyester could have formed an internal barrier for water penetration and thus substantially retarded the dispersion process in water.

Table 1. Water Disintegration Test Results of Water-Dispersible Films

Materials	*Water Dispersion Time (Seconds)*
1	10
2	20
3	30
4	30
5	60
6	60
7	>1 hr.

Materials: 1. Thermoplastic modified starch ether (TPSE: Glucosol 800/sorbitol 70/30). 2. Plasticized PVOH (p-PVOH). 3. TMSE/p-PVOH/copolyester 60/30/10. 4. TPSE/p-PVOH/copolyester 70/20/10. 5. TPSE/p-PVOH/copolyester 63/27/10. 6. TPSE/p-PVOH/copolyester 56/24/20. 7. TPSE/p-PVOH/copolyester 49/21/30.

Publication Date (Web): November 22, 2013 | doi: 10.1021/bk-2013-1144.ch027

Conclusion

This article described water-dispersible films from renewable, modified starch. Starch ester and starch ether were converted into thermoplastic modified starch (TPMS). The rheology of TPMS was dependent on the type of modified starch (e.g. etherification or esterification), the type of plasticizers, and the amount of plasticizers. The films made from TPMS were too brittle for practical applications.

Binary polymer blends comprising of TPMS and an aliphatic-aromatic copolyester (polybutylene adipate terephthalate, PBAT) were prepared and characterized, it was found that the binary blends had good processability for making thin films; the films were very anisotropic, i.e. with a large property difference between the machine and cross directions (MD and CD).

Further experiments led to the invention of tertiary blend films. It was found that the addition of a synthetic water-soluble polymer, polyvinyl alcohol (PVOH), to the binary systems was critical to obtain thin films with balanced mechanical properties in MD and CD. The tertiary blend films had good ductility (~200% strain to break) even in the presence of brittle thermoplastic modified starch in majority. It was further determined that the water dispersion time of the tertiary blend films depended on the amount of water-insoluble copolyester present. This article has demonstrated the challenges and success in developing high-value functional materials from renewable starch-based polymers.

In Green Polymer Chemistry: Biocatalysis and Materials II; Cheng, H., et al.;
ACS Symposium Series; American Chemical Society: Washington, DC, 2013.

Publication Date (Web): November 22, 2013 | doi: 10.1021/bk-2013-1144.ch027

Acknowledgments

The authors would like to thank Irene Hall for study on modified starches, Gregory Wideman for assistance in extrusion process, and Mike Shlepr for scanning electron microscopy (SEM).

References

1. Fink, J. K. *Handbook of Engineering and Specialty Thermoplastics, Water Soluble Polymers*; John Wiley and Sons and Scrivener: Hoboken, NJ, 2011.
2. Wang, J. H.; Schertz, D. M. Method of Modifying Poly(Ethylene Oxide). U.S. Patent 6,117,947, 2000.
3. Wang, J. H.; Schertz, D. M.; Soerens, D. A. Grafted Poly(Ethylene Oxide) Compositions. U.S. Patent. 6,172,177 B1, 2001.
4. Wang, J. H.; Schertz, D. M.; Pomplun, W. S. Methods of Making Unmodified Polyvinyl Alcohol Fibers. U.S. Patent. 6,197,238 B1, 2001.
5. Wang, J. H.; Schertz, D. M. Melt Processable Poly(Ethylene Oxide) Fibers. U.S. Patent. 6,372,850 B2, 2002.
6. Wang, J. H.; Topolkaraev, V. A.; Balogh, B. A. Methods of Making Polymer/Dispersed Modifier Compositions. U.S. Patent. 6,403,706 B1, 2002.
7. Wang, J. H.; Topolkaraev, V. A.; Balogh, B. A. Polymer/Dispersed Modifier Compositions, U.S. Patent. 6,607,819 B1, 2003.
8. Wang, J. H.; Schertz, D. M.; Pomplun, W. S. Unmodified Polyvinyl Alcohol Films and Fibers and Methods of Making the Same. U.S. Patent 6,020,425, 2000.
9. Wang, J. H.; Schertz, D. M.; Pomplun, W. S. Methods of Making Unmodified Polyvinyl Alcohol Fibers. U.S. Patent 6,197,238 B1, 2001.
10. Wang, J. H.; Schertz, D. M.; Pomplun, W. S. Unmodified Polyvinyl Alcohol Fibers. U.S. Patent 6,203,903 B1, 2001.
11. Shi, B.; Wideman, G.; Wang, J. H. *Int. Polym. Proc.* **2012**, *27*, 231.
12. Stevens, E. S. *Green Plastics*; Princeton University Press: Princeton, NJ, 2002; p 3.
13. Stevens, C.; Verhe, R. *Renewable Bioresources*; John Wiley & Sons: 2004.
14. Wang, J. H.; Shi, B. U.S. Paent Application 2008/0147034, 2008.
15. Wang, J. H.; Shi, B. U.S. Patent Application 2009/0054548A1, 2009.
16. Wang, J. H.; Shi, B. *Proceeding of 18th European Biomass Conference and Exhibition* **2010**, 1472DOI:10.5071/18thEUBCE2010-10.2.

Publication Date (Web): November 22, 2013 | doi: 10.1021/bk-2013-1144.ch028

Chapter 28

Use of Cotton Gin Trash and Compatibilizers in Polyethylene Composites

H. N. Cheng,*[,1] M. K. Dowd,[1] V. L. Finkenstadt,[2] G. W. Selling,[2] R. L. Evangelista,[2] and Atanu Biswas*[,2]

[1]Southern Regional Research Center, USDA Agricultural Research Service, 1100 Robert E. Lee Blvd., New Orleans, Louisiana 70124, U.S.A.
[2]National Center for Agricultural Utilization Research, USDA Agricultural Research Service, 1815 N. University St, Peoria, Illinois 61604, U.S.A.
***E-mail: hn.cheng@ars.usda.gov (H.N.C.); atanu.biswas@ars.usda.gov (A.B.)**

The ginning of cotton produces 15–42% of foreign materials, called "cotton gin trash", including cotton burr, stems, leaf fragment, and dirt. In this work we examined the mechanical properties of composites of low density polyethylene (LDPE) and cotton burr. The burr was ground into powder and separated by size into several fractions. These were separately blended with the polymer and then injection molded. Four compatibilizing polymers (polyethylene-g-maleic anhydride, polyethylene-co-methacrylic acid, and polyethylene-co-acrylic acid at two acrylic acid levels) were included to observe their effects on the mechanical properties. In general, the addition of these fillers to LDPE reduced tensile strength and elongation, but enhanced Young's modulus. Improvement in tensile strength was observed for samples containing two of the tested compatibilizers. The results suggested that LDPE-cotton burr-compatibilizer composites may be useful in applications where reduced cost is desirable and reductions in mechanical properties are acceptable.

In Green Polymer Chemistry: Biocatalysis and Materials II; Cheng, H., et al.; ACS Symposium Series; American Chemical Society: Washington, DC, 2013.

Publication Date (Web): November 22, 2013 | doi: 10.1021/bk-2013-1144.ch028

Introduction

Fillers are often used in polymers to lower product cost and to enhance the end-use properties of the polymers. There has been a lot of recent interest to incorporate natural renewable materials as fillers in polymers to form biocomposites (*1–3*). One of the polymers often studied is low-density polyethylene (LDPE). Fillers from many natural renewable materials have been studied with LDPE, including starch (*4–12*), cellulose (*13–17*), kenaf (*18*), agar (*19*), nutshells (*20–22*), edible beans (*23*), and cotton byproducts (*24*). For LDPE, fillers from renewable materials can often improve the polymer's hydrophilicity, gas permeability, and dyability (*7*, *8*, *23*). Another benefit of fillers is to incorporate a large amount of biodegradable material into the blend, which can help to degrade the matrix over time and can accelerate disintegration of the entire matrix (*4*, *5*, *8*, *9*). It has also been reported that the physical properties of LDPE-filler composites are improved when maleic anhydride is grafted onto polyethylene (*9*, *13*).

Among natural renewable raw materials being studied as fillers are byproducts of cotton production and processing (*25*). The ginning of spindle-harvested cotton typically results in 15–42% by weight of foreign materials, commonly referred to as "cotton gin trash", comprising cotton burrs, pieces of stems, leaf fragments, immature cottonseed, and dirt. Previously, cotton byproducts were studied as fillers in poly(lactic acid) and LDPE (*24*). In the present study, a closer look was made of LDPE-cotton burr composites with and without compatibilizers. Compatibilizers are materials that usually enhance the adhesion between the polymeric matrix and the filler (*26–28*). The compatibilizers used in this work were polyethylene-g-maleic anhydride, polyethylene-co-methacrylic acid, and two ethylene-acrylic acid copolymers (with 5 wt% and 15 wt% acrylic acid). These compatibilizers were chosen because they were commercially available or have been previously studied in various biocomposites (*6*, *10*, *11*).

Experimental

Low-density polyethylene (Tradename: Petrothene) was purchased from Quantum Chemical Corp. (Cincinnati, OH). Compatibilizing polymers were acquired from Sigma-Aldrich (Milwaukee, WI) and included polyethylene grafted with 3 wt% maleic anhydride (C1), ethylene-methacrylic acid random copolymer (15 wt% methacrylic acid) (C2), ethylene-acrylic acid copolymer (15 wt% acrylic acid) (C3), and ethylene-acrylic acid copolymer (5 wt% acrylic acid) (C4). Cotton burr was collected as part of the cotton trash fraction obtained from a harvesting cotton stripper. Most of the stem, leaf and other foreign matter were removed to leave a relatively clean burr fraction. The sample was ground with a laboratory-scale Wiley mill. Four fractions (F1, F2, F3, and F4) varying in particle size were produced from the ground sample. Fraction F4 passed through a 100-mesh screen (<149 μm). Fraction F3 did not passed through a 100-mesh screen but passed through a 50-mesh screen (between 149 and 297 μm). Fraction F2 did not pass through a 50-mesh screen but passed through a 40-mesh screen (between 297 and 400 μm). Fraction F1 did not pass through 40-mesh screen

In Green Polymer Chemistry: Biocatalysis and Materials II; Cheng, H., et al.;
ACS Symposium Series; American Chemical Society: Washington, DC, 2013.

(>400 μm) and consisted mostly of fibrous materials. Polymer composites were formulated in a design shown in Table 1.

For burr fractions F2, F3, and F4, the formulation included 70% by weight of LDPE, 25% by weight of burr fraction, and 5% by weight of compatibilizer. Because the fibrous fraction F1 had a low bulk density, a reduced level was used, and the formulation comprised 92% LDPE, 3% F1, and 5% compatibilizer. Each mixture of materials was manually blended and fed into a single screw extruder (C. W. Brabender, South Hackensack, NJ) with a high shear screw and 1-inch ribbon slit. The extruded temperature profile was set from the feed end to the die end as 110, 120, 115, and 110 °C. Screw speed was set at 25 rpm. Sample was fed through a feed throat attached to an air chiller. A conveyor belt was used to take up the ribbon at the same speed as the ribbon sample was produced.

Dog-bone-shaped samples were cut from 1-inch extruded ribbons with a stamp press (MS Instrument Inc., Castledon on Hudson, NY), in accordance with ASTM method D638 Type V. Samples were conditioned for at least 48 h at room temperature (23 °C) and 50% relative humidity. The thickness of the test samples was measured along the neck at five locations with a Precision micrometer (Model No. 49-63, Testing Machines Inc., Amityville, NY), and averaged values were used. Tensile strength, Young's modulus, and elongation at breakage were evaluated with a Universal Testing System (Model 4201, Instron Corp., Norwood, MA). These mechanical tests were measured with a cross-head speed of 10 mm/min, a gauge length of 7.62 mm, grip distance of 50 mm, and a 1-kg load cell. Five specimens were tested for each composite, and both the average values and the standard deviations were used in data analyses.

Publication Date (Web): November 22, 2013 | doi: 10.1021/bk-2013-1144.ch028

Results and Discussions

Twenty-five composite samples were prepared as given in Table 1. The mechanical properties of the LDPE blends and compatibilizers (without cotton burr) are shown as samples 1–5 (Table 2). Under the experimental conditions employed, LDPE had a tensile strength of 6.8 N/mm^2, 287% elongation at break, and a Young's modulus of 31 MPa. Addition of 5% compatibilizers did not significantly affect the mechanical properties of the blends (Table 2).

The mechanical properties of LDPE composites with 3% burr fraction F1 are shown as samples 6, 10, 14, 18, and 22 (Table 2). In this case, LDPE with burr F1 alone (sample 6) had lower tensile strength and elongation than LDPE without the filler (sample 1), but its Young's modulus was unchanged. The use of compatibilizers C1 and C2 (samples 10 and 14, respectively) increased tensile strength and elongation but had no noticeable effect on the Young's modulus. The compatibilizers C3 and C4 (samples 18 and 22) had no significant effect on tensile strength, elongation, or Young's modulus, relative to the samples without compatibilizer (sample 6).

In Green Polymer Chemistry: Biocatalysis and Materials II; Cheng, H., et al.;
ACS Symposium Series; American Chemical Society: Washington, DC, 2013.

Table 1. Composition of LDPE-burr-compatibilizer composites (in wt%)

Sample Number	*LDPE*	*Cotton Burr*				*Compatibilizer*			
		F4	*F3*	*F2*	*F1*	*C1*	*C2*	*C3*	*C4*
1	100								
2	95					5			
3	95						5		
4	95							5	
5	95								5
6	75	25							
7	75		25						
8	75			25					
9	97				3				
10	70	25				5			
11	70		25			5			
12	70			25		5			
13	92				3	5			
14	70	25					5		
15	70		25				5		
16	70			25			5		
17	92				3		5		
18	70	25						5	
19	70		25					5	
20	70			25				5	
21	92				3			5	
22	70	25							5
23	70		25						5
24	70			25					5
25	92				3				5

Publication Date (Web): November 22, 2013 | doi: 10.1021/bk-2013-1144.ch028

Table 2. Mechanical properties of LDPE-burr-compatibilizer composites[a]

Sample No.	*Description*	*Thickness (mm)*	*Tensile Strength (N/mm^2)*	*Elon-gation (%)*	*Young's Modulus (MPa)*
1	LDPE	1.91 (0.05)	6.8 (0.1)	287 (45)	31 (2)
2	LDPE + C1	1.70 (0.02)	6.6 (0.04)	228 (37)	32 (2)
3	LDPE + C2	1.75 (0.03)	7.0 (0.1)	286 (48)	30 (1)
4	LDPE + C3	1.79 (0.06)	6.5 (0.1)	270 (-)[b]	30 (1)
5	LDPE + C4	1.85 (0.03)	6.5 (0.1)	293 (26)	32 (2)
6	LDPE + F1	1.74 (0.02)	5.5 (0.2)	100 (15)	31 (1)
10	LDPE + F1 + C1	1.70 (0.03)	6.2 (0.2)	105 (34)	33 (1)
14	LDPE + F1 + C2	2.23 (0.05)	6.3 (0.1)	126 (13)	29 (1)
18	LDPE + F1 + C3	1.89 (0.01)	5.8 (0.1)	110 (14)	29 (1)
22	LDPE + F1 + C4	2.03 (0.07)	5.7 (0.2)	96 (19)	29 (1)
7	LDPE + F2	1.52 (0.04)	3.7 (0.1)	31 (3)	43 (2)
11	LDPE + F2 + C1	1.66 (0.05)	4.5 (0.1)	26 (2)	43 (1)
15	LDPE + F2 + C2	1.63 (0.03)	4.4 (0.3)	36 (5)	39 (2)
19	LDPE + F2 + C3	1.84 (0.03)	3.7 (0.1)	38 (5)	37 (0.3)
23	LDPE + F2 + C4	1.78 (0.01)	3.6 (0.2)	25 (2)	43 (2)
8	LDPE + F3	1.62 (0.12)	3.5 (0.1)	32 (3)	39 (2)
12	LDPE + F3 + C1	1.61 (0.01)	4.1 (0.2)	24 (2)	37 (1)
16	LDPE + F3 + C2	1.69 (0.05)	3.5 (0.04)	31 (2)	34 (1)
20	LDPE + F3 + C3	1.80 (0.04)	3.2 (0.03)	32 (2)	35 (2)
24	LDPE + F3 + C4	1.83 (0.03)	3.3 (0.1)	30 (2)	36 (2)
9	LDPE + F4	1.55 (0.09)	3.4 (0.2)	27 (3)	35 (3)
13	LDPE + F4 + C1	1.64 (0.23)	3.8 (0.2)	24 (2)	33 (2)
17	LDPE + F4 + C2	1.72 (0.05)	3.0 (0.3)	20 (4)	29 (1)
21	LDPE + F4 + C3	1.83 (0.20)	3.1 (0.2)	24 (4)	30 (2)
25	LDPE + F4 + C4	1.87 (0.04)	3.5 (0.1)	22 (3)	36 (2)

[a] Standard deviations are given in parentheses. Compatibilizer C1 = polyethylene grafted with 3 wt% maleic anhydride; C2 = polyethylene methacrylic acid random copolymer (15% methacrylic acid); C3 = polyethylene-acrylic acid copolymer (15 wt% acrylic acid); C4 = polyethylene-acrylic acid copolymer (5 wt% acrylic acid). [b] Data partly lost.

Publication Date (Web): November 22, 2013 | doi: 10.1021/bk-2013-1144.ch028

The mechanical properties of LDPE composites shown for burr fraction F2 as samples 7, 11, 15, 19, and 23; for burr fraction F3 as samples 8, 12, 16, 20, and 24; and for burr fraction F4 as samples 9, 13, 17, 21, and 25 (Table 2). LDPE with the burr fractions F2, F3, or F4 alone (samples 7, 8, and 9, respectively) had lower tensile and elongation but higher Young's modulus than LDPE without filler (sample 1). This was consistent with our earlier study of LDPE blended with cotton burr (*24*). The mechanical properties of LDPE-burr composites with compatibilizers C3 and C4 did not show noticeable improvements over the LDPE-burr composites without compatibilizers. However, incorporation of the compatibilizers C1 and C2 seemed to have beneficial effects on tensile strength for most of the samples. Elongation was not affected and the Young's modulus either stayed the same or was slightly reduced with the inclusion of compatibilizers C1 and C2.

The effect of burr particle size on the mechanical properties can be seen by plotting tensile strength, elongation, and Young's modulus separately (Figures 1–3). It may be reminded that for F1 the filler level was 3%, whereas for F2, F3, and F4, the filler level was 25%. Moreover, the average particle size for fillers decreased in the order F1 > F2 > F3 > F4. Thus, an increasing value on the x-axis in Figures 1–3 represents decreasing particle size. The tensile strength of the composites decreased by about 10% when fraction F1 was added at 3%, but decreased to about 50% when 25% of F2, F3, or F4 was added (Figure 1). As filler particle size decreased (from F2 to F4), tensile strength also decreased slightly (Figure 1). This weakening of the composites was probably due to poor bonding between filler particles and LDPE polymer, with each particle serving as a weak point that reduces tensile strength. At the same 25% filler level, filler with smaller particles contain more particles resulting in greater surface areas with the base polymer, thereby leading to more weak points. The use of compatibilizer partly remedied this effect. Compatibilizer C1 appeared to have the most beneficial effect, followed by compatibilizer C2.

Elongation decreased as filler was added (Figure 2), similar to the trends observed with tensile strength. The effect of filler particle size and compatibilizer addition on elongation was less apparent. Different behavior was observed for the Young's modulus (Figure 3), which exhibited a maximum with burr fraction F2 but decreased with fractions F3 and F4. This indicates that the presence of larger filler particles enhances the stiffness of LDPE; but if the filler particles are too small, they became less effective in stiffening the polyethylene matrix. The addition of a compatibilizer did not appear to be beneficial for Young's modulus; among the four compatibilizers, C1 gave the best results.

Thus, the addition of cotton burr fractions F2, F3, and F4 as fillers in LDPE reduced tensile strength and elongation but generally improved the Young's modulus of the composites. The use of C1 and C2 compatibilizers improved tensile strength in most samples. Filler particle size had an important effect on the composite's mechanical properties. In particular, the Young's modulus of the composite could be optimized by using filler with an appropriate particle size.

Publication Date (Web): November 22, 2013 | doi: 10.1021/bk-2013-1144.ch028

In Green Polymer Chemistry: Biocatalysis and Materials II; Cheng, H., et al.;
ACS Symposium Series; American Chemical Society: Washington, DC, 2013.

Publication Date (Web): November 22, 2013 | doi: 10.1021/bk-2013-1144.ch028

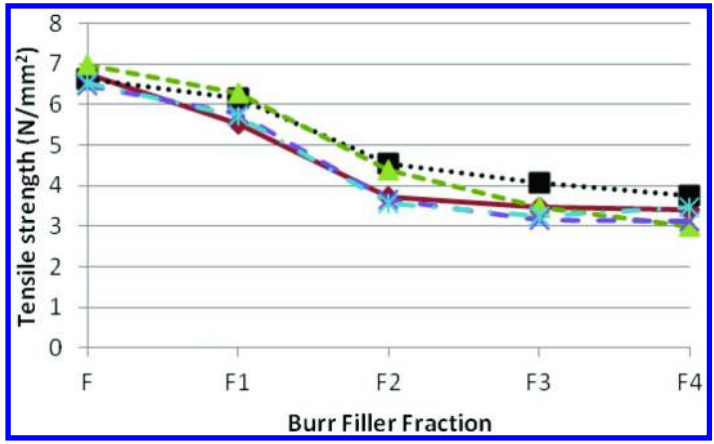

*Figure 1. Effect of filler size on tensile strength of LDPE composites: LDPE (no compatibilizer), solid brown line, diamond markers; LDPE with C1, dotted black line, square markers; LDPE with C2, short dashed green line, triangle markers; LDPE with C3, long dashed purple line, X markers; LDPE with C4, dashed-dotted blue line, * markers. On x-axis, F = LDPE without filler.*

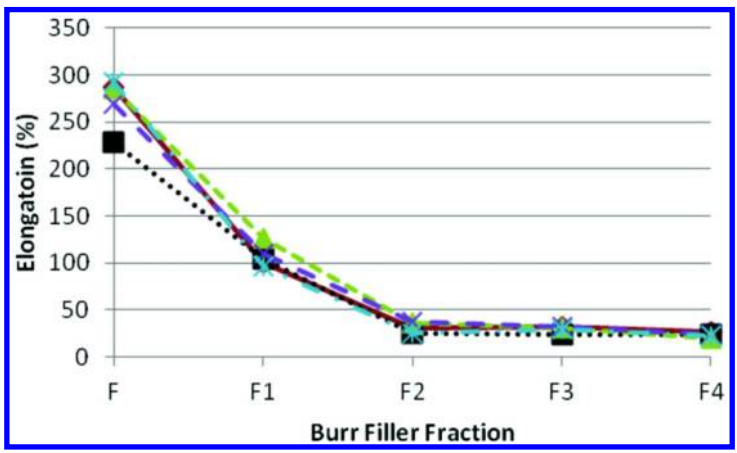

*Figure 2. Effect of filler size on elongation for LDPE composites: LDPE (no compatibilizer), solid brown line, diamond markers; LDPE with C1, dotted black line, square markers; LDPE with C2, short dashed green line, triangle markers; LDPE with C3, long dashed purple line, X markers; LDPE with C4, dashed-dotted blue line, * markers. On x-axis, F = LDPE without filler.*

In Green Polymer Chemistry: Biocatalysis and Materials II; Cheng, H., et al.;
ACS Symposium Series; American Chemical Society: Washington, DC, 2013.

Publication Date (Web): November 22, 2013 | doi: 10.1021/bk-2013-1144.ch028

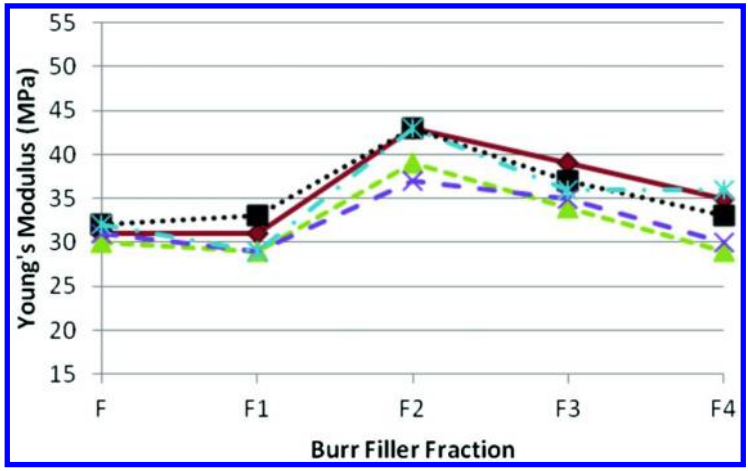

*Figure 3. Effect of filler size on Young's modulus for LDPE composites: LDPE (no compatibilizer), solid brown line, diamond markers; LDPE with C1, dotted black line, square markers; LDPE with C2, short dashed green line, triangle markers; LDPE with C3, long dashed purple line, X markers; LDPE with C4, dashed-dotted blue line, * markers. On x-axis, F = LDPE without filler.*

In summary, LDPE-cotton burr composites have modified properties that may serve some niche uses. If there is an application for LDPE where a stiffer and somewhat cheaper material is needed, the use of cotton burr filler with a compatibilizer may be considered.

Acknowledgments

The authors would like to thank Janet Berfield for technical assistance, and Gary Grose and Paulette Smith for help with extrusion. Mention of trade names or commercial products in this publication is solely for the purpose of providing specific information and does not imply recommendation or endorsement by the U.S. Department of Agriculture. USDA is an equal opportunity provider and employer.

References

1. Xanthos, M. *Functional Fillers for Plastics*; Wiley-VCH: Weinheim, Germany, 2010.
2. Wool, R. P.; Sun, X. S. *Bio-Based Polymers and Composites*; Elsevier: Burlington, MA, 2005.
3. Bledzki, A. K.; Reihmane, S.; Gassan, J. *Polym.-Plast. Technol. Eng.* **1998**, *37* (4), 451–468.
4. Peanasky, J. S.; Long, J. M.; Wool, R. P. *J. Polym. Sci.: Part B: Polym. Phys.* **1991**, *29*, 565–579 and references therein.

5. Albertsson, A.-C.; Barenstedt, C.; Karlsson, S. *J. Appl. Polym. Sci.* **1994**, *51*, 1097–1105.
6. Willett, J. L. *J. Appl. Polym. Sci.* **1994**, *54*, 1685–1695.
7. Willett, J. L. *Polym. Eng. Sci.* **1995**, *35*, 1184–1190.
8. Arvanitoyannis, I.; Biliaderis, C. G.; Ogawa, H.; Kawasaki, N. *Carbohydr. Polym.* **1998**, *36*, 89–104.
9. Yoo, Y.-D.; Kim,Y.-W.; Cho, W.-Y. U.S. Patent 5,461,093.
10. Girija, B. G.; Sailaja, R. R. N. *J. Appl. Polym. Sci.* **2006**, *101* (2), 1109–1120.
11. Gupta, A. P.; Kumar, V.; Sharma, M.; Shukla, S. K. *Polym.-Plast. Technol. Eng.* **2009**, *48* (6), 587–594.
12. Gupta, A. P.; Kumar, V.; Sharma, M. *J. Polym. Environ.* **2010**, *18*, 484–491.
13. Kim, T.-J.; Lee, Y.-M.; Im, S.-S. *Polym. Compos.* **1997**, *18* (3), 273–282.
14. Ołdak, D.; Kaczmarek, H.; Buffeteau, T.; Sourisseau, C. *J. Mater. Sci.* **2005**, *40* (16), 4189–4198.
15. Kaczmarek, H.; Ołdak, D. *Polym. Degrad. Stab.* **2006**, *91* (10), 2282–2291.
16. Lomakin, S. M.; Rogovina, S. Z.; Grachev, A. V.; Prut, E. V.; Alexanyan, C. V. *Thermochim. Acta* **2011**, *521*, 66–73.
17. de Menezes, A. J.; Siqueira, G.; Curvelo, A. A. S.; Dufresne, A. *Polymer* **2009**, *50*, 4552–4563.
18. Tajeddin, B.; Rahman, R. A.; Abdulah, L. C.; Ibrahim, N. A.; Yusof, Y. A. *Eur. J. Sci. Res.* **2009**, *32* (2), 223–230.
19. Madera-Santana, T. J.; Robledo, D.; Azamar, J. A.; Rios-Soberanis, C. R.; Freile-Pelegrin, Y. *Polym. Eng. Sci.* **2010**, *50* (3), 585–591.
20. Raj, R. G.; Kokta, B. V.; Nizio, J. D. *J. Appl. Polym. Sci.* **1992**, *45* (1), 91–101.
21. Beyer, C. D. *US Patent* 5,755,836.
22. Sutivisedsak, N.; Cheng, H. N.; Burks, C. S.; Johnson, J. A.; Siegel, J. P.; Civerolo, E. L.; Biswas, A. *J. Polym. Environ.* **2012**, *20*, 305–314.
23. Sutivisedsak, N.; Cheng, H. N.; Liu, S.; Lesch, W. C.; Finkenstadt, V. L.; Biswas, A. *J. Biobased Mater. Bioenergy* **2012**, *6* (1), 59–68.
24. Sutivisedsak, N.; Cheng, H. N.; Dowd, M. K.; Selling, G. W.; Biswas, A. *Ind. Crops Prod.* **2012**, *36*, 127–134.
25. Bailey, A. E. *Cottonseed and Cottonseed Products*; Wiley-Interscience: New York, 1948; pp 873−893.
26. Hausmann, K. In *Concise Polymeric Materials Encyclopedia*; Salamone, J. C., Ed.; CRC Press: Boca Raton, FL, 1999; pp 273–276.
27. Koning, C.; Van Duin, M.; Pagnoulle, C.; Jerome, R. *Prog. Polym. Sci.* **1998**, *23*, 707–757.
28. Bicerano, J. A Practical Guide to Polymeric Compatibilizers for Polymer Blends, Composites and Laminates. www.plas2006.com/UploadFile/TopicFile/20063112235119.doc.

Publication Date (Web): November 22, 2013 | doi: 10.1021/bk-2013-1144.ch028

Subject Index

Publication Date (Web): November 22, 2013 | doi: 10.1021/bk-2013-1144.ix002

In Green Polymer Chemistry: Biocatalysis and Materials II; Cheng, H., et al.;
ACS Symposium Series; American Chemical Society: Washington, DC, 2013.

Publication Date (Web): November 22, 2013 | doi: 10.1021/bk-2013-1144.ix002

E

F

G

H

In Green Polymer Chemistry: Biocatalysis and Materials II; Cheng, H., et al.;
ACS Symposium Series; American Chemical Society: Washington, DC, 2013.

L

M

In Green Polymer Chemistry: Biocatalysis and Materials II; Cheng, H., et al.;
ACS Symposium Series; American Chemical Society: Washington, DC, 2013.

Publication Date (Web): November 22, 2013 | doi: 10.1021/bk-2013-1144.ix002

N

O

P

In Green Polymer Chemistry: Biocatalysis and Materials II; Cheng, H., et al.;
ACS Symposium Series; American Chemical Society: Washington, DC, 2013.

S

In Green Polymer Chemistry: Biocatalysis and Materials II; Cheng, H., et al.;
ACS Symposium Series; American Chemical Society: Washington, DC, 2013.

Publication Date (Web): November 22, 2013 | doi: 10.1021/bk-2013-1144.ix002

T

U

V

X

In Green Polymer Chemistry: Biocatalysis and Materials II; Cheng, H., et al.;
ACS Symposium Series; American Chemical Society: Washington, DC, 2013.

Publication Date (Web): November 22, 2013 | doi: 10.1021/bk-2013-1144.ix002

Y

Publication Date (Web): November 22, 2013 | doi: 10.1021/bk-2013-1144.ix002

In Green Polymer Chemistry: Biocatalysis and Materials II; Cheng, H., et al.;
ACS Symposium Series; American Chemical Society: Washington, DC, 2013.